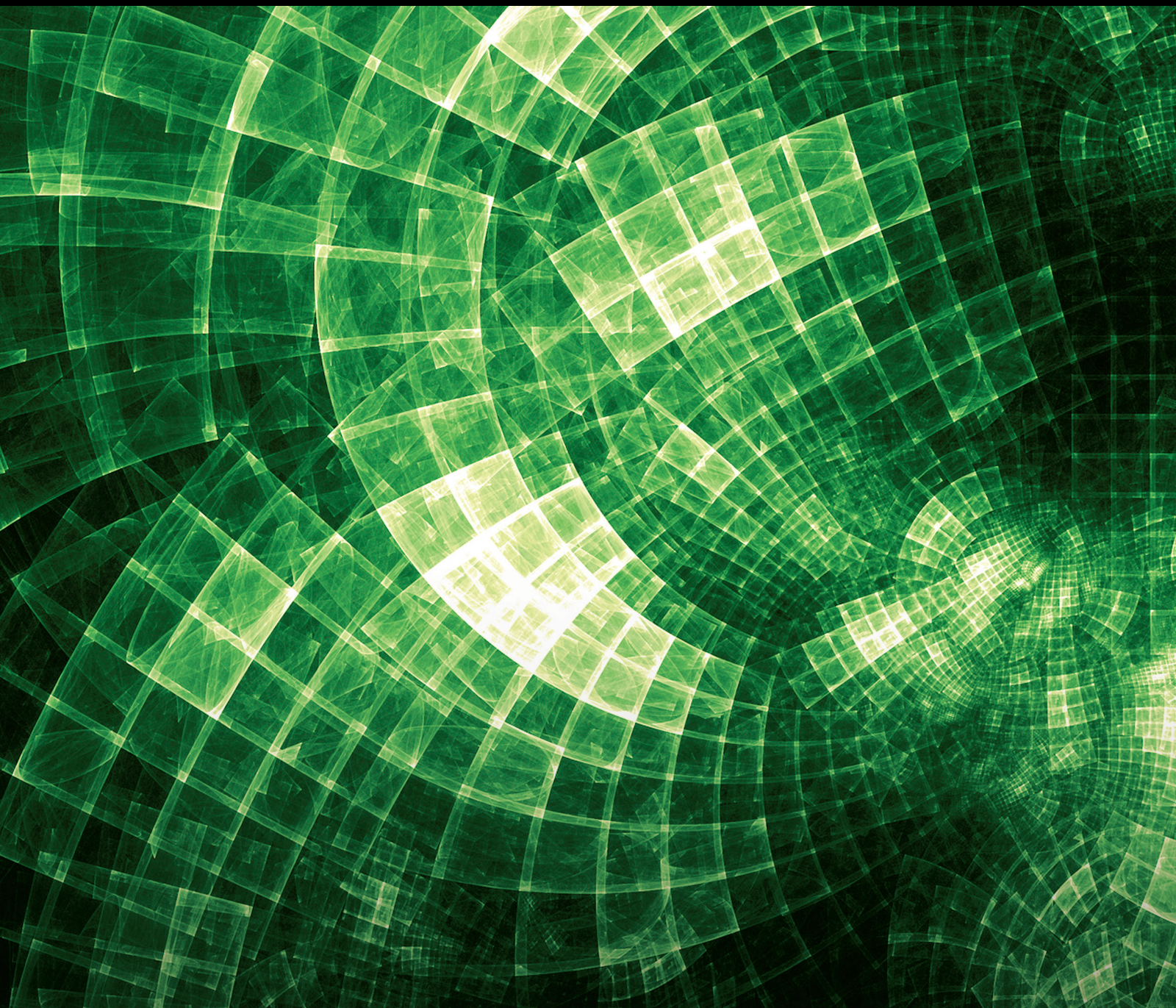


Journal of Mathematics

Graphics and Computation for Engineering Design

Lead Guest Editor: Ghulam Mustafa

Guest Editors: Jiansong Deng and Muhammad Aslam





Graphics and Computation for Engineering Design

Journal of Mathematics

Graphics and Computation for Engineering Design

Lead Guest Editor: Ghulam Mustafa

Guest Editors: Jiansong Deng and Muhammad
Aslam



Copyright © 2023 Hindawi Limited. All rights reserved.

This is a special issue published in "Journal of Mathematics." All articles are open access articles distributed under the Creative Commons Attribution License, which permits unrestricted use, distribution, and reproduction in any medium, provided the original work is properly cited.

Chief Editor

Jen-Chih Yao, Taiwan

Algebra

SEÇİL ÇEKEN , Turkey
Faranak Farshadifar , Iran
Marco Fontana , Italy
Genni Fragnelli , Italy
Xian-Ming Gu, China
Elena Guardo , Italy
Li Guo, USA
Shaofang Hong, China
Naihuan Jing , USA
Xiaogang Liu, China
Xuanlong Ma , China
Francisco Javier García Pacheco, Spain
Francesca Tartarone , Italy
Fernando Torres , Brazil
Zafar Ullah , Pakistan
Jiang Zeng , France

Geometry

Tareq Al-shami , Yemen
R.U. Gobithaasan , Malaysia
Erhan Güler , Turkey
Ljubisa Kocinac , Serbia
De-xing Kong , China
Antonio Masiello, Italy
Alfred Peris , Spain
Santi Spadaro, Italy

Logic and Set Theory

Ghous Ali , Pakistan
Kinkar Chandra Das, Republic of Korea
Jun Fan , Hong Kong
Carmelo Antonio Finocchiaro, Italy
Radomír Halaš, Czech Republic
Ali Jaballah , United Arab Emirates
Baoding Liu, China
G. Muhiuddin , Saudi Arabia
Basil K. Papadopoulos , Greece
Musavarah Sarwar, Pakistan
Anton Setzer , United Kingdom
R Sundareswaran, India
Xiangfeng Yang , China

Mathematical Analysis

Ammar Alsinai , India
M.M. Bhatti, China
Der-Chen Chang, USA
Phang Chang , Malaysia
Mengxin Chen, China
Genni Fragnelli , Italy
Willi Freeden, Germany
Yongqiang Fu , China
Ji Gao , USA
A. Ghareeb , Egypt
Victor Ginting, USA
Azhar Hussain, Pakistan
Azhar Hussain , Pakistan
Ömer Kişi , Turkey
Yi Li , USA
Stefan J. Linz , Germany
Ming-Sheng Liu , China
Dengfeng Lu, China
Xing Lü, China
Gaetano Luciano , Italy
Xiangyu Meng , USA
Dimitri Mugnai , Italy
A. M. Nagy , Kuwait
Valeri Obukhovskii, Russia
Humberto Rafeiro, United Arab Emirates
Luigi Rarità , Italy
Hegazy Rezk, Saudi Arabia
Nasser Saad , Canada
Mohammad W. Alomari, Jordan
Guotao Wang , China
Qiang Wu, USA
Çetin YILDIZ , Turkey
Wendong Yang , China
Jun Ye , China
Agacik Zafer, Kuwait

Operations Research

Ada Che , China
Nagarajan Deivanayagam Pillai, India
Sheng Du , China
Nan-Jing Huang , China
Chiranjibe Jana , India
Li Jin, United Kingdom
Mehmet Emir Koksal, Turkey
Palanivel M , India

Stanislaw Migorski , Poland
Predrag S. Stanimirović , Serbia
Balendu Bhooshan Upadhyay, India
Ching-Feng Wen , Taiwan
K.F.C. Yiu , Hong Kong
Liwei Zhang, China
Qing Kai Zhao, China

Probability and Statistics

Mario Abundo, Italy
Antonio Di Crescenzo , Italy
Jun Fan , Hong Kong
Jiancheng Jiang , USA
Markos Koutras , Greece
Fawang Liu , Australia
Barbara Martinucci , Italy
Yonghui Sun, China
Niansheng Tang , China
Efthymios G. Tsionas, United Kingdom
Bruce A. Watson , South Africa
Ding-Xuan Zhou , Hong Kong

Contents






Retracted: Evaluation of SMEs' Credit Decision Based on Support Vector Machine-Logistics

Regression

Journal of Mathematics

Retraction (1 page), Article ID 9809741, Volume 2023 (2023)

The Family of Multiparameter Quaternary Subdivision Schemes

Ghulam Mustafa , Muhammad Asghar , Shafqat Ali , Arzoo Qamar , and Jia-Bao Liu 



Research Article (12 pages), Article ID 4732464, Volume 2021 (2021)

A New Double Truncated Generalized Gamma Model with Some Applications

Awad A. Bakery , Wael Zakaria , and OM Kalthum S. K. Mohamed 






Research Article (27 pages), Article ID 5500631, Volume 2021 (2021)

Optimal Intersection Curves for Surfaces

Jiwen Gao, Faiza Sarfraz , Misbah Irshad, and Jia-Bao Liu 

Research Article (9 pages), Article ID 9945984, Volume 2021 (2021)

Subdivision Collocation Method for One-Dimensional Bratu's Problem

Ghulam Mustafa , Syeda Tehmina Ejaz , Sabila Kouser , Shafqat Ali , and Muhammad Aslam 


Research Article (8 pages), Article ID 3497017, Volume 2021 (2021)

Number of Distinct Homomorphic Images in Coset Diagrams

Muhammad Aamir , Muhammad Awais Yousaf , and Abdul Razaq 



Research Article (39 pages), Article ID 6669459, Volume 2021 (2021)

Research on DNA Nanostructures Based on the Hybrid Chain Reaction for the Assignment Problem

Risheng Wang, Zhixiang Yin , Jing Yang, Xinmu Yang, and Zhen Tang








Research Article (6 pages), Article ID 5570737, Volume 2021 (2021)

A Class of Sextic Trigonometric Bézier Curve with Two Shape Parameters

Salma Naseer, Muhammad Abbas , Homan Emadifar , Samia Bi Bi, Tahir Nazir, and Zaheer Hussain Shah

Research Article (16 pages), Article ID 9989810, Volume 2021 (2021)

Research on Revenue Insurance Premium Ratemaking of Jujube Based on Copula-Stochastic Optimization Model

Li-Mei Qi , Ruo-Yu Yao , Xing-Zhe Zhang , Yu-Jing Zhang , Xiao-Yin Wang , Jian-Ping Tao , and Jia-Ming Zhu 




Research Article (8 pages), Article ID 9959638, Volume 2021 (2021)

Recursive Process for Constructing the Refinement Rules of New Combined Subdivision Schemes and Its Extended Form






Rabia Hameed , Ghulam Mustafa , Jiansong Deng , and Shafqat Ali 

Research Article (23 pages), Article ID 6639706, Volume 2021 (2021)

On Distance-Based Topological Descriptors of Chemical Interconnection Networks

Min Hu, Haidar Ali , Muhammad Ahsan Binyamin , Bilal Ali, Jia-Bao Liu , and Chengmei Fan
Research Article (10 pages), Article ID 5520619, Volume 2021 (2021)


A Family of Optimal Eighth Order Iteration Functions for Multiple Roots and Its Dynamics

Saima Akram , Faiza Akram , Moin-ud-Din Junjua , Misbah Arshad , and Tariq Afzal 
Research Article (18 pages), Article ID 5597186, Volume 2021 (2021)

[Retracted] Evaluation of SMEs' Credit Decision Based on Support Vector Machine-Logistics Regression

Rui Xie , Rui Liu , Xian-Bei Liu , and Jia-Ming Zhu 
Research Article (10 pages), Article ID 5541436, Volume 2021 (2021)

A Modified Hybrid Conjugate Gradient Method for Unconstrained Optimization

Minglei Fang , Min Wang, Min Sun, and Rong Chen
Research Article (9 pages), Article ID 5597863, Volume 2021 (2021)

Some Graph-Based Encryption Schemes

Baizhu Ni, Rabiha Qazi, Shafiq Ur Rehman , and Ghulam Farid 
Research Article (8 pages), Article ID 6614172, Volume 2021 (2021)

Some Algebraic Properties of a Class of Integral Graphs Determined by Their Spectrum

Jia-Bao Liu , S. Morteza Mirafzal , and Ali Zafari 
Research Article (5 pages), Article ID 6632206, Volume 2021 (2021)

A New Paradigm to Design a Class of Combined Ternary Subdivision Schemes

Humaira Mustanira Tariq , Rabia Hameed , and Ghulam Mustafa 
Research Article (19 pages), Article ID 6679201, Volume 2021 (2021)

A Nonstationary Ternary 4-Point Shape-Preserving Subdivision Scheme

Jieqing Tan and Guangyue Tong 
Research Article (10 pages), Article ID 6694241, Volume 2021 (2021)

Inverse Numerical Iterative Technique for Finding all Roots of Nonlinear Equations with Engineering Applications

Mudassir Shams , Naila Rafiq , Babar Ahmad, and Nazir Ahmad Mir
Research Article (10 pages), Article ID 6643514, Volume 2021 (2021)

Retraction

Retracted: Evaluation of SMEs' Credit Decision Based on Support Vector Machine-Logistics Regression

Journal of Mathematics

Received 15 August 2023; Accepted 15 August 2023; Published 16 August 2023

Copyright © 2023 Journal of Mathematics. This is an open access article distributed under the Creative Commons Attribution License, which permits unrestricted use, distribution, and reproduction in any medium, provided the original work is properly cited.

This article has been retracted by Hindawi following an investigation undertaken by the publisher [1]. This investigation has uncovered evidence of one or more of the following indicators of systematic manipulation of the publication process:

- (1) Discrepancies in scope
- (2) Discrepancies in the description of the research reported
- (3) Discrepancies between the availability of data and the research described
- (4) Inappropriate citations
- (5) Incoherent, meaningless and/or irrelevant content included in the article
- (6) Peer-review manipulation

The presence of these indicators undermines our confidence in the integrity of the article's content and we cannot, therefore, vouch for its reliability. Please note that this notice is intended solely to alert readers that the content of this article is unreliable. We have not investigated whether authors were aware of or involved in the systematic manipulation of the publication process.

Wiley and Hindawi regrets that the usual quality checks did not identify these issues before publication and have since put additional measures in place to safeguard research integrity.

We wish to credit our own Research Integrity and Research Publishing teams and anonymous and named external researchers and research integrity experts for contributing to this investigation.

The corresponding author, as the representative of all authors, has been given the opportunity to register their agreement or disagreement to this retraction. We have kept a record of any response received.

References

- [1] R. Xie, R. Liu, X. Liu, and J. Zhu, "Evaluation of SMEs' Credit Decision Based on Support Vector Machine-Logistics Regression," *Journal of Mathematics*, vol. 2021, Article ID 5541436, 10 pages, 2021.

Research Article

The Family of Multiparameter Quaternary Subdivision Schemes

Ghulam Mustafa ¹, Muhammad Asghar ¹, Shafqat Ali ¹, Arzoo Qamar ²,
and Jia-Bao Liu ³

¹Department of Mathematics, The Islamia University of Bahawalpur, Bahawalpur, Pakistan

²Department of Mathematics, NCBA & E Sub-Campus Bahawalpur, Bahawalpur, Pakistan

³School of Mathematics and Physics, Anhui Jianzhu University, Hefei 230601, China

Correspondence should be addressed to Jia-Bao Liu; liujiabaoad@163.com

Received 8 May 2021; Revised 28 September 2021; Accepted 19 October 2021; Published 14 December 2021

Academic Editor: Efthymios G. Tsionas

Copyright © 2021 Ghulam Mustafa et al. This is an open access article distributed under the Creative Commons Attribution License, which permits unrestricted use, distribution, and reproduction in any medium, provided the original work is properly cited.

In the field of subdivision, the smoothness increases as the arity of schemes increases. The family of high arity schemes gives high smoothness comparative to low arity schemes. In this paper, we propose a simple and generalized formula for a family of multiparameter quaternary subdivision schemes. The conditions for convergence of subdivision schemes are also presented. Moreover, we derive subdivision schemes after substituting the different values of parameters. We also analyzed the important properties of the proposed family of subdivision schemes. After comparison with existing schemes, we analyze that the proposed family of subdivision schemes gives better smoothness and approximation compared with the existing subdivision schemes.

1. Introduction

Subdivision schemes are the backbone of Computer Aided Geometric Design (CAGD). Subdivision schemes are used for the generation of smooth curves from the initial polygon. If the rules of subdivision schemes are four, then subdivision schemes are called quaternary subdivision schemes.

In 2009, a 4-point quaternary scheme is presented in [1]. The proposed scheme has C^3 -continuity. A family of quaternary schemes is presented in [2]. They used the Cox–De Boor recursion formula for the construction of quaternary schemes. In 2013, Ghaffar et al. [3] presented a generalized formula for the generation of 4-point subdivision schemes of binary, ternary, and quaternary subdivision schemes. In the same year, Amat and Liandrat [4] presented a 4-point scheme for the elimination of the Gibbs phenomenon.

In 2018, Pervaz [5] presented a 4-point quaternary scheme. They discuss the shape preserving properties of the subdivision scheme. Ashraf et al. [6, 7] presented and analyzed the geometrical properties of four point interpolating subdivision schemes. Hameed et al. [8] presented a 4-point subdivision scheme for regular curves and surfaces design.

Hussain et al. [9] presented a generalized formula for 5-point subdivision schemes of any arity. Khan et al. [10] presented a computational method for the generation of subdivision schemes. Conti and Romani [11] presented an algebraic technique for the generation of m -ary subdivision schemes. Romani [12] presented an algorithm for the generation of dual interpolating m -ary subdivision schemes. Romani and Viscardi [13] presented a new class of univariate stationary interpolating subdivision schemes of arity m . Recently, Mustafa et al. [14] presented a family of integer-point ternary parametric subdivision schemes.

1.1. Our Contributions. In the field of subdivision, as arity increases, the smoothness also increases. The main purpose of this work is to present a simple and generalized formula for derivation of multiparametric quaternary subdivision schemes based on Laurent polynomial. The conditions for the construction of subdivision schemes are also presented. Our schemes give better approximation and smoothness compared to the same type of existing subdivision schemes (see Figures 1 and 2).

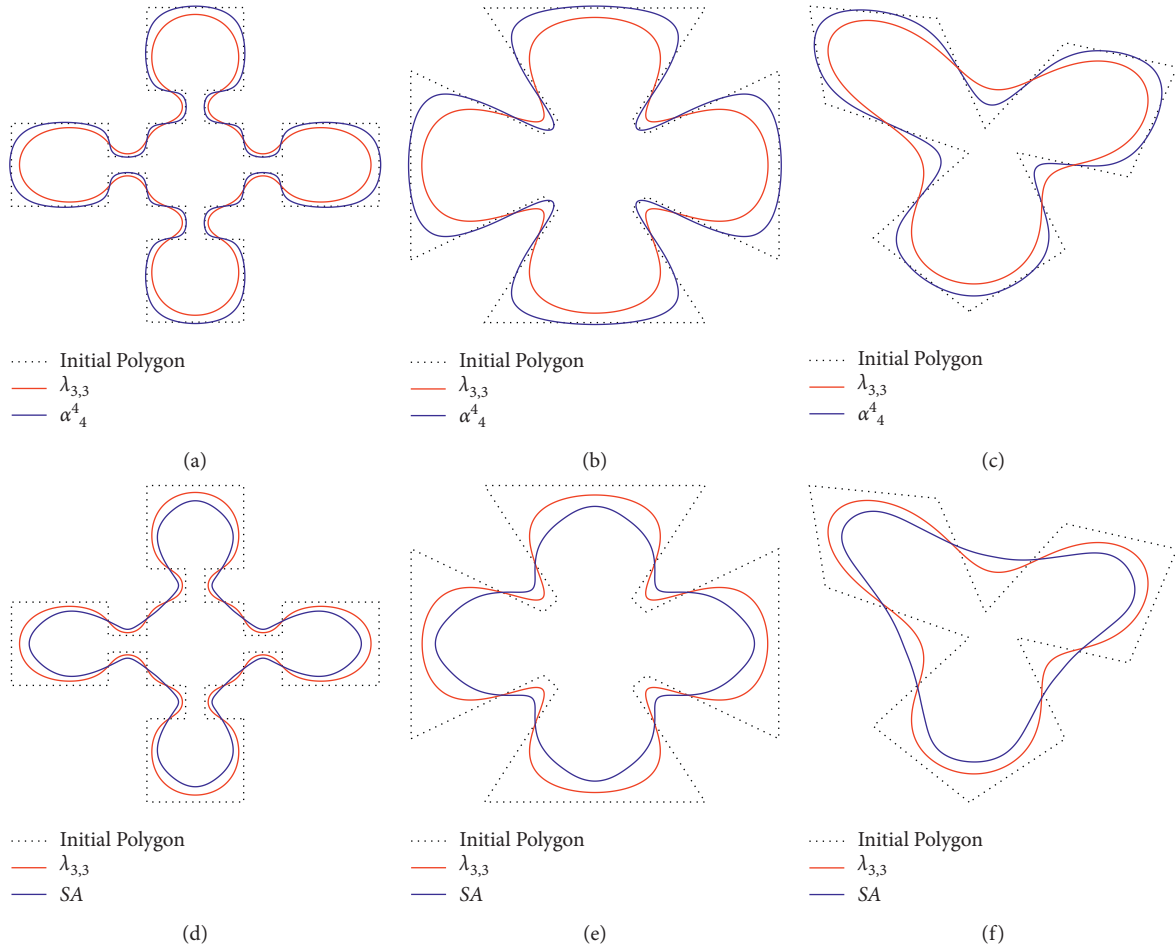


FIGURE 1: (a–c) Comparison of limit curves for close polygons produced by 4-point schemes $\lambda_{3,3}$ and α_4^4 .

The paper is organized as follows. In Section 2, we present the general formula with different cases of a family of quaternary subdivision schemes. Analysis of the proposed family is presented in Section 3. Section 4 is for the comparison of the proposed family of subdivision schemes with existing subdivision schemes. Conclusions are drawn in Section 5.

2. General Formula for Multiparameter Family of Quaternary Subdivision Schemes

In this section, we present a general formula for the multiparameter family of quaternary approximating subdivision schemes based on Laurent polynomial. The general formula is

$$\lambda_{l,q}(z) = (1 + z + z^2 + z^3)^{l+1} (a_0 + a_1z + a_2z^2 + \dots + a_qz^q). \tag{1}$$

The value of l controls the complexity and that of q controls the parameters in subdivision schemes. By using different values of l and q , we get the Laurent polynomial of family of $(l + 1)$ -point quaternary $(q + 1)$ parametric subdivision schemes. Here, we will discuss the different cases and conditions for family of quaternary subdivision schemes.

Case 1. By putting $l = 2, q = 1$ and $a_0 + a_1 = 1/16$, with $a_0 < 1/4, a_1 < 1/4$, in (1), we can obtain the Laurent polynomial of subdivision scheme

$$\begin{aligned} \lambda_{2,1}(z) = & a_1z^{10} + (a_0 + 3a_1)z^9 + (3a_0 + 6a_1)z^8 + (6a_0 + 10a_1)z^7 \\ & + (10a_0 + 12a_1)z^6 + (12a_0 + 12a_1)z^5 + (12a_0 + 10a_1)z^4 + (10a_0 + 6a_1)z^3 \\ & + (6a_0 + 3a_1)z^2 + (a_1 + 3a_0)z + a_0. \end{aligned} \tag{2}$$

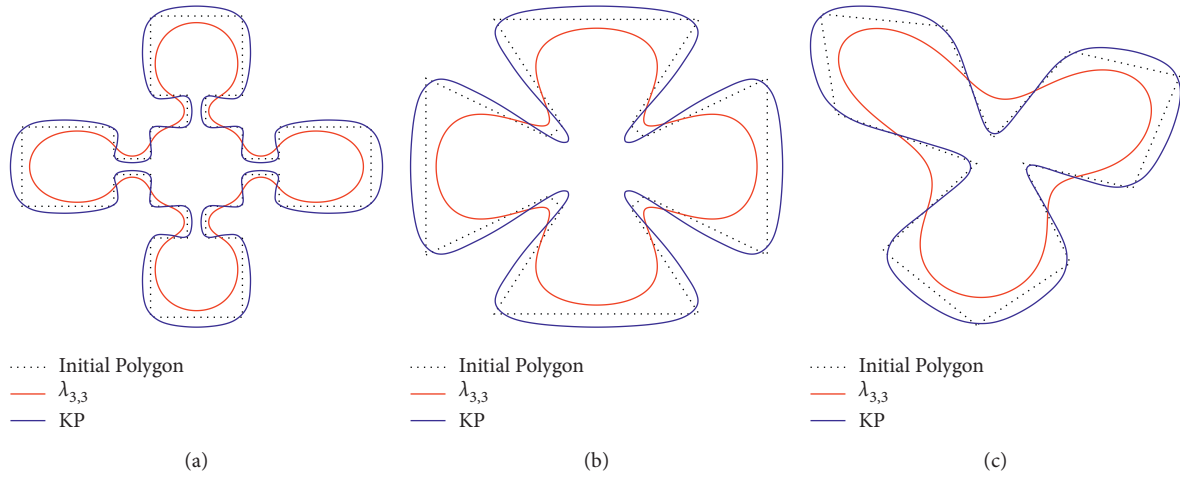


FIGURE 2: (a–c) Comparison of limit curves for close polygons produced by 4-point schemes $\lambda_{3,3}$ and KP .

The mask of the scheme corresponding to the Laurent polynomial $\lambda_{2,1}(z)$ is

$$\lambda_{2,1} = \left\{ \begin{array}{l} a_1, (a_0 + 3a_1), (3a_0 + 6a_1), (6a_0 + 10a_1), (10a_0 + 12a_1), (12a_0 + 12a_1), \\ (12a_0 + 10a_1), (10a_0 + 6a_1), (6a_0 + 3a_1), (3a_0 + a_1), a_0 \end{array} \right\}. \quad (3)$$

The scheme corresponding to mask (3) is

$$\begin{aligned} P_{4i}^{k+1} &= (10a_0 + 6a_1)P_{i-1}^k + (6a_0 + 10a_1)P_i^k, \\ P_{4i+1}^{k+1} &= (6a_0 + 3a_1)P_{i-1}^k + (10a_0 + 12a_1)P_i^k + a_1P_{i+1}^k, \\ P_{4i+2}^{k+1} &= (3a_0 + a_1)P_{i-1}^k + (12a_0 + 12a_1)P_i^k + (a_0 + 3a_1)P_{i+1}^k, \\ P_{4i+3}^{k+1} &= a_0P_{i-1}^k + (12a_0 + 10a_1)P_i^k + (3a_0 + 6a_1)P_{i+1}^k. \end{aligned} \quad (4)$$

Case 2. By setting $l = 2, q = 2$ and $a_0 + a_1 + a_2 = 1/16$ with $a_0 < 1/4, a_1 < 1/4, a_2 < 1/4$ in (2), we get the Laurent polynomial of 3-point scheme

$$\begin{aligned} \lambda_{2,2}(z) &= a_2z^{11} + (a_1 + 3a_2)z^{10} + (a_0 + 3a_1 + 6a_2)z^9 + (3a_0 + 6a_1 + 10a_2)z^8 \\ &\quad + (6a_0 + 10a_1 + 12a_2)z^7 + (10a_0 + 12a_1 + 12a_2)z^6 + (12a_0 + 12a_1 + 10a_2)z^5 \\ &\quad + (12a_0 + 10a_1 + 6a_2)z^4 + (10a_0 + 6a_1 + 3a_2)z^3 + (6a_0 + a_2 + 3a_1)z^2 \\ &\quad + (a_1 + 3a_0)z + a_0. \end{aligned} \quad (5)$$

The mask of the scheme corresponding to the Laurent polynomial (5) is

TABLE 1: The mask of the unified family of quaternary curve subdivision schemes corresponding to different values of l and q .

l, q	Complexity	Mask
2, 1	3-point	$\{a_1, (a_0 + 3a_1), (3a_0 + 6a_1), (6a_0 + 10a_1), (10a_0 + 12a_1),$ $(12a_0 + 12a_1), (12a_0 + 10a_1), (10a_0 + 6a_1), (6a_0 + 3a_1),$ $(3a_0 + a_1), a_0\}.$
2, 2	3-point	$\{a_2, (3a_2 + a_1), (a_0 + 3a_1 + 6a_2), (3a_0 + 6a_1 + 10a_2), (6a_0 + 10a_1 + 12a_2),$ $(10a_0 + 12a_1 + 12a_2), (12a_0 + 12a_1 + 10a_2), (12a_0 + 10a_1 + 6a_2), (10a_0 + 6a_1 + 3a_2),$ $(6a_0 + a_2 + 3a_1), (a_1 + 3a_0), a_0\}.$
3, 2	4-point	$\{a_2, (4a_2 + a_1), (a_0 + 4a_1 + 10a_2), (4a_0 + 10a_1 + 20a_2), (10a_0 + 20a_1 + 31a_2),$ $(20a_0 + 31a_1 + 40a_2), (31a_0 + 40a_1 + 44a_2), (40a_0 + 44a_1 + 40a_2),$ $(44a_0 + 40a_1 + 31a_2), (40a_0 + 20a_2 + 31a_1), (20a_1 + 31a_0 + 10a_2),$ $(20a_0 + 10a_1 + 4a_2), (10a_0 + 4a_1 + a_2), (4a_0 + a_1), a_0\}.$
3, 3	4-point	$\{a_3, (4a_3 + a_2), (a_1 + 4a_2 + 10a_3), (a_0 + 4a_1 + 10a_2 + 20a_3), (4a_0 + 10a_1 + 20a_2 + 31a_3),$ $(10a_0 + 20a_1 + 31a_2 + 40a_3), (20a_0 + 31a_1 + 40a_2 + 44a_3), (31a_0 + 40a_1 + 44a_2 + 40a_3),$ $(40a_0 + 44a_1 + 40a_2 + 31a_3), (44a_0 + 40a_1 + 31a_2 + 20a_3), (40a_0 + 31a_1 + 20a_2 + 10a_3),$ $(31a_0 + 20a_1 + 10a_2 + 4a_3), (20a_0 + 10a_1 + 4a_2 + a_3), (10a_0 + 4a_1 + a_2), (4a_0 + a_1), a_0\}.$

TABLE 2: The degree of generation of family of unified quaternary curve subdivision scheme for different cases.

Cases	l, q	D_g	Values of $a_{q's}$	τ	Parametrization
1	$l = 2, q = 1$	2	$a_0 = -(3/32), a_1 = 5/32$ $a_0 = 5/32, a_1 = -(3/32)$	7 3	Primal Primal
2	$l = 2, q = 2$	2	$a_0 = a_2 = -(15/128), a_1 = 19/64$	$\frac{11}{2}$	Dual
3	$l = 3, q = 2$	3	$a_0 = a_2 = -(5/128), a_1 = 3/32$	7	Primal
4	$l = 3, q = 3$	3	$a_0 = a_3 = w, a_1 = a_2 = 1/128 - w$	$\frac{15}{2}$	Dual

$$\lambda_{2,2} = \left\{ \begin{array}{l} a_2, (3a_2 + a_1), (a_0 + 3a_1 + 6a_2), (3a_0 + 6a_1 + 10a_2), (6a_0 + 10a_1 + 12a_2), \\ (10a_0 + 12a_1 + 12a_2), (12a_0 + 12a_1 + 10a_2), (12a_0 + 10a_1 + 6a_2), (10a_0 + 6a_1 + 3a_2), \\ (6a_0 + a_2 + 3a_1), (a_1 + 3a_0), a_0 \end{array} \right\}. \quad (6)$$

The scheme corresponding to mask (6) is

$$\begin{aligned} P_{4i}^{k+1} &= (10a_0 + 6a_1 + 3a_2)P_{i-1}^k + (6a_0 + 10a_1 + 12a_2)P_i^k + a_2P_{i+1}^k, \\ P_{4i+1}^{k+1} &= (6a_0 + 3a_1 + a_2)P_{i-1}^k + (10a_0 + 12a_1 + 12a_2)P_i^k + (a_1 + 3a_2)P_{i+1}^k, \\ P_{4i+2}^{k+1} &= (3a_0 + a_1)P_{i-1}^k + (12a_0 + 12a_1 + 10a_2)P_i^k + (a_0 + 3a_1 + 6a_2)P_{i+1}^k, \\ P_{4i+3}^{k+1} &= a_0P_{i-1}^k + (6a_2 + 10a_1 + 12a_2)P_i^k + (3a_0 + 6a_1 + 10a_2)P_{i+1}^k. \end{aligned} \quad (7)$$

Case 3. By setting $l = 3, q = 2$, and $a_0 + a_1 + a_2 = 1/64$, with $a_0 < 1/4, a_1 < 1/4, a_2 < 1/4$ in (2), we can obtain the Laurent polynomial of 4-point scheme

$$\begin{aligned} \lambda_{3,2}(z) &= a_2z^{14} + (a_1 + 4a_2)z^{13} + (a_0 + 4a_1 + 10a_2)z^{12} + (4a_0 + 10a_1 + 20a_2)z^{11} \\ &\quad + (10a_0 + 20a_1 + 31a_2)z^{10} + (20a_0 + 31a_1 + 40a_2)z^9 + (31a_0 + 40a_1 + 44a_2)z^8 \\ &\quad + (40a_0 + 44a_1 + 40a_2)z^7 + (44a_0 + 40a_1 + 31a_2)z^6 + (40a_0 + 20a_2 + 31a_1)z^5 \\ &\quad + (31a_0 + 20a_1 + 10a_2)z^4 + (20a_0 + 10a_1 + 4a_2)z^3 + (10a_0 + 4a_1 + a_2)z^2 \\ &\quad + (4a_0 + a_1)z + a_0. \end{aligned} \quad (8)$$

The mask of the scheme corresponding to the Laurent polynomial (8) is

$$\lambda_{3,2} = \left\{ \begin{array}{l} a_2, (4a_2 + a_1), (a_0 + 4a_1 + 10a_2), (4a_0 + 10a_1 + 20a_2), (10a_0 + 20a_1 + 31a_2), \\ (20a_0 + 31a_1 + 40a_2), (31a_0 + 40a_1 + 44a_2), (40a_0 + 44a_1 + 40a_2), (44a_0 + 40a_1 + 31a_2), \\ (40a_0 + 20a_2 + 31a_1), (20a_1 + 31a_0 + 10a_2), (20a_0 + 10a_1 + 4a_2), (10a_0 + 4a_1 + a_2), (4a_0 + a_1), a_0 \end{array} \right\}. \quad (9)$$

The scheme corresponding to mask (9) is

$$\begin{aligned}
P_{4i}^{k+1} &= (20a_0 + 10a_1 + 4a_2)P_{i-1}^k + (40a_0 + 44a_1 + 40a_2)P_i^k + (4a_0 + 10a_1 + 20a_2)P_{i+1}^k, \\
P_{4i+1}^{k+1} &= (10a_0 + 4a_1 + a_2)P_{i-1}^k + (44a_0 + 40a_1 + 31a_2)P_i^k + (10a_0 + 20a_1 + 31a_2)P_{i+1}^k + a_2P_{i+2}^k, \\
P_{4i+2}^{k+1} &= (4a_0 + a_1)P_{i-1}^k + (40a_0 + 20a_2 + 31a_1)P_i^k + (20a_0 + 31a_1 + 40a_2)P_{i+1}^k + (4a_2 + a_1)P_{i+2}^k, \\
P_{4i+3}^{k+1} &= a_0P_{i-1}^k + (20a_1 + 31a_0 + 10a_2)P_i^k + (31a_0 + 40a_1 + 44a_2)P_{i+1}^k + (a_0 + 4a_1 + 10a_2)P_{i+2}^k.
\end{aligned} \tag{10}$$

Case 4. By putting $l = 3, q = 3$, and $a_0 + a_1 + a_2 + a_3 = 1/64$, with $a_0 < 1/4, a_1 < 1/4, a_2 < 1/4, a_3 < 1/4$ in (2), we can obtain the Laurent polynomial of 4-point scheme

$$\begin{aligned}
\lambda_{3,3}(z) &= a_3z^{15} + (a_2 + 4a_3)z^{14} + (a_1 + 4a_2 + 10a_3)z^{13} + (a_0 + 4a_1 + 10a_2 + 20a_3)z^{12} \\
&\quad + (4a_0 + 10a_1 + 20a_2 + 31a_3)z^{11} + (10a_0 + 20a_1 + 31a_2 + 40a_3)z^{10} \\
&\quad + (20a_0 + 40a_2 + 44a_3 + 31a_1)z^9 + (31a_0 + 40a_1 + 44a_2 + 40a_3)z^8 \\
&\quad + (40a_0 + 44a_1 + 40a_2 + 31a_3)z^7 + (44a_0 + 31a_2 + 40a_1 + 20a_3)z^6 \\
&\quad + (31a_1 + 20a_2 + 10a_3 + 40a_0)z^5 + (20a_1 + 10a_2 + 4a_3 + 31a_0)z^4 \\
&\quad + (20a_0 + 10a_1 + 4a_2 + a_3)z^3 + (4a_1 + 10a_0 + a_2z)^2 + (4a_0 + a_1)z + a_0.
\end{aligned} \tag{11}$$

The mask of the scheme corresponding to the Laurent polynomial (11) is

$$\lambda_{3,3} = \left\{ \begin{array}{l} a_3, (4a_3 + a_2), (a_1 + 4a_2 + 10a_3), (a_0 + 4a_1 + 10a_2 + 20a_3), (4a_0 + 10a_1 + 20a_2 + 31a_3), \\ (10a_0 + 20a_1 + 31a_2 + 40a_3), (20a_0 + 31a_1 + 40a_2 + 44a_3), (31a_0 + 40a_1 + 44a_2 + 40a_3), \\ (40a_0 + 44a_1 + 40a_2 + 31a_3), (44a_0 + 40a_1 + 31a_2 + 20a_3), (40a_0 + 31a_1 + 20a_2 + 10a_3), \\ (31a_0 + 20a_1 + 10a_2 + 4a_3), (20a_0 + 10a_1 + 4a_2 + a_3), (10a_0 + 4a_1 + a_2), (4a_0 + a_1), a_0 \end{array} \right\}. \tag{12}$$

The scheme corresponding to the mask is

$$\begin{aligned}
P_{4i}^{k+1} &= (20a_0 + 10a_1 + 4a_2 + a_3)P_{i-1}^k + (40a_0 + 44a_1 + 40a_2 + 31a_3)P_i^k \\
&\quad + (4a_0 + 10a_1 + 20a_2 + 31a_3)P_{i+1}^k + a_3P_{i+2}^k, \\
P_{4i+1}^{k+1} &= (10a_0 + 4a_1 + a_2)P_{i-1}^k + (44a_0 + 40a_1 + 31a_2 + 20a_3)P_i^k + (10a_0 + 20a_1 + 31a_2 + 40a_3)P_{i+1}^k \\
&\quad + (4a_3 + a_2)P_{i+2}^k, \\
P_{4i+2}^{k+1} &= (4a_0 + a_1)P_{i-1}^k + (40a_0 + 31a_1 + 20a_2 + 10a_3)P_i^k + (20a_0 + 31a_1 + 40a_2 + 40a_3)P_{i+1}^k \\
&\quad + (4a_2 + a_1 + 10a_3)P_{i+2}^k, \\
P_{4i+3}^{k+1} &= a_0P_{i-1}^k + (31a_0 + 20a_1 + 10a_2 + 4a_3)P_i^k + (31a_0 + 40a_1 + 44a_2 + 40a_3)P_{i+1}^k \\
&\quad + (a_0 + 4a_1 + 10a_2 + 20a_3)P_{i+2}^k.
\end{aligned} \tag{13}$$

Scheme (13) is the general 4-point quaternary scheme with 4 parameters.

Similarly for different values of l and q , we get the $l+1$ -point quaternary approximating subdivision schemes

having $(q + 1)$ parameters. In Table 1, we present the mask of family members of quaternary schemes for different values of l and q .

4-point scheme. After substituting the values of $a_0 = w$, $a_1 = 1/128 - w$, $a_2 = 1/128 - w$, and $a_3 = w$ in (13), we get a 4-point parametric scheme

3. Analysis of the Unified Family of Quaternary Curve Subdivision Schemes

This section contains the analysis of important properties of the proposed subdivision schemes. For this, we consider the

$$\begin{aligned}
 P_{4i}^{k+1} &= \left(7w + \frac{7}{64}\right)P_{i-1}^k + \left(\frac{21}{32} - 13w\right)P_i^k + \left(5w + \frac{15}{64}\right)P_{i+1}^k + wP_{i+2}^k, \\
 P_{4i+1}^{k+1} &= \left(5w + \frac{5}{128}\right)P_{i-1}^k + \left(\frac{71}{128} - 7w\right)P_i^k + \left(\frac{51}{128} - w\right)P_{i+1}^k + \left(3w + \frac{1}{128}\right)P_{i+2}^k, \\
 P_{4i+2}^{k+1} &= \left(3w + \frac{1}{128}\right)P_{i-1}^k + \left(\frac{51}{128} - w\right)P_i^k + \left(\frac{71}{128} - 7w\right)P_{i+1}^k + \left(5w + \frac{5}{128}\right)P_{i+2}^k, \\
 P_{4i+3}^{k+1} &= wP_{i-1}^k + \left(5w + \frac{15}{64}\right)P_i^k + \left(\frac{21}{32} - 13w\right)P_{i+1}^k + \left(7w + \frac{7}{64}\right)P_{i+2}^k.
 \end{aligned}
 \tag{14}$$

The Laurent polynomial corresponding to scheme (14) is

$$\lambda(z) = \frac{1}{128}(1 + z + z^2 + z^3)^4(1 + z)(128w + (1 - 256w)z + 128wz^2),
 \tag{15}$$

The Laurent polynomial method [15] is used to compute the degree of generation, degree of reproduction, and continuity analysis. Moreover, Rioul’s method [16] is used to compute lower and upper bounds on Hölder regularity of scheme (14). The analysis of other schemes is similar.

Theorem 1. A 4-point quaternary subdivision scheme (14) has cubic reproduction with respect to the dual parametrization for $w = -(21/1024)$.

Proof. By taking the derivative of (15) with respect to z , we get

$$\begin{aligned}
 \lambda'(z) &= 4(1 + z + z^2 + z^3)^3(1 + 2z + 3z^2)\left(w + \left(\frac{1}{128} - w\right)z + \left(\frac{1}{128} - w\right)z^2 + wz^3\right) \\
 &\quad + (1 + z + z^2 + z^3)^4\left(\left(\frac{1}{128} - w\right) + 2\left(\frac{1}{128} - w\right)z + 3wz^2\right),
 \end{aligned}
 \tag{16}$$

After substituting $z = 1$ in (15) and (16), we get $\lambda(1) = 4$ and $\lambda'(1) = 30$. The value of shift parameter $\tau = \lambda'(1)/4 = 15/2$. Hence, by [15], the subdivision scheme (14) has dual parametrization. Further, we can easily verify that

proposed family of quaternary subdivision schemes. Here, l, q, D_g , values of $a_{q's}$, τ , and parametrization denote the positive integer, degree of generation, parameter values, shift parameter, and parametrization of the scheme, respectively.

$$\lambda^k(1) = 4 \prod_{j=0}^{k-1} \left(\frac{15}{2} - j\right) \quad \text{for } k = 0, 1, 2, 3 \text{ with } w = -\frac{21}{1024},
 \tag{17}$$

Theorem 2. A 4-point quaternary subdivision scheme (14) has C^3 continuity for $w \in (-1/128, 2/128)$.

Proof. Consider the Laurent polynomial

Hence, by [15], the scheme corresponding to $\lambda(z)$ has cubic reproduction with respect to the dual parametrization. \square

$$\lambda^1(z) = \left(\frac{4z^3}{1 + z + z^2 + z^3}\right)^4 \lambda(z),
 \tag{18}$$

Table 2 summarizes the results of degree of generation, values of parameters, shift parameter, and parametrization of a

where $\lambda(z)$ is defined in (15). This implies

$$\lambda^1(z) = \left(\frac{4z^3}{1+z+z^2+z^3}\right)^4 (1+z+z^2+z^3)^4 \left(w + \left(\frac{1}{128} - w\right)z + \left(\frac{1}{128} - w\right)z^2 + wz^3\right), \tag{19}$$

After simplification, we get

$$\lambda^1(z) = 256z^{12} \left[w + \left(\frac{1}{128} - w\right)z + \left(\frac{1}{128} - w\right)z^2 + wz^3 \right]. \tag{20}$$

Let λ^1 be the mask of the scheme S^1 corresponding to $\lambda^1(z)$, then we have

$$\lambda^1 = 256 \left[w, \frac{1}{128} - w, \frac{1}{128} - w, w \right], \tag{21}$$

The scheme corresponding to $\lambda(z)$ is C^3 continuous if $\|1/4S^1\|_\infty < 1$; for this, we have to check that

$$\left\| \frac{1}{4}S^1 \right\|_\infty = \max \frac{1}{4} \{ |256w|, |2 - 256w|, |2 - 256w|, |256w| \}. \tag{22}$$

If $w \in (-1/128, 2/128)$, then $\|1/4S^1\|_\infty < 1$. Then, by [15], the scheme corresponding to $\lambda(z)$ has C^3 continuity, which completes the proof. \square

Theorem 3. *The Hölder regularity of a 4-point scheme (14) is $r = 4 - \log_4(\mu)$, where μ is defined as*

$$\begin{cases} \mu = 2 - 256w, & \text{if } -\frac{1}{128} < w \leq \frac{1}{256}, \\ \mu = 256w, & \text{if } \frac{1}{256} < w < \frac{2}{128}. \end{cases} \tag{23}$$

Proof. The Laurent polynomial (15) can be written as

$$\lambda(z) = \left(\frac{1+z+z^2+z^3}{4}\right)^4 b(z), \tag{24}$$

where

$$b(z) = [256w + (2 - 256w)z + (2 - 256w)z^2 + 256wz^3]. \tag{25}$$

From (25), the coefficients of z in $b(z)$ are $b_0 = 256w$, $b_1 = 2 - 256w$, $b_2 = 2 - 256w$, and $b_3 = 256w$. The number of factors in $\lambda(z)$ is $k = 4$. The matrices B_n has order 3×3 where $n = 0, 1, 2$ and 3 . The elements of the matrices B_0, B_1, B_2 , and B_3 can be derived by $(B_n)_{ij} = b_{(3+n)+i-4j}$, for $i, = 1, 2$, and 3 ; then, we have

$$B_0 = \begin{pmatrix} 256w & 0 & 0 \\ 2 - 256w & 0 & 0 \\ 2 - 256w & 0 & 0 \end{pmatrix},$$

$$B_1 = \begin{pmatrix} 2 - 256w & 0 & 0 \\ 2 - 256w & 0 & 0 \\ 256w & 0 & 0 \end{pmatrix},$$

$$B_2 = \begin{pmatrix} 2 - 256w & 0 & 0 \\ 256w & 0 & 0 \\ 0 & 256w & 0 \end{pmatrix}, \tag{26}$$

$$B_3 = \begin{pmatrix} 256w & 0 & 0 \\ 0 & 256w & 0 \\ 0 & 2 - 256w & 0 \end{pmatrix}.$$

The eigenvalues of B_0, B_1, B_2 , and B_3 are $\{0, 0, 256w\}, \{0, 0, 2 - 256w\}, \{0, 0, 2 - 256w\}$, and $\{0, 256w, 256w\}$, respectively. For bounds on Hölder regularity, we calculate $\max\{\rho(B_0), \rho(B_1), \rho(B_2), \rho(B_3)\} \leq \mu \leq \max\{\|(B_0)\|, \|(B_1)\|, \|(B_2)\|, \|(B_3)\|\}$, with $\|\cdot\|$ denoting the infinity norm, since μ is bounded from below by the spectral radii and from above by the infinity norm of the matrices B_0, B_1, B_2, B_3 . So $\max\{\rho(B_3), \rho(B_1), \rho(B_2), \rho(B_0)\} = \max(|2 - 256w|, |256w|)$ and $\max(\|B_0\|, \|B_1\|, \|B_2\|, \|B_3\|) = \max(|2 - 256w|, |256w|)$. Then by [16], we have $\mu = \max(|2 - 256w|, |256w|)$. So Hölder regularity of the scheme S is computed by $r = 4 - \log_4(\mu)$, where μ is defined as

$$\begin{cases} \mu = 2 - 256w & \text{if } -\frac{1}{128} < w \leq \frac{1}{256}, \\ \mu = 256w & \text{if } \frac{1}{256} < w < \frac{2}{128}, \end{cases} \tag{27}$$

which completes the proof. \square

Corollary 1. *The 4-point scheme (14) is C^3 continuous if and only if $1 \leq \mu < 4$, i.e., if and only if $-1/128 < w < 2/128$.*

Theorem 4. *The limit stencils providing the evaluations of the basic limit function of the 4-point scheme (14) at integers and half integers are $\{(128w^2/15 + 7w/12 + 1/5120), (31w/5 - 512w^2/15 + 223/1280), (256w^2/5 - 407w/30 + 1667/2560), (31w/5 - 512w^2/15 + 223/1280), (128w^2/15 + 7w/12 + 1/5120)\}$ and $\{(64w/15 + 1/40), (19/40 - 64w/15), (19/40 - 64w/15), (64w/15 + 1/40)\}$, respectively.*

Proof. The local subdivision matrices for limit stencils of 4-point scheme (14) at integers and half integers are $P_I^{k+1} = S_I P_I^k$ and $P_{I/2}^{k+1} = S_{I/2} P_{I/2}^k$, respectively, with

$$S_I = \begin{bmatrix} \frac{1}{128} + 3w & \frac{51}{128} - w & \frac{71}{128} - 7w & \frac{5}{128} + 5w & 0 \\ w & \frac{15}{64} + 5w & \frac{21}{32} - 13w & \frac{7}{64} + 7w & 0 \\ 0 & \frac{7}{64} + 7w & \frac{21}{32} - 13w & \frac{15}{64} + 5w & w \\ 0 & \frac{5}{128} + 5w & \frac{71}{128} - 7w & \frac{51}{128} - w & \frac{1}{128} + 3w \end{bmatrix}, \tag{28}$$

$$P_I^{k+1} = \begin{bmatrix} P_{-2}^{k+1} \\ P_{-1}^{k+1} \\ P_0^{k+1} \\ P_1^{k+1} \end{bmatrix}, \quad P_I^k = \begin{bmatrix} P_{-2}^k \\ P_{-1}^k \\ P_0^k \\ P_1^k \\ P_2^k \end{bmatrix},$$

$$S_{I/2} = \begin{bmatrix} 7w + \frac{7}{64} & \frac{21}{32} - 13w & 5w + \frac{15}{64} & w \\ 5w + \frac{5}{128} & \frac{71}{128} - 7w & \frac{51}{128} - w & 3w + \frac{1}{128} \\ 3w + \frac{1}{128} & \frac{51}{128} - w & \frac{71}{128} - 7w & 5w + \frac{5}{128} \\ w & 5w + \frac{15}{64} & \frac{21}{32} - 13w & 7w + \frac{7}{64} \end{bmatrix}, \tag{29}$$

$$P_{I/2}^{k+1} = \begin{bmatrix} P_{-(3/2)}^{k+1} \\ P_{-(1/2)}^{k+1} \\ P_{1/2}^{k+1} \\ P_{3/2}^{k+1} \end{bmatrix} \text{ and } P_{I/2}^k = \begin{bmatrix} P_{-(3/2)}^k \\ P_{-(1/2)}^k \\ P_{1/2}^k \\ P_{3/2}^k \end{bmatrix}.$$

The eigenvalues of the matrix $S_{I/2}$ are $\{1/16, 1, 1/64, 1/4\}$. The eigenvectors of local subdivision matrix $S_{I/2}$ corresponding to eigenvalues are

$$Q_{I/2} = \begin{bmatrix} 1 & 1 & -1 & -1 \\ \frac{512w+3}{512w-57} & 1 & -\frac{128w+2}{384w-9} & -\frac{1}{3} \\ \frac{512w+3}{512w-57} & 1 & \frac{128w+2}{384w-9} & \frac{1}{3} \\ 1 & 1 & 1 & 1 \end{bmatrix}. \tag{30}$$

The inverse of $Q_{I/2}$ is

$$Q_{I/2}^{-1} = \begin{bmatrix} \frac{19}{40} - \frac{64w}{15} & -\frac{19}{40} + \frac{64w}{15} & -\frac{19}{40} + \frac{64w}{15} & \frac{19}{40} - \frac{64w}{15} \\ \frac{1}{40} + \frac{64w}{15} & \frac{19}{40} - \frac{64w}{15} & \frac{19}{40} - \frac{64w}{15} & \frac{1}{40} - \frac{64w}{15} \\ -\frac{3}{10} + \frac{64w}{5} & \frac{9}{10} - \frac{192w}{5} & -\frac{9}{10} + \frac{192w}{5} & \frac{3}{10} - \frac{64w}{5} \\ -\frac{1}{5} - \frac{64w}{5} & -\frac{9}{10} + \frac{192w}{5} & \frac{9}{10} - \frac{192w}{5} & \frac{1}{5} + \frac{64w}{5} \end{bmatrix}. \tag{31}$$

For the decomposition of matrix $S_{I/2}$, we need $\Delta_{I/2}$, where $\Delta_{I/2}$ is the scalar matrix in which eigenvalues are arranged diagonally; therefore, we now compute $\lim_{k \rightarrow \infty} \Delta_{I/2}^k$

$$\Delta_{1/2}^k = \begin{bmatrix} \left(\frac{1}{16}\right)^k & 0 & 0 & 0 \\ 0 & 1 & 0 & 0 \\ 0 & 0 & \left(\frac{1}{64}\right)^k & 0 \\ 0 & 0 & 0 & \left(\frac{1}{4}\right)^k \end{bmatrix} \quad \text{and} \quad \lim_{k \rightarrow \infty} \Delta_{1/2}^k = \begin{bmatrix} 0 & 0 & 0 & 0 \\ 0 & 1 & 0 & 0 \\ 0 & 0 & 0 & 0 \\ 0 & 0 & 0 & 0 \end{bmatrix}. \quad (32)$$

$P_{1/2}^{k+1} = S_{1/2} P_{1/2}^k$; therefore, $P_{1/2}^{k+1} = S_{1/2}^k P_{1/2}^0$. This implies

$$\begin{bmatrix} P_{-(3/2)}^\infty \\ P_{-(1/2)}^\infty \\ P_{1/2}^\infty \\ P_{3/2}^\infty \end{bmatrix} = \begin{bmatrix} \frac{1}{40} + \frac{64}{15}w & \frac{19}{40} - \frac{64}{15}w & \frac{19}{40} - \frac{64}{15}w & \frac{1}{40} + \frac{64}{15}w \\ \frac{1}{40} + \frac{64}{15}w & \frac{19}{40} - \frac{64}{15}w & \frac{19}{40} - \frac{64}{15}w & \frac{1}{40} + \frac{64}{15}w \\ \frac{1}{40} + \frac{64}{15}w & \frac{19}{40} - \frac{64}{15}w & \frac{19}{40} - \frac{64}{15}w & \frac{1}{40} + \frac{64}{15}w \\ \frac{1}{40} + \frac{64}{15}w & \frac{19}{40} - \frac{64}{15}w & \frac{19}{40} - \frac{64}{15}w & \frac{1}{40} + \frac{64}{15}w \end{bmatrix} \begin{bmatrix} P_{-(3/2)}^0 \\ P_{-(1/2)}^0 \\ P_{1/2}^0 \\ P_{3/2}^0 \end{bmatrix}. \quad (33)$$

Since the subdivision scheme is dual, after computing the limit stencil at half integers by the local matrix $S_{1/2}$, the limit stencil at integers must be computed as

$$\text{limit stencil integers} = \text{limit stencil half integers} \times S_I. \quad (34)$$

The matrix of limit stencils at half integers is

$$S_{1/2}^\infty = \begin{bmatrix} \frac{1}{40} + \frac{64}{15}w & \frac{19}{40} - \frac{64}{15}w & \frac{19}{40} - \frac{64}{15}w & \frac{1}{40} + \frac{64}{15}w \\ \frac{1}{40} + \frac{64}{15}w & \frac{19}{40} - \frac{64}{15}w & \frac{19}{40} - \frac{64}{15}w & \frac{1}{40} + \frac{64}{15}w \\ \frac{1}{40} + \frac{64}{15}w & \frac{19}{40} - \frac{64}{15}w & \frac{19}{40} - \frac{64}{15}w & \frac{1}{40} + \frac{64}{15}w \\ \frac{1}{40} + \frac{64}{15}w & \frac{19}{40} - \frac{64}{15}w & \frac{19}{40} - \frac{64}{15}w & \frac{1}{40} + \frac{64}{15}w \end{bmatrix}. \quad (35)$$

After multiplying the matrix of limit stencil at half integers $S_{1/2}^\infty$ with local subdivision matrix S_I , we get

$$S_I^\infty = \begin{bmatrix} l_1 & l_2 & l_3 & l_4 & l_5 \\ l_1 & l_2 & l_3 & l_4 & l_5 \\ l_1 & l_2 & l_3 & l_4 & l_5 \\ l_1 & l_2 & l_3 & l_4 & l_5 \end{bmatrix}, \quad (36)$$

with

$$\begin{aligned} l_1 &= \frac{128w^2}{15} + \frac{7w}{12} + \frac{1}{5120}, \\ l_2 &= \frac{31w}{5} - \frac{512w^2}{15} + \frac{223}{1280}, \\ l_3 &= \frac{256w^2}{5} - \frac{407w}{30} + \frac{1667}{2560}, \\ l_4 &= \frac{31w}{5} - \frac{512w^2}{15} + \frac{223}{1280}, \\ l_5 &= \frac{128w^2}{15} + \frac{7w}{12} + \frac{1}{5120}. \end{aligned} \quad (37)$$

Hence, the limit stencils providing the evaluations of the basic limit functions of the 4-point scheme (14) at integers and half integers are

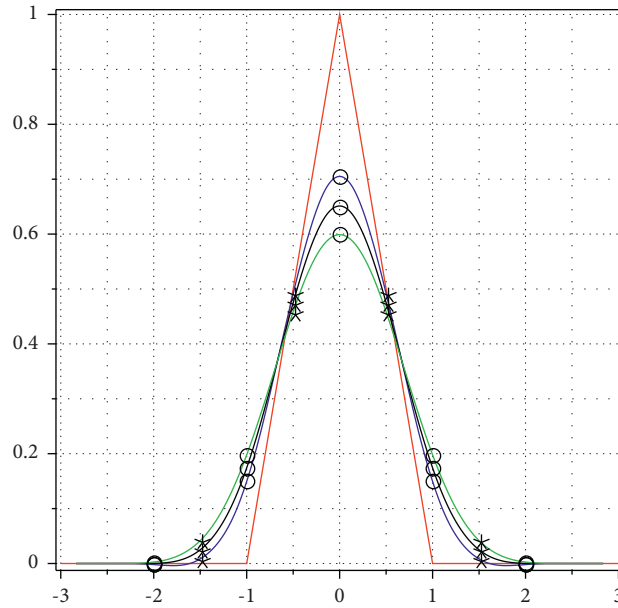


FIGURE 3: Basic limit functions produced by the 4-point scheme corresponding to (14) for different values of parameter w . The red lines denote the initial polyline, and the blue, black, and green lines represent the basic limit functions produced with $w = -1/256, 0, 1/256$ respectively. The circles denote the evaluations of the basic limit function at integers, and the asterisks denote the evaluations of the basic limit function at half integers.

$$\left\{ \begin{array}{l} (128w^2/15 + 7w/12 + 1/5120), (31w/5 - 512w^2/15 + 223/1280), (256w^2/5 - 407w/30 + 1667/2560), \\ (31w/5 - 512w^2/15 + 223/1280), (128w^2/15 + 7w/12 + 1/5120) \end{array} \right\}, \quad (38)$$

$$\{(64w/15 + 1/40), (19/40 - 64w/15), (19/40 - 64w/15), (64w/15 + 1/40)\}$$

respectively, which completes the proof. □

In Figure 3, we present the basic limit functions of the proposed 4-point quaternary approximating subdivision scheme for different values of w and show its evaluations at integers and half integers which coincide with the limit stencils computed in Theorem 4.

4. Comparison with Existing Schemes

Here we will present the comparison of our proposed family of quaternary subdivision schemes with existing quaternary subdivision schemes in visual performance. In Figure 1, we present the comparison of proposed 4-point scheme $\lambda_{3,3}$ with 4-point scheme α_4^4 presented in [1] ((a), (b)&(c)) and 4-point scheme presented in [4] ((d), (e)&(f)), respectively. Here, black dotted lines show the initial polygon, red solid lines are the limit curves of 4-point scheme $\lambda_{3,3}$, and blue solid lines are the limit curves of 4-point scheme α_4^4 presented in [1] and 4-point scheme presented in [4]. We see that, our proposed schemes $\lambda_{3,3}$ give maximum smoothness and best approximation compared with the schemes presented in [1, 4].

In Figure 2, we present the comparison of proposed 4-point scheme $\lambda_{3,3}$ with 4-point scheme KP presented in [5]. Here, black dotted lines show the initial polygon, red solid lines are the limit curve of 4-point scheme $\lambda_{3,3}$, and blue solid lines are the limit curve of 4-point scheme KP

presented in [5]. We see that the approximating scheme KP presented in [5] gives interpolating behavior, but our proposed schemes $\lambda_{3,3}$ give maximum smoothness and best approximation compared with the schemes presented in [5].

5. Conclusions

In this paper, we have presented a general formula for the derivation of multiparametric family of quaternary subdivision schemes. We present the complete analysis of the proposed family of the multiparametric quaternary subdivision schemes. We also present the comparison with existing quaternary subdivision schemes. The comparison shows that our proposed family gives maximum smoothness compared with existing quaternary subdivision schemes.

Data Availability

The data used to support the findings of the study are available within this paper.

Conflicts of Interest

The authors declare that there are no conflicts of interest regarding the publication of this study.

References

- [1] G. Mustafa and F. Khan, "A new 4-point C^3 quaternary approximating subdivision scheme," *Abstract and Applied Analysis*, vol. 2009, Article ID 301967, 14 pages, 2009.
- [2] S. S. Siddiqi and M. Younis, "The m-point quaternary approximating subdivision schemes," *American Journal of Computational Mathematics*, vol. 3, pp. 6–10, 2013.
- [3] A. Ghaffar, G. Mustafa, and K. Qin, "The 4-point a-ary approximating subdivision scheme," *Open Journal of Applied Sciences*, vol. 3, pp. 106–111, 2013.
- [4] S. Amat and J. Liandrat, "On a nonlinear 4-point quaternary approximating subdivision scheme eliminating the Gibbs phenomenon," *SeMA Journal*, vol. 62, pp. 15–25, 2013.
- [5] K. Pervez, "Shape preservation of the stationary 4-point quaternary subdivision schemes," *Communications in Mathematics and Applications*, vol. 9, no. 3, pp. 249–264, 2018.
- [6] P. Ashraf, B. Nawaz, D. Baleanu et al., "Analysis of geometric properties of ternary four-point rational interpolating subdivision scheme," *Mathematics*, vol. 8, pp. 1–19, 2020.
- [7] P. Ashraf, M. Sabir, A. Ghaffar, K. S. Nisar, and I. Khan, "Shape-preservation of the four-point ternary interpolating non-stationary subdivision scheme," *Frontiers in Physics*, vol. 2020, pp. 1–10, 2020.
- [8] R. Hameed, G. Mustafa, A. Liaqat et al., "A new approach to increase the flexibility of curves and regular surfaces produced by 4-point ternary subdivision scheme," *Mathematical Problems in Engineering*, vol. 2020, Article ID 6096545, 17 pages, 2020.
- [9] S. M. Hussain, A. Rehman, D. Baleanu, K. S. Nisar, A. Ghaffar, and S. A. A. Karim, "Generalized 5-point approximating subdivision scheme of varying arity," *Mathematics*, vol. 8, 2020.
- [10] F. Khan, G. Mustafa, A. Shahzad, D. Baleanu, and M. M. Al-Qurashi, "A computational method for subdivision depth of ternary schemes," *Mathematics*, vol. 8, no. 5, 2020.
- [11] C. Conti and L. Romani, "Dual univariate m-ary subdivision schemes of de Rham-type," *Journal of Mathematical Analysis and Applications*, vol. 407, pp. 443–456, 2013.
- [12] L. Romani, "Interpolating m-refinable functions with compact support: The second generation class," *Applied Mathematics and Computation*, vol. 361, pp. 735–746, 2019.
- [13] L. Romani and A. Viscardi, "Dual univariate interpolatory subdivision of every arity: Algebraic characterization and construction," *Journal of Mathematical Analysis and Applications*, vol. 484, Article ID 123713, 2020.
- [14] G. Mustafa, M. Asghar, A. Afzal, and J.-B. Liu, "A family of integer-point ternary parametric subdivision schemes," *Journal of Mathematics*, vol. 2021, Article ID 9281006, 10 pages, 2021.
- [15] N. Dyn and D. Levin, "Subdivision schemes in geometric modelling," *Acta Numerica*, vol. 11, pp. 73–144, 2002.
- [16] O. Rioul, "Simple regularity criteria for subdivision schemes," *SIAM Journal on Mathematical Analysis*, vol. 23, no. 6, pp. 1544–1576, 1992.

Research Article

A New Double Truncated Generalized Gamma Model with Some Applications

Awad A. Bakery ^{1,2}, Wael Zakaria ², and OM Kalthum S. K. Mohamed ^{1,3}

¹University of Jeddah, College of Science and Arts at Khulis, Department of Mathematics, Jeddah, Saudi Arabia

²Department of Mathematics, Faculty of Science, Ain Shams University, P.O. Box 1156, Abbassia, Cairo 11566, Egypt

³Academy of Engineering and Medical Sciences, Department of Mathematics, Khartoum, Sudan

Correspondence should be addressed to OM Kalthum S. K. Mohamed; om_kalsoom2020@yahoo.com

Received 7 May 2021; Accepted 6 August 2021; Published 17 August 2021

Academic Editor: Ghulam Mustafa

Copyright © 2021 Awad A. Bakery et al. This is an open access article distributed under the Creative Commons Attribution License, which permits unrestricted use, distribution, and reproduction in any medium, provided the original work is properly cited.

The generalized Gamma model has been applied in a variety of research fields, including reliability engineering and lifetime analysis. Indeed, we know that, from the above, it is unbounded. Data have a bounded service area in a variety of applications. A new five-parameter bounded generalized Gamma model, the bounded Weibull model with four parameters, the bounded Gamma model with four parameters, the bounded generalized Gaussian model with three parameters, the bounded exponential model with three parameters, and the bounded Rayleigh model with two parameters, is presented in this paper as a special case. This approach to the problem, which utilizes a bounded support area, allows for a great deal of versatility in fitting various shapes of observed data. Numerous properties of the proposed distribution have been deduced, including explicit expressions for the moments, quantiles, mode, moment generating function, mean variance, mean residual lifespan, and entropies, skewness, kurtosis, hazard function, survival function, r th order statistic, and median distributions. The delivery has hazard frequencies that are monotonically increasing or declining, bathtub-shaped, or upside-down bathtub-shaped. We use the Newton Raphson approach to approximate model parameters that increase the log-likelihood function and some of the parameters have a closed iterative structure. Six actual data sets and six simulated data sets were tested to demonstrate how the proposed model works in reality. We illustrate why the Model is more stable and less affected by sample size. Additionally, the suggested model for wavelet histogram fitting of images and sounds is very accurate.

1. Introduction

The gamma (GM) model, including Weibull, gamma, exponential, and Rayleigh as special submodels, among others, is a very popular distribution for modeling lifetime data and for modeling phenomenon with monotone failure rates. An advantage of GM is that it requires a little measure of parameters for learning. Also, these parameters can be measured by getting the expectation maximization (EM) algorithm [1, 2] to maximize the log-likelihood function. The early generalization of gamma distribution can be traced back to Amoroso [3] who discussed a generalized gamma distribution and applied it to fit income rates. Johnson et al. [4] gave a four parameter generalized gamma

distribution which reduces to the generalized gamma distribution defined by Stacy [2] when the location parameter is set to zero. Mudholkar and Srivastava [5] introduced the exponentiated method to derive a distribution. The generalized gamma defined by Stacy [2] is a three-parameter exponentiated gamma distribution. Agarwal and Al-Saleh [6] applied generalized gamma to study hazard rates. Balakrishnan and Peng [7] applied this distribution to develop generalized gamma frailty model. Cordeiro et al. [8] derived another generalization of Stacys generalized gamma distribution using exponentiated method and applied it to life time and survival analysis. Nadarajah and Gupta [9] proposed another type of generalized gamma distribution with application to fit drought

data. As of late, Chen et al. [10] used generalized gamma distribution with three parameters for flood frequency analysis, Zhao et al. [11] used generalized gamma distribution with three parameters to give the statistical characterizes of high-resolution SAR images, and Mead et al. [12] defined modified generalized gamma distribution so as to investigate greater flexibility in modeling data from a practical viewpoint and they derived multifarious identities and properties of this distribution, including explicit expressions for the moments, quantiles, mode, moment generating function, mean deviation, mean residual lifetime, and expression of the entropies. We extend all the past models with five parameters to range \mathbb{R} (real numbers) or any bounded subset of \mathbb{R} . Fulger et al. [13] generate random numbers within any arbitrary interval. We introduce in this paper the high flexibility of a bounded generalized Gamma model with five parameters (BGGM) for analyzing data. The BGGM Model is of noticeable significance for image coding, compression applications, sound system, wind speed data, and breast cancer data fitting. This new distribution has a flexibility to fit any kind of observed data whose pdf is monotonically increasing, decreasing, bathtub, and upside down bathtub-shaped depending on the parameter values and bounded support regions. The remainder of this paper is organized as follows: The BGGM with its sub models and some shapes describe the hazard rate function are defined in Section 2. Some properties of the BGGM distribution are studied in Section 3 including, quantile, mode, moments, moment generating function, mean deviation, mean residual life and entropy. Section 4 presents the parameter estimation. Section 5 sets out the experimental results. Section 6 presents our conclusions.

2. The Bounded Generalized Gamma Model and Its Special Models

The standard form of gamma function is

$$\Gamma(\eta) = \int_0^{\infty} x^{\eta-1} e^{-x} dx, \quad \eta > 0. \quad (1)$$

The incomplete gamma function is defined by

$$\Gamma(\eta, s) = \frac{1}{\Gamma(\eta)} \int_0^s x^{\eta-1} e^{-x} dx, \quad \eta > 0 \text{ and } s \geq 0. \quad (2)$$

The probability density function (pdf) of the generalized gamma distribution is given by

$$T(x|\Theta) = \frac{\lambda\beta^\eta}{2\delta\Gamma(\eta)} \left(\frac{|x-u|}{\delta}\right)^{\eta\lambda-1} e^{-\beta(|x-u|/\delta)^\lambda}, \quad (3)$$

for all $x \in \mathbb{R}$, where $\Theta = (u, \delta, \beta, \eta, \lambda)'$, $\delta, \eta, \lambda, \beta > 0$ and $u \in \mathbb{R}$. The cumulative distribution function (cdf) of generalized gamma distribution defined as follows:

$$\begin{aligned} D(z) &= \int_{-\infty}^z T(x|\Theta) dx = \int_{-\infty}^z \frac{\lambda\beta^\eta}{2\delta\Gamma(\eta)} \left(\frac{|x-u|}{\delta}\right)^{\eta\lambda-1} e^{-\beta(|x-u|/\delta)^\lambda} dx \\ &= \frac{1}{2} + \frac{1}{2} \text{sign}(z-u) \left[\Gamma\left(\eta, \beta\left(\frac{|z-u|}{\delta}\right)^\lambda\right) - \Gamma\left(\eta, \beta\left(\frac{|u|}{\delta}\right)^\lambda\right) \right]. \end{aligned} \quad (4)$$

Let $\Omega = [a, b] \subseteq \mathbb{R}$ and we denote the indicator function by

$$1_\Omega(x) = \begin{cases} 1, & \text{if } x \in \Omega, \\ 0, & \text{if otherwise.} \end{cases} \quad (5)$$

We define the pdf of the bounded generalized gamma distribution (BGGM) as

$$\begin{aligned} Y &= Y(x|\Theta) = \frac{T(x|\Theta)}{\int_\Omega T(x|\Theta) dx} \\ &= \frac{\lambda\beta^\eta/2\delta\Gamma(\eta) (|x-u|/\delta)^{\eta\lambda-1} e^{-\beta(|x-u|/\delta)^\lambda}}{\int_\Omega T(x|\Theta) dx}, \text{ for all } x \in \Omega. \end{aligned} \quad (6)$$

In another form, we can write the pdf of the bounded generalized gamma distribution (BGGM) as

$$Y = \frac{\lambda\beta^\eta/2\delta\Gamma(\eta) (|x-u|/\delta)^{\eta\lambda-1} e^{-\beta(|x-u|/\delta)^\lambda}}{D(b) - D(a)}, \quad (7)$$

where

$$\begin{aligned} D(b) - D(a) &= \frac{1}{2} \text{sign}(b-u) \left[\Gamma\left(\eta, \beta\left(\frac{|b-u|}{\delta}\right)^\lambda\right) - \Gamma\left(\eta, \beta\left(\frac{|u|}{\delta}\right)^\lambda\right) \right] \\ &\quad - \frac{1}{2} \text{sign}(a-u) \left[\Gamma\left(\eta, \beta\left(\frac{|a-u|}{\delta}\right)^\lambda\right) - \Gamma\left(\eta, \beta\left(\frac{|u|}{\delta}\right)^\lambda\right) \right]. \end{aligned} \quad (8)$$

It is clear to see that

$$Y \geq 0 \text{ and } \int_\Omega Y(x|u, \delta, \beta, \eta, \lambda) dx = 1. \quad (9)$$

Hence, the cdf of the bounded generalized gamma distribution (BGGM) is given by

$$\begin{aligned} \Phi(x) &= \frac{D(x) - D(a)}{D(b) - D(a)} \\ &= \frac{\text{sign}(x-u) \left[\Gamma\left(\eta, \beta(|x-u|/\delta)^\lambda\right) - \Gamma\left(\eta, \beta(|u|/\delta)^\lambda\right) \right] - \text{sign}(a-u) \left[\Gamma\left(\eta, \beta(|a-u|/\delta)^\lambda\right) - \Gamma\left(\eta, \beta(|u|/\delta)^\lambda\right) \right]}{\text{sign}(b-u) \left[\Gamma\left(\eta, \beta(|b-u|/\delta)^\lambda\right) - \Gamma\left(\eta, \beta(|u|/\delta)^\lambda\right) \right] - \text{sign}(a-u) \left[\Gamma\left(\eta, \beta(|a-u|/\delta)^\lambda\right) - \Gamma\left(\eta, \beta(|u|/\delta)^\lambda\right) \right]} \end{aligned} \quad (10)$$

The parameters $u(\delta, \beta)$ and (η, λ) are corresponding to the location, scale, and shape parameters, respectively. Note that $Y(x|\Theta)$ can be any kind of distribution, for example, in exponential distribution (ED) [14, 15] be $\phi(x|u, \delta, \beta)$, Weibull distribution (WD) [16–18] be $T(x|u, \delta, \beta, \lambda)$, Rayleigh distribution (RD) [19, 20] be $T(x|u, \delta)$, generalized Gaussian distribution (GGD) [21] be $T(x|u, \delta, \lambda)$, Gaussian distribution (GD) [15] be $T(x|u, \delta)$, Laplacian distribution (LD) [22] be $T(x|u, \delta)$ and Gamma distribution (ΓD) [1] be $T(x|u, \delta, \eta, \beta)$. These distributions are all unbounded with support range $(0, \infty)$. We extend all the past models with range $(-\infty, \infty)$ also to the bounded case. The BGFM has several models as special cases, which makes it distinguishable scientific importance from other models. We investigate the various special models of the BGFM as listed in Table 1. The survival function and hazard rate function for BGFM are, respectively, given by

TABLE 1: The comparative models are special cases of the BGFM.

GFM	BGFM: $\Omega = \mathbb{R}$
BGM	BGFM: $\lambda = 1$
GM	BGFM: $\Omega = \mathbb{R}$ and $\lambda = 1$
BWM	BGFM: $\eta = 1$
WM	BGFM: $\Omega = \mathbb{R}, \eta = 1$
BGGM	BGFM: $\eta = 1/\lambda$ and $\beta = (\Gamma(3/\lambda)/\Gamma(1/\lambda))^{\lambda/2}$
GGM	BGFM: $\Omega = \mathbb{R}, \eta = 1/\lambda$ and $\beta = (\Gamma(3/\lambda)/\Gamma(1/\lambda))^{\lambda/2}$
BEM	BGFM: $\lambda = 1$, and $\eta = 1$
EM	BGFM: $\Omega = \mathbb{R}, \lambda = 1$, and $\eta = 1$
BGM	BGFM: $\lambda = 2, \eta = 0.5$ and $\beta = 0.5$
GM	BGFM: $\Omega = \mathbb{R}, \lambda = 2, \eta = 0.5$ and $\beta = 0.5$
BRM	BGFM: $\lambda = 2, \eta = 1$ and $\beta = 0.5$
RM	BGFM: $\Omega = \mathbb{R}, \lambda = 2, \eta = 1$ and $\beta = 0.5$
BLM	BGFM: $\lambda = 1, \eta = 1$ and $\beta = \sqrt{2}$
LM	BGFM: $\Omega = \mathbb{R}, \lambda = 1, \eta = 1$ and $\beta = \sqrt{2}$

$$S(x) = 1 - \Phi(x)$$

$$= \frac{\text{sign}(b-u) [\Gamma(\eta, \beta(|b-u|/\delta)^\lambda) - \Gamma(\eta, \beta(|u|/\delta)^\lambda)] - \text{sign}(x-u) [\Gamma(\eta, \beta(|x-u|/\delta)^\lambda) - \Gamma(\eta, \beta(|u|/\delta)^\lambda)]}{\text{sign}(b-u) [\Gamma(\eta, \beta(|b-u|/\delta)^\lambda) - \Gamma(\eta, \beta(|u|/\delta)^\lambda)] - \text{sign}(a-u) [\Gamma(\eta, \beta(|a-u|/\delta)^\lambda) - \Gamma(\eta, \beta(|u|/\delta)^\lambda)]}$$

$$\wedge(x) = \frac{Y(x|\Theta)}{S(x)} \tag{11}$$

$$= \frac{\lambda\beta^\eta/2\delta\Gamma(\eta)(|x-u|/\delta)^{\eta\lambda-1}e^{-\beta(|x-u|/\delta)^\lambda}}{\text{sign}(b-u) [\Gamma(\eta, \beta(|b-u|/\delta)^\lambda) - \Gamma(\eta, \beta(|u|/\delta)^\lambda)] - \text{sign}(x-u) [\Gamma(\eta, \beta(|x-u|/\delta)^\lambda) - \Gamma(\eta, \beta(|u|/\delta)^\lambda)]}$$

In Figures 1 and 2, we display the plots of the pdf of BGFM for various parameters. Figure 3 displays the BGFM failure rate function which can be increasing, decreasing, bathtub, and upside down bathtub-shaped depending on the parameter values.

deviation, mean residual life and mean waiting time, Rényi entropy, and order statistics.

3. Properties of BGFM

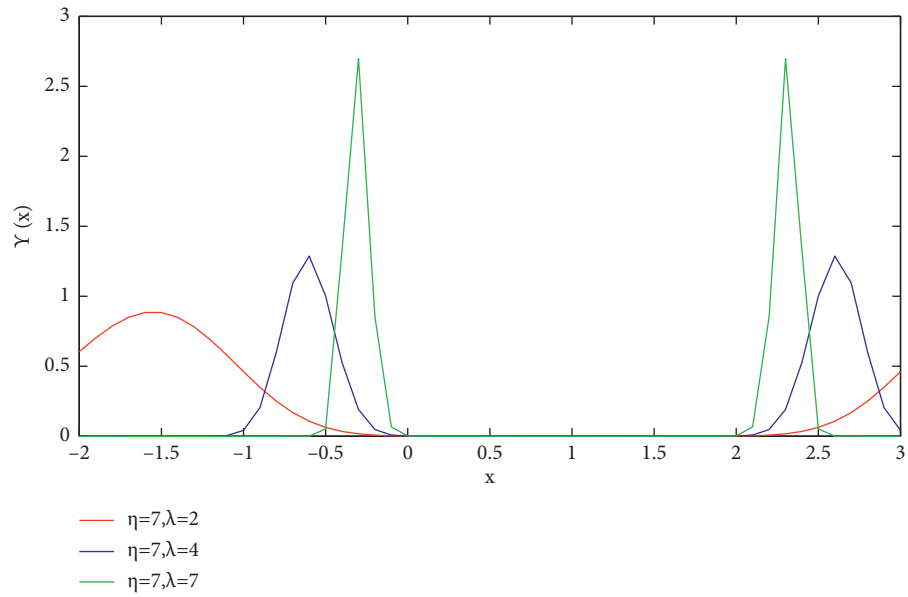
3.1. Mode and Quantile. The p^{th} quantile function of the BGFM is the solution of

In this section, we provide some general properties of the BGFM including quantile function, mode, moments, mean

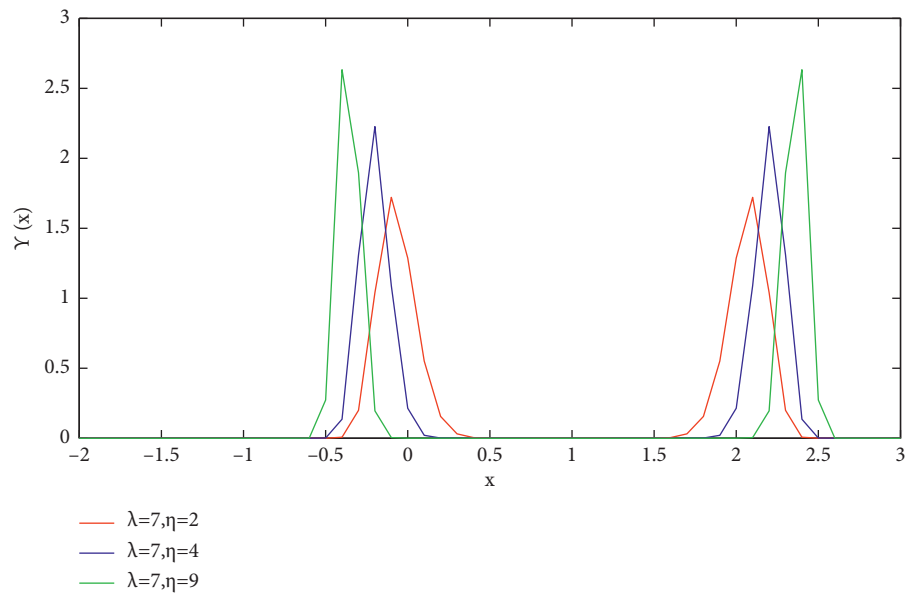
$$\Phi(x_p) = \frac{D(x_p) - D(a)}{D(b) - D(a)} = p \Rightarrow$$

$$\frac{\text{sign}(x_p-u) [\Gamma(\eta, \beta(|x_p-u|/\delta)^\lambda) - \Gamma(\eta, \beta(|u|/\delta)^\lambda)] - \text{sign}(a-u) [\Gamma(\eta, \beta(|a-u|/\delta)^\lambda) - \Gamma(\eta, \beta(|u|/\delta)^\lambda)]}{\text{sign}(b-u) [\Gamma(\eta, \beta(|b-u|/\delta)^\lambda) - \Gamma(\eta, \beta(|u|/\delta)^\lambda)] - \text{sign}(a-u) [\Gamma(\eta, \beta(|a-u|/\delta)^\lambda) - \Gamma(\eta, \beta(|u|/\delta)^\lambda)]} = p. \tag{12}$$

The median, denoted by μ^* , can be obtained by substituting $p = 0.5$ in 10 and solving the equation

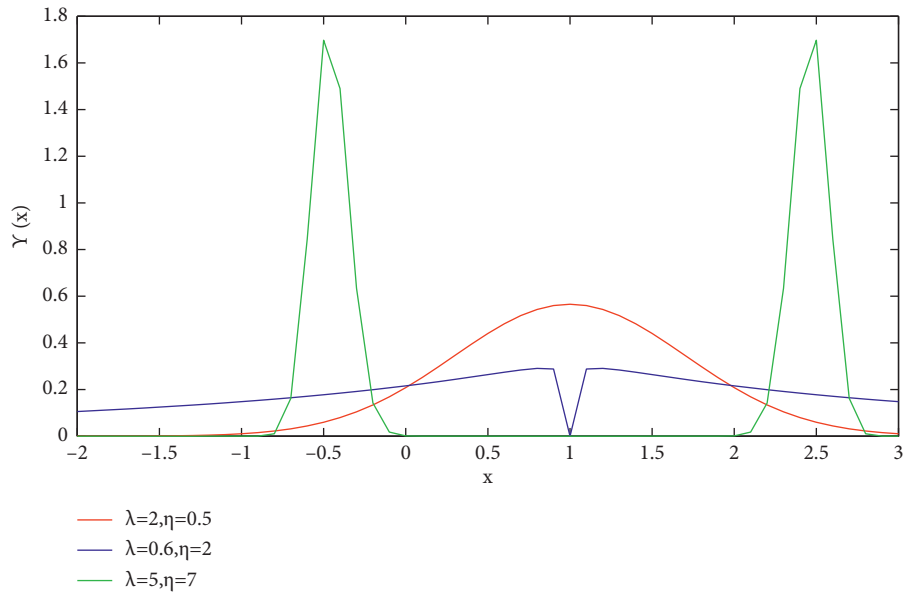


(a)



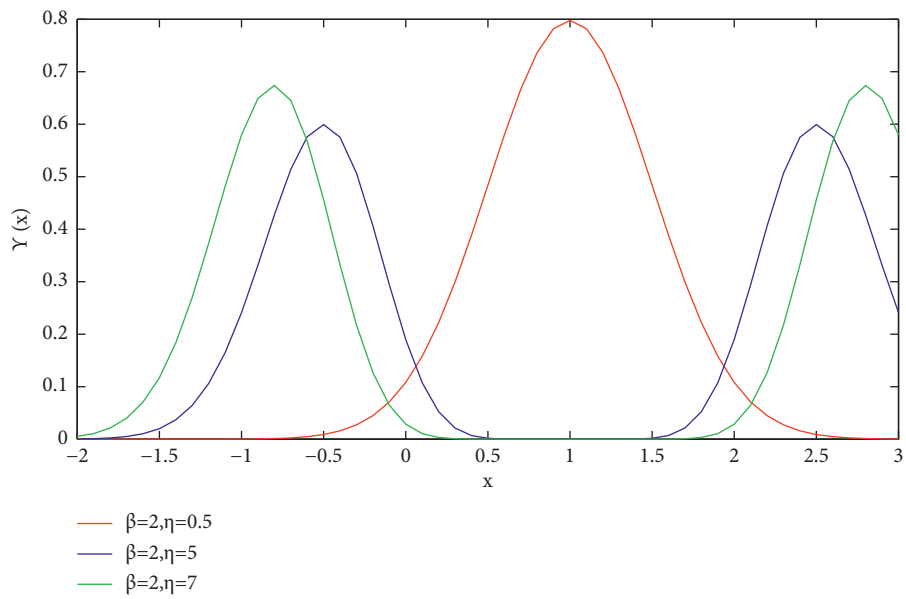
(b)

FIGURE 1: Continued.



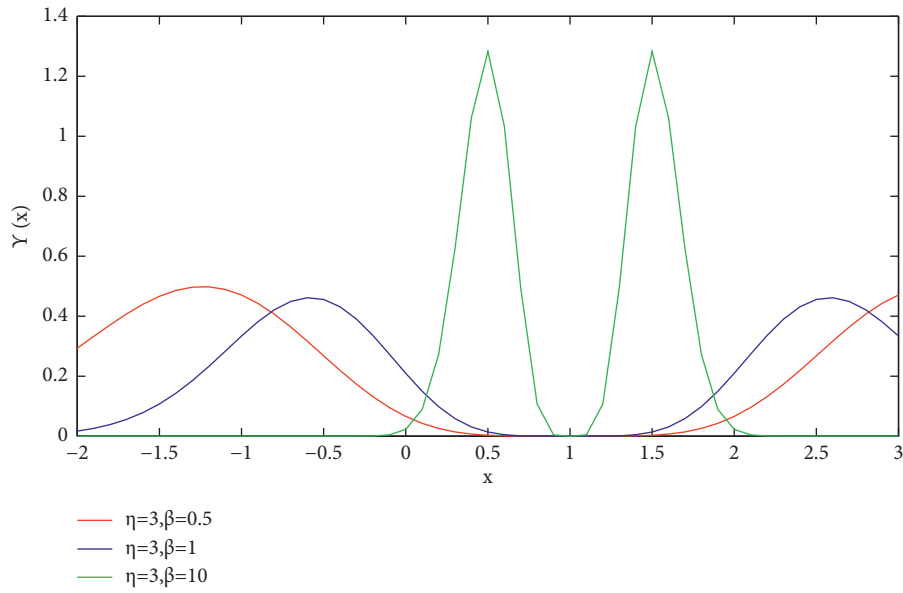
(c)

FIGURE 1: The pdf of BGTM for $a = -2, b = 3, u = 1, \delta = 1, \beta = 1$ and (a) $\eta = 7$ and $\lambda = 2, 4, 7$; (b) $\lambda = 7$ and $\eta = 2, 4, 9$; (c) $(\eta = 0.5, \lambda = 2)$, $(\eta = 2, \lambda = 0.6)$ and $(\eta = 7, \lambda = 5)$.

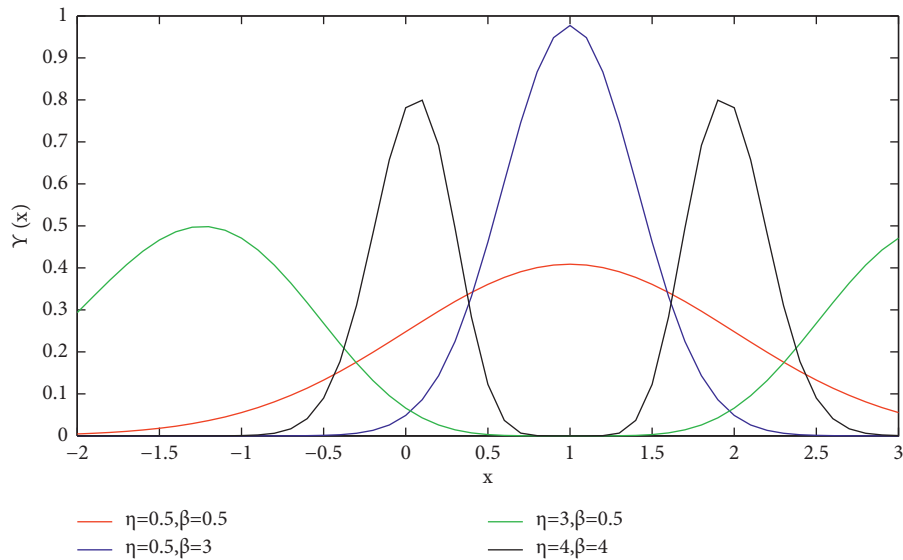


(a)

FIGURE 2: Continued.



(b)



(c)

FIGURE 2: The pdf of BGGM for $a = -2, b = 3, u = 1, \delta = 1, \lambda = 2$ and (a) $\beta = 2$ and $\eta = 0.5, 5, 7$; (b) $\eta = 3$ and $\beta = 0.5, 1, 10$; (c) ($\eta = 0.5, \beta = 0.5$), ($\eta = 0.5, \beta = 3$), ($\eta = 3, \beta = 0.5$) and ($\eta = 4, \beta = 4$).

$$\frac{\text{sign}(\mu^* - u) \left[\Gamma(\eta, \beta(|\mu^* - u|/\delta)^\lambda) - \Gamma(\eta, \beta(|u|/\delta)^\lambda) \right] - \text{sign}(a - u) \left[\Gamma(\eta, \beta(|a - u|/\delta)^\lambda) - \Gamma(\eta, \beta(|u|/\delta)^\lambda) \right]}{\text{sign}(b - u) \left[\Gamma(\eta, \beta(|b - u|/\delta)^\lambda) - \Gamma(\eta, \beta(|u|/\delta)^\lambda) \right] - \text{sign}(a - u) \left[\Gamma(\eta, \beta(|a - u|/\delta)^\lambda) - \Gamma(\eta, \beta(|u|/\delta)^\lambda) \right]} = 0.5. \quad (13)$$

The mode, denoted by x_m of the BGM distribution, is given by

$$x_m = u \pm \delta \left(\frac{\eta\lambda - 1}{\beta\lambda} \right)^{1/\lambda}, \text{ such that } Y''(x_m|\Theta) < 0. \quad (14)$$

Remark 1

- (1) If $\eta\lambda = 1$, then the BGM distribution is unimodal distribution
- (2) If $\eta\lambda > 1$, then the BGM distribution is multimodal distribution

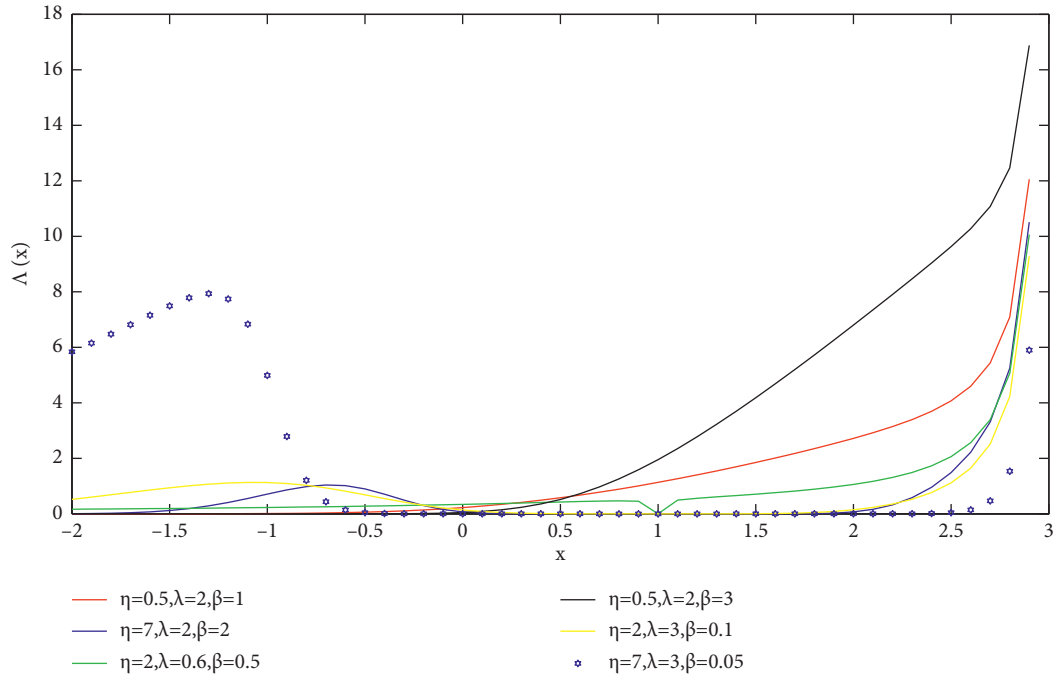


FIGURE 3: The hazard plots of BGM for $a = -2, b = 3, u = 1, \delta = 1$ and different values of β, η and λ .

3.2. Moments, Generating Function, and Mean Deviation. The r^{th} moment about zero of BGF distribution is

$$\begin{aligned}
 E(x^r) &= \int_a^b x^r \Upsilon(x|\Theta) dx \\
 &= \frac{\pm \sum_{n=0}^r \binom{r}{n} u^n (\pm \delta / \beta^{1/\lambda})^{r-n} \Gamma(\eta + (r - n/\lambda)) \left[\Gamma(\eta + (r - n/\lambda), \beta(|b - u|/\delta)^\lambda) - \Gamma(\eta + (r - n/\lambda), \beta(|a - u|/\delta)^\lambda) \right]}{2\Gamma(\eta)(D(b) - D(a))}.
 \end{aligned} \tag{15}$$

The mean μ of the BGF distribution is given by

$$\begin{aligned}
 \mu &= E(x) \\
 &= \frac{\pm 1}{2\Gamma(\eta)(D(b) - D(a))} \pm \delta \beta^{1/\lambda} \Gamma\left(\eta + \frac{1}{\lambda}\right) \left[\Gamma\left(\eta + \frac{1}{\lambda}, \beta\left(\frac{|b - u|}{\delta}\right)^\lambda\right) - \Gamma\left(\eta + \frac{1}{\lambda}, \beta\left(\frac{|a - u|}{\delta}\right)^\lambda\right) \right] \\
 &\quad + u \Gamma(\eta) \left[\Gamma\left(\eta, \beta\left(\frac{|b - u|}{\delta}\right)^\lambda\right) - \Gamma\left(\eta, \beta\left(\frac{|a - u|}{\delta}\right)^\lambda\right) \right].
 \end{aligned} \tag{16}$$

The variance σ^2 of the BGF distribution is given by

$$\begin{aligned}
\sigma^2 &= E(x^2) - E^2(x) \\
&= \frac{\pm 1}{2\Gamma(\eta)(D(b) - D(a))} \left\{ \frac{\delta^2}{\beta^{2/\lambda}} \Gamma\left(\eta + \frac{2}{\lambda}\right) \left[\Gamma\left(\eta + \frac{2}{\lambda}, \beta\left(\frac{|b-u|}{\delta}\right)^\lambda\right) - \Gamma\left(\eta + \frac{2}{\lambda}, \beta\left(\frac{|a-u|}{\delta}\right)^\lambda\right) \right] \right. \\
&\quad \pm \frac{2u\delta}{\beta^{1/\lambda}} \Gamma\left(\eta + \frac{1}{\lambda}\right) \left[\Gamma\left(\eta + \frac{1}{\lambda}, \beta\left(\frac{|b-u|}{\delta}\right)^\lambda\right) \right. \\
&\quad \left. \left. - \Gamma\left(\eta + \frac{1}{\lambda}, \beta\left(\frac{|a-u|}{\delta}\right)^\lambda\right) \right] \right\} \\
&\quad + u^2 \Gamma(\eta) \left[\Gamma\left(\eta, \beta\left(\frac{|b-u|}{\delta}\right)^\lambda\right) - \Gamma\left(\eta, \beta\left(\frac{|a-u|}{\delta}\right)^\lambda\right) \right] - \mu^2.
\end{aligned} \tag{17}$$

The central moments of BGF distribution can be obtained as follows

$$\begin{aligned}
E((x - \mu)^r) &= \int_a^b (x - \mu)^r Y(x|\Theta) dx \\
&= \frac{\pm 1}{2\Gamma(\eta)(D(b) - D(a))} \sum_{n=0}^r \binom{r}{n} u^n \left(\frac{\pm \delta}{\beta^{1/\lambda}}\right)^{r-n} \Gamma\left(\eta + \frac{r-n}{\lambda}\right) \left[\Gamma\left(\eta + \frac{r-n}{\lambda}, \beta\left(\frac{|b-u|}{\delta}\right)^\lambda\right) \right. \\
&\quad \left. - \Gamma\left(\eta + \frac{r-n}{\lambda}, \beta\left(\frac{|a-u|}{\delta}\right)^\lambda\right) \right] \sum_{j=0}^r \binom{r}{j} (-\mu)^{r-j}, \\
\gamma_1 &= \frac{E((x - \mu)^3)}{\sigma^3}, \\
\gamma_2 &= \frac{E((x - \mu)^4)}{\sigma^4}.
\end{aligned} \tag{18}$$

The moment generating function $M_x(t)$ of BGF distribution is

$$\begin{aligned}
M_x(t) &= \int_a^b e^{tx} Y(x|\Theta) dx \\
&= \frac{\pm \sum_{r=0}^{\infty} t^r / r! \sum_{n=0}^r \binom{r}{n} u^n (\pm \delta / \beta^{1/\lambda})^{r-n} \Gamma(\eta + (r-n)/\lambda) \left[\Gamma(\eta + (r-n)/\lambda, \beta(|b-u|/\delta)^\lambda) - \Gamma(\eta + (r-n)/\lambda, \beta(|a-u|/\delta)^\lambda) \right]}{2\Gamma(\eta)(D(b) - D(a))}.
\end{aligned} \tag{19}$$

The mean deviation Md of BGF distribution can be derived as

$$\begin{aligned}
 Md &= E(|x - \mu|) = \int_a^b |x - \mu|Y(x|\Theta)dx = 2 \left[\mu\Phi(\mu) - \int_a^\mu xY(x|\Theta)dx \right] \\
 &= \frac{2\mu \operatorname{sign}(\mu - u) \left[\Gamma(\eta, \beta(|\mu - u|/\delta)^\lambda) - \Gamma(\eta, \beta(|u|/\delta)^\lambda) \right] - \operatorname{sign}(a - u) \left[\Gamma(\eta, \beta(|a - u|/\delta)^\lambda) - \Gamma(\eta, \beta(|u|/\delta)^\lambda) \right]}{\operatorname{sign}(b - u) \left[\Gamma(\eta, \beta(|b - u|/\delta)^\lambda) - \Gamma(\eta, \beta(|u|/\delta)^\lambda) \right] - \operatorname{sign}(a - u) \left[\Gamma(\eta, \beta(|a - u|/\delta)^\lambda) - \Gamma(\eta, \beta(|u|/\delta)^\lambda) \right]} \\
 &\quad - \frac{1}{\Gamma(\eta)(D(b) - D(a))} \frac{\delta}{\beta^{1/\lambda}} \Gamma\left(\eta + \frac{1}{\lambda}\right) \left[\Gamma\left(\eta + \frac{1}{\lambda}, \beta\left(\frac{|\mu - u|}{\delta}\right)^\lambda\right) - \Gamma\left(\eta + \frac{1}{\lambda}, \beta\left(\frac{|a - u|}{\delta}\right)^\lambda\right) \right] \\
 &\quad \Gamma(\eta) \left[\Gamma\left(\eta, \beta\left(\frac{|\mu - u|}{\delta}\right)^\lambda\right) - \Gamma\left(\eta, \beta\left(\frac{|a - u|}{\delta}\right)^\lambda\right) \right].
 \end{aligned} \tag{20}$$

In Table 2, the Median, Mode, Mean, Variance, Skewness, and Kurtosis of BGM have given for $a = -2$, $b = 3$, $u = 1$, $\delta = 1$, and $\beta = 1$ and various values of η and λ . From Table 2, we note that for fixed values of a, b, u, δ, β , and η , the Kurtosis is decreasing function of λ . Also, for fixed values of a, b, u, δ, β , and λ , the Mode 1, Variance, and Skewness are increasing function and the Mode 2 and Mean are decreasing function of η . In Table 3, Median, Mode, Mean, Variance, Skewness, and Kurtosis of BGM have given for $a = -2$, $b = 3$, $u = 1$, $\delta = 1$, and $\lambda = 2$ and various values of η

and β . From Table 3, we note that for fixed values of a, b, u, δ, λ , and η , Mode 1 is decreasing, Median, Mode 2, and Mean are increasing functions of β . Also, for fixed values of a, b, u, δ, β , and η , Mode 1 and Skewness are increasing and Mode 2 and Mean are decreasing functions of η .

3.3. Mean Residual Life and Mean Waiting Time. The mean residual life function, say $\varphi(t)$, is given by

$$\begin{aligned}
 \varphi(t) &= E(\tau - t | \tau > t) \\
 &= \frac{\left(\operatorname{sign}(b - u) \left[\Gamma(\eta, \beta(|b - u|/\delta)^\lambda) - \Gamma(\eta, \beta(|u|/\delta)^\lambda) \right] - \operatorname{sign}(a - u) \left[\Gamma(\eta, \beta(|a - u|/\delta)^\lambda) - \Gamma(\eta, \beta(|u|/\delta)^\lambda) \right] \right)}{\left(\operatorname{sign}(b - u) \left[\Gamma(\eta, \beta(|b - u|/\delta)^\lambda) - \Gamma(\eta, \beta(|u|/\delta)^\lambda) \right] - \operatorname{sign}(t - u) \left[\Gamma(\eta, \beta(|t - u|/\delta)^\lambda) - \Gamma(\eta, \beta(|u|/\delta)^\lambda) \right] \right)} \\
 &\quad \times \frac{1}{2\Gamma(\eta)(D(b) - D(a))} \left\{ \frac{\delta}{\beta^{1/\lambda}} \Gamma\left(\eta + \frac{1}{\lambda}\right) \left[\Gamma\left(\eta + \frac{1}{\lambda}, \beta\left(\frac{|b - u|}{\delta}\right)^\lambda\right) - \Gamma\left(\eta + \frac{1}{\lambda}, \beta\left(\frac{|t - u|}{\delta}\right)^\lambda\right) \right] \right. \\
 &\quad \left. \pm u\Gamma(\eta) \left[\Gamma\left(\eta, \beta\left(\frac{|b - u|}{\delta}\right)^\lambda\right) - \Gamma\left(\eta, \beta\left(\frac{|t - u|}{\delta}\right)^\lambda\right) \right] \right\} - t.
 \end{aligned} \tag{21}$$

The mean waiting time of BGM distribution, say $\bar{\varphi}(t)$, can be derived as

$$\begin{aligned}
 \bar{\varphi}(t) &= t - \frac{\int_a^t xY(x|\Theta)dx}{\Phi(t)} \\
 &= t - \frac{1}{2\Gamma(\eta)(D(b) - D(a))} \left\{ \frac{\delta}{\beta^{1/\lambda}} \Gamma\left(\eta + \frac{1}{\lambda}\right) \left[\Gamma\left(\eta + \frac{1}{\lambda}, \beta\left(\frac{|t - u|}{\delta}\right)^\lambda\right) - \Gamma\left(\eta + \frac{1}{\lambda}, \beta\left(\frac{|a - u|}{\delta}\right)^\lambda\right) \right] \right. \\
 &\quad \left. \pm u\Gamma(\eta) \left[\Gamma\left(\eta, \beta\left(\frac{|t - u|}{\delta}\right)^\lambda\right) - \Gamma\left(\eta, \beta\left(\frac{|a - u|}{\delta}\right)^\lambda\right) \right] \right\} \\
 &\quad \times \frac{\operatorname{sign}(b - u) \left[\Gamma(\eta, \beta(|b - u|/\delta)^\lambda) - \Gamma(\eta, \beta(|u|/\delta)^\lambda) \right] - \operatorname{sign}(a - u) \left[\Gamma(\eta, \beta(|a - u|/\delta)^\lambda) - \Gamma(\eta, \beta(|u|/\delta)^\lambda) \right]}{\operatorname{sign}(t - u) \left[\Gamma(\eta, \beta(|t - u|/\delta)^\lambda) - \Gamma(\eta, \beta(|u|/\delta)^\lambda) \right] - \operatorname{sign}(a - u) \left[\Gamma(\eta, \beta(|a - u|/\delta)^\lambda) - \Gamma(\eta, \beta(|u|/\delta)^\lambda) \right]}.
 \end{aligned} \tag{22}$$

TABLE 2: Median, Mode, Mean, Variance, Skewness, and Kurtosis of BGM.

η	λ	Median	Mode1	Mode2	Mean	Variance	Skewness	Kurtosis
0.5	2	0.9979	1	1	0.9949	0.4895	-0.0525	2.8857
0.5	4	1.0037	1.7071	0.2929	1	0.5642	0	1.5708
0.5	7	0.9909	1.8632	0.1368	1	0.6661	0	1.2251
2	2	0.4207	2.2248	-0.2248	0.8932	1.8297	0.0117	1.4184
2	4	0.8071	2.1502	-0.1502	1	1.3293	0	1.13176489
2	7	0.9244	2.0925	-0.0924	1	1.1568	0	1.04581787
7	2	-1.3817	3.5495	-1.5495	-0.9009	2.0185	2.0649	5.7078
7	4	-0.1453	2.6119	-0.6119	0.9959	2.5958	0.0035	1.0358
7	7	0.9785	2.3166	-0.3166	1	1.7181	0	1.0121

TABLE 3: Median, Mode, Mean, Variance, Skewness, and Kurtosis of BGM.

η	β	Median	Mode1	Mode2	Mean	Variance	Skewness	Kurtosis
0.5	0.5	0.9732	1	1	0.9492	0.8732	-0.1824	2.6472
0.5	2	1	1	1	0.9999	0.2499	-0.002	2.993
0.5	7	1	1	1	1	0.0714	0	3
2	0.5	-0.2227	2.7321	-0.7321	0.4599	2.7085	0.2947	1.4377
2	2	0.8327	1.866	0.134	0.9968	0.9946	-0.0052	1.4863
2	7	1.001	1.4629	0.5371	1	0.2857	0	1.5
7	0.5	-1.722	4.6056	-2.6056	-1.547	0.5886	4.8737	28.0326
7	2	-0.483	2.8028	-0.8028	0.5854	3.0344	0.3259	1.2304
7	7	1.0855	1.9636	0.0364	1	1	0	1.1429

3.4. Entropy. The entropy of a random variable X measures the variation of the uncertainty. The Rényi entropy of BGM distribution, say $RE_X(\nu)$ for $\nu \neq 1$ and $\nu > 0$, is derived as

$$\begin{aligned}
 RE_X(\nu) &= \frac{\ln \int_a^b x \Upsilon^\nu(x|\Theta) dx}{1-\nu} \\
 &= -\ln \lambda - \frac{\nu \ln 2}{1-\nu} + \ln \delta - \frac{\nu \ln \Gamma(\eta)}{1-\nu} \\
 &\quad - \frac{\nu \ln(D(b) - D(a))}{1-\nu} - \frac{\ln \beta}{\lambda} - \left(\frac{1}{\lambda} + \frac{\nu \eta}{1-\nu} \right) \ln \nu \\
 &\quad + \frac{1}{1-\nu} \ln \Gamma\left(\nu \eta - \frac{\nu-1}{\lambda}\right) + \frac{1}{1-\nu} \ln \left\{ \pm \Gamma\left(\nu \eta - \frac{\nu-1}{\lambda}, \beta \nu \left(\frac{|b-u|}{\delta}\right)^\lambda\right) \mp \Gamma\left(\nu \eta - \frac{\nu-1}{\lambda}, \beta \nu \left(\frac{|a-u|}{\delta}\right)^\lambda\right) \right\}.
 \end{aligned}
 \tag{23}$$

3.5. Order Statistics. Let $X_{1:n}, X_{2:n}, \dots, X_{n:n}$ denote the order statistics obtained from a random sample of size n

from BGM distribution. The probability density function of i^{th} order statistics is given by

$$\begin{aligned}
 f_{i:n}(x) &= \frac{n!}{(i-1)!(n-i)!} (\Phi(x))^{i-1} (1-\Phi(x))^{n-i} \Upsilon(x|\Theta) \\
 &= \frac{n! \lambda \beta^\eta (|x-u|/\delta)^{\eta \lambda - 1} e^{-\beta(|x-u|/\delta)^\lambda} (D(x) - D(a))^{i-1} (D(b) - D(x))^{n-i}}{2(i-1)!(n-i)! \delta \Gamma(\eta) (D(b) - D(a))^n}.
 \end{aligned}
 \tag{24}$$

The pdf of the minimum and the maximum order statistics of BGT distribution can be obtained, respectively, as follows:

$$f_{1:n}(x) = \frac{n\lambda\beta^\eta (|x-u|/\delta)^{\eta\lambda-1} e^{-\beta(|x-u|/\delta)^\lambda} (D(b)-D(x))^{n-1}}{2\delta\Gamma(\eta)(D(b)-D(a))^n},$$

$$f_{n:n}(x) = \frac{n\lambda\beta^\eta (|x-u|/\delta)^{\eta\lambda-1} e^{-\beta(|x-u|/\delta)^\lambda} (D(x)-D(a))^{n-1}}{2\delta\Gamma(\eta)(D(b)-D(a))^n}.$$

(25)

If n is odd. The pdf of BGT distribution of the median is obtained by substituting $i = (n + 1)/2$ in equation (24) as follows:

$$f_{(n+1/2):n}(x) = \frac{n!\lambda\beta^\eta (|x-u|/\delta)^{\eta\lambda-1} e^{-\beta(|x-u|/\delta)^\lambda} (D(x)-D(a))^{n-1/2} (D(b)-D(x))^{n-1/2}}{2((n-1/2)!)^2\delta\Gamma(\eta)(D(b)-D(a))^n}.$$

(26)

The joint pdf of the i^{th} and the l^{th} order statistics for $x < y$ can be written as

$$f_{i,l:n}(x) = \frac{n!}{(i-1)!(l-i-1)!(n-l)!} (\Phi(x))^{i-1} (1-\Phi(y))^{n-l} (\Phi(y)-\Phi(x))^{l-i-1} Y(x|\Theta)Y(y|\Theta).$$

(27)

So the joint pdf of the i^{th} and the l^{th} order statistics of BGT distribution is

$$f_{i,l:n}(x) = \frac{n!\lambda^2\beta^{2\eta} (D(x)-D(a))^{i-1} (D(b)-D(y))^{n-l} (D(y)-D(x))^{l-i-1}}{4\delta^2\Gamma^2(\eta)(D(b)-D(a))^n (i-1)!(l-i-1)!(n-l)!}$$

$$\times \left(\frac{|x-u||y-u|}{\delta^2}\right)^{\eta\lambda-1} e^{-\beta((|x-u|/\delta)^\lambda+(|y-u|/\delta)^\lambda)}.$$

(28)

4. Maximizing the Log-Likelihood Function

Here, we consider the estimation of the unknown parameters of the BGT distribution by the method of maximum likelihood. Let x_1, x_2, \dots, x_N be a random sample from the BGT distribution. The total log-likelihood ($L(\Theta)$) is given by

$$L(\Theta) = \sum_{i=1}^N \left[\ln T(x_i|u, \delta, \beta, \eta, \lambda) - \ln \int_{\Omega} T(x|u, \delta, \beta, \eta, \lambda) dx \right].$$

(29)

4.1. Location Parameter Estimation. To maximize the likelihood function in (28), we consider the derivation of L with the location u at the $(t + 1)$ iteration step. We have

$$\frac{\partial L}{\partial u} = \sum_{i=1}^N \left\{ \left((u-x_i)|u-x_i|^{-2} \left(\eta\lambda - 1 - \frac{\beta\lambda}{\delta^\lambda} (|u-x_i|)^\lambda \right) \right) \right.$$

$$\left. \frac{\int_{\Omega} \left(\text{sign}(u-x_i)|u-x_i|^{-1} \left(\eta\lambda - 1 - \beta\lambda/\delta^\lambda (|u-x_i|)^\lambda \right) \right) T(x|\Theta) dx}{\int_{\Omega} T(x|\Theta) dx} \right\}.$$

(30)

At that point as [23], we have

$$\int_{\Omega} T(x|\Theta)dx \approx \frac{1}{M} \sum_{i=1}^M 1_{\Omega}(v_i), \tag{31}$$

where $v_i \sim T(x|\Theta^{(t)})$ indicates the random variable that is drawn from the probability distribution $T(x|\Theta^{(t)})$, with $\Theta^{(t)} = (u^{(t)}, \delta^{(t)}, \beta^{(t)}, \eta^{(t)}, \lambda^{(t)})$ and M is the number of random variables v_i . We use $M = 10^6$, for our experiments. In the same manner, we can write

$$\begin{aligned} & \int_{\Omega} \left(\text{sign}(u - x_i) |u - x_i|^{-1} \left(\eta \lambda - 1 - \frac{\beta \lambda}{\delta^\lambda} (|u - x_i|)^\lambda \right) \right) T(x|\Theta) dx \\ & \approx \frac{1}{M} \sum_{i=1}^M 1_{\Omega}(v_i) \left(\text{sign}(u^{(t)} - v_i) |u^{(t)} - v_i|^{-1} \left(\eta^{(t)} \lambda^{(t)} - 1 - \frac{\beta^{(t)} \lambda^{(t)}}{(\delta^{(t)})^{\lambda^{(t)}}} (|u^{(t)} - v_i|)^{\lambda^{(t)}} \right) \right). \end{aligned} \tag{32}$$

By using (31) and (32), we can rewrite (30) as

$$\frac{\partial L}{\partial u} \Big|_{u=u^{(t)}} \approx \sum_{i=1}^N |u^{(t)} - x_i|^{-2} \left\{ \left((u^{(t)} - x_i) \left(\eta^{(t)} \lambda^{(t)} - 1 - \frac{\beta^{(t)} \lambda^{(t)}}{(\delta^{(t)})^{\lambda^{(t)}}} (|u^{(t)} - x_i|)^{\lambda^{(t)}} \right) \right) - H |u^{(t)} - x_i|^2 \right\}, \tag{33}$$

where

$$H = \frac{\sum_{i=1}^M 1_{\Omega}(v_i) \text{sign}(u^{(t)} - v_i) |u^{(t)} - v_i|^{-1} \left(\eta^{(t)} \lambda^{(t)} - 1 - \frac{\beta^{(t)} \lambda^{(t)}}{(\delta^{(t)})^{\lambda^{(t)}}} (|u^{(t)} - v_i|)^{\lambda^{(t)}} \right)}{\sum_{i=1}^M 1_{\Omega}(v_i)}. \tag{34}$$

According to the theory of robust statistics [24], any estimate u is defined by an implicit equation:

$$\sum_i F(x_i - u) = 0. \tag{35}$$

$$u = \frac{\sum_i \omega_i x_i}{\sum_i \omega_i}; \text{ where } \omega_i = \frac{F(x_i - u)}{x_i - u}. \tag{36}$$

Now, we can apply (35) to $\partial L/\partial u$ in (33), and the solution of $\partial L/\partial u = 0$ gives the solutions of u at the $(t + 1)$ step:

This gives a numerical solution of the location of u as a weighted mean:

$$u^{(t+1)} = \frac{\sum_{i=1}^N \left[|u^{(t)} - x_i|^{-2} x_i \left(\eta^{(t)} \lambda^{(t)} - 1 - \frac{\beta^{(t)} \lambda^{(t)}}{(\delta^{(t)})^{\lambda^{(t)}}} (|u^{(t)} - x_i|)^{\lambda^{(t)}} \right) (|u^{(t)} - x_i|)^{\lambda^{(t)}} \right] + H}{\sum_{i=1}^N \left[|u^{(t)} - x_i|^{-2} \left(\eta^{(t)} \lambda^{(t)} - 1 - \frac{\beta^{(t)} \lambda^{(t)}}{(\delta^{(t)})^{\lambda^{(t)}}} (|u^{(t)} - x_i|)^{\lambda^{(t)}} \right) (|u^{(t)} - x_i|)^{\lambda^{(t)}} \right]}. \tag{37}$$

4.2. *Scale Parameters Estimation.* Putting the derivative of the log-likelihood function L with respect to the scale parameter δ at the $(t + 1)$ iteration step, we have

$$\frac{\partial L}{\partial \delta} = \delta^{-1} \sum_{i=1}^N \left[\beta \lambda \delta^{-\lambda} |u - x_i|^\lambda - \eta \lambda - \frac{\int_{\Omega} (\beta \lambda \delta^{-\lambda} |u - x_i|^\lambda - \eta \lambda) T(x|\Theta) dx}{\int_{\Omega} T(x|\Theta) dx} \right]. \quad (38)$$

Similarly as (31) and (32), we can rewrite $\partial L/\partial \delta$ as

$$\frac{\partial L}{\partial \delta} = \delta^{-1} \sum_{i=1}^N \left[\beta \lambda \delta^{-\lambda} |u - x_i|^\lambda - \eta \lambda - G \right], \quad (39)$$

where

$$G = \frac{\sum_{i=1}^M \left[\beta^{(t)} \lambda^{(t)} (\delta^{(t)})^{-\lambda^{(t)}} |u^{(t)} - v_i|^\lambda - \eta^{(t)} \lambda^{(t)} \right] \mathbf{1}_{\Omega}(v_i)}{\sum_{i=1}^M \mathbf{1}_{\Omega}(v_i)}. \quad (40)$$

The solution of $\partial L/\partial \delta = 0$ yields the solutions of δ at the $(t + 1)$ step:

$$\delta^{(t+1)} = \left(\frac{\beta^{(t)} \lambda^{(t)} \sum_{i=1}^N |u^{(t)} - x_i|^{\lambda^{(t)}}}{\sum_{i=1}^N (\eta^{(t)} \lambda^{(t)} + G)} \right)^{1/\lambda^{(t)}}. \quad (41)$$

The next step is to update the estimate of the scale parameter β . This includes fixing the other parameters and improving the estimate of β by using the Newton Raphson method [25]. Every cycle requires the first and second derivatives of $L(\Theta)$ with respect to the parameter β .

$$\beta^{(t+1)} = \beta^{(t)} - \frac{\partial L/\partial \beta}{(\partial^2 L/\partial \beta^2) + \varepsilon} \Big|_{\beta=\beta^{(t)}}, \quad (42)$$

where ε is a scaling element. The derivative of the function $L(\Theta)$ regarding β is given by

$$\frac{\partial L}{\partial \beta} = \sum_{i=1}^N \left\{ f(x_i, \Theta) - \frac{\int_{\Omega} f(x, \Theta) T(x|\Theta) dx}{\int_{\Omega} T(x|\Theta) dx} \right\}, \quad (43)$$

where

$$f(x_i, \Theta) = \frac{1}{T(x_i|\Theta)} \frac{\partial T(x_i|\Theta)}{\partial \beta} = \frac{\eta}{\beta} - \left(\frac{|u - x_i|}{\delta} \right)^\lambda. \quad (44)$$

The term $\partial L/\partial \beta$ can be approximated as

$$\frac{\partial L}{\partial \beta} \Big|_{\beta=\beta^{(t)}} \approx \sum_{i=1}^N \left\{ f(x_i, \Theta^{(t)}) - \frac{\sum_{i=1}^M \mathbf{1}_{\Omega}(v_i) f(v_i, \Theta^{(t)})}{\sum_{i=1}^M \mathbf{1}_{\Omega}(v_i)} \right\}. \quad (45)$$

The term $\partial^2 L/\partial \beta^2$ is given by

$$\frac{\partial^2 L}{\partial \beta^2} = \sum_{i=1}^N \left\{ \frac{\partial f(x, \Theta)}{\partial \beta} + \frac{(\int_{\Omega} T(x|\Theta) f dx)^2}{(\int_{\Omega} T(x|\Theta) dx)^2} - \frac{\int_{\Omega} ((\partial f/\partial \beta) + f^2) T(x|\Theta) dx}{\int_{\Omega} T(x|\Theta) dx} \right\}, \quad (46)$$

where

$$\frac{\partial f}{\partial \beta} = \frac{-\eta}{\beta^2}. \quad (47)$$

Also the term $\partial^2 L/\partial \beta^2$ can be approximated as

$$\frac{\partial^2 L}{\partial \beta^2} \Big|_{\beta=\beta^{(t)}} \approx \sum_{i=1}^N \left\{ \frac{-\eta^{(t)}}{(\beta^{(t)})^2} + \frac{(\sum_{i=1}^M \mathbf{1}_{\Omega}(v_i) (f(v_i, \Theta^{(t)})))^2}{(\sum_{i=1}^M \mathbf{1}_{\Omega}(v_i))^2} - \frac{\sum_{i=1}^M \mathbf{1}_{\Omega}(v_i) \left(-\eta^{(t)}/(\beta^{(t)})^2 + (f(v_i, \Theta^{(t)}))^2 \right)}{\sum_{i=1}^M \mathbf{1}_{\Omega}(v_i)} \right\}. \quad (48)$$

4.3. *Shape Parameters Estimation.* For shape parameter estimation η by using the Newton Raphson method, we have

$$\eta^{(t+1)} = \eta^{(t)} - \frac{\partial L/\partial \eta}{(\partial^2 L/\partial \eta^2) + \varepsilon} \Big|_{\eta=\eta^{(t)}}. \quad (49)$$

The derivative of the function $L(\Theta)$ with respect to η is given by

$$\frac{\partial L}{\partial \eta} = \sum_{i=1}^N \left\{ g(x_i|\Theta) - \frac{\int_{\Omega} g(x|\Theta) T(x|\Theta) dx}{\int_{\Omega} T(x|\Theta) dx} \right\}, \quad (50)$$

where

$$g(x_i|\Theta) = \frac{1}{T(x_i|\Theta)} \frac{\partial T(x_i|\Theta)}{\partial \eta} = \ln \beta - \Psi(\eta) + \lambda (\ln |u - x_i| - \ln \delta). \quad (51)$$

The term $\partial L/\partial \eta$ can be approximated as

$$\frac{\partial L}{\partial \eta} \Big|_{\eta=\eta^{(t)}} \approx \sum_{i=1}^N \left\{ g^{(t)}(x_i|\Theta) - \frac{\sum_{m=1}^M \mathbf{1}_{\Omega}(v_m) g^{(t)}(v_m|\Theta)}{\sum_{i=1}^M \mathbf{1}_{\Omega}(v_i)} \right\}, \quad (52)$$

where

$$g^{(t)}(x_i|\Theta) = \ln \beta^{(t)} - \Psi(\eta^{(t)}) + \lambda^{(t)} (\ln |u^{(t)} - x_i| - \ln \delta^{(t)}). \quad (53)$$

The calculation of the term $\partial^2 L/\partial \eta^2$ is obtained as

$$\frac{\partial^2 L}{\partial \eta^2} = \sum_{i=1}^N \left\{ \frac{\partial g(x_i|\Theta)}{\partial \eta} + \frac{\left(\int_{\Omega} T(x|\Theta) g(x|\Theta) dx \right)^2}{\left(\int_{\Omega} T(x|\Theta) dx \right)^2} \right. \\ \left. - \frac{\int_{\Omega} (\partial g(x|\Theta)/\partial \eta + g^2(x|\Theta)) T(x|\Theta) dx}{\int_{\Omega} T(x|\Theta) dx} \right\}, \quad (54)$$

where

$$\frac{\partial g}{\partial \eta} = -\Psi'(\eta). \quad (55)$$

The term $\partial^2 L/\partial \eta^2$ can be approximated as

$$\frac{\partial^2 L}{\partial \eta^2} \Big|_{\eta=\eta^{(t)}} \approx \sum_{i=1}^N \left\{ \left(\frac{\partial g(x_i|\Theta)}{\partial \eta} \right)^{(t)} + \frac{\left(\sum_{m=1}^M 1_{\Omega}(v_m) g^{(t)}(v_m|\Theta) \right)^2}{\left(\sum_{i=1}^M 1_{\Omega}(v_i) \right)^2} \right. \\ \left. - \frac{\sum_{m=1}^M 1_{\Omega}(v_m) \left((\partial g(v_m|\Theta)/\partial \eta)^{(t)} + (g^{(t)}(v_m|\Theta))^2 \right)}{\sum_{i=1}^M 1_{\Omega}(v_i)} \right\}, \quad (56)$$

where

$$\left(\frac{\partial g(x_i|\Theta)}{\partial \eta} \right)^{(t)} = -\Psi'(\eta^{(t)}). \quad (57)$$

For shape parameter estimation λ by using the Newton Raphson method, we have

$$\lambda^{(t+1)} = \lambda^{(t)} - \frac{\partial L/\partial \lambda}{\partial^2 L/\partial \lambda^2 + \varepsilon} \Big|_{\lambda=\lambda^{(t)}}. \quad (58)$$

The derivative of the function $L(\Theta)$ with respect to λ is given by

$$\frac{\partial L}{\partial \lambda} = \sum_{i=1}^N \left\{ h(x_i|\Theta) - \frac{\int_{\Omega} h(x|\Theta) T(x|\Theta) dx}{\int_{\Omega} T(x|\Theta) dx} \right\}, \quad (59)$$

where

$$h(x_i|\Theta) = \frac{1}{T(x_i|\Theta)} \frac{\partial T(x_i|\Theta)}{\partial \lambda} \\ = \frac{1}{\lambda} + \left(\eta - \beta \left(\frac{|u - x_i|}{\delta} \right)^{\lambda} \right) \ln \left(\frac{|u - x_i|}{\delta} \right). \quad (60)$$

The term $\partial L/\partial \lambda$ can be approximated as

$$\frac{\partial L}{\partial \lambda} \Big|_{\lambda=\lambda^{(t)}} \approx \sum_{i=1}^N \left\{ h^{(t)}(x_i|\Theta) - \frac{\sum_{m=1}^M 1_{\Omega}(v_m) h^{(t)}(v_m|\Theta)}{\sum_{m=1}^M 1_{\Omega}(v_m)} \right\}, \quad (61)$$

where

$$h^{(t)}(x_i|\Theta) = \frac{1}{\lambda^{(t)}} + \left(\eta^{(t)} - \beta^{(t)} \left(\frac{|u^{(t)} - x_i|}{\delta^{(t)}} \right)^{\lambda^{(t)}} \right) \ln \left(\frac{|u^{(t)} - x_i|}{\delta^{(t)}} \right). \quad (62)$$

The calculation of the term $\partial^2 L/\partial \lambda^2$ is obtained as

$$\frac{\partial^2 L}{\partial \lambda^2} = \sum_{i=1}^N \left\{ \frac{\partial h(x_i|\Theta)}{\partial \lambda} + \frac{\left(\int_{\Omega} T(x|\Theta) h(x|\Theta) dx \right)^2}{\left(\int_{\Omega} T(x|\Theta) dx \right)^2} N \right. \\ \left. - \frac{\int_{\Omega} ((\partial h(x|\Theta)/\partial \lambda) + h^2(x|\Theta)) T(x|\Theta) dx}{\int_{\Omega} T(x|\Theta) dx} \right\}, \quad (63)$$

where

$$\frac{\partial h}{\partial \lambda} = \frac{-1}{\lambda^2} - \beta \left(\frac{|u - x_i|}{\delta} \right)^{\lambda} \ln^2 \left(\frac{|u - x_i|}{\delta} \right). \quad (64)$$

The term $\partial^2 L/\partial \lambda^2$ can be approximated as

$$\frac{\partial^2 L}{\partial \lambda^2} \Big|_{\lambda=\lambda^{(t)}} \approx \sum_{i=1}^N \left\{ \left(\frac{\partial h(x_i|\Theta)}{\partial \lambda} \right)^{(t)} + \frac{\left(\sum_{m=1}^M 1_{\Omega}(v_m) h^{(t)}(v_m|\Theta) \right)^2}{\left(\sum_{m=1}^M 1_{\Omega}(v_m) \right)^2} \right. \\ \left. - \frac{\sum_{m=1}^M 1_{\Omega}(v_m) \left((\partial h(v_m|\Theta)/\partial \lambda)^{(t)} + (h^{(t)}(v_m|\Theta))^2 \right)}{\sum_{m=1}^M 1_{\Omega}(v_m)} \right\}. \quad (65)$$

4.4. Algorithm. To study the stability of our model, we have to find the set of initial points that generate a convergent sequence which called stable points of the dynamical system, i.e., we have to find $u^{(0)}, \delta^{(0)}, \beta^{(0)}, \eta^{(0)}, \lambda^{(0)}$ such that $\lim_{t \rightarrow \infty} u^{(t)}, \lim_{t \rightarrow \infty} \delta^{(t)}, \lim_{t \rightarrow \infty} \beta^{(t)}, \lim_{t \rightarrow \infty} \eta^{(t)}$, and $\lim_{t \rightarrow \infty} \lambda^{(t)}$ exist. Indeed for fixed initial, it is difficult to predict how the approximation sequence behaves; hence, for this purpose, we take a random numbers of initial points until the convergence is verified (two successive approximations of each parameter correct to 4 decimal places). The various steps of the proposed model can be summarized as follows:

Step 1: Initialize the parameters $\Theta(u, \delta, \beta, \eta, \lambda)$.

Step 2: Reestimate the parameters $\Theta(u, \delta, \beta, \eta, \lambda)$, where the most common value of scaling parameter ε is 10^{-30} for our experiments.

+Update the parameter u in (37).

+Update the parameter δ in (41).

+Update the parameter β in (42).

+Update the parameter η in (49).

+Update the parameter λ in (58).

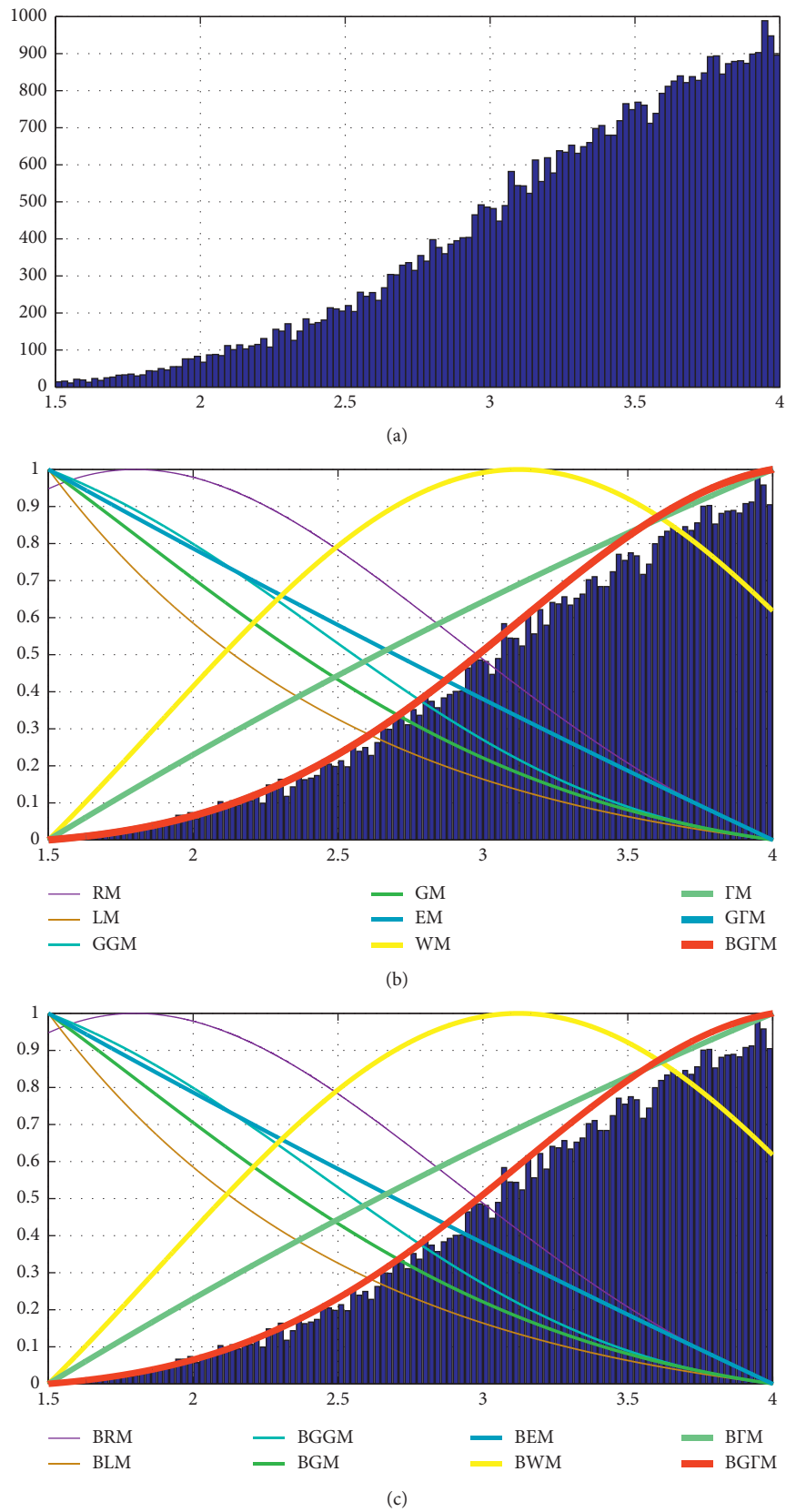
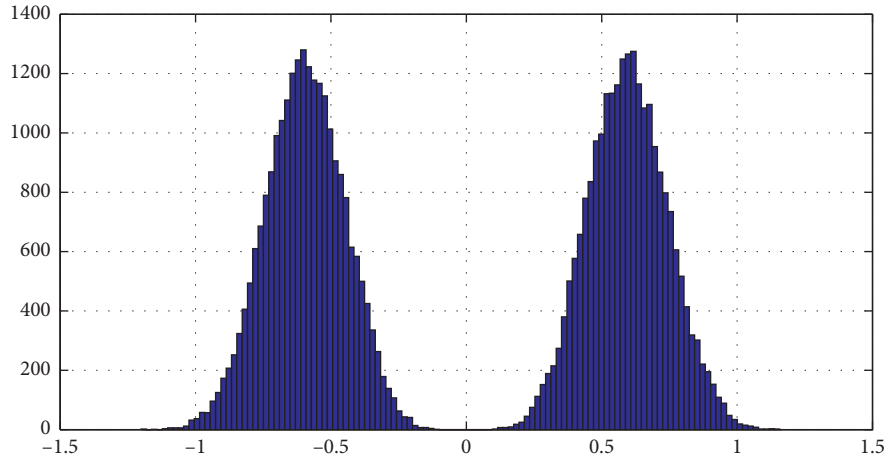
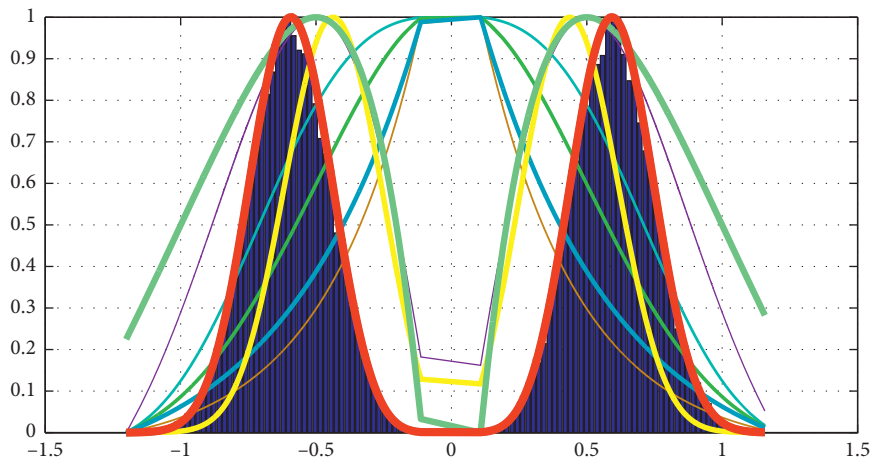


FIGURE 4: The estimated histogram (a) the histogram of the observed data with $u = 0.3$; $\delta = 1.5$; $\eta = 2$, $\lambda = 3$ and $\beta = 0.1$ in the interval (1.5, 4); (b) the estimated histogram of RM, LM, WM, GM, EM, GGM, Γ M, GFM, and BGM; (c) the estimated histogram of BRM, BLM, BWM, BGM, BEM, BGGM, BFM, and BGFm.

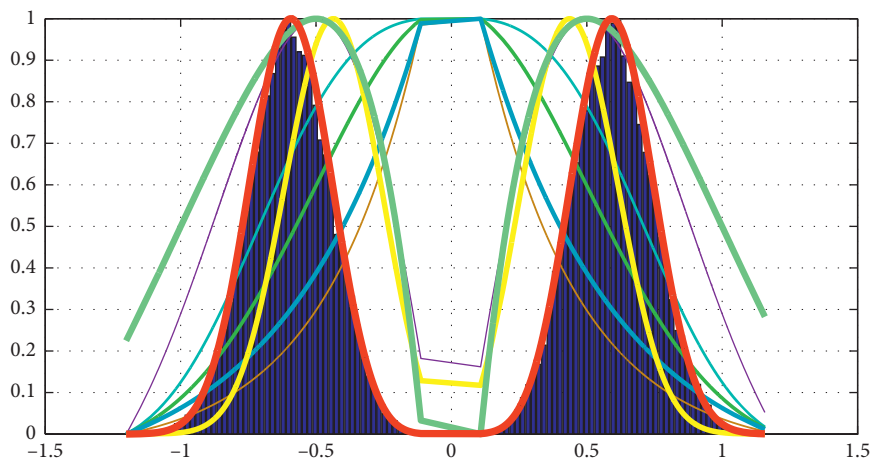


(a)



RM
 GM
 ΓM
 LM
 EM
 GΓM
 GGM
 WM
 BGΓM

(b)



BRM
 BGGM
 BEM
 BΓM
 BLM
 BGM
 BWM
 BGΓM

(c)

FIGURE 5: The estimated histogram. (a) The histogram of the observed data with $u = 0$; $\delta = 0.5$; $\eta = 2$, $\lambda = 3$ and $\beta = 1$ in the interval $(-1.5, 1.5)$; (b) the estimated histogram of RM, LM, WM, GM, EM, GGM, Γ M, G Γ M, and G Γ M; (c) the estimated histogram of BRM, BLM, BWM, BGM, BEM, BGGM, B Γ M, and BG Γ M.

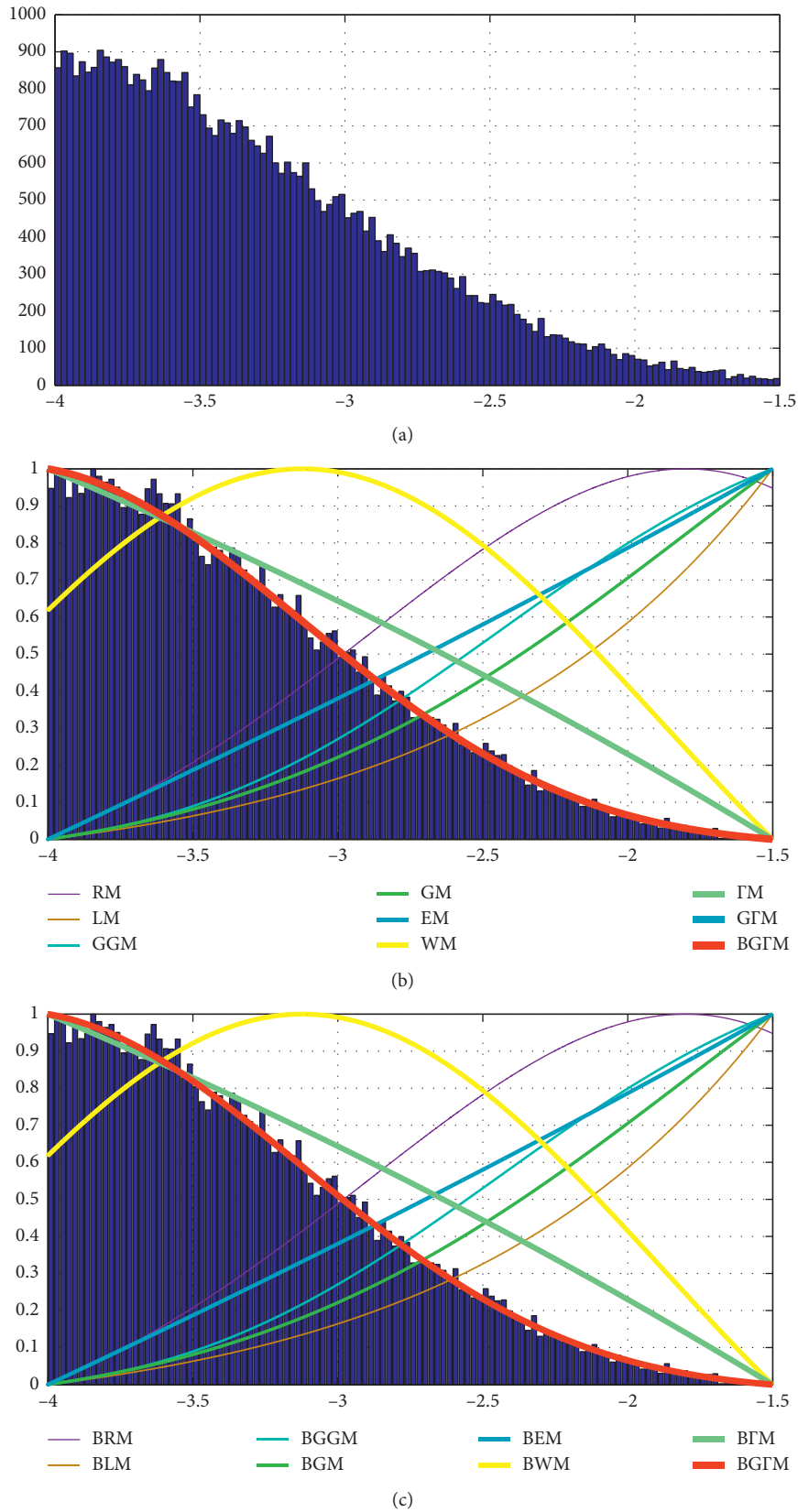


FIGURE 6: The estimated histogram. (a) The histogram of the observed data with $u = -0.3$; $\delta = 1.5$; $\eta = 2$, $\lambda = 3$ and $\beta = 0.1$ in the interval $(-4, -1.5)$; (b) the estimated histogram of RM, LM, WM, GM, EM, GGM, Γ M, GFM, and GFM; (c) the estimated histogram of BRM, BLM, BWM, BGM, BEM, BGGM, BFM, and BGFM.

TABLE 4: The corresponding $-2L$ values of models fitted to simulated data in Figures 4–6.

Model	Figure 4	Figure 5	Figure 6
LM	340369.6	127185.1	339937.1
RM	236056.8	58161.5	235563.1
GM	321759.5	93056.9	321116.7
EM	342290.4	113226.3	342259.8
GGM	328885.3	79528	327945.2
WM	172977.9	59251.4	172863.8
GM	496904.9	99792	497023.3
GFM	199109.3	18948.2	199442.2
BLM	157338.1	123729.1	156760.5
BRM	132502.2	52067.8	132867
BGM	321759.5	93056.9	321116.7
BEM	89868.5	103830.2	90370.9
BGGM	189787.7	59251.4	188722.3
BWM	76569.8	78813.4	76857.7
BFM	71019.3	63381.9	70210
BGFM	55227.9	18944.4	55581

Step 3: Check the convergence, if $|\partial L(\Theta)/\partial \Theta_i|_{\Theta=\Theta^{(i)}} < 10^{-4}$, for all $1 \leq i \leq 5$ under the constrains $AL(\Theta^{(i)})$ is negative definite, where

$$AL(\Theta) = \begin{pmatrix} \frac{\partial^2 L}{\partial u^2} & \frac{\partial^2 L}{\partial u \partial \delta} & \frac{\partial^2 L}{\partial u \partial \beta} & \frac{\partial^2 L}{\partial u \partial \eta} & \frac{\partial^2 L}{\partial u \partial \lambda} \\ \frac{\partial^2 L}{\partial u \partial \delta} & \frac{\partial^2 L}{\partial \delta^2} & \frac{\partial^2 L}{\partial \delta \partial \beta} & \frac{\partial^2 L}{\partial \delta \partial \eta} & \frac{\partial^2 L}{\partial \delta \partial \lambda} \\ \frac{\partial^2 L}{\partial u \partial \beta} & \frac{\partial^2 L}{\partial \delta \partial \beta} & \frac{\partial^2 L}{\partial \beta^2} & \frac{\partial^2 L}{\partial \beta \partial \eta} & \frac{\partial^2 L}{\partial \beta \partial \lambda} \\ \frac{\partial^2 L}{\partial u \partial \eta} & \frac{\partial^2 L}{\partial \delta \partial \eta} & \frac{\partial^2 L}{\partial \beta \partial \eta} & \frac{\partial^2 L}{\partial \eta^2} & \frac{\partial^2 L}{\partial \eta \partial \lambda} \\ \frac{\partial^2 L}{\partial u \partial \lambda} & \frac{\partial^2 L}{\partial \delta \partial \lambda} & \frac{\partial^2 L}{\partial \beta \partial \lambda} & \frac{\partial^2 L}{\partial \eta \partial \lambda} & \frac{\partial^2 L}{\partial \lambda^2} \end{pmatrix}. \quad (66)$$

Then evaluate the function in (29). When the convergence is not verified, then go to step 1 to update the initial point.

Recall that since the matrix $AL(\Theta)$ be an 5×5 symmetric matrix and let $A_k L(\Theta)$ be the submatrix of $AL(\Theta)$ obtained by taking the upper left-hand corner 5×5 submatrix of $AL(\Theta)$. Furthermore, let $\Delta_k = \det(A_k L(\Theta))$, the k^{th} principal minor of $AL(\Theta)$. Then $AL(\Theta)$ is negative definite if and only if $(-1)^k \Delta_k > 0$ for $k = 1, 2, 3, 4, 5$. In comparison with the standard EM algorithm, our methodology can make it simple to evaluate the parameters β , η , and λ by maximizing the higher bound on the data log-likelihood function as appeared in (42), (49), and (58) separately. In the following section, we will explain the robustness, accuracy, and effectiveness of the proposed model, as compared with other models.

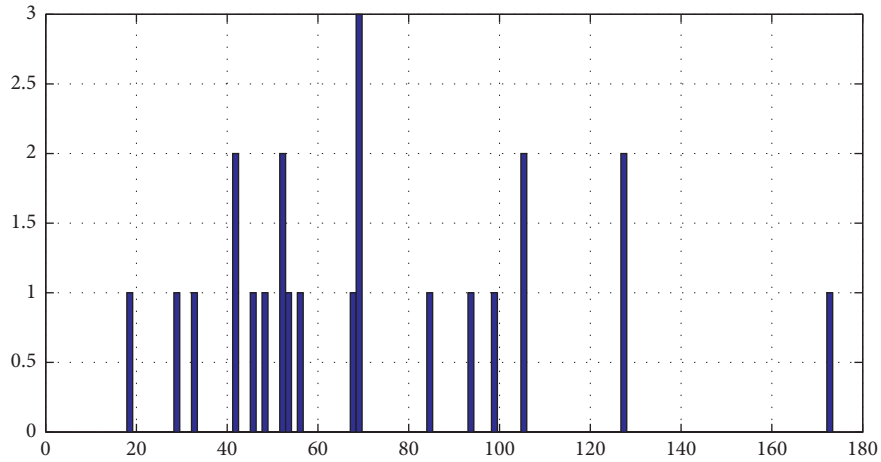
5. Experiments

We explain the proposed technique in different examinations. The execution of BGFM is compared with the WM [16], RM [19], EM [14], LM [22], GM [15], GGM [25], GM [1], GFM [2], BWMM [26], BRM [27], BEM [28], BLM [22], BGM [29, 30], BGGM [22], and BFM [31]. To measure the fitting precision of every model, we use the corresponding -2 Log-likelihood ($-2L$) values of models fitted to data. In general, the smaller values of ($-2L$), is the better fit to the data.

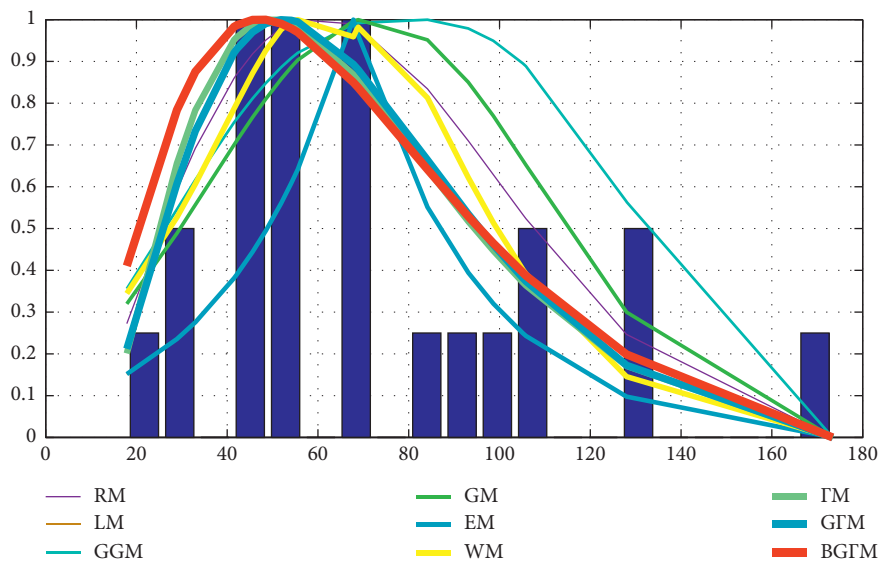
5.1. Simulation Study. We generate 40000 random numbers from BGFM with different parameters and bounded support regions see Figures 4–6. The corresponding $-2L$ values of models fitted to simulated data are listed in Table 4. We find that BGFM is the most powerful and has the least $-2L$. The pdf of BGFM is monotonically increasing, decreasing, bathtub, and upside down bathtub-shaped depending on the parameter values and bounded support regions. So this model is of noticeable importance for image coding and compression applications [32, 33].

5.2. Real Data Study. We give here six real data as follows:

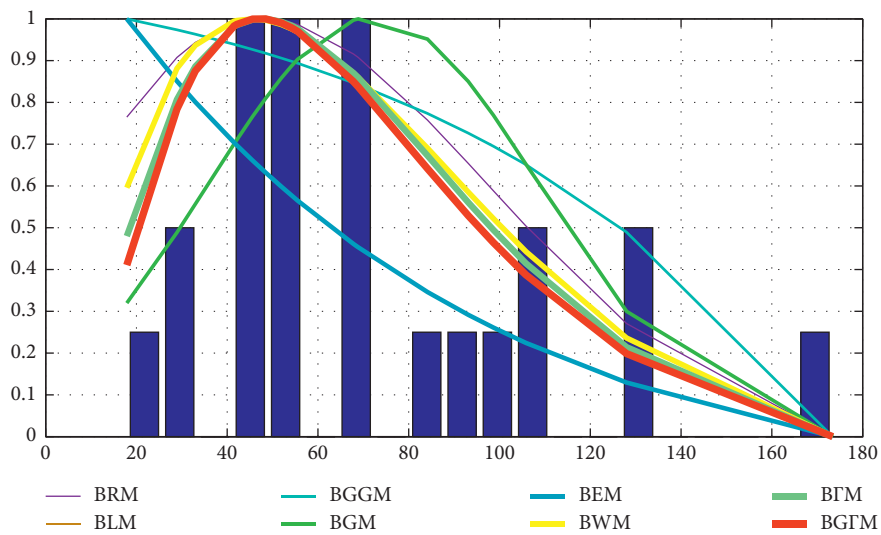
- (1) The first data set arose in tests on endurance of deep groove ball bearings which is from Lawless (1982, p. 288). The data set is 17.88, 28.92, 33, 41.52, 42.12, 45.6, 48.48, 51.84, 51.96, 54.12, 55.56, 67.80, 68.64, 68.64, 68.88, 84.12, 93.12, 98.64, 105.12, 105.84, 127.92, 128.04, 173.40.
- (2) The second data set of the yearly maximum wind speed data in miles/hour, used in this study has been quoted from Castillo (1988) [34].
- (3) The third data set of the tensile strength of 100 observations of carbon fibers, the data was obtained from Ref [35]. The data are 3.7, 2.74, 2.73, 2.5, 3.6,



(a)

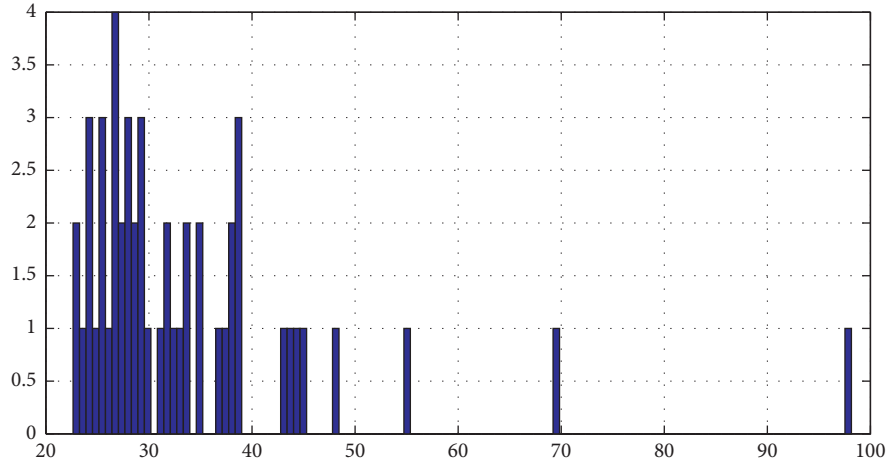


(b)

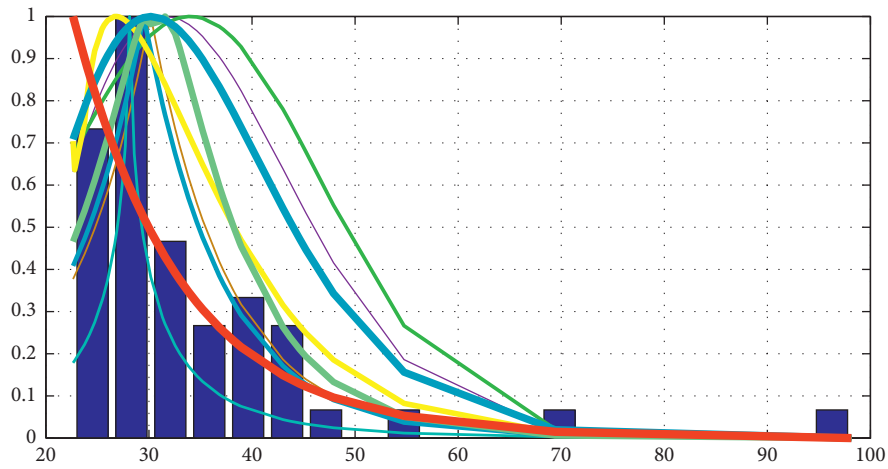


(c)

FIGURE 7: The estimated histogram. (a) The histogram of the tests on endurance of deep groove ball bearings; (b) the estimated histogram of RM, LM, WM, GM, EM, GGM, Γ M, Γ M, and Γ M; (c) the estimated histogram of BRM, BLM, BWM, BGM, BEM, BGGM, Γ M, and Γ M.

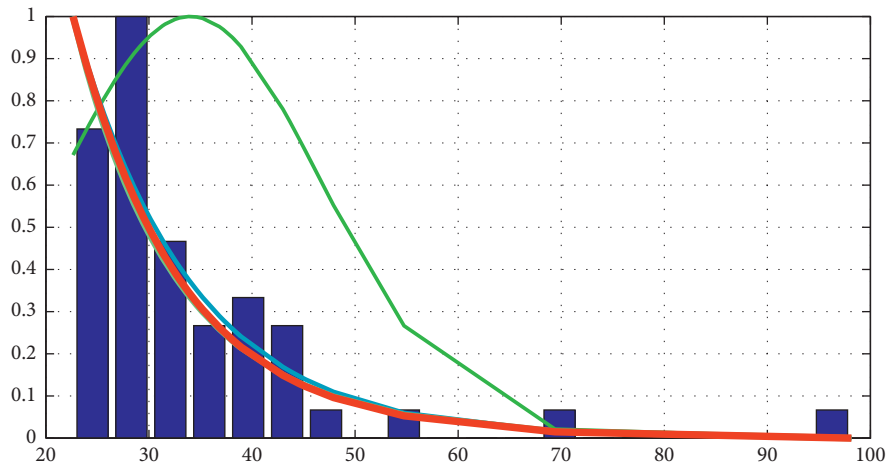


(a)



- RM
- GM
- FM
- LM
- EM
- GFM
- GGM
- WM
- BGFM

(b)



- BRM
- BGGM
- BEM
- BFM
- BLM
- BGM
- BWM
- BGFM

(c)

FIGURE 8: The estimated histogram. (a) The histogram of the yearly maximum wind speed data; (b) the estimated histogram of RM, LM, WM, GM, EM, GGM, FM, GFM, and GFM; (c) the estimated histogram of BRM, BLM, BWM, BGM, BEM, BGGM, BFM, and BGFM.

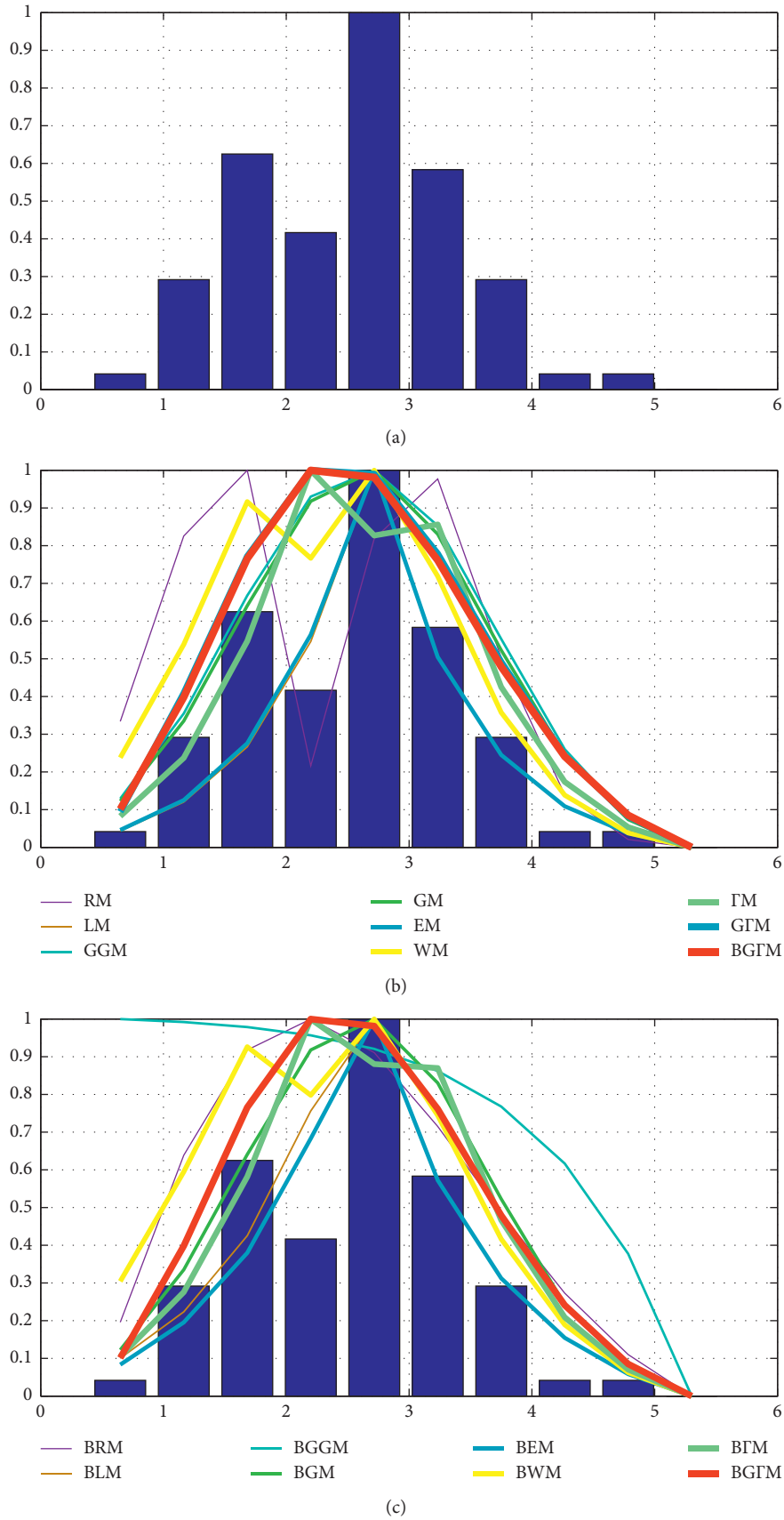
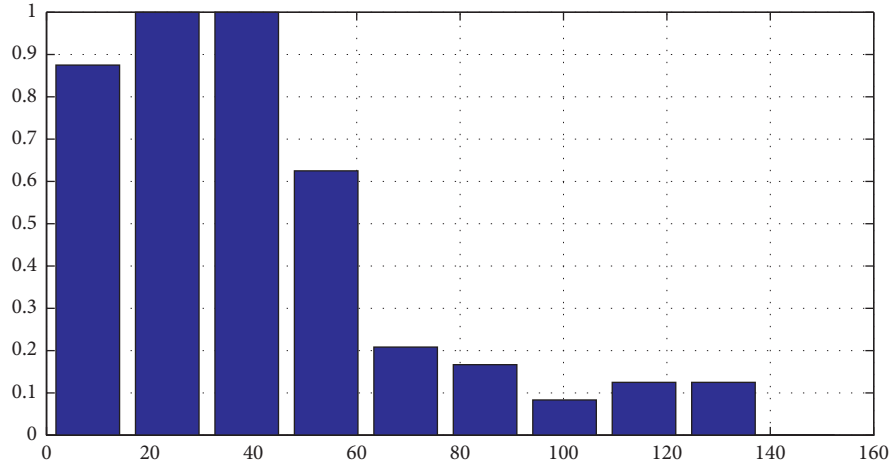
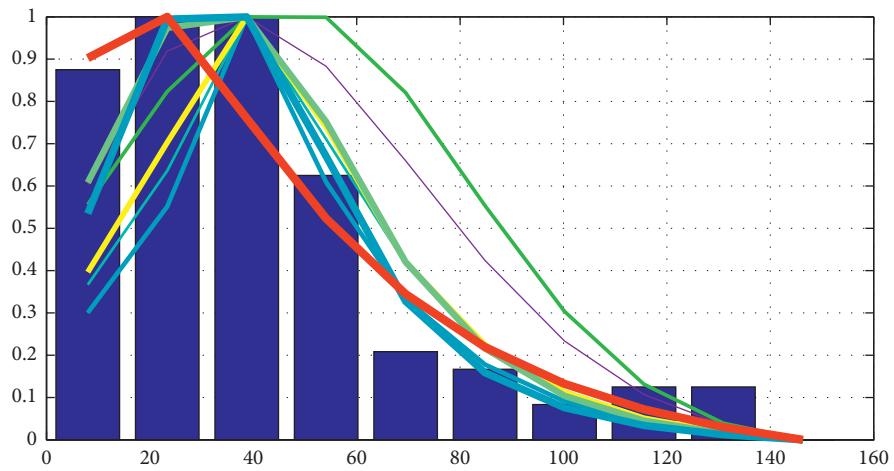


FIGURE 9: The estimated histogram. (a) The histogram of the tensile strength of 100 observations of carbon fibers; (b) the estimated histogram of RM, LM, WM, GM, EM, GGM, IM, GIM, and BGM; (c) the estimated histogram of BRM, BLM, BWM, BGM, BEM, BGGM, BFM, and BGTM.

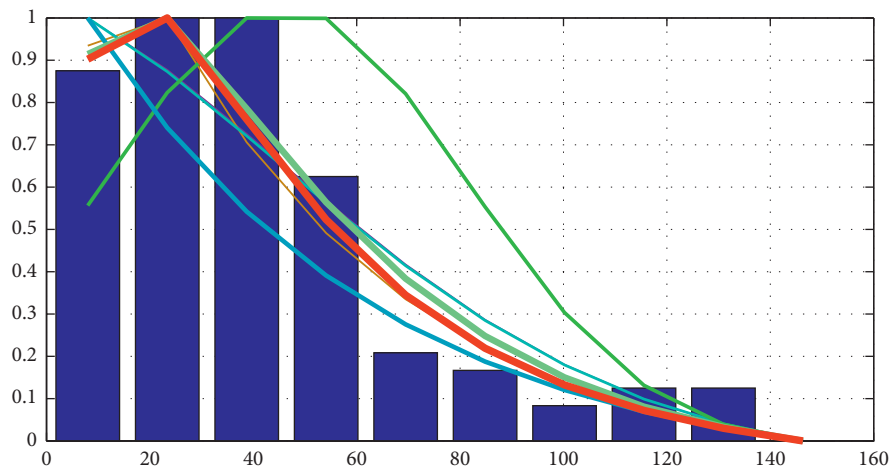


(a)



- RM
- LM
- GGM
- GM
- EM
- WM
- IM
- GFM
- BGM

(b)



- BRM
- BLM
- BGM
- BGGM
- BEM
- BWM
- BFM
- BGM

(c)

FIGURE 10: The estimated histogram. (a) The histogram of the survival times of 121 patients with breast cancer; (b) the estimated histogram of RM, LM, WM, GM, EM, GGM, IM, GFM, and BGM; (c) the estimated histogram of BRM, BLM, BWM, BGM, BEM, BGGM, BFM, and BGM.

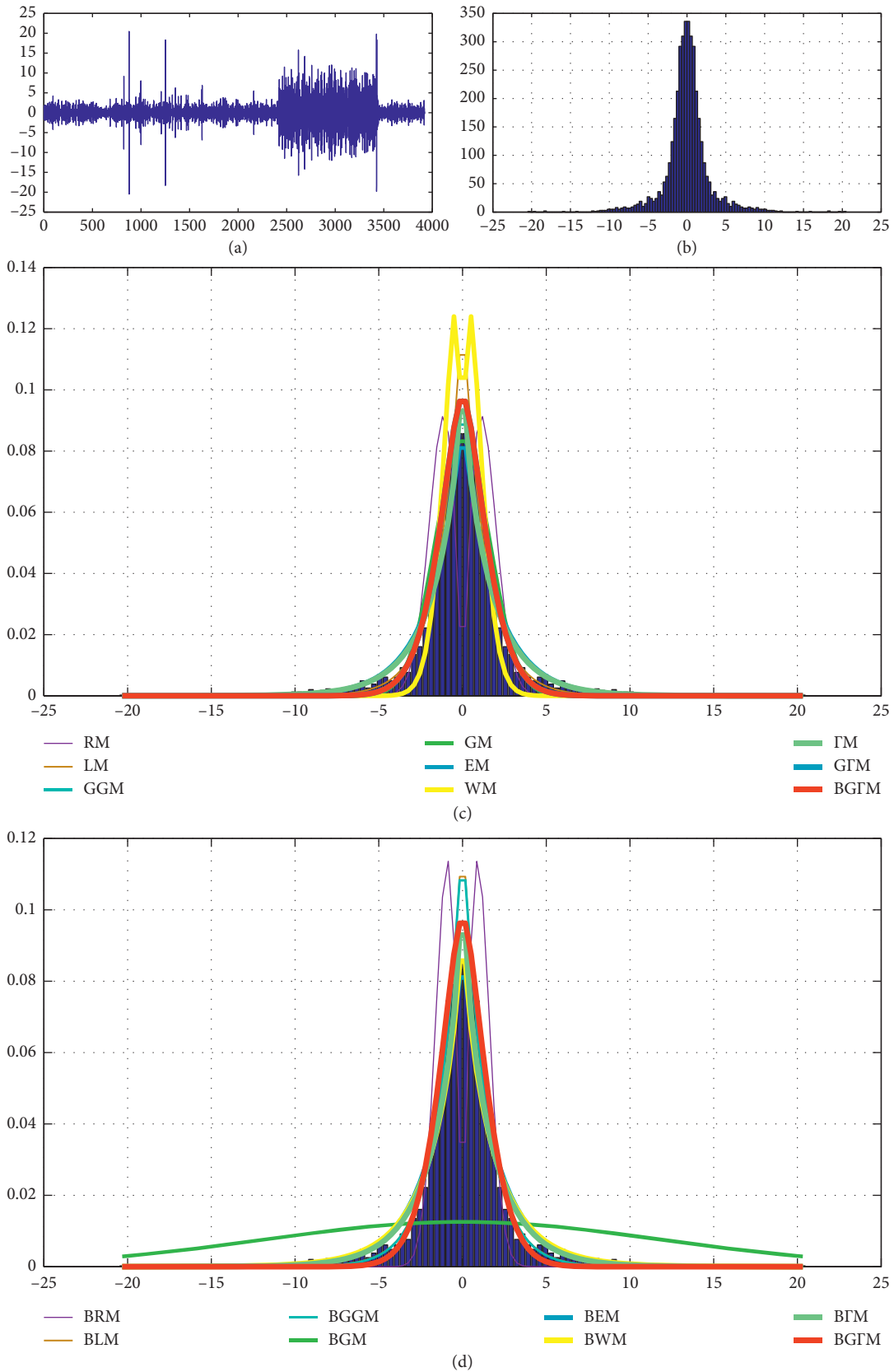


FIGURE 11: Approximation of the wavelet coefficients. (a) “Leleccum.wav”(leleccum (1 : 3920)); (b) approximation of the wavelet coefficient (db1, CD, level 1) of “leleccum.wav;” (c) the estimated histogram of RM, LM, WM, GM, EM, GGM, IM, GFM, and BGM; (d) the estimated histogram of BRM, BLM, BWM, BGM, BEM, BGGM, BFM, and BGM.

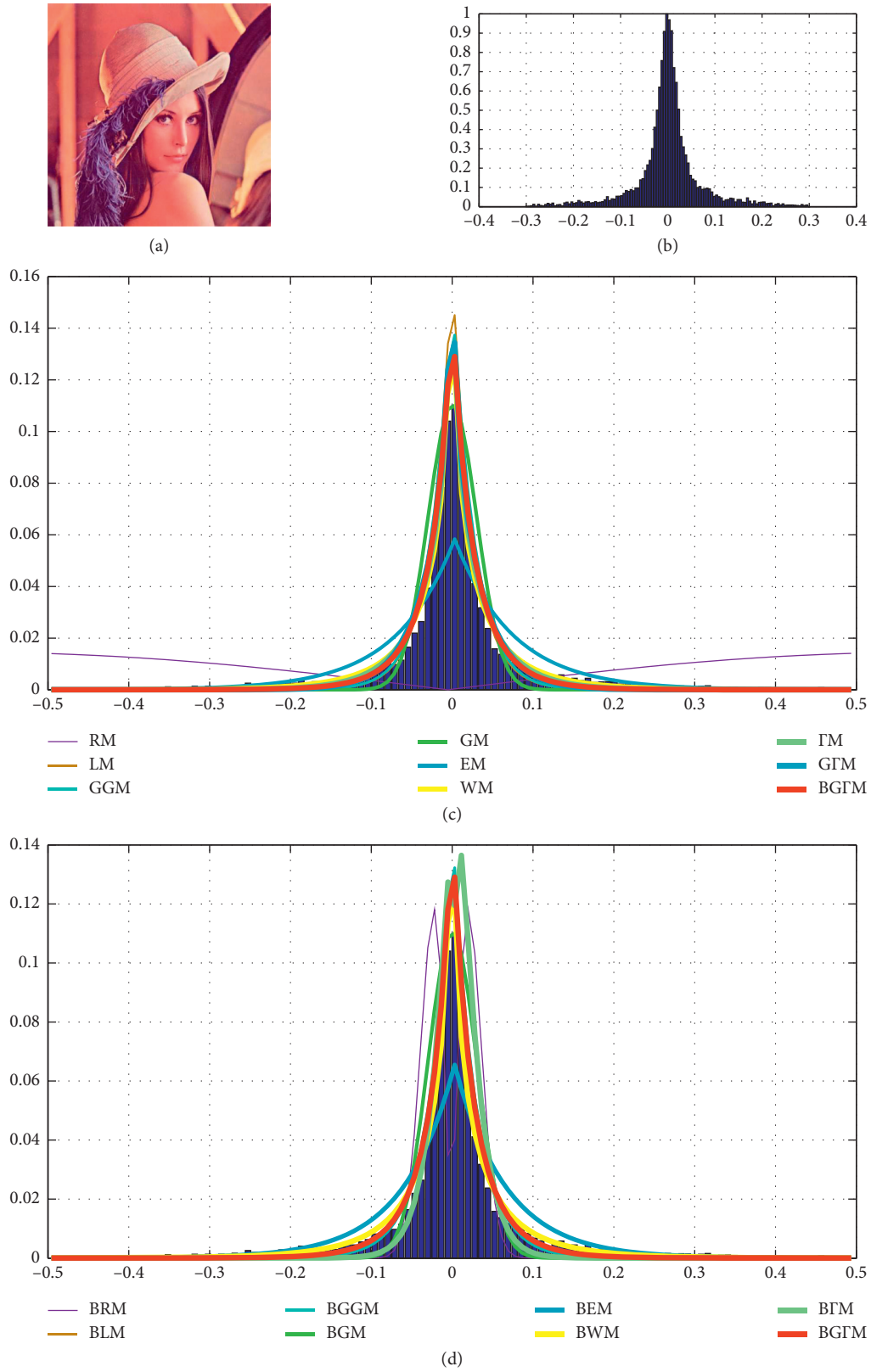


FIGURE 12: Approximation of the wavelet coefficients. (a) The original image (lena); (b) the wavelet coefficient (db4, CD, level 1) of lena image in $(-0.5, 0.5)$; (c) the estimated histogram of RM, LM, WM, GM, EM, GGM, Γ M, GFM, and GFM; (d) the estimated histogram of BRM, BLM, BWM, BGM, BEM, BGGM, BFM, and BGFM.

TABLE 5: The corresponding $-2L$ values of models fitted to real data in Figures 7–12.

Model	Figure 7	Figure 8	Figure 9	Figure 10	Figure 11	Figure 12
LM	231.689	372.636	294.201	1202.9	2054.7969	1622.7872
RM	258.488	445.485	311.805	1343.8	12980.3354	20236.904
GM	230.955	396.412	285.541	1204.7	6672.0221	10248.145
EM	231.691	372.636	294.201	1202.9	1597.1747	1.4026
GGM	231.743	370.125	285.727	1201.7	4469.5735	1.6748
WM	230.41	415.379	287.88	1202.2	7595.6214	534.9312
FM	305.696	373.761	314.142	1218.7	3552.8825	739.3194
GFM	257.824	441.071	421.314	1198.6	1557.8015	440.4421
BLM	225.714	343.052	282.126	1152	2020.3745	1294.9581
BRM	224.418	343.064	285.874	1154.8	20206.6427	20527.3021
BGM	224.632	343.072	281.674	1155	6672.0221	10248.145
BEM	225.714	343.052	282.098	1156.6	1597.168	881.9213
BGGM	232.148	342.794	328.575	1154.9	2104.6441	1361.9667
BWM	224.164	432.44	279.486	1155.7	3551.7368	515.5414
BFM	245.613	346.724	296.563	11741.7	1557.7918	626.7688
BGFM	223.82	342.289	280.608	1151.3	1493.2769	366.1614

TABLE 6: The corresponding AIC, BIC, and CAIC on real data 4.

Model	AIC	BIC	CAIC
BGFM	1161.308	1175.288	1161.831
McLL	1164.661	1178.64	1165.183

3.11, 3.27, 2.87, 1.47, 3.11, 4.42, 2.41, 3.19, 3.22, 1.69, 3.28, 3.09, 1.87, 3.15, 4.9, 3.75, 2.43, 2.95, 2.97, 3.39, 2.96, 2.53, 2.67, 2.93, 3.22, 3.39, 2.81, 4.2, 3.33, 2.55, 3.31, 3.31, 2.85, 2.56, 3.56, 3.15, 2.35, 2.55, 2.59, 2.38, 2.81, 2.77, 2.17, 2.83, 1.92, 1.41, 3.68, 2.97, 1.36, 0.98, 2.76, 4.91, 3.68, 1.84, 1.59, 3.19, 1.57, 0.81, 5.56, 1.73, 1.59, 2, 1.22, 1.12, 1.71, 2.17, 1.17, 5.08, 2.48, 1.18, 3.51, 2.17, 1.69, 1.25, 4.38, 1.84, 0.39, 3.68, 2.48, 0.85, 1.61, 2.79, 4.7, 2.03, 1.8, 1.57, 1.08, 2.03, 1.61, 2.12, 1.89, 2.88, 2.82, 2.05, 3.65.

- (4) The fourth data set of the survival times of 121 patients with breast cancer, the data was obtained from Ref [36].
- (5) In this part “leleccum.wav”(leleccum (1 : 3920)) is disintegrated into three high-pass subbands (CH, CV, CD) and one low-pass subband (CA). The Daubechies channel bank (db1) is used. The fifth data set is the approximation of the wavelet coefficient (db1, CD, level 1) of “leleccum.wav” in the interval $(-20.32, 20.32)$.
- (6) The wavelet approximation coefficient is an essential issue in computer vision as it assumes an important part in an extensive range of applications. The image of (lena) is decomposed into three high-pass subbands (CH, CV, CD) and one low-pass subband (CA). The Daubechies filter bank (db4) is used. The sixth data set is the wavelet coefficients of the high-pass subband (CD), level 1 in the interval $(-0.5, 0.5)$.

The histogram for all real sets and their estimated pdfs for the fitted models are displayed in Figure 7–12. The corresponding $-2L$ values of models fitted to real data are listed in Table 5. Therefore, the proposed model provides a

better fit to these data and has the least $-2L$. Secondly, if we compare the power of our model with modified generalized gamma distribution (MGG) having 6-parameters defined and studied in [12] on real data 3, we have $-2L = 280.608$ and $-2L = 282.692$, respectively. Hence, BGFM is high flexible than MGG for this data. Furthermore, we compare McDonald log-logistic distribution (McLL) [36] with our model BGFM. The model selection is carried out using the following statistics: AIC (Akaike information criterion), CAIC (consistent Akaike information criterion), and BIC (Bayesian information criterion). The corresponding values of models fitted to real data 4 are listed in Table 6. We find that BGFM is more flexible than McLL in this case.

6. Conclusions

A bounded generalized Gamma model with five parameters, whose hazard function can be monotonically increasing, decreasing, bathtub, and upside down bathtub-shaped depending on the parameter values, has been introduced and studied. Some mathematical and statistical properties of the new model are investigated. We estimate the model parameters using maximum log-likelihood function and find a closed form of some parameters by the Newton Raphson method. The predictive ability of our model is found to be comparable or superior to widely accepted distributions. The performance of the model has the smallest $-2L$ values. A simulation study was carried out to evaluate the predictive ability of our model to fit any kind of data with bounded support regions and compare it with other distributions. The power of the new model is illustrated by means of application to six real data sets. The BGFM performs significantly better than the others distributions when sample sizes are

small. Thus, it is less affected by sample size and is more robust. Also the accuracy of the proposed model for wavelet histogram fitting of image and sound is high. We hope that this model may attract wider applications on the modeling of the probability density function of the data via BGF in video coding and image denoising as a future work.

Data Availability

The data used to support the findings of this study are available from the corresponding author upon request.

Ethical Approval

This article does not contain any studies with human participants or animals performed by any of the authors.

Conflicts of Interest

The authors declare that they have no competing interests.

Authors' Contributions

All the authors contributed equally to the writing of this paper. All authors read and approved the final manuscript.

References

- [1] J. M. Nicolas and F. Tupin, "Gamma mixture modeled with second kind statistics: application to SAR image processing," in *Proceedings of the IGARSS*, pp. 2489–2491, Toronto, Canada, June 2002.
- [2] E. W. Stacy, "A generalization of the gamma distribution," *The Annals of Mathematical Statistics*, vol. 33, no. 3, pp. 1187–1192, 1962.
- [3] L. Amoroso, "Ricerche intorno alla curva dei redditi," *Annali di Matematica Pura ed Applicata*, vol. 2, no. 1, pp. 123–159, 1925.
- [4] N. L. Johnson, S. Kotz, and N. Balakrishnan, *Continuous Univariate Distributions*, Vol. 1, Wiley and Sons, Inc., New York, NY, USA, 2nd edition, 1994.
- [5] G. S. Mudholkar and D. K. Srivastava, "Exponentiated Weibull family for analyzing bathtub failure-rate data," *IEEE Transactions on Reliability*, vol. 42, no. 2, pp. 299–302, 1993.
- [6] S. K. Agarwal and J. A. Al-Saleh, "Generalized gamma type distribution and its hazard rate function," *Communications in Statistics - Theory and Methods*, vol. 30, no. 2, pp. 309–318, 2001.
- [7] N. Balakrishnan and Y. Peng, "Generalized gamma frailty model," *Statistics in Medicine*, vol. 25, no. 16, pp. 2797–2816, 2006.
- [8] G. M. Cordeiro, E. M. M. Ortega, and G. O. Silva, "The exponentiated generalized gamma distribution with application to lifetime data," *Journal of Statistical Computation and Simulation*, vol. 81, no. 7, pp. 827–842, 2012.
- [9] S. Nadarajah and A. K. Gupta, "A generalized gamma distribution with application to drought data," *Mathematics and Computers in Simulation*, vol. 74, no. 1, pp. 1–7, 2007.
- [10] L. Chen, V. Singh, and F. Xiong, "An entropy-based generalized gamma distribution for flood frequency analysis," *Entropy*, vol. 19, no. 6, p. 239, 2017.
- [11] Z. Zhao, L. Guo, M. Jia, and L. Wang, "The generalized gamma-DBN for high-resolution SAR image classification," *Remote Sensing*, vol. 10, no. 6, p. 878, 2018.
- [12] M. Mead, M. Nassar, and S. Dey, "A generalization of generalized gamma distributions," *Pakistan Journal of Statistics and Operation Research*, vol. 1, no. 14, pp. 121–138, 2018.
- [13] D. Fulger, E. Scalas, and G. Germano, "Random numbers from the tails of probability distributions using the transformation method," *Fractional Calculus and Applied Analysis*, vol. 16, no. 2, pp. 332–353, 2013.
- [14] A. Feldmann and W. Whitt, "Fitting mixtures of exponentials to long-tail distributions to analyze network performance models," *Performance Evaluation*, vol. 31, no. 3–4, pp. 245–279, 1998.
- [15] G. McLachlan and D. Peel, *Finite Mixture Models*, John Wiley & Sons, New York, NY, USA, 2000.
- [16] L. Attardi, M. Guida, and G. Pulcini, "A mixed-Weibull regression model for the analysis of automotive warranty data," *Reliability Engineering & System Safety*, vol. 87, no. 2, pp. 265–273, 2005.
- [17] T. Bučar, D. M. Nago, and M. Jdiga, "Reliability approximation using finite Weibull mixture distributions," *Reliability Engineering & System Safety*, vol. 84, pp. 241–251, 2004.
- [18] J. A. Carta and P. Ramírez, "Analysis of two-component mixture Weibull statistics for estimation of wind speed distributions," *Renewable Energy*, vol. 32, no. 3, pp. 518–531, 2007.
- [19] K. V. Sorensen and S. V. Andersen, "Rayleigh mixture model-based hidden markov modeling and estimation of noise in noisy speech signals," *IEEE Transactions on Audio Speech and Language Processing*, vol. 15, no. 3, pp. 901–917, 2007.
- [20] J. Seabra, F. Ciompi, P. Radeva, and J. Miguel Sanches, "A Rayleigh mixture model for IVUS imaging," *Ultrasound Imaging. Advances and Applications*, Springer-Verlag New York, New York, NY, USA, 2012.
- [21] M. N. Do and M. Vetterli, "Wavelet-based texture retrieval using generalized Gaussian density and Kullback-Leibler distance," *IEEE Transactions on Image Processing*, vol. 11, no. 2, pp. 146–158, 2002.
- [22] T. M. Nguyen, Q. M. Jonathan Wu, and H. Zhang, "Bounded generalized Gaussian mixture model," *Pattern Recognition*, vol. 47, no. 9, pp. 3132–3142, 2014.
- [23] C. M. Bishop, *Pattern Recognition and Machine Learning*, Springer, Berlin, Germany, 2006.
- [24] P. J. Huber, *Robust Statistics*, Vol. 43, Wiley, New York, NY, USA, 1981.
- [25] M. Allili, "Wavelet modeling using finite mixtures of generalized Gaussian distributions: application to texture discrimination and retrieval," *IEEE Transactions on Image Processing*, vol. 21, no. 4, pp. 1452–1464, 2012.
- [26] T. Zhang and M. Xie, "On the upper truncated Weibull distribution and its reliability implications," *Reliability Engineering & System Safety*, vol. 96, no. 1, pp. 194–200, 2011.
- [27] A. R. Sudamani Ramaswamy and S. Jayasri, "Time truncated chain sampling plans for generalized Rayleigh distribution," *International Refereed Journal of Engineering and Science (IRJES)*, vol. 3, no. 2, pp. 49–53, 2014.
- [28] M. Raschke, "Inference for the truncated exponential distribution," *Stochastic Environmental Research and Risk Assessment*, vol. 26, no. 1, pp. 127–138, 2012.
- [29] P. Hedelin and J. Skoglund, "Vector quantization based on Gaussian mixture models," *IEEE Transactions on Speech and Audio Processing*, vol. 8, no. 4, pp. 385–401, 2000.

- [30] J. Lindblom and J. Samuelsson, "Bounded support Gaussian mixture modeling of speech spectra," *IEEE Transactions on Speech and Audio Processing*, vol. 11, no. 1, pp. 88–99, 2003.
- [31] C. S. Coffey and K. E. Muller, "Properties of doubly-truncated gamma variables," *Communications in Statistics-Theory and Methods*, vol. 29, no. 4, pp. 851–857, 2000.
- [32] S. G. Chang, B. Bin Yu, and M. Vetterli, "Adaptive wavelet thresholding for image denoising and compression," *IEEE Transactions on Image Processing*, vol. 9, no. 9, pp. 1532–1546, 2000.
- [33] S. Kasaei, M. Deriche, and B. Boashash, "A novel fingerprint image compression technique using wavelets packets and pyramid lattice vector quantization," *IEEE Transactions on Image Processing*, vol. 11, no. 12, pp. 1365–1378, 2002.
- [34] E. Castillo, *Extreme Value Theory In Engineering*, Vol. 334, Academic Press, London, UK, 1988.
- [35] D. F. Andrews and A. M. Herzberg, *Data: A Collection of Problems from Many Fields for the Student and Research Worker*, Springer Series in Statistics, New York, NY, USA, 1985.
- [36] M. H. Tahir, M. Mansoor, M. Zubair, and G. G. Hamedani, "McDonald log-logistic distribution with an application to breast cancer data," *Journal of Statistical Theory and Applications*, vol. 1, no. 13, pp. 65–82, 2014.

Research Article

Optimal Intersection Curves for Surfaces

Jiwen Gao,¹ Faiza Sarfraz ,² Misbah Irshad,² and Jia-Bao Liu ³

¹College of Modern Service Industry, Hefei College of Finance & Economics, Hefei 230601, China

²Department of Mathematics, Lahore College for Women University, Lahore, Pakistan

³School of Mathematics and Physics, Anhui Jianzhu University, Hefei 230601, P.R., China

Correspondence should be addressed to Faiza Sarfraz; faizasarfraz03@yahoo.com

Received 17 March 2021; Revised 27 May 2021; Accepted 13 June 2021; Published 17 August 2021

Academic Editor: Ghulam Mustafa

Copyright © 2021 Jiwen Gao et al. This is an open access article distributed under the Creative Commons Attribution License, which permits unrestricted use, distribution, and reproduction in any medium, provided the original work is properly cited.

In this article, an algorithm has been established to approximate parametric-parametric, explicit-implicit, and explicit-explicit surface intersection. Foremost, it extracts the characteristic points (boundary and turning points) from the sequence of intersection points and fits an optimal cubic spline curve to these points. Moreover, this paper utilizes genetic algorithm (GA) for optimization of shape parameters in the portrayal of cubic spline so that the error is minimal. The proposed algorithm is demonstrated with different types of surfaces to analyze its robustness and proficiency. In the end, all illustrations show the effectiveness of the algorithm which makes it more influential to resolve all complexities arises during intersection with a minimal error.

1. Introduction

Surface/surface intersection (SSI) has enormous applications in diverse fields while dealing with two surfaces/curves' intersection problems. It is a fundamental ingredient in computer graphics to develop different shapes of ultrasonic machines (3D images from ultrasonic machines can be joined with CAD images for good results), airplanes, architecture designs, etc., via a variety of surfaces. With the advancement in 3D technologies, such as in laser scanning, one can scan more precisely even at a significant distance. Similarly, in engineering, curve of intersection (COI) is achieved by the intersection of different solids such as prism-prism, prism-cone, and cone-cone. It deals with complex mathematical geometry which arises in designing of automotive at large scale. A huge collection of work, extending back quite a few years, addresses the issues related to SSI. This is still an important issue in industrial engineering and mathematical fields. Usually, nonempty intersection intends to find an error bound for approximation of intersection curves, see, for example, [1–5] and references therein.

The algorithm proposed in [6] focused on evaluating intersection curves of rational polynomial parametric surface patches, which is based on a validated ordinary

differential equation system solver. Later on, they emphasized on the marching method [7] for solving problems which offer remarkable advantages, but still their approach is facing some problems because of complicated initial and boundary values. In the same way, an approach in [8] worked on solving differential geometry problems of hypersurfaces; also, they are doing this research [9] by increasing dimensions of surfaces which take more time for showing results. Extracting boundary and turning points of parametric surface intersection curves by the GK method are discussed in [10, 11]. Their topology is still confronting problems of error that come up through surface intersection. Also, the methodology in [12] is used for finding characteristics points, but excess of points are calculated for appropriate results.

Explicit and implicit surfaces are not extensively used in a variety of fields, but researchers did remarkable work whatever the circumstances occurred during research. In the medical field, scientists used an explicit surface-based method for the cortical thickness of the brain [13]; still, they are doing their work on that purpose. In CAD, hybrid models can be merged with explicit models [14] for removing ambiguities and getting better graphic results. The problems occurring in ocean-free surface models can be

solved explicitly or implicitly. In explicit surfaces, scaling behavior on parallel systems is better than implicit schemes [15] because baro-clinic time steps are used in implicit surfaces and are larger than the time-stepping scheme in explicit surfaces.

Collectively, methods involving implicit surfaces are quite diffusive because global communication in each iteration makes the method's scale poorer; while explicit surface methods have flexibility to resolve all possible difficulties during the iteration process. The combination of these surfaces is good for intersection because if one surface is creating some problem during intersection the other may overcome the situation.

Soft computing behavior such as computational intelligence, is a blend of different techniques such as fuzzy logic [16], simulated annealing, genetic algorithm, numerical technics [17], etc., whose objective is to solve computational problems which is based on natural evolution theory [18], which is not easily demonstrated numerically. In this research work, a genetic algorithm is utilized, which is useful in getting optimal outcomes.

While a lot of work has been done on SSI issues, still there is hardly any established algorithm which can deal intersection of all types of surfaces. Each approach that was discussed in the previous section has its own disadvantages and limits. This motivated us to develop an optimal technique using genetic algorithm and cubic spline function, which can be used to approximate intersections of wider range of surfaces. The technique proposed in this paper works equally well to approximate intersection curves for following three cases of intersection of surfaces:

- 1 Intersection of two explicit surfaces
- 2 Intersection of one implicit and one explicit surface
- 3 Intersection of two parametric surfaces

This paper is organized as follows. Section 2 includes the materials and methods of proposed approach. Genetic algorithm is discussed in Section 3. Results and discussion is given in Section 4. This paper is concluded in Section 5.

2. Materials and Methods

The proposed approach takes two surfaces as input. These surfaces may consist of two explicit surfaces s_1 and s_2 in R^3 , which are defined as

$$\begin{aligned} s_1: \{a_1 = G_1(x, y): a = x = b, c = y = d\}, \\ s_2: \{a_2 = G_2(x, y): a = x = b, c = y = d\}, \end{aligned} \quad (1)$$

where $a, b, c, d \in R$.

One implicit and one explicit surface h_1 and h_2 are represented by

$$\begin{aligned} h_1: \{K_1(x, y, z) = 0: a = x = b, c = y = d, e = z = f\}, \\ h_2: \{z = K_2(x, y): a = x = b, c = y = d, e = z = f\}, \end{aligned} \quad (2)$$

where $a, b, c, d, e, f \in R$.

Two parametric surfaces z_1 and z_2 in R^3 are denoted as

$$\begin{aligned} z_1 = \{F_1(x(s, t), y(s, t), z(s, t)): a = s = b, c = t = d\}, \\ z_2 = \{F_2(x(r, w), y(r, w), z(r, w)): a = r = b, c = w = d\}, \end{aligned} \quad (3)$$

where $a, b, c, d \in R$.

In order to find sequence of intersection points of all above surfaces, the solution of the following equations is required, respectively:

$$\begin{cases} a_1 - a_2 = 0, \\ z - K_1(x, y, z) = 0, \\ F_1 - F_2 = 0. \end{cases} \quad (4)$$

Additionally, its nonempty intersection contains isolated sequence points and curves of intersected pieces.

2.1. Characteristic Points. Characteristic points are the subset of the sequence of intersection points which helps to identify the shape of intersection curves, including all the turning and boundary points.

2.1.1. Boundary Points. The boundary points can be determined by imposing the following conditions: $x = a, x = b, y = c, y = d, z = e$, and $z = f$ in equation (4).

2.1.2. Turning Point. A point where curve changes its direction or where intersected curve makes a sharp turn is called turning point. The turning points can be estimated by finding

- (i) The inflection point of equation (4)
- (ii) The points where curve (4) has slope 0, 1, or -1
- (iii) Where the function changes its curvature
- (iv) When derivative changes its sign

2.2. Cubic Spline Interpolant. Cubic spline function [19] is used to fit the curve at the points obtained in the previous section. Let F_i and F_{i+1} , $i = 1, 2, \dots, n-1$, be distinct characteristic points. Moreover, the slope of tangent associated to these points is denoted by D_i, D_{i+1} , and v_i and w_i are shape control parameters. Then, the cubic function is considered as

$$\begin{cases} P_i(t) = U_i(1-t)^3 + 3V_i(1-t)^2t + 3W_i(1-t)t^2 + X_it^3, \\ h_i = t_{i+1} - t_i, \quad i = 1, 2, \dots, n-1, \end{cases} \quad (5)$$

satisfying the following properties:

$$\begin{aligned} P(t_i) &= F_i, \\ P(t_{i+1}) &= F_{i+1}, \\ P^{(1)}(t_i) &= v_i D_i, \\ P^{(1)}(t_{i+1}) &= w_i D_{i+1}, \end{aligned} \quad (6)$$

where $P^{(1)}$ denotes first derivative with respect to t , which yields interpolating conditions as

$$\begin{aligned} U_i &= F_i, \\ X_i &= F_{i+1}, \\ V_i &= \left(F_i + \frac{h_i D_i v_i}{3} \right), \\ W_i &= \left(F_{i+1} - \frac{h_i D_{i+1} w_i}{3} \right). \end{aligned} \tag{7}$$

So, $P_i(t)$ takes the form:

$$\begin{aligned} P_i(t) &= F_i(1-t)^3 + 3\left(f_i + \frac{h_i D_i v_i}{3} \right)(1-t)^2 t \\ &+ 3\left(f_{i+1} - \frac{h_i D_{i+1} w_i}{3} \right)(1-t)t^2 + F_{i+1}t^3. \end{aligned} \tag{8}$$

The above equation can be rewritten as

$$P_i(t) = R_{0,i}(t)F_i + R_{1,i}(t)V_i + R_{2,i}(t)W_i + R_{3,i}(t)F_{i+1}, \tag{9}$$

where $R_{0,i} = (1-t)^3$, $R_{1,i} = 3t(1-t)^2$, $R_{2,i} = 3t^2(1-t)$, and $R_{3,i} = t^3$.

The functions $R_{j,i}$, $j = 0, 1, 2, 3$, are like Bernstein Bezier basis functions such that

$$\sum_{j=0}^3 R_{j,i}(t) = 1. \tag{10}$$

Two cases of optimal intersection curve are discussed below.

In order to achieve optimal curve fitted to characteristic points, the sum of squares of distances between data (intersection) points $P'_{i,j} = (x_{i,j}, y_{i,j})$ and approximated points using cubic spline $P(t_j)$ should be minimized, i.e.,

$$S_i = \sum_{j=1}^{m_i} [P_i(t_{i,j}) - P'_{i,j}]^2, \quad i = 1, 2, \dots, n, \tag{11}$$

where chord length parameterization which is used for parameter t needs to be minimized.

In this procedure, such values of the shape control parameters v_i and w_i must be chosen with the help of genetic algorithm so that S_i (equation (11)) is minimal and the following two cases may arise to do so.

Case 1. $v_i = w_i$

Shape parameters are taken as equal in this case, so the objective function (11) depends on one variable only.

Case 2. $v_i \neq w_i$

Shape parameters are not taken as equal in this case. The process of finding the best curve is the same as above by taking objective function (11) as a function of two variables.

Moreover, in this paper, results are obtained using case 2 as case 1 is special case of case 2.

3. Genetic Algorithm

As cubic spline has two parameters v_i and w_i , in case of achieving optimal values of v and w , a soft computing technique, i.e., genetic algorithm (GA) [18] is used. Genetic algorithm is one of the powerful evolutionary-based optimization technique to tackle complicated optimization problems. It forms adaptive patterns of searching, based on natural genetics and designs of natural selection. Natural evolution process works under some genetic operators (selection, crossover, and mutation). This procedure moves from one parent population (chromosomes) to another by using genetic operators where every chromosome consists of more than one bit strings. Selection operator helps selecting chromosome which allowed to reproduce and would die out. Crossover operator generates new chromosomes by exchanging some area of two bit strings (chromosomes) mutually. Mutation operator disseminates some new characteristics among the bit strings for more variety of chromosomes. Figure 1 shows an example of crossover and mutation operator for some particular choice of chromosomes.

GA does not need any lengthy mathematical formulation for better results and rise as a significant technique which solves complex problems in short time with appropriate results. GA choses random values of the parameters v_i, w_i from certain population and application of iterated process of GA along with genetic operators, selection, mutation, and crossover which specifically fit the optimal curve to intersection points by finding optimal values of shape control parameters v_i, w_i .

For best curve fitted to given data, those values of shape parameters are required, for which the sums S_i should be minimized. GA is used to optimize the values of parameters which help in minimizing the error.

In literature, different methods are used for finding the error. The error occurs when approximated points do not lie on the exact location. The error calculated by the proposed technique in this paper is shown in Tables 1–3. The minimized error gives best approximated curve which shows the efficiency of the proposed approach. Table 4 displays values of parameters which are used for GA.

3.1. Proposed Algorithm Steps. The overall proposed scheme can be described in the form of an algorithm.

Step 1: input surface data

Step 2: find intersection of surfaces by the method mentioned in Section 2

Step 3: extract the characteristics points through criteria given in Section 2

Step 4: fit the spline curve to the points attained in Step 3

Step 5: compute the best optimal value of parameters v and w by using GA

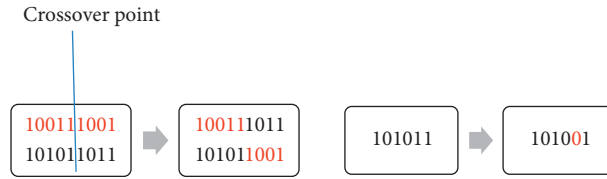


FIGURE 1: Execution of crossover and mutation operator.

TABLE 1: Iterative values with characteristic points of Example 1.

	SPV	TE (seconds)	E (SSE)	TOIP	CP
	$\nu = 0.22$				
1 st iteration	$w = 0.31$	0.047	0.02941	762	(-1.85,-0.39) (0.19, 0.82) (-0.15,-0.39) (2, 1.77) (-2, 0.5)
2 nd iteration	$\nu = 0.41$ $w = 0.56$	0.039	0.00572		
Optimal curve	$\nu = 0.9$ $w = 0.9$	0.023	6.7×10^{-5}		

TABLE 2: Iterative values with characteristics points of Example 2.

	SPV	TE (seconds)	E (SSE)	TOIP	CP
	$\nu = 1.06$				
1 st iteration	$w = 1.17$	0.124	0.00365	217	(0, 1.249, 1.562) (0, -1.249, 1.562) (1.249, 0, -1.562) (-1.249, 0, -1.562) (1.414, 1.414, 0) (-1.414, -1.414, 0) (1.414, -1.414, 0) (-1.414, 1.414, 0)
2 nd iteration	$\nu = 1.22$ $w = 1.34$	0.086	0.00021		
Optimal curve	$\nu = 3.82$ $w = 3.82 = 3.82$	0.135	1.1×10^{-7}		

TABLE 3: Iterative values with characteristics points of Example 3.

	SPV	TE (seconds)	E (SSE)	TNIP	CS
1 st iteration	$\nu = 1.49$ $w = 1.56$	0.049	0.0169	167	(1/3, 1/3) (0.993, 0.284)
2 nd iteration	$\nu = 1.67$ $w = 1.77$	0.052	0.00021		
Optimal curve	$\nu = 2.99$ $w = 2.99$	0.047	1.8×10^{-8}		

TABLE 4: Parameters utilized for GA.

Sr. no.	Name	Values
1	Population size	25-30
2	Genome length	15
3	Selection rate	0.5
4	Mutation rate	0.01

Step 6: if the optimal curve has been accomplished in Step 5, then go to Step 7, otherwise go to Step 4 and repeat these steps until the desired optimal curve is achieved

Step 7: Stop

4. Results and Discussion

The execution of proposed approach on intersection of explicit-explicit, implicit-explicit, and parametric-parametric surfaces has been shown in the following examples.

Example 1. Two explicit surfaces are given by

$$\begin{aligned} s_1: \{z = y^2 + 2x | 0 \leq x, y \leq 1\}, \\ s_2: \{z = 2y^3 - x^2 | 0 \leq x, y \leq 1\}. \end{aligned} \tag{12}$$

Both explicit surfaces are shown in Figures 2 and 3. Figure 4 depicts intersection of surfaces, while Figure 5 epitomizes the xy -view of intersection along with boundary and turning points which extracted through criteria given in Section 2. Approximation of sequence of points is displayed in Figure 6. Figures 7 and 8 show how cubic spline is used to fit the curve through 1st and 2nd iterations of GA. The best optimal curve is given in Figure 9 and achieved in 20th iteration of GA.

Example 2. Implicit and explicit surfaces are given by

$$\begin{aligned} s_1: \{x^2 + y^2 + z^2 = 4 | 0 \leq x, y, z \leq 1\}, \\ s_2: \{-x^2 + y^2 = z | 0 \leq x, y, z \leq 1\}. \end{aligned} \tag{13}$$

Explicit and implicit surfaces are displayed in Figures 10 and 11. Figure 12 portrays intersection of surfaces, while Figure 13 denotes the xy -view of intersection along with boundary and turning points which are extracted through criteria given in Section 2. Approximation of sequence of points is publicized in Figure 14. Figures 15 and 16 represent how cubic spline is used to fit the curve through 1st and 2nd iterations of GA. The best optimal curve is shown in Figure 17 and obtained after 24th iteration of GA.

Example 3. Two parametric surfaces with parameters x, y are given by

$$\begin{aligned} s_1: \{(3x, 3y, 18xy(x-1)(y-1)) | 0 \leq x, y \leq 1\}, \\ s_2: \{(3x+1, -18x^3y^2 + 18x^3y + 27x^2y^2 - 27x^2y - 9xy^2 + 9xy + 1, 3y-1) | 0 \leq x, y \leq 1\}. \end{aligned} \tag{14}$$

Both parametric surfaces are shown in Figures 18 and 19. Figure 20 illustrates intersection of surfaces, while Figure 21 demonstrates the xy -view of intersection along with boundary and turning points which extracted through criteria given in Section 2. Approximation of sequence of points is shown in Figure 22. Figures 23 and 24 exemplify how cubic spline is used to fit the curve through 1st and 2nd iterations of GA. The best optimal curve is depicted in Figure 25 and produced in 31st iteration.



FIGURE 2: Explicit surface 1.



FIGURE 3: Explicit surface 2.



FIGURE 4: Intersection of both surfaces.

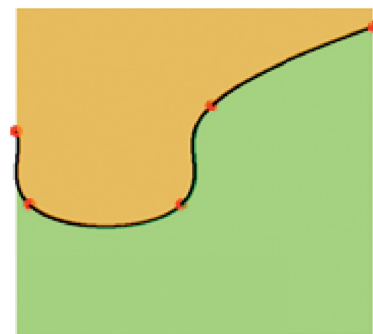


FIGURE 5: xy -view of intersection along with boundary and turning points.

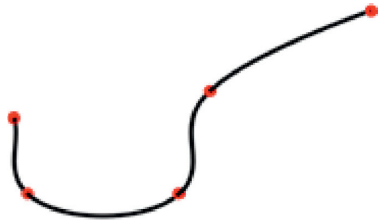


FIGURE 6: Sequence of points.

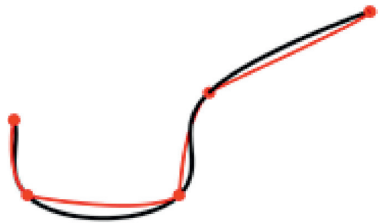


FIGURE 7: Cubic spline fitted for 1st iteration of GA.

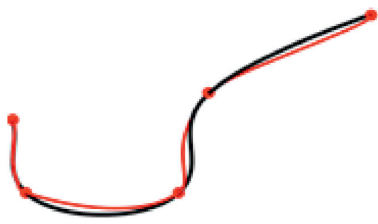


FIGURE 8: Cubic spline fitted for 2nd iteration of GA.

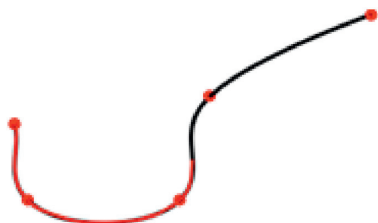


FIGURE 9: Best optimal curve achieved.



FIGURE 10: Implicit surface.

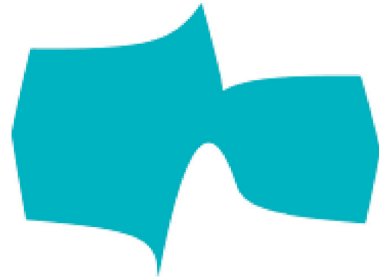


FIGURE 11: Explicit surface.

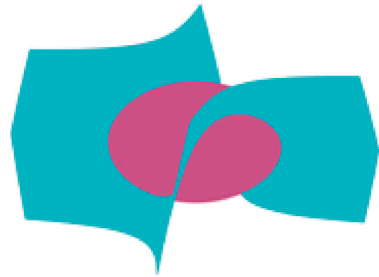


FIGURE 12: Intersection of both surfaces.

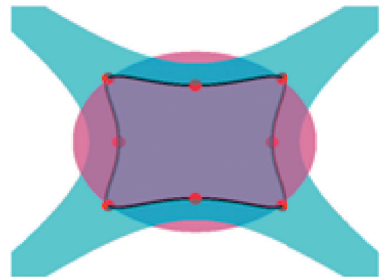


FIGURE 13: xy -view of intersection along with boundary and turning points.

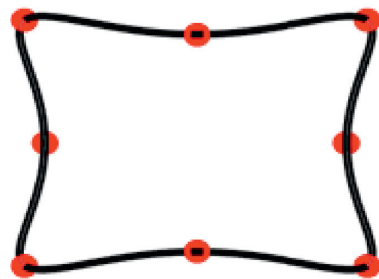


FIGURE 14: Sequence of points.

Some randomly selected values of shape parameters by GA and characteristics points of Example 1–3 are shown in Tables 1–3. In these tables, CS denotes characteristics points, TNIP denotes the total number of intersection points, E denotes the error, TE denotes time elapsed, and SPV denotes shape parameter values.

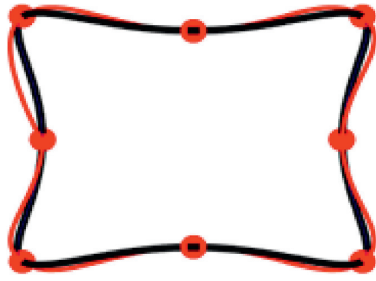


FIGURE 15: Cubic spline fitted for 1st iteration of GA.



FIGURE 19: Explicit surface.

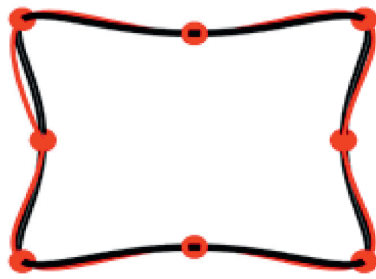


FIGURE 16: Cubic spline fitted for 2nd iteration of GA.

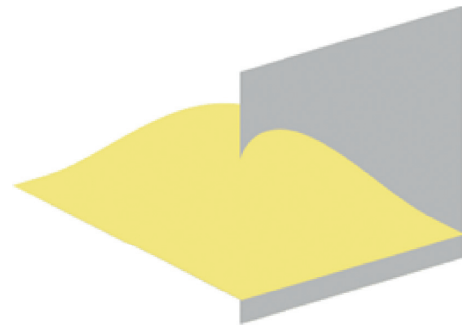


FIGURE 20: Intersection of both surfaces.

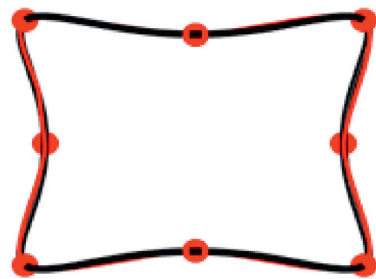


FIGURE 17: Best optimal curve achieved.

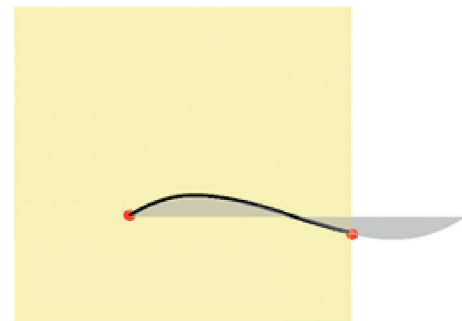


FIGURE 21: xy -view of intersection along with boundary and turning points.

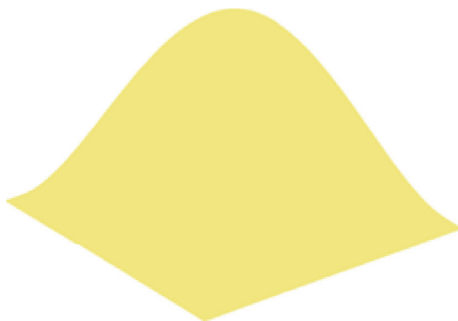


FIGURE 18: Implicit surface.



FIGURE 22: Sequence of points.



FIGURE 23: Cubic spline fitted for 1st iteration of GA.



FIGURE 24: Cubic spline fitted for 2nd iteration of GA.



FIGURE 25: Best optimal curve achieved.

5. Conclusion

A new scheme together with a genetic algorithm has been introduced to approximate surface to surface (parametric-parametric, explicit-implicit, and implicit-implicit) intersection curves. Characteristics points are evaluated from sequence points of surface intersection and fit optimal curve using cubic spine. Finest shape parameter values in cubic spline are selected by genetic algorithm. Moreover, it does not include any extra points for approximation. Finally, the optimal outcomes from the proposed technique suggested that it is more reliable scheme with GA in order to overcome surface intersection problems.

Data Availability

All data required for this research is included within this paper.

Conflicts of Interest

Authors declare that they have no conflicts of interest.

Authors' Contributions

All authors contributed equally in this paper.

Acknowledgments

This work was supported by the Key Teaching Research Project of Quality Engineering in Colleges and Universities in Anhui Province and Hefei College of Finance & Economics Guangzhou Zhuoya Education Investment Co., Ltd. Practical Education Base (subject no. 2020sjjd093).

References

- [1] D. Ritelli and G. Spaletta, "Trinomial equation: The hypergeometric way," *Open Journal of Mathematical Sciences*, vol. 5, no. 1, pp. 236–247, 2021.
- [2] I. Kovcs and T. Vradý, "Constrained fitting with free-form curves and surfaces," *Computer-Aided Design*, vol. 122, Article ID 102816, 2020.
- [3] S. Motta, A. Montenegro, M. Gattass, and D. Roehl, "A 3D sketch-based formulation to model salt bodies from seismic data," *Computers & Geosciences*, vol. 142, Article ID 104457, 2020.
- [4] S. Foschi and D. Ritelli, "The lambert function, the quintic equation and the proactive discovery of the implicit function theorem," *Open Journal of Mathematical Sciences*, vol. 5, no. 1, pp. 94–114, 2021.
- [5] F. Liang, C. Kang, and F. Fang, "A smooth tool path planning method on NURBS surface based on the shortest boundary geodesic map," *Journal of Manufacturing Processes*, vol. 58, pp. 646–658, 2020.
- [6] H. Mukundun, T. Maekawa, T. Sakkalis, and N. Patrikalakis, "Tracing surface intersections with validated ODE system solver," *ACM Symposium on Solid Modeling and Applications*, vol. 4, 2004.
- [7] N. M. Patrikalakis, T. Maekawa, K. H. Ko, and H. Mukundan, "Surface to surface intersections," *Computer Aided Design and Applications*, vol. 1, pp. 449–457, 2013.
- [8] N. H. Abdel-All, S. A. N. Badr, M. A. Soliman, and S. A. Hassan, "Intersection curves of hypersurfaces in," *Computer Aided Geometric Design*, vol. 29, no. 2, pp. 99–108, 2012.
- [9] M. Salem, O. Alessio, M. Jamali, and M. Hassan, "Transversal intersection curves of hyper-surfaces in R^5 ," 2007, <https://arxiv.org/abs/1601.04252>.
- [10] S. Hur, M. Oh, and T. W. Oh, "Approximation of surface-to-surface intersection curves within a prescribed error bound satisfying G continuity," *Computer-Aided Design*, vol. 41, no. 1, pp. 37–46, 2009.
- [11] S. Hur, M. Oh, and T. W. Oh, "Classification and resolution of critical cases in grandine and klein's topology determination using a perturbation method," *Computer Aided Geometric Design*, vol. 26, no. 2, pp. 243–258, 2009.
- [12] M. Sarfraz, M. Irshad, F. Sarfraz, and M. Zawwar, "A novel approach for surface to surface intersection approximation," in *Proceedings of the Information Visualisation 17th International Conference*, London, England, July 2013.

- [13] A. Gutman, "Intersection of neuroscience, ethics, and society," *Presidential Commission for the Study of Bioethical*, vol. 2, 2015.
- [14] S. Ilic and P. Fua, *From Explicit to Implicit Surfaces for Visualization. Animation and Modelling*, Computer Vision Lab, Swiss Federal Institute of Technology, Zürich, Switzerland, 2008.
- [15] M. A. Latif, H. Abdel, S. Ali, and S. A. Naeim, "Intersection curves of implicit and parametric surfaces in R^3 ," *Applied Mathematics*, vol. 2, 2011.
- [16] I. Silambarasan, "Generalized orthopair fuzzy sets based on hamacher T-norm and T-conorm," *Open Journal of Mathematical Sciences*, vol. 5, no. 1, pp. 44–64, 2021.
- [17] U. K. Qureshi, A. A. Shaikhi, F. K. Shaikhi, S. K. Shaikh, S. K. Hazarewal, and T. A. Laghari, "New simpson type method for solving nonlinear equations," *Open Journal of Mathematical Sciences*, vol. 5, no. 1, pp. 94–100, 2021.
- [18] G. Renner and A. Ekárt, "Genetic algorithms in computer aided design," *Computer-Aided Design*, vol. 35, no. 8, pp. 709–726, 2003.
- [19] M. Sarfraz, Z. Hussain, and F. S. Chaudary, "Shape preserving cubic spline for data visualization," *Computer Graphics and CAD/CAM*, vol. 1, no. 6, pp. 185–193, 2005.

Research Article

Subdivision Collocation Method for One-Dimensional Bratu's Problem

Ghulam Mustafa ¹, Syeda Tehmina Ejaz ², Sabila Kouser ², Shafqat Ali ¹
 and Muhammad Aslam ³

¹Department of Mathematics, The Islamia University of Bahawalpur, Bahawalpur, Pakistan

²Department of Mathematics, The Government Sadiq College Women University Bahawalpur, Bahawalpur, Pakistan

³Department of Mathematics, Lock Haven University of Pennsylvania, Lock Haven, PA, USA

Correspondence should be addressed to Ghulam Mustafa; ghulam.mustafa@iub.edu.pk

Received 17 April 2021; Revised 16 July 2021; Accepted 22 July 2021; Published 3 August 2021

Academic Editor: Sumit Chandok

Copyright © 2021 Ghulam Mustafa et al. This is an open access article distributed under the Creative Commons Attribution License, which permits unrestricted use, distribution, and reproduction in any medium, provided the original work is properly cited.

The purpose of this article is to employ the subdivision collocation method to resolve Bratu's boundary value problem by using approximating subdivision scheme. The main purpose of this researcher is to explore the application of subdivision schemes in the field of physical sciences. Our approach converts the problem into a set of algebraic equations. Numerical approximations of the solution of the problem and absolute errors are compared with existing methods. The comparison shows that the proposed method gives a more accurate solution than the existing methods.

1. Introduction

The general expression of Liouville–Bratu–Gelfand equation [1, 2]:

$$\begin{cases} \Delta\chi(r) + \alpha \exp(\chi(r)) = 0, & r \in \Omega_1, \\ \chi(r) = 0, & r \in \partial\Omega_1, \end{cases} \quad (1)$$

where parameter $\alpha > 0$ and Ω_1 is a bounded domain. We consider the Bratu's boundary value problem in one-dimensional planar coordinates [2–4] of the form

$$\chi''(r) + \alpha \exp(\chi(r)) = 0, \quad 0 < r < 1, \alpha > 0, \quad (2)$$

with conditions at the ends of the domain

$$\begin{cases} \chi(0) = 0, \\ \chi(1) = 0. \end{cases} \quad (3)$$

The detailed information of problem (2) is given in [4, 5]. The exact solution of (2) is

$$\chi(r) = -2 \ln \left[\frac{\cosh(0.5\theta(r-0.5))}{\cosh(0.25\theta)} \right], \quad \text{where } \theta = \sqrt{2\alpha} \cosh(0.25\theta). \quad (4)$$

The exponential term guarantees nonlinearity and the bifurcation phenomenon that follows up. In particular, one can verify the following for different values of α , i.e., problem (2) has no solution for $\alpha > \alpha_c$, unique solution for $\alpha = \alpha_c$, and two bifurcated solutions have been obtained for $0 < \alpha < \alpha_c$, where α_c is the critical value given as $\alpha_c = 3.51380719$. It is the solution of $1 = 0.25\sqrt{2\alpha_c} \sinh(0.25\theta)$.

In science and engineering, Bratu's problem is often used to characterize complex physical and chemical models. For example, Bratu's problem is used in a wide range of applications, including the thermal combustion theory's fuel ignition model, the model of the thermal reaction mechanism, the Chandrasekhar model of the universe's expansion, chemical reaction theory, radiative heat transfer, and nanotechnology.

Many researchers have developed analytical and numerical methods to solve the Bratu's problem, including the B-spline method [6], Adomian decomposition method

[7, 8], Chebyshev polynomial approximation method [2], homotopy analysis method [9], homotopy perturbation method [10, 11], differential transform method [12], Laplace transformed decomposition method [13], method of weighted residuals [14], and variational iteration method [15, 16]. Moreover, the solutions of the problem have been reported by Jalilian [17] using the nonpolynomial spline method, by Boyd [18] with the one-point pseudospectral collocation method, and by Abbasbandy et al. [19] with the Lie-group shooting method.

Our goal is to make use of subdivision schemes for solving Bratu’s problem. Subdivision schemes-based algorithms are not frequently used to find numerical solutions of boundary value problems. The approximate solutions of boundary value problems have been found by subdivision-based algorithms. Initially, these algorithms were constructed by Qu and Agarwal [20, 21]. Their constructed algorithms were based on an interpolatory subdivision algorithm and formulated only for the second-order two-point boundary value problems. After that, Ejaz et al. [22, 23] constructed subdivision schemes-based algorithm for solutions of boundary value problems of third and fourth order. We present a subdivision collocation algorithm for solving Bratu’s problem in this paper.

We organize our paper in the following way. In Section 2, we present some important properties of 6-point binary approximating subdivision scheme. In Section 3, subdivision collocation algorithm is formulated for the solution of (2). The convergence and error estimation of the proposed algorithm are also discussed in this section. Numerical results based on the proposed algorithm, comparison with other existing methods, and conclusion based on the obtained results are given in Section 4.

2. Subdivision Scheme and Derivatives of Its Two-Scale Relation

In this section, we define 6-point binary approximating subdivision scheme (6PBASS) [24] as

$$\begin{cases} Z_{2i}^{k+1} = a_0 Z_{i-2}^k + a_1 Z_{i-1}^k + a_2 Z_i^k + a_3 Z_{i+1}^k + a_4 Z_{i+2}^k, \\ Z_{2i+1}^{k+1} = b_0 Z_{i-2}^k + b_1 Z_{i-1}^k + b_2 Z_i^k + b_3 Z_{i+1}^k + b_4 Z_{i+2}^k + b_5 Z_{i+3}^k, \end{cases} \quad (5)$$

with $a_0 = a_4 = -(1/32)\alpha$, $a_1 = a_3 = (1/8)\alpha$, $a_2 = (1 - (3/16)\alpha)$, $b_0 = b_5 = (1 - \alpha)\beta$, $b_1 = b_4 = -(1/16) - 3\beta(1 - \alpha)$, $b_2 = b_3 = (9/16) + 2\beta(1 - \alpha)$, where α and β are tension parameters. The 6PBASS scheme possesses some of the following properties:

- (i) The scheme (5) is C^2 -continuous for $\alpha = (1/5)$, $\beta = (13/1000)$.
- (ii) It has support width (5, 5).
- (iii) Its approximation order is fourth.
- (iv) Its fundamental solution is

$$\nu(i) = \begin{cases} 1, & \text{for } i = 0, \\ 0, & \text{for } i \neq 0, \end{cases} \quad (6)$$

and it satisfies the two-scale relation

$$\nu(x) = \sum_k a_k \nu(2x - k), \quad (7)$$

where a_k is the mask of the scheme (5). Since 6PBASS is C^2 -continuous by [24], so its 2-scale relations $\nu(x)$ are also C^2 -continuous.

- (v) For the computation of the first- and second-order derivatives of (7), we adopt similar approach of [22, 23].

The first two derivatives of (7) are given in the following equations:

$$\left\{ \begin{array}{l} \nu''(0) = 0, \\ \nu''(\pm 1) = \pm \frac{308375375}{103575526}, \\ \nu'(\pm 2) = \mp \frac{89875573}{155363289}, \\ \nu'(\pm 3) = \pm \frac{6037875}{1035755526}, \\ \nu'(\pm 4) = \pm \frac{186056}{155363289}, \end{array} \right. \quad (8)$$

$$\left\{ \begin{array}{l} \nu'(0) = -\frac{2030241008}{65127633}, \\ \nu''(\pm 1) = \frac{1259384000}{65127633}, \\ \nu''(\pm 2) = \frac{96510000}{21709211}, \\ \nu''(\pm 3) = \frac{43501000}{65127633}, \\ \nu''(\pm 4) = \frac{1765504}{65127633}. \end{array} \right. \quad (9)$$

3. Subdivision Collection Algorithm for Bratu’s Problem

In this section, we have constructed a subdivision collocation algorithm for the solution of (2), which is based upon the fundamental solution of the subdivision scheme and its derivatives. Convergence and error estimations results are also presented in this section.

3.1. Formulation of Subdivision Collection Algorithm for Bratu’s Problem. The detail of the proposed algorithm is given as follows:

Let

$$\mathbb{W}(y) = \sum_{i=-4}^{N+4} w_i \gamma \left(\frac{y - y_i}{h} \right), \quad 0 \leq y \leq 1, \quad (10)$$

be an approximate solution of (2) and N must be greater than or equal to four, h is the step size and is defined as $h = (1/N)$, $y_i = ih$, where $i = -4$ to $N + 4$, and w_i are the unknowns to be determined. From (10), we get

$$D^2 \mathbb{W}(y_i) = \frac{1}{h^2} \sum_{i=-4}^{N+4} w_i \gamma'' \left(\frac{y - y_i}{h} \right). \quad (11)$$

By using (10) and (11) in (2), we get

$$\frac{1}{h^2} \left[\sum_{i=-4}^{N+4} w_i \gamma'' \left(\frac{y_j - y_i}{h} \right) \right] + \alpha \exp \left[\sum_{i=-4}^{N+4} w_i \gamma \left(\frac{y_j - y_i}{h} \right) \right] = 0, \quad (12)$$

where $j = 0, 1, \dots, N$, and the conditions given at the ends of the domain (3) become

$$\begin{aligned} \mathbb{W}(0) &= w_0 = 0, \\ \mathbb{W}(1) &= w_N = 0. \end{aligned} \quad (13)$$

The matrix representation of equation (12) is

$$\mathcal{A}\mathbb{W} + \alpha \mathbb{D}_1 = 0, \quad (14)$$

where

$$\mathbb{A} = \begin{pmatrix} \ddot{\nu}_4 & \ddot{\nu}_3 & \ddot{\nu}_2 & \ddot{\nu}_1 & \ddot{\nu}_0 & \ddot{\nu}_{-1} & \ddot{\nu}_{-2} & \cdots & 0 & 0 & 0 \\ 0 & \ddot{\nu}_4 & \ddot{\nu}_3 & \ddot{\nu}_2 & \ddot{\nu}_1 & \ddot{\nu}_0 & \ddot{\nu}_{-1} & \cdots & 0 & 0 & 0 \\ 0 & 0 & \ddot{\nu}_4 & \ddot{\nu}_3 & \ddot{\nu}_2 & \ddot{\nu}_1 & \ddot{\nu}_0 & \cdots & 0 & 0 & 0 \\ \vdots & & & & & & & & & & \\ 0 & 0 & 0 & 0 & 0 & 0 & 0 & \cdots & \ddot{\nu}_{N-3} & \ddot{\nu}_{N-4} & 0 \\ 0 & 0 & 0 & 0 & 0 & 0 & 0 & \cdots & \ddot{\nu}_{N-2} & \ddot{\nu}_{N-3} & \ddot{\nu}_{N-4} \end{pmatrix}_{N+1 \times N+9}, \quad (15)$$

$$\mathbb{W} = (w_{-4}, w_{-3}, \dots, w_{N+3}, w_{N+4})^T, \quad (16)$$

$$\mathbb{D}_1 = h^2 \times (\exp(\mathbb{W}(y_0)), \exp(\mathbb{W}(y_1)), \dots, \exp(\mathbb{W}(y_{N-1})), \exp(\mathbb{W}(y_N)))^T. \quad (17)$$

Since system (14) is underdetermined because it has fewer equations than unknowns, so it requires eight more equations to get a unique solution. Two conditions are given in (13) at the ends of the domain of (2) and the detail of the remaining six conditions is given in the next section.

3.2. Forced Conditions. As we require six more conditions to get a unique solution of (14), so we will construct three conditions at the left and three conditions at the right end of the domain. Since 6PBASS reproduces third degree polynomial with order of approximation four, so the order of new conditions is four and these conditions are known as forced conditions. Let w_{-3}, w_{-2}, w_{-1} and $w_{N+1}, w_{N+2}, w_{N+3}$ represent the left end points and right end points. These left and right end points can be computed by using polynomial of degree three which interpolates the data (y_i, w_i) , for $0 \leq i \leq 3$, i.e., left end conditions are obtained from

$$w_{-i} = S(-y_i), \quad i = 1, 2, 3, \quad (18)$$

where

$$S(y_i) = \sum_{j=1}^4 \binom{4}{j} (-1)^{j+1} \mathbb{W}(y_{i-j}). \quad (19)$$

Since by (10), $\mathbb{W}(y_i) = w_i$ for $i = 1, 2, 3$ and substituting y_i by $-y_i$ in (19), we have

$$S(-y_i) = \sum_{j=1}^4 \binom{4}{j} (-1)^{j+1} w_{j-i}. \quad (20)$$

So, the following conditions can be used at the left end and

$$\sum_{j=0}^4 \binom{4}{j} (-1)^j w_{j-i} = 0, \quad i = 3, 2, 1. \quad (21)$$

Similarly, at the right end, we have the following conditions:

$$\sum_{j=0}^4 \binom{4}{j} (-1)^j w_{i-j} = 0, \quad i = N + 3, N + 2, N + 1. \quad (22)$$

Finally, we get system of $(N + 9) \times (N + 9)$ nonlinear equations

$$\mathbb{J}_c \mathbb{W} + \alpha \mathbb{D} = 0, \tag{23}$$

or

$$\mathbb{J}_c \mathbb{W} = -\alpha \mathbb{D}(w), \tag{24}$$

where

$$\mathbb{J}_c = (\mathbb{J}_{c_0}^T, \mathbb{A}^T, \mathbb{J}_{c_N}^T), \tag{25}$$

where \mathbb{A} is defined in (15) and \mathbb{J}_{c_0} and \mathbb{J}_{c_N} are constrained as follows: the matrix \mathbb{J}_{c_0} is obtained from all the conditions defined at the left end of the domain, i.e., first three rows obtained from (21) and fourth row of \mathbb{J}_{c_0} obtained from (13) at $\mathbb{W}(0) = w_0 = 0$. Similarly, the matrix \mathbb{J}_{c_N} is obtained from all the conditions defined at the right end of the domain, i.e., first row comes from (13) at $\mathbb{W}(1) = w_N = 0$ and remaining rows come from (22). Hence,

$$\mathbb{J}_{c_0} = \begin{pmatrix} 0 & 1 & -4 & 6 & -4 & 1 & 0 & 0 & \dots & 0 \\ 0 & 0 & 1 & -4 & 6 & -4 & 1 & 0 & \dots & 0 \\ 0 & 0 & 0 & 1 & -4 & 6 & -4 & 1 & \dots & 0 \\ 0 & 0 & 0 & 0 & 1 & 0 & 0 & 0 & \dots & 0 \end{pmatrix}, \tag{26}$$

$$\mathbb{J}_{c_N} = \begin{pmatrix} 0 & \dots & 0 & 0 & 0 & 1 & 0 & 0 & 0 & 0 \\ 0 & \dots & 1 & -4 & 6 & -4 & 1 & 0 & 0 & 0 \\ 0 & \dots & 0 & 1 & -4 & 6 & -4 & 1 & 0 & 0 \\ 0 & \dots & 0 & 0 & 1 & -4 & 6 & -4 & 1 & 0 \end{pmatrix}.$$

The column vector \mathbb{W} is defined in (16) and \mathbb{D} is defined as

$$\mathbb{D} = (0, 0, 0, \mathbb{W}(0), \mathbb{D}_1^T, \mathbb{W}(N), 0, 0, 0)^T, \tag{27}$$

where \mathbb{D}_1 is given in (17).

3.3. Iterative Algorithm. To find the numerical solutions of nonlinear system of equation (24), we define an iterative algorithm. The iterative algorithm includes the following steps:

- (i) Formulation of initial solution: the initial approximate solution \mathbb{W}^0 is selected to find the following system:

$$\mathbb{J}_c \mathbb{W}^0 = -\alpha \mathbb{R}^0, \tag{28}$$

where

$$\begin{cases} \mathbb{R}^0 = (0, 0, 0, \mathbb{W}(0), \delta_0, \delta_1, \dots, \delta_N, \mathbb{W}(N), 0, 0, 0)^T, \\ \delta_i = h^3 \mathbb{D}_i(y_i, \mathbb{L}_i, \mathbb{D}_0^*), \\ \mathbb{L}_i = \mathbb{W}(0) + 3ih(\mathbb{W}(N) - \mathbb{W}(0)), \\ \mathbb{D}_0^* = \mathbb{W}(N) - \mathbb{W}(0), \end{cases} \tag{29}$$

where $i \in \{0, 1, \dots, N\}$. The column vector \mathbb{R}^0 is the linear approximation of the column vector (27).

- (ii) Iterative scheme: the following iterative scheme is used to find the approximate solution \mathbb{W}^* ,

$$\mathbb{J}_c \mathbb{W}^{k+1} = \mathbb{D}(w^k), \quad k = 0, 1, 2, \dots \tag{30}$$

- (iii) Terminating criteria: the following condition is used to stop the iteration at k -th level, for any ε ; let $\varepsilon = 10^{-4}$,

$$\|\mathbb{W}^{k+1} - \mathbb{W}^k\|_{\infty} \leq \varepsilon. \tag{31}$$

3.4. Convergence and Error Estimation. In this section, we present results of convergence and error estimation of the proposed iterative algorithm. The convergence of the iterative algorithm is guaranteed by the following proposition.

Proposition 1. *The approximate solution $\{\mathbb{W}^k\}$ founded by (28) and (30) linearly converges to the approximate solution \mathbb{W}^* of (24) with the supposition that step size and the Lipschitz constants r_0, r_1 are small, i.e.,*

$$\|\mathbb{J}_c^{-1}\|_{\infty} \left(r_0 h^2 + r_1 h \frac{29773}{10000} \right) \leq 1. \tag{32}$$

The proof is similar to [23].

The main result of error estimation is given by the following proposition.

Theorem 1. *Let exact solution $g(y) \in C^4[0, 1]$ and w_i be obtained by solving (24) with the fourth order boundary treatment at the end points. Then, we have*

$$\|w(y_j) - g(y_j)\|_{\infty} = O(h^{4-j}), \quad j = 0, 1, 2. \tag{33}$$

4. Numerical Examples and Comparison

The numerical technique discussed previously is illustrated in this section by applying subdivision collection algorithm to the planar one-dimensional Bratu's problem (2) for three distinct values of α , which guarantee the existence of two locally unique solutions. We have created comparison tables using $\alpha = 1, 2$ and 3.51 to show the consistency of our approach in comparison to the exact solution as well as the solutions of other methods. All calculations have been performed using MATLAB .

- (i) The fact regarding the solution of Bratu's problem for $\alpha = 1$ is obtained after third iteration, as shown in Table 1. Comparison between the numerical results and absolute errors obtained by our subdivision collection algorithm and decomposition method [25] are presented in Tables 2 and 3, respectively. From the tabulated results, we observed that the numerical results obtained by our subdivision collection algorithm are better than the decomposition method [25].
- (ii) The fact regarding the solution of Bratu's problem for $\alpha = 2$ is obtained after fifth iteration, as shown in

TABLE 1: Numerical results of (2) by subdivision collection algorithm for case $\alpha = 1$.

x	Exact solution	By subdivision collection algorithm	Absolute error
0.0	0.0000000000	0.0000000000000000	0.0000000000000000
0.1	0.0498467900	0.049835942666664	$1.08473333363529e-5$
0.2	0.0891899350	0.089157036980790	$3.28980192095263e-5$
0.3	0.1176090956	0.117560379925558	$4.87156744417711e-5$
0.4	0.1347902526	0.134731783666151	$5.84689338488098e-5$
0.5	0.1405392142	0.140477341442747	$6.18727572535005e-5$
0.6	0.1347902526	0.134731783666151	$5.84689338488931e-5$
0.7	0.1176090956	0.117560379925558	$4.87156744419098e-5$
0.8	0.0891899350	0.089157036980790	$3.28980192097483e-5$
0.9	0.0498467900	0.049835942666663	$1.08473333366513e-5$
1.0	0.0000000000	0.0000000000000000	$0.00000000000085e-5$

TABLE 2: Comparison between the numerical results of (2) for $\alpha = 1$.

x	Exact solution	By [25]	By subdivision collection algorithm
0.0	0.0000000000	0.0000000000	0.0000000000000000
0.1	0.0498467900	0.0471616875	0.049835942666664
0.2	0.0891899350	0.0871680000	0.089157036980790
0.3	0.1176090956	0.1177614375	0.117560379925558
0.4	0.1347902526	0.1369920000	0.134731783666151
0.5	0.1405392142	0.1435546875	0.140477341442747
0.6	0.1347902526	0.1369920000	0.134731783666151
0.7	0.1176090956	0.1177614375	0.117560379925558
0.8	0.0891899350	0.0871680000	0.089157036980790
0.9	0.0498467900	0.0471616875	0.049835942666663
1.0	0.0000000000	0.0000000000	0.0000000000000000

TABLE 3: Comparison between the absolute errors of (2) for case $\alpha = 1$.

x	By [25]	By subdivision collection algorithm
0.0	0.000000000000000000	0.0000000000000000
0.1	$2.6851025000000001e-3$	$1.08473333363529e-5$
0.2	$2.0219350000000003e-3$	$3.28980192095263e-5$
0.3	$1.523418999999915e-4$	$4.87156744417711e-5$
0.4	$2.2017474000000009e-3$	$5.84689338488098e-5$
0.5	$3.015473299999988e-3$	$6.18727572535005e-5$
0.6	$2.2017474000000009e-3$	$5.84689338488931e-5$
0.7	$1.523418999999915e-4$	$4.87156744419098e-5$
0.8	$2.0219350000000003e-3$	$3.28980192097483e-5$
0.9	$2.6851025000000001e-3$	$1.08473333366513e-5$
1.0	0.0000000000000000	$0.00000000000085e-5$

TABLE 4: Numerical results of (2) for case $\alpha = 2$.

x	Exact solution	By subdivision collection algorithm	Absolute error
0.0	0.0000000000	0.0000000000000000	0.0000000000000000
0.1	0.1144107440	0.114588772999854	$1.78028999853849e-4$
0.2	0.2064191156	0.206717298179522	$2.98182579522244e-4$
0.3	0.2738793116	0.274280205962876	$4.00894362875881e-4$
0.4	0.3150893646	0.315559243360757	$4.69878760757103e-4$
0.5	0.3289524214	0.329446300901418	$4.93879501417605e-4$
0.6	0.3150893646	0.315559243360757	$4.69878760757159e-4$
0.7	0.2738793116	0.274280205962876	$4.00894362875992e-4$
0.8	0.2064191156	0.206717298179522	$2.98182579522410e-4$
0.9	0.1144107440	0.114588772999854	$1.78028999854057e-4$
1.0	0.0000000000	0.0000000000000000	$0.0000000000017e-4$

TABLE 5: Comparison between numerical results of (2) for case $\alpha = 2$.

x	Exact solution	By subdivision collection algorithm	By [25]	By [5]
0.0	0.0000000000	0.0000000000000000	0.0000000000	0.0000000000
0.1	0.1144107440	0.114248449272834	0.0991935000	0.1122817141
0.2	0.2064191156	0.206065066411653	0.1917440000	0.2022094162
0.3	0.2738793116	0.273375407642615	0.2679915000	0.2676925058
0.4	0.3150893646	0.314489410524746	0.3183360000	0.3070874506
0.5	0.3289524214	0.328319028557975	0.3359375000	0.3193532294
0.6	0.3150893646	0.314489410524746	0.3183360000	0.3041598403
0.7	0.2738793116	0.273375407642615	0.2679915000	0.2619458909
0.8	0.2064191156	0.206065066411653	0.1917440000	0.1940413072
0.9	0.1144107440	0.114248449272835	0.0991935000	0.1035373785
1.0	0.0000000000	0.0000000000000000	0.0000000000	0.0000000000

TABLE 6: Comparison between absolute errors of (2) for case $\alpha = 2$.

x	By subdivision collection algorithm	By [25]	By [5]
0.0	0.00000000000200e-4	0.000000000000000000	0.000000000000000000
0.1	1.78028999853849e-4	1.5217243999999999e-2	2.1290298999999999e-3
0.2	2.98182579522244e-4	1.467511560000001e-2	4.209699400000017e-3
0.3	4.00894362875881e-4	5.887811600000015e-3	6.186805800000028e-3
0.4	4.69878760757103e-4	3.246635400000031e-3	8.001913999999999e-3
0.5	4.93879501417605e-4	6.985078600000028e-3	9.599191999999979e-3
0.6	4.69878760757159e-4	3.246635400000031e-3	1.092952429999999e-2
0.7	4.00894362875992e-4	5.887811600000015e-3	1.193342070000003e-2
0.8	2.98182579522410e-4	1.467511560000001e-2	1.237780840000000e-2
0.9	1.78028999854057e-4	1.521724399999999e-2	1.087336650000000e-2
1.0	0.0000000000017e-4	0.000000000000000000	0.000000000000000000

TABLE 7: Numerical results of (2) for case $\alpha = 3.51$.

x	Exact solution	By subdivision collection algorithm	Absolute error
0.0	0.0000000000	0.0000000000000002	0.0000000000000002
0.1	0.3958056990	0.395838508425970	0.000032809425970
0.2	0.7390974100	0.739653867710330	0.000556457710330
0.3	1.0087582600	1.009642835147183	0.000884575147183
0.4	1.1825366600	1.183595191371533	0.001058531371533
0.5	1.2427426900	1.243855461630791	0.001112771630791
0.6	1.1825366600	1.183595191371532	0.001058531371532
0.7	1.0087582600	1.009642835147182	0.000884575147182
0.8	0.7390974100	0.739653867710329	0.000556457710329
0.9	0.3958056990	0.395838508425968	0.000032809425968
1.0	0.0000000000	0.0000000000000000	0.0000000000000000

TABLE 8: Comparison between absolute errors of (2) for case $\alpha = 3.51$.

x	By [6]	By subdivision collection algorithm
0.0	0.0000000000000000	0.0000000000000002
0.1	3.84172369550e-2	3.280942597000e-5
0.2	7.48135367780e-2	5.564577103300e-4
0.3	1.05827422823e-1	8.845751471830e-4
0.4	1.27116880861e-1	1.058531371533e-3
0.5	1.34752877607e-1	1.112771630791e-3
0.6	1.27116880861e-1	1.058531371532e-3
0.7	1.05827422823e-1	8.845751471820e-4
0.8	7.48135367780e-2	5.564577103290e-4
0.9	3.84172369550e-2	3.280942596800e-5
1.0	0.0000000000000000	0.0000000000000000

Table 4. Comparison between the numerical results and absolute errors obtained by our subdivision collection algorithm, decomposition [25], and Laplace method [5] are presented in Tables 5 and 6, respectively. From the tabulated results, we observed that the numerical results obtained by our subdivision collection algorithm are better than [5, 25].

- (iii) The fact regarding the solution of Bratu's problem for $\alpha = 3.15$ is obtained after forty-two iterations, as shown in Table 7. Comparisons between the absolute errors obtained by our subdivision collection algorithm and B-spline [6] method are presented in Table 8. From the tabulated results, we observed that the numerical results obtained by our subdivision collection algorithm give better approximation than [6].

5. Concluding Remarks

In this paper, we have established a subdivision collocation algorithm for the solution of one-dimensional nonlinear Bratu's problem. The numerical results obtained by subdivision collection algorithm showed that the algorithm is suitable for the approximate solution of (2). We have concluded that the numerical results converge to the exact solution for the small step size. We have also presented a comparison of absolute errors of the solution obtained from subdivision collection algorithm with decomposition method [25], Laplace method, [5] and B-spline method [6] for different values of α . We conclude that our algorithm gives smaller absolute errors as compared with the other existing methods [5, 6, 25].

Data Availability

The data used to support the findings of the study are available within this paper.

Conflicts of Interest

The authors declare that there are no conflicts of interest regarding the publication of this paper.

References

- [1] U. M. Ascher, R. M. Mattheij, and R. D. Russell, *Numerical Solution of Boundary Value Problems for Ordinary Differential Equations*, Society for Industrial and Applied Mathematics (SIAM), Philadelphia, PA, USA, Classics in Applied Mathematics, 1995.
- [2] J. P. Boyd, "Chebyshev polynomial expansions for simultaneous approximation of two branches of a function with application to the one-dimensional bratu equation," *Applied Mathematics and Computation*, vol. 143, no. 2-3, pp. 189–200, 2003.
- [3] R. Buckmire, "Investigations of nonstandard, mickens-type, finite-difference schemes for singular boundary value problems in cylindrical or spherical coordinates," *Numerical Methods for Partial Differential Equations*, vol. 19, no. 3, pp. 380–398, 2003.
- [4] J. Jacobsen and K. Schmitt, "The liouville-bratu-gelfand problem for radial operators," *Journal of Differential Equations*, vol. 184, no. 1, pp. 283–298, 2002.
- [5] J. S. McGough, "Numerical continuation and the gelfand problem," *Applied Mathematics and Computation*, vol. 89, no. 1-3, pp. 225–239, 1998.
- [6] H. Caglar, N. Caglar, M. Özer, A. Valaristos, and A. N. Anagnostopoulos, "B-spline method for solving bratu's problem," *International Journal of Computer Mathematics*, vol. 87, no. 8, pp. 1885–1891, 2010.
- [7] E. Deeba, S. A. Khuri, and S. Xie, "An algorithm for solving boundary value problems," *Journal of Computational Physics*, vol. 159, no. 2, pp. 125–138, 2000.
- [8] A.-M. Wazwaz, "Adomian decomposition method for a reliable treatment of the bratu-type equations," *Applied Mathematics and Computation*, vol. 166, no. 3, pp. 652–663, 2005.
- [9] S. Abbasbandy and E. Shivanian, "Prediction of multiplicity of solutions of nonlinear boundary value problems: novel application of homotopy analysis method," *Communications in Nonlinear Science and Numerical Simulation*, vol. 15, no. 12, pp. 3830–3846, 2010.
- [10] X. Feng, Y. He, and J. Meng, "Application of homotopy perturbation method to the bratu-type equations," *Topological Methods in Nonlinear Analysis*, vol. 31, no. 2, pp. 243–252, 2008.
- [11] M. C. Wang, X. S. Zhao, and X. Liu, "Analytic solutions of a class of nonlinearly dynamic systems," *Journal of Physics: Conference Series*, vol. 96, no. 1, Article ID 012174, 2008.
- [12] I. H. A.-H. Hassan and V. S. Erturk, "Applying differential transformation method to the one-dimensional planar bratu problem," *International Journal of Contemporary Mathematical Sciences*, vol. 2, no. 30, pp. 1493–1504, 2007.
- [13] S. A. Khuri, "A new approach to bratu's problem," *Applied Mathematics and Computation*, vol. 147, no. 1, pp. 131–136, 2004.
- [14] Y. A. S. Aregbesola, "Numerical solution of bratu problem using the method of weighted residual," *Electronic Journal of Southern African Mathematical Sciences Association*, vol. 3, no. 1, pp. 1–7, 2003.
- [15] J.-H. He, "Some asymptotic methods for strongly nonlinear equations," *International Journal of Modern Physics B*, vol. 20, no. 10, pp. 1141–1199, 2006.
- [16] J. H. He, "Variational approach to the bratu's problem," *Journal of Physics: Conference Series*, vol. 96, no. 1, Article ID 012087, 2008.
- [17] R. Jalilian, "Non-polynomial spline method for solving bratu's problem," *Computer Physics Communications*, vol. 181, no. 11, pp. 1868–1872, 2010.
- [18] J. P. Boyd, "One-point pseudospectral collocation for the one-dimensional bratu equation," *Applied Mathematics and Computation*, vol. 217, no. 12, pp. 5553–5565, 2011.
- [19] S. Abbasbandy, M. S. Hashemi, and C.-S. Liu, "The lie-group shooting method for solving the bratu equation," *Communications in Nonlinear Science and Numerical Simulation*, vol. 16, no. 11, pp. 4238–4249, 2011.
- [20] R. Qu and R. P. Agarwal, "Solving two point boundary value problems by interpolatory subdivision algorithms," *International Journal of Computer Mathematics*, vol. 60, no. 3-4, pp. 279–294, 1996.
- [21] R. Qu and R. P. Agarwal, "A subdivision approach to the construction of approximate solutions of boundary-value problems with deviating arguments," *Computers & Mathematics with Applications*, vol. 35, no. 11, pp. 121–135, 1998.

- [22] S. T. Ejaz and G. Mustafa, "A subdivision based iterative collocation algorithm for nonlinear third order boundary value problems," *Advances in Mathematical Physics*, vol. 2016, p. 15, Article ID 5026504, 2016.
- [23] G. Mustafa, M. Abbas, S. T. Ejaz, A. I. M. Ismail, and F. Khan, "A numerical approach based on subdivision schemes for solving non-linear fourth order boundary value problems," *Journal of Computational Analysis and Applications*, vol. 23, no. 4, pp. 607–623, 2017.
- [24] K. Rehan and S. S. Siddiqi, "A combined binary 6-point subdivision scheme," *Applied Mathematics and Computation*, vol. 270, pp. 130–135, 2015.
- [25] S. Liao and Y. Tan, "A general approach to obtain series solutions of nonlinear differential equations," *Studies in Applied Mathematics*, vol. 119, no. 4, pp. 297–354, 2007.

Research Article

Number of Distinct Homomorphic Images in Coset Diagrams

Muhammad Aamir ¹, Muhammad Awais Yousaf ¹, and Abdul Razaq ²

¹Department of Mathematics, The Islamia University of Bahawalpur, Bahawalpur 63100, Pakistan

²Division of Science and Technology, Department of Mathematics, University of Education, Lahore 54000, Pakistan

Correspondence should be addressed to Muhammad Aamir; aamir.math.hed@gmail.com

Received 12 December 2020; Accepted 28 March 2021; Published 2 August 2021

Academic Editor: Elena Guardo

Copyright © 2021 Muhammad Aamir et al. This is an open access article distributed under the Creative Commons Attribution License, which permits unrestricted use, distribution, and reproduction in any medium, provided the original work is properly cited.

The representation of the action of $\text{PGL}(2, \mathbb{Z})$ on $F_t \cup \{\infty\}$ in a graphical format is labeled as coset diagram. These finite graphs are acquired by the contraction of the circuits in infinite coset diagrams. A circuit in a coset diagram is a closed path of edges and triangles. If one vertex of the circuit is fixed by $(pq)^{\Delta_1} (pq^{-1})^{\Delta_2} (pq)^{\Delta_3} \dots (pq^{-1})^{\Delta_m} \in \text{PSL}(2, \mathbb{Z})$, then this circuit is titled to be a length- m circuit, denoted by $(\Delta_1, \Delta_2, \Delta_3, \dots, \Delta_m)$. In this manuscript, we consider a circuit Δ of length 6 as $(\Delta_1, \Delta_2, \Delta_3, \Delta_4, \Delta_5, \Delta_6)$ with vertical axis of symmetry, that is, $\Delta_2 = \Delta_6, \Delta_3 = \Delta_5$. Let Γ_1 and Γ_2 be the homomorphic images of Δ acquired by contracting the vertices a, u and b, v , respectively, then it is not necessary that Γ_1 and Γ_2 are different. In this study, we will find the total number of distinct homomorphic images of Δ by contracting its all pairs of vertices with the condition $\Delta_1 > \Delta_2 > \Delta_3 > \Delta_4$. The homomorphic images are obtained in this way having versatile applications in coding theory and cryptography. One can attain maximum nonlinearity factor using this in the encryption process.

1. Introduction

It is prominent that the finite presentation $\langle p, q; p^2 = q^3 = 1 \rangle$ is known as the modular group $\text{PSL}(2, \mathbb{Z})$ generated by the linear fractional transformations $p: \chi \rightarrow (-1/\chi)$ and $q: \chi \rightarrow ((\chi - 1)/\chi)$. In [1], Akbas discussed sub-orbitalgraphs for the modular group by showing that these graphs contains no circuit if and only if it contains no triangles. If we insert an extra generator $r = (1/\chi)$ with p and q , another group is emerged, denoted as $\text{PGL}(2, \mathbb{Z})$ [2], an extension of $\text{PSL}(2, \mathbb{Z})$ with the finite presentation as

$$\langle p, q, r; p^2 = q^3 = r^2 = (pr)^2 = (qr)^2 = 1 \rangle. \quad (1)$$

In 1978, Professor Graham Higman propounds an unfamiliar type of a graph, titled as coset diagram, which presents the action of $\text{PGL}(2, \mathbb{Z})$ on $\text{PL}(F_t)$, where F_t is a finite field and t shows a prime power. In 1983, this foundation is laid by Qaisar Mushtaq [3]. Small triangles are proposed for the cycle q^3 , such that q permutes the vertices of triangles in the opposite direction of rotation of clock and an edge is attached to any two vertices that are interchanged by p . Heavy dots represent the

fixed points of p and q . Note that $(pr)^2 = 1$ equals $rqr = q^{-1}$, which means r reverses the triangle orientation proposed for the cycle q^3 . For that reason, the diagram need not to be made more perplexing by interjecting r edges.

A coset diagram (subdiagram) Γ_1 is said to be a homomorphic image of the coset diagram (subdiagram) Γ_2 if and only if $|V(\Gamma_1)| < |V(\Gamma_2)| \forall a \in V(\Gamma_2)$ with $(a)h = a$, where $h \in \text{PSL}(2, \mathbb{Z})$, there exist a vertex u in $V(\Gamma_1)$ such that $(u)h = u$.

Coset diagrams obtained from the action of $\text{PSL}(2, \mathbb{Z})$ over Q_ϵ are infinite graphs [4], where $Q_\epsilon = \{a_1 + a_2\sqrt{\epsilon}; a_1, a_2 \in \mathbb{Q} \text{ and } \epsilon \in \mathbb{Z}^+ \text{ is a square free}\}$. These diagrams are not easy to study because they are infinite. Thence, coset diagrams are considered as important for the action of $\text{PSL}(2, \mathbb{Z})$ on $\text{PL}(F_q)$ because this action presents finite graphs. The number $((x_1 + \sqrt{\epsilon})/x_2)$ is an expression of the number $a_1 + a_2\sqrt{\epsilon} \in Q_\epsilon$, where $(x_1, x_2, ((x_1^2 - \epsilon)/x_2)) = 1$. These finite coset diagrams are the homomorphic images of the coset diagrams for $((x_1 + \sqrt{\epsilon})/x_2)$, where $\epsilon \equiv z^2 \pmod{p}$ for some $z \in N$.

To explain more, coset diagram in Figure 1 illustrates the action on $\text{PL}(F_{17})$ by $\text{PGL}(2, \mathbb{Z})$ with permutation

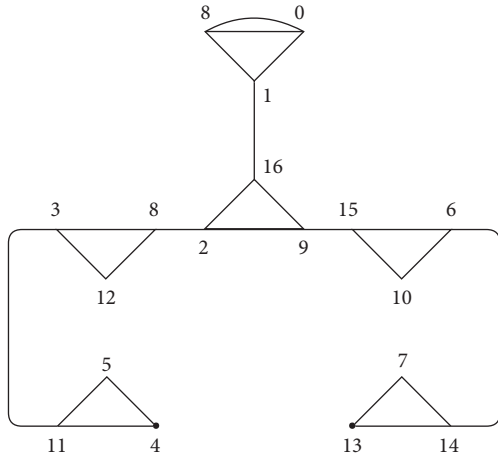


FIGURE 1: Coset diagram for the action of $PGL(2, \mathbb{Z})$ on $PL(F_{17})$.

representations p, q , and r by $(\chi)p = (-1/\chi)$, $(\chi)q = ((\chi - 1)/\chi)$, and $(\chi)r = (1/\chi)$, respectively, as

- p : $(0 \infty), (1 \ 16), (2 \ 8), (3 \ 11), (4), (5 \ 10), (6 \ 14), (7 \ 12), (9 \ 15), (13),$
- q : $(0 \infty \ 1), (29 \ 16), (3 \ 12 \ 8), (4 \ 5 \ 11), (6 \ 15 \ 10), (7 \ 13 \ 14),$ (2)
- r : $(0 \infty), (1), (2 \ 9), (3 \ 6), (4 \ 13), (5 \ 7), (8 \ 15), (10 \ 12), (11 \ 14), (16).$

Thus, $13 = 8^2 \pmod{17}$ gives that the coset diagram $PGL(2, 17)$ is a homomorphic image of the coset diagram for $((x_1 + \sqrt{13})/x_2)$.

Coset diagrams obtained from the action of $PSL(2, \mathbb{Z})$ on \mathbb{Q}_ε have some attractive narrative. In [5], the quadratic irrational numbers are classified by taking prime modulus that proved helpful in investigating the modular group action on the real quadratic field. The number $\bar{B} = ((x_1 - \sqrt{\varepsilon})/x_2)$ is called the conjugate of $B = ((x_1 + \sqrt{\varepsilon})/x_2)$, where x_1 and x_2 are integers and ε is a fixed number from \mathbb{Z}^+ , which is not a perfect square. B is said to be an ambiguous number [6], if the sign of B is different from the sign of \bar{B} . B is said to be a totally negative (positive) if B and \bar{B} both have the same signs. For a fixed ε , the number of ambiguous numbers of the form $B = ((x_1 + \sqrt{\varepsilon})/x_2)$ is finite and that segment of the coset diagram attained by the ambiguous numbers forms a closed path (circuit) and it is the only closed path in B -orbit [4]. With the help of coset diagram, Anna Torstensson not only described the applications to study the finitely presented group but also discussed the one-relator quotients of the modular group [7].

A closed path of triangles and edges in a coset diagram is called a circuit. In a coset diagram, a circuit is said to be a length- k circuit, denoted by $(\Delta_1, \Delta_2, \Delta_3, \dots, \Delta_k)$, if its one vertex is fixed by

$$(ax)^{\Delta_1} (ax^{-1})^{\Delta_2} (ax)^{\Delta_3} \dots (ax^{-1})^{\Delta_k} \in PSL(2, \mathbb{Z}). \quad (3)$$

Alternatively, it means that one vertex of the Δ_1 triangles lies outside of the circuit and one vertex of the Δ_2 triangles lies inside of the circuit and likewise. Since $(\Delta_1, \Delta_2, \Delta_3, \dots, \Delta_k)$ is a cycle, so it does not matter if one

vertex of the Δ_1 triangles lies inside of the circuit and one vertex of the Δ_2 triangles lies outside of the circuit and likewise. Note that k is always even.

The circuit of the type $(\Delta_1, \Delta_2, \Delta_3, \dots, \Delta_l, \Delta_1, \Delta_2, \Delta_3, \dots, \Delta_l, \dots, \Delta_1, \Delta_2, \Delta_3, \dots, \Delta_l)$ is termed as a periodic circuit with period of length l .

Note 1. By $V(\Delta)$, we mean the collection of vertices lies on the circuit $\Delta = (\Delta_1, \Delta_2, \Delta_3, \dots, \Delta_k)$.

Let $a, u \in V(\Delta)$ be any two vertices fixed by the words h_1 and h_2 , that is, $(a)h_1 = a$ and $(u)h_2 = u$. Suppose h_3 is the word that maps a to u , then $(a)h_1^{-1}h_3 = u$. Note that h_3 and $h_1^{-1}h_3$ are the only two paths that assign a to u . Now, by contraction of the pair of vertices a and u , we mean that a and u melt together to become one node $s = a = u$ such that $(s)h_3 = (s)h_1^{-1}h_3 = s$. As a result of this contraction, a closed path Γ is created that contains the vertex s fixed by h_3 and $h_1^{-1}h_3$. This closed path Γ is the homomorphic image of the circuit Δ . It is important to note that a and u is not the only pair of contraction in Δ that creates homomorphic image Γ . There are also many pairs of contraction other than a and u that create the same homomorphic image Γ . The following theorems proved in [8] will help us to find the total number of such contracted pairs that produce the same homomorphic image Γ of Δ .

Theorem 1. *Let the vertices a and u in Δ are contracted and a homomorphic image Γ of Δ is evolved, then Γ is also obtainable if the vertices $(a)h$ and $(u)h$ in Δ are contracted.*

Theorem 2. *If a and u are contracted to obtain Γ , then during this process $|E|$ number of pairs are contracted all together, where E is the collection of words such that $\forall h \in E, (a)h$ and $(u)h$ are contained by Δ .*

Example 1. Let us contract the vertices a and u from the circuit $(3, 4, 2, 4, 2, 4)$ (Figure 2) and acquire a homomorphic Γ (Figure 3) of the circuit $(3, 4, 2, 4, 2, 4)$. Thus, $h_1 = q(pq)$ and $h_2 = (pq)(pq^{-1})^4(pq)^2(pq^{-1})^4(pq)^2(pq^{-1})^4p$ are the two possible paths between a and u that are fixing the vertex $s = a = u$ in Γ .

Let E be the family of words such that for all $h \in E$ implies $(a)h$ and $(u)h$ lie on the circuit $(3, 4, 2, 4, 2, 4)$, then $E = \{e, q, q^{-1}, p, pq, pq^{-1}, (pq)p, (pq)^2, (pq)pq^{-1}\}$. Then by Theorem 2, the cardinality of E implies that there are 9 pairs of vertices contracted to generate the homomorphic image Γ .

Note that the cardinality of E does not give the total number of contracted pairs to generate the homomorphic image Γ . In the following, we will discuss the process to find the total number of contracted pairs to generate Γ .

Let Γ^* denote itself as the mirror image of Γ . Thus, the permutation r ensures that the coset diagram is symmetric along the vertical axis. This implies Γ^* will assuredly occur.

If $u = pq^{\pi_1}pq^{\pi_2} \dots pq^{\pi_n}(\pi_i = 1 \text{ or } -1)$ is a word, then $u^* = pq^{-\pi_1}pq^{-\pi_2} \dots pq^{-\pi_n}$. If the word h fixes the vertex s , then the vertex s^* is fixed by u^* .

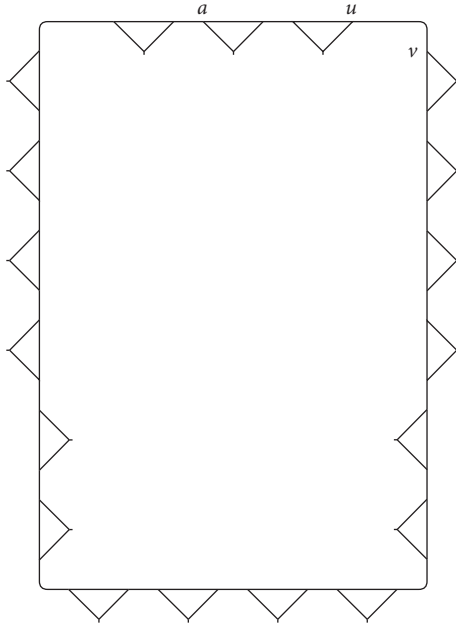


FIGURE 2: Circuit (3, 4, 2, 4, 2, 4).

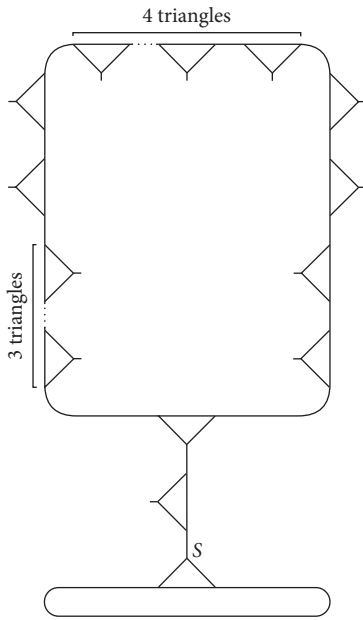


FIGURE 3: Homomorphic image Γ .

A homomorphic image Γ has a symmetry with respect to vertical axis if and only if by contracting a and u , the vertices a^* and u^* are also contracted.

Remark 1. In coset diagrams, r reverses the orientation of the triangles representing the three cycles of q (as reflection does). So corresponding to each vertex s fixed by the pair h_1, h_2 , there is a vertex s^* in Γ^* (mirror image of Γ) such that s^* is a fixed point of h_1^*, h_2^* . In other words, it is created by contracting a^* and u^* . There are certain Γ 's which have a vertical symmetry and so have the same orientations as those of their mirror images. The homomorphic image Γ of a circuit $\Delta = (\Delta_1, \Delta_2, \Delta_3, \Delta_4, \Delta_5, \Delta_6)$, which has a vertex s fixed

by the pair h_1, h_2 , has the same orientation as that of its mirror image if and only if there is a vertex s^* in Γ such that $(s^*)h_1 = (s^*)h_2 = s^*$.

1.1. Counting the Number of Pairs of Contracting Vertices of a Homomorphic Image. Let Γ be a homomorphic image of the circuit Δ acquired by the contraction of pair of vertices a and u of Δ . Then by Theorem 2, Γ has $|E|$ number of pairs of vertices. To find the total number of pairs of vertices, one should follow the following steps.

To know how many total pairs of contracting vertices are there, special precaution must be taken.

- (1) If by contracting a and u to create Γ , the pair of vertices a^* and u^* are not contracted, then Γ has different orientation from its mirror image Γ^* . So, there are $|E|$ number of more pairs of vertices for the mirror image of Γ .
- (2) If by contracting a and u to create Γ , the pair of vertices a^* and u^* are also contracted, then Γ has the same orientation as that of its mirror image Γ^* . So, in this case, Γ has $|E|$ number of pairs of contracted vertices.

Consider a circuit of length 6 as $\Delta = (\Delta_1, \Delta_2, \Delta_3, \Delta_4, \Delta_5, \Delta_6)$ (Figure 4) with vertical axis of symmetry, that is, $\Delta_2 = \Delta_6, \Delta_3 = \Delta_5$. Suppose $\Delta_1 > \Delta_2 > \Delta_3 > \Delta_4$. The coset diagrams are composed of circuits. The vertices of the circuits in infinite diagrams are contracted in a certain way, and a finite coset diagram evolves. It is therefore necessary to ask how many distinct homomorphic images are obtained if we contract all the pairs of vertices of the circuit Δ ? We not only give the answer to this question for a circuit Δ but also mention those pairs of vertices which are “important”. There is no need to contract the pairs which are not mentioned as “important”. If we contract those, we obtain a homomorphic image, which we have already obtained by contracting “important” pairs.

Note 2. It is clear from Figure 4 that

- (1) The mirror image of the vertex e_l^k is e_l^{2-k} , that is, $e_l^{k*} = e_{3\Delta_k - (l-1)}^{2-k}$
- (2) The vertex a_{3m+1}^k is fixed by the word $(pq^{-1})^m (pq)^{\Delta_{k+5}} (pq^{-1})^{\Delta_{k+4}} (pq)^{\Delta_{k+3}} (pq^{-1})^{\Delta_{k+2}} (pq)^{\Delta_{k+1}} (pq^{-1})^{\Delta_{k-m}}$
- (3) The vertex x_{3m}^k is fixed by the word $(pq)^{\Delta_{k-m}} (pq^{-1})^{\Delta_{k+1}} (pq)^{\Delta_{k+2}} (pq^{-1})^{\Delta_{k+3}} (pq)^{\Delta_{k+4}} (pq^{-1})^{\Delta_{k+5}} (pq)^m$, where

$$k \in \{1, 2, 3, 4, 5, 6\}; l = 1, 2, 3, \dots, \Delta_k; m =$$

$$1, 2, 3, \dots, \Delta_k - 1, \underline{n} = \begin{cases} 6, & \text{if } n = 0, 6 \\ n \pmod{6} & \text{otherwise} \end{cases}$$

$$\text{and } \pm = \begin{cases} + & \text{if } k \text{ is odd} \\ - & \text{otherwise} \end{cases}$$

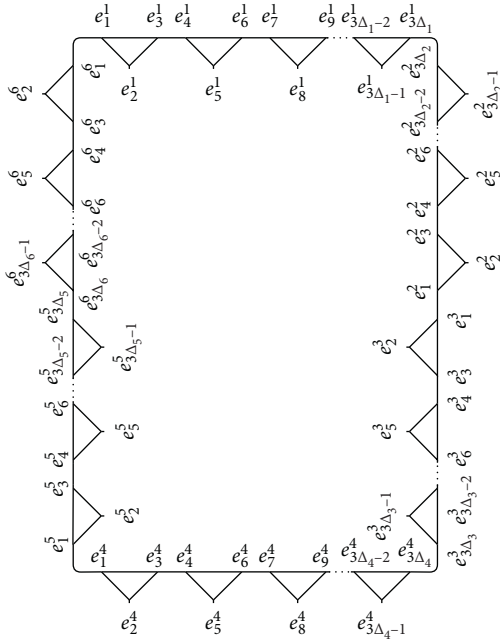


FIGURE 4: The circuit $\Delta = (\Delta_1, \Delta_2, \Delta_3, \Delta_4, \Delta_5, \Delta_6)$.

Lemma 1. *If we contract the vertices $e_{3l_1+1}^1: l_1 = 0, 1, 2, \dots, \Delta_2 - 1$, with the vertex $e_{3\Delta_1}^1$ in the circuit Δ , then there arise Δ_2 distinct homomorphic images of Δ and $3(l_1 + 2)$ pairs of contracted vertices create each homomorphic image. Moreover, the number of total pairs of contracted vertices to generate all Δ_2 and their mirror homomorphic images of Δ is $3(\Delta_2^2 + 3\Delta_2 - 2)$.*

Proof. Let $H_1 = \{\Omega_{l_1}^1; l_1 = 0, 1, 2, \dots, \Delta_2 - 1\}$ (Figure 5) be the collection of homomorphic images of Δ acquired by the contraction of the vertices $e_{3l_1+1}^1: l_1 = 0, 1, 2, \dots, \Delta_2 - 1$ with the vertex $e_{3\Delta_1}^1$ in Δ , where $e_{3l_1+1}^1$ and $e_{3\Delta_1}^1$ are fixed by the words $(pq)^{l_1}(pq^{-1})^{\Delta_6}(pq)^{\Delta_5}(pq^{-1})^{\Delta_4}(pq)^{\Delta_3}(pq^{-1})^{\Delta_2}(pq)^{\Delta_1-l_1}$ and $(pq)^{\Delta_2}(pq^{-1})^{\Delta_3}(pq)^{\Delta_4}(pq^{-1})^{\Delta_5}(pq)^{\Delta_6}(pq^{-1})^{\Delta_1}$. It is easy to verify that $P_1 = q^{-1}(pq^{-1})^{\Delta_1-l_1-1}$ and $P_2 = (pq)^{\Delta_2}(pq^{-1})^{\Delta_3}(pq)^{\Delta_4}(pq^{-1})^{\Delta_5}(pq)^{\Delta_6}(pq^{-1})^{l_1}p$ are the possible paths between $e_{3l_1+1}^1$ and $e_{3\Delta_1}^1$ (Figure 4). This implies that for each l_1 , the homomorphic image $\Omega_{l_1}^1$ has a vertex s fixed by P_1 and P_2 .

Thus,

$$E_1 = \{e, q, q^{-1}, p, pq, pq^{-1}, pq^2, pq^3, \dots,$$

$$(pq)^{l_1}p, (pq)^{l_1+1}, (pq)^{l_1}pq^{-1}\} \quad (4)$$

is the family of elements in $\text{PSL}(2, \mathbb{Z})$ such that $\forall x \in E, \Delta$ contains the vertices $(e_{3l_1+1}^1)x$ and $(e_{3\Delta_1}^1)x$. This gives that the cardinality of E_1 , that is, $3(l_1 + 2)$ is the number of contracted pairs of vertices to produce the homomorphic image $\Omega_{l_1}^1$ (Theorem 2). For $m \neq n$, let Ω_m^1 and Ω_n^1 be any two elements of H_1 , then the number of triangles in Ω_m^1 and Ω_n^1 are not equal (Figure 5). This implies that all the elements in H_1 are different and no one is the mirror image of the other. This

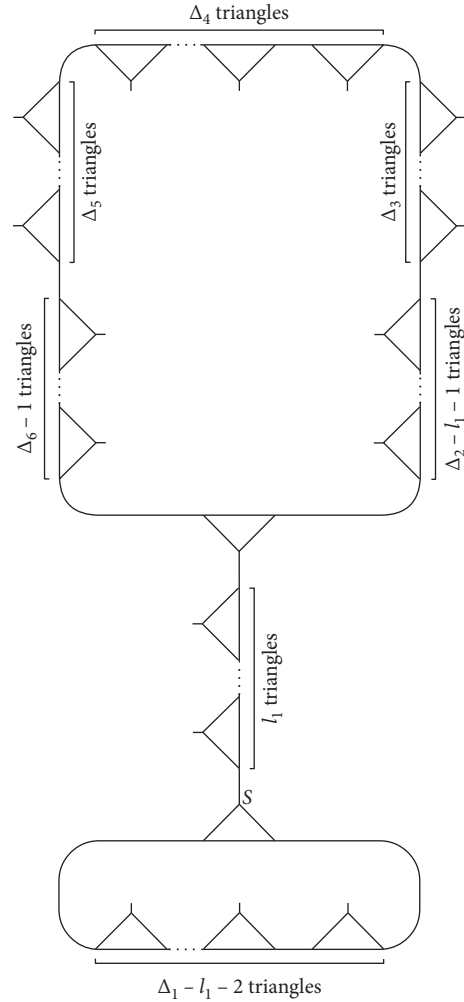


FIGURE 5: Homomorphic images $\Omega_{l_1}^1$.

further forms the result as $|H_1| = \Delta_2$. Thence, the number of contracted pairs of vertices of Δ to create all the elements of H_1 is $\sum_{l_1=0}^{\Delta_2-1} 3(l_1 + 2)$.

From Figure 5, it is also clear that no element of H_1 except Ω_0^1 has vertical axis of symmetry. So, Ω_0^1 is the only homomorphic image whose orientation is not different from its mirror image Ω_0^{1*} and all the remaining $\Delta_2 - 1$ elements of H_1 have different orientations from their mirror images. Hence, there are

$$6 \sum_{l_1=1}^{\Delta_2-1} (l_1 + 2) + 6 = 3(\Delta_2^2 + 3\Delta_2 - 2) \quad (5)$$

pairs of contracted vertices to produce all the homomorphic images in H_1 . \square

Lemma 2. *If we contract the vertices $e_{3l_1+1}^2: l_1 = 0, 1, 2, \dots, \Delta_2 - 1$, with the vertex $e_{3\Delta_1}^1$ in the circuit Δ , then there arise Δ_2 distinct homomorphic images of Δ and $3(l_1 + 2)$ pairs of contracted vertices create each homomorphic image. Moreover, the number of total pairs of contracted vertices to generate all Δ_2 and their mirror homomorphic images of Δ is $3(\Delta_2^2 + 3\Delta_2)$.*

Let $H_2 = \{\Omega_{l_1}^2; l_1 = 0, 1, 2, \dots, \Delta_2 - 1\}$ be the collection of homomorphic images of Δ acquired by the contraction of the vertices $e_{3l_1+1}^2; l_1 = 0, 1, 2, \dots, \Delta_2 - 1$ with the vertex $e_{3\Delta_1}^1$ in Δ . Suppose r shows itself as the remainder of $(l_1/(\Delta_2 - l_1))$. Then, graphically we make four partitions of H_2 as follows:

- (i) $\Omega_{l_1}^2: \Delta_2 - 2l_1 > 1$ (Figure 6(a))
- (ii) $\Omega_{l_1}^2: \Delta_2 - 2l_1 = 1$ (Figure 6(b))
- (iii) $\Omega_{l_1}^2: \Delta_2 - 2l_1 < 1$ and $\Delta_2 - l_1 > r + 1$ (Figure 6(c))
- (iv) $\Omega_{l_1}^2: \Delta_2 - 2l_1 < 1$ and $\Delta_2 - l_1 = r + 1$ (Figure 6(d))

From all the homomorphic images presented in these figures, it is not intricated to check that no one is the mirror image of itself. This lemma can be proved by using the same procedure as that for Lemma 1.

Let $k_1 \in \{3, 4, 5\}$.

Lemma 3. *If we contract the vertices $e_{3l_{(2,k_1)+1}}^{k_1}; l_{(2,k_1)} = 0, 1, 2, \dots, \Delta_{k_1} - 1$, with the vertex $e_{3\Delta_1}^1$ in the circuit Δ , then for each k_1 , there arise Δ_{k_1} distinct homomorphic images of Δ and $3(l_{(2,k_1)} + 2)$ pairs of contracted vertices that create each homomorphic image. Moreover, the number of total pairs of contracted vertices to generate all Δ_{k_1} and their mirror homomorphic images of Δ is $3(\Delta_{k_1}^2 + 3\Delta_{k_1})$.*

For a fix value of k_1 , let $H_3^{k_1} = \{\Omega_{l_{(2,k_1)}}^3; l_{(2,k_1)} = 0, 1, 2, \dots, \Delta_{k_1} - 1\}$ be the collection of homomorphic images of Δ acquired by the contraction of the vertices $e_{3l_{(2,k_1)+1}}^{k_1}; l_{(2,k_1)} = 0, 1, 2, \dots, \Delta_{k_1} - 1$, with the vertex $e_{3\Delta_1}^1$ in Δ . Figures 7–9 present $H_3^{k_1}$ graphically. From all the homomorphic images presented in these figures, it is not intricated to check that no one is the mirror image of itself.

This lemma can be proved by using the same procedure as that for Lemma 1.

Lemma 4. *If we contract the vertices $e_{3l_3+1}^6; l_3 = 0, 1, 2, \dots, \Delta_6 - 1$, with the vertex $e_{3\Delta_1}^1$ in the circuit Δ , then there arise Δ_6 distinct homomorphic images of Δ and $3(l_3 + 2)$ pairs of contracted vertices create each homomorphic image. Moreover, the number of total pairs of contracted vertices to generate all Δ_6 and their mirror homomorphic images of Δ is $(3/2)(\Delta_6^2 + 3\Delta_6)$.*

Let $H_4 = \{\Omega_{l_3}^4; l_3 = 0, 1, 2, \dots, \Delta_6 - 1\}$ be the collection of homomorphic images of Δ acquired by the contraction of the vertices $e_{3l_3+1}^4; l_3 = 0, 1, 2, \dots, \Delta_6 - 1$ with the vertex $e_{3\Delta_1}^1$ in Δ . Figure 10 presents H_4 graphically. From all the homomorphic images presented in Figure 10, it is not intricated to check that every one is the mirror image of itself.

This lemma can be proved by using the same procedure as that for Lemma 1.

Lemma 5. *If we contract the vertices $e_{3l_4+1}^1; l_4 = 1, 2, \dots, \Delta_1 - 1$, with the vertex $e_{3\Delta_2}^2$ in the circuit Δ , then there arise $\Delta_1 - 1$ distinct homomorphic images of Δ and $3(l_4 + 2)$ pairs of contracted vertices create each homomorphic image. Moreover, the number of total pairs of contracted vertices to*

generate all $\Delta_1 - 1$ and their mirror homomorphic images of Δ is $(3/2)(\Delta_1^2 + 3\Delta_1 - 4)$.

Let $H_5 = \{\Omega_{l_4}^5; l_4 = 1, 2, \dots, \Delta_1 - 1\}$ be the collection of homomorphic images of Δ acquired by the contraction of the vertices $e_{3l_4+1}^1; l_4 = 1, 2, \dots, \Delta_1 - 1$, with the vertex $e_{3\Delta_2}^2$ in Δ . Suppose r shows itself as the remainder of $(l_4/(\Delta_1 - l_4))$, then graphically, we make four partitions of H_5 as follows:

- (i) $\Omega_{l_4}^5: \Delta_1 - 2l_4 > 1$ (Figure 11(a))
- (ii) $\Omega_{l_4}^5: \Delta_1 - 2l_4 = 1$ (Figure 11(b))
- (iii) $\Omega_{l_4}^5: \Delta_1 - 2l_4 < 1$ and $\Delta_1 - l_4 > r + 1$ (Figure 11(c))
- (iv) $\Omega_{l_4}^5: \Delta_1 - 2l_4 < 1$ and $\Delta_1 - l_4 = r + 1$ (Figure 11(d))

From all the homomorphic images presented in these figures, it is not intricated to check that every one is the mirror image of itself. This lemma can be proved by using the same procedure as that for Lemma 1.

Lemma 6. *If we contract the vertices $e_{3l_5+1}^2; l_5 = 1, 2, \dots, \Delta_2 - 1$, with the vertex $e_{3\Delta_2}^2$ in the circuit Δ , then there arise $\Delta_2 - 1$ distinct homomorphic images of Δ and $3(l_5 + 2)$ pairs of contracted vertices create each homomorphic image. Moreover, the number of total pairs of contracted vertices to generate all $\Delta_2 - 1$ and their mirror homomorphic images of Δ is $3(\Delta_2^2 + 3\Delta_2 - 4)$.*

Let $H_6 = \{\Omega_{l_5}^6; l_5 = 1, 2, \dots, \Delta_2 - 1\}$ be the collection of homomorphic images of Δ acquired by the contraction of the vertices $e_{3l_5+1}^2; l_5 = 1, 2, \dots, \Delta_2 - 1$, with the vertex $e_{3\Delta_2}^2$ in Δ . Graphically, we make two partitions of H_5 as follows:

- (i) $\Omega_{l_5}^6: l_5 < \Delta_2 - 1$ (Figure 12(a))
- (ii) $\Omega_{l_5}^6: l_5 = \Delta_2 - 1$ (Figure 12(b))

From all the homomorphic images presented in Figures 12(a) and 12(b), it is not intricated to check that no one is the mirror image of itself. This lemma can be proved by using the same procedure as that for Lemma 1.

Let $k_1 \in \{3, 4, 5\}$.

Lemma 7. *If we contract the vertices $e_{3l_{(6,k_1)+1}}^{k_1}; l_{(6,k_1)} = 1, 2, \dots, \Delta_{k_1} - 1$, with the vertex $e_{3\Delta_2}^2$ in the circuit Δ , then for each k_1 , there arise $\Delta_{k_1} - 1$ distinct homomorphic images of Δ and $3(l_{(6,k_1)} + 2)$ pairs of contracted vertices create each homomorphic image. Moreover, the number of total pairs of contracted vertices to generate all $\Delta_{k_1} - 1$ and their mirror homomorphic images of Δ is $3(\Delta_{k_1}^2 + 3\Delta_{k_1} - 4)$.*

For a fix value of k_1 , let $H_7^{k_1} = \{\Omega_{l_{(6,k_1)}}^7; l_{(6,k_1)} = 1, 2, \dots, \Delta_{k_1} - 1\}$ be the collection of homomorphic images of Δ acquired by the contraction of the vertices $e_{3l_{(6,k_1)+1}}^{k_1}; l_{(6,k_1)} = 1, 2, \dots, \Delta_{k_1} - 1$, with the vertex $e_{3\Delta_2}^2$ in Δ . Figures 13–15 present $H_7^{k_1}$ graphically. From all the homomorphic images presented in these figures, it is not intricated to check that no one is the mirror image of itself. This lemma can be proved by using the same procedure as that for Lemma 1.

Lemma 8. *If we contract the vertices $e_{3l_7+1}^3; l_7 = 1, 2, \dots, \Delta_4 - 1$, with the vertex $e_{3\Delta_3}^3$ in the circuit Δ , then there arise*

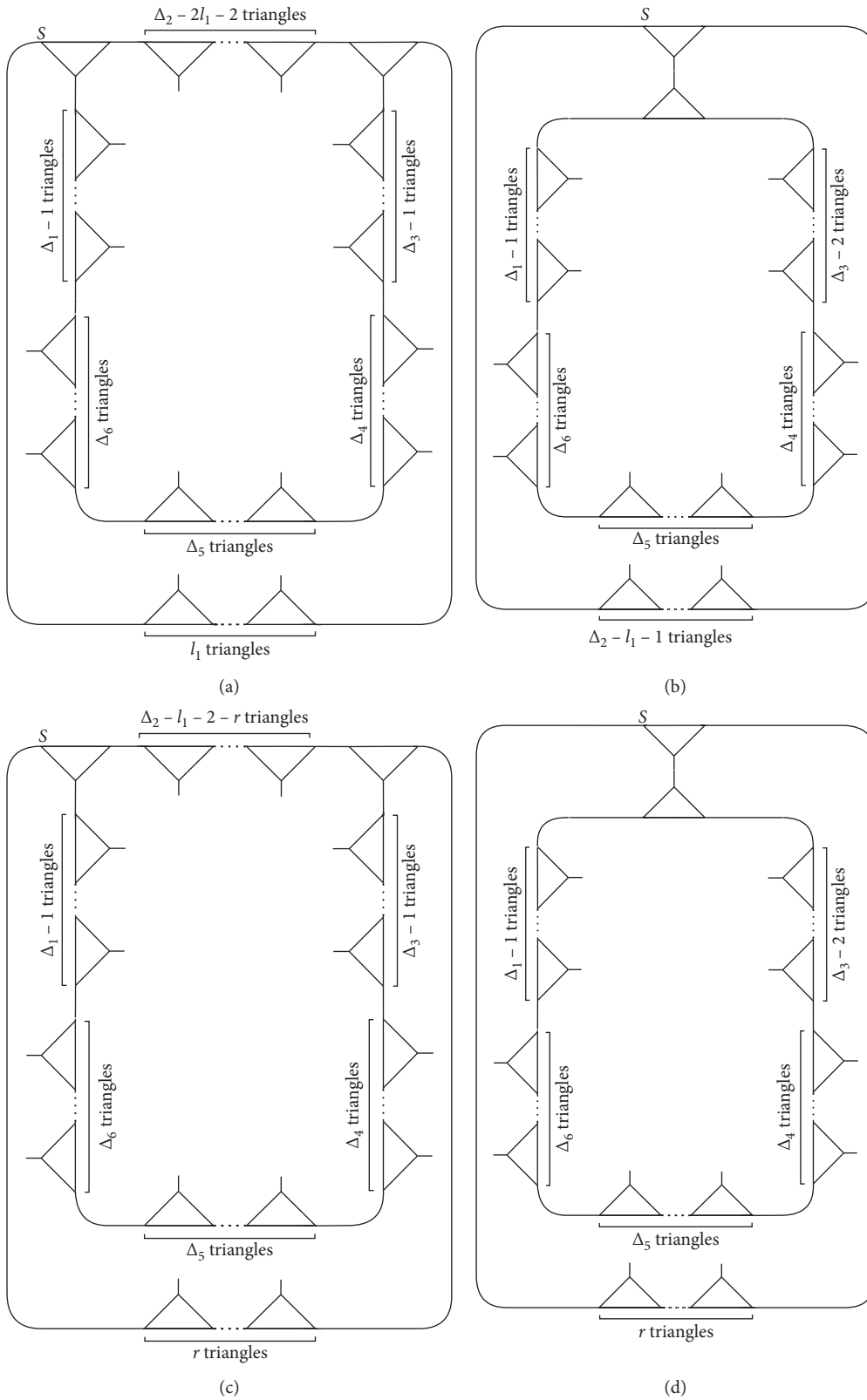


FIGURE 6: (a) Homomorphic images $\Omega_{l_1}^2: \Delta_2 - 2l_1 > 1$. (b) Homomorphic images $\Omega_{l_1}^2: \Delta_2 - 2l_1 = 1$. (c) Homomorphic images $\Omega_{l_1}^2: \Delta_2 - 2l_1 < 1$ and $\Delta_2 - l_1 > r + 1$. (d) Homomorphic images $\Omega_{l_1}^2: \Delta_2 - 2l_1 < 1$ and $\Delta_2 - l_1 = r + 1$.

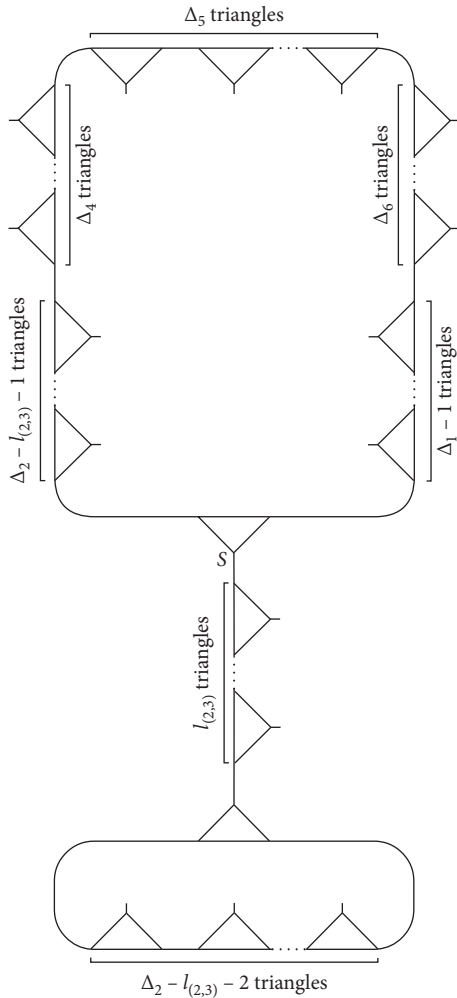


FIGURE 7: Homomorphic images $\Omega_{l_{(2,3)}}^3$.

$\Delta_4 - 1$ distinct homomorphic images of Δ and $3(l_7 + 2)$ pairs of contracted vertices create each homomorphic image. Moreover, the number of total pairs of contracted vertices to generate all $\Delta_4 - 1$ and their mirror homomorphic images of Δ is $3(\Delta_4^2 + 3\Delta_4 - 4)$.

Let $H_8 = \{\Omega_{l_7}^8; l_7 = 1, 2, \dots, \Delta_4 - 1\}$ be the collection of homomorphic images of Δ acquired by the contraction of the vertices $e_{3l_7+1}^3; l_7 = 1, 2, \dots, \Delta_4 - 1$, with the vertex $e_{3\Delta_3}^3$ in Δ . Figure 16 presents H_8 graphically. From all the homomorphic images presented in Figure 16, it is not intricate to check that no one is the mirror image of itself. This lemma can be proved by using the same procedure as that for Lemma 1.

Lemma 9. If we contract the vertices $e_{3l_7+1}^4; l_7 = 1, 2, \dots, \Delta_4 - 1$, with the vertex $e_{3\Delta_3}^4$ in the circuit Δ , then there arise $\Delta_4 - 1$ distinct homomorphic images of Δ and $3(l_7 + 2)$ pairs of contracted vertices create each homomorphic image. Moreover, the number of total pairs of contracted vertices to generate all $\Delta_1 - 1$ and their mirror homomorphic images of Δ is $(3/2)(\Delta_4^2 + 3\Delta_4 - 4)$.

Let $H_9 = \{\Omega_{l_7}^9; l_7 = 1, 2, \dots, \Delta_4 - 1\}$ be the collection of homomorphic images of Δ acquired by the contraction of the

vertices $e_{3l_7+1}^4; l_7 = 1, 2, \dots, \Delta_4 - 1$, with the vertex $e_{3\Delta_3}^4$ in Δ . Suppose r shows itself as the remainder of $(l_7/\Delta_4 - l_7)$, then graphically we make four partitions of H_9 as follows:

- (i) $\Omega_{l_7}^9: \Delta_4 - 2l_7 > 1$ (Figure 17(a))
- (ii) $\Omega_{l_7}^9: \Delta_4 - 2l_7 = 1$ (Figure 17(b))
- (iii) $\Omega_{l_7}^9: \Delta_4 - 2l_7 < 1$ and $\Delta_4 - l_7 > r + 1$ (Figure 17(c))
- (iv) $\Omega_{l_7}^9: \Delta_4 - 2l_7 < 1$ and $\Delta_4 - l_7 = r + 1$ (Figure 17(d))

From all the homomorphic images presented in these figures, it is not intricate to check that every one is the mirror image of itself. This lemma can be proved by using the same procedure as that for Lemma 1.

Lemma 10. If we contract the vertices $e_{3l_8+1}^4; l_8 = 0, 1, 2, \dots, \Delta_4 - 1$, with the vertex $e_{3\Delta_4}^4$ in the circuit Δ , then there arise Δ_4 distinct homomorphic images of Δ and $3(l_8 + 2)$ pairs of contracted vertices create each homomorphic image. Moreover, the number of total pairs of contracted vertices to generate all Δ_4 and their mirror homomorphic images of Δ is $3(\Delta_4^2 + 3\Delta_4 - 2)$.

Let $H_{10} = \{\Omega_{l_8}^{10}; l_8 = 0, 1, 2, \dots, \Delta_4 - 1\}$ be the collection of homomorphic images of Δ acquired by the contraction of the vertices $e_{3l_8+1}^4; l_8 = 0, 1, 2, \dots, \Delta_4 - 1$, with the vertex $e_{3\Delta_4}^4$ in Δ . Graphically, we make two partitions of H_{10} as follows:

- (i) $\Omega_{l_8}^{10}: l_8 < \Delta_4 - 1$ (Figure 18(a))
- (ii) $\Omega_{l_8}^{10}: l_8 = \Delta_4 - 1$ (Figure 18(b))

From all the homomorphic images presented in these figures, it is not intricate to check that no one is the mirror image of itself except Ω_0^{10} . This lemma can be proved by using the same procedure as that for Lemma 1.

Lemma 11. If we contract the vertices $e_{3l_9+1}^5; l_9 = 0, 1, 2, \dots, \Delta_5 - 1$, with the vertex $e_{3\Delta_4}^5$ in the circuit Δ , then there arise Δ_5 distinct homomorphic images of Δ and $3(l_9 + 2)$ pairs of contracted vertices create each homomorphic image. Moreover, the number of total pairs of contracted vertices to generate all Δ_5 and their mirror homomorphic images of Δ is $(3/2)(\Delta_5^2 + 3\Delta_5)$.

Let $H_{11} = \{\Omega_{l_9}^{11}; l_9 = 0, 1, 2, \dots, \Delta_5 - 1\}$ be the collection of homomorphic images of Δ acquired by the contraction of the vertices $e_{3l_9+1}^5; l_9 = 0, 1, 2, \dots, \Delta_5 - 1$, with the vertex $e_{3\Delta_4}^5$ in Δ . Figure 19 presents H_{11} graphically. From all the homomorphic images presented in Figure 19, it is not intricate to check that every one is the mirror image of itself. This lemma can be proved by using the same procedure as that for Lemma 1.

Lemma 12. If we contract the vertices $e_{3l_{10}+1}^3; l_{10} = 0, 1, 2, \dots, \Delta_3 - 1$, with the vertex $e_{3\Delta_4}^4$ in the circuit Δ , then there arise Δ_3 distinct homomorphic images of Δ and $3(l_{10} + 2)$ pairs of contracted vertices create each homomorphic image. Moreover, the number of total pairs of contracted vertices to generate all Δ_3 and their mirror homomorphic images of Δ is $3(\Delta_3^2 + 3\Delta_3)$.

Let $H_{12} = \{\Omega_{l_{10}}^{12}; l_{10} = 0, 1, 2, \dots, \Delta_3 - 1\}$ be the collection of homomorphic images of Δ acquired by the contraction of the vertices $e_{3l_{10}+1}^3; l_{10} = 0, 1, 2, \dots, \Delta_3 - 1$, with the vertex $e_{3\Delta_4}^4$

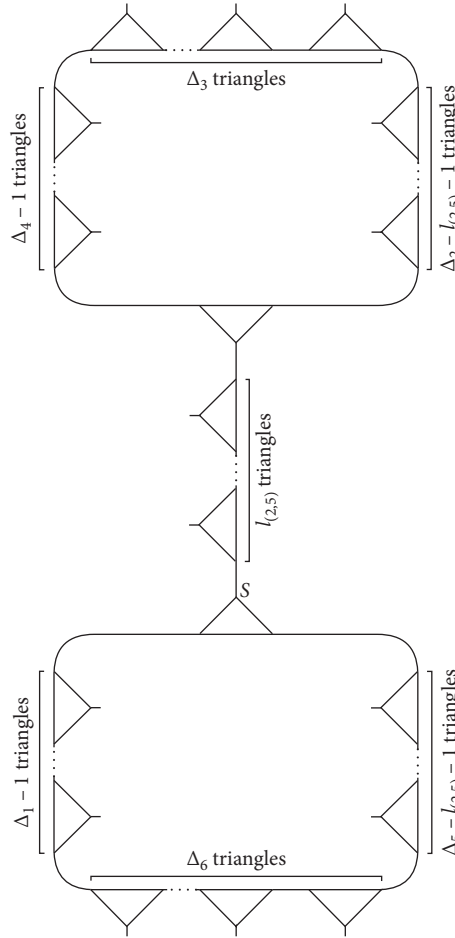


FIGURE 8: Homomorphic images $\Omega_{l(2,5)}^3$.

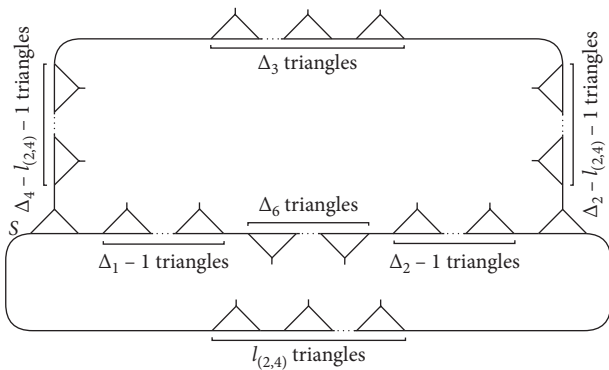


FIGURE 9: Homomorphic images $\Omega_{l(2,4)}^3$.

in Δ . Suppose r shows itself as the remainder of $(l_{10}/(\Delta_3 - l_{10}))$, then graphically we make four partitions of H_{12} as follows:

- (i) $\Omega_{l_{10}}^{12}$: $\Delta_3 - 2l_{10} > 1$ (Figure 20(a))
- (ii) $\Omega_{l_{10}}^{12}$: $\Delta_3 - 2l_{10} = 1$ (Figure 20(b))
- (iii) $\Omega_{l_{10}}^{12}$: $\Delta_3 - 2l_{10} < 1$ and $\Delta_3 - l_{10} > r + 1$ (Figure 20(c))
- (iv) $\Omega_{l_{10}}^{12}$: $\Delta_3 - 2l_{10} < 1$ and $\Delta_3 - l_{10} = r + 1$ (Figure 20(d))

From all the homomorphic images presented in these figures, it is not intricate to check that no one is the mirror

image of itself. This lemma can be proved by using the same procedure as that for Lemma 1.

Lemma 13. If we contract the vertices $e_{3l_1+1}^2$; $l_1 = 0, 1, 2, \dots, \Delta_2 - 1$, with the vertex $e_{3\Delta_5}^5$ in the circuit Δ , then there arise Δ_2 distinct homomorphic images of Δ and $3(l_1 + 2)$ pairs of contracted vertices create each homomorphic image. Moreover, the number of total pairs of contracted vertices to generate all Δ_2 and their mirror homomorphic images of Δ is $(3/2)(\Delta_2^2 + 3\Delta_2)$.

Let $H_{13} = \{\Omega_{l_1}^{13}; l_1 = 0, 1, 2, \dots, \Delta_2 - 1\}$ be the collection of homomorphic images of Δ acquired by the contraction of the vertices $e_{3l_1+1}^2$; $l_1 = 0, 1, 2, \dots, \Delta_2 - 1$, with the vertex $e_{3\Delta_5}^5$ in Δ . Figure 21 presents H_{13} graphically. From all the homomorphic images presented in Figure 21, it is not intricate to check that every one is the mirror image of itself. This lemma can be proved by using the same procedure as that for Lemma 1.

Lemma 14. If we contract the vertices $e_{3l_1+1}^3$; $l_1 = 0, 1, 2, \dots, \Delta_3 - 1$, with the vertex $e_{3\Delta_5}^5$ in the circuit Δ , then there arise Δ_3 distinct homomorphic images of Δ and $3(l_{11} + 2)$ pairs of contracted vertices create each homomorphic image. Moreover, the number of total pairs of

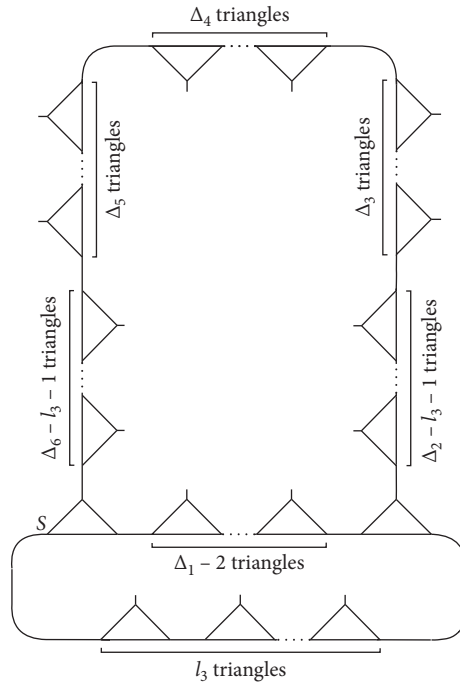


FIGURE 10: Homomorphic images Ω_3^4 .

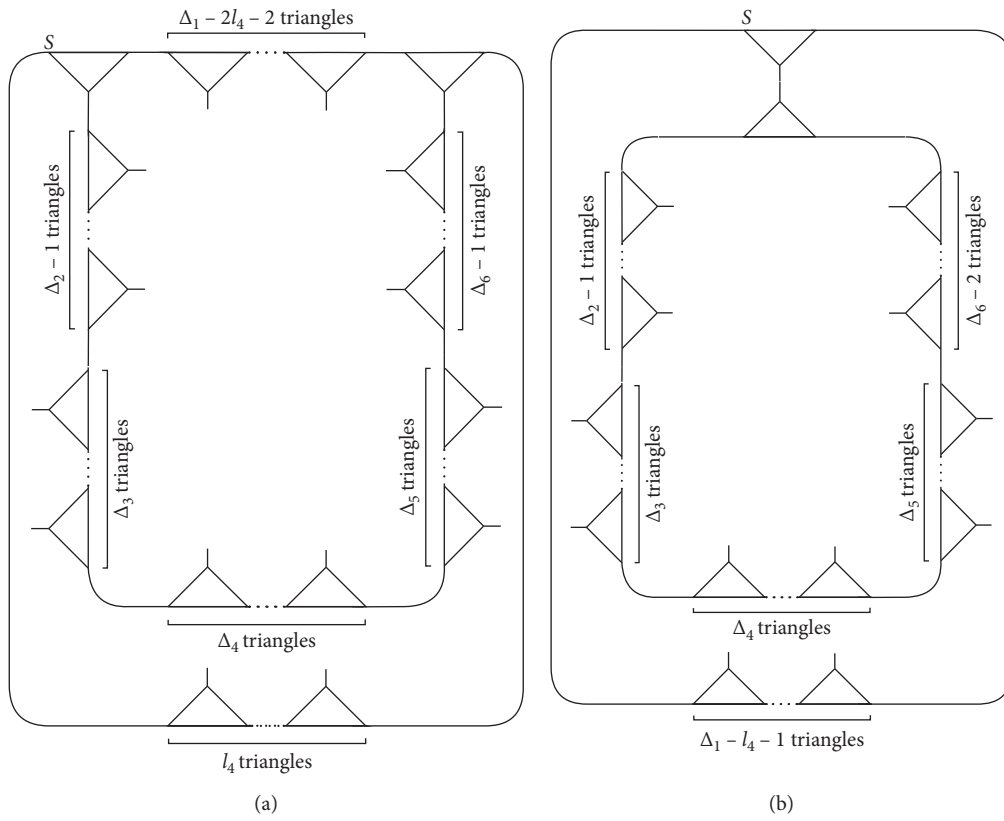


FIGURE 11: Continued.

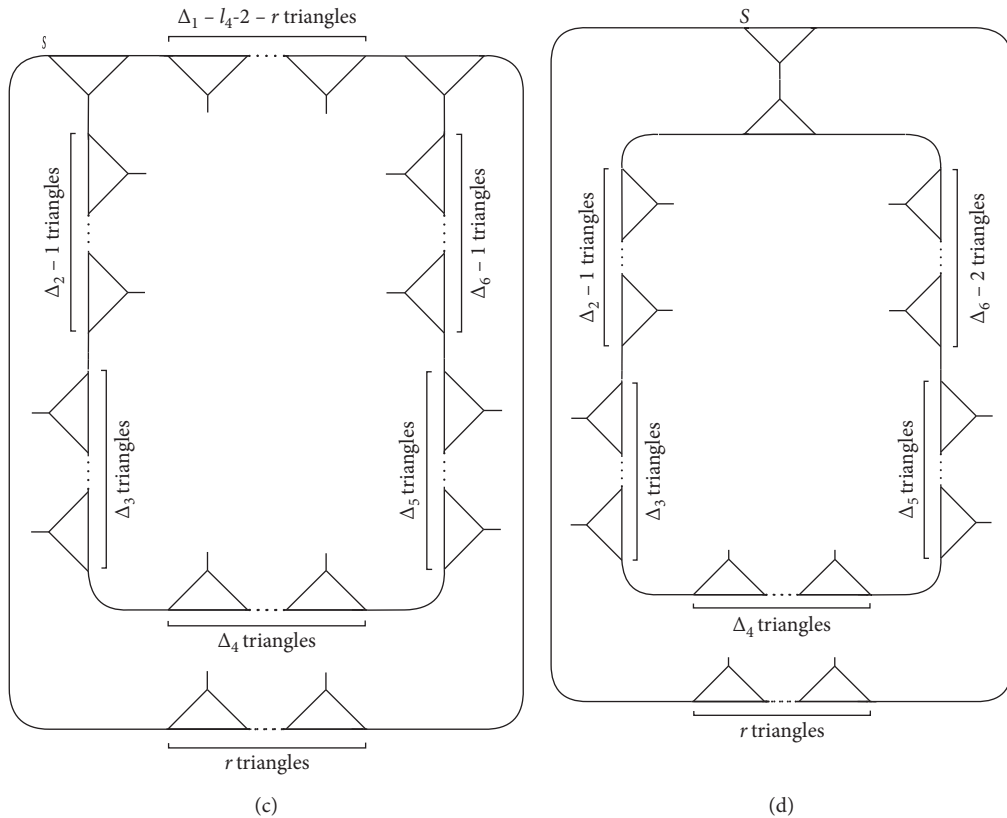


FIGURE 11: (a) Homomorphic images Ω_4^5 : $\Delta_1 - 2l_4 > 1$. (b) Homomorphic images Ω_4^5 : $\Delta_1 - 2l_4 = 1$. (c) Homomorphic images Ω_4^5 : $\Delta_1 - 2l_4 < 1$ and $\Delta_1 - l_4 > r + 1$. (d) Homomorphic images Ω_4^5 : $\Delta_1 - 2l_4 < 1$ and $\Delta_1 - l_4 = r + 1$

contracted vertices to generate all Δ_3 and their mirror homomorphic images of Δ is $3(\Delta_3^2 + 3\Delta_3 - 2)$.

Let $H_{14} = \{\Omega_{l_{11}}^{14}; l_{11} = 0, 1, 2, \dots, \Delta_3 - 1\}$ be the collection of homomorphic images of Δ acquired by the contraction of the vertices $e_{3l_{11}+1}^3$: $l_{11} = 0, 1, 2, \dots, \Delta_3 - 1$, with the vertex $e_{3\Delta_5}^5$ in Δ . Figure 22 presents H_{14} graphically. From all the homomorphic images presented in Figure 22, it is not intricate to check that no one is the mirror image of itself except Ω_0^{14} . This lemma can be proved by using the same procedure as that for Lemma 1.

Lemma 15. If we contract the vertices $e_{3l_7+1}^4$: $l_7 = 1, 2, \dots, \Delta_4 - 1$, with the vertex $e_{3\Delta_5}^5$ in the circuit Δ , then there arise $\Delta_4 - 1$ distinct homomorphic images of Δ and $3(l_7 + 2)$ pairs of contracted vertices create each homomorphic image. Moreover, the number of total pairs of contracted vertices to generate all $\Delta_4 - 1$ and their mirror homomorphic images of Δ is $3(\Delta_4^2 + 3\Delta_4 - 4)$.

Let $H_{15} = \{\Omega_{l_7}^{15}; l_7 = 1, 2, \dots, \Delta_4 - 1\}$ be the collection of homomorphic images of Δ acquired by the contraction of the vertices $e_{3l_7+1}^4$: $l_7 = 1, 2, \dots, \Delta_4 - 1$, with the vertex $e_{3\Delta_5}^5$ in Δ . Figure 23 presents H_{15} graphically. From all the homomorphic images presented in Figure 23, it is not intricate to check that no one is the mirror image of itself.

This lemma can be proved by using the same procedure as that for Lemma 1.

Lemma 16. If we contract the vertices $e_{3l_{12}+1}^5$: $l_{12} = 0, 1, 2, \dots, \Delta_5 - 1$, with the vertex $e_{3\Delta_5}^5$ in the circuit Δ , then there arise Δ_5 distinct homomorphic images of Δ and $3(l_{12} + 2)$ pairs of contracted vertices create each homomorphic image. Moreover, the number of total pairs of contracted vertices to generate all Δ_5 and their mirror homomorphic images of Δ is $3(\Delta_5^2 + 3\Delta_5)$.

Let $H_{16} = \{\Omega_{l_{12}}^{16}; l_{12} = 0, 1, 2, \dots, \Delta_5 - 1\}$ be the collection of homomorphic images of Δ acquired by the contraction of the vertices $e_{3l_{12}+1}^5$: $l_{12} = 0, 1, 2, \dots, \Delta_5 - 1$, with the vertex $e_{3\Delta_5}^5$ in Δ . Graphically, we make two partitions of H_{16} as follows:

- (i) $\Omega_{l_{12}}^{16}$: $l_{12} < \Delta_5 - 1$ (Figure 24(a))
- (ii) $\Omega_{l_{12}}^{16}$: $l_{12} = \Delta_5 - 1$ (Figure 24(b))

From all the homomorphic images presented in these figures, it is not intricate to check that no one is the mirror image of itself. This lemma can be proved by using the same procedure as that for Lemma 1.

Lemma 17. If we contract the vertices $e_{3l_{13}+1}^3$: $l_{13} = 1, 2, \dots, \Delta_3 - 1$, with the vertex $e_{3\Delta_6}^6$ in the circuit Δ , then there arise $\Delta_3 - 1$ distinct homomorphic images of Δ and $3(l_{13} + 2)$ pairs of contracted vertices create each homomorphic image. Moreover, the number of total pairs of contracted vertices to generate all $\Delta_3 - 1$ and their mirror homomorphic images of Δ is $(3/2)(\Delta_3^2 + 3\Delta_3 - 4)$.

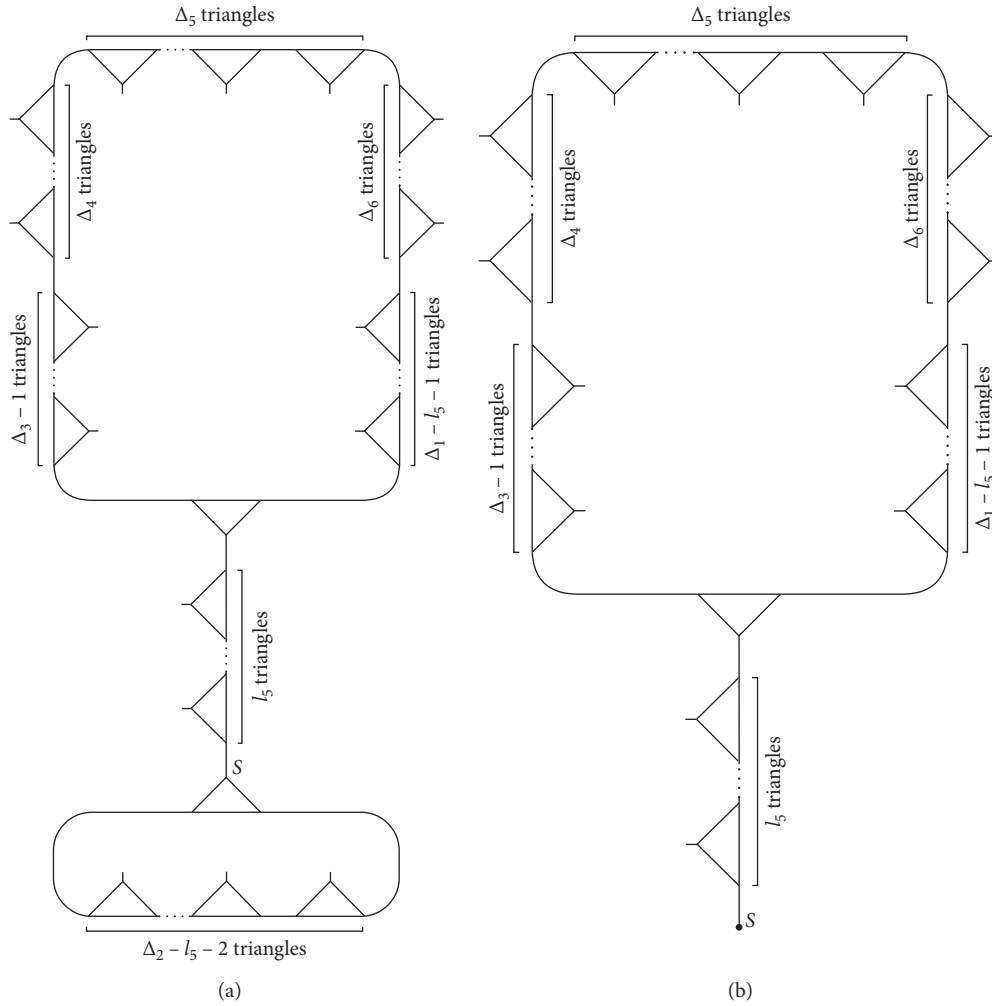


FIGURE 12: (a) Homomorphisms $\Omega_i^6: l_5 < \Delta_2 - 1$. (b) Homomorphisms $\Omega_i^6: l_5 = \Delta_2 - 1$.

Let $H_{17} = \{\Omega_{l_{13}}^{17}; l_{13} = 1, 2, \dots, \Delta_3 - 1\}$ be the collection of homomorphisms of Δ acquired by the contraction of the vertices $e_{3l_{13}+1}^3: l_{13} = 1, 2, \dots, \Delta_3 - 1$, with the vertex $e_{3\Delta_6}^6$ in Δ . Figure 25 presents H_{17} graphically. From all the homomorphisms presented in Figure 25, it is not intricate to check that every one is the mirror image of itself. This lemma can be proved by using the same procedure as that for Lemma 1.

Lemma 18. If we contract the vertices $e_{3l_{14}+1}^1: l_{14} = \Delta_2 + 1, \Delta_2 + 2, \dots, \Delta_1 - 1$, with the vertex $e_{3\Delta_1}^1$ in the circuit Δ , then there arise $\Delta_1 - \Delta_2 - 1$ distinct homomorphisms of Δ and $3(\Delta_2 + 2)$ pairs of contracted vertices create each homomorphism image. Moreover, the number of total pairs of contracted vertices to generate all $\Delta_1 - \Delta_2 - 1$ and their mirror homomorphisms of Δ is $6(\Delta_2 + 2)(\Delta_1 - \Delta_2 - 1)$.

Proof. Let $H_{18} = \{\Omega_{l_{14}}^{18}; l_{14} = \Delta_2 + 1, \Delta_2 + 2, \dots, \Delta_1 - 1\}$ (Figure 26) be the collection of homomorphisms of Δ acquired by the contraction of the vertices $e_{3l_{14}+1}^1: l_{14} = \Delta_2 + 1, \Delta_2 + 2, \dots, \Delta_1 - 1$, with the vertex $e_{3\Delta_1}^1$ in Δ , where $e_{3l_{14}+1}^1$ and $e_{3\Delta_1}^1$ are fixed by the words $(pq)^{\Delta_1 - l_{14}}(pq^{-1})^{\Delta_6}(pq)^{\Delta_5}(pq^{-1})^{\Delta_4}(pq)^{\Delta_3}(pq^{-1})^{\Delta_2}(pq)^{l_{14}}$ and

$(pq)^{\Delta_2}(pq^{-1})^{\Delta_3}(pq)^{\Delta_4}(pq^{-1})^{\Delta_5}(pq)^{\Delta_2}(pq^{-1})^{\Delta_3}(pq)^{\Delta_4}(pq^{-1})^{\Delta_5}(pq)^{\Delta_6}(pq^{-1})^{\Delta_1}$. It is easy to verify that $P_1 = q^{-1}(pq^{-1})^{\Delta_1 - l_{14} - 1}$ and $P_2 = (pq)^{\Delta_2}(pq^{-1})^{\Delta_3}(pq)^{\Delta_4}(pq^{-1})^{\Delta_5}(pq)^{\Delta_6}(pq^{-1})^{l_{14}}p$ are the possible paths between $e_{3l_{14}+1}^1$ and $e_{3\Delta_1}^1$ (Figure 4). This implies that, for each l_{14} , the homomorphism image $\Omega_{l_{14}}^{18}$ has a vertex s fixed by P_1 and P_2 . Thus,

$$E_{18} = \{e, q, q^{-1}, p, pq, pq^{-1}, pqp, (pq)^2, pqpq^{-1}, \dots, (pq)^{\Delta_2}p, (pq)^{\Delta_2+1}, (pq)^{\Delta_2}pq^{-1}\} \quad (6)$$

is the family of elements in $\text{PSL}(2, \mathbb{Z})$ such that $\forall x \in E_{18}, \Delta$ contains the vertices $(e_{3l_{14}+1}^1)x$ and $(e_{3\Delta_1}^1)x$. This gives that the cardinality of E_{18} , that is, $3(\Delta_2 + 2)$ is the number of contracted pairs of vertices to produce the homomorphism image $\Omega_{l_{14}}^{18}$ (Theorem 2).

Now, we will prove that all the homomorphisms in H_{18} are distinct and no one is the mirror image of itself.

Let Ω_m^{18} and Ω_n^{18} be any two elements of H_{18} , then Ω_m^{18} is produced by contraction of e_{3m+1}^1 and $e_{3\Delta_1}^1$ and Ω_n^{18} is produced by contraction of e_{3n+1}^1 and $e_{3\Delta_1}^1$. Suppose Ω_m^{18} and Ω_n^{18} are the same. This concludes that Ω_m^{18} is procurable also

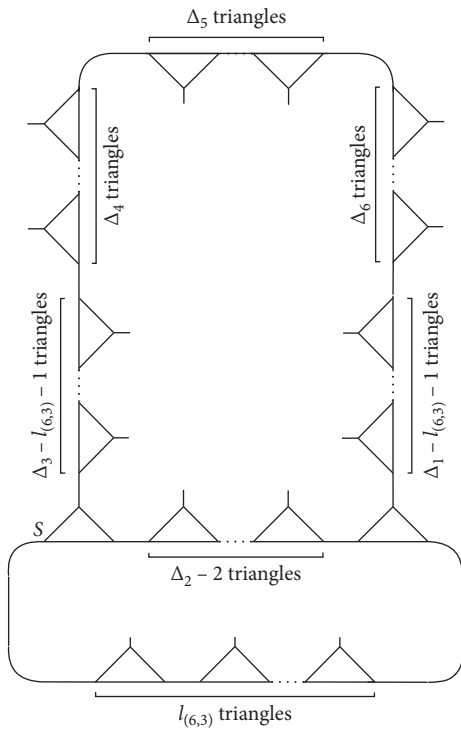


FIGURE 13: Homomorphic images $\Omega_{l_{(6,3)}}^7$.

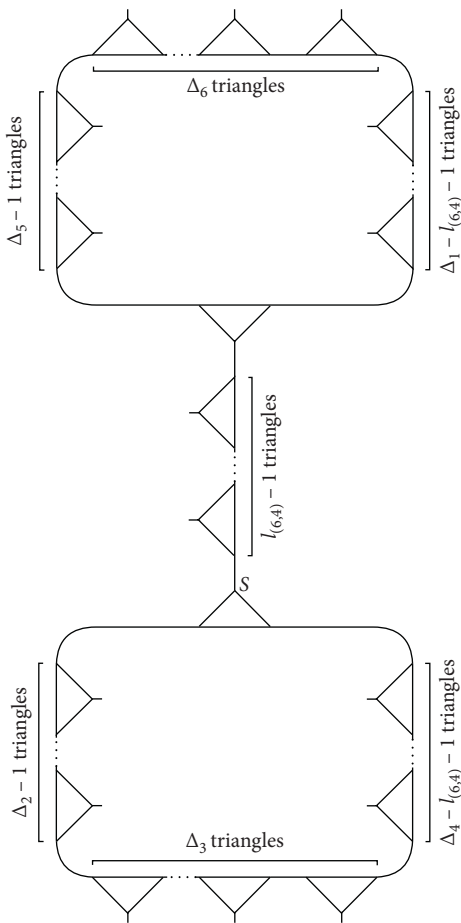


FIGURE 14: Homomorphic images $\Omega_{l_{(6,4)}}^7$.

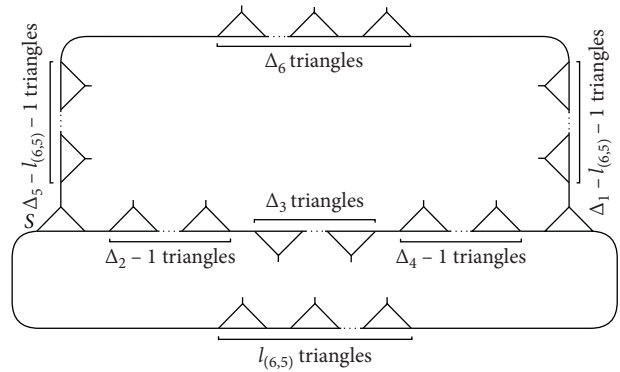


FIGURE 15: Homomorphic images $\Omega_{l_{(6,5)}}^7$.

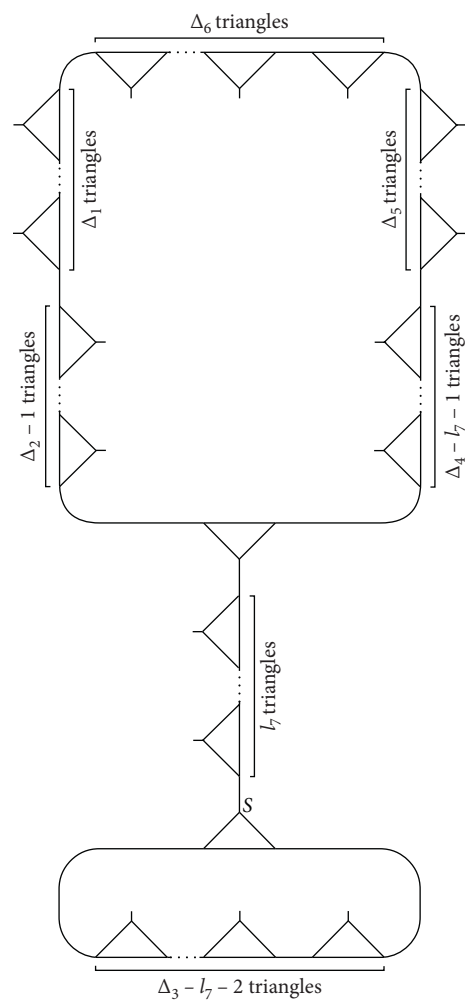


FIGURE 16: Homomorphic images $\Omega_{l_7}^8$.

by contracting e_{3n+1}^1 and $e_{3\Delta_1}^1$, implying that $e_{3n+1}^1 \leftrightarrow e_{3\Delta_1}^1$ is one of the pairs of contracted vertices for Ω_m^{18} . Then there must exist an element $w \in E_{18}$ such that $(e_{3m+1}^1)w = e_{3n+1}^1$ and $(e_{3\Delta_1}^1)w = e_{3\Delta_1}^1$. $e \in E_{18}$ is the only element such that $(e_{3\Delta_1}^1)e = e_{3\Delta_1}^1$ but $(e_{3m+1}^1)e \neq e_{3n+1}^1$. Thus, Ω_m^{18} and Ω_n^{18} are not the same, that is, by contracting e_{3m+1}^1 and $e_{3\Delta_1}^1$ to produce Ω_m^{18} , e_{3n+1}^1 and $e_{3\Delta_1}^1$ are not contracted. Now, if Ω_m^{18} and Ω_n^{18}

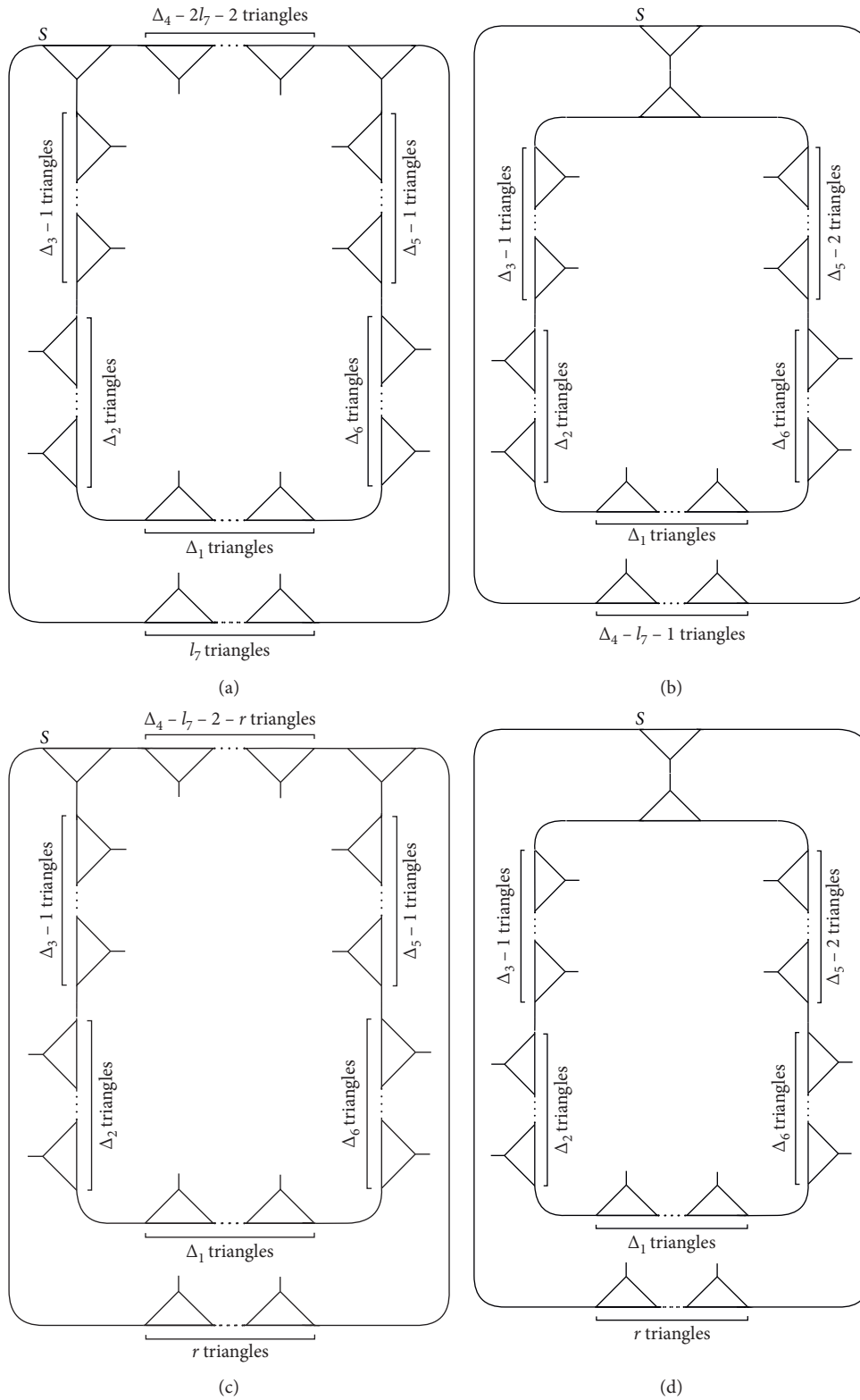


FIGURE 17: (a) Homomorphic images $\Omega_{l_7}^9$: $\Delta_4 - 2l_7 > 1$. (b) Homomorphic images $\Omega_{l_7}^9$: $\Delta_4 - 2l_7 = 1$. (c) Homomorphic images $\Omega_{l_7}^9$: $\Delta_4 - 2l_7 < 1$ and $\Delta_4 - l_7 > r + 1$. (d) Homomorphic images $\Omega_{l_7}^9$: $\Delta_4 - 2l_7 < 1$ and $\Delta_4 - l_7 = r + 1$.

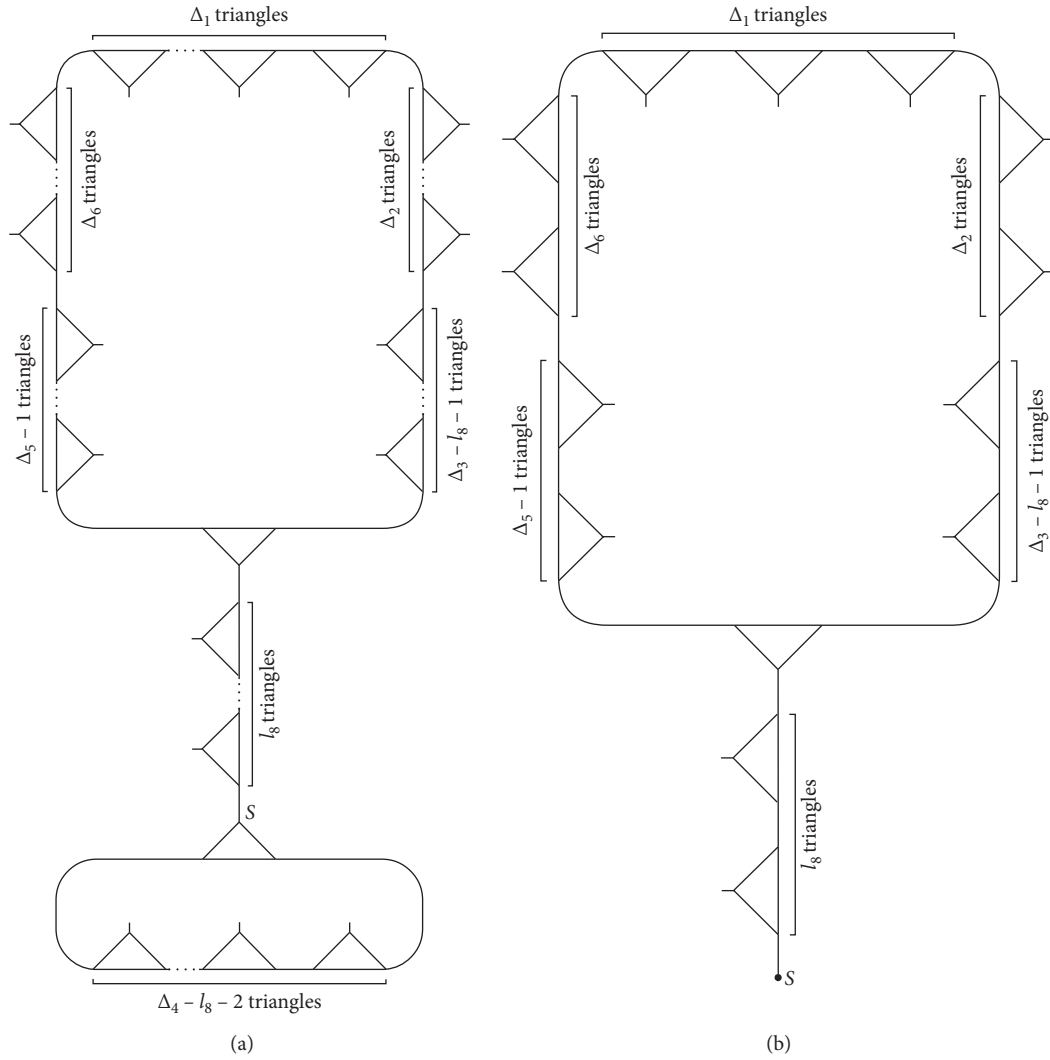


FIGURE 18: (a) Homomorphic images $\Omega_{l_8}^{10}$; $l_8 < \Delta_4 - 1$. (b) Homomorphic images $\Omega_{l_8}^{10}$; $l_8 = \Delta_4 - 1$.

are the same, then there must exist an element $w \in E_{18}$ such that $(e_{3m+1}^1)w = e_{3m+1}^{1*}$ and $(e_{3\Delta_1}^1)w = e_{3\Delta_1}^{1*}$. But there does not such an element exist in E_{18} . Thus, Ω_m^{18} is not the same as the mirror image of Ω_m^{18} , that is, by contracting e_{3m+1}^1 and $e_{3\Delta_1}^1$ to create Ω_m^{18} , e_{3m+1}^{1*} and $e_{3\Delta_1}^{1*}$ are not contracted. This implies that all the elements in H_{18} are distinct. Thus, $H_{18} = \{\Omega_{l_{14}}^{18}; l_{14} = \Delta_2 + 1, \Delta_2 + 2, \dots, \Delta_1 - 1\}$ gives $|H_{18}| = \Delta_1 - \Delta_2 - 1$.

To check does any element of H_{18} is the mirror image of itself, we suppose Ω_m^{18} is the same to its mirror image Ω_m^{18*} . Then by definition, there must exist an element $w \in E_{18}$ such that $(e_{3m+1}^1)w = e_{3m+1}^{1*}$ and $(e_{3\Delta_1}^1)w = e_{3\Delta_1}^{1*}$. But there does not such an element exist in E_{18} . Thus, Ω_m^{18} is not the same as its mirror image, that is, by contracting e_{3m+1}^1 and $e_{3\Delta_1}^1$ to create Ω_m^{18} , e_{3m+1}^{1*} and $e_{3\Delta_1}^{1*}$ are not contracted. Hence, there are

$$2 \times |E_{18}| \times |H_{18}| = 6(\Delta_2 + 2)(\Delta_1 - \Delta_2 - 1) \quad (7)$$

pairs of contracting vertices to produce all the homomorphic images in H_{18} .

$$\text{Let } \eta_1 = \begin{cases} 0, & \text{if } \Delta_1 + \Delta_4 = 0 \pmod{2} \\ 1, & \text{otherwise.} \end{cases} \quad \square$$

Lemma 19. *If we contract the vertices $e_{3l_{15}+1}^1$: $l_{15} = \Delta_4 + 1, \Delta_4 + 2, \dots, ((\Delta_1 + \Delta_4 - \eta_1)/2)$, with the vertex $e_{3\Delta_3}^3$ in the circuit Δ , then there arise $((\Delta_1 - \Delta_4 - \eta_1)/2)$ distinct homomorphic images of Δ and $3(\Delta_4 + 2)$ pairs of contracted vertices create each homomorphic image. Moreover, the number of total pairs of contracted vertices to generate all $((\Delta_1 - \Delta_4 - \eta_1)/2)$ and their mirror homomorphic images of Δ is $3(\Delta_4 + 2)(\Delta_1 - \Delta_4 - 1)$.*

Proof. Let

$H_{19} = \{\Omega_{l_{15}}^{19}; l_{15} = \Delta_4 + 1, \Delta_4 + 2, \dots, ((\Delta_1 + \Delta_4 - \eta_1)/2)\}$ (Figure 27) be the collection of homomorphic images of Δ acquired by the contraction of the vertices $e_{3l_{15}+1}^1$: $l_{15} = \Delta_4 + 1, \Delta_4 + 2, \dots, ((\Delta_1 + \Delta_4 - \eta_1)/2)$, with the vertex $e_{3\Delta_3}^3$ in Δ , where $e_{3l_{15}+1}^1$ and $e_{3\Delta_3}^3$ are fixed by the words $(pq)^{\Delta_1 - l_{15}} (pq^{-1})^{\Delta_6} (pq)^{\Delta_5} (pq^{-1})^{\Delta_4} (pq)^{\Delta_3} (pq^{-1})^{\Delta_2} (pq)^{l_{15}}$ and $(pq)^{\Delta_4} (pq^{-1})^{\Delta_5} (pq)^{\Delta_6} (pq^{-1})^{\Delta_1} (pq)^{\Delta_2} (pq^{-1})^{\Delta_3}$. It is easy to verify that $P_1 = q^{-1} (pq^{-1})^{\Delta_1 - l_{15} - 1} (pq)^{\Delta_2} (pq^{-1})^{\Delta_3}$ and $P_2 = (pq)^{\Delta_4} (pq^{-1})^{\Delta_5} (pq)^{\Delta_6} (pq^{-1})^{l_{15}} p$ are the possible paths between $e_{3l_{15}+1}^1$ and $e_{3\Delta_3}^3$ (Figure 4). This implies that,

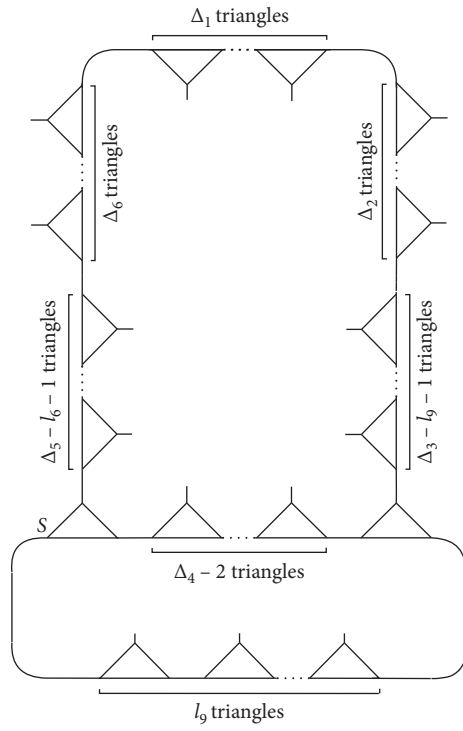


FIGURE 19: Homomorphic images $\Omega_{l_9}^{11}$.

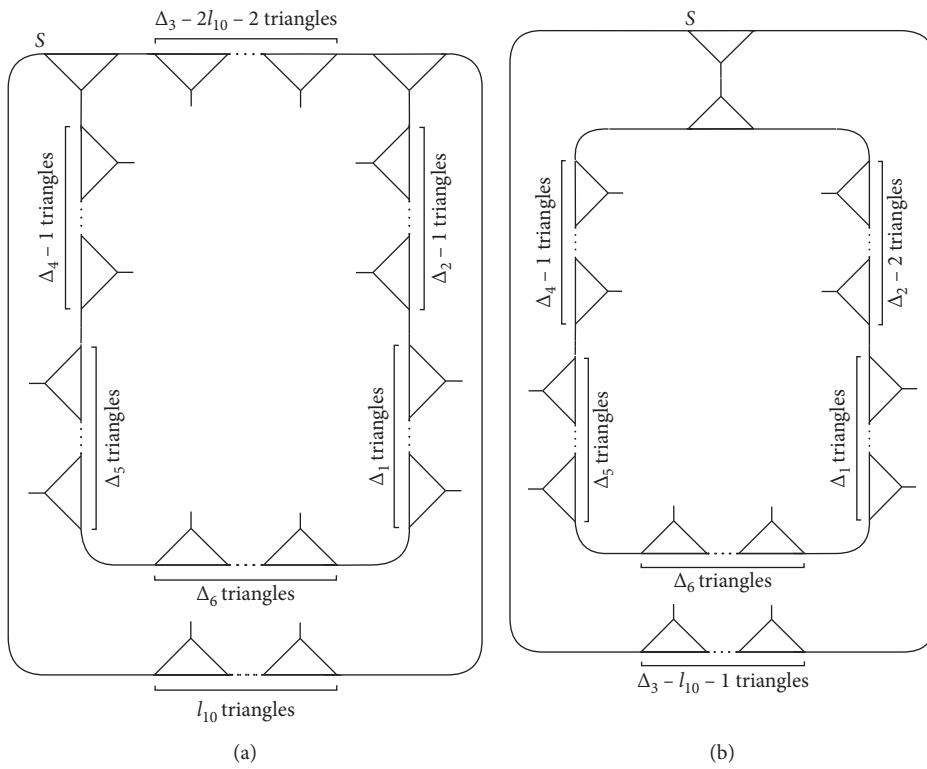


FIGURE 20: Continued.

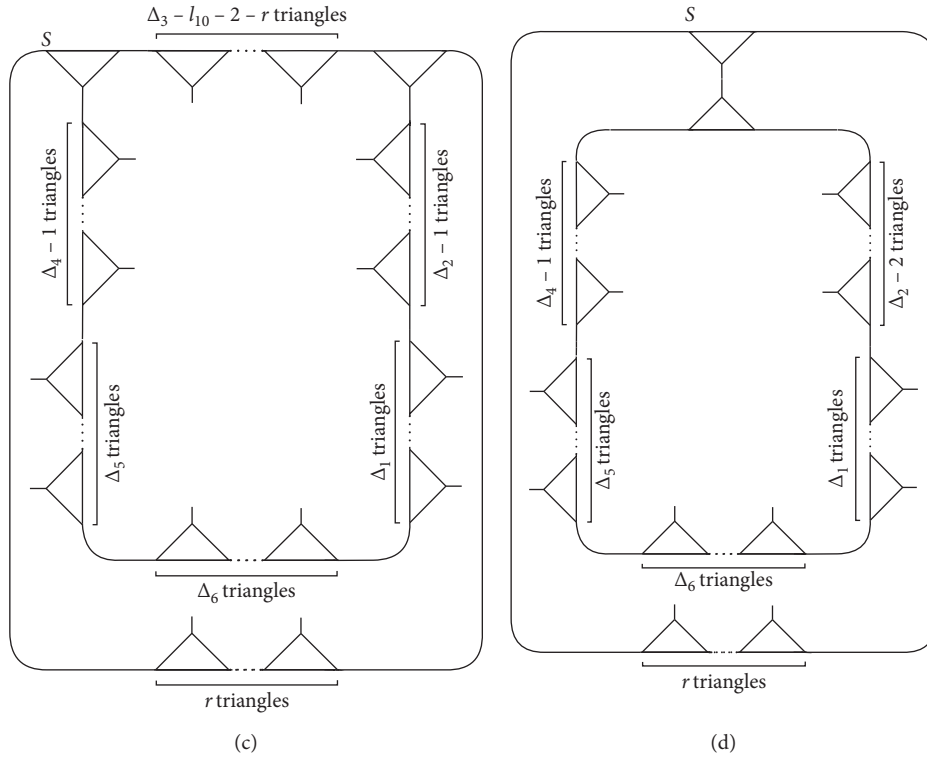


FIGURE 20: (a) Homomorphic images $\Omega_{l_{10}}^{12}$: $\Delta_3 - 2l_{10} > 1$. (b) Homomorphic images $\Omega_{l_{10}}^{12}$: $\Delta_3 - 2l_{10} = 1$. (c) Homomorphic images $\Omega_{l_{10}}^{12}$: $\Delta_3 - 2l_{10} < 1$ and $\Delta_3 - l_{10} > r + 1$. (d) Homomorphic images $\Omega_{l_{10}}^{12}$: $\Delta_3 - 2l_{10} < 1$ and $\Delta_3 - l_{10} = r + 1$.

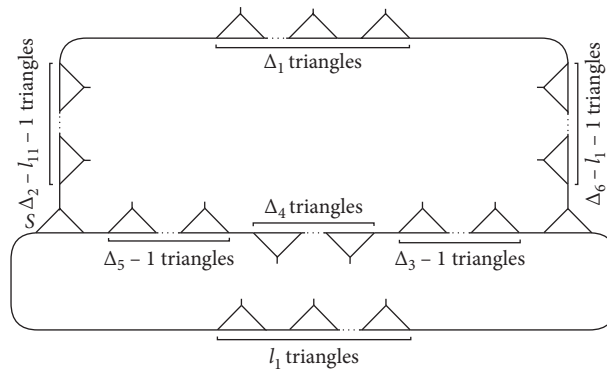


FIGURE 21: Homomorphic images $\Omega_{l_1}^{13}$.

for each l_{15} , the homomorphic image $\Omega_{l_{15}}^{19}$ has a vertex s fixed by P_1 and P_2 . Thus,

$$E_{19} = \{e, q, q^{-1}, p, pq, pq^{-1}, pqp, (pq)^2, pqpq^{-1}, \dots, (pq)^{\Delta_4} p, (pq)^{\Delta_4+1}, (pq)^{\Delta_4} pq^{-1}\} \quad (8)$$

is the family of elements in $\text{PSL}(2, \mathbb{Z})$ such that $\forall x \in E_{19}, \Delta$ contains the vertices $(e_{3l_{15}+1}^1)x$ and $(e_{3\Delta_3}^3)x$. This gives that the cardinality of E_{19} , that is, $3(\Delta_4 + 2)$ is the number of contracted pairs of vertices to produce the homomorphic image $\Omega_{l_{15}}^{19}$ (Theorem 2).

Now, we will prove that (i) for $\Delta_1 + \Delta_4 = 1 \pmod{2}$, all the homomorphic images in H_{19} are distinct and no one is

the mirror image of itself, and (ii) for $\Delta_1 + \Delta_4 = 0 \pmod{2}$, all the homomorphic images in H_{19} are distinct and only Ω_{m}^{19} is the mirror image of itself.

Let Ω_m^{19} and Ω_n^{19} be any two elements of H_{19} , then Ω_m^{19} is produced by contraction of e_{3m+1}^1 and $e_{3\Delta_3}^3$ and Ω_n^{19} is produced by contraction of e_{3n+1}^1 and $e_{3\Delta_3}^3$.

Suppose Ω_m^{19} and Ω_n^{19} are the same. This concludes that Ω_m^{19} is procurable also by contracting e_{3n+1}^1 and $e_{3\Delta_3}^3$, implying that $e_{3n+1}^1 \leftrightarrow e_{3\Delta_3}^3$ is one of the pairs of contracted vertices for Ω_m^{19} . Then there must exist an element $w \in E_{19}$ such that $(e_{3m+1}^1)w = e_{3n+1}^1$ and $(e_{3\Delta_3}^3)w = e_{3\Delta_3}^3$. $e \in E_{19}$ is the only element such that $(e_{3\Delta_3}^3)e = e_{3\Delta_3}^3$ but $(e_{3m+1}^1)e \neq e_{3m+1}^1$. Thus, Ω_m^{19} and Ω_n^{19} are not the same, that is, by contracting e_{3m+1}^1 and $e_{3\Delta_3}^3$ to produce Ω_m^{19} , e_{3n+1}^1 and $e_{3\Delta_3}^3$ are not contracted.

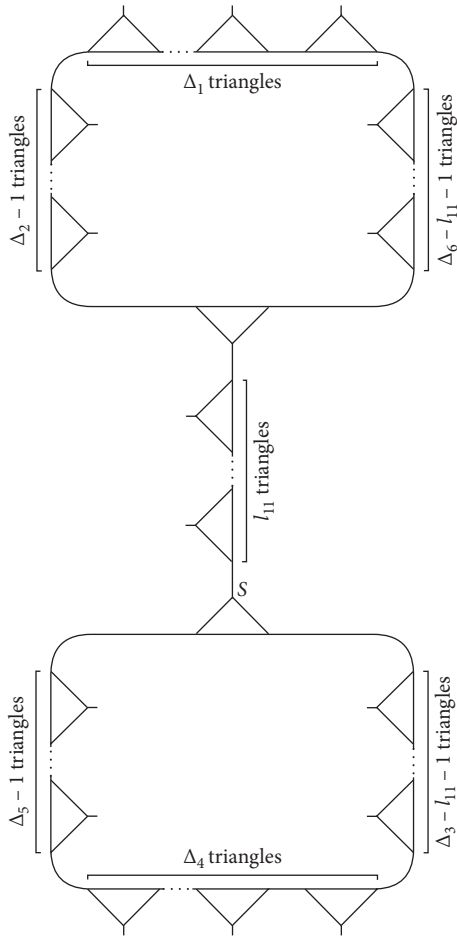


FIGURE 22: Homomorphic images $\Omega_{l_{11}}^{14}$.

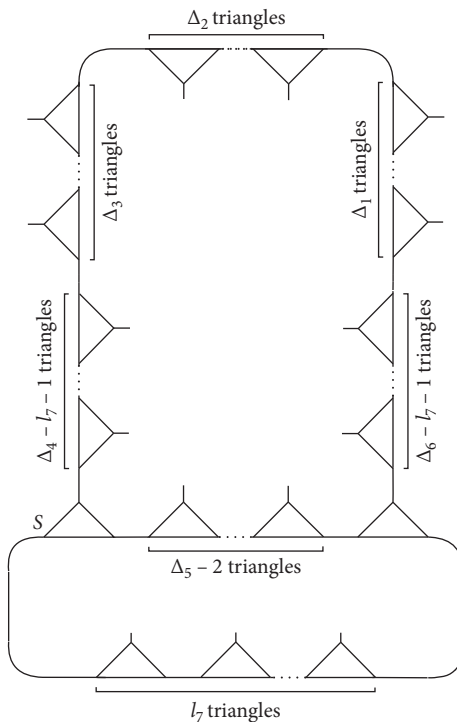


FIGURE 23: Homomorphic images $\Omega_{l_7}^{15}$.

Now, if Ω_m^{19} and Ω_n^{19*} are the same, then there must exist an element $w \in E_{19}$ such that $(e_{3m+1}^1)w = e_{3m+1}^{1*}$ and $(e_{3\Delta_3}^3)w = e_{3\Delta_3}^{3*}$. $(pq)^{\Delta_4}p \in E_{19}$ is the only element such that $(e_{3\Delta_3}^3)(pq)^{\Delta_4}p = e_{3\Delta_3}^{3*}$ and $(e_{3m+1}^1)(pq)^{\Delta_4}p = e_{3(\Delta_1+\Delta_4-m)+1}^{1*}$. This implies that Ω_m^{19} and Ω_n^{19} are the mirror images of each other if and only if $n = \Delta_1 + \Delta_4 - m$ and Ω_m^{19} is the mirror image of itself if and only if $m = \Delta_1 + \Delta_4 - m$, that is, $m = ((\Delta_1 + \Delta_4)/2)$. Now,

- (i) If $\Delta_1 + \Delta_4 = 1 \pmod{2}$, then $\forall m \in l_{15}$, $\Delta_1 + \Delta_4 - m > ((\Delta_1 + \Delta_4 - 1)/2)$, implying that $\Omega_{\Delta_1+\Delta_4-m}^{19} \notin H_{19}$. This states that no homomorphic image in H_{19} is the mirror image of other. Hence, all the homomorphic images in H_{19} are distinct. Thus, $H_{19} = \{\Omega_{l_{15}}^{19}; l_{15} = \Delta_4 + 1, \Delta_4 + 2, \dots, ((\Delta_1 + \Delta_4 - 1)/2)\}$ gives $|H_{19}| = ((\Delta_1 - \Delta_4 - 1)/2)$.

Also, $((\Delta_1 + \Delta_4)/2) > ((\Delta_1 + \Delta_4 - 1)/2)$ gives that no homomorphic image in H_{19} is the mirror image of itself. Hence, there are

$$2 \times |E_{19}| \times |H_{19}| = 6(\Delta_4 + 2) \left(\frac{\Delta_1 - \Delta_4 - 1}{2} \right) \tag{9}$$

$$= 3(\Delta_4 + 2)(\Delta_3 - \Delta_4 - 1)$$

pairs of contracting vertices to produce all the homomorphic images in H_{19} .

- (ii) If $\Delta_1 + \Delta_4 = 0 \pmod{2}$, then $\forall m \in (l_{15}/\{(\Delta_1 + \Delta_4)/2\})$, $\Delta_1 + \Delta_4 - m > ((\Delta_1 + \Delta_4)/2)$, implying that $\Omega_{\Delta_1+\Delta_4-m}^{19} \notin H_{19}$. This states that no homomorphic image in H_{19} is the mirror image of other. Hence, all the homomorphic images in H_{19} are distinct. Thus, $H_{19} = \{\Omega_{l_{15}}^{19}; l_{15} = \Delta_4 + 1, \Delta_4 + 2, \dots, ((\Delta_1 + \Delta_4)/2)\}$ gives $|H_{19}| = ((\Delta_1 - \Delta_4)/2)$.

For $m = ((\Delta_1 + \Delta_4)/2)$, we have $\Delta_1 + \Delta_4 - m = ((\Delta_1 + \Delta_4)/2) \in l_{15}$ gives $\Omega_{(\Delta_1+\Delta_4)/2}^{19} \in H_{19}$ is the mirror image of itself. Hence, there are

$$2 \times |E_{19}| \times (|H_{19}| - 1) + |E_{19}| = 6(\Delta_4 + 2) \left(\frac{\Delta_1 - \Delta_4}{2} - 1 \right) \tag{10}$$

$$+ 3(\Delta_4 + 2) = 3(\Delta_4 + 2)(\Delta_3 - \Delta_4 - 1)$$

pairs of contracting vertices to produce all the homomorphic images in H_{19} .

Let $k_2 \in \{2, 3\}$. □

Lemma 20. *If we contract the vertices $e_{3l_{(3,k_2)}^{k_2}+1}^{k_2}; l_{(3,k_2)} = \Delta_4 + 1, \Delta_4 + 2, \dots, \Delta_{k_2} - 1$, with the vertex $e_{3\Delta_3}^3$ in the circuit Δ , then for each k_2 , there arise $\Delta_{k_2} - \Delta_4 - 1$ distinct homomorphic images of Δ and $3(\Delta_4 + 2)$ pairs of contracted vertices create each homomorphic image. Moreover, the number of total pairs of contracted vertices to generate all $\Delta_{k_2} - \Delta_4 - 1$ and their mirror homomorphic images of Δ is $6(\Delta_4 + 2)(\Delta_{k_2} - \Delta_4 - 1)$.*

For a fix value of k_2 , let $H_{20}^{k_2} = \{\Omega_{l_{(3,k_2)}^{k_2}}^{20}; l_{(3,k_2)} = \Delta_4 + 1, \Delta_4 + 2, \dots, \Delta_{k_2} - 1\}$ be the collection of homomorphic images of Δ acquired by the contraction of the vertices $e_{3l_{(3,k_2)}^{k_2}}$

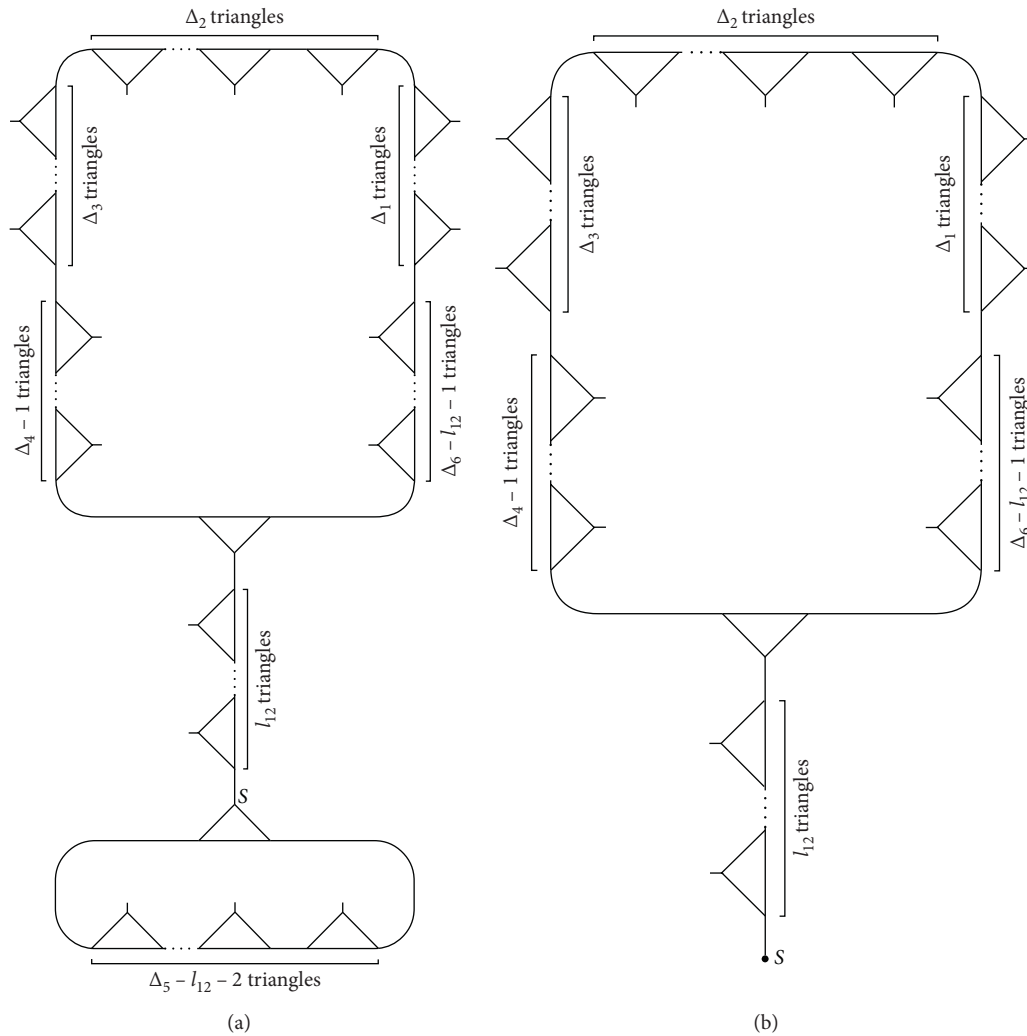


FIGURE 24: (a) Homomorphic images $\Omega_{l_{12}}^{16}$: $l_{12} < \Delta_5 - 1$. (b) Homomorphic images $\Omega_{l_{12}}^{16}$: $l_{12} = \Delta_5 - 1$.

$+1^{k_2}$: $l_{(3,k_2)} = \Delta_4 + 1, \Delta_4 + 2, \dots, \Delta_{k_2} - 1$, with the vertex $e_{3\Delta_3}^3$ in Δ . Figures 28 and 29 present $H_3^{k_2}$ graphically. From all the homomorphic images presented in these figures, it is not intricate to check that no one is the mirror image of itself.

This lemma can be proved by using the same procedure as that for Lemma 18.

Lemma 21. If we contract the vertices $e_{3l_{16}+1}^2$: $l_{16} = \Delta_3 + 1, \Delta_3 + 2, \dots, \Delta_2 - 1$, with the vertex $e_{3\Delta_4}^4$ in the circuit Δ , then there arise $\Delta_2 - \Delta_3 - 1$ distinct homomorphic images of Δ and $3(\Delta_3 + 2)$ pairs of contracted vertices create each homomorphic image. Moreover, the number of total pairs of contracted vertices to generate all $\Delta_2 - \Delta_3 - 1$ and their mirror homomorphic images of Δ is $6(\Delta_3 + 2)(\Delta_2 - \Delta_3 - 1)$.

Let $H_{21} = \{\Omega_{l_{16}}^{21}; l_{16} = \Delta_3 + 1, \Delta_3 + 2, \dots, \Delta_2 - 1\}$ be the collection of homomorphic images of Δ acquired by the contraction of the vertices $e_{3l_{16}+1}^2$: $l_{16} = \Delta_3 + 1, \Delta_3 + 2, \dots, \Delta_2 - 1$, with the vertex $e_{3\Delta_4}^4$ in Δ . Figure 30 presents H_{21} graphically. From all the homomorphic images presented in Figure 30, it is not intricate to check

that no one is the mirror image of itself. This lemma can be proved by using the same procedure as that for Lemma 18.

Let $k_3 \in \{1, 2\}$.

Lemma 22. If we contract the vertices $e_{3l_{(4,k_3)}+1}^{k_3}$: $l_{(4,k_3)} = \Delta_5 + 1, \Delta_5 + 2, \dots, \Delta_{k_3} - 1$, with the vertex $e_{3\Delta_6}^6$ in the circuit Δ , then for each k_3 , there arise $\Delta_{k_3} - \Delta_5 - 1$ distinct homomorphic images of Δ and $3(\Delta_5 + 2)$ pairs of contracted vertices create each homomorphic image. Moreover, the number of total pairs of contracted vertices to generate all $\Delta_{k_3} - \Delta_5 - 1$ and their mirror homomorphic images of Δ is $6(\Delta_5 + 2)(\Delta_{k_3} - \Delta_5 - 1)$.

For a fix value of k_3 , let $H_{22}^{k_3} = \{\Omega_{l_{(4,k_3)}}^{22}; l_{(4,k_3)} = \Delta_5 + 1, \Delta_5 + 2, \dots, \Delta_{k_3} - 1\}$ be the collection of homomorphic images of Δ acquired by the contraction of the vertices $e_{3l_{(4,k_3)}+1}^{k_3}$: $l_{(4,k_3)} = \Delta_5 + 1, \Delta_5 + 2, \dots, \Delta_{k_3} - 1$, with the vertex $e_{3\Delta_6}^6$ in Δ . Figures 31 and 32 present $H_{22}^{k_3}$ graphically. From all the homomorphic images presented in these figures, it is not intricate to check that no

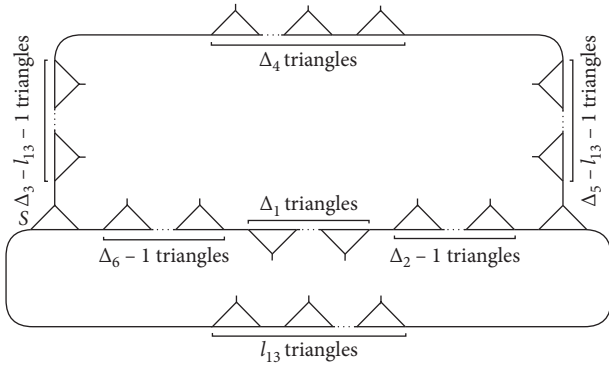


FIGURE 25: Homomorphic images $\Omega_{l_{13}}^{17}$.

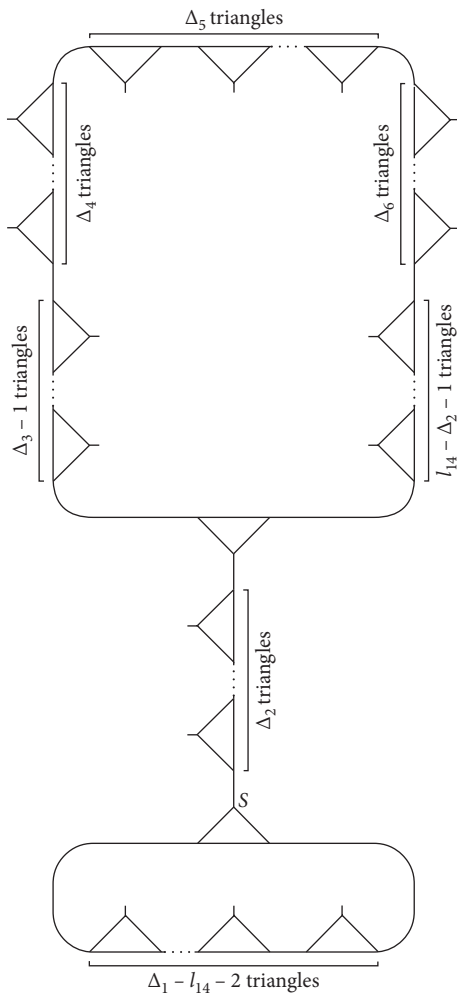


FIGURE 26: Homomorphic images $\Omega_{l_{14}}^{18}$.

one is the mirror image of itself. This lemma can be proved by using the same procedure as that for Lemma 18.

Let $k_2 \in \{2, 3\}$.

Lemma 23. *If we contract the vertices $e_{3l_4+1}^1; l_4 = 1, 2, \dots, \Delta_1 - 1$, with the vertices $e_{3l_{(5,k_2)}}^{k_2}; l_{(5,k_2)} = 1, 2, \dots, \Delta_{k_2} - 1$, in the circuit Δ , then for each k_2 , there arise $(\Delta_1 - 1)(\Delta_{k_2} - 1)$*

distinct homomorphic images of Δ and 6 pairs of contracted vertices create each homomorphic image. Moreover, the number of total pairs of contracted vertices to generate all $(\Delta_1 - 1)(\Delta_{k_2} - 1)$ and their mirror homomorphic images of Δ is $12(\Delta_1 - 1)(\Delta_{k_2} - 1)$.

Proof. For $k_2 = 2$, let $H_{23}^2 = \left\{ \Omega_{(l_4, l_{(5,2)})}^{23}; l_4 = 1, 2, \dots, \Delta_1 - 1; l_{(5,2)} = 1, 2, \dots, \Delta_2 - 1 \right\}$ (Figure 33) be the collection of homomorphic images of Δ acquired by the contraction of the vertices $e_{3l_4+1}^1$ with the vertex $e_{3l_{(5,2)}}^2$ in Δ , where $e_{3l_4+1}^1$ and $e_{3l_{(5,2)}}^2$ are fixed by the words $(pq)^{\Delta_4} (pq^{-1})^{\Delta_6} (pq)^{\Delta_5} (pq^{-1})^{\Delta_4} (pq)^{\Delta_3} (pq^{-1})^{\Delta_2} (pq)^{\Delta_1 - l_4}$ and $(pq^{-1})^{\Delta_2 - l_{(5,2)}} (pq)^{\Delta_1} (pq^{-1})^{\Delta_6} (pq)^{\Delta_5} (pq^{-1})^{\Delta_4} (pq)^{\Delta_3} (pq^{-1})^{l_{(5,2)}}$. It is easy to verify that $P_1 = (pq^{-1})^{\Delta_2 - l_{(5,2)}} (pq)^{\Delta_1 - l_4}$ and $P_2 = (pq)^{l_4} (pq^{-1})^{\Delta_6} (pq)^{\Delta_5} (pq^{-1})^{\Delta_4} (pq)^{\Delta_3} (pq^{-1})^{l_{(5,2)}}$ are the possible paths between $e_{3l_4+1}^1$ and $e_{3l_{(5,2)}}^2$ (Figure 4). This implies that the homomorphic image $\Omega_{(l_4, l_{(5,2)})}^{23}$ has a vertex x fixed by P_1 and P_2 . Thus,

$$E_{23}^2 = \{e, q, q^{-1}, p, pq, pq^{-1}\} \tag{11}$$

is the family of elements in $\text{PSL}(2, \mathbb{Z})$ such that $\forall x \in E_{23}^2, \Delta$ contains the vertices $(e_{3l_4+1}^1)x$ and $(e_{3l_{(5,2)}}^2)x$. This gives that the cardinality of E_{23}^2 , that is, 6 is the number of contracted pairs of vertices to produce the homomorphic image $\Omega_{(l_4, l_{(5,2)})}^{23}$ (Theorem 2).

Now, we will prove that all the homomorphic images in H_{23}^2 are distinct and no one is the mirror image of itself.

Let $\Omega_{(m_1, m_2)}^{23}$ and $\Omega_{(n_1, n_2)}^{23}$ be any two elements of H_{23}^2 , then $\Omega_{(m_1, m_2)}^{23}$ is produced by contraction of $e_{3m_1+1}^1$ and $e_{3m_2}^2$ and $\Omega_{(n_1, n_2)}^{23}$ is produced by contraction of $e_{3n_1+1}^1$ and $e_{3n_2}^2$.

Suppose $\Omega_{(m_1, m_2)}^{23}$ and $\Omega_{(n_1, n_2)}^{23}$ are the same. This concludes that $\Omega_{(m_1, m_2)}^{23}$ is procurable also by contracting $e_{3n_1+1}^1$ and $e_{3n_2}^2$, implying that $e_{3n_1+1}^1 \leftrightarrow e_{3n_2}^2$ is one of the pairs of contracted vertices for $\Omega_{(m_1, m_2)}^{23}$. Then there must exist an element $w \in E_{23}^2$ such that $(e_{3m_1+1}^1)w = e_{3n_1+1}^1$ and $(e_{3m_2}^2)w = e_{3n_2}^2$. $pq^{-1} \in E_5^2$ is the only element such that $(e_{3m_2}^2)pq^{-1} = e_{3(m_2+1)}^2$ but $(e_{3m_1+1}^1)pq^{-1} \neq e_{3n_1+1}^1$. Thus, $\Omega_{(m_1, m_2)}^{23}$ and $\Omega_{(n_1, n_2)}^{23}$ are not the same, that is, by contracting $e_{3m_1+1}^1$ and $e_{3m_2}^2$ to produce $\Omega_{(m_1, m_2)}^{23}$, $e_{3n_1+1}^1$ and $e_{3n_2}^2$ are not contracted. Now, if $\Omega_{(m_1, m_2)}^{23}$ and $\Omega_{(n_1, n_2)}^{23*}$ are the same, then there must exist an element $w \in E_{23}^2$ such that $(e_{3m_1+1}^1)w = e_{3n_1+1}^{1*}$ and $(e_{3m_2}^2)w = e_{3n_2}^{2*}$. $p \in E_{23}^2$ is the only element such that $(e_{3m_1+1}^1)p = e_{3(\Delta_1 - m_1) + 1}^{1*}$ but $(e_{3m_2}^2)p \neq e_{3n_2}^{2*}$. This implies that $\Omega_{(m_1, m_2)}^{23}$ and $\Omega_{(n_1, n_2)}^{23*}$ are not the mirror images of each other, that is, by contracting $e_{3m_1+1}^1$ and $e_{3m_2}^2$ to produce $\Omega_{(m_1, m_2)}^{23}$, $e_{3n_1+1}^{1*}$ and $e_{3n_2}^{2*}$ are not contracted. Hence, all the homomorphic images in H_{23}^2 are distinct. Thus,

$$H_{23}^2 = \left\{ \Omega_{(l_4, l_{(5,2)})}^{23}; l_4 = 1, 2, \dots, \Delta_1 - 1; l_{(5,2)} = 1, 2, \dots, \Delta_2 - 1 \right\}$$

gives $|H_{23}^2| = (\Delta_1 - 1)(\Delta_2 - 1)$.

Suppose $\Omega_{(m_1, m_2)}^{23}$ is the mirror image of itself, then there must exist an element $w \in E_{23}^2$ such that $(e_{3m_1+1}^1)w = e_{3m_1+1}^{1*}$ and $(e_{3m_2}^2)w = e_{3m_2}^{2*}$. $p \in E_{23}^2$ is the only element such that

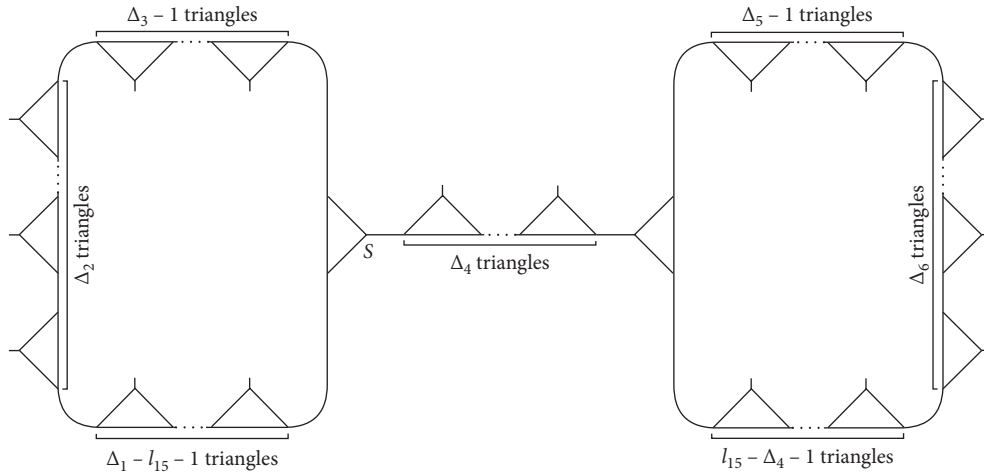


FIGURE 27: Homomorphisms $\Omega_{l_{15}}^{19}$.

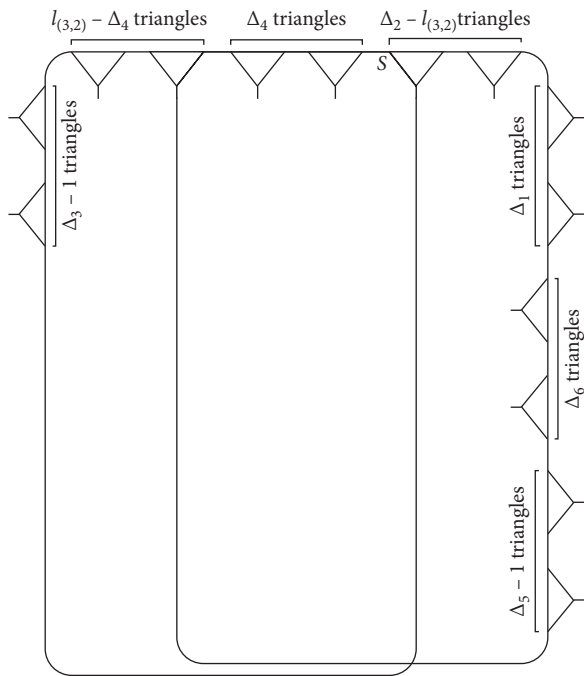


FIGURE 28: Homomorphisms $\Omega_{l_{(3,2)}}^{20}$.

$(e_{3m_1+1}^1)p = e_{3(\Delta_1-m_1)+1}^{1*}$ but $(e_{3m_2}^2)p \neq e_{3m_2}^{2*}$. This implies that $\Omega_{(m_1, m_2)}^{23}$ is not the same as $\Omega_{(m_1, m_2)}^{23*}$, that is, by contracting $e_{3m_1+1}^1$ and $e_{3m_2}^2$ to produce $\Omega_{(m_1, m_2)}^{23}$, $e_{3m_1+1}^{1*}$ and $e_{3m_2}^{2*}$ are not contracted.

Hence, there are

$$2 \times |E_{23}^2| \times |H_{23}^2| = 12(\Delta_1 - 1)(\Delta_2 - 1) \quad (12)$$

pairs of contracting vertices to produce all the homomorphisms in H_{23}^2 .

We can prove this lemma for $k_2 = 3$ (Figure 34) in similar way as that for $k_2 = 2$.

Let $\eta_2 = \begin{cases} 0 & \text{if } \Delta_4 = 0 \pmod{2} \\ 1 & \text{otherwise} \end{cases}$ and $\eta_3 = \begin{cases} 0 & \text{if } \Delta_1 = 0 \pmod{2} \\ 1 & \text{otherwise} \end{cases}$. □

Lemma 24. *If we contract the vertices $e_{3l_{17}+1}^1: l_{17} = \begin{cases} 1, 2, \dots, ((\Delta_1 - \eta_3)/2), & \text{if } l_{18} = (\Delta_4/2) \\ 1, 2, \dots, \Delta_1 - 1 & \text{otherwise} \end{cases}$, with the vertices $e_{3l_{18}}^4: l_{18} = 1, 2, \dots, ((\Delta_4 - \eta_2)/2)$, in the circuit Δ , then there arise $\begin{cases} (1/2)(\Delta_1 - 1)(\Delta_4 - 1) & \text{if } \Delta_4 = 1 \pmod{2} \\ (1/2)[(\Delta_1 - 1)(\Delta_4 - 1) + 1 - \eta_3] & \text{if } \Delta_4 = 0 \pmod{2} \end{cases}$ distinct homomorphisms of Δ and 6 pairs of contracted vertices create each homomorphism. Moreover, the number of total pairs of contracted vertices to generate all these homomorphisms and their mirror homomorphisms of Δ is $6(\Delta_1 - 1)(\Delta_4 - 1)$.*

Proof. Let $H_{24} = \{\Omega_{(l_{17}, l_{18})}^{24}; l_{17} = \{1, 2, \dots, ((\Delta_1 - \eta_3)/2), \text{ if } l_{18} = (\Delta_4/2), 1, 2, \dots, \Delta_1 - 1 \text{ otherwise}\}$ (Figure 35) be the collection of homomorphisms of Δ acquired by the contraction of the vertices $e_{3l_{17}+1}^1$ with the vertices $e_{3l_{18}}^4$ in Δ , where $e_{3l_{17}+1}^1$ and $e_{3l_{18}}^4$ are fixed by the words $(pq)^{l_{17}}(pq^{-1})^{\Delta_6}(pq)^{\Delta_5}(pq^{-1})^{\Delta_4}(pq)^{\Delta_3}(pq^{-1})^{\Delta_2}(pq)^{\Delta_1-l_{18}}$ and $(pq^{-1})^{\Delta_4-l_{18}}(pq)^{\Delta_3}(pq^{-1})^{\Delta_2}(pq)^{\Delta_1-l_{17}}$ are the possible paths between $e_{3l_{17}+1}^1$ and $e_{3l_{18}}^4$ (Figure 4). This implies that the homomorphism $\Omega_{(l_{17}, l_{18})}^{24}$ has a vertex s fixed by P_1 and P_2 . Thus,

$$E_{24} = \{e, q, q^{-1}, p, pq, pq^{-1}\} \quad (13)$$

is the family of elements in $\text{PSL}(2, \mathbb{Z})$ such that $\forall x \in E_{24}, \Delta$ contains the vertices $(e_{3l_{17}+1}^1)x$ and $(e_{3l_{18}}^4)x$. This gives that the cardinality of E_{24} , that is, 6 is the number of contracted pairs of vertices to produce the homomorphism $\Omega_{(l_{17}, l_{18})}^{24}$ (Theorem 2).

Now, we prove that (i) for $\Delta_4 = 0 \pmod{2}$, all the elements in H_{24} are distinct and no one is the mirror image of itself, and (ii) for $\Delta_4 = 1 \pmod{2}$, all the elements in H_{24} are distinct and the homomorphism $\Omega_{((\Delta_1/2), (\Delta_4/2))}^{24}$ is the mirror image of itself.

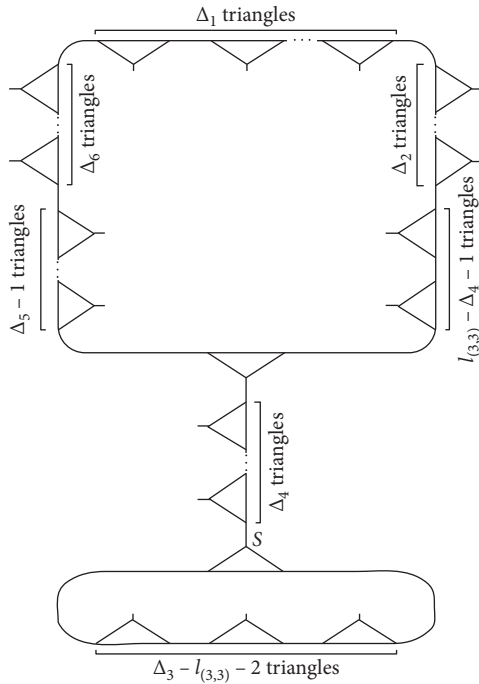


FIGURE 29: Homomorphic images $\Omega_{l_{(3,3)}}^{20}$.

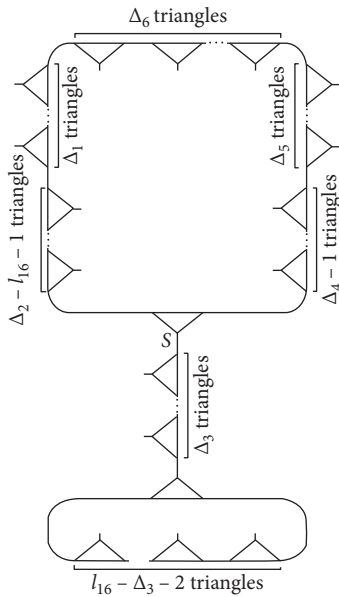


FIGURE 30: Homomorphic images $\Omega_{l_{16}}^{21}$.

Suppose $\Omega_{(m_1, m_2)}^{24}$ and $\Omega_{(n_1, n_2)}^{24}$ are the same. This concludes that $\Omega_{(m_1, m_2)}^{24}$ is procurable also by contracting $e_{3m_1+1}^1$ and $e_{3m_2}^4$, implying that $e_{3m_1+1}^1 \leftrightarrow e_{3m_2}^4$ is one of the pairs of contracted vertices for $\Omega_{(m_1, m_2)}^{24}$. Then there must exist an element $w \in E_{24}$ such that $(e_{3m_1+1}^1)w = e_{3m_1+1}^1$ and $(e_{3m_2}^4)w = e_{3m_2}^4$. $pq^{-1} \in E_{24}$ is the only element such that $(e_{3m_2}^4)pq^{-1} = e_{3(m_2+1)}^4$ but $(e_{3m_1+1}^1)pq^{-1} \neq e_{3m_1+1}^1$. Thus, $\Omega_{(m_1, m_2)}^{24}$ and $\Omega_{(n_1, n_2)}^{24}$ are not the same, that is, by contracting $e_{3m_1+1}^1$ and $e_{3m_2}^4$ to produce $\Omega_{(m_1, m_2)}^{24}$, $e_{3m_1+1}^1$ and $e_{3m_2}^4$ are not contracted. Now, if $\Omega_{(m_1, m_2)}^{24}$ and $\Omega_{(n_1, n_2)}^{24}$ are the same, then there must exist an element $w \in E_{24}$ such that $(e_{3m_1+1}^1)w =$

$e_{3m_1+1}^{1*}$ and $(e_{3m_2}^4)w = e_{3m_2}^{4*}$. $p \in E_{24}$ is the only element such that $(e_{3m_1+1}^1)p = e_{3(\Delta_1 - m_1) + 1}^{1*}$ and $(e_{3m_2}^4)p = e_{3(\Delta_4 - m_2)}^{4*}$. This implies that $\Omega_{(m_1, m_2)}^{24}$ and $\Omega_{(n_1, n_2)}^{24}$ are the mirror images of each other if and only if $n_1 = \Delta_1 - m_1$ and $n_2 = \Delta_4 - m_2$, that is, by contracting $e_{3m_1+1}^1$ and $e_{3m_2}^4$ to produce $\Omega_{(m_1, m_2)}^{24}$, $e_{3m_1+1}^{1*}$ and $e_{3m_2}^{4*}$ are also contracted and the homomorphic image $\Omega_{(m_1, m_2)}^{24}$ is the mirror image of itself if and only if $m_1 = \Delta_1 - m_1$ and $m_2 = \Delta_4 - m_2$ that is $m_1 = (\Delta_1/2)$ and $m_2 = (\Delta_4/2)$. Now,

- (1) If $\Delta_4 = 1 \pmod{2}$ then $\forall m_2 \in l_{18}$, we get $\Delta_4 - m_2 > ((\Delta_4 - 1)/2)$ implies $\Omega_{(\Delta_1 - m_1, \Delta_4 - m_2)}^{24} \notin H_{24}$. This indicates that no homomorphic image in H_{24} is the mirror image of other. Hence, all the elements in H_{24} are distinct. Thus, $H_{24} = \{\Omega_{(l_{17}, l_{18})}^{24}; l_{17} = \{1, 2, \dots, ((\Delta_1 - \eta_3)/2) \text{ if } l_{18} = (\Delta_4/2), l_{18} = 1, 2, \dots, ((\Delta_4 - \eta_2)/2)1, 2, \dots, \Delta_1 - 1 \text{ otherwise}\}$, implying that

$$|H_{24}| = \frac{1}{2} (\Delta_1 - 1)(\Delta_4 - 1). \quad (14)$$

Also, $(\Delta_4/2) > ((\Delta_4 - 1)/2)$ implies no homomorphic image in H_{24} is the mirror image of itself. Hence, there are

$$2 \times |E_{24}| \times |H_{24}| = 6(\Delta_1 - 1)(\Delta_4 - 1) \quad (15)$$

pairs of contracting vertices to produce all the homomorphic images in H_{24} .

- (2) If $\Delta_4 = 0 \pmod{2}$, then only for $m_2 = (\Delta_4/2)$, $\Delta_4 - m_2 = (\Delta_4/2) \in l_{18}$ and $\forall m_1 \in l_{17} \{ \Delta_1/2 \}$, $\Delta_1 - m_1 \notin l_{17}$, implying that $\Omega_{(\Delta_1 - m_1, (\Delta_4/2))}^{24} \notin H_{24}$. Hence, all the elements in H_{24} are distinct. Thus, $H_{24} = \{\Omega_{(l_{17}, l_{18})}^{24}; l_{17} = \{1, 2, \dots, ((\Delta_1 - \eta_3)/2) \text{ if } l_{18} = (\Delta_4/2); l_{18} = 1, 2, \dots, ((\Delta_4 - \eta_2)/2)1, 2, \dots, \Delta_1 - 1 \text{ otherwise}\}$, implying that

$$\begin{aligned} |H_{24}| &= \frac{1}{2} (\Delta_1 - 1)(\Delta_4 - 2) + \frac{1}{2} (\Delta_1 - \eta_3) \\ &= \frac{1}{2} [(\Delta_1 - 1)(\Delta_4 - 1) + 1 - \eta_3]. \end{aligned} \quad (16)$$

Now,

- (a). If Δ_1 is odd, then $(\Delta_1/2) \notin l_{17}$, implying that $\Omega_{((\Delta_1/2), (4/2))}^{24} \notin H_{24}$. So, no homomorphic image in H_{24} is the mirror image of itself. Hence, there are

$$2 \times |E_{24}| \times |H_{24}| = 6(\Delta_1 - 1)(\Delta_4 - 1) \quad (17)$$

pairs of contracting vertices to produce all the homomorphic images in H_{24} .

- (b) If Δ_1 is even, then $(\Delta_1/2) \in l_{17}$, implying that $\Omega_{((\Delta_1/2), (\Delta_4/2))}^{24} \in H_{24}$ is the mirror image of itself. Hence, there are

$$2 \times |E_{24}| \times (|H_{24}| - 1) + |E_{24}| = 6(\Delta_1 - 1)(\Delta_4 - 1) \quad (18)$$

pairs of contracting vertices to produce all the homomorphic images in H_{24} .

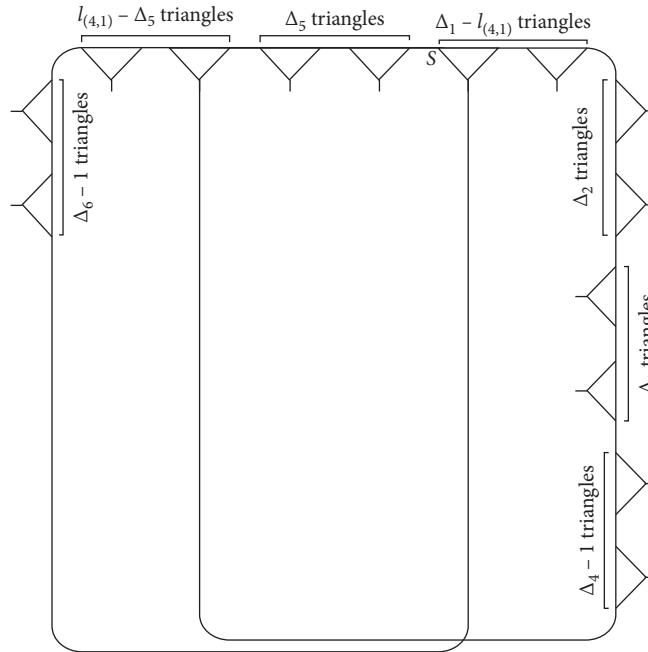


FIGURE 31: Homomorphic images $\Omega_{l_{(4,1)}}^{22}$.

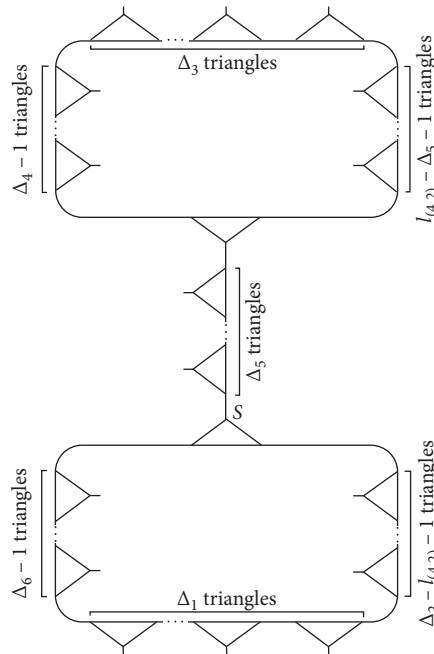


FIGURE 32: Homomorphic images $\Omega_{l_{(4,2)}}^{22}$.

Let $k_1 \in \{3, 4, 5\}$.

□

Lemma 25. *If we contract the vertices $e_{3l_5+1}^{k_1}$; $l_5 = 1, 2, \dots, \Delta_2 - 1$, with the vertices $e_{3l_{(6,k_1)}}^{k_1}$; $l_{(6,k_1)} = 1, 2, \dots, \Delta_{k_1} - 1$, in the circuit Δ , then for each k_5 , there arise $(\Delta_2 - 1)(\Delta_{k_1} - 1)$ distinct homomorphic images of Δ and 6 pairs of contracted vertices create each homomorphic image. Moreover, the*

number of total pairs of contracted vertices to generate all $(\Delta_2 - 1)(\Delta_{k_1} - 1)$ and their mirror homomorphic images of Δ is $12(\Delta_2 - 1)(\Delta_{k_1} - 1)$.

For a fix value of k_1 , let $H_{25}^{k_1} = \{\Omega_{(l_5, l_{(6,k_1)})}^{25}; l_5 = 1, 2, \dots, \Delta_2 - 1; l_{(6,k_1)} = 1, 2, \dots, \Delta_{k_1} - 1\}$ be the collection of homomorphic images of Δ acquired by the contraction of the vertices $e_{3l_5+1}^{k_1}$ with the vertices $e_{3l_{(6,k_1)}}^{k_1}$ in Δ . Figures 36, 37, and

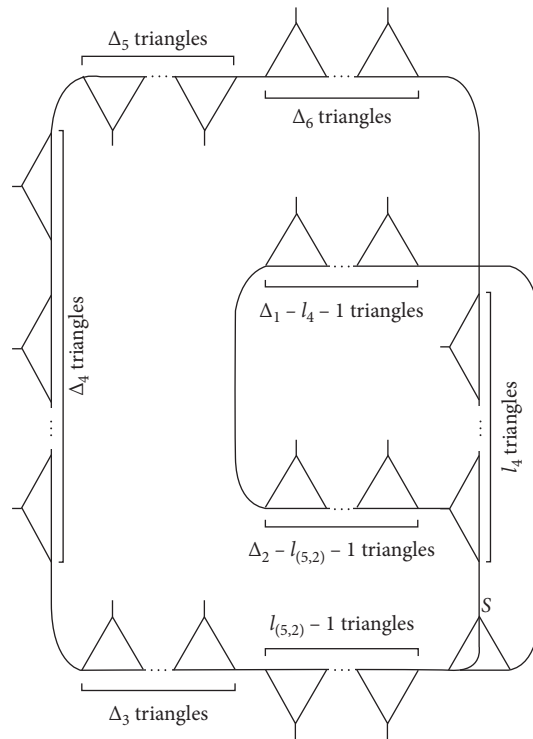


FIGURE 33: Homomorphic images $\Omega_{(l_4, l_{(5,2)})}^{23}$.

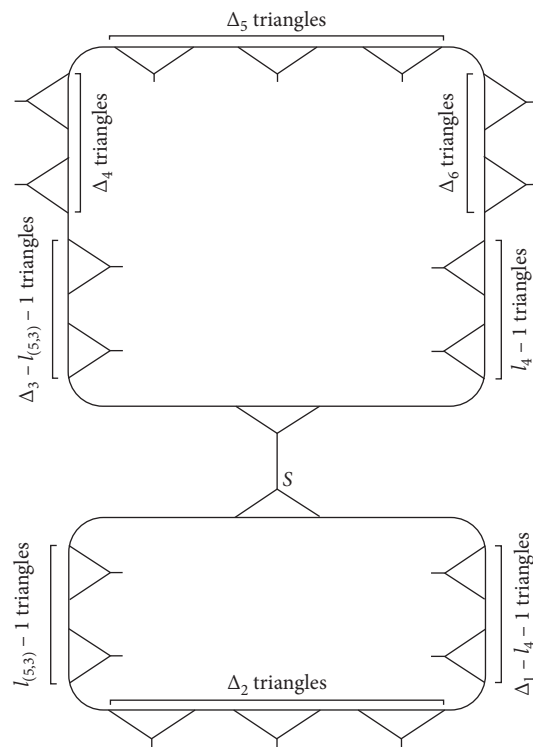


FIGURE 34: Homomorphic images $\Omega_{(l_4, l_{(5,3)})}^{23}$.

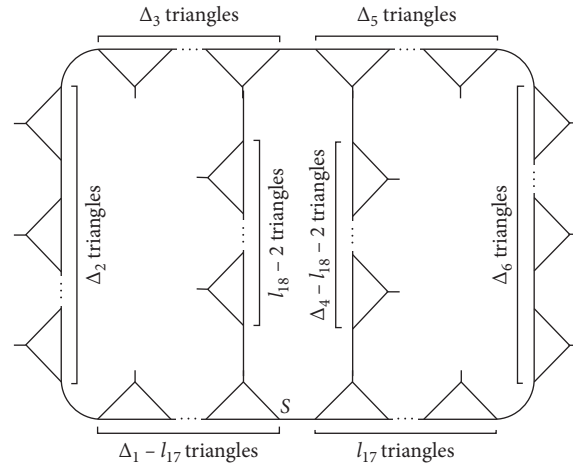


FIGURE 35: Homomorphic images $\Omega_{(l_{17}, l_{18})}^{24}$.

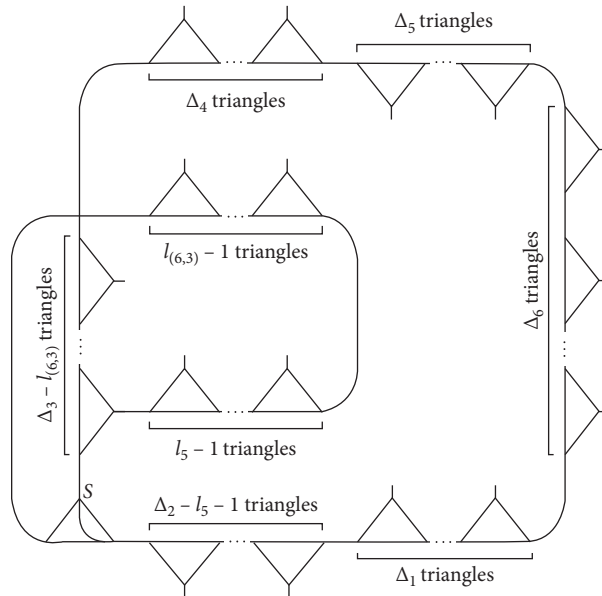


FIGURE 36: Homomorphic images $\Omega_{(l_5, l_{(6,3)})}^{25}$.

38 present $H_{25}^{k_1}$ graphically. From all the homomorphic images presented in these figures, it is not intricated to check that no one is the mirror image of itself.

This lemma can be proved by using the same procedure as that for Lemma 23.

Lemma 26. If we contract the vertices $e_{3l_{13}+1}^3: l_{13} = 1, 2, \dots, \Delta_3 - 1$, with the vertices $e_{3l_7}^4: l_7 = 1, 2, \dots, \Delta_4 - 1$, in the circuit Δ , then there arise $(\Delta_3 - 1)(\Delta_4 - 1)$ distinct homomorphic images of Δ and 6 pairs of contracted vertices create each homomorphic image. Moreover, the number of total pairs of contracted vertices to generate all $(\Delta_3 - 1)(\Delta_4 - 1)$ and their mirror homomorphic images of Δ is $12(\Delta_3 - 1)(\Delta_4 - 1)$.

Let $H_{26} = \{\Omega_{(l_{13}, l_7)}^{26}; l_{13} = 1, 2, \dots, \Delta_3 - 1; l_7 = 1, 2, \dots, \Delta_4 - 1\}$ be the collection of homomorphic images of Δ acquired by the contraction of the vertices $e_{3l_{13}+1}^3$ with the vertices $e_{3l_7}^4$ in Δ . Figure 39 presents H_{26} graphically. From all the homomorphic images presented in Figure 39, it is not intricated to check that no

one is the mirror image of itself. This lemma can be proved by using the same procedure as that for Lemma 23.

Let $\bar{k}_2 = 8 - k_2$.

Lemma 27. If we contract the vertices $e_{3l_{(7, k_2)}+1}^{k_2}: l_{(7, k_2)} = 1, 2, \dots, \Delta_{k_2} - 1$, with the vertices $e_{3l_{(8, k_2)}}^{k_2}: l_{(8, k_2)} = 1, 2, \dots, \Delta_{k_2} - l_{(7, k_2)}$, in the circuit Δ , then for each k_3 , there arise $(1/2)\Delta_{k_2}(\Delta_{k_2} - 1)$ distinct homomorphic images of Δ and 6 pairs of contracted vertices create each homomorphic image. Moreover, the number of total pairs of contracted vertices to generate all $(1/2)\Delta_{k_2}(\Delta_{k_2} - 1)$ and their mirror homomorphic images of Δ is $6(\Delta_{k_2} - 1)^2$.

Proof. For $k_2 = 2$, let $H_{27}^2 = \{\Omega_{(l_{(7,2)}, l_{(8,2)})}^{27}; l_{(7,2)} = 1, 2, \dots, \Delta_2 - 1; l_{(8,2)} = 1, 2, \dots, \Delta_2 - l_{(7,2)}\}$ (Figure 40) be the collection of homomorphic images of Δ acquired by the contraction of the vertices $e_{3l_{(7,2)}+1}^2$ with the vertex $e_{3l_{(8,2)}}^6$ in Δ , where $e_{3l_{(7,2)}+1}^2$ and $e_{3l_{(8,2)}}^6$ are fixed by the words

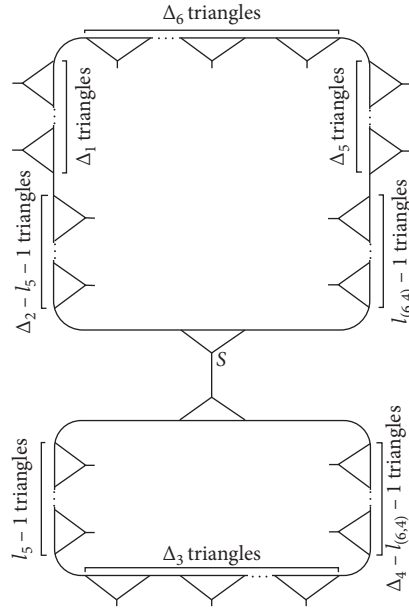


FIGURE 37: Homomorphic images $\Omega_{(l_5, l_{(6,4)})}^{25}$.

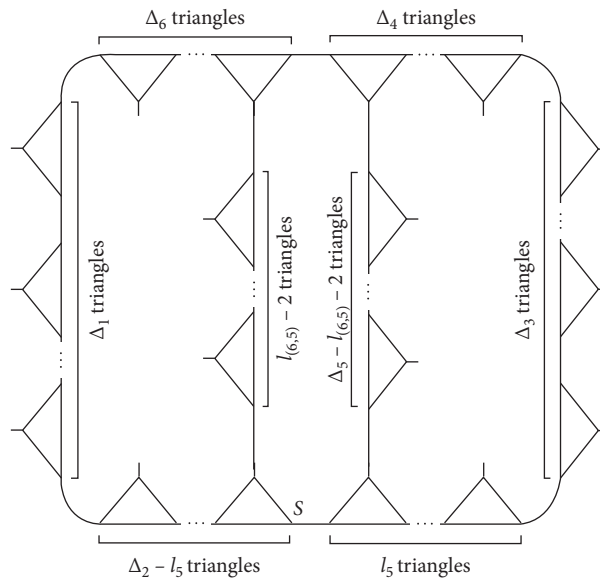


FIGURE 38: Homomorphic images $\Omega_{(l_5, l_{(6,5)})}^{25}$.

$(pq)^{l_{(7,2)}} (pq^{-1})^{\Delta_3} (pq)^{\Delta_4} (pq^{-1})^{\Delta_5} (pq)^{\Delta_6} (pq^{-1})^{\Delta_1} (pq)^{\Delta_2 - l_{(7,2)}}$ and $(pq^{-1})^{\Delta_6 - l_{(8,2)}} (pq)^{\Delta_5} (pq^{-1})^{\Delta_4} (pq)^{\Delta_3} (pq^{-1})^{\Delta_2} (pq)^{\Delta_1} (pq^{-1})^{l_{(8,2)}}$. It is easy to verify that $P_1 = (pq)^{l_{(7,2)}} (pq^{-1})^{\Delta_3} (pq)^{\Delta_4} (pq^{-1})^{\Delta_5} (pq)^{\Delta_6 - l_{(8,2)}} p$ and $P_2 = q (pq)^{l_{(8,2)} - 1} (pq^{-1})^{\Delta_1} (pq)^{\Delta_2 - l_{(7,2)}}$ are the possible paths between $e_{3l_{(7,2)}+1}^2$ and $e_{3l_{(8,2)}}^6$ (Figure 4). This implies that the homomorphic image $\Omega_{(l_{(7,2)}, l_{(8,2)})}^{27}$ has a vertex s fixed by P_1 and P_2 . Thus,

$$E_{27}^2 = \{e, q, q^{-1}, p, pq, pq^{-1}\} \quad (19)$$

is the family of elements in $\text{PSL}(2, \mathbb{Z})$ such that $\forall w \in E_{27}^2, \Delta$ contains the vertices $(e_{3l_{(7,2)}+1}^2)w$ and $(e_{3l_{(8,2)}}^6)w$. This gives that the cardinality of E_{27}^2 , that is, 6 is the number of contracted pairs of vertices to produce each homomorphic image $\Omega_{(l_{(7,2)}, l_{(8,2)})}^{27}$ (Theorem 2).

Suppose $\Omega_{(m_1, m_2)}^{27}$ and $\Omega_{(n_1, n_2)}^{27}$ are the same. This concludes that $\Omega_{(m_1, m_2)}^{27}$ is procurable also by contracting $e_{3n_1+1}^2$ and $e_{3n_2}^6$, implying that $e_{3n_1+1}^2 \leftrightarrow e_{3n_2}^6$ is one of the pairs of contracted vertices for $\Omega_{(m_1, m_2)}^{27}$. Then there must exist an element $w \in E_{27}^2$ such that $(e_{3m_1+1}^2)w = e_{3n_1+1}^2$ and $(e_{3m_2}^6)w = e_{3n_2}^6 \cdot pq^{-1} \in E_{27}^2$ is the only element such that $(e_{3m_2}^6)pq^{-1} = e_{3(m_2+1)}^6$ but $(e_{3m_1+1}^2)pq^{-1} \neq e_{3n_1+1}^2$. Thus, $\Omega_{(m_1, m_2)}^{27}$ and $\Omega_{(n_1, n_2)}^{27}$ are not the same, that is, by contracting $e_{3m_1+1}^2$ and $e_{3m_2}^6$ to produce $\Omega_{(m_1, m_2)}^{27}$, $e_{3n_1+1}^2$ and $e_{3n_2}^6$ are not contracted. Now, if $\Omega_{(m_1, m_2)}^{27}$ and $\Omega_{(n_1, n_2)}^{27}$ are the same, then there must exist an element $w \in E_{27}^2$ such that $(e_{3m_1+1}^2)w = e_{3n_1+1}^{2*}$ and $(e_{3m_2}^6)w = e_{3n_2}^{6*}$ or $(e_{3m_1+1}^2)w = e_{3n_1+1}^{6*}$ and $(e_{3m_2}^6)w = e_{3n_2}^{2*}$. $p \in E_{27}^2$ is the only element such that $(e_{3m_1+1}^2)p = e_{3m_1}^6 = e_{3(\Delta_2 - m_1) + 1}^{6*}$ and $(e_{3m_2}^6)p = e_{3m_2+1}^6 = e_{3(\Delta_2 - m_2)}^{2*}$. This implies that $\Omega_{(m_1, m_2)}^{27}$ and

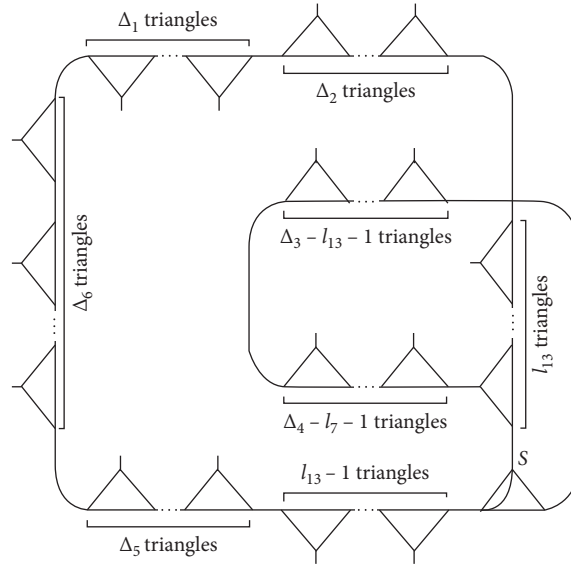


FIGURE 39: Homomorphic images $\Omega_{(l_{13}, l_7)}^{26}$.

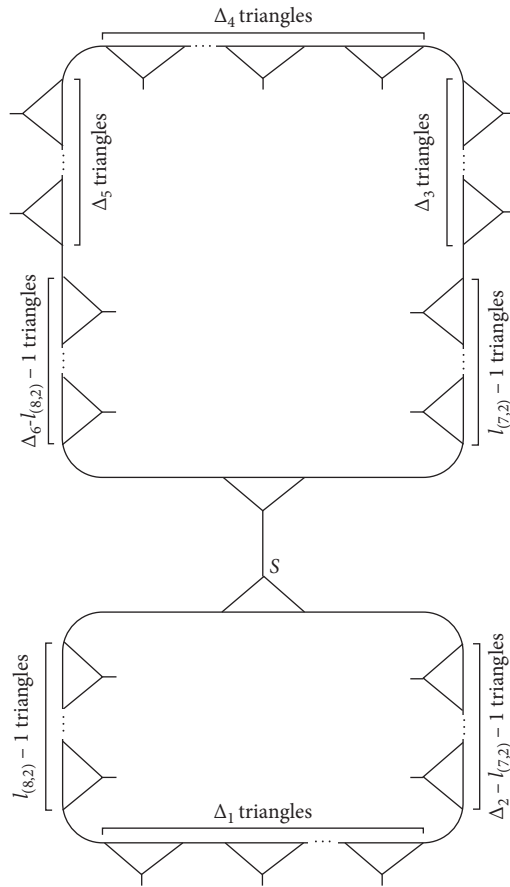


FIGURE 40: Homomorphic images $\Omega_{(l_{(7,2)}, l_{(8,2)})}^{27}$.

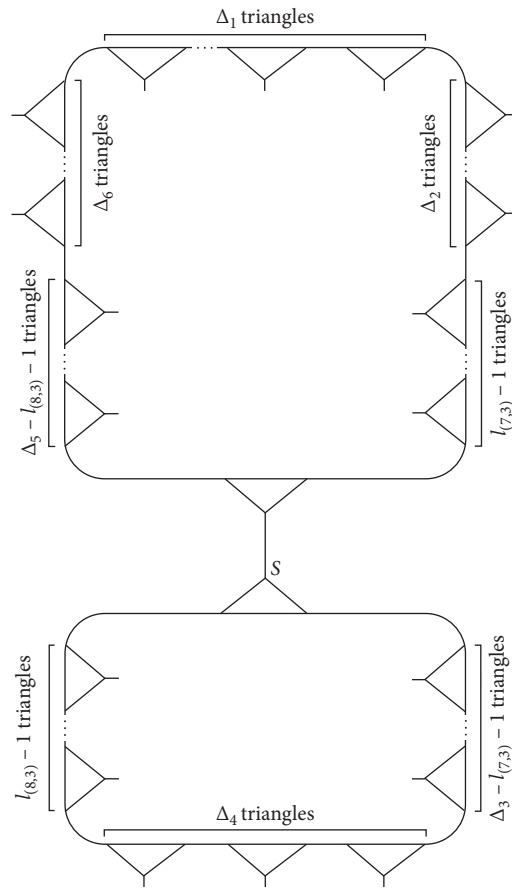


FIGURE 41: Homomorphic images $\Omega_{(l_{(7,3)}^1)l_{(8,3)}}^{27}$.

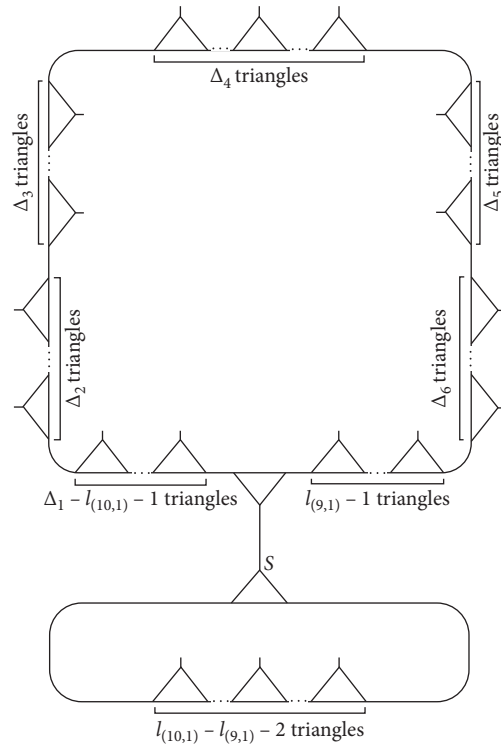


FIGURE 42: Homomorphic images $\Omega_{(l_{(9,1)}^1)l_{(10,1)}}^{28}$.

$\Omega_{(n_1, n_2)}^{27}$ are the mirror images of each other if and only if $n_1 = \Delta_2 - m_2$ and $n_2 = \Delta_2 - m_1$, that is, by contracting $e_{3m_1+1}^2$ and $e_{3m_2}^6$ to produce $\Omega_{(m_1, m_2)}^{27}$, $e_{3m_1+1}^{2*}$ and $e_{3m_2}^{6*}$ are also contracted. For a fix $m_1 \in l_{(7,2)}$ and for all $m_2 \in l_{(8,2)} \setminus \{\Delta_2 - m_1\}$, $\Omega_{(\Delta_2 - m_2, \Delta_2 - m_1)}^{27} \notin H_{27}^2$, implying that $\Omega_{(m_1, m_2)}^{27}$ and $\Omega_{(n_1, n_2)}^{27}$ are not the mirror images of each other. This implies that all the homomorphic images in H_{27}^2 are distinct. Thus, $H_{27}^2 = \left\{ \Omega_{(l_{(7,2)}, l_{(8,2)})}^{27}; l_{(7,2)} = 1, 2, \dots, \Delta_2 - 1; l_{(8,2)} = 1, 2, \dots, \Delta_2 - l_{(7,2)} \right\}$ implies

$$|H_{27}^2| = \frac{1}{2} \Delta_2 (\Delta_2 - 1). \tag{20}$$

Let $\Omega_{(m_1, m_2)}^{27}$ be the mirror image of itself, then from Figure 40, we have $m_1 - 1 = \Delta_2 - m_2 - 1$ and $m_2 - 1 = \Delta_2 - m_1 - 1$, implying $m_2 = \Delta_2 - m_1$. Now, $\forall m_1 \in l_{(7,2)}, \Delta_2 - m_1 \in l_{(8,2)}$, implying that $\Omega_{(m_1, \Delta_2 - m_1)}^{27} \in H_{27}^2$ is the mirror image of itself. So, out of $(1/2)\Delta_2(\Delta_2 - 1)$ homomorphic images in H_{27}^2 , $\Delta_2 - 1$ are the mirror images of itself. Hence, there are

$$2 \times |E_{27}^2| \times [|H_{27}^2| - (\Delta_2 - 1)] + |E_{27}^2| \times (\Delta_2 - 1) = 6(\Delta_2 - 1)^2 \tag{21}$$

pairs of contracting vertices to produce all the homomorphic images in H_{27}^2 . We can prove this lemma for $k_2 = 3$ (Figure 41) in similar way as that for $k_2 = 2$.

$$\text{Let } k_4 = \{1, 4\} \text{ and } \eta_{(4, k_4)} = \begin{cases} 0 & \text{if } \Delta_{k_4} = 0 \pmod{2} \\ 1 & \text{otherwise} \end{cases}. \quad \square$$

Lemma 28. *If we contract the vertices $e_{3l_{(7, k_4)}+1}^{k_4} : l_{(9, k_4)} = 1, 2, \dots, ((\Delta_{k_4} - 2 - \eta_{(4, k_4)})/2)$, with the vertices $e_{3l_{(10, k_4)}}^{k_4} : l_{(10, k_4)} = l_{(9, k_4)} + 1, l_{(9, k_4)} + 2, \dots, \Delta_{k_4} - l_{(9, k_4)}$, in the circuit Δ , then for each k_4 , there arise $(1/4)(\Delta_{k_4}^2 - 2\Delta_{k_4} + \eta_{(4, k_4)})$ distinct homomorphic images of Δ and 6 pairs of contracted vertices create each homomorphic image. Moreover, the number of total pairs of contracted vertices to generate all $(1/4)(\Delta_{k_4}^2 - 2\Delta_{k_4} + \eta_{(4, k_4)})$ and their mirror homomorphic images of Δ is $3(\Delta_{k_4}^2 - 3\Delta_{k_4} + 2)$.*

Proof. For $k_4 = 1$, let $H_{28}^1 = \left\{ \Omega_{(l_{(9,1)}, l_{(10,1)})}^{28}; l_{(9,1)} = 1, 2, \dots, ((\Delta_1 - 2 - \eta_{(4,1)})/2); l_{(10,1)} = l_{(9,1)} + 1, l_{(9,1)} + 2, \dots, \Delta_1 - l_{(9,1)} \right\}$ (Figure 42) be the

$$H_{28}^1 = \left\{ \Omega_{(l_{(9,1)}, l_{(10,1)})}^{28}; l_{(9,1)} = 1, 2, \dots, \frac{\Delta_1 - 2 - \eta_{(4,1)}}{2}; l_{(10,1)} = l_{(9,1)} + 1, l_{(9,1)} + 2, \dots, \Delta_1 - l_{(9,1)} \right\} \tag{23}$$

implies

$$\begin{aligned} |H_{28}^1| &= (\Delta_1 - 2) + (\Delta_2 - 4) + (\Delta_2 - 6) + \dots + (4 - \eta_{(4,1)}) \\ &+ (2 - \eta_{(4,1)}), \\ &= \frac{1}{4} (\Delta_1^2 - 2\Delta_1 + \eta_{(4,1)}). \end{aligned} \tag{24}$$

collection of homomorphic images of Δ acquired by the contraction of the vertices $e_{3l_{(9,1)}+1}^1$ with the vertices $e_{3l_{(10,1)}}^1$ in Δ , where $e_{3l_{(9,1)}+1}^1$ and $e_{3l_{(10,1)}}^1$ are fixed by the words $(pq)^{l_{(9,1)}}(pq^{-1})^{\Delta_6}(pq)^{\Delta_5}(pq^{-1})^{\Delta_4}(pq)^{\Delta_3}(pq^{-1})^{\Delta_2}(pq)^{\Delta_1-l_{(9,1)}}$ and $(pq^{-1})^{\Delta_1-l_{(10,1)}}$. It is easy to verify that $P_1 = (pq)^{l_{(9,1)}}(pq^{-1})^{\Delta_6}(pq)^{\Delta_5}(pq^{-1})^{\Delta_4}(pq)^{\Delta_3}(pq^{-1})^{\Delta_2}(pq)^{\Delta_1-l_{(10,1)}}p$ and $P_2 = q(pq)^{l_{(10,1)}-l_{(9,1)}-1}$ are the possible paths between $e_{3l_{(9,1)}+1}^1$ and $e_{3l_{(10,1)}}^1$ (Figure 4). This implies that the homomorphic image $\Omega_{(l_{(9,1)}, l_{(10,1)})}^{28}$ has a vertex s fixed by P_1 and P_2 . Thus,

$$E_{28}^1 = \{e, q, q^{-1}, p, pq, pq^{-1}\} \tag{22}$$

is the family of elements in $\text{PSL}(2, \mathbb{Z})$ such that $\forall w \in E_{28}^1, \Delta$ contains the vertices $(e_{3l_{(9,1)}+1}^1)w$ and $(e_{3l_{(10,1)}}^1)w$. This gives that the cardinality of E_{28}^1 , that is, 6 is the number of contracted pairs of vertices to produce each homomorphic image $\Omega_{(l_{(9,1)}, l_{(10,1)})}^{28}$ (Theorem 2).

Suppose $\Omega_{(m_1, m_2)}^{28}$ and $\Omega_{(n_1, n_2)}^{28}$ are the same. This concludes that $\Omega_{(m_1, m_2)}^{28}$ is procurable also by contracting $e_{3m_1+1}^1$ and $e_{3m_2}^1$, implying that $e_{3m_1+1}^1 \leftrightarrow e_{3m_2}^1$ is one of the pairs of contracted vertices for $\Omega_{(m_1, m_2)}^{28}$. Then there must exist an element $w \in E_{28}^1$ such that $(e_{3m_1+1}^1)w = e_{3m_1+1}^1$ and $(e_{3m_2}^1)w = e_{3m_2}^1$. $pq, pq^{-1} \in E_{28}^1$ are the only element such that $(e_{3m_1+1}^1)pq = e_{3(m_1-1)+1}^1$ and $(e_{3m_2}^1)pq^{-1} = e_{3(m_2+1)}^1$ but $(e_{3m_2}^1)pq \neq e_{3m_2}^1$ and $(e_{3m_1+1}^1)pq^{-1} \neq e_{3m_1+1}^1$. $\Omega_{(m_1, m_2)}^{28}$ and $\Omega_{(n_1, n_2)}^{28}$ are not the same, that is, by contracting $e_{3m_1+1}^1$ and $e_{3m_2}^1$ to produce $\Omega_{(m_1, m_2)}^{28}$, $e_{3m_1+1}^1$ and $e_{3m_2}^1$ are not contracted. Now, if $\Omega_{(m_1, m_2)}^{28}$ and $\Omega_{(n_1, n_2)}^{28*}$ are same, then there must exist an element $w \in E_{28}^1$ such that $(e_{3m_1+1}^1)w = e_{3n_1+1}^{1*}$ and $(e_{3m_2}^1)w = e_{3n_2}^{1*}$. $p \in E_{28}^1$ is the only element such that $(e_{3m_1+1}^1)p = e_{3m_1}^{1*} = e_{3(\Delta_1 - m_1) + 1}^{1*}$ and $(e_{3m_2}^1)p = e_{3m_2+1}^{1*} = e_{3(\Delta_1 - m_2)}^{1*}$. This implies that $\Omega_{(m_1, m_2)}^{28}$ and $\Omega_{(n_1, n_2)}^{28}$ are the mirror images of each other if and only if $n_1 = \Delta_1 - m_1$ and $n_2 = \Delta_1 - m_2$, that is, by contracting $e_{3m_1+1}^1$ and $e_{3m_2}^1$ to produce $\Omega_{(m_1, m_2)}^{28}$, $e_{3m_1+1}^{1*}$ and $e_{3m_2}^{1*}$ are also contracted. For all $m_1 \in l_{(9,1)}, \Delta_1 - m_1 > ((\Delta_1 - 2 - \eta_{(4,1)})/2)$, implying that $\Omega_{(n_1, n_2)}^{28} = \Omega_{(\Delta_2 - m_2, \Delta_2 - m_1)}^{28} \notin H_{28}^1$ and that $\Omega_{(m_1, m_2)}^{28}$ and $\Omega_{(n_1, n_2)}^{28}$ are not the mirror images of each other. This implies that all the homomorphic images in H_{28}^1 are distinct. Thus,

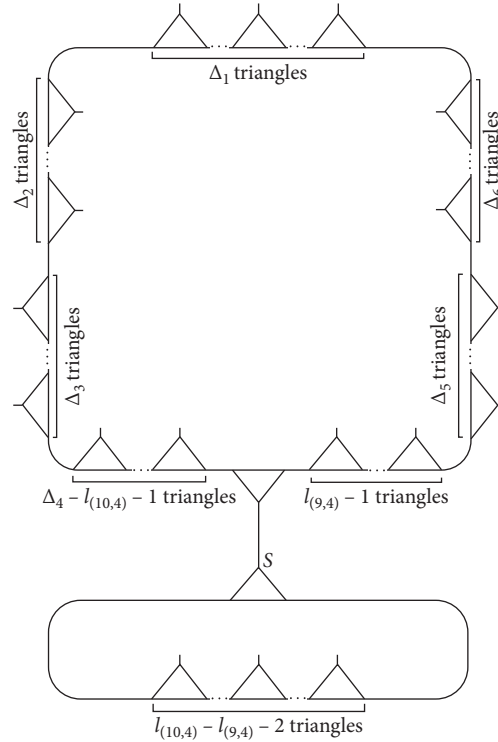


FIGURE 43: Homomorphic images $\Omega_{(l(9,4)l(10,4))}^{28}$.

$$2 \times |E_{28}^2| \times \left[|H_{28}^2| - \frac{\Delta_1 - 2 - \eta_{(4,1)}}{2} \right] + |E_{28}^2| \times \frac{\Delta_1 - 2 - \eta_{(4,1)}}{2} = 3(\Delta_1^2 - 3\Delta_1 + 2) \tag{25}$$

pairs of contracting vertices to produce all the homomorphic images in H_{28}^1 . We can prove this lemma for $k_4 = 4$ (Figure 43) in similar way as that for $k_4 = 1$. \square

Lemma 29. *If we contract the vertices $e_{3l(11,k_2)+1}^{k_2} : l_{(11,k_2)} = 1, 2, \dots, \Delta_{k_2} - 1$, with the vertices $e_{3l(12,k_2)}^{k_2} : l_{(12,k_2)} = 1, 2, \dots, \Delta_{k_2} - l_{(11,k_2)}$, in the circuit Δ , then for each k_2 , there arise $(1/6)(\Delta_{k_2} - 1)(\Delta_{k_2} - 2)$ distinct homomorphic images of Δ and 6 pairs of contracted vertices create each homomorphic image. Moreover, the number of total pairs of contracted vertices to generate all $(1/2)(\Delta_{k_2} - 1)(\Delta_{k_2} - 2)$ and their mirror homomorphic images of Δ is $6(\Delta_{k_2} - 1)(\Delta_{k_2} - 2)$.*

For a fix value of k_2 , let $H_{29}^{k_2} = \left\{ \Omega_{(l(11,k_2)l(12,k_2))}^{30} ; l_{(11,k_2)} = 1, 2, \dots, \Delta_{k_2} - 1 ; l_{(12,k_2)} = 1, 2, \dots, \Delta_{k_2} - l_{(11,k_2)} \right\}$ be the collection of homomorphic images of Δ acquired by the contraction of the vertices $e_{3l(11,k_2)+1}^{k_2}$ with the vertices $e_{3l(12,k_2)}^{k_2}$ in Δ . Figures 44 and 45 present $H_{29}^{k_2}$ graphically. From all the homomorphic images presented in these figures, it is not intricated to check that no one is the mirror image of itself. This lemma can be proved by using the same procedure as that for Lemma 23.

$$\text{Let } k_4 = \{1, 4\} \text{ and } \eta_{(4,k_4)} = \begin{cases} 0 & \text{if } \Delta_{k_4} = 0 \pmod{2} \\ 1 & \text{otherwise} \end{cases}.$$

Lemma 30. *If we contract the vertices $e_{3l(13,k_4)+1}^{k_4} : l_{(13,k_4)} = 1, 2, \dots, ((\Delta_{k_4} - \eta_{(4,k_4)})/2)$, with the vertices $e_{3l(13,k_4)}^{k_4}$ in the circuit Δ , then for each k_4 , there arise $(1/2)(\Delta_{k_4} - \eta_{(4,k_4)})$ distinct homomorphic images of Δ and 3 pairs of contracted vertices create each homomorphic image. Moreover, the number of total pairs of contracted vertices to generate all $(1/2)(\Delta_{k_4} - \eta_{(4,k_4)})$ and their mirror homomorphic images of Δ is $3(\Delta_{k_4} - 1)$.*

For a fix value of k_4 , let $H_{30}^{k_4} = \left\{ \Omega_{(l(13,k_4)l(13,k_4))}^{30} ; l_{(13,k_4)} = 1, 2, \dots, ((\Delta_{k_4} - \eta_{(4,k_4)})/2) \right\}$ be the collection of homomorphic images of Δ acquired by the contraction of the vertices $e_{3l(13,k_4)+1}^{k_4}$ with the vertices $e_{3l(13,k_4)}^{k_4}$ in Δ . Figures 46 and 47 present $H_{30}^{k_4}$ graphically. From all the homomorphic images presented in these figures, it is not intricated to check that if $\Delta_{k_2} = 0 \pmod{2}$, then $\Omega_{((\Delta_{k_2}/2), (\Delta_{k_2}/2))}^{30}$ is the only homomorphic image which is the mirror image of itself; otherwise, no one is the mirror image of itself.

This lemma can be proved by using the same procedure as that for Lemma 28.

Lemma 31. *If we contract the vertices $e_{3l(11,k_2)+1}^{k_2} : l_{(11,k_2)} = 1, 2, \dots, \Delta_{k_2} - 1$, with the vertices $e_{3l(11,k_2)}^{k_2}$ in the circuit Δ , then for each k_2 , there arise $\Delta_{k_2} - 1$ distinct homomorphic images of Δ and 3 pairs of contracted vertices create each homomorphic image. Moreover, the number of total pairs of contracted vertices to generate all $\Delta_{k_2} - 1$ and their mirror homomorphic images of Δ is $6(\Delta_{k_2} - 1)$.*

For a fix value of k_2 , let $H_{31}^{k_2} = \left\{ \Omega_{(l(11,k_2)l(11,k_2))}^{31} ; l_{(11,k_2)} = 1, 2, \dots, \Delta_{k_2} - 1 \right\}$ be the collection of homomorphic images of Δ acquired by the

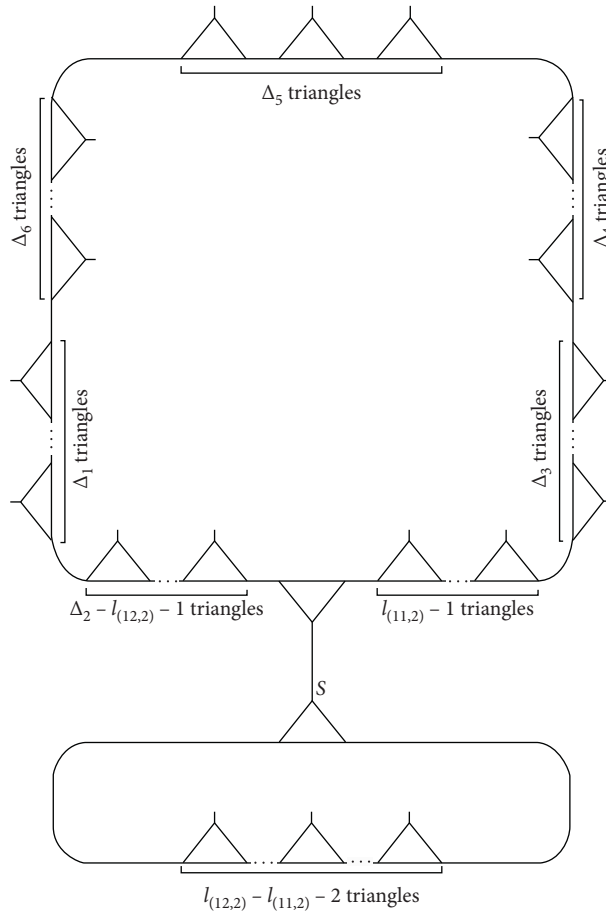


FIGURE 44: Homomorphic images $\Omega_{(l(11,2), l(12,2))}^{29}$.

contraction of the vertices $e_{3l(11,k_2)}^{k_2}$ with the vertices $e_{3l(11,k_2)}^{k_2}$ in Δ . Figures 48 and 49 present $H_{31}^{k_2}$ graphically. From all the homomorphic images presented in these figures, it is not intricate to check that no one is the mirror image of itself. This lemma can be proved by using same procedure as that for Lemma 23.

Let $k_5 = \{2, 4\}$.

Lemma 32. For each k_5 , there are $6(\Delta_{k_5} + \Delta_{k_5+1} + 2)$ pairs of contracting vertices to produce the homomorphic image of Δ by contracting the vertex e_1^1 with the vertex $e_1^{k_5}$.

For $k_5 = 2$, let Ω_2^{32} be the homomorphic image of Δ acquired by contracting the vertex e_1^1 with the vertex e_1^2 in Δ , where e_1^1 and e_1^2 are fixed by the words $(pq^{-1})^{\Delta_6}(pq)^{\Delta_5}(pq^{-1})^{\Delta_4}(pq)^{\Delta_3}(pq^{-1})^{\Delta_2}(pq)^{\Delta_1}$ and $(pq^{-1})^{\Delta_3}(pq)^{\Delta_4}(pq^{-1})^{\Delta_5}(pq)^{\Delta_6}(pq^{-1})^{\Delta_1}(pq)^{\Delta_2}$. It is easy to verify that $P_1 = (pq^{-1})^{\Delta_6}(pq)^{\Delta_5}(pq^{-1})^{\Delta_4}(pq)^{\Delta_3}p$ and $P_2 = q^{-1}(pq^{-1})^{\Delta_2-1}(pq)^{\Delta_1}$ are the possible paths between e_1^1 and e_1^2 (Figure 4). This implies that the homomorphic image Ω_2^{32} has a vertex s fixed by P_1 and P_2 . Thus,

$$E_2^{32} = \left\{ \begin{array}{l} e, q, q^{-1}, p, pq, (pq^{-1})^1, (pq^{-1})^1 p, (pq^{-1})^1 pq, (pq^{-1})^2, \dots, (pq^{-1})^{\Delta_3} p, (pq^{-1})^{\Delta_3} pq, \\ (pq^{-1})^{\Delta_3+1}, (q^{-1}p)^1, (q^{-1}p)^1 q, (q^{-1}p)^1 q^{-1}, \dots, (q^{-1}p)^{\Delta_2}, (q^{-1}p)^{\Delta_2} q, (q^{-1}p)^{\Delta_2} q^{-1} \end{array} \right\} \quad (26)$$

is the family of elements in $PSL(2, \mathbb{Z})$ such that $\forall w \in E_2^{32}, \Delta$ contains the vertices $(e_1^1)w$ and $(e_1^2)w$. This gives that the cardinality of E_2^{32} , that is, $3(\Delta_2 + \Delta_3 + 2)$ is the number of contracted pairs of vertices to produce the homomorphic image Ω_2^{32} (Theorem 2). From Figure 50, it is not intricate to

check that Ω_2^{32} and its mirror image Ω_2^{32*} are not the same. Hence, there are

$$2 \times |E_{32}^2| = 3(\Delta_2 + \Delta_3 + 2), \quad (27)$$

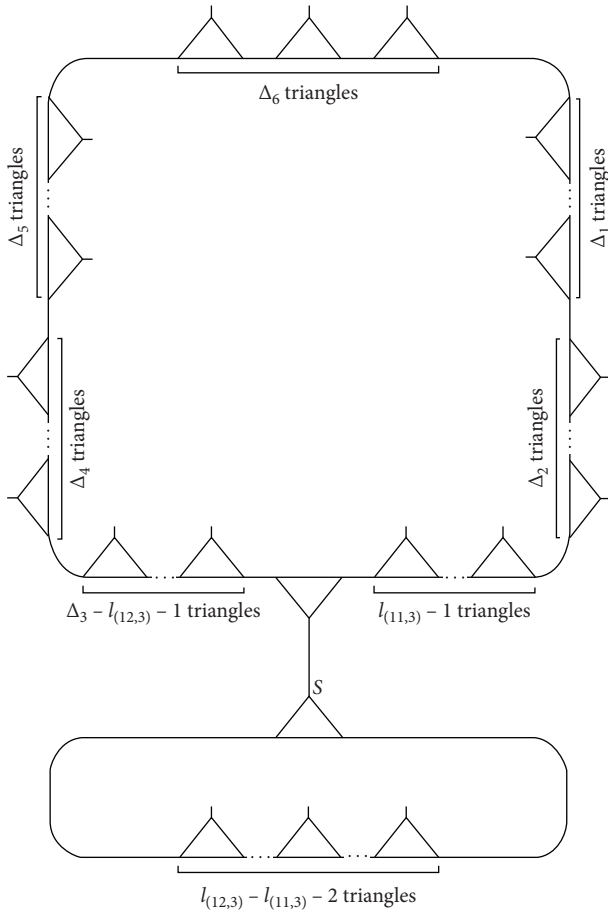


FIGURE 45: Homomorphic images $\Omega_{(l_{(11,3)}, l_{(12,3)})}^{29}$.

pairs of contracting vertices to produce the homomorphic images Ω_2^{32} .

We can prove this lemma for $k_5 = 4$ (Figure 51) in similar way as that for $k_5 = 2$.

Lemma 33. For each k_3 , there are $6 (\Delta_4 + \Delta_5 + 2)$ pairs of contracting vertices to produce the homomorphic image of Δ by contracting the vertex $e_1^{k_3}$ with the vertex $e_1^{k_3}$.

For a fix value of k_3 , let $\Omega_{k_3}^{33}$ be the homomorphic image of Δ acquired by the contraction of the vertex $e_1^{k_3}$ with the vertex $e_1^{k_3}$ in Δ . Figures 52 and 53 present $\Omega_{k_3}^{33}$ graphically. From these figures, it is not intricated to check that $\Omega_{k_3}^{33}$ is not the mirror image of itself.

This lemma can be proved by using the same procedure as that for Lemma 32.

$$\text{Let } k_6 = \{1, 2, 5\} \text{ and } \bar{k}_6 = \begin{cases} 6 & \text{if } k_6 = 1, \\ 3 & \text{if } k_6 = 2, \\ 4 & \text{if } k_6 = 5. \end{cases}$$

Lemma 34. For each k_6 , there are $6 (\Delta_{\bar{k}_6} + 1)$ pairs of contracting vertices to produce the homomorphic image of Δ by contracting the vertex $e_1^{k_6}$ with the vertex $e_1^{k_6}$.

For a fix value of k_6 , let $\Omega_{k_6}^{34}$ be the homomorphic image of Δ acquired by the contraction of the vertex $e_1^{k_6}$ with the vertex $e_1^{k_6}$ in Δ . Figures 54, 55, and 56 present $\Omega_{k_6}^{34}$ graphically. From these figures, it is not intricated to check that $\Omega_{k_6}^{34}$ is not the mirror image of itself. This lemma can be proved by using the same procedure as that for Lemma 32.

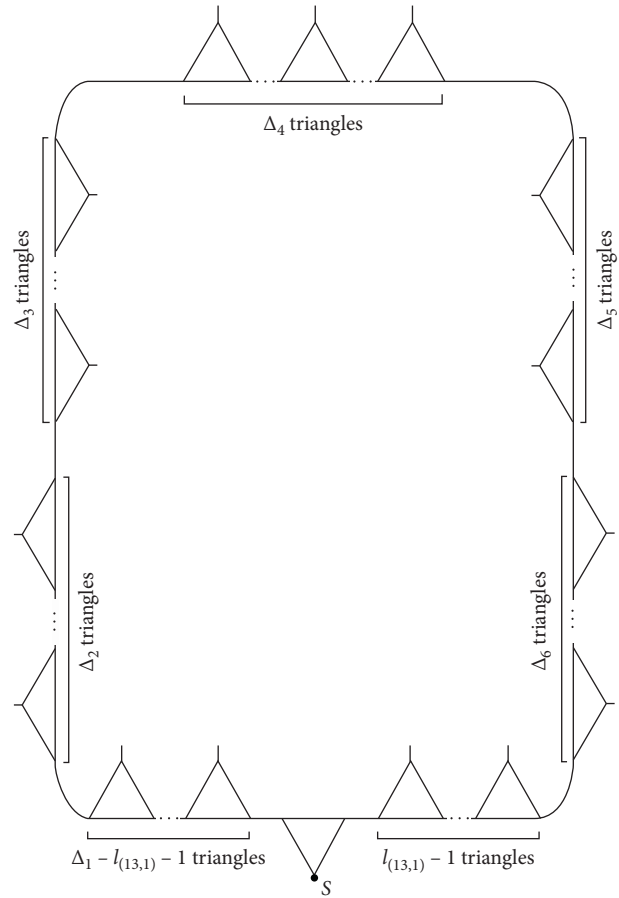


FIGURE 46: Homomorphic images $\Omega_{(l_{(13,1)}, l_{(13,1)})}^{30}$.

Lemma 35. For each k_3 , there are $3 (\Delta_{k_3+1} + 2\Delta_{k_3+2} + 2)$ pairs of contracting vertices to produce the homomorphic image of Δ by contracting the vertex $e_1^{k_3}$ with the vertex $e_1^{k_3+2}$.

For a fix value of k_3 , let $\Omega_{k_3}^{35}$ be the homomorphic image of Δ acquired by the contraction of the vertex $e_1^{k_3}$ with the vertex $e_1^{k_3+2}$ in Δ . Figures 57(a), 57(b), and 57(c) present $\Omega_{k_3}^{35}$ and Figure 58 presents $\Omega_{k_3}^{35}$ graphically. From these figures, it is not intricated to check that $\Omega_{k_3}^{35}$ is the mirror image of itself. This lemma can be proved by using the same procedure as that for Lemma 32.

Let $V(\Delta \times \Delta) = \{(a, b); a, b \in V(\Delta) \text{ and } a \neq b\}$, then

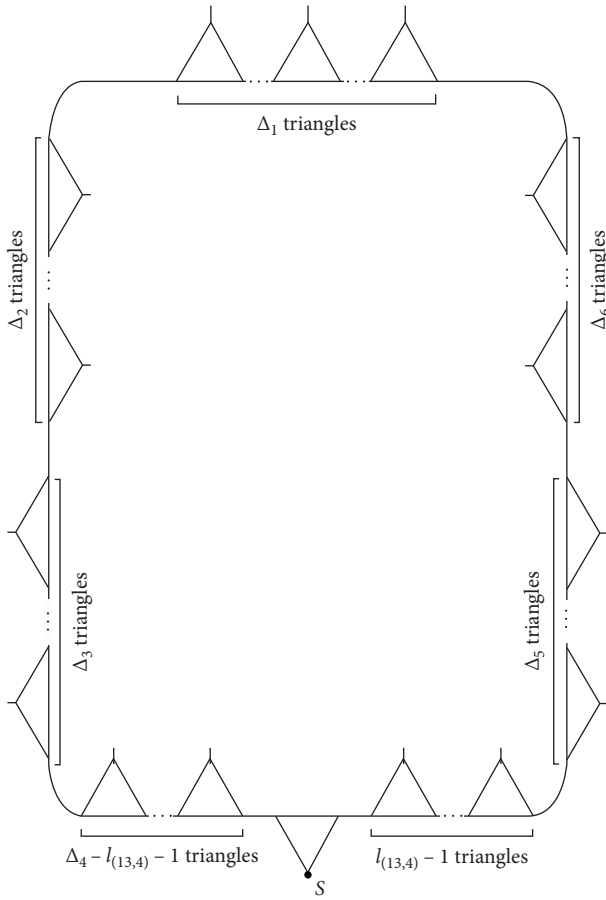
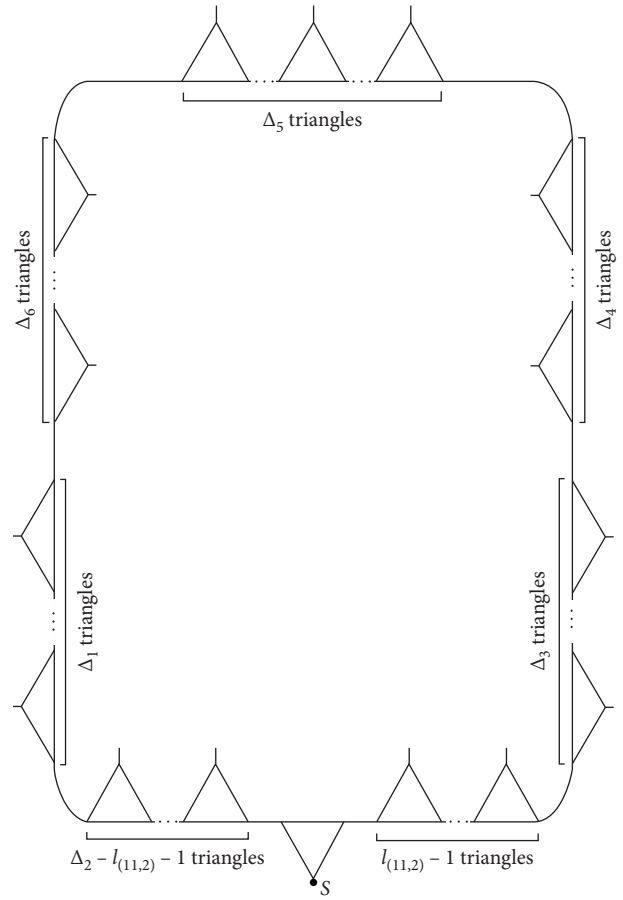
$$|V(\Delta \times \Delta)| = \frac{1}{2} [9(\Delta_1 + 2\Delta_2 + 2\Delta_3 + \Delta_4) - 3(\Delta_1 + 2\Delta_2 + 2\Delta_3 + \Delta_4)]. \tag{28}$$

We are now able to prove our primary outcome. Let

$$\eta = \begin{cases} 4, & \text{if } (\Delta_1, \Delta_4) = (E, E), \\ 0, & \text{if } (\Delta_1, \Delta_4) = (O, O), \\ -1, & \text{otherwise.} \end{cases} \tag{29}$$

where E and O stand for even and odd, respectively.

Theorem 5. There are $(1/4)[(\Delta_1 + 2\Delta_2 + 2\Delta_3 + \Delta_4)^2 + 4(\Delta_1 + 2\Delta_2 + 2\Delta_3 + \Delta_4) + 4\Delta_4 + \eta]$ number of distinct

FIGURE 47: Homomorphic images $\Omega_{(l(13,4), l(13,4))}^{30}$.FIGURE 48: Homomorphic images $\Omega_{(l(11,2), l(11,2))}^{31}$.

homomorphic images acquired by the contraction of all pairs of vertices of the circuit Δ .

Proof. Let us collect all the pairs of contracting vertices of Δ mentioned in Lemma 1 to Lemma 35 in the form of set S as

$$S = \left\{ \begin{array}{l} (e_{3l_1+1}^1, e_{3\Delta_1}^1), (e_{3l_1+1}^2, e_{3\Delta_1}^2), (e_{3l_{(2,k_1)}+1}^{k_1}, e_{3\Delta_1}^1), (e_{3l_5+1}^6, e_{3\Delta_1}^1), (e_{3l_4+1}^1, e_{3\Delta_2}^2), (e_{3l_5+1}^2, e_{3\Delta_2}^2), (e_{3l_{(6,k_1)}+1}^{k_1}, e_{3\Delta_2}^2), \\ (e_{3l_7+1}^3, e_{3\Delta_3}^3), (e_{3l_7+1}^4, e_{3\Delta_3}^3), (e_{3l_8+1}^4, e_{3\Delta_4}^4), (e_{3l_9+1}^5, e_{3\Delta_4}^4), (e_{3l_{10}+1}^3, e_{3\Delta_4}^4), (e_{3l_1+1}^2, e_{3\Delta_5}^5), (e_{3l_{11}+1}^3, e_{3\Delta_5}^5), (e_{3l_7+1}^4, e_{3\Delta_5}^5), \\ (e_{3l_{12}+1}^5, e_{3\Delta_5}^5), (e_{3l_{13}+1}^3, e_{3\Delta_6}^6), (e_{3l_{14}+1}^1, e_{3\Delta_1}^1), (e_{3l_{15}+1}^1, e_{3\Delta_3}^3), (e_{3l_{(3,k_2)}+1}^{k_2}, e_{3\Delta_3}^3), (e_{3l_{16}+1}^2, e_{3\Delta_4}^4), (e_{3l_{(4,k_3)}+1}^3, e_{3\Delta_6}^6), \\ (e_{3l_4+1}^1, e_{3l_{(5,k_2)}+1}^{k_2}), (e_{3l_4+1}^1, e_{3l_{17}+1}^4), (e_{3l_5+1}^2, e_{3l_{(6,k_1)}+1}^{k_1}), (e_{3l_{13}+1}^3, e_{3l_7+1}^4), (e_{3l_{(7,k_2)}+1}^{k_2}, e_{3l_{(8,k_2)}+1}^{\bar{k}_2}), (e_{3l_{(7,k_4)}+1}^{k_4}, e_{3l_{(10,k_4)}+1}^{k_4}), (e_{3l_{(11,k_2)}+1}^3, e_{3l_{(12,k_2)}+1}^{k_2}), \\ (e_{3l_{(13,k_4)}+1}^{k_4}, e_{3l_{(13,k_4)}+1}^{k_4}), (e_{3l_{(11,k_2)}+1}^{k_2}, e_{3l_{(11,k_2)}+1}^{k_2}), (e_1^{k_3}, e_1^1), (e_1^{k_3}, e_1^1), (e_1^{k_6}, e_1^{\bar{k}_6}), (e_1^{k_3}, e_1^{k_3+2}) \end{array} \right\}. \quad (30)$$

Let H be the set of homomorphic images obtained by contracting each element of S , then

$$H = \left\{ \begin{array}{l} \Omega_{l_1}^1, \Omega_{l_1}^2, \Omega_{l_{(2,k_1)}}^3, \Omega_{l_3}^4, \Omega_{l_4}^5, \Omega_{l_5}^6, \Omega_{l_{(6,k_1)}}^7, \Omega_{l_7}^8, \Omega_{l_7}^9, \Omega_{l_8}^{10}, \Omega_{l_9}^{11}, \Omega_{l_{10}}^{12}, \Omega_{l_1}^{13}, \Omega_{l_{11}}^{14}, \Omega_{l_7}^{15}, \Omega_{l_{12}}^{16}, \Omega_{l_{13}}^{17}, \\ \Omega_{l_{14}}^{18}, \Omega_{l_{15}}^{19}, \Omega_{l_{(3,k_2)}}^{20}, \Omega_{l_{16}}^{21}, \Omega_{l_{(4,k_3)}}^{22}, \Omega_{l_{(5,k_2)}}^{23}, \Omega_{l_{(4,l_{17})}}^{24}, \Omega_{l_{(5,l_{(6,k_1)})}}^{25}, \Omega_{l_{(13,l_7)}}^{26}, \Omega_{l_{(7,k_2), l_{(8,k_2)}}}^{27}, \\ \Omega_{l_{(9,k_4), l_{(10,k_4)}}}^{28}, \Omega_{l_{(11,k_2), l_{(12,k_2)}}}^{29}, \Omega_{l_{(13,k_4), l_{(13,k_4)}}}^{30}, \Omega_{l_{(11,k_2), l_{(11,k_2)}}}^{31}, \Omega_{k_5}^{32}, \Omega_{k_3}^{33}, \Omega_{k_6}^{34}, \Omega_{k_3}^{35} \end{array} \right\}. \quad (31)$$

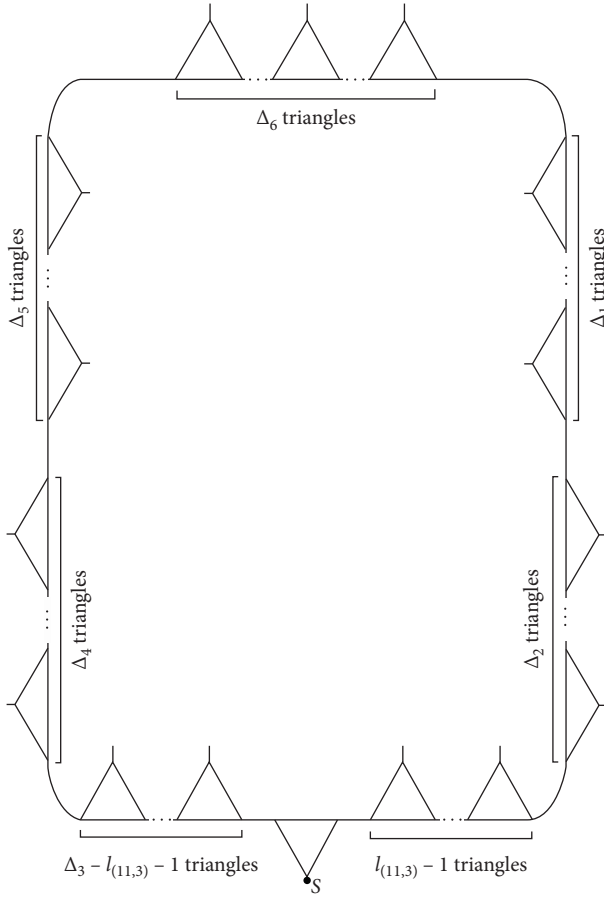


FIGURE 49: Homomorphic images $\Omega_{(l_{(11,3)}, l_{(11,3)})}^{31}$.

Let S' be the sum of contracted pairs obtained by contracting each element of S , then

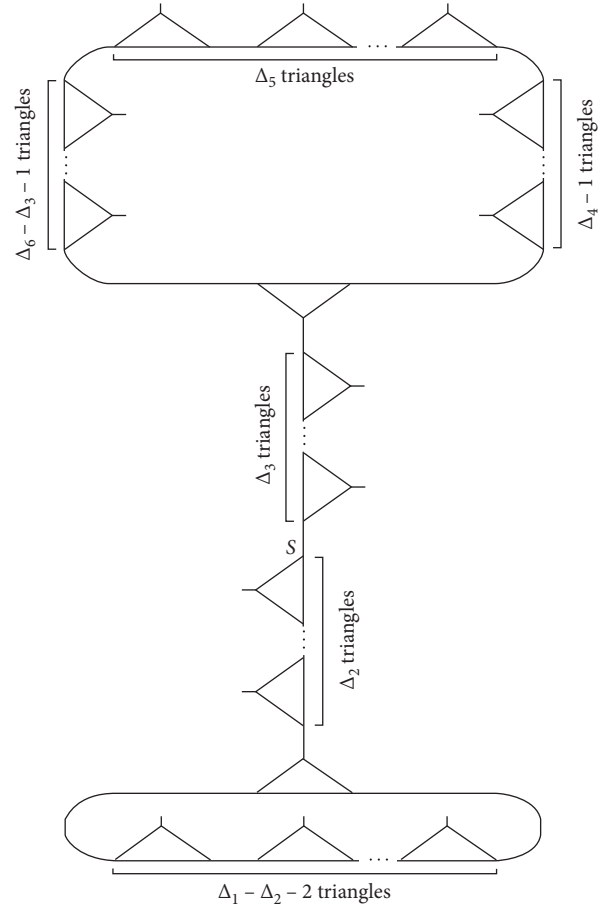


FIGURE 50: Homomorphic image Ω_2^{32} .

$$\begin{aligned}
 S' &= 3(\Delta_2^2 + 3\Delta_2 - 2) + 3(\Delta_2^2 + 3\Delta_2) + \frac{3}{2}(\Delta_6^2 + 3\Delta_6) + \frac{3}{2}(\Delta_1^2 + 3\Delta_1 - 4) + 3(\Delta_2^2 + 3\Delta_2 - 4) + 3(\Delta_4^2 + 3\Delta_4 - 4) \\
 &+ \frac{3}{2}(\Delta_4^2 + 3\Delta_4 - 4) + 3(\Delta_4^2 + 3\Delta_4 - 2) + \frac{3}{2}(\Delta_5^2 + 3\Delta_5) + 3(\Delta_3^2 + 3\Delta_3) + \frac{3}{2}(\Delta_2^2 + 3\Delta_2) + 3(\Delta_3^2 + 3\Delta_3 - 2) \\
 &+ 3(\Delta_4^2 + 3\Delta_4 - 4) + 3(\Delta_5^2 + 3\Delta_5) + \frac{3}{2}(\Delta_3^2 + 3\Delta_3 - 4) + 6(\Delta_2 + 2)(\Delta_1 - \Delta_2 - 1) \\
 &+ 3(\Delta_4 + 2)(\Delta_1 - \Delta_4 - 1) \\
 &+ 6(\Delta_3 + 2)(\Delta_2 - \Delta_3 - 1) \\
 &+ 6(\Delta_1 - 1)(\Delta_4 - 1) + 12(\Delta_3 - 1)(\Delta_4 - 1) + \sum_{k_1=3}^5
 \end{aligned}$$

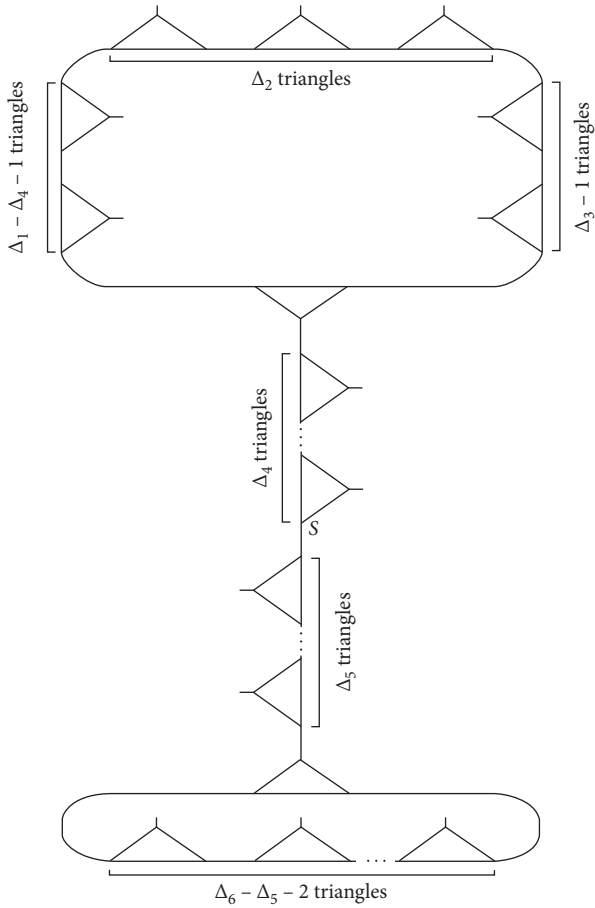


FIGURE 51: Homomorphic image Ω_4^{32} .

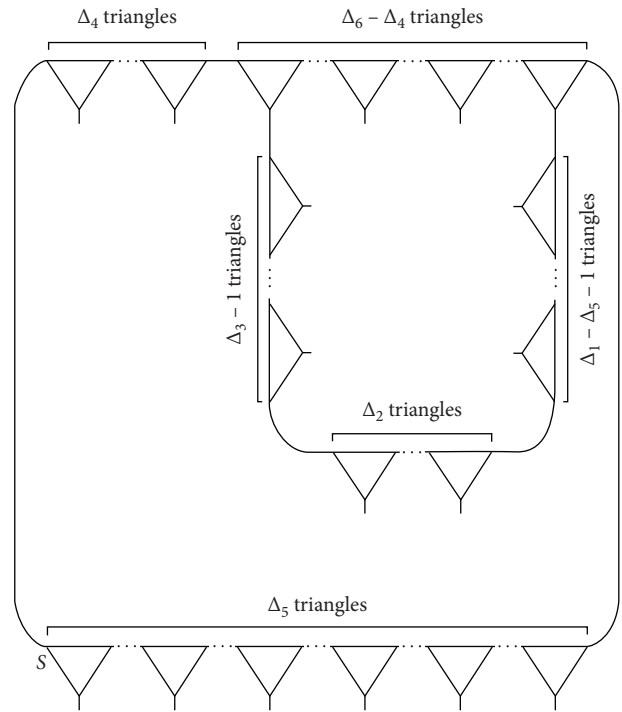


FIGURE 52: Homomorphic image Ω_1^{33} .

$$\begin{aligned}
 & [3(\Delta_{k_1}^2 + 3\Delta_{k_1}) + 3(\Delta_{k_1}^2 + 3\Delta_{k_1} - 4) + 12(\Delta_2 - 1)(\Delta_{k_1} - 1)] \\
 & + \sum_{k_2=2}^3 [6(\Delta_4 + 2)(\Delta_{k_2} - \Delta_4 - 1) + 12(\Delta_1 - 1)(\Delta_{k_2} - 1) + 6(\Delta_{k_2} - 1)^2 + 6(\Delta_{k_2} - 1)(\Delta_{k_2} - 2) + 6(\Delta_{k_2} - 1)] \\
 & + \sum_{k_3=1}^2 [6(\Delta_5 + 2\Delta_{k_3} - \Delta_5 - 1) + 6(\Delta_4 + \Delta_5 + 2) + 3(\Delta_{k_3+1} + 2\Delta_{k_3+2} + 2)] + \sum_{k_4=1}^4 [3(\Delta_{k_4}^2 - 3\Delta_{k_4} + 2) + 3(\Delta_{k_4} - 1)] \\
 & + \sum_{k_5=2,4} [6(\Delta_{k_5} + \Delta_{k_5+1} + 2)] + \sum_{k_6=1,2,5} [6(\Delta_{k_6} + 1)] \\
 & = \frac{1}{2} [9(\Delta_1 + 2\Delta_2 + 2\Delta_3 + \Delta_4) - 3(\Delta_1 + 2\Delta_2 + 2\Delta_3 + \Delta_4)].
 \end{aligned} \tag{32}$$

shows that each element of $V(\Delta \times \Delta)$ is contracted.

Now,

$$\begin{aligned}
 |H| &= \Delta_2 + \Delta_2 + \Delta_6 + (\Delta_1 - 1) + (\Delta_2 - 1) + (\Delta_4 - 1) + (\Delta_1 - 1) + \Delta_4 + \Delta_5 + \Delta_3 + \Delta_2 + \Delta_3 + (\Delta_4 - 1) + \Delta_5 + (\Delta_3 - 1) \\
 &+ (\Delta_1 - \Delta_2 - 1) + \frac{\Delta_1 - \Delta_4 - \eta_1}{2} + (\Delta_2 - \Delta_3 - 1) + \begin{cases} \frac{1}{2}(\Delta_1 - 1)(\Delta_4 - 1) & \text{if } \Delta_4 = 1 \pmod{2} \\ \frac{1}{2}[(\Delta_1 - 1)(\Delta_4 - 1) + 1 - \eta_3] & \text{if } \Delta_4 = 0 \pmod{2} \end{cases} + (\Delta_3 - 1)(\Delta_4 - 1)
 \end{aligned}$$

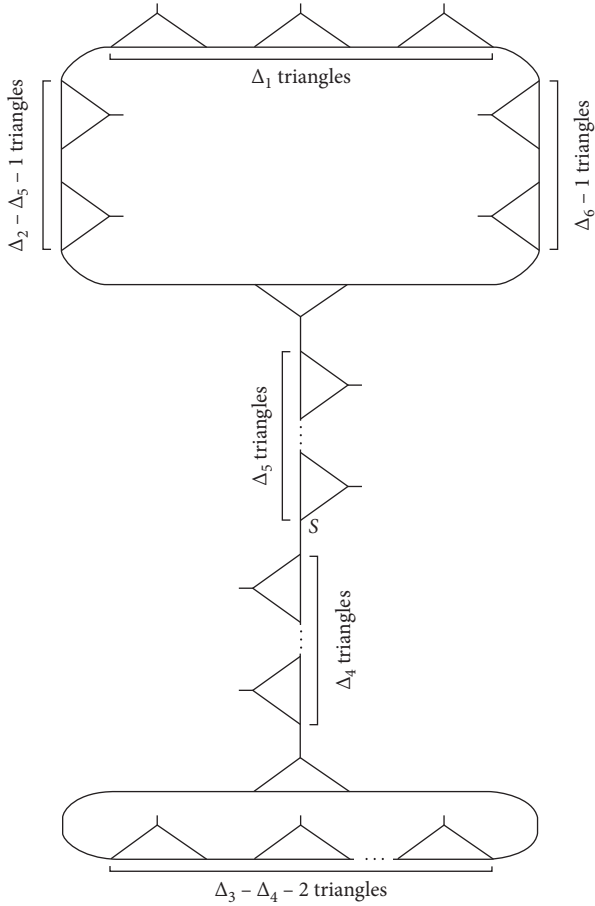


FIGURE 53: Homomorphic image Ω_2^{33} .

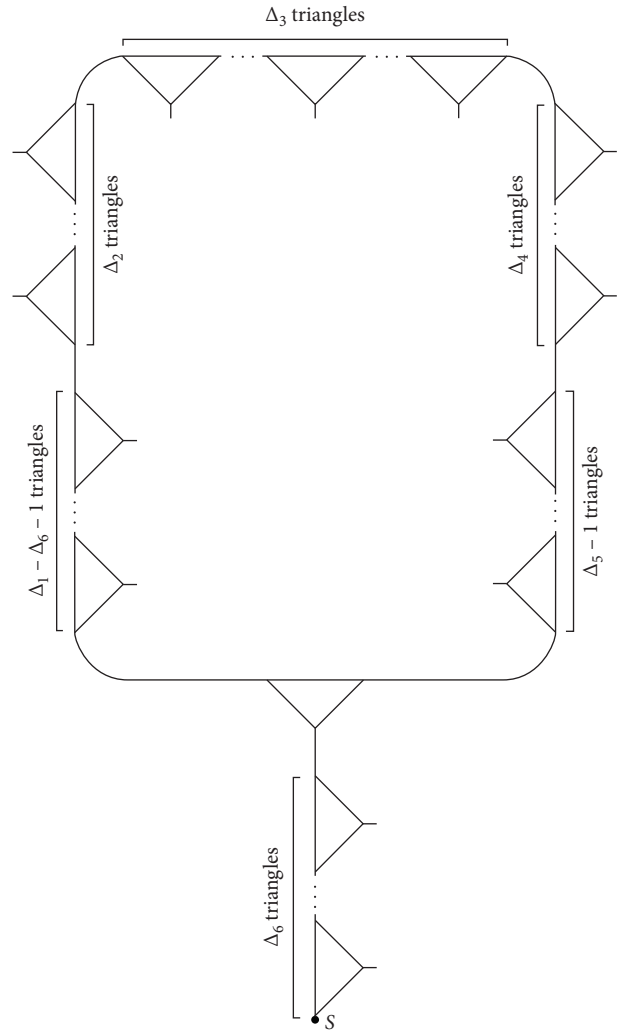


FIGURE 54: Homomorphic image Ω_1^{34} .

$$\begin{aligned}
 & + \sum_{k_1=3}^5 [\Delta_{k_1} + (\Delta_{k_1} - 1) + (\Delta_2 - 1)(\Delta_{k_1} - 1)] + \sum_{k_1=3}^5 [(\Delta_{k_2} - \Delta_4 - 1) + (\Delta_1 - 1)(\Delta_{k_2} - 1) + \frac{1}{2}\Delta_{k_2}(\Delta_{k_2} - 1) + (\Delta_{k_2} - 1) \\
 & + \frac{1}{2}(\Delta_{k_2} - 1)(\Delta_{k_2} - 2)] \\
 & + \sum_{k_3=1}^2 [\Delta_{k_3} - \Delta_5 - 1 + 1 + 1] + \sum_{k_4=1,4} \left[\frac{1}{4}(\Delta_{k_4}^2 - 2\Delta_{k_4} + \Delta_{(4,k_4)}) + \frac{1}{2}(\Delta_{k_4} - \eta_{(4,k_4)}) \right] + \sum_{k_5=2,4} [1] + \sum_{k_6=1,2,5} [1] \\
 & = \frac{1}{4} [(\Delta_1 + 2\Delta_2 + 2\Delta_3 + \Delta_4)^2 + 4(\Delta_1 + 2\Delta_2 + 2\Delta_3 + \Delta_4) + 4\Delta_4 + \eta].
 \end{aligned}$$

(33)

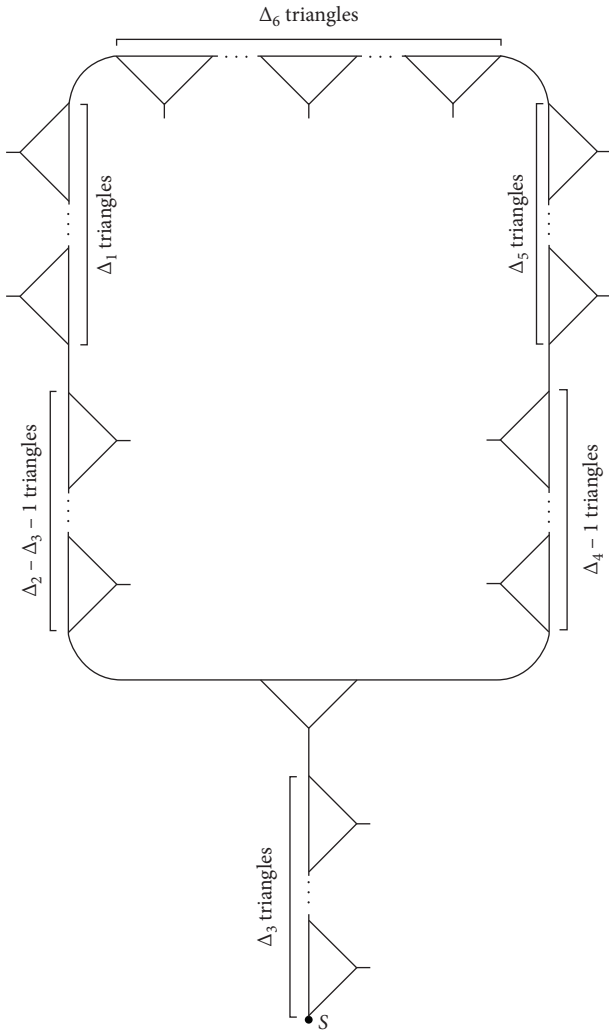


FIGURE 55: Homomorphic image Ω_2^{34} .

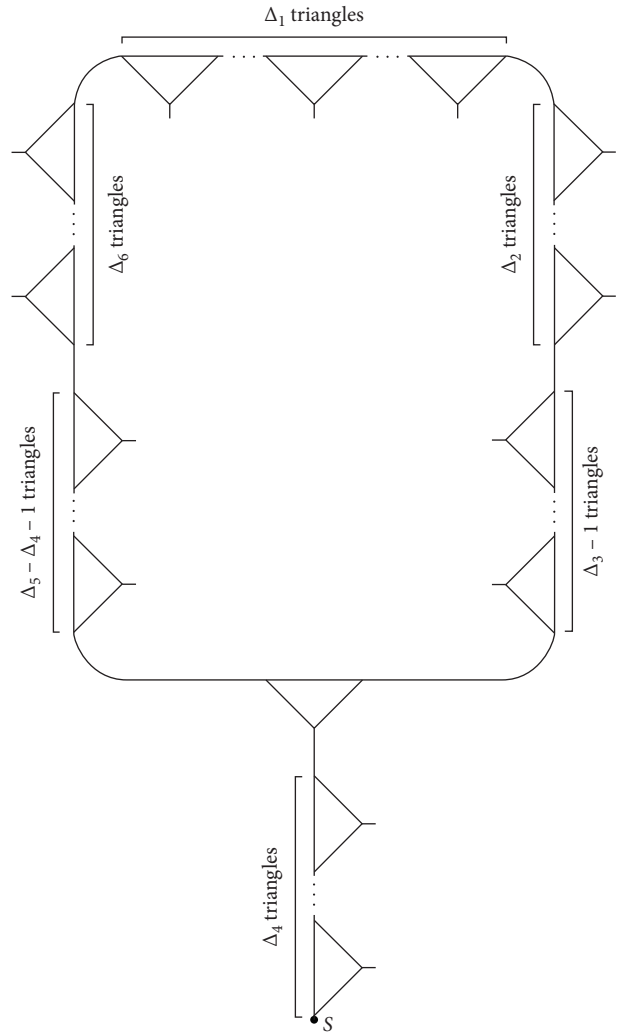


FIGURE 56: Homomorphic image Ω_5^{34} .

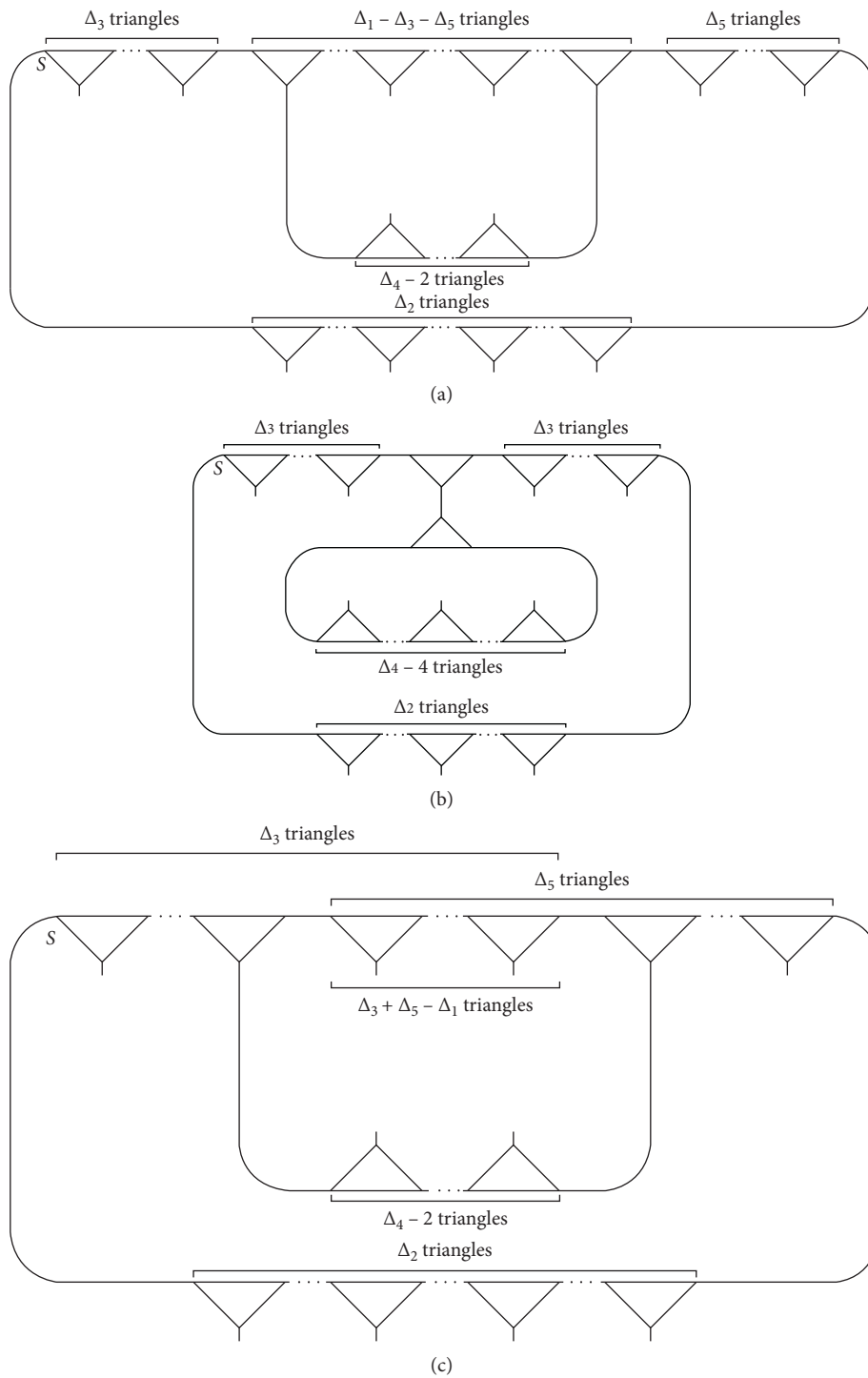


FIGURE 57: (a) Homomorphic image Ω_1^{35} : $\Delta_1 > \Delta_3 + \Delta_5 + 1$. (b) Homomorphic image Ω_1^{35} : $\Delta_1 = \Delta_3 + \Delta_5 + 1$. (c) Homomorphic image Ω_1^{35} : $\Delta_1 < \Delta_3 + \Delta_5 + 1$.

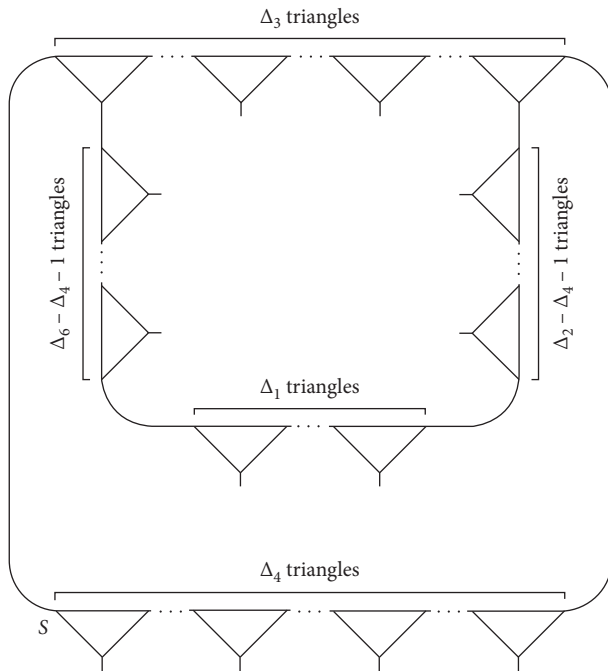


FIGURE 58: Homomorphic image Ω_2^{35} .

The value of $|H|$ gives the total number of homomorphic images produced in the contraction of all pairs of vertices of Δ . The value of S' guaranteed that the set H contains all homomorphic images. \square

2. Conclusion

Thus, there are total $(1/2)[9(\Delta_1 + 2\Delta_2 + 2\Delta_3 + \Delta_4) - 3(\Delta_1 + 2\Delta_2 + 2\Delta_3 + \Delta_4)]$ number of elements in $V(\Delta \times \Delta)$. To find all distinct homomorphic images, we do not need to contract each pair of vertices of $V(\Delta \times \Delta)$. We have to contract only those pairs of vertices, which are in set S and they are $(1/4)[(\Delta_1 + 2\Delta_2 + 2\Delta_3 + \Delta_4)^2 + 4(\Delta_1 + 2\Delta_2 + 2\Delta_3 + \Delta_4) + 4\Delta_4 + \eta]$ in numbers because if we contract the pair which is not belong to set S , we attain the homomorphic image, which we already acquired by contracting the element of set S .

3. Applications of Homomorphic Copies in Lightweight Cryptography and Chemistry

The construction of any product by using minimum resources without compromising on quality is primary objective of scientists.

The coset diagrams with 256 vertices are used in the construction of strong 8×8 S-boxes [9]. In present-day block ciphers, cryptographically secure S-boxes are designed to attain the requirements of Shannon's necessity for perplexity. Substitution boxes are the fundamental segments in numerous Feistel network-based block cryptosystems or substitution-permutation (S-P) networks. The use of 8×8 S-boxes in block cipher is excessively costly. So, it is not surprising that we are seeing strong progress in the field of lightweight cryptography in recent years, for instance

PRESENT. Lightweight cryptographic calculations are utilized in business items, including DESL, PRINTCIPHER, SEA, HIGHT, PRESENT, LED, and KATAN/KTANTAN. For instance, Keeloq is a 32-bit block cipher frequently utilized in the automobile business. Digital signature transponder is a 40-bit block cipher, implemented in wireless authentication systems. Since a homomorphic copy of a graph is smaller graph with the same algebraic structure, it can be quite handy to generate small sized S-boxes by using homomorphic copies of the coset diagram having 256 vertices.

Interrelation of certain types of coset graphs and structure of carbon allotropes not only highlights the connection but also improvises applications in many fields.

Several forms of carbon can be found in nature. One of the most important allotropes of carbon is fullerene which was discovered in 1985. Fullerenes are carbon-cage-like polyhedral molecules in which a large number of carbon atoms are bonded in a nearly spherical symmetric configuration. Fullerenes C_n can be drawn for $n = 20$ and for all even $n \geq 24$. They have n carbon atoms, $(3n/2)$ bonds, 12 pentagonal faces, and $(n/2) - 10$ hexagonal faces. The most important member of the family of fullerenes is C_{60} . Fullerenes can be classified in terms of their groups of symmetries. These groups are also known as point groups. Every element of a point group is an isometry of the Euclidian space and so it is either a rotation around an axis or it is a reflection in a plane. The list of all 28 fullerene point groups is: $I_h, I, T_h, T_d, T, D_{6h}, D_{6d}, D_6, D_{5h}, D_{5d}, D_5, D_{3h}, D_{3d}, D_3, D_{2h}, D_{2d}, D_2, S_6, S_4, C_{3h}, C_{2h}, C_{3v}, C_3, C_{2v}, C_2, C_s, C_i$, and C_1 [10]. Fullerene C_{60} has icosahedral symmetry, that is, the symmetry group is isomorphic to A_5 . A constructive enumeration of fullerenes has been dealt in detail in [11]. The structure of coset graphs of fullerene C_{60} , symmetry group $PSL(2, 5)$ and adjacency matrix has been explored through the action of modular group in [12]. Another carbon allotrope with high permutational symmetry is allotrope D_{168} Schwarzite, proposed by Vanderbilt and Tersoff, which has an automorphism group of order 168. In [13], it has been shown that coset diagram for $PSL(2, 7)$ points has interesting relation with carbon allotrope with negative curvature D_{168} Schwarzite. The future studies may extend the present study by investigating the homomorphic copies of the coset graphs for $PSL(2, 5)$ and $PSL(2, 7)$ and their related chemical structures.

Data Availability

No datasets were generated or analyzed during the current study.

Conflicts of Interest

The authors declare that they have no conflicts of interest.

References

- [1] M. Akbas, "On suborbital graphs for the modular group," *Bulletin of the London Mathematical Society*, vol. 33, no. 3, pp. 647–652, 2001.

- [2] Ö. Koruoğlu, “The determination of parabolic points in modular and extended modular groups by continued fractions,” *Bulletin of the Malaysian Mathematical Sciences Society*, vol. 33, no. 3, pp. 439–445, 2010.
- [3] Q. Mushtaq, *Coset Diagrams for the Modular Group*, University of Oxford, Oxford, UK, 1983.
- [4] Q. Mushtaq, “Modular group acting on real quadratic fields,” *Bulletin of the Australian Mathematical Society*, vol. 37, no. 2, pp. 303–309, 1988.
- [5] M. A. Malik and M. A. Zafar, “Real quadratic irrational numbers and modular group action,” *Southeast Asian Bulletin of Mathematics*, vol. 35, no. 3, pp. 439–445, 2011.
- [6] S. M. Husnine, M. A. Malik, and A. Majeed, “On ambiguous numbers of an invariant subset under the action of the modular group $\text{St u diaPSL}(2, \mathbb{Z})$,” *Scientiarum Mathematicarum Hungarica*, vol. 42, no. 4, pp. 401–412, 2005.
- [7] A. Torstensson, “Coset diagrams in the study of finitely presented groups with an application to quotients of the modular group,” *Journal of Commutative Algebra*, vol. 2, no. 4, pp. 501–514, 2010.
- [8] Q. Mushtaq and A. Razaq, “Equivalent pairs of words and points of connection,” *The Scientific World Journal*, vol. 2014, Article ID 505496, 8 pages, 2014.
- [9] A. Razaq, A. Yousaf, U. Shuaib, N. Siddiqui, A. Ullah, and A. Waheed, “A novel construction of substitution box involving coset diagram and a bijective map,” *Security and Communication Networks*, vol. 2017, Article ID 5101934, 16 pages, 2017.
- [10] P. W. Fowler and D. E. Manolopoulos, “An atlas of fullerenes,” *Courier Corporation*, 2007.
- [11] G. Brinkmann and A. W. M. Dress, “A constructive enumeration of fullerenes,” *Journal of Algorithms*, vol. 23, no. 2, pp. 345–358, 1997.
- [12] Q. Mushtaq and A. Rafiq, “Adjacency matrices of $\text{PSL}(2, 5)$ and resemblance of its coset diagrams with fullerene C_{60} ,” in *Academy of Mathematics and Systems Science, Chinese Academy of Sciences*, vol. 20, pp. 541–552, no. No. 04, Suzhou University, Suzhou, China, 2013.
- [13] Q. Mushtaq and N. Mumtaz, “ $\text{PSL}(2, 7)$ and carbon allotrope D_{168} Schwarzite,” *Journal of Mathematical Chemistry*, vol. 56, no. 8, pp. 2485–2494, 2018.

Research Article

Research on DNA Nanostructures Based on the Hybrid Chain Reaction for the Assignment Problem

Risheng Wang,¹ Zhixiang Yin ,² Jing Yang,¹ Xinmu Yang,¹ and Zhen Tang¹

¹Anhui University of Science and Technology, Huainan, China

²Shanghai University of Engineering Science, Shanghai, China

Correspondence should be addressed to Zhixiang Yin; 2308182296@qq.com

Received 8 February 2021; Revised 23 March 2021; Accepted 15 April 2021; Published 12 July 2021

Academic Editor: Ghulam Mustafa

Copyright © 2021 Risheng Wang et al. This is an open access article distributed under the Creative Commons Attribution License, which permits unrestricted use, distribution, and reproduction in any medium, provided the original work is properly cited.

Nanostructures with information processing play an important role in many fields. It is an excellent approach to the application that DNA nanostructures represented by DNA origami molecules combine with the hybrid chain reaction. In this paper, the assignment problem is mapped to a combinatorial graph on the DNA origami substrate. The graph has several modules corresponding to the time efficiency matrix of the assignment problem. The starting chain of the corresponding module is hybridized with the hairpin structure of the starting point, and the corresponding module is opened to emit light. The feasible solution to the problem can be obtained by observing the light-emitting fluorescent numbers of the opened modules. The fluorescent numbers of all the opened modules are added up on the same origami substrate, then different opening methods in different test tubes are compared, and the optimal solution is obtained.

1. Introduction

DNA nanostructure is being studied by more and more scholars, and it has become the main way to construct nanomaterials. DNA nanostructures from one-dimensional to two-dimensional and three-dimensional structures play an increasingly important role in related issues [1–4]. In 2006, Rothmund proposed a new DNA nano-self-assembly method—DNA origami [5]. DNA origami is a kind of phage DNA chain as a scaffold. We call it scaffold chain folding back and forth using multiple stapling chains to fix the shape, and we can get a sophisticated two-dimensional structure. DNA origami has the advantages of high assembly efficiency, nanostructure programmability, and nanostructure addressability. DNA origami can construct many complex and diverse nanostructures, and its substrate has great advantages in assembling functional carbon nanotubes, nanoparticles, and proteins [6, 7]. Ke et al. designed and constructed a tetrahedral three-dimensional molecular container by DNA origami. The three-dimensional molecular cage has high stability and has potential application prospects in the nanofield [8]. Tikhomirov and his team

proposed a fractal assembly method for micron-scale DNA origami arrays with arbitrary patterns. In this paper, square DNA origami tiles with patterns on the surface are used as basic building units to construct patterns such as Mona Lisa and rooster. The construction and successful implementation of this assembly method demonstrate the addressability of DNA origami [9]. Wang et al. used DNA origami nanostructures to visually observe cell uptake and metastasis of tumor cells [10]. DNA origami can construct highly complex nanostructures, which has a wide range of potential applications in the nanofield. In fact, DNA origami has been widely used in logic operation, single-molecule detection, and other fields [11, 12]. DNA origami has been used as the basic template, carbon nanotubes, and protein structure for the assembly of functional metal nanoparticles [13–15].

Hybrid chain reaction (HCR) is a DNA molecular structure interaction method proposed by Dirks and Pierce in 2004. It uses competitive hybridization between nucleic acid probes as the energy source to self-assemble a nucleic acid nanostructure to realize signal amplification [16]. Hybridized chain reaction can take place at room temperature. It is easy to operate and has lower experimental cost.

By combining HCR with G-quadruplex, Dong et al. designed a fluorescent sensor for unlabeled detection of target DNA. When the target DNA strand exists, it opens two hairpin probes and hybridizes them as a trigger chain. HCR forms long double chains and releases G-quadruplex to detect target DNA by changing the fluorescence intensity before and after the reaction [17]. Xiao et al. designed a variety of chemiluminescent imaging technologies aiming at the hybridization chain reaction amplification of DNA microarrays and adjacent binding [18]. In this paper, the correct solution of logical circuit can be obtained on the basis of hybrid chain reaction. Chao et al. integrated DNA origami with the hybrid chain reaction to design a single-molecule DNA navigator to solve the maze problem. In this design, the 2D origami model is used as the base, and the near-end-chain exchange cascade reaction based on the hybrid chain reaction is used for unidirectional amplification on the base. Finally, the correct route of the maze problem is obtained through the atomic force microscope observation [19]. It has been proved to have good application prospects like hybrid chain reaction combined with DNA origami structure [20–32].

DNA nanostructure and hybrid chain reaction were used to design the graph on the origami substrate. The starting chain was put into the reaction solution and hybridized with the hairpin structure to open the corresponding module. The sequence of the DNA strand in the model is carefully designed, which ensures that the system is stable in solution without any reaction. By reacting with the hairpin structure on the origami substrate in the solution, the corresponding module is opened, and the fluorescence emits light. By adding up the fluorescent numbers of the opened modules on the same origami substrate, we can get the feasible solution.

2. Background Knowledge

2.1. DNA Origami and Hybrid Chain Reaction. DNA origami is to fold a long M13mp18 phage DNA strand back and forth and to use multiple short chains to fix the shape to obtain the fine and complex structure. The design of the DNA chain is relatively simple, and the assembly efficiency is high. The site selection can be achieved by redesigning the staple chain (short chain) and scaffold chain (long chain) to complement each other.

Hybrid chain reaction (HCR) is a new signal amplification method proposed by Dirks and Pierce. It designs different oligonucleotides and uses a small nucleotide chain as an initiator to induce oligonucleotides to hybridize with each other to form DNA with spatial structure. The reaction conditions are mild, and the operation is simple. The reaction principle is shown in Figure 1.

C_1 and C_2 are two hairpin DNA strands that are stable in solution. They are composed of sticky ends, double-stranded “stems,” and single-stranded loops, as shown in the left side of Figure 1. T is the starting strand, which is a single strand of DNA composed of two parts. When the starting chain is added, its two segments hybridize with the sticky end, and the stem of C_1 and the hairpin segment of C_1 are opened, as

shown in the middle of Figure 1. The exposed section of C_1 hybridizes with C_2 , and the hairpin section of C_2 is opened, as shown in the right side of Figure 1. The exposed section of C_2 continues to hybridize with the next C_1 , open up the clamp structure, and repeat the reaction in turn until C_1 and C_2 in the solution are exhausted. Finally, a long DNA nanowire assembled spontaneously by alternate hybridization of C_1 and C_2 is formed. Each priming strand is equivalent to the growth site of a DNA nanowire.

2.2. Assignment Problem. The assignment problem is a special integer programming problem. There are a certain number of tasks and the same number of people. Each person can complete the task, but the time cost is different. So, we need to find a way of assignment to minimize the total time (or the total efficiency of completing the tasks is the highest). Such problems are called assignment problems.

It is often encountered in life. Each person has different expertise and completes the task differently, so the efficiency is also different. In an actual assignment problem, the cost for the i -th person to complete the j -th task is C_{ij} . Then, n individuals and n tasks are combined one by one to get n^2 costs, which are listed into a matrix to get the coefficient matrix of the assignment problem.

3. DNA Origami Model

3.1. Model Composition and Design. For the assignment problem, we present a combinatorial graph of the hairpin structure on DNA origami. It is mapped to the efficiency or time matrix of the assignment problem. The combination has $n \times n$ modules, and each module has a corresponding number of hairpin structures, corresponding to the efficiency or time required for a person to complete a task in the problem. In each module of the graph, the first chain is a common hairpin structure, and the rest are molecular beacons with fluorescent group and quenching group markers, as shown in Figure 2. The origami substrate is represented by gray in the figure. On the origami substrate, there are staple chains (light purple in the figure) extending at corresponding distances, and they connect molecular beacons and ordinary hairpin structures. The distance between adjacent hairpin structures in each module is just the distance that can be connected by opening the auxiliary chain (intermediate chain). Enough space is provided between modules, which enables the same module to react completely and avoids the interaction of different modules.

Molecular beacon and hairpin structure: they are composed of several oligoglycosidic acid segments. A “ring” is a single chain, two complementary segments form a double chain, and the other segment is complementary to the sticky end of a staple chain extending from the origami base to fix the chain on the origami substrate. The molecular beacon has two more sticky ends with the luminescent fluorescent group and quenching group than the ordinary hairpin structure. They do not light up when they are not turned on; they are only turned on while the starting chain and auxiliary chain are added. The molecular beacon fixed

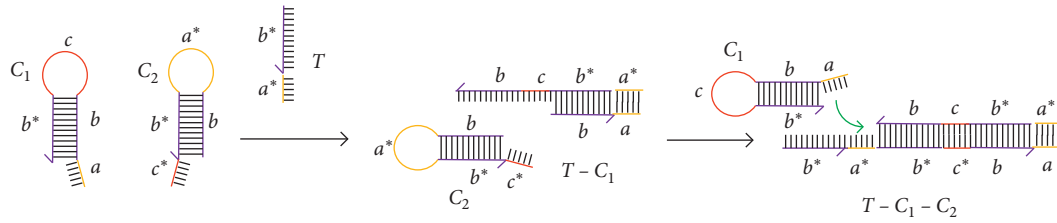


FIGURE 1: Basic principle of the hybrid chain reaction.

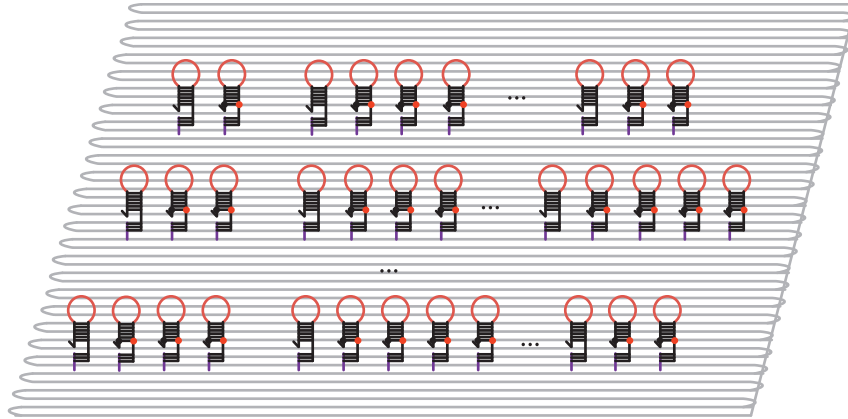


FIGURE 2: The diagram of the origami substrate and hairpin structure.

on the origami substrate can represent the efficiency (the time required) of the assignment problem. In this way, it can be used for graphic design to solve the optimal problem.

The DNA origami substrate with the hairpin structure can be stable in solution. To open the hairpin structure, the corresponding starting chain is added, whose structure is composed of two oligonucleotide fragments, as shown in Figure 3(a). Only the corresponding starting chain can open the corresponding hairpin structure. After opening the first hairpin structure of each module, the intermediate chain needs to open all the other molecular beacons in the module. The intermediate chain can also exist stably in the solution without adding the starting chain. The intermediate chain is composed of four oligoglycosidic acid segments, as shown in Figure 3(b).

3.2. Model Graphic Realization. According to the composition of the model, the combination graph reflecting the assignment problem matrix is designed. The graph has n^n modules. Each module starts with an ordinary hairpin structure followed by the molecular beacons. The base of the hairpin structure at the beginning of each module is different, while the other molecular beacons are the same. Here, because the hairpin structure of the first starting point of each module can only be opened by adding the corresponding starting chain, we will design the molecular beacon of all modules after the hairpin structure of the starting point to be the same, which can greatly simplify the design and model construction. The hairpin structure base of the starting point is mostly the same as the molecular beacon

base; only the base of the molecular beacon at the binding marker and the one at the junction of the starting chain are different, as shown in Figure 4. In the composite pattern on the origami substrate, all the starting hairpin structures can be regarded as composed of five oligoglycosidic acid fragments, and the subsequent molecular beacon can be regarded as composed of five oligoglycosidic acid fragments, fluorescent groups and quenching groups. One of them complements the sticky end of the staple chain extending from the base, and all the hairpins in this section have the same structure. The rest of the segments are shown in the hairpin structure in Figure 4, and we mark them with letters. The design of three sections is the same for all hairpin structures. There are two complementary segments forming a double chain, named s and s^* segments, respectively, and one segment is a ring structure, named o segment. Compared with the hairpin structure of the starting point, the two sticky ends of the s and s^* segments of the latter molecular beacon have luminescent fluorescent groups and absorbable fluorescence quenching groups. However, the oligoglycosidic acid fragment is different that binds the starting chain and the hairpin structure at the beginning of each module, which is labeled a_i, b_i, c_i, \dots . For other molecular beacons, the design of this segment is the same, and we mark it as segment e .

Origami base and intermediate chain have been in the solution in advance, and then the starting chain corresponding to the opening module is added to the solution. When the start chain is added, it opens the hairpin structure of the starting point. The opening process is shown in Figure 5. The corresponding section of the starting chain

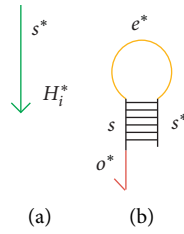


FIGURE 3: Starting chain (a) and intermediate chain (b).

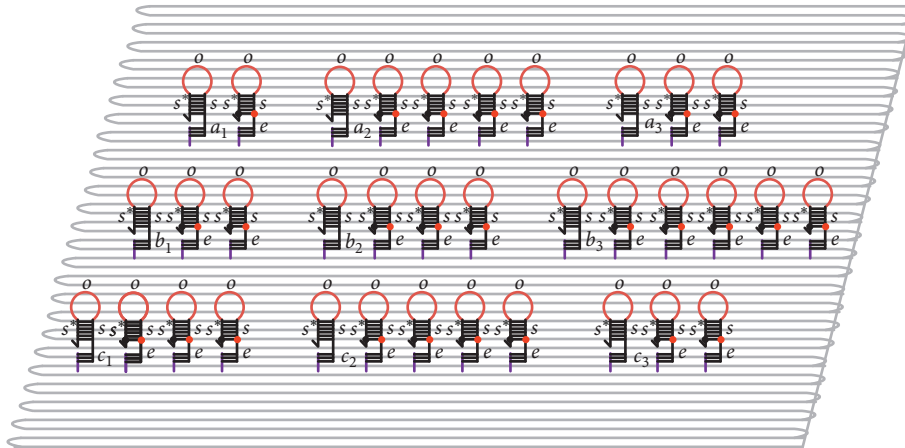


FIGURE 4: Hairpin structure designed on the origami substrate.



FIGURE 5: Opening process after adding the starting chain.

complements the corresponding section of the starting hairpin structure to open the hairpin structure. Correspondingly, the starting hairpin structure and the intermediate chain complement each other and then open the intermediate chain. The intermediate chain can continue to complement the molecular beacon, open the molecular beacon, and make the hairpin luminescent.

The biological algorithm based on the calculation model of the hybrid chain reaction assignment problem is as follows:

- (1) For the assignment problem with n implementers and n tasks, all possible solutions are $n!$, corresponding to $n!$ different opening modules' combinations of the DNA strand.
- (2) Construct the combinatorial graph on DNA origami (n) of corresponding variables, and put them in the test tubes ($n!$ in total). Add a set of DNA start strands to each test tube, and perform the DNA hybrid chain reaction.
- (3) After the reaction is completed, each test tube has a combination mode of opening the hairpin structure

module, corresponding to a task completion mode, which is the feasible solution of the problem.

- (4) By comparing the light-emitting fluorescent number in different test tubes, the efficiency of different ways is obtained, and then the optimal solution is determined.

3.3. Case Analysis. To illustrate the feasibility of DNA computing to solve the assignment problem, an example of an assignment problem is given to verify it.

The calculation process of the assignment problem with an efficiency value in Table 1 is as follows.

It can be seen from the above algorithm that, for the assignment problem of three implementers completing three tasks, all possible solutions are $3! = 6$, corresponding to the DNA origami base combination graph composed of nine modules. Each module is composed of a common hairpin structure at the starting point and a luminous molecular beacon at the back. The number of molecular beacons corresponds to the efficiency of an implementer to complete a task. Because the possible solutions are 6, the designed

TABLE 1: Assignment problem efficiency c_{ij} data.

Number of people	Task		
	1	2	3
1	1	4	1
2	2	3	2
3	3	4	1

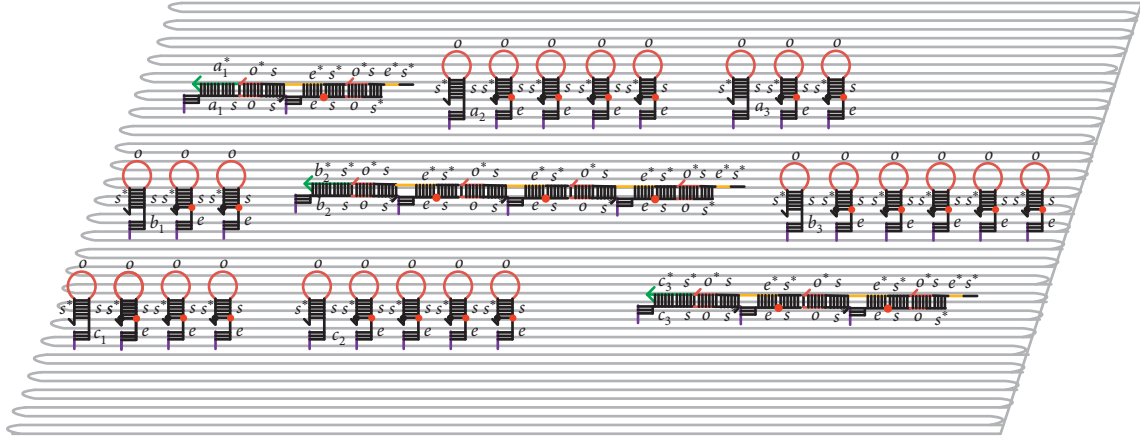


FIGURE 6: Optimal solution of the origami substrate after the reaction.

origami substrate is put into 6 test tubes. A set of promoter chains were added to each tube and hybridized at room temperature. Each group of chains is the starting chain corresponding to three modules in different rows and columns. In this way, in each test tube, three modules in different rows and columns are opened to emit light. After the reaction, the DNA strand on the origami substrate is shown in Figure 6. By observing the fluorescent number of each tube, the one with the least fluorescent number is the optimal solution. Finally, the origami base with the least open fluorescent number is a_1, b_2, c_3 , that is, the optimal solution is (1, 0, 0, 0, 1, 0, 0, 0, 0, 1).

4. Simulation

In this paper, a DNA origami model based on the DNA nanostructure is constructed, which can be used to solve assignment problems. The simulation results are consistent with the expected results of the system. The molecular beacon was used as reactant, and the reaction concentration gradually approached 0. The concentration of intermediate chain tends to be stable. The simulation results show that the model has good performance compared with the previous work.

5. Conclusion

In this paper, DNA nanostructures are combined with the hybrid chain reaction to establish a DNA origami model that solves the assignment problem. We design the hairpin structure on the origami base, which can solve simple assignment problems. By adding the starting chain, the corresponding module is opened to obtain the optimal solution.

With the development of molecular biology and bioengineering, this method is expected to have more progress in reusability and can be further expanded to solve more complex problems.

Data Availability

The data used to support the findings of this study are available from the corresponding author upon request.

Conflicts of Interest

The authors declare that they have no conflicts of interest.

References

- [1] E. Winfree, *Algorithmic Self-Assembly of DNA*, California Institute of Technology, CA, USA, 1998.
- [2] T. H. LaBean, "Another dimension for DNA art," *Nature*, vol. 459, no. 7245, pp. 331-332, 2009.
- [3] P. Yin, H. M. T. Choi, C. R. Calvert, and N. A. Pierce, "Programming biomolecular self-assembly pathways," *Nature*, vol. 451, no. 7176, pp. 318-322, 2008.
- [4] P. Yin, R. F. Hariadi, S. Sahu et al., "Programming DNA tube circumferences," *Science*, vol. 321, no. 5890, pp. 824-826, 2008.
- [5] P. W. K. Rothemund, "Folding DNA to create nanoscale shapes and patterns," *Nature*, vol. 440, no. 7082, pp. 297-302, 2006.
- [6] F. Zhang, J. Nangreave, Y. Liu, and H. Yan, "Reconfigurable DNA origami to generate quasifractal patterns," *Nano Letters*, vol. 12, no. 6, pp. 3290-3295, 2012.

- [7] B. Wei, M. Dai, and P. Yin, "Complex shapes self-assembled from single-stranded DNA tiles," *Nature*, vol. 485, no. 7400, pp. 623–626, 2012.
- [8] Y. Ke, J. Sharma, M. Liu, K. Jahn, Y. Liu, and H. Yan, "Scaffolded DNA origami of a DNA tetrahedron molecular container," *Nano Letters*, vol. 9, no. 6, pp. 2445–2447, 2009.
- [9] G. Tikhomirov, P. Petersen, and L. Qian, "Fractal assembly of micrometre-scale DNA origami arrays with arbitrary patterns," *Nature*, vol. 552, no. 7683, pp. 67–71, 2017.
- [10] P. Wang, M. A. Rahman, Z. Zhao et al., "Visualization of the cellular uptake and trafficking of DNA origami nanostructures in cancer cells," *Journal of the American Chemical Society*, vol. 140, no. 7, pp. 2478–2484, 2018.
- [11] C. Zhang, J. Yang, S. Jiang, Y. Liu, and H. Yan, "DNAzyme-based logic gate-mediated DNA self-assembly," *Nano Letters*, vol. 16, no. 1, pp. 736–741, 2016.
- [12] D. Wang, Y. Fu, J. Yan et al., "Molecular logic gates on DNA origami nanostructures for microRNA diagnostics," *Analytical Chemistry*, vol. 86, no. 4, pp. 1932–1936, 2014.
- [13] H. Yan, S. H. Park, G. Finkelstein, J. H. Reif, and T. H. LaBean, "DNA-templated self-assembly of protein arrays and highly conductive nanowires," *Science*, vol. 301, no. 5641, pp. 1882–1884, 2003.
- [14] N. V. Voigt, T. Tørring, A. Rotaru et al., "Single-molecule chemical reactions on DNA origami," *Nature Nanotechnology*, vol. 5, no. 3, pp. 200–203, 2010.
- [15] H. T. Maune, S.-P. Han, R. D. Barish et al., "Self-assembly of carbon nanotubes into two-dimensional geometries using DNA origami templates," *Nature Nanotechnology*, vol. 5, no. 1, pp. 61–66, 2010.
- [16] R. M. Dirks and N. A. Pierce, "From the cover: triggered amplification by hybridization chain reaction," *Proceedings of the National Academy of Sciences*, vol. 101, no. 43, pp. 15275–15278, 2004.
- [17] J. Dong, X. Cui, Y. Deng, and Z. Tang, "Amplified detection of nucleic acid by G-quadruplex based hybridization chain reaction," *Biosensors and Bioelectronics*, vol. 38, no. 1, pp. 258–263, 2012.
- [18] Q. Xiao, J. Wu, P. Dang, and H. Ju, "Multiplexed chemiluminescence imaging assay of protein biomarkers using DNA microarray with proximity binding-induced hybridization chain reaction amplification," *Analytica Chimica Acta*, vol. 1032, pp. 130–137, 2018.
- [19] J. Chao, J. Wang, F. Wang et al., "Solving mazes with single-molecule DNA navigators," *Nature Materials*, vol. 18, no. 3, pp. 273–279, 2019.
- [20] M. Xiao, W. Lai, T. Man et al., "Rationally engineered nucleic acid architectures for biosensing applications," *Chemical Reviews*, vol. 119, no. 22, pp. 11631–11717, 2019.
- [21] S. Shah, A. K. Dubey, and J. Reif, "Improved optical multiplexing with temporal DNA barcodes," *ACS Synthetic Biology*, vol. 8, no. 5, pp. 1100–1111, 2019.
- [22] S. D. Mason, Y. Tang, Y. Li, X. Xie, and F. Li, "Emerging bioanalytical applications of DNA walkers," *TrAC Trends in Analytical Chemistry*, vol. 107, pp. 212–221, 2018.
- [23] K. Chen, J. Zhu, F. Bošković, and U. F. Keyser, "Nanopore-based DNA hard drives for rewritable and secure data storage," *Nano Letters*, vol. 20, no. 5, pp. 3754–3760, 2020.
- [24] Z. Zeng, R. Zhou, R. Sun et al., "Nonlinear hybridization chain reaction-based functional DNA nanostructure assembly for biosensing, bioimaging applications," *Biosensors and Bioelectronics*, vol. 173, p. 112814, 2021.
- [25] A. E. Kiouche, M. Bessedik, F. Benbouzid-SiTayeb, and M. R. Keddar, "An efficient hybrid multi-objective memetic algorithm for the frequency assignment problem," *Engineering Applications of Artificial Intelligence*, vol. 87, p. 103265, 2020.
- [26] Z. Zhang, Y. Yang, F. Pincet, M. C. Llaguno, and C. Lin, "Placing and shaping liposomes with reconfigurable DNA nanocages," *Nature Chemistry*, vol. 9, no. 7, pp. 653–659, 2017.
- [27] X. Song and J. Reif, "Nucleic acid databases and molecular-scale computing," *ACS Nano*, vol. 13, no. 6, pp. 6256–6268, 2019.
- [28] J. O'Brien and A. Murugan, "Temporal pattern recognition through analog molecular computation," *ACS Synthetic Biology*, vol. 8, no. 4, pp. 826–832, 2019.
- [29] G. Chatterjee, N. Dalchau, R. A. Muscat, A. Phillips, and G. Seelig, "A spatially localized architecture for fast and modular DNA computing," *Nature Nanotechnology*, vol. 12, no. 9, pp. 920–927, 2017.
- [30] K. Sergio, W. J. Paschoalino, and L. T. Kubota, "Supramolecular DNA origami nanostructures for use in bioanalytical applications," *TrAC Trends in Analytical Chemistry*, vol. 108, pp. 88–97, 2018.
- [31] K. E. Bujold, A. Lacroix, and H. F. Sleiman, "DNA nanostructures at the interface with biology," *Chem*, vol. 4, no. 3, pp. 495–521, 2018.
- [32] T. Fu, Y. Lyu, H. Liu et al., "DNA-based dynamic reaction networks," *Trends in Biochemical Sciences*, vol. 43, no. 7, pp. 547–560, 2018.

Research Article

A Class of Sextic Trigonometric Bézier Curve with Two Shape Parameters

Salma Naseer,¹ Muhammad Abbas ,¹ Homan Emadifar ,² Samia Bi Bi,³ Tahir Nazir,¹ and Zaheer Hussain Shah⁴

¹Department of Mathematics, University of Sargodha, Sargodha 40100, Pakistan

²Department of Mathematics, Islamic Azad University, Hamedan Branch, Hamedan, Iran

³School of Mathematical Sciences, Universiti Sains Malaysia, Gelugor, Penang 11800, Malaysia

⁴Department of Physics, University of Management and Technology, Lahore, Pakistan

Correspondence should be addressed to Homan Emadifar; homan_emadi@yahoo.com

Received 25 April 2021; Revised 5 June 2021; Accepted 19 June 2021; Published 28 June 2021

Academic Editor: Muhammad Aslam

Copyright © 2021 Salma Naseer et al. This is an open access article distributed under the Creative Commons Attribution License, which permits unrestricted use, distribution, and reproduction in any medium, provided the original work is properly cited.

In this paper, we present a new class of sextic trigonometric Bernstein (ST-Bernstein, for short) basis functions with two shape parameters along with their geometric properties which are similar to the classical Bernstein basis functions. A sextic trigonometric Bézier (ST-Bézier, for short) curve with two shape parameters and their geometric characteristics is also constructed. The continuity constraints for the connection of two adjacent ST-Bézier curves segments are discussed. Shape control parameters can provide an opportunity to modify the shape of curve as designer desired. Some open and closed curves are also part of this study.

1. Introduction

A Bézier curve is a parametric curve that is used to draw the shapes in the fields of computer graphics and computer-aided geometric design. The Bézier curve is usually followed by the defining polygon. The tangent vectors direction at the end is the same as the vector defined by the first and last segment of the Bézier curves. It is useful in many industrial and engineering fields with various applications. Since Bézier curve always mimics the shape of its control polygon, designers can easily attain the required shape for designing purposes.

The trigonometric Bézier curves got a lot of attention in the fields of computer graphics and computer-aided geometric design due to their construction of conic section. Bézier curve with two parameters and control point was introduced by Kun [1], but the behavior of curve was not symmetric. The generalized Bézier-like curve with all of its geometric characteristics and continuity conditions is described by Yan and Liang [2]. They also applied the generalized Bézier-like curve for the tensor product surfaces to

gain access for triangular surfaces as well. The modeling of innovative surfaces based on stream curves was described by Liu et al. [3]. By extending the concept of Bézier curve, Li [4] defined alpha-Bézier-like curves of degree n with shape control parameters. The properties and applications of alpha-Bézier-like curves are also given. Han et al. [5–7] introduced some cubic and quartic trigonometric Bézier curves. They created an ellipse by using a cubic trigonometric Bézier curve and some designing and geometric modeling also made by continuity conditions. The behavior of shape control parameters also examined on these Bézier curves. Xiujuan et al. [8] investigated special revolution surfaces and their dramatic improvement. Bashir et al. [9] derived a class of quasi-quartic trigonometric Bézier curves with two shape parameters and proved their geometric features. The properties of the basis functions and curves are established, and the effect of the shape control parameters is also discussed. Practical applications of Bézier curves in geometric modeling and engineering are limited due to their shortcomings, and much work has been done to resolve these shortcomings [10–16].

BiBi et al. [17, 18] suggested a new method for solving the problem of constructing symmetric curves and surfaces by using GHT-Bézier curves with four different shape parameters. The shape of curves can easily be modified by using different values of shape parameters. They generated some free-form complex curves with parametric continuity conditions by using GHT-Bézier curves to demonstrate the efficiency of modeling. Yan and Liang [2] used the recursive technique to create the rectangular Bézier curve and surface based on a new class of polynomial basis functions with one shape parameter. Hu et al. [19] presented a novel scheme to generate free-form complex figures using shape-adjustable generalized (SG) Bézier curves with some geometric continuities conditions. They constructed the necessary and sufficient constraints for G^1 and G^2 continuity for connection of two adjacent SG-Bézier curves to overcome the difficulty that most of the composite curves in engineering cannot often be constructed by using only a single curve. Majeed and Qayyum [20] presented the cubic and rational cubic trigonometric B-spline curves using new trigonometric functions with shape parameter. The proposed curves inherit the basic properties of classical B-spline and have been proved. Misro et al. [21] developed the general technique to construct S- and C-shaped transition curves using cubic trigonometric Bézier Curve with two shape parameters which satisfy G^2 Hermite condition. Misro et al. [22] constructed a new quintic trigonometric Bézier curve that has the potential to estimate the maximum driving speed allowed for safe driving on roads. The shape parameters used in this trigonometric Bézier function provided more flexibility for users in designing highways. The trigonometric Bézier curve of fifth degree with two shape parameters has been presented by Misro et al. [23]. Shape parameters provided more control on the shape of the curve compared to the classical Bézier curve. Juhász and Róth [24] presented a scheme for interpolating the given set of data points with C^n continuous trigonometric spline curves of order $n + 1$ which are produced by blending elliptical arcs with global parameter $\alpha \in (0, \pi)$. Zhu and Han [25] constructed four new trigonometric Bernstein-like basis functions with two exponential shape parameters, based on which a class of trigonometric Bézier-like curves, similar to the cubic Bézier curves, have also been developed. The trigonometric Bézier-like curves corner cutting algorithm was also constructed. Yan and Liang [26] presented a new kind of algebraic-trigonometric blended spline curve, called xyB curves. The proposed curves not only inherit most properties of classical cubic B-spline curves in polynomial space but also enjoy some other advantageous properties for modeling.

In this article, the research begins with the development of new ST-Bernstein basis functions with two shape control parameters. This study also provides a guarantee to construct a new ST-Bézier curve with two shape parameters. The newly constructed curves share all geometric properties of classical Bézier curves except the shape modification property, which is superior to the classical Bézier curve. The C^2 and G^2 continuity constraints are constructed to connect the two adjacent ST-Bézier curves segments. Moreover, in contrast with classical Bézier curves, our proposed scheme gives more

shape adjustability in curve designing. Several examples are presented to show that the proposed method has high applied values in geometric modeling in terms of some closed and open curves.

The remainder of the paper is organized as follows. In Section 2, the new ST-Bernstein basis functions with two parameters are presented, which possess all geometric properties. In Section 3, the graphical representation of ST-Bézier curve with all geometric properties is given. The parametric and geometric continuity conditions with shape control parameters are given in Section 5. Shape control on ST-Bézier curve via shape parameters is given in Section 4. In Section 6, some application to construction of some closed and open curves is given with multiple shape control parameters. Finally, concluding remarks of this work are given in Section 7.

2. Sextic Trigonometric Bernstein Basis Functions

In this section, the ST-Bernstein basis function with two shape parameters μ, ω and their geometric properties is discussed.

Definition 1. For $\eta \in [0, \pi/2]$, the ST-Bernstein basis function with two shape parameters $\mu, \omega \in [-4, 1]$ is defined by

$$\begin{cases} \Phi_0(\eta) = (1 - \sin \eta)^4 (1 - \mu \sin \eta), \\ \Phi_1(\eta) = \sin \eta (1 - \sin \eta)^3 (4 + \mu(1 - \sin \eta)), \\ \Phi_2(\eta) = \sin^2 \eta (1 - \sin \eta)^2 (6 + \mu(1 - \sin \eta)), \\ \Phi_3(\eta) = 1 - \Phi_0(\eta) - \Phi_1(\eta) - \Phi_2(\eta) - \Phi_4(\eta) - \Phi_5(\eta) - \Phi_6(\eta), \\ \Phi_4(\eta) = \cos^2 \eta (1 - \cos \eta)^2 (6 + \omega(1 - \cos \eta)), \\ \Phi_5(\eta) = \cos \eta (1 - \cos \eta)^3 (4 + \omega(1 - \cos \eta)), \\ \Phi_6(\eta) = (1 - \cos \eta)^4 (1 - \omega \cos \eta). \end{cases} \quad (1)$$

The graphical representation of ST-Bernstein basis functions is given in Figure 1. By changing the values of shape control parameters, the variation in graphs of ST-Bernstein basis function is obvious. In Figure 1(a), the ST-Bernstein basis functions are drawn as $\mu = \omega = 1$ (thick red), $\mu = \omega = 0.5$ (dotted, blue), $\mu = \omega = 0$ (dot dashed, green), $\mu = \omega = -1$ (dashed, pink), $\mu = \omega = -2$ (thick, purple), $\mu = \omega = 3$ (thick, black), and $\mu = \omega = -4$ (thick, yellow). In Figure 1(b), the ST-Bernstein basis functions are drawn as $\mu = \omega = 1$ (thick, red), $\mu = 1, \omega = 0.5$ (dotted, blue), $\mu = 1, \omega = 0$ (dot dashed, green), $\mu = 1, \omega = -1$ (dashed, pink), $\mu = 1, \omega = -2$ (thick, purple), $\mu = 1, \omega = -3$ (thick, black), and $\mu = 1, \omega = -4$ (thick, yellow). In Figure 1(c), the ST-Bernstein basis functions are drawn as $\mu = \omega = 1$ (thick, red), $\mu = 0.5, \omega = 1$ (dotted, blue), $\mu = 0, \omega = 1$ (dot dashed, green), $\mu = -1, \omega = 1$ (dashed, pink), $\mu = -2, \omega = 1$ (thick, purple), $\mu = -3, \omega = 1$ (thick, black), and $\mu = -4, \omega = 1$ (thick, gray).

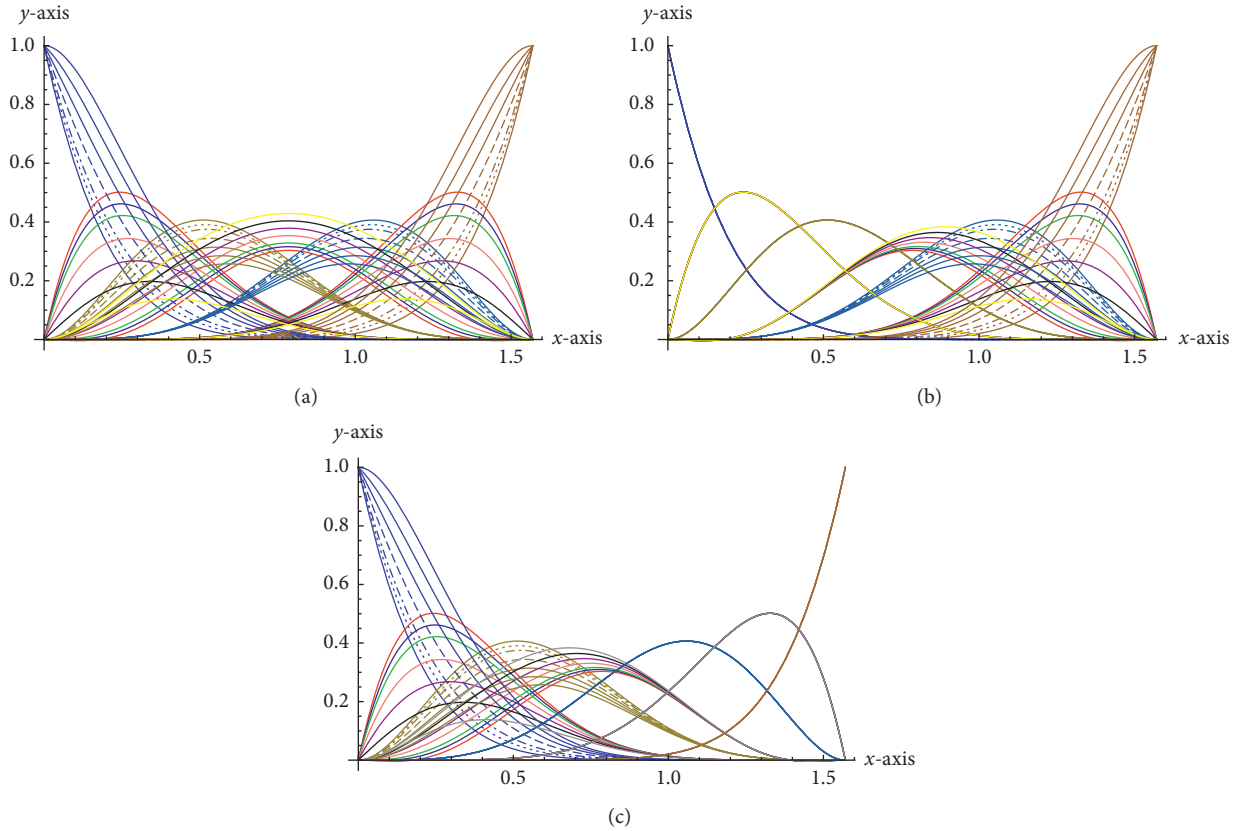


FIGURE 1: ST-Bernstein basis functions with shape parameters.

Theorem 1. *The ST-Bernstein basis functions in equation (1) have the following geometric characteristics:*

- (1) *Nonnegativity:* $\Phi_i(\eta) \geq 0 (i = 0, 1, \dots, 6)$
- (2) *Partition of unity:* $\sum_{i=0}^6 \Phi_i(\eta) = 1$
- (3) *Symmetry:* $\Phi_i(\eta; \mu, \omega) = \Phi_{6-i}(\pi/2 - \eta; \mu, \omega) (i = 0, 1, \dots, 6)$
- (4) *Monotonicity:* *for the given value of the shape parameter μ, ω , $\Phi_0(\eta)$ is monotonically decreasing and $\Phi_6(\eta)$ is monotonically increasing*
- (5) *Terminal property:* $\Phi_0(0) = 1, \Phi_i(0) = 0, \Phi_i(\pi/2) = 0, \Phi_6(\pi/2) = 1, i = 0, 1, 2, \dots, 5$

Proof

- (1) For $\eta \in [0, \pi/2]$ and $-4 \leq \mu, \omega \leq 1$, since $(1 \pm \sin \eta) \geq 0, (1 - \mu \sin \eta) \geq 0, (1 \pm \cos \eta) \geq 0$ and $(1 - \omega \cos \eta) \geq 0, \sin \eta \geq 0, \cos \eta \geq 0, \sin^2 \eta \geq 0, \cos^2 \eta \geq 0$, this shows that $\Phi_i(\eta) \geq 0, (i = 0, 1, 2, \dots, 6)$.
- (2) It is obvious by Definition 1.
- (3) For $i = 0$,

$$\Phi_0(\eta) = (1 - \sin \eta)^4 (1 - \mu \sin \eta) = \left(1 - \cos\left(\frac{\pi}{2} - \eta\right)\right)^4 \left(1 - \omega \cos\left(\frac{\pi}{2} - \eta\right)\right) = \Phi_6(\eta). \tag{2}$$

For $i = 1$,

$$\Phi_1(\eta) = \sin \eta (1 - \sin \eta)^3 (4 + \omega (1 - \sin \eta)) = \cos\left(\frac{\pi}{2} - \eta\right) \left(1 - \cos\left(\frac{\pi}{2} - \eta\right)\right)^3 \left(4 + \omega \left(1 - \cos\left(\frac{\pi}{2} - \eta\right)\right)\right) = \Phi_5(\eta). \tag{3}$$

For $i = 2$,

$$\Phi_2(\eta) = \sin^2 \eta (1 - \sin \eta)^2 (6 + \mu(1 - \sin \eta)) = \cos^2\left(\frac{\pi}{2} - \eta\right) \left(1 - \cos\left(\frac{\pi}{2} - \eta\right)\right)^2 \left(6 + \omega\left(1 - \cos\left(\frac{\pi}{2} - \eta\right)\right)\right) = \Phi_4(\eta). \quad (4)$$

- (4) For any $\eta_0, \eta_1 \in [0, \pi/2]$ such that if $\eta_0 \leq \eta_1$ then $\Phi_0(\eta_0) \geq \Phi_0(\eta_1)$, this means that $\Phi_0(\eta)$ is monotonically decreasing similarly when $\eta_0 \leq \eta_1$ and $\Phi_6(\eta_0) \geq \Phi_6(\eta_1)$, which shows that $\Phi_6(\eta)$ is monotonically increasing. Let $f_1(\eta) = \Phi_0'(\eta) = -\mu \cos \eta (1 - \sin \eta)^4 - 4 \cos \eta (1 - \sin \eta)^3 (1 - \mu \sin \eta)$ and $f_2(\eta) = \Phi_6'(\eta) = \omega (1 - \cos \eta)^4 \sin \eta + 4 (1 - \cos \eta)^3 (1 - \omega \cos \eta) \sin \eta$, where $\eta \in [0, \pi/2]$. From the figures of the functions $f_1(\eta)$ and $f_2(\eta)$, we can see $f_1(\eta) \leq 0$ and $f_2(\eta) \geq 0$ when $\eta \in [0, \pi/2]$. Therefore, $\Phi_0(\eta)$ and $\Phi_6(\eta)$ are monotonically decreasing and increasing about η , respectively. This can also be shown graphically in Figure 1.
- (5) When we put $\eta = 0$ and $\eta = \pi/2$ in Definition 1, we get $\Phi_0(0) = 1, \Phi_i(0) = 0 (i = 1, 2, \dots, 6), \Phi_i(\pi/2) = 0 (i = 0, 1, 2, \dots, 6), \Phi_6(\pi/2) = 1$ and the first derivatives of these basis functions at their end points are given as follows:

$$\Phi_i'(0) = \begin{cases} -4 - \mu, & i = 0, \\ 4 + \mu, & i = 1, \\ 0, & i = 2, \dots, 6, \end{cases} \quad (5)$$

$$\Phi_i'\left(\frac{\pi}{2}\right) = \begin{cases} 4 + \omega, & i = 6, \\ -4 - \omega, & i = 5, \\ 0, & i = 0, \dots, 4. \end{cases}$$

Similarly, the second derivatives of these basis functions at their end points are given as follows (see Figure 2):

$$\Phi_i''(0) = \begin{cases} 12 + 8\mu, & i = 0, \\ -12 - 8\mu, & i = 1, \\ 2(6 + \mu), & i = 2, \\ -2\mu, & i = 3, \\ 0, & i = 4, 5, 6, \end{cases} \quad (6)$$

$$\Phi_i''\left(\frac{\pi}{2}\right) = \begin{cases} 12 + 8\omega, & i = 6, \\ -12 - 8\omega, & i = 5, \\ 2(6 + \omega), & i = 4, \\ -2\omega, & i = 3, \\ 0, & i = 0, 1, 2. \end{cases} \quad \square$$

3. Sextic Trigonometric Bézier Curves with Two Shape Parameters

In this section, the ST-Bézier curves with two shape parameters μ, ω and their geometric properties are discussed.

Definition 2. For the given control points $S_i (i = 0, 1, 2, \dots, 6)$, the curve

$$\alpha(\eta) = \sum_{i=0}^6 S_i \Phi_i(\eta), \quad \eta \in \left[0, \frac{\pi}{2}\right], \mu, \omega \in [-4, 1], \quad (7)$$

is called ST-Bézier curve, where $\Phi_i(\eta) (i = 0, 1, 2, \dots, 6)$ are called ST-Bernstein basis functions and μ, ω are the shape parameters.

Some graphical results of ST-Bézier curve are discussed as follows: when shape parameters vary equally, Figure 3 is generated, while, by keeping one parameter fixed to 1, Figure 4 is generated. In Figure 4(a), when $\mu = 1$ and ω varies, then influence of shape parameters can be seen on the left side of the figure. Meanwhile when we consider $\omega = 1$ and parameter μ varies, the influence of these parameters can be observed on the right side of Figure 4(b).

Theorem 2. *The ST-Bézier curves in equation (7) have the following geometric properties:*

(1) *End point properties:*

$$\left\{ \begin{array}{l} \alpha(0) = S_0, \\ \alpha\left(\frac{\pi}{2}\right) = S_6, \\ \alpha'(0) = (4 + \mu)(S_1 - S_0), \\ \alpha'\left(\frac{\pi}{2}\right) = (4 + \omega)(S_6 - S_5), \\ \alpha''(0) = 2(2(3 + 2\mu)S_0 - 2(3 + 2\mu)S_1 + (6 + \mu)S_2 - \mu S_3), \\ \alpha''\left(\frac{\pi}{2}\right) = 2(2(3 + 2\omega)S_6 - 2(3 + 2\omega)S_5 + (6 + \omega)S_4 - \omega S_3). \end{array} \right. \quad (8)$$

(2) *Symmetry: the control points S_i define the same ST-Bézier curve having symmetric influence in different parameterizations, such as*

$$\alpha(\eta; \mu, \omega; S_0, \dots, S_6) = \alpha\left(\frac{\pi}{2} - \eta; \mu, \omega; S_6, \dots, S_0\right). \quad (9)$$

(3) *Geometric invariance: the shape of ST-Bézier curve is independent from the coordinate axis, which means*

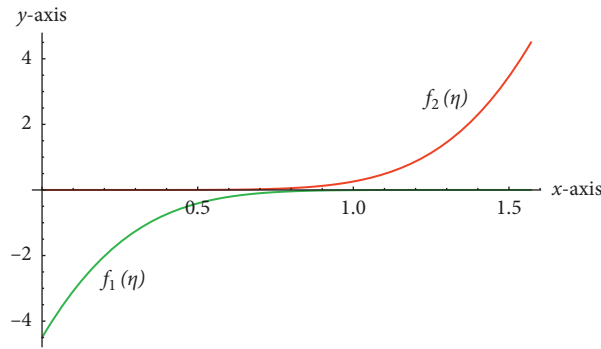


FIGURE 2: Functions $f_1(\eta)$ and $f_2(\eta)$ on $\eta \in [0, \pi/2]$.

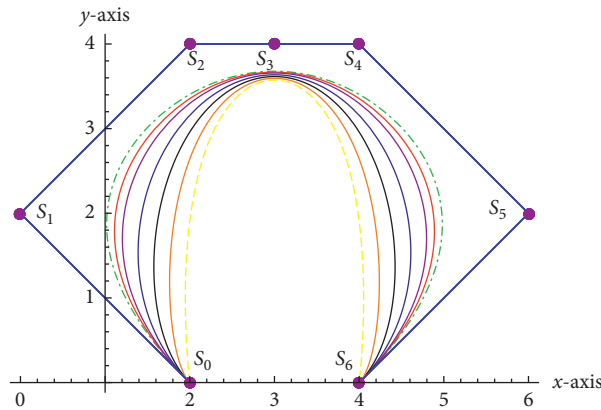


FIGURE 3: ST-Bézier curves with some shape parameters when $\mu = \omega = 1, 0.5, 0, -1, -2, -3, -4$.

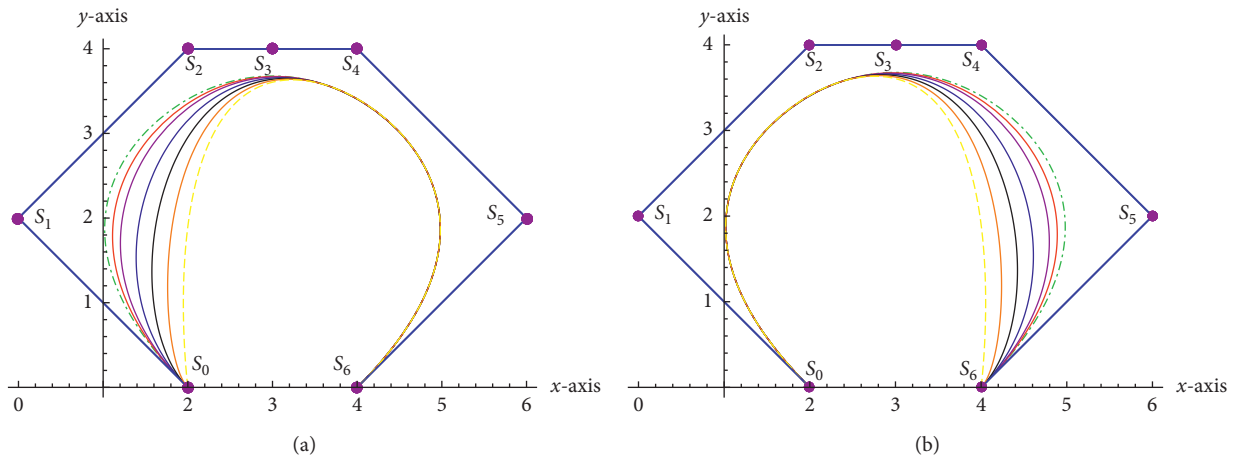


FIGURE 4: ST-Bézier curves with different shape parameters. (a) $\mu = 1, \omega = 1, 0.5, 0, -1, -2, -3, -4$. (b) $\omega = 1, \mu = 1, 0.5, 0, -1, -2, -3, -4$.

that the curve defined in equation (7) satisfies the two following equations:

$$\begin{aligned} \alpha(\eta; \mu, \omega; S_0 + \vartheta, \dots, S_6 + \vartheta) &= \alpha(\eta; \mu, \omega; S_0, \dots, S_6) + \vartheta, \\ \alpha(\eta; \mu, \omega; S_0 \times \rho, \dots, S_6 \times \rho) &= \alpha(\eta; \mu, \omega; S_0, \dots, S_6) \times \rho. \end{aligned} \tag{10}$$

(4) *Shape control property:* the shape of classical Bézier curve cannot be modified due to absence of shape

control parameters, while the ST-Bézier curve possesses two shape parameters by which we can modify the curve easily.

(5) *Convex hull property:* the ST-Bézier curve must be confined inside the convex polygon spanned by its control points.

(6) *Linearly independent:* for any $b_i \in R (i = 0, 1, \dots, 6)$, consider a linear combination as follows:

$$\sum_{i=0}^6 b_i \Phi_i(\eta) = 0, \quad \eta \in \left[0, \frac{\pi}{2}\right]. \quad (11)$$

Taking 1st, 2nd, 3rd, ..., 6th derivatives of the above equation with respect to η on each side yields the following equations:

$$\left\{ \begin{array}{l} \sum_{i=0}^6 b_i \Phi_i'(\eta) = 0, \\ \sum_{i=0}^6 b_i \Phi_i''(\eta) = 0, \\ \sum_{i=0}^6 b_i \Phi_i'''(\eta) = 0, \\ \sum_{i=0}^6 b_i \Phi_i^{(iv)}(\eta) = 0, \\ \sum_{i=0}^6 b_i \Phi_i^{(v)}(\eta) = 0, \\ \sum_{i=0}^6 b_i \Phi_i^{(vi)}(\eta) = 0. \end{array} \right. \quad (12)$$

When $\eta = 0$, we have

$$\left\{ \begin{array}{l} \sum_{i=0}^6 b_i \Phi_i'(0) = 0, \\ \sum_{i=0}^6 b_i \Phi_i''(0) = 0, \\ \sum_{i=0}^6 b_i \Phi_i'''(0) = 0, \\ \sum_{i=0}^6 b_i \Phi_i^{(iv)}(0) = 0, \\ \sum_{i=0}^6 b_i \Phi_i^{(v)}(0) = 0, \\ \sum_{i=0}^6 b_i \Phi_i^{(vi)}(0) = 0. \end{array} \right. \quad (13)$$

By using the values of the 1st, 2nd, 3rd, ..., 6th-order derivatives of ST-Bernstein basis functions at $\eta = 0$, we get $b_i = 0 (i = 0, 1, \dots, 6)$; this fact shows that $\Phi_i(\eta) (i = 0, 1, \dots, 6)$ are linearly independent.

4. Shape Control of the ST-Bézier Curve

As we know, the shape parameters help us to modify the shape of the curve within which lies inside the control polygon. So, by using these shape control parameters, the ST-Bézier curves can be modified wherever the shape does not change at all. The shape parameters μ, ω cause local

change in the curve; see Figure 5. In Figure 5(a), the effect on shape of the curve is observed when $\mu = \omega = \{1$ (dot dashed, green), 0.5 (thick, red), 0 (thick, purple), -1 (thick, blue), -2 (thick, black), -3 (thick, orange), and -4 (dashed, yellow)}. In Figure 5(b), the influence of ST-Bézier curve can be seen on the left-hand side when $\omega = 1$ is fixed and μ varies in the interval $[-4, 1]$ as $\mu = 1$ (thick, pink), $\mu = 0.5$ (thick, red), $\mu = 0$ (thick, green), $\mu = -1$ (thick, black), $\mu = -3$ (thick, orange), and $\mu = -4$ (dashed, yellow). Similarly, Figure 5(c) is determined with influence on the right-hand side of the figure when $\mu = 1$ is fixed and ω varies as $\omega = 1$ (thick, pink), $\omega = 0.5$ (thick, red), $\omega = 0$ (thick, green), $\omega = -1$ (thick, black), $\omega = -3$ (thick, orange), and $\omega = -4$ (dashed, yellow).

5. Continuity Conditions for ST-Bézier Curve Segments

In this section, the continuity conditions are derived for smooth joining of two ST-Bézier curves segments.

Lemma 1 (see [15]). *The necessary and sufficient conditions for smooth joining of two ST-Bézier curve segments $\alpha(\eta) = \sum_{i=0}^6 S_i \Phi_i(\eta)$ with control points S_0, \dots, S_6 and shape parameters μ, ω and $\alpha_1(\eta) = \sum_{i=0}^6 T_i \Phi_i(\eta)$ with control points T_0, \dots, T_6 and shape parameters μ_1, ω_1 via parametric continuity are as follows:*

- (1) $S_6 = T_0$, for C^0 continuity
- (2) $S_6 = T_0, \alpha'(\pi/2) = \alpha_1'(0)$, for C^1 continuity
- (3) $S_6 = T_0, \alpha'(\pi/2) = \alpha_1'(0), \alpha''(\pi/2) = \alpha_1''(0)$, for C^2 continuity

Lemma 2 (see [15]). *The necessary and sufficient conditions for smooth joining of two ST-Bézier curve segments $\alpha(\eta) = \sum_{i=0}^6 S_i \Phi_i(\eta)$ with control points S_0, \dots, S_6 and shape parameters μ, ω and $\alpha(\eta) = \sum_{i=0}^6 T_i \Phi_i(\eta)$ with control points T_0, \dots, T_6 and shape parameters μ_1, ω_1 via geometric continuity are as follows:*

- (1) $S_6 = T_0$, for G^0 continuity
- (2) $S_6 = T_0, \alpha' = \lambda \alpha_1'(\pi/2), \lambda > 0$, for G^1 continuity
- (3) $S_6 = T_0, \alpha'(\pi/2) = \lambda \alpha_1'(\pi/2), \lambda > 0$ and the curvature $\kappa(\pi/2) = |\alpha'(\pi/2) \times \alpha''(\pi/2)| / |\alpha'(\pi/2)|^3 = |\alpha_1'(\pi/2) \times \alpha_1''(\pi/2)| / |\alpha_1'(\pi/2)|^3 = \kappa_1(\pi/2)$, for G^2 continuity

Theorem 3. *Suppose that any two adjacent segments of ST-Bézier curves $\alpha(\eta) = \sum_{i=0}^6 S_i \Phi_i(\eta)$ and $\alpha(\eta) = \sum_{i=0}^6 T_i \Phi_i(\eta)$ with control points S_0, \dots, S_6 and T_0, \dots, T_6 reach $C^k, k = 0, 1, 2$ smooth continuities at joint point if they match the following necessary and sufficient conditions:*

- (1) $S_6 = T_0$ for C^0 continuity.
- (2) For C^1 continuity,

$$S_6 = T_0, T_1 = \frac{-4S_5 - \omega S_5 + 8S_6 + \mu 1S_6 + \omega S_6}{4 + \mu 1}. \quad (14)$$

- (3) For C^2 continuity,

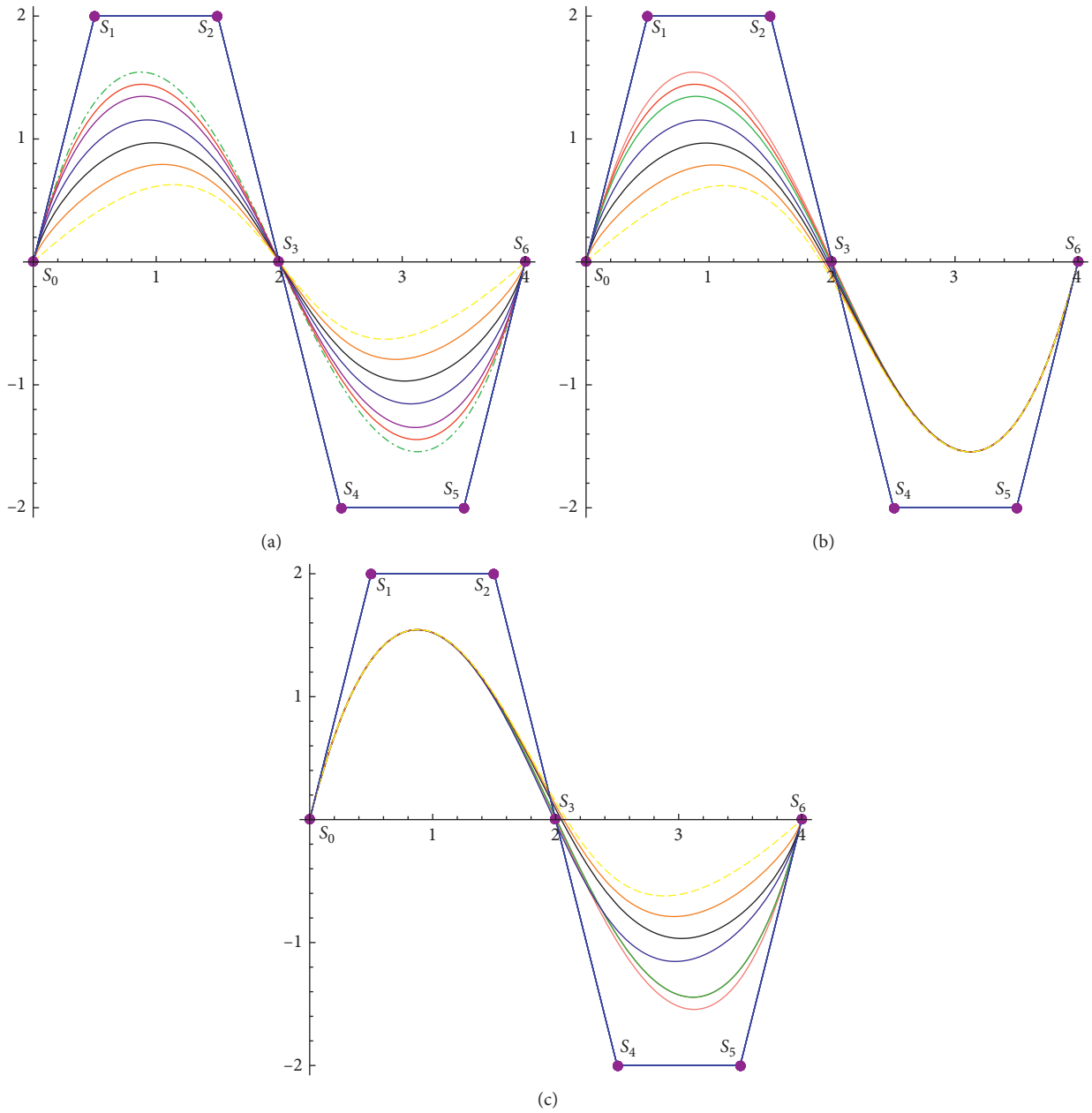


FIGURE 5: Effect on shape of the curve by changing the shape parameters. (a) $\omega = \mu = 1, 0.5, 0, -1, -2, -3, -4$. (b) $\mu = 1$ and $\omega = 1, 0.5, 0, -1, -2, -3, -4$. (c) $\omega = 1$ and $\mu = 1, 0.5, 0, -1, -2, -3, -4$.

$$\begin{aligned}
 S_6 &= T_0, \\
 T_1 &= \frac{-4S_5 - \omega S_5 + 8S_6 + \mu 1 S_6 + \omega S_6}{4 + \mu 1}, \\
 T_2 &= \frac{6(4 + \mu 1)S_3 - 4(24 + 7\omega + \mu 1(7 + 2\omega))(S_5 - S_6) + \mu 1(4 + \mu 1)T_3}{(4 + \mu 1)(6 + \mu 1)}.
 \end{aligned}
 \tag{15}$$

Proof

(1) Using $\alpha(\pi/2) = \alpha_1(0)$, we get $S_6 = T_0$. C^0 continuity is achieved.

(2) For C^1 continuity, we must have C^0 continuity first to get $S_6 = T_0$, and $\alpha'(\pi/2) = \alpha'_1(0)$ can be used to get $T_1 = -4S_5 - \omega S_5 + 8S_6 + \mu 1 S_6 + \omega S_6 / 4 + \mu 1$.

- (3) For C^2 continuity, we must have C^0 continuity and C^1 continuity conditions; additionally the condition $\alpha''(\pi/2) = \alpha_1''(0)$ is used to get

$$\begin{aligned} S_6 &= T_0, \\ T_1 &= \frac{-4S_5 - \omega S_5 + 8S_6 + \mu 1 S_6 + \omega S_6}{4 + \mu 1}, \\ T_2 &= \frac{6(4 + \mu 1)S_3 - 4(24 + 7\omega + \mu 1(7 + 2\omega))(S_5 - S_6) + \mu 1(4 + \mu 1)T_3}{(4 + \mu 1)(6 + \mu 1)}. \end{aligned} \quad (16)$$

□

5.1. C^0 Continuity of ST-Bézier Curve. For C^0 parametric continuity, we consider any two ST-Bézier curve segments having the same joint point. In this case, the last control point of initial curve and the first control point of second curve are the same. By changing the values of control parameters, we can see the variation in figures. The values of different shape control parameters are used to modify the shape of values; see Figure 6.

5.2. C^1 Continuity of ST-Bézier Curve. For parametric continuity of degree 1, consider two adjacent ST-Bézier curve segments with shape control parameters. In this case, we should have common tangents of the two curve segments at joint point. The first two control points of second curve can be achieved as given in Theorem 3. Figures 7(a)–7(c) can be obtained by varying the shape control parameters via C^1 continuity constraints.

5.3. C^2 Continuity of ST-Bézier Curve. The C^2 continuity can be achieved by connecting two adjacent ST-Bézier curve segments if they fulfill the C^0 and C^1 continuity conditions. The second derivative of these segments at joint point must be the same as that of C^2 continuity. The control points of the first curve can be chosen according to the designer's

requirement, while the control points for the second curve can be obtained from Theorem 3. Different values of shape control parameters can be used to obtain different curves as given in Figure 8.

6. Geometric Continuity of ST-Bézier Curve

To get more smoothness between any two adjacent ST-Bézier curves, geometric continuity conditions have been derived. In geometric continuity conditions, one extra parameter is involved, which is used for the modification of the curve.

Theorem 4. Suppose that two adjacent segments of ST-Bézier curve $\alpha(\eta) = \sum_{i=0}^6 S_i \Phi_i(\eta)$ and $\alpha(\eta) = \sum_{i=0}^6 T_i \Phi_i(\eta)$ with control points S_0, \dots, S_6 and T_0, \dots, T_6 , respectively, can be connected via G^k , $k = 0, 1, 2$ smooth continuities at joint point if they match the following necessary and sufficient conditions:

- (1) $S_6 = T_0$, for G^0 continuity.
- (2) $S_6 = T_0, T_1 = \frac{-4S_5 - \omega S_5 + 4S_6 + \omega S_6 + 4\lambda S_6 + \mu 1 S_6}{(4 + \mu 1)\lambda}$, for G^1 continuity.
- (3) $S_6 = T_0, T_1 = \frac{-4S_5 - \omega S_5 + 4S_6 + \omega S_6 + 4\lambda S_6 + \mu 1 \lambda S_6}{(4 + \mu 1)\lambda}$,

$$\begin{aligned} T_2 &= \left\{ \frac{1}{2(4 + \mu 1)(6 + \mu 1)\lambda^3} \left(12(4 + \mu 1)\lambda S_3 + ((4 + \mu 1)(4 + \omega)\beta - 8(4 + \mu 1)(3 + \omega)\lambda - 8(3 + \mu 1)(4 + \omega)\lambda^2) S_5 \right. \right. \\ &\quad \left. \left. + \left(-(4 + \mu 1)(4 + \omega)\beta + 4\lambda \left(\begin{array}{c} (4 + \mu 1)(3 + 2\omega) \\ + 2(3 + \mu 1)(4 + \omega)\lambda + 3(4 + \mu 1)\lambda^2 \end{array} \right) \right) S_6 + 2\mu 1(4 + \mu 1)\lambda^3 T_3 \right) \right\}, \end{aligned} \quad (17)$$

for G^2 continuity.

Proof

1. For G^0 continuity, $\alpha(\pi/2) = \alpha_1(0)$ yields $S_6 = T_0$.
- (2) For G^1 continuity, the expressions $\alpha(\pi/2) = \alpha_1(0)$ and $\alpha'(\pi/2) = \lambda \alpha_1'(0)$, $\lambda > 0$, yield $S_6 = T_0$,

$$T_1 = \frac{-4S_5 - \omega S_5 + 4S_6 + \omega S_6 + 4\lambda S_6 + \mu 1 \lambda S_6}{(4 + \mu 1)\lambda}.$$

- (3) For G^2 continuity, as we know that $\alpha(\pi/2) = S_6 = T_0 = \alpha_1(0)$, $\alpha'(\pi/2) = \lambda \alpha_1'(0)$, $\lambda > 0$, and the reverse normal vector $D = \alpha'(\pi/2) \times \alpha''(\pi/2)$ of $\alpha(\eta)$ and vice normal vector $D_1 = \alpha_1'(0) \times \alpha_1''(0)$ of $\alpha_1(\eta)$ in $\eta = \pi/2$ have the same

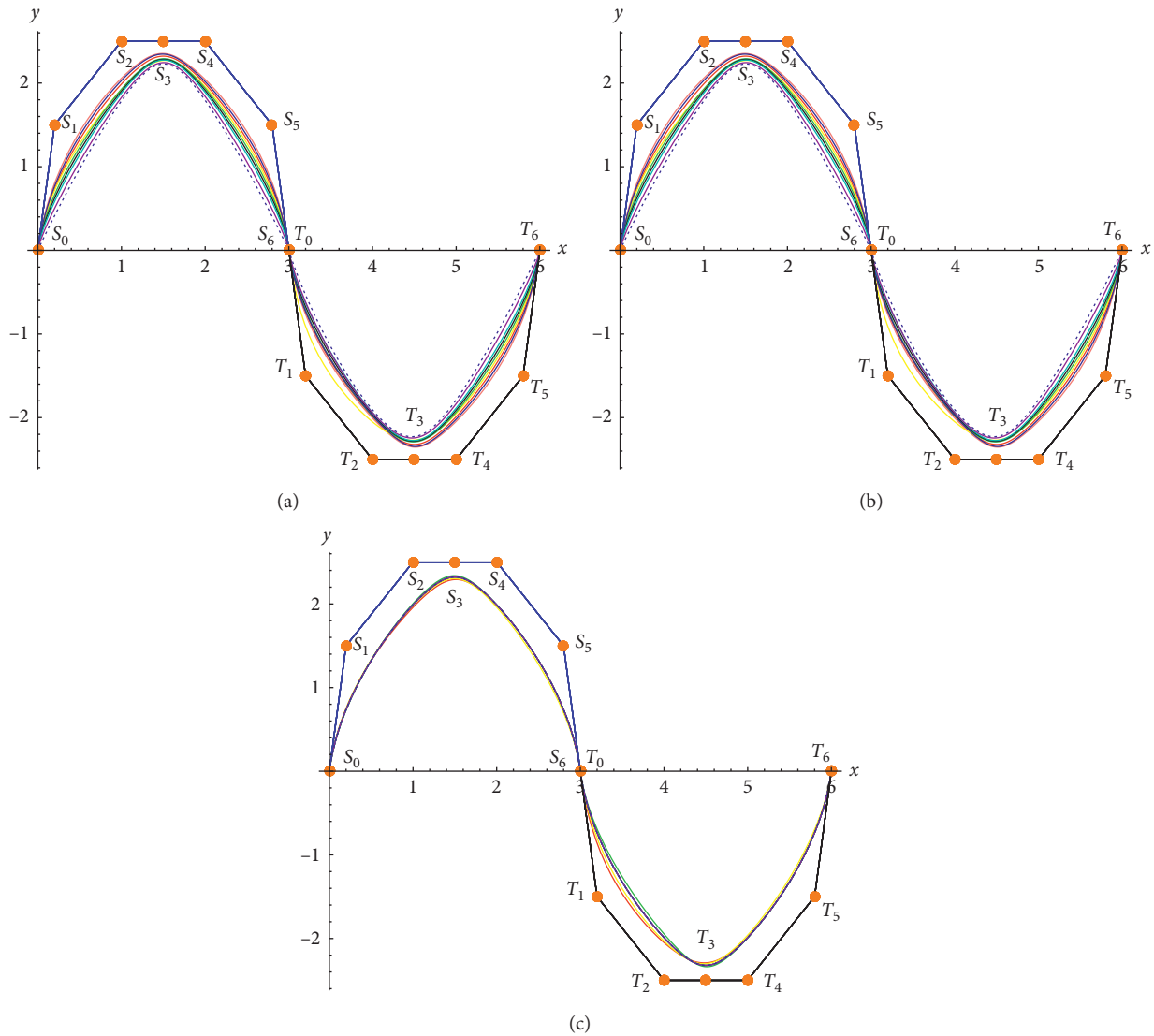


FIGURE 6: C^0 continuity of ST-Bézier curve segments with various shape parameters.

direction, the four vectors $\alpha'(\pi/2), \alpha'(0), \alpha''(\pi/2), \alpha''(0)$ are coplanar. So, we consider $\alpha''(\pi/2) = \mu\alpha'_1(0) + \beta\alpha'_1(0)$, where $\mu, \beta > 0$ are

arbitrarily constants. Since the curvatures at the final point of the first curve and at the initial point of the second curve are the same,

$$\kappa\left(\frac{\pi}{2}\right) = \frac{|\alpha'(\pi/2) \times \alpha''(\pi/2)|}{|\alpha'(\pi/2)|^3} = \frac{\lambda\mu|\alpha'_1(0) \times \alpha''_1(0)|}{\lambda^3|\alpha'_1(0)|^3} = \frac{|\alpha'_1(0) \times \alpha''_1(0)|}{|\alpha'_1(0)|^3} = \kappa_1(0), \quad (18)$$

where $\mu = \lambda^2$, to meet the G^2 continuity conditions. \square

values of shape control parameters, the variation in figures can be seen.

6.1. G^1 Continuity of ST-Bézier Curve. C^0 and G^0 both have the same significance. For G^1 continuity, the tangents of the first curve and the second curve at joint point are the same. The parameter λ is any positive scale factor which is used for modification of curves. In Figure 9, by having different

6.2. G^2 Continuity of ST-Bézier Curve. The geometric continuity of degree 2 between any two adjacent ST-Bézier curves is given here. Different figures display the behavior of various shape parameters and scale factors. In Figures 9(a)–9(c), the shape parameters for both curves vary, while the scale factors remain fixed. In Figures 10(a)–10(d), the shape

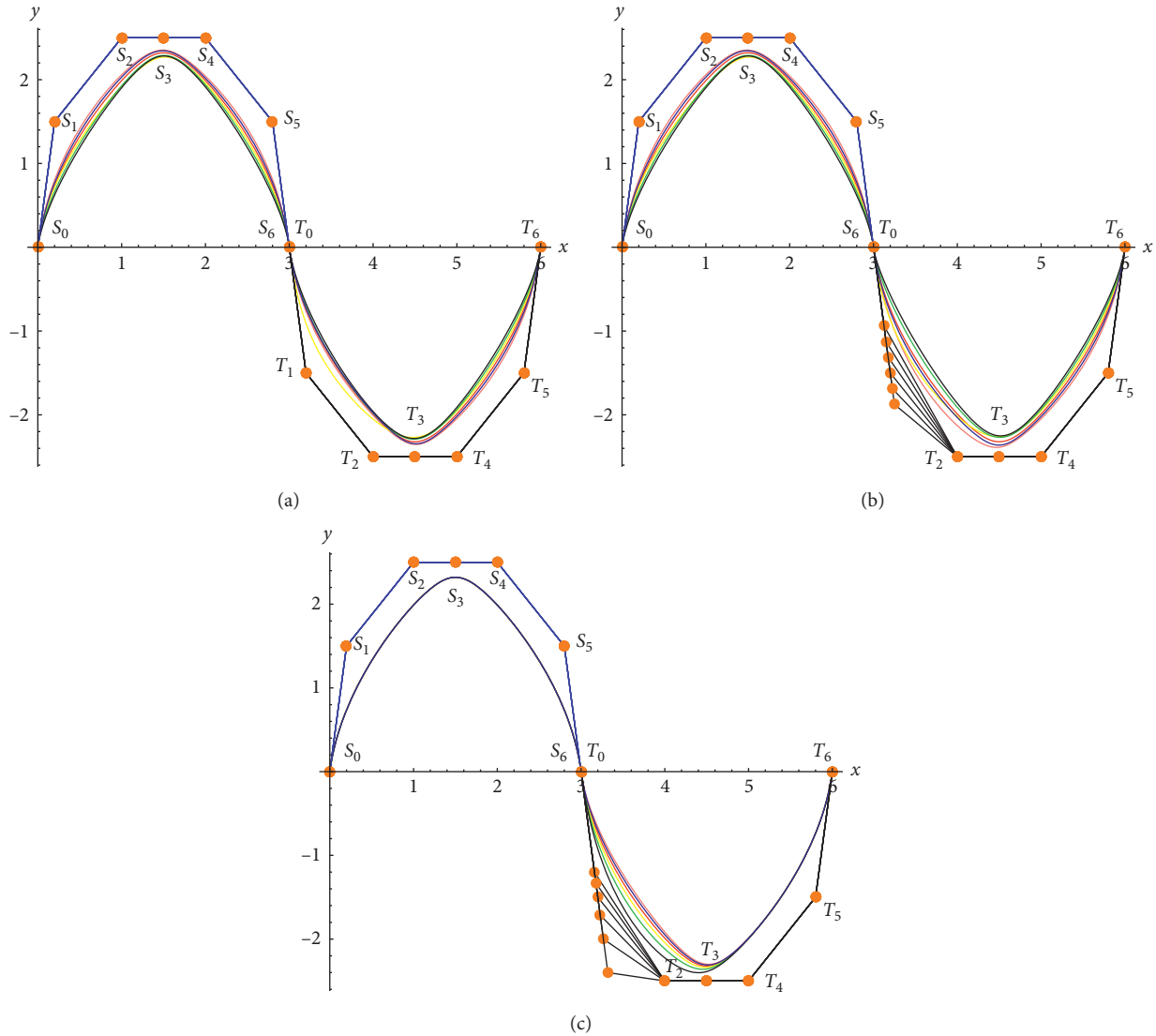


FIGURE 7: C^1 continuity of ST-Bézier curve segments with various shape parameters. (a) $\mu = \omega = \mu_1 = \omega_1 = 1, 0, 0.5, 1, -0.5, -1, -1.5$. (b) $\mu = \omega = 0, 0.5, 1, 0.5, -1, -1.5, \mu_1 = \omega_1 = 0$. (c) $\mu_1 = \omega_1 = 0, 0.5, 1, -0.5, -1, -1.5, \mu_1 = \omega_1 = 0$.

parameters for both curves remain the same, while by changing the scale factors of the second curve the variation in the figures is obvious.

7. Construction of Some Closed and Open Curves

Modeling and shape designing play a very important role in CAGD/CAD. ST-Bézier curves are also very useful for modeling and construction. So, by using ST-Bézier curves with various shape control parameters, we can construct some closed curves as shown in Figure 11. In Figure 11(a), closed curves are generated by using ST-Bézier curve when $\mu = \omega = 1$ (dot dashed, green), 0.5 (thick, red), 0 (thick, purple), -1 (thick, blue), -2 (thick, black), -3 (thick, orange), and -4 (dashed, yellow). Similarly, in Figures 11(b) and 11(c), some closed curves are obtained by continuity conditions when $\mu = \omega = 1$ (dot dashed, green), $\omega = 1, \mu =$

0.5 (thick, red), $\omega = 1, \mu = 0$ (thick, purple), $\omega = 1, \mu = 1$ (thick, blue), $\omega = 1, \mu = -2$ (thick, black), $\omega = 1, \mu = -3$ (thick, orange), and $\omega = 1, \mu = -4$ (dashed, yellow). By having different values of shape parameters, the influence can be seen as in Figures 11(a)–11(c). By using ST-Bézier curves with various shape parameters, we can construct some open curves as shown in Figure 12. In Figure 12(a), the open curve is generated by using ST-Bézier curve when $\mu = \omega = 1$ (dot dashed, green), 0.5 (thick, red), 0 (thick, purple), -1 (thick, blue), -2 (thick, black), -3 (thick, orange), and -4 (dashed, yellow). Similarly, in Figures 12(b) and 12(c), some open curves are obtained by continuity conditions when $\mu = \omega = 1$ (dot dashed, green), $\omega = 1, \mu = 0.5$ (thick, red), $\omega = 1, \mu = 0$ (thick, purple), $\omega = 1, \mu = 1$ (thick, blue), $\omega = 1, \mu = -2$ (thick, black), $\omega = 1, \mu = -3$ (thick, orange), and $\omega = 1, \mu = -4$ (dashed, yellow). By having different values of shape parameters, the influence can be seen as in Figures 12(a)–12(c).

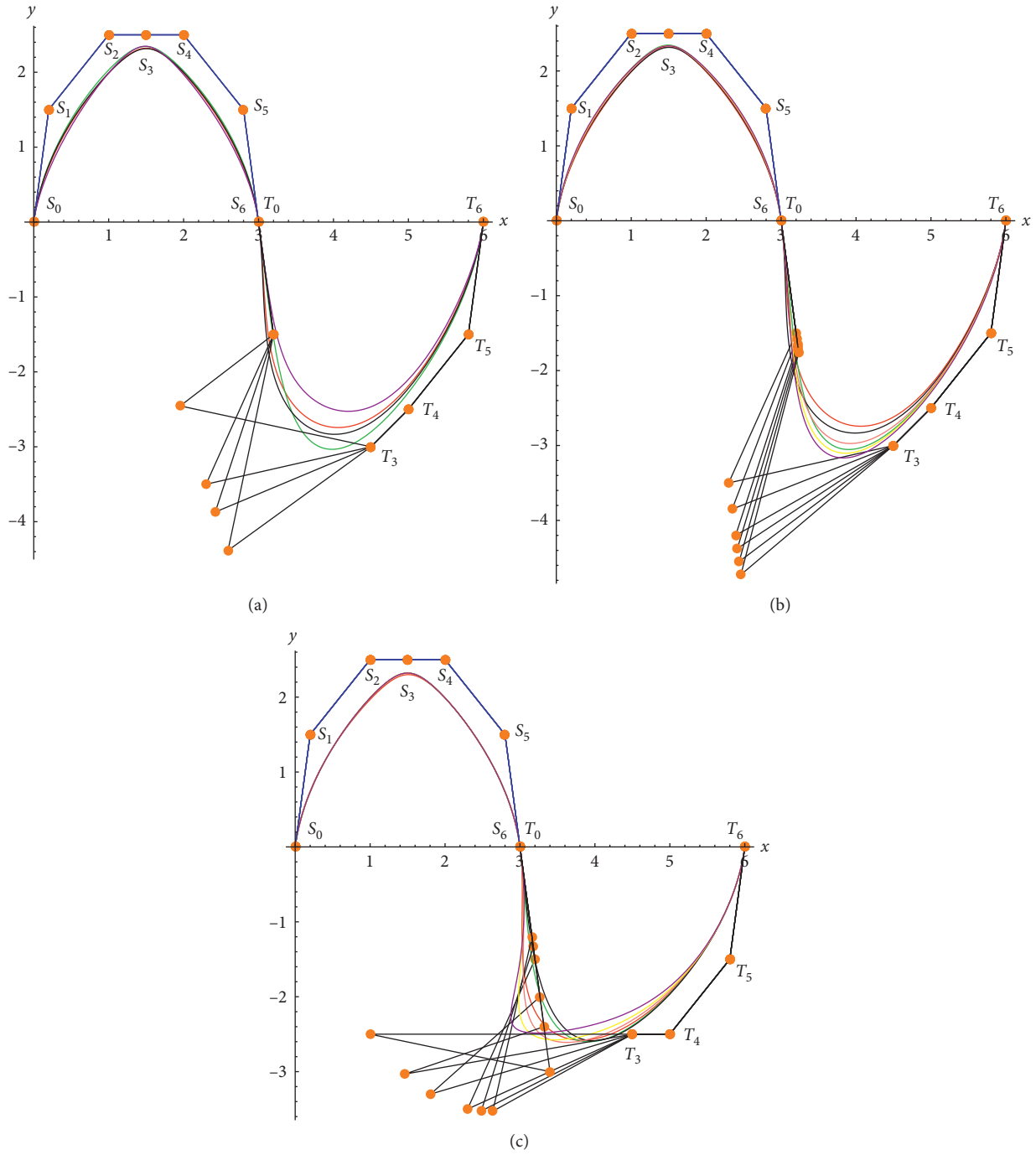


FIGURE 8: C^2 continuity of ST-Bézier curve segments with various shape parameters. (a) $\mu = \omega = \mu_1 = \omega_1 = 0, 0.5, 0.2, -0.5$. (b) $\mu = \omega = 0, 0.2, 0.4, 0.5, 0.6, 0.7, \mu_1 = \omega_1 = 1$. (c) $\mu = \omega = 0, \mu_1 = \omega_1 = 0, 0.5, 1, -1, -1.5, -2$.

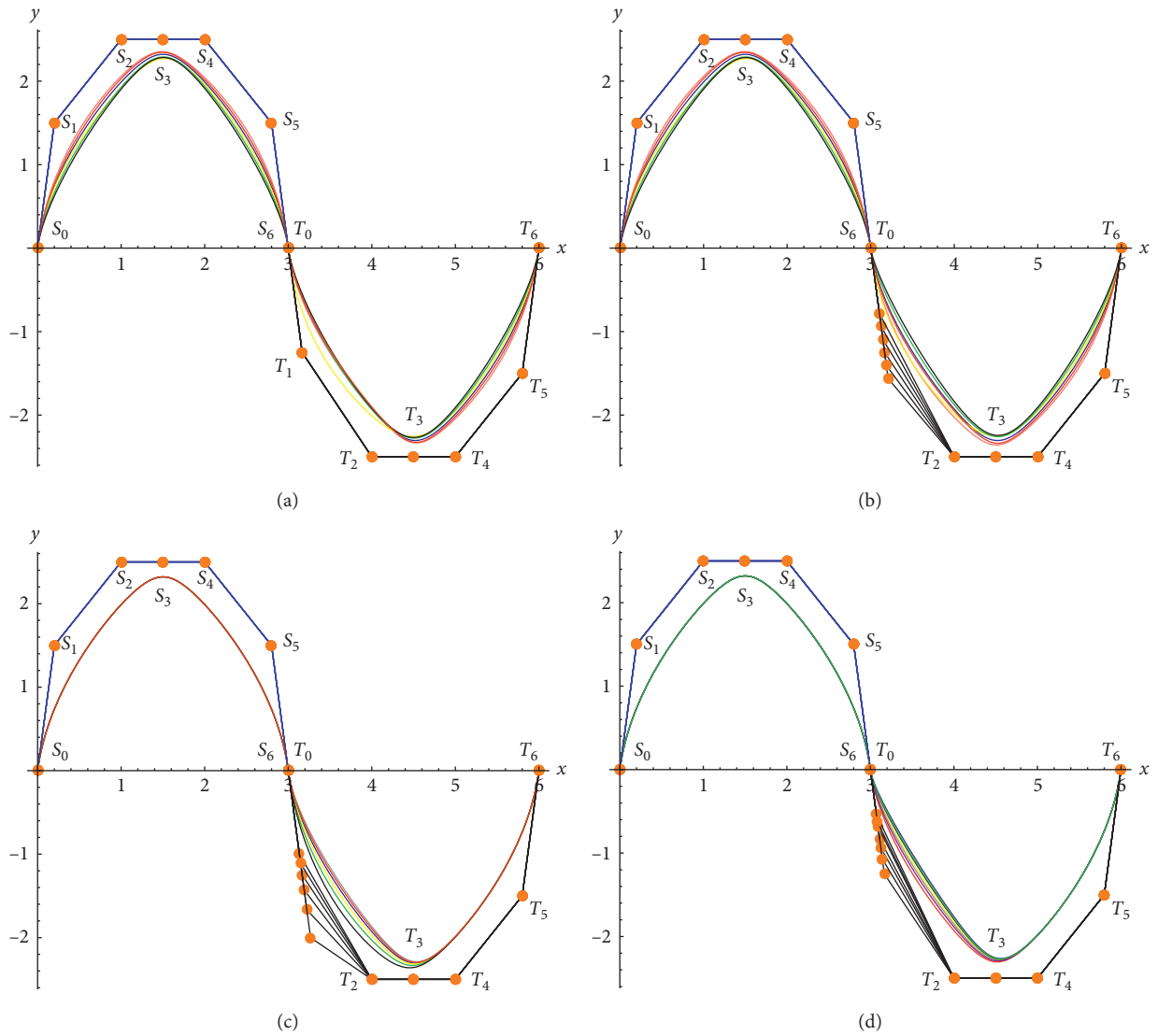


FIGURE 9: G^1 continuity of ST-Bézier curve segments with various shape parameters. (a) $\mu = \omega = \mu_1 = \omega_1 = 0, 0.5, 1, -1, -1.5, -2, \lambda = 1.2$. (b) $\mu = \omega = 0, 0.5, 1, -0.5, -1, -1.5, \mu_1 = \omega_1 = 0, \lambda = 1.2$. (c) $\mu_1 = \omega_1 = 0, 0.5, 1, -0.5, -1, 1.5, \mu = \omega = 0, \lambda = 1.2$. (d) $\mu_1 = \omega_1 = \mu = \omega = 0, \lambda = 1.2, 1.4, 1.6, 1.8, 2.2, 2.4, 2.8$.

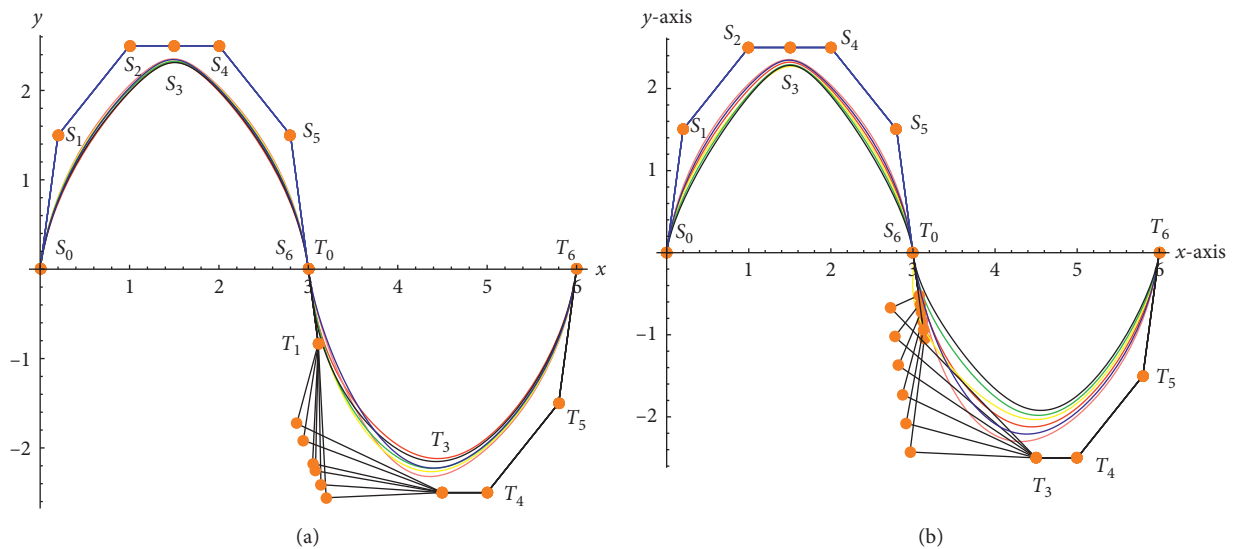


FIGURE 10: Continued.

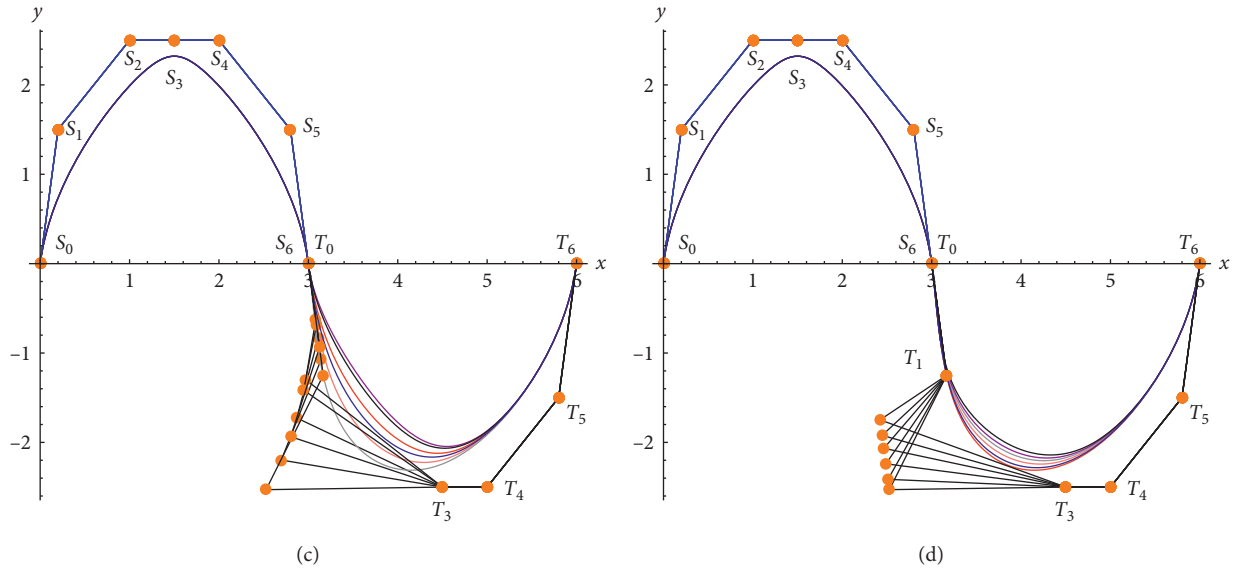


FIGURE 10: G^2 continuity of ST-Bézier curve segments with various shape parameters. (a) $\mu = \omega = \mu_1 = \omega_1 = 0, 0.2, 0.5, 0.6, 0.8, \lambda = 1.8, \beta = 1.1$. (b) $\mu_1 = \omega_1 = 0, \lambda = 1.8, \beta = 1.1, \mu = \omega = 0, 0.2, 0.5, 0.6, 0.8$. (c) $\mu = \omega = \mu_1 = \omega_1 = 0, \beta = 1.1, \lambda = 1.2, 1.4, 1.6, 1.8, 2.2, 2.4$. (d) $\mu = \omega = \mu_1 = \omega_1 = 0, \beta = 1.1, 1.5, 2.1, 2.7, 3.2, 3.8, \lambda = 1.2$.

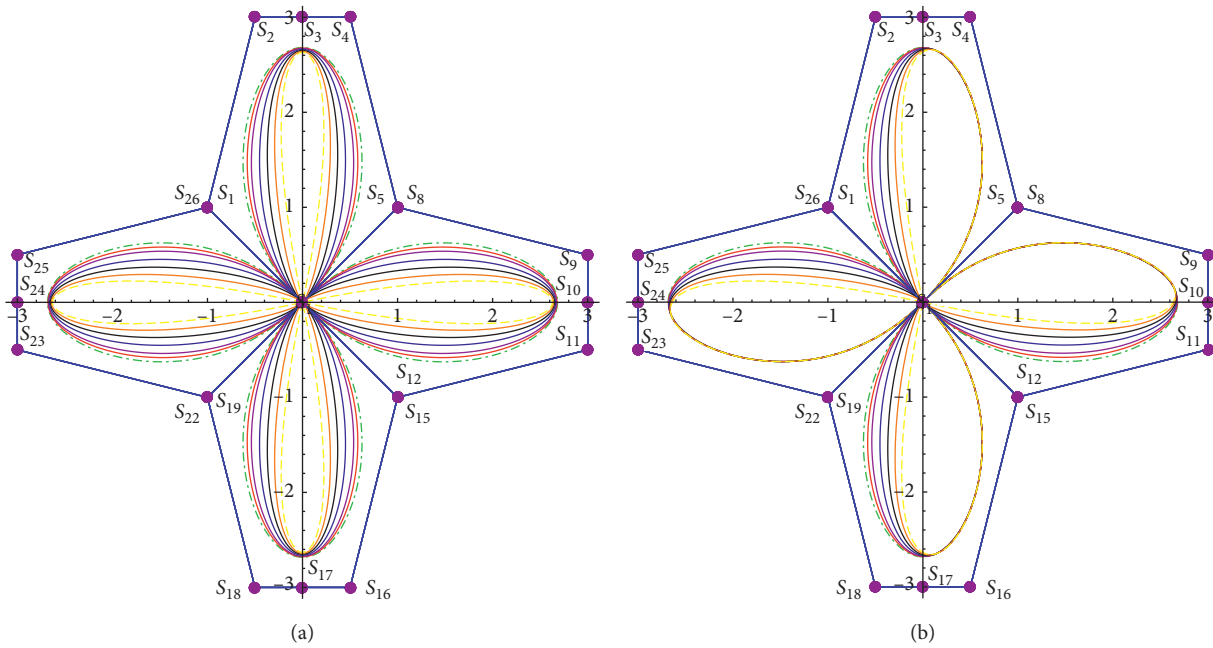


FIGURE 11: Continued.

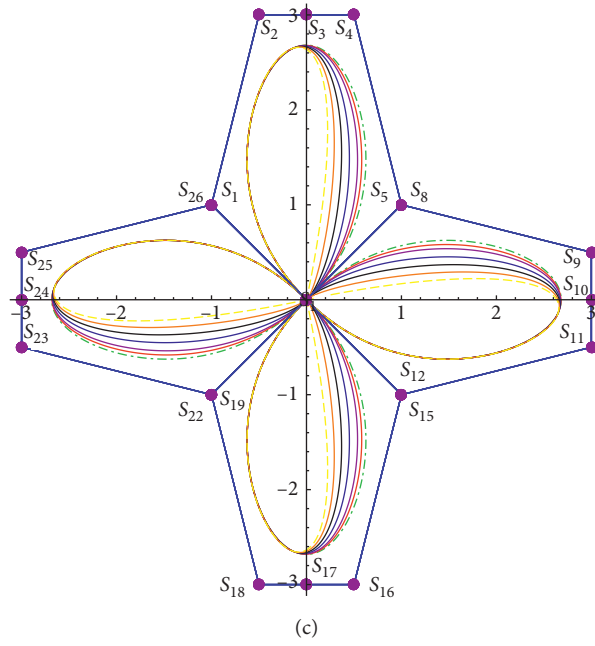


FIGURE 11: Construction of some closed curves by different values of shape parameters. (a) $\mu = \omega = 1, 0.5, 0, -1, -2, -3, -4$. (b) $\omega = 1, 0.5, 0, -1, -2, -3, -4, \mu = 1$. (c) $\mu = 1, 0.5, 0, -1, -2, -3, -4, \omega = 1$.

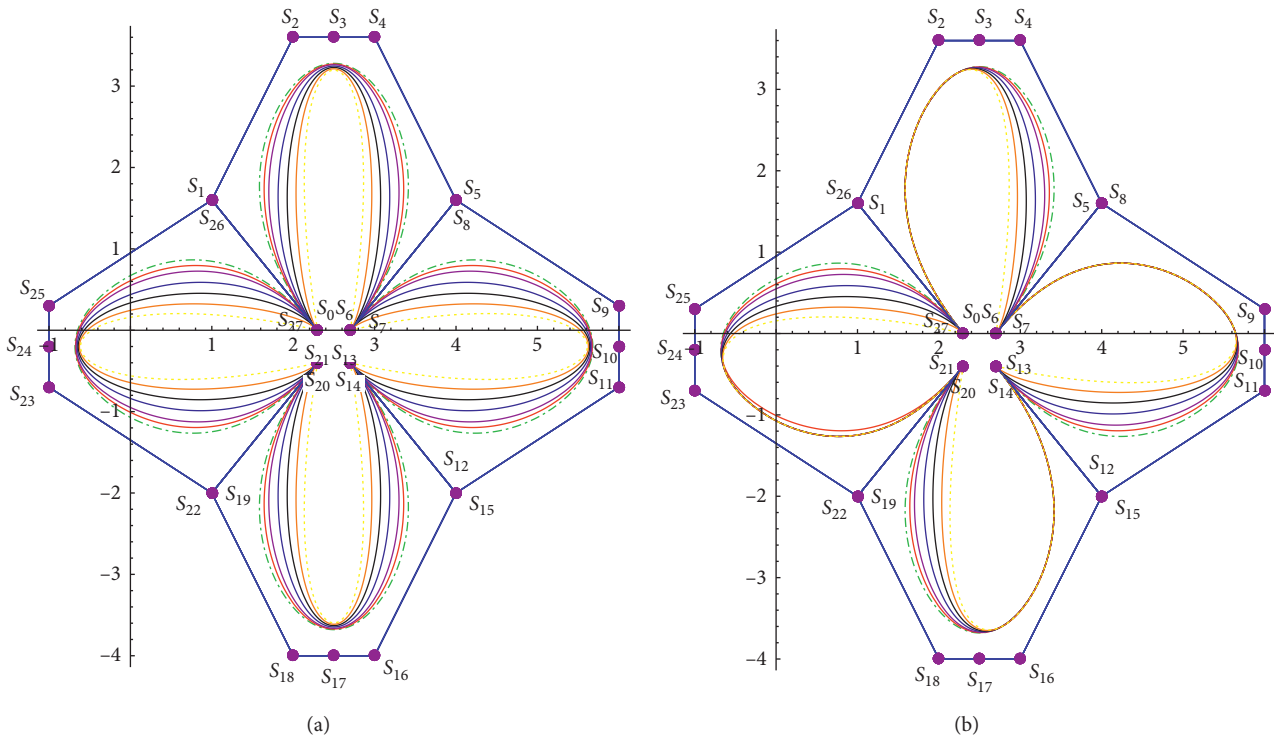


FIGURE 12: Continued.

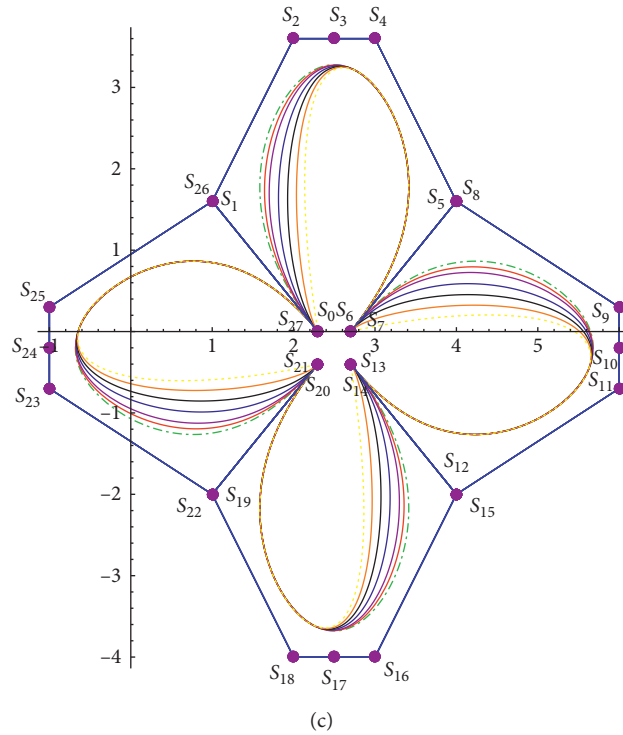


FIGURE 12: Construction of some open curves by different values of shape parameters. (a) $\mu = \omega = 1, 0.5, 0, -1, -2, -3, -4$. (b) $\mu = 1, 0.5, 0, -1, -2, -3, -4, \omega = 1$. (c) $\omega = 1, 0.5, 0, -1, -2, -3, -4, \mu = 1$.

8. Conclusions

In this research, a newly constructed ST-Bernstein basis and Bézier curve with two shape parameters has been proposed. It can be concluded that its geometric properties are similar to those of the classical Bézier curve. The shape of the curve can be regulated by changing the values of shape parameters. The suggested curve can be used to create open and closed curves with different values of shape parameter. The parametric and geometric continuities for two adjacent ST-Bézier curves are also presented, which demonstrate the efficiency of adjoining the ST-Bézier curves.

Data Availability

The experimental data used to support the findings of this study are included within the paper.

Conflicts of Interest

The authors declare that they have no conflicts of interest regarding this study.

Authors' Contributions

All authors equally contributed to this work and read and approved the final manuscript.

Acknowledgments

The authors thank Dr. Muhammad Kashif Iqbal for his assistance in proofreading of the manuscript.

References

- [1] L. X. Kun, "Bernstein-Bézier class curves and a re-parametrization method of Bézier curve," *Journal of Computer Research and Development*, vol. 6, pp. 1-16, 2004.
- [2] L. Yan and J. Liang, "An extension of the Bézier model," *Applied Mathematics and Computation*, vol. 218, no. 6, pp. 2863-2879, 2011.
- [3] H. Liu, L. Li, D. Zhang, and H. Wang, "Cubic trigonometric polynomial B-spline curves and surfaces with shape parameter," *Journal of Information & Computational Science*, vol. 9, no. 4, pp. 989-996, 2012.
- [4] J. Li, "A novel Bézier curve with a shape parameter of the same degree," *Results in Mathematics*, vol. 73, no. 4, p. 159, 2018.
- [5] X.-A. Han, Y. Ma, and X. Huang, "The cubic trigonometric Bézier curve with two shape parameters," *Applied Mathematics Letters*, vol. 22, no. 2, pp. 226-231, 2009.
- [6] M. Dube and R. Sharma, "Quartic trigonometric Bézier curve with a shape parameter," *International Journal of Mathematics and Computer Applications Research*, vol. 3, no. 3, pp. 89-96, 2013.
- [7] Y. Zhu, X. Han, and J. Han, "Quartic trigonometric Bézier curves and shape preserving interpolation curves," *Journal of Computational Information Systems*, vol. 8, no. 2, pp. 905-914, 2012.
- [8] L. Xiujuan, L. Hao, H. Gang, and L. Wenhe, "Generation and shape adjustment of revolution surface based on stream

- curve," *Mechanical Science and Technology*, vol. 27, no. 3, p. 326, 2008.
- [9] U. Bashir, M. Abbas, M. N. Hj Awang, and J. Ali, "A class of quasi-quintic trigonometric Bézier curve with two shape parameters," *ScienceAsia*, vol. 39S, no. 1, pp. 11–15, 2013.
- [10] X.-A. Han, Y. Ma, and X. Huang, "A novel generalization of Bézier curve and surface," *Journal of Computational and Applied Mathematics*, vol. 217, no. 1, pp. 180–193, 2008.
- [11] L. Yang and X.-M. Zeng, "Bézier curves and surfaces with shape parameters," *International Journal of Computer Mathematics*, vol. 86, no. 7, pp. 1253–1263, 2009.
- [12] T. Xiang, Z. Liu, W. Wang, and P. Jiang, "A novel extension of Bézier curves and surfaces of the same degree," *Journal of Information and Computing Science*, vol. 7, pp. 2080–2089, 2010.
- [13] Z. Liu, X. Chen, and P. Jiang, "A class of generalized bézier curves and surfaces with multiple shape parameters," *Journal of Computer-Aided Design & Computer Graphics*, vol. 22, no. 5, pp. 838–844, 2010.
- [14] X. Han, "A class of general quartic spline curves with shape parameters," *Computer Aided Geometric Design*, vol. 28, no. 3, pp. 151–163, 2011.
- [15] X. Qin, G. Hu, N. Zhang, X. Shen, and Y. Yang, "A novel extension to the polynomial basis functions describing Bezier curves and surfaces of degree n with multiple shape parameters," *Applied Mathematics and Computation*, vol. 223, pp. 1–16, 2013.
- [16] A. Ahmad, A. H. Amat, and J. Ali, "A generalization of Bézier-like curve," *Educatum-journal of Science, Mathematics and Technology*, vol. 1, no. 2, pp. 56–68, 2014.
- [17] S. BiBi, M. Abbas, M. Y. Misro, and G. Hu, "A novel approach of hybrid trigonometric Bézier curve to the modeling of symmetric revolutionary curves and symmetric rotation surfaces," *IEEE Access*, vol. 7, pp. 165779–165792, 2019.
- [18] S. BiBi, M. Abbas, K. T. Miura, and M. Y. Misro, "Geometric modeling of novel generalized hybrid trigonometric Bézier-like curve with shape parameters and its applications," *Mathematics*, vol. 8, no. 6, p. 967, 2020.
- [19] G. Hu, C. Bo, J. Wu, G. Wei, and F. Hou, "Modeling of free-form complex curves using SG-bézier curves with constraints of geometric continuities," *Symmetry*, vol. 10, p. 545, 2018.
- [20] A. Majeed and F. Qayyum, "New rational cubic trigonometric B-spline curves with two shape parameters," *Journal of Computational and Applied Mathematics*, vol. 39, pp. 1–24, 2020.
- [21] M. Y. Misro, A. Ramli, and J. M. Ali, "S-shaped and C-shaped transition curve using cubic trigonometric Bézier," *AIP Conference Proceedings*, vol. 1870, no. 1, Article ID 050005, 2017.
- [22] M. Y. Misro, A. Ramli, and J. M. Ali, "Quintic trigonometric Bézier curve and its maximum speed estimation on highway designs," *AIP Conference Proceedings*, vol. 1974, no. 1, Article ID 020089, 2018.
- [23] M. Y. Misro, A. Ramli, and J. M. Ali, "Quintic trigonometric bézier curve with two shape parameters," *Sains Malaysiana*, vol. 46, no. 5, pp. 825–831, 2017.
- [24] I. Juhász and A. Róth, "A scheme for interpolation with trigonometric spline curves," *Journal of Computational and Applied Mathematics*, vol. 263, pp. 246–261, 2014.
- [25] Y. P. Zhu and X. L. Han, "New trigonometric basis possessing exponential shape parameters," *Journal of Computational Mathematics*, vol. 33, pp. 642–684, 2015.
- [26] L. Yan and J. Liang, "A class of algebraic-trigonometric blended splines," *Journal of Computational and Applied Mathematics*, vol. 235, no. 6, pp. 1713–1729, 2011.

Research Article

Research on Revenue Insurance Premium Ratemaking of Jujube Based on Copula-Stochastic Optimization Model

Li-Mei Qi ^{1,2}, Ruo-Yu Yao ³, Xing-Zhe Zhang ⁴, Yu-Jing Zhang ³, Xiao-Yin Wang ³,
Jian-Ping Tao ¹ and Jia-Ming Zhu ⁵

¹College of Economics and Management, Huazhong Agricultural University, Wuhan 430070, China

²College of Information Engineering, Tarim University, Alaer 843300, China

³School of Mathematical Sciences, Tiangong University, Tianjin 300387, China

⁴School of Computer Science and Technology, Tiangong University, Tianjin 300387, China

⁵School of Statistics and Applied Mathematics, Anhui University of Finance & Economics, Bengbu 233030, China

Correspondence should be addressed to Jian-Ping Tao; tx2021new@126.com and Jia-Ming Zhu; zhujm1973@163.com

Received 29 March 2021; Accepted 6 May 2021; Published 18 May 2021

Academic Editor: Ghulam Mustafa

Copyright © 2021 Li-Mei Qi et al. This is an open access article distributed under the Creative Commons Attribution License, which permits unrestricted use, distribution, and reproduction in any medium, provided the original work is properly cited.

During the process of jujube planting, there are not only natural risks caused by natural disasters but also market risks caused by price factors. In the study, firstly, wavelet analysis method was used to stabilize the jujube yield per unit area and the jujube price from 1997 to 2018 in Aksu region, Xinjiang, China. Secondly, EasyFit software was used to fit the distribution functions of yield per unit area and price, respectively. Thirdly, the optimal Copula function which connects the marginal distribution functions and its joint distribution function was selected with the principle of “the minimum square distance from the empirical Copula function.” Finally, taking the premium rate and the insurance amount as two decision variables, the farmer’s risk minimization as the objective function, around the four constraints of functions and role of insurance, the nonspeculative nature of insurance, the sustainability of insurance, and the moral hazard factors and the farmers’ willing to participate in insurance, the Copula-stochastic optimization model was set up to determine the premium rate of jujube revenue insurance in Aksu region.

1. Introduction

“The world’s red dates are in China, and China’s red dates are in Xinjiang.” China’s jujube planting area and output rank first in the world. As the largest fruit industry in Xinjiang, the jujube industry is a new growth point of rural economy in southern Xinjiang and an important way to increase farmers’ income. However, due to the existence of natural disasters such as harmful organisms, low temperature and freezing damage, strong wind and dust, and market price, the development of the jujube industry in southern Xinjiang is directly affected. For this reason, the local governments actively explore safeguard measures. In years of production practice, the importance of agricultural insurance in the development of Xinjiang characteristic fruit industry has been gradually recognized [1].

In 2018, Xinjiang’s jujube planting area accounted for nearly 50% of China’s total, and the planting area of jujube in Xinjiang was mainly concentrated around the Tarim Basin in southern Xinjiang, and Aksu region accounted for about 20%. Aiming at the situation of rapid development of fruit industry in Aksu region, in order to ensure fruit growers’ income and prevent natural disasters, Xinjiang government launched pilot insurance policy for characteristic fruit industry in 2010. Aksu city was selected as the pilot county and city. It adopted the form of fixed insurance with an insurance amount of 15,000 Yuan per hectare, with a premium rate of 9%, covering jujube, apple, pear, etc., and the premium subsidy ratio was 65% from the regional government, 15% from the regional and municipal government, and 20% from farmers. In 2020, the policy of policy-based forest and fruit industry insurance award and subsidy benefiting the people

implemented in Aksu region, with an insurance amount of 24,000 Yuan per hectare and a premium rate of 6%. The insurance premium subsidy ratio was 30% subsidized by the central government, 35% subsidized by the autonomous region, 15% subsidized by the prefectural and county governments (no more than 5% in counties or cities), and 20% subsidized by fruit farmers. Reasonable premium rate will directly affect whether the local fruit insurance can be carried out smoothly and directly determine whether agricultural insurance can play a role in escorting the fruit industry.

Agricultural insurance is an effective mechanism for avoiding and apportioning agricultural risks, which is one of the effective tools for promoting agricultural development and one of the core ways of modern agricultural risk management [2, 3]. And, agricultural insurance belongs to the “green box policy” of WTO. Revenue insurance, which combines yield risk with price risk, has become one of the most popular types of insurance in the United States [4, 5]. Since 2007, agricultural insurance has appeared in China’s Document No. 1 of the Central Government for many consecutive years. China has appeared for many years in a row. In 2016, it was proposed to explore the revenue insurance pilot, and in 2019, it was proposed to promote the revenue insurance pilot program for agricultural products [6].

At present, the literature and materials for the determination of crop revenue insurance rate all adopt the mode of “fitting the marginal distribution functions of yield per unit area and price—selecting the optimal Copula function—Monte Carlo simulation” to determine the rate [7–17]. But the Monte Carlo simulation method is a computer simulation method, and its basic idea is to replace the probability with the frequency of random events and obtain some digital characteristics of the random variable through the generation of random number. The Monte Carlo simulation method is easy to implement and can obtain the estimate of these digital features through a large number of “experiments,” but the results are not stable and will be certain deviation with the difference of “number of experiments.”

Stochastic optimization method is an optimization method with random variables [18]. Compared with the Monte Carlo simulation method, the stochastic optimization method preserves the randomness of random variables in the model to a greater extent. By analyzing the correlation of random variables, determining decision variables, defining the objective function, and constructing the constraint conditions, the stochastic optimization model is established to obtain the final results.

2. Copula Functions

The Copula function (also known as the join or dependent function) is a function that connects the marginal distributions and the joint distribution. In 1959, Sklar first proposed Copula theory, and Elizabeth applied it in the field of crop yield insurance in 2002. In recent years, it has been gradually applied in the field of income insurance. In 2006,

Nelsen [19] gave the definition of 2-element copulas—a 2-element copula is a function with the following properties: (i) the domain of definition is $[0, 1]^2$; (ii) C is grounded and is 2-increasing; (iii) For every u and v in $[0, 1]$, $C(u, 1) = u$ and $C(1, v) = v$.

2.1. Sklar’s Theorem [19]. Let H is a joint distribution function with margins F and G . Then, there exists a Copula C such that, for all $x, y \in (-\infty, +\infty)$ and $H(x, y) = C(F(x), G(y))$. If F and G are continuous, then C is unique; otherwise, C is uniquely determined on $\text{Ran}F \times \text{Ran}G$. Conversely, if C is a copula and F and G are distribution functions, then the function H defined by $H(x, y) = C(F(x), G(y))$ is a joint distribution function with margins F and G .

Sklar’s theorem guarantees the existence and uniqueness of copulas, through which the edge distribution of crop yield per unit area and price can be connected to its joint distribution function.

3. Data Source and Processing

3.1. Data Source. In this paper, the data of planting area, output value, and yield of jujube are all from Aksu Statistical Yearbook (1998–2019), and the sample time is from 1997 to 2018. The jujube is not divided into varieties or grades. The data of jujube in Aksu region uniformly adopts the sum of the data of 7 counties and 2 cities under the jurisdiction of Aksu region as the corresponding data. According to the growth law of jujube, the grafted jujube trees will bear fruit in the same year (the second year after planting) and enter the full fruit period from the 4th year, and the yield is relatively stable from about the 6th year after planting. In this paper, the jujube output value in the current year is divided by the jujube yield as the jujube price in the current year. Since jujube is a perennial fruit tree, the calculation of yield per unit area is different from that of annual crops. The increase of nonbearing jujube trees and the reduction of the age of jujube trees is not clear, and other problems all affect the yield per unit area of jujube trees. And, considering the actual situation of Chinese jujube cultivation of Aksu region in Xinjiang and the situation of steady production after bear fruit, we calculated the yield per unit area of jujube by referring to the calculation method of apple yield per unit area used by Wu and Wang [7] in the study of apple insurance rate calculation in Aksu region. In other words, the planting area of jujube trees in 1997 was taken as the planting area of actual output of jujube trees in 2002, and then it was calculated in turn with a period of 6 years.

3.2. Data Processing. Since the Copula function is used, the per unit area yield and price data are required to be stable. Therefore, SAS software is first used to conduct a stabilization test on the yield per unit area and price data of jujube trees, and it is found that these two sequences are not stable. The following is to consider the stabilization processing of the data.

For the stabilization of time series, there are both time domain analysis for the time trend of the series, such as

various linear or nonlinear trend models and frequency domain analysis for the fluctuation frequency of the stationary series at specific time points, such as Fourier transform. However, in actual production, the variation law of crop yield per unit area and price series is often more complex, which not only increases with the improvement of agricultural technology but also randomly fluctuates due to natural disasters and other conditions. Therefore, it is biased to adopt a simple time-domain analysis or frequency-domain analysis [20]. Wavelet analysis has the characteristics of multiresolution, which can decompose the signal into low frequency region and high frequency region. The analysis in time domain and frequency domain is more suitable for the stabilization of time series.

In this paper, wavelet multiresolution analysis is used to decompose the time series into multiple layers to separate the trend term and fluctuation term. Its essence is to decompose and reconstruct the nonstationary time series. The time series is decomposed into large-scale components (low-frequency signals, i.e., trend items) and small-scale components (high-frequency signals, i.e., wave items), and the superposition of the corresponding large-scale components and small-scale components is the original sequence, i.e.,

$$S = A_1 + D_1 = A_2 + D_1 + D_2 = A_3 + D_1 + D_2 + D_3 = \dots, \tag{1}$$

where S represents the original nonstationary time series, $A_i (i = 1, 2, \dots)$ represents the trend term of the nonstationary time series, and $D_j (j = 1, 2, \dots)$ represents the fluctuation term of the nonstationary time series.

Using the wavelet toolbox of MATLAB software, the tightly supported orthogonal wavelet SMY8 wavelet was selected to carry out wavelet multiresolution analysis on the yield per unit area of jujube and the price of jujube in Aksu region. It was found that the wave terms after two-layer wavelet decomposition and reconstruction all passed the ADF stabilization test. Considering the dimensional differences between the yield per unit area and the price, Z-score normalization was conducted for the stabilized sequence of fluctuation terms, and the data are shown in Table 1.

4. Establishment of Copula-Stochastic Optimization Model

4.1. *Fit Distribution Functions of Yield per Unit Area and Price of Jujube Tree.* EasyFit software was used to fit the distribution functions of the data series after the stabilization of yield per unit area and price of jujube in Aksu region, respectively. The results are shown in Table 2.

As can be seen from Table 2, both unit yield and price are subject to log-logistic (3P) function, and their distribution function is

$$F(y) = \left[1 + \left(\frac{\beta}{y - \gamma} \right)^\alpha \right]^{-1}, \quad y \geq \gamma, \tag{2}$$

and the probability density function is

$$f(y) = \frac{\alpha((y - \gamma)/\beta)^{\alpha-1}}{\beta[1 + ((y - \gamma)/\beta)^\alpha]^2}. \tag{3}$$

4.2. *Select the Optimal Copula Function.* Among the Gaussian Copula function, t-Copula function, Gumbel Copula function, Clayton Copula function, and Frank Copula function, the optimal Copula function was selected with the principle of minimum the square Euclidean distance from the empirical Copula function (as shown in Figure 1).

Empirical Copula [21]: let $(x_i, y_i) (i = 1, 2, \dots, n)$ be a sample taken from a 2-dimensional population (X, Y) . The empirical distribution function of X is $F_n(x)$, and the empirical distribution function of Y is $G_n(y)$, and the empirical Copula function is as follows:

$$\hat{C}_n(u, v) = \frac{1}{n} \sum_{i=1}^n I_{[F_n(x_i) \leq u]} I_{[G_n(y_i) \leq v]}, \quad u, v \in [0, 1], \tag{4}$$

where $I_{[\cdot]}$ is an indicator function,

$$I_{[F_n(x_i) \leq u]} = \begin{cases} 1, & F_n(x_i) \leq u, \\ 0, & F_n(x_i) > u, \end{cases} \quad \text{and}$$

$$I_{[G_n(y_i) \leq v]} = \begin{cases} 1, & G_n(y_i) \leq v, \\ 0, & G_n(y_i) > v. \end{cases}$$

MATLAB software was used to calculate the square Euclidean distances between the five Copula functions and the empirical Copula functions, respectively [21]. So, Frank Copula function was selected as the optimal Copula function adopting the principle of minimum the square Euclidean distance from the empirical Copula function. The results are shown in Table 3.

The distribution function of Frank Copula function is expressed as follows:

$$C_F^\alpha(u, v) = -\frac{1}{\alpha} \ln \left[1 + \frac{(e^{-\alpha u} - 1)(e^{-\alpha v} - 1)}{e^{-\alpha} - 1} \right], \tag{5}$$

and the probability density function is expressed as follows:

$$c_F^\alpha(u, v) = \frac{\alpha(1 - e^{-\alpha})e^{-\alpha(u+v)}}{[(1 - e^{-\alpha}) - (1 - e^{-\alpha u})(1 - e^{-\alpha v})]^2}. \tag{6}$$

Frank Copula function (Figure 2) has a symmetrical tail feature, which indicates that the yield per unit area and price of jujube trees are asymptotically independent. Kendall's rank correlation coefficient is -0.1626 , indicating that there is a very weak negative correlation between yield per unit area and price of jujube trees.

4.3. *Model Preparation.* Before establishing the stochastic optimization model, variables such as compensation amount, jujube farmers' income, and jujube farmers' risk should be further clarified.

TABLE 1: Z-score normalized data of fluctuation items in yield per unit area and price of jujube in Aksu region.

Time/year	2002	2003	2004	2005	2006	2007	2008	2009	2010
Yield per unit area	0.9209	-1.2248	-0.7132	-0.4427	2.96	-1.1104	-1.0053	-0.3387	0.8537
Price	-1.4635	2.3301	-0.9486	0.3199	-0.3625	0.2797	-0.2522	-0.9188	1.5111
Time/year	2011	2012	2013	2014	2015	2016	2017	2018	—
Yield per unit area	0.6656	-0.5131	0.1116	-0.3877	-0.2682	-0.0334	0.1674	0.3584	—
Price	-0.0232	0.1822	-1.1625	-0.3641	1.4938	-0.0033	-0.5163	-0.1018	—

TABLE 2: Distribution functions and parameters of jujube yield per unit area and price in Aksu region.

The data sequence	Distribution function	Parameters
Yield per unit area	Log-logistic	$\alpha = 3.40740, \beta = 1.60040, \gamma = -1.80370$
Price	Log-logistic	$\alpha = 4.48300, \beta = 2.28600, \gamma = -2.45590$

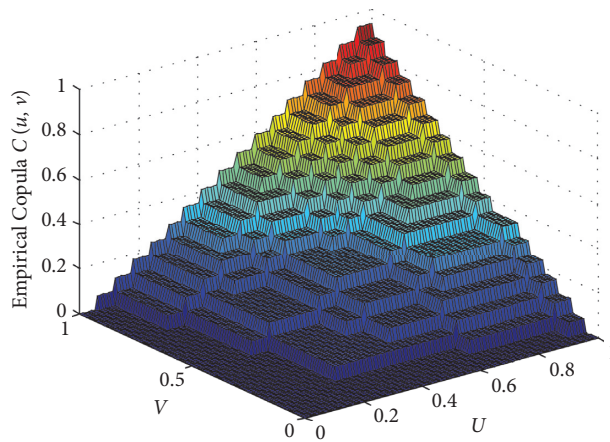


FIGURE 1: Empirical Copula function.

TABLE 3: Estimation results of the optimal Copula function.

Copula function	Parameter	Kendall rank correlation coefficient	Euclidean distance squared
Frank	-1.4956	-0.1626	0.0120
Gumbel	1.0000	$1.3575e - 06$	0.0125
Clayton	$1.4509e - 06$	$7.2543e - 07$	0.0125
Gaussian	-0.3024	-0.1955	0.0142
<i>t</i>	-0.3050	-0.1973	0.0143

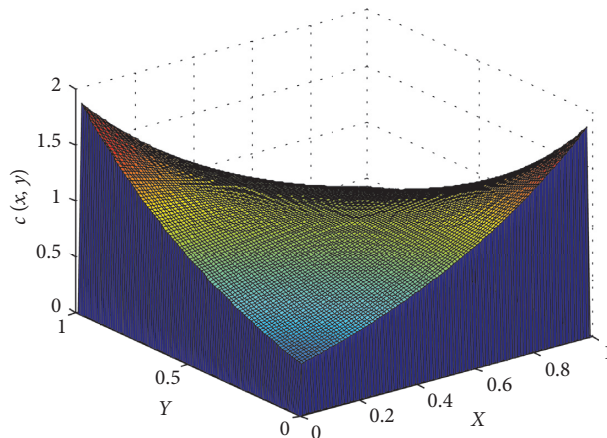


FIGURE 2: Probability density function of Frank Copula function.

4.3.1. *Compensation Amount.* After the jujube harvest period, when the actual income of jujube farmers (the insured) H is lower than the expected income agreed in the contract (insurance amount) \bar{H} due to the risk, the insurance company starts the claim settlement procedure, verify the cause of the loss and the extent of the loss, and pays the compensation.

Compensation amount is the cost that insurance company compensates to farmer: compensation amount $I = \text{insurance amount } \bar{H} - \text{jujube farmer's actual income } H$.

4.3.2. *Risk.* Risk is the core of this paper. How to define risk will directly affect the result of stochastic optimization.

The risk of jujube farmers is mainly reflected in the volatility of yield per unit area and price of jujube trees, which can be described by the variance of variables. The greater the variance is, the greater the risk is.

In this paper, the variance of date farmers' income from planting dates is selected to represent the risk of jujube farmers before insurance. Then,

$$S_0 = E(H^2) - [E(H)]^2. \tag{7}$$

Select the variance of the jujube farmer's income of planting jujube trees H plus the compensation amount I minus the insurance premium F (i.e., $H + I - F$) as the risk after insurance. Then,

$$S(x, y, Z, F) = E[(H + I - F)^2] - [E(H + I - F)]^2. \tag{8}$$

Substitute $F = ZM$ into the above equation, and the risks of jujube farmers after insurance $S(x, y, Z, F)$ are sorted out as $S(x, y, Z, M)$.

4.3.3. *Revenue.* Assuming that there is no moral hazard, the cost L of fertilizer, pesticide, labor, and other costs of planting one hectare of jujube is fixed. Let the probability density function of the yield per unit area of jujube tree x is $f_x(x)$, the probability density function of the price y is $f_y(y)$, and the joint probability density function of the yield per unit area and the price is $f(x, y)$. Select the mathematical expectation $E(H)$ of the jujube farmer's income H of planting

jujube trees minus the cost sL as the revenue $N_0(x, y)$ of jujube farmers noninsured, i.e.,

$$N_0(x, y) = E(H) - sL, \\ = \iint_{R^+} rp \times rq \times s \times f(x, y) dx dy - sL. \tag{9}$$

After the jujube farmers purchase insurance, the additional expenditure is the insurance premium F and the additional income is the compensation amount I . Thus, the revenue of the farmers $N(x, y)$ insured is obtained:

$$N(x, y) = N_0(x, y) + I - F. \tag{10}$$

4.4. Determine Constraint Conditions

- (1) Determination of decision variables

In this paper, select premium rate and insurance amount as decision variables

- (2) Determination of objective function

The target of insurance products is jujube farmers. It is assumed that there is no moral hazard. It is assumed that the cost of fertilizer, pesticide, labor, and other costs per hectare for each hectare are fixed cost L . Assume the income of the jujube farmer with the planting area s is H and the fixed cost is sL . Assume the expenditure is only the insurance premium. Then, the objective function of the optimization model is $S(x, y, Z, M)$ (i.e., the risk of jujube farmers insured).

- (3) Establishment of constraint conditions

First of all, the risk of jujube farmers insured should be lower than that of the noninsured, so as to establish constraint 1:

$$S(x, y, Z, M) < S_0(x, y). \tag{11}$$

Secondly, in order to avoid the speculative nature of insurance, the revenue of jujube farmers insured is limited, so that the revenue of jujube farmers insured is lower than that noninsured so as to establish constraint 2:

$$\iint_{\{(x,y)|x,y \in R^+, xy < Z\}} (xy - F + I) f(x, y) dx dy + \iint_{\{(x,y)|x,y \in R^+, xy < Z\}} (xy - F) f(x, y) dx dy \leq \iint_{\{(x,y)|x,y \in R^+\}} xy f(x, y) dx dy. \tag{12}$$

Thirdly, farmers' revenue should be improved as much as possible; on the other hand, in order to ensure the sustainability of insurance company operation, the earning of insurance company should

be positive and from 0+ tend to 0. In the optimization algorithm, in order to expand the feasible region of the algorithm, the earning interval of the insurance company is extended to $[-0.5, 0.5]$, which

TABLE 4: Premium rate and risk of jujube revenue insurance in Aksu region.

Guarantee level	100 (%)	95 (%)	90 (%)	85 (%)	80 (%)	75 (%)	70 (%)
Pure premium rate	11.33	10.06	8.81	7.61	6.43	5.31	4.24
Gross premium rate	16.42	14.58	12.77	11.03	9.32	7.69	6.14
Risk reduction ratio insured	47.03	41.75	36.45	31.21	26.08	21.15	16.51

Note. gross rate = net rate × (1 + safety factor) × (1 + operating expense factor) × (1 + predetermined savings rate), safety factor is 15%, operating expense factor is 20%, and predetermined savings rate is 5% [22].

is conducive to finding the optimal solution so as to establish constraint 3:

$$-0.5 \leq \iint_{\{(x,y)|x,y \in R^+, xy < Z\}} (F - I)f(x, y)dx dy + \iint_{\{(x,y)|x,y \in R^+, xy \geq Z\}} Ff(x, y)dx dy \leq 0.5. \tag{13}$$

Finally, the excessively high insurance amount will promote the emergence of moral hazard behavior of jujube farmers and also lead to the excessively high insurance premium, which will affect the insurance willingness of jujube farmers. Therefore, the insurance amount per hectare needs to be constrained.

According to relevant materials, the material cost of jujube tree planting in Aksu city is 18,000 Yuan per hectare, and the labor cost is about 12,000 Yuan per hectare. Therefore, the limited insurance amount is 18,000–30,000 Yuan per hectare, so as to establish constraint 4:

$$18000 \leq Z \leq 30000. \tag{14}$$

4.5. Solve the Stochastic Optimization Model

Step 1. Use MATLAB software, according to the probability density functions of yield per unit area and price. The random numbers of yield per unit area and price were generated by simple random sampling and selection sampling method, respectively.

Step 2. Use the random number obtained in Step 1 to solve the income of jujube.

Step 3. Call the “FMINCON” function library, set the initial value of insurance amount and premium rate as 22000 and 0.1, respectively, set the lower limit as 0 and the upper limit as 100000 and 0.5, and solve the model.

Step 4. Calculate the risk of noninsured and insured farmers’ by using the insurance amount and premium rate obtained.

Use MATLAB software to solve the stochastic optimization model and obtain that, at the 100% guarantee level, the insurance amount is 30000Yuan per hectare, the pure premium rate is 11.33%, the gross premium rate is 16.42%, and the premium is 4926 Yuan per hectare (according to the subsidy ratio of the current insurance award and subsidy

scheme, jujube farmers only need to bear 985.2 Yuan per hectare), and the risk of jujube farmers has decreased by 47.03% compared with that noninsured. The results are shown in Table 4.

5. Conclusions and Policy Recommendations

5.1. Conclusions

- (i) The stochastic optimization method can be used to determine the crop revenue insurance rate, which is more stable than such simulation methods as Monte Carlo simulation.
- (ii) The yield per unit area and the price of jujube in Aksu region are asymptotically independent, and there is a weak positive correlation.
- (iii) Revenue insurance plays a very important role in risk diversification of jujube farmers, and the risk after insurance is nearly 50% lower than that before insurance.
- (iv) Compared with the calculation result in this paper, “under the 80% guarantee level, the insurance amount is 24,000 Yuan per hectare, and the gross premium rate is 9.32%,” the current policy-based premium rate of 6% for fruit insurance is low. This may be because the current policy requires comprehensive consideration of the six main tree varieties of walnut, jujube, apricot, almond, apple, and grape, rather than just a single variety of jujube, so the insurance amount and premium formulated are not targeted enough for different trees and fruits [23].

5.2. Policy Recommendations

- (1) *Carry Out Jujube Revenue Insurance to Boost the Development of the Jujube Industry.* As the main producing area of jujube in Aksu, Xinjiang is vulnerable to natural disasters such as hail and wind damage. Market risks such as price factors cannot be ignored. In recent years, the price fluctuation of

Xinjiang jujube market is very violent, which seriously affects the healthy development of jujube industry and directly affects the economic income of jujube farmers. In order to prevent jujube farmers from going back to poverty again, carrying out jujube revenue insurance is necessary on the basis of the current policy-based insurance reward and subsidy policy of characteristic fruit industry, so as to boost the development of jujube industry and increase the income of jujube farmers in Xinjiang.

- (2) *Formulate Agricultural Insurance Policies in View of Different Fruit Trees.* Since 2010, Aksu has successively implemented the characteristic fruit industry insurance policies, which are unified insurance amount and unified premium rate for jujube, apple, and other major varieties. It is convenient to calculate and highly operable, but it is easy to promote moral hazard and adverse selection which is not conducive to the development of fruit industry [24]. Moreover, with the development of various fruit industries, the differences in cost and price are increasing. Therefore, it is necessary to formulate different agricultural insurance policies for different fruit varieties.
- (3) *Establish the Database of Fruit Industry.* The fruit industry is of great significance for Xinjiang farmers to get rid of poverty, but there is not too much data about the fruit industry. Considering the formulation of relevant policies such as agricultural insurance pricing, as well as the early warning research on industrial development and disaster early warning, it is suggested to establish a database for the fruit industry, which includes the disaster data of natural disasters, the product price, and planting cost data.
- (4) *The Government Needs to Continue to Provide Financial Subsidies for Agricultural Insurance and Support the Development of Agricultural Insurance such as Revenue Insurance.* The income of Xinjiang fruit growers is still lower in the whole country. Considering the insurance cost in fruit industry, insurance will increase the burden of fruit farmers, which may affect the fruit farmers to participate in the initiative to protect all kinds of risks. Therefore, finance of all levels of government may adopt the insurance premium award and subsidy policy implemented in the pilot at present and share the proportion of the insurance premium of fruit farmers [25].
- (5) *Increase Publicity to Enhance the Awareness of Risk and Insurance Participation of Fruit Farmers.* In addition to the pricing factors of agricultural insurance, such as insurance amount and premium, farmers' risk awareness and insurance participation consciousness also directly affect the implementation of agricultural insurance system and fundamentally determine whether the fruit insurance policy formulated can really play the role of guarantee.

Therefore, the government may organize professionals to popularize various professional knowledge and possible planting risks for fruit farmers and to increase the publicity of the fruit industry insurance, which can enhance the risk awareness and insurance participation awareness of fruit farmers and fully mobilize their enthusiasm for insurance participation, so that agricultural insurance can really play a role in protecting the fruit industry.

Data Availability

The data used to support the findings of this study are included within the article.

Conflicts of Interest

The authors declare that there are no conflicts of interest regarding the publication of this paper.

Acknowledgments

This study was funded by Southern Xinjiang Research Center of Agricultural Information, Institute of Agricultural Information, Chinese Academy of Agricultural Sciences (Study on Zoning of Planting Risk of Jujube in Southern Xinjiang, no. zx2015003), Tarim University-Chinese Academy of Agricultural Sciences Joint Fund Project (Study on Xinjiang Cotton Price Early Warning Model under the Background of Big Data, no. NJZX201601, and National Innovation and Entrepreneurship Program (Determination of Jujube Income Premium Rate Based on Copula and Stochastic Optimization Model, no. 202010058004).

References

- [1] J.Z. Gu, "Research on demand and model of fruit industry insurance in Xinjiang," Master Dissertation, Xinjiang Agricultural University, Ürümqi, China, 2016.
- [2] G. Z. Tuo and J. S. Zhu, "Revenue insurance: an important means to perfect the farm produce price formation mechanism reform," *Insurance Studies*, vol. 6, pp. 3–11, 2016.
- [3] B. L. Wang, J. Sun, and C. G. Jiang, "Research on the economic effect of introducing agricultural income insurance in China," *Insurance Studies*, vol. 3, pp. 71–89, 2017.
- [4] B. W. Wang and Q. Zhang, "Scale evolution of the U.S. crop revenue insurance and its prospect," *Agricultural Outlook*, vol. 6, pp. 34–40, 2018.
- [5] B. K. Goodwin and A. Hungerford, "Copula-based models of systemic risk in U.S. agriculture: implications for crop insurance and reinsurance contracts," *American Journal of Agricultural Economics*, vol. 97, no. 3, pp. 879–896, 2014.
- [6] S. C. Liu and Y. W. Liu, "The analysis of the crop revenue insurance and pricing: on apple industry in Shandong province," *China Soft Science*, vol. 9, pp. 185–192, 2018.
- [7] Y. H. Wu and J. Wang, "An empirical analysis of the rationality of the apple premium rate in Aksu pilot region," *Issues of Forestry Economics*, vol. 31, no. 6, pp. 475–478, 2011.
- [8] F. J. Xie, "Pricing models and empirical studies of crop insurance," Doctoral Dissertation, Dalian University of Technology, Dalian, China, 2011.

- [9] Q. Zhang, K. Wang, Y. Li et al., "Necessity and possible scheme of revenue insurance pilot for main grains in China—taking wheat in Hebei province as an example," *Agricultural Outlook*, vol. 7, pp. 18–24, 2015.
- [10] S. W. Chen and L. Yan, "Meteorological index insurance design for regional apple low temperature freezing disaster: with a case study of Qixia city in Shandong province," *Insurance Studies*, vol. 12, pp. 78–87, 2015.
- [11] T. T. Xu, R. Sun, and W. W. Cui, "Analysis of the cash crop revenue insurance and its pricing—take Shaanxi apples as an example," *Insurance Studies*, vol. 11, pp. 33–43, 2017.
- [12] Y. H. Guo, "Research on the problem of corn revenue insurance," Master Dissertation, Hebei University of Economics and Business, Shijiazhuang, China, 2017.
- [13] N. N. Chao, "Premium rating for cotton revenue insurance in Xinjiang Uygur Autonomous Region of China," Doctoral Dissertation, China Agricultural University, Beijing, China, 2018.
- [14] L. Zhang, "Rate making for agricultural revenue insurance products—a case study of Shandong winter wheat," Master Dissertation, Shandong Agricultural University, Tai'an, China, 2018.
- [15] W. J. Zhang, "Research on corn income insurance in Yunnan Province," Master Dissertation, Yunnan University of Finance and Economics, Kunming, China, 2018.
- [16] G. D. Wang and K. Pang, "Calculation of economic crop income insurance rate based on the copula function—a case study of apples in Gansu province," *Exploration of Financial Theory*, vol. 3, pp. 62–70, 2019.
- [17] J. L. Peng and X. R. Xu, "Copula-based rate determination of crop revenue insurance a case study of early indica rice in Hu'nan province," in *Proceeding of the 2020 International Conference on Management, Economy and Law, Advances in Economics, Business and Management Research*, vol. 153, pp. 37–42, Krasnodar, Russia, October 2020.
- [18] S. B. Yang, Z. F. Tan, Z. X. Liu et al., "A multi-objective stochastic optimization model for electricity retailers with energy storage system considering uncertainty and demand response," *Journal of Cleaner Production*, vol. 277, pp. 1–17, 2020.
- [19] R. B. Nelsen, *An Introduction to Copulas*, Springer, Berlin, Germany, 2nd edition, 2006.
- [20] J. Feng, "The area-based crop yield insurance premium rate estimation based on wavelet analysis," Master Dissertation, Ocean University of China, Qingdao, China, 2014.
- [21] Z. H. Xie, *MATLAB statistical analysis and application: 40 case*, Beihang University Press, Beijing, China, 2nd edition, 2016.
- [22] G. Z. Tuo and J. Li, *Agriculture insurance*, China Renmin University Press, Beijing, China, 2005.
- [23] J. B. Liu, J. Zhao, and J. Min, "On the Hosoya index of graphs formed by a fractal graph," *Fractals-Complex Geometry Patterns and Scaling in Nature and Society*, vol. 27, no. 8, pp. 19–35, 2019.
- [24] J.-M. Zhu, Y. Chen, and S. Zhang, "Analysis of the impact of climate change on national vulnerability based on fuzzy comprehensive evaluation," *Discrete Dynamics in Nature and Society*, vol. 2020, Article ID 3527540, 10 pages, 2020.
- [25] F. Xu, Y.-A. Du, H. Chen et al., "Prediction of fish migration caused by ocean warming based on SARIMA model," *Complexity*, vol. 2021, Article ID 5553935, 9 pages, 2021.

Research Article

Recursive Process for Constructing the Refinement Rules of New Combined Subdivision Schemes and Its Extended Form

Rabia Hameed ¹, Ghulam Mustafa ², Jiansong Deng ³, and Shafqat Ali ²

¹Department of Mathematics, The Government Sadiq College Women University Bahawalpur, Bahawalpur, Punjab 63100, Pakistan

²Department of Mathematics, The Islamia University of Bahawalpur, Bahawalpur, Punjab 63100, Pakistan

³School of Mathematical Sciences, University of Science and Technology of China, Hefei, Anhui 230026, China

Correspondence should be addressed to Ghulam Mustafa; ghulam.mustafa@iub.edu.pk

Received 12 December 2020; Accepted 26 March 2021; Published 16 April 2021

Academic Editor: Efthymios G. Tsionas

Copyright © 2021 Rabia Hameed et al. This is an open access article distributed under the Creative Commons Attribution License, which permits unrestricted use, distribution, and reproduction in any medium, provided the original work is properly cited.

In this article, we present a new method to construct a family of $(2N + 2)$ -point binary subdivision schemes with one tension parameter. The construction of the family of schemes is based on repeated local translation of points by certain displacement vectors. Therefore, refinement rules of the $(2N + 2)$ -point schemes are recursively obtained from refinement rules of the $2N$ -point schemes. Thus, we get a new subdivision scheme at each iteration. Moreover, the complexity, polynomial reproduction, and polynomial generation of the schemes are increased by two at each iteration. Furthermore, a family of interproximate subdivision schemes with tension parameters is also introduced which is the extended form of the proposed family of schemes. This family of schemes allows a different tension value for each edge and vertex of the initial control polygon. These schemes generate curves and surfaces such that some initial control points are interpolated and others are approximated.

1. Introduction

Subdivision schemes are efficient tools for generating smooth curves/surfaces as the limit of an iterative process based on simple refinement rules starting from certain control points defining a control polygon/mesh. In recent years, subdivision schemes have been an important research area. These schemes provide an efficient way to describe curves, surfaces, and related geometric objects. Generally, subdivision schemes are classified as interpolatory or approximating, depending on whether the limit curve passes through all the given initial control points or not. Although approximating schemes yield smoother curves with higher order continuity, interpolating schemes are more useful for engineering applications as they preserve the shape of the coarse mesh. The special family of interpolatory schemes consists of the schemes with refinement rules that preserve the points associated with the coarse mesh and only generate new points related to the additional vertices of the refined mesh. An important family of interpolatory schemes was

introduced by Deslauriers and Dubuc [1], and latest tools for its analysis were introduced by Amat et al. [2] whereas an important family of approximating subdivision schemes that is the dual counterparts of the schemes of Deslauriers and Dubuc [1] was proposed by Dyn et al. [3]. In 2017, Hameed and Mustafa [4] introduced an oscillation-free family of a -point b -ary subdivision schemes which can produce approximating curves with high continuity and less complexity.

However, there also exist the parametric subdivision schemes, which can produce family of smooth approximating curves for special choices of the tension parameters. The families of such schemes were introduced in [5–8]. Furthermore, a parametric subdivision scheme can be converted to the nonuniform subdivision scheme by defining the local tension parameter. Mustafa and Hameed [6, 7] converted their families of univariate and bivariate subdivision schemes to nonuniform approximating subdivision schemes by defining local tension parameters. A parametric subdivision scheme which can produce both

interpolatory and approximating curves is called the combined subdivision scheme. If a combined subdivision scheme is capable to convert in the nonuniform form such that it can interpolate only certain initial control points and approximate all the other initial control points, then such a scheme will be interproximate scheme. Pan et al. [9] and Novara and Romani [10] presented the combined ternary subdivision schemes to fit interpolatory and approximating curves. However, they did not present the nonuniform form of their combined subdivision schemes.

Li and Zheng [11] combined the 4-point scheme of Dyn et al. [12] and the cubic B-spline binary refinement scheme to construct an interproximate subdivision scheme. Tan et al. [13] combined the 4-point scheme of Dyn et al. [12] and a 2-point corner cutting scheme to construct another interproximate subdivision scheme. However, these schemes give interproximate behavior but are not easy to implement and analyze. Nowadays, surface modeling is also modifying to fulfill the previous gaps. Pan et al. [14] presented a surface formulation method of multipatches based on rational splines. Nguyen-Thanh et al. [15] gave a subdivision approach for the minimal surface models on planar domains.

In this paper, we present a recursive method to construct the $(2N + 2)$ -point combined subdivision schemes with one tension parameter to control the given points of the initial polygon. The construction of combined subdivision schemes by a recursive method is a new trend in CAGD. We also present an extended form of this family of combined schemes by defining another tension parameter to control the insertion of new point between the given points in order to smooth the given polygon. Thus, the involvement of two tension parameters increases the flexibility in curves and surfaces fitting. Furthermore, we analyze the behavior of these combined subdivision schemes mathematically and show that these schemes not only give optimal smoothness but also give a desired reproduction degree. The results are then verified geometrically. Furthermore, we convert our schemes to interproximate schemes that generate smooth and oscillation-free curves and surfaces such that some initial control points are interpolated and others are approximated.

This article is organized as follows. Section 2 deals with some basic definitions and results. In Section 3, we construct three families of primal subdivision schemes. Section 4 deals with some important properties of the proposed families of schemes. In Section 5, numerical examples and comparisons are presented. A family of interproximate subdivision schemes and associated numerical examples are presented in Section 6. Conclusions are given in Section 7.

2. Preliminaries

A general compact form of linear, uniform, and stationary binary univariate subdivision scheme S_a which maps a polygon $f^k = \{f_i^k, i \in \mathbb{Z}\}$ to a refined polygon $f^{k+1} = \{f_i^{k+1}, i \in \mathbb{Z}\}$ is defined as

$$f_i^{k+1} = \sum_{j \in \mathbb{Z}} a_{i-2j} f_j^k, \quad i \in \mathbb{Z}. \quad (1)$$

Since the subdivision scheme (1) is a binary scheme, the two rules for defining the new control points are as follows:

$$\begin{aligned} f_{2i}^{k+1} &= \sum_{j \in \mathbb{Z}} a_{2i-2j} f_j^k = \sum_{\gamma \in \mathbb{Z}} a_{2\gamma} f_{i-\gamma}^k, \quad i \in \mathbb{Z}, \\ f_{2i+1}^{k+1} &= \sum_{j \in \mathbb{Z}} a_{2i+1-2j} f_j^k = \sum_{\gamma \in \mathbb{Z}} a_{2\gamma+1} f_{i-\gamma}^k, \quad i \in \mathbb{Z}. \end{aligned} \quad (2)$$

The symbol of the above subdivision scheme is given by the Laurent polynomial:

$$a(z) = \sum_{i \in \mathbb{Z}} a_i z^i, \quad z \in \mathbb{C} \setminus \{0\}, \quad (3)$$

where $a = \{a_i, i \in \mathbb{Z}\}$ is called the mask of the subdivision scheme. Detailed information about refinement rules, Laurent polynomials, and convergence of a subdivision scheme can be found in [16–18]. The necessary condition for the convergence of the subdivision scheme (2) is that $\sum_{\gamma \in \mathbb{Z}} a_{2\gamma} = \sum_{\gamma \in \mathbb{Z}} a_{2\gamma+1} = 1$. The continuity of the subdivision schemes can be analyzed by the following theorems.

Theorem 1 (see [17]). *A convergent subdivision scheme S_a corresponding to the symbol*

$$a(z) = \left(\frac{1+z}{2z}\right)^n b(z), \quad (4)$$

is C^n -continuous iff the subdivision scheme S_b corresponding to the symbol $b(z)$ is convergent.

Theorem 2 (see [17]). *The scheme S_b corresponding to the symbol $b(z)$ is convergent iff its difference scheme S_c corresponding to the symbol $c(z)$ is contractive, where $b(z) = (1+z)c(z)$. The scheme S_c is contractive if*

$$\|c^l\|_{\infty} = \max \left\{ \sum_i |c_{j-2i}^l| : 0 \leq j < 2^l \right\} < 1, \quad l \in \mathbb{N}, \quad (5)$$

where c_i^l are the coefficients of the scheme S_c^l with symbol

$$c^l(z) = c(z)c(z^2), \dots, c(z^{2^{l-1}}). \quad (6)$$

In a geometric context, subdivision schemes are further categorized into primal and dual subdivision schemes. The primal binary subdivision schemes are the schemes that leave or modify the old vertex points and create one new point at each old edge. Primal schemes can be interpolatory, approximating, or combined. Dual binary subdivision schemes on the other hand are the schemes that create two new points at the old edges and discard the old points. Most of the dual schemes are approximating subdivision schemes; however, recently Romani [19, 20] introduced interpolatory subdivision schemes that are dual in nature. Detailed information about the primal and dual subdivision schemes can be found in [16]. Furthermore, if one refinement rule of an approximating binary subdivision scheme (2) uses the affine combination of $\xi = \{\xi_1 > 2: \xi_1 \in \mathbb{Z}\}$ control points at level k to get a new control point at level $k + 1$ whereas the other refinement rule of (2) uses the affine combination of

control points less than ξ at level k to get a new point at level $k + 1$, then that binary scheme is called the primal binary scheme. Moreover, every primal binary scheme is the relaxed subdivision scheme. Mathematical definition of primal and dual subdivision schemes is presented as follows.

Definition 1. Let the symbol of the symmetric subdivision scheme (2) defined in (3) can particularly be written as $a(z) = \dots + a_{-3}z^{-3} + a_{-2}z^{-2} + a_{-1}z^{-1} + a_0z^0 + a_1z^1 + a_2z^2 + a_3z^3 + \dots$. If the symbol $a(z)$ defined in (3) corresponding to the scheme S_a satisfies the following condition:

$$a(z) = a(z^{-1}), \quad (7)$$

then S_a is said to be a primal subdivision scheme. On the other hand, if it satisfies following condition:

$$za(z) = a(z^{-1}), \quad (8)$$

then S_a is said to be a dual subdivision scheme.

The combined subdivision schemes are the schemes which depend on one or more tension parameters. Moreover, at the specific values of these parameters, these schemes can be regarded either as an approximating subdivision scheme or an interpolatory one. Interproximate subdivision schemes (see [11]) are the schemes which generate the limit curves that interpolate some of the vertices of the given control polygons, while approximate the other vertices of the given control polygons.

Generation and reproduction degrees are used to check the behaviors of a subdivision scheme when the original data points lie on the graph of a polynomial. Suppose that the original data points are taken from a polynomial of degree d . If the control points of the limit curve lie on graph of the polynomial having same degree (i.e., d), then we say that the subdivision scheme generates polynomials of degree d . If the control points of the limit curve lie on graph of the same polynomial, then we say that the subdivision scheme reproduces polynomials of degree d . Mathematically, let Π_d denote the space of polynomials of degree d and $g, h \in \Pi_d$; an operator \mathbf{O} generates polynomials of degree d if $\mathbf{O}g = h \forall g, h \in \Pi_d$, whereas \mathbf{O} reproduces polynomials of degree d if $\mathbf{O}g = g \forall g \in \Pi_d$. Furthermore, the generation degree of a subdivision scheme is the maximum degree of polynomials that can theoretically be generated by the scheme, provided that the initial data are taken correctly. Evidently, it is not less than the reproduction degree. For exact definitions of polynomial generation and reproduction, the readers can consult [16, 21]. The following theorem is used to check the generation and reproduction degrees of the subdivision schemes in this paper.

Theorem 3 (see [21]). *A univariate convergent binary subdivision scheme S_a performs the following functions:*

(i) *Generates polynomials up to degree d if and only if*

$$\begin{aligned} a(1) &= 2, \\ a(-1) &= 0, \\ D^{(m)}a(z)|_{z=-1} &= 0, \quad m = 1, 2, \dots, d, \end{aligned} \quad (9)$$

where $D^{(m)}a(z)|_{z=-1}$ denotes the m -th derivative of $a(z)$ with respect to z evaluated at a point $z = -1$.

(ii) *Reproduces polynomials up to degree d with respect to the parametrization $\{t_i^{(k)} = (i + \tau/2^k)\}_{i \in \mathbb{Z}}$ with $\tau = (1/2)D^{(1)}(z)|_{z=1}$ if and only if it generates polynomials of degree d and*

$$D^{(m)}a(z)|_{z=1} = 2 \prod_{h=0}^{m-1} (\tau - h), \quad m = 1, 2, \dots, d. \quad (10)$$

The support of a basic limit function and a subdivision scheme is the area of the limit curve that will be affected by the displacement of a single control point from its initial place. The part which is dependent on that given control point is called the support width of the given subdivision scheme. By following the approach of [22], we give following theorem to calculate the support width of a relaxed binary combined scheme or an interpolatory binary scheme.

Theorem 4. *The support width of a ξ -point binary relaxed subdivision scheme S_a is 2ξ where $\xi = \{\xi_1 > 2: \xi_1 \in \mathbb{Z}\}$, which implies that it vanishes outside the interval $[-\xi, \xi]$. The support width of a ξ -point interpolatory binary scheme S_a is $2\xi - 2$, which implies that it vanishes outside the interval $[-\xi + 1, \xi - 1]$.*

3. Construction of the Families of Subdivision Schemes

In this section, we present a family of $(2N + 2)$ -point relaxed combined subdivision schemes that is based on repeated local translation of points by using certain displacement vectors. Thus, the refinement rules of a member of the proposed family is recursively obtained by the refinement rules of one other member of this family, i.e., the refinement rules of a $(2N + 2)$ -point scheme for $N = M$ are recursively obtained from the refinement rules of the $(2N + 2)$ -point scheme for $N = M - 1$. We propose a new family of $(2N + 3)$ -point relaxed combined schemes with two tension parameters by extending the points of the family of $(2N + 2)$ -point relaxed combined schemes. Then, we modify the family of $(2N + 3)$ -point relaxed schemes to a family of $(2N + 4)$ -point interpolatory schemes by removing one of its tension parameters. Construction process for the family of $(2N + 2)$ -point relaxed combined schemes with one tension parameter is given as follows.

3.1. Framework for the Construction of a Family of $(2N + 2)$ -Point Relaxed Schemes. The family of $(2N + 2)$ -point combined subdivision schemes $S_{a_{2N+2}}$ which maps the polygon $f_{N+1}^k = \{f_{i,N+1}^k: i \in \mathbb{Z}\}$ to the refined polygon $f_{N+1}^{k+1} = \{f_{i,N+1}^{k+1}: i \in \mathbb{Z}\}$ is defined by the set of following refinement rules:

$$\left\{ \begin{aligned} f_{2i,N+1}^{k+1} &= \sum_{j=-N-1}^{N+1} a_{2j,N+1} f_{i+j,N+1}^k, \\ f_{2i+1,N+1}^{k+1} &= \sum_{j=-N-1}^N a_{2j+1,N+1} f_{i+j+1,N+1}^k, \end{aligned} \right. \quad (11)$$

where $N \in \mathbb{N}_0 = \mathbb{N} \cup \{0\}$ is used to calculate the complexity (number of control points at k -th subdivision level used in the insertion of a new point at $(k + 1)$ -th subdivision level is called the complexity) of the subdivision schemes and $k \in \mathbb{N}$ denotes the number of times subdivision is applied on the original data points. Hence, for each N , the set $\{f_{i,N+1}^{k+1} : i \in \mathbb{Z}\}$ represents the $(k + 1)$ -th level subdivided points obtained by applying $(k + 1)$ -times the $(2N + 2)$ -point relaxed subdivision scheme (11) on the initial data points $\{f_i^0 = f_{i,N+1}^0 : i \in \mathbb{Z}\}$, and $a = [a_{j,N+1} : j = -2(N + 1), \dots, 2(N + 1)]$ is mask of the scheme (11) which is same at each level of refinement for a fix value of N . The schematic sketches of both rules defined in (11) are presented in Figures 1(a) and 1(b).

The construction process of these rules is given as follows.

If $N = 0$, the two refinement rules of the 2-point relaxed scheme are obtained from (12). Hence, $\{f_{i,1}^1 : i \in \mathbb{Z}\}$ are the control points at first subdivision level obtained by the 2-point relaxed subdivision scheme on the initial control points $\{f_i^0 = f_{i,1}^0 : i \in \mathbb{Z}\}$. These two refinement rules are the initial refinement rules used to calculate the other

refinement rules of proposed family of schemes for each successive value of N . The initial refinement rules are defined as

$$\left\{ \begin{aligned} f_{2i,1}^1 &= f_{i,1}^0 + \alpha_0(f_{i-1,1}^0 - 2f_{i,1}^0 + f_{i+1,1}^0), \\ f_{2i+1,1}^1 &= \frac{1}{2}f_{i,1}^0 + \frac{1}{2}f_{i+1,1}^0, \end{aligned} \right. \quad (12)$$

where $\alpha_0 \in (-1, 1)$.

Now, we calculate points $\{f_{2i+\ell,N+1}^1 : \ell = 0, 1\}_{i \in \mathbb{Z}}$ of the (HTML translation failed)-point relaxed subdivision scheme for $N \geq 1$. Hence, for a fix value of N , the points $\{f_{2i+\ell,N+1}^1 : \ell = 0, 1\}_{i \in \mathbb{Z}}$ of the $(2N + 2)$ -point relaxed subdivision scheme are obtained by moving the points $\{f_{2i+\ell,N}^1 : \ell = 0, 1\}_{i \in \mathbb{Z}}$ to the new position according to the displacement vectors $\{\alpha_\ell \vec{C}_{2i+\ell,N+1} : \ell = 0, 1\}_{i \in \mathbb{Z}}$, where α_ℓ is the tension parameter with $\alpha_1 = 1$ and $\alpha_0 = \alpha$.

Mathematically, for $N \geq 1$, the two refinement rules of the family of $(2N + 2)$ -point relaxed subdivision schemes at first level of subdivision are obtained by the following recurrence relation:

$$f_{2i+\ell,N+1}^1 = f_{2i+\ell,N}^1 + \alpha_\ell \vec{C}_{2i+\ell,N+1}, \quad \ell = 0, 1, \quad (13)$$

where the vectors $\vec{C}_{2i+\ell,N+1} : \ell = 0, 1$ are calculated by the following recurrence relation:

$$\left\{ \begin{aligned} \vec{C}_{2i,N+1} &= (\vec{C}_{2i,N} - \vec{C}_{2(i+1),N}) + (\vec{C}_{2i,N} - \vec{C}_{2(i-1),N}), \\ \vec{C}_{2i+1,N+1} &= \frac{1}{N} \left(\frac{N}{4} - \frac{1}{8} \right) \left((\vec{C}_{2i+1,N} - \vec{C}_{2(i+1)+1,N}) + (\vec{C}_{2i+1,N} - \vec{C}_{2(i-1)+1,N}) \right), \end{aligned} \right. \quad (14)$$

and initial values for relation (14) are

$$\left\{ \begin{aligned} \vec{C}_{2i,1} &= f_{i-1,1}^0 - f_{i,1}^0 + f_{i+1,1}^0, \\ \vec{C}_{2i+1,1} &= \frac{1}{2}(f_{i,1}^0 + f_{i+1,1}^0). \end{aligned} \right. \quad (15)$$

Here, $f_i^0 = f_{i,1}^0 = f_{i,2}^0 = f_{i,3}^0 = \dots = f_{i,N+1}^0$ are the initial control points.

While the points $f_{i,1}^1, f_{i,2}^1, f_{i,3}^1$, and $f_{i,4}^1$ are the initial points of the 4-point, 6-point, and 8-point relaxed subdivision schemes obtained by substituting the values of N equal to 1, 2, and 3, respectively, in (13) and (14). Since the proposed subdivision schemes are stationary, the refinement rules are same at each level of subdivision. Therefore, for other subdivision levels, we apply (11) while the coefficients of points $f_{i,N+1}^k$ remain same as the coefficients of points $f_{i,N+1}^0 = f_i^0$ obtained from (13). Also, $f_{i,1}^{k+1}, f_{i,2}^{k+1}, f_{i,3}^{k+1}$, and $f_{i,4}^{k+1}$ are the control points at $(k + 1)$ -th subdivision level obtained by applying the 2-point, 4-point, 6-point, and 8-

point relaxed subdivision schemes on the k -th level points $f_{i,1}^k, f_{i,2}^k, f_{i,3}^k$, and $f_{i,4}^k$, respectively. Moreover, the points other than the initial control points hold the relation $f_{i,N}^k \neq f_{i,N+1}^k \forall N \in \mathbb{N}$.

At each iteration, i.e., by substituting $N = 1, 2, 3, \dots$ in (11), (13), and (14), we get a new binary primal $(2N + 2)$ -point subdivision scheme. The masks of these $(2N + 2)$ -point schemes by defining $\alpha_0 = \alpha$ are tabulated in Table 1.

Remark 1. If $\alpha = 0$, the family of scheme (11) reduces to the family of $(2N + 2)$ -point interpolatory schemes with symbol

$$a(z) = 1 + \sum_{j=-N-1}^N a_{2j+1,N+1} z^{2j+1}, \quad (16)$$

which is proposed by Deslauriers and Dubuc [1]. The continuity of $(2N + 2)$ -point interpolatory schemes is C^N for $0 \leq N \leq 4$ and $C^{\approx (83/200)(N+1)}$ for $N \geq 5$.

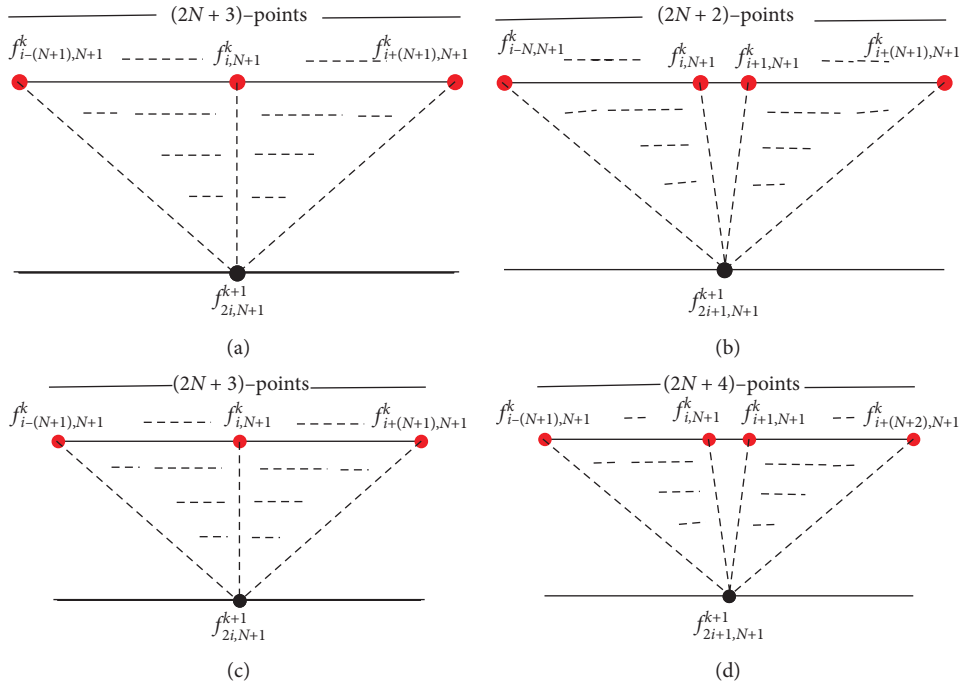


FIGURE 1: Graphical sketches of the rules of $(2N + 2)$ -point primal schemes in (a-b) and of $(2N + 3)$ -point primal schemes in (c-d), respectively. (a) Vertex rule. (b) Edge rule. (c) Vertex rule. (d) Edge rule.

TABLE 1: Mask of the $(2N + 2)$ -point schemes $S_{a_{2N+2}}$.

N	Mask
0	$(1/2)[2\alpha, 1, 2 - 4\alpha, 1, 2\alpha]$
1	$(1/16)[-16\alpha, -1, 64\alpha, 9, 16 - 96\alpha, 9, 64\alpha, -1, -16\alpha]$
2	$(1/256) \begin{bmatrix} 256\alpha, 3, -1536\alpha, -25, 3840\alpha, 150, 256 - 5120\alpha, 150, 3840\alpha, \\ 25, -1536\alpha, 3, 256\alpha \end{bmatrix}$
3	$(1/2048) \begin{bmatrix} -2048\alpha, -5, 16384\alpha, 49, -57344\alpha, -245, 114688\alpha, 1225, 2048 - \\ 143360\alpha, 1225, 114688\alpha, -245, -57344\alpha, 49, 16384\alpha, -5, -2048\alpha \end{bmatrix}$
4	$(1/65536) \begin{bmatrix} 65536\alpha, 35, -655360\alpha, -405, 2949120\alpha, 2268, -7864320\alpha \\ -8820, 13762560\alpha, 39690, 65536 - 16515072\alpha, 39690, 13762560\alpha, \\ -8820, -7864320\alpha, 2268, 2949120\alpha, -405, -655360\alpha, 35, 65536\alpha \end{bmatrix}$
5	$(1/524288) \begin{bmatrix} -524288\alpha, -63, 6291456\alpha, 847, -34603008\alpha, -5445, 115343360\alpha, \\ 22869, -259522560\alpha, -76230, 415236096\alpha, 320166, 524288, \\ -484442112\alpha, 320166, 415236096\alpha, -76230, -259522560\alpha, 22869, \\ 115343360\alpha, -5445, -34603008\alpha, 847, 6291456\alpha, -63, -524288\alpha \end{bmatrix}$

3.2. Interpretation of Framework 3.1 for $N = 1$. The refinement rules of the initial subdivision scheme defined in (12) are

$$\begin{cases} f_{2i,1}^1 = \alpha f_{i-1}^0 + (1 - 2\alpha)f_i^0 + \alpha f_{i+1}^0, \\ f_{2i+1,1}^1 = \frac{1}{2}f_i^0 + \frac{1}{2}f_{i+1}^0. \end{cases} \quad (17)$$

Moreover, the initial values $\left\{ \vec{C}_{2i+\ell,1} : \ell = 0, 1 \right\}$ which will be used to calculate the vectors $\left\{ \vec{C}_{2i+\ell,N+1} : \ell = 0, 1 \right\}_{N \in \mathbb{N}}$ defined in (15) are

$$\begin{cases} \vec{C}_{2i,1} = f_{i-1}^0 - f_i^0 + f_{i+1}^0, \\ \vec{C}_{2i+1,1} = \frac{1}{2}f_i^0 + \frac{1}{2}f_{i+1}^0. \end{cases} \quad (18)$$

Now, we use initial relations (17) and (18) to calculate the refinement rules of 4-point relaxed scheme which will be obtained by putting $N = 1$ in (13) and (14). Hence, for $N = 1$, we get

$$\begin{cases} f_{2i,2}^1 = f_{2i,1}^1 + \alpha_0 \vec{C}_{2i,2}, \\ f_{2i+1,2}^1 = f_{2i+1,1}^1 + \alpha_1 \vec{C}_{2i+1,2}, \end{cases} \quad (19)$$

where

$$\begin{cases} \vec{C}_{2i,2} = (\vec{C}_{2i,1} - \vec{C}_{2(i+1),1}) + (\vec{C}_{2i,1} - \vec{C}_{2(i-1),1}), \\ \vec{C}_{2i+1,2} = \frac{1}{8} [(\vec{C}_{2i+1,1} - \vec{C}_{2(i+1)+1,1}) + (\vec{C}_{2i+1,1} - \vec{C}_{2(i-1)+1,1})]. \end{cases} \quad (20)$$

By using (18) in (20), we get

$$\begin{cases} \vec{C}_{2i,2} = -f_{i-2}^0 + 3f_{i-1}^0 - 4f_i^0 + 3f_{i+1}^0 - f_{i+2}^0, \\ \vec{C}_{2i+1,2} = \frac{1}{16} (-f_{i-1}^0 + f_i^0 + f_{i+1}^0 - f_{i+2}^0). \end{cases} \quad (21)$$

Now, firstly we put $\alpha_0 = \alpha$ and $\alpha_1 = 1$ in (19) and then we use (17) and (21) in (19). Hence, we get the following 4-point relaxed subdivision scheme:

$$\begin{cases} f_{2i,2}^1 = -\alpha f_{i-2}^0 + 4\alpha f_{i-1}^0 + (1 - 6\alpha) f_i^0 + 4\alpha f_{i+1}^0 - \alpha f_{i+2}^0, \\ f_{2i+1,2}^1 = \frac{1}{16} (-f_{i-1}^0 + 9f_i^0 + 9f_{i+1}^0 - f_{i+2}^0). \end{cases} \quad (22)$$

By using (22) in (11), we get

$$\begin{cases} f_{2i,2}^{k+1} = -\alpha f_{i-2}^k + 4\alpha f_{i-1}^k + (1 - 6\alpha) f_i^k + 4\alpha f_{i+1}^k - \alpha f_{i+2}^k, \\ f_{2i+1,2}^{k+1} = \frac{1}{16} (-f_{i-1}^k + 9f_i^k + 9f_{i+1}^k - f_{i+2}^k). \end{cases} \quad (23)$$

Step by step geometrical representations of the above procedure are shown in Figures 2 and 3. The description of Figure 2 is as follows. In Figure 2(a), the implementation of the initial subdivision scheme defined in (17) is given. In Figure 2(b), blue bullets show the points obtained by the relations defined in (18). Here, $\vec{C}_{2i-2,1} = f_{i-2}^0 - f_{i-1}^0 + f_i^0$, $\vec{C}_{2i-1,1} = (1/2)(f_{i-1}^0 + f_i^0)$, $\vec{C}_{2i,1} = f_{i-1}^0 - f_i^0 + f_{i+1}^0$, $\vec{C}_{2i+1,1} = (1/2)(f_i^0 + f_{i+1}^0)$, $\vec{C}_{2i+2,1} = f_i^0 - f_{i+1}^0 + f_{i+2}^0$, and $\vec{C}_{2i+3,1} = (1/2)(f_{i+1}^0 + f_{i+2}^0)$. In Figure 2(c), $\vec{C}_{2i,2}$ is the resultant vector of two vectors $\vec{C}_{2i,1} - \vec{C}_{2(i+1),1}$ and $\vec{C}_{2i,1} - \vec{C}_{2(i-1),1}$. Similarly, $\vec{C}_{2i+1,2}$ is the resultant vector of $\vec{C}_{2i+1,1} - \vec{C}_{2(i+1)+1,1}$ and $\vec{C}_{2i+1,1} - \vec{C}_{2(i-1)+1,1}$. The resultant vectors are obtained by adding two vectors using head to tail

rule. The resultant vectors are denoted by blue solid lines while the other vectors are denoted by blue dashed lines. Moreover, the description of Figure 3 is as follows, In Figure 3(a), the geometrical representation of the vectors defined in (20) is given. Here, $\vec{C}_{2i+1,2} = (1/8)\vec{C}\vec{C}_{2i+1,2}$; In Figure 3(b), the translation of the points $f_{2i,1}^1$ and $f_{2i+1,1}^1$ is shown by using vectors $\alpha\vec{C}_{2i,2}$ and $\vec{C}_{2i+1,2}$ to obtain the points $f_{2i,2}^1$ and $f_{2i+1,2}^1$ denoted by green bullets; In Figure 3(c), green bullets show the points of the subdivision scheme (21) constructed by the proposed framework.

3.3. *Extended Form of Framework 3.1 for Constructing a Family of $(2N + 3)$ -Point Relaxed Schemes.* When $\ell = 1$, we add these weights

$$\begin{aligned} & \sum_{j=-N-1}^N (-1)^{j+N+1} \binom{2j+1}{N-j+1} \binom{2N+2}{N+j+2} \beta \\ & \cdot (1-\alpha) f_{i+j+1, N+1}^0 + \beta(1-\alpha) (f_{i-N-1, N+1}^0 + f_{i+N+2, N+1}^0), \end{aligned} \quad (24)$$

in (13), where $-1 < \alpha < 1$ & $-1 < \beta < 1$. Hence, we get the family of $(2N + 3)$ -point combined relaxed schemes $S_{a_{2N+3}}$ associated with the following refinement rules:

$$\begin{cases} f_{2i, N+1}^{k+1} = \sum_{j=-N-1}^{N+1} b_{2j} f_{i+j, N+1}^k, \\ f_{2i+1, N+1}^{k+1} = \sum_{j=-N-2}^{N+1} b_{2j+1} f_{i+j+1, N+1}^k, \end{cases} \quad (25)$$

where

$$b_{2j} = a_{2j, N+1} \quad \text{for } j = -(N+1), -N, \dots, (N+1),$$

$$\begin{aligned} b_{2j+1} &= a_{2j+1, N+1} + (-1)^{j+N+1} \binom{2j+1}{N-j+1} \binom{2N+2}{N+j+2} \beta \\ &\cdot (1-\alpha) \quad \text{for } j = -(N+1), -N, \dots, N \text{ and} \end{aligned}$$

$$b_{2j+1} = \beta(1-\alpha) \quad \text{for } j = -(N+2)(N+1). \quad (26)$$

The schematic sketches of these rules are given in Figures 1(c) and 1(d), and mask of the first three members of this family of schemes is given as follows:

(i) When $N = 0$, (25) gives the primal 3-point relaxed scheme with mask

$$\left[\beta(1-\alpha), \alpha, \frac{1}{2} - \beta(1-\alpha), 1 - 2\alpha, \frac{1}{2} - \beta(1-\alpha), \alpha, \beta(1-\alpha) \right]. \quad (27)$$

(ii) When $N = 1$, (25) gives the primal 5-point relaxed scheme with mask

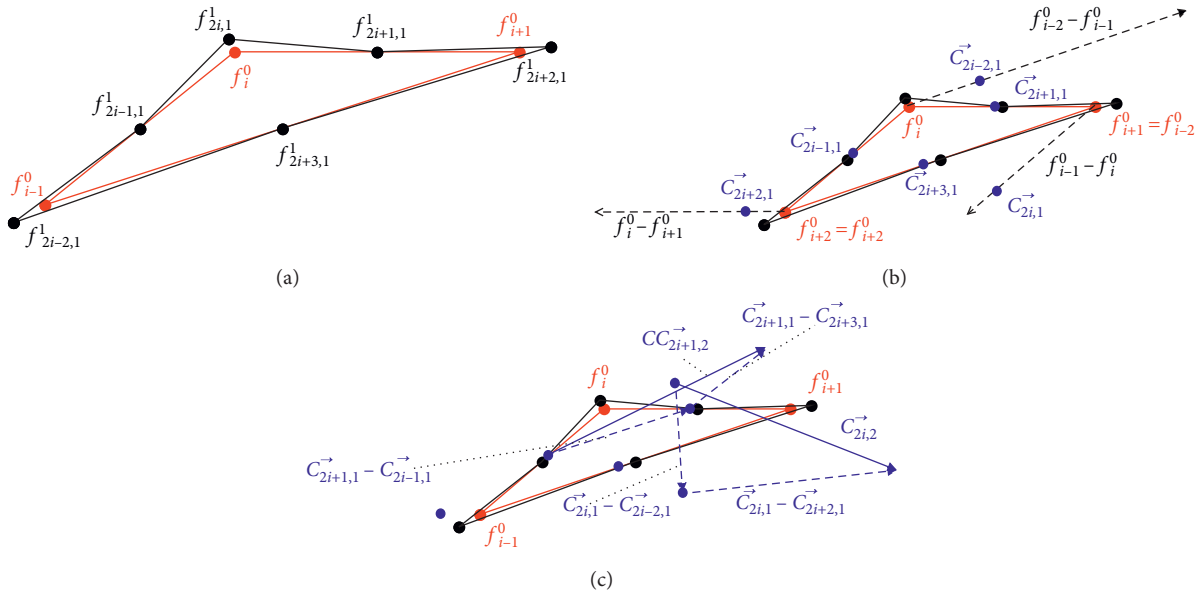


FIGURE 2: Geometrical interpretation of the proposed framework. Red bullets and red lines represent initial points and initial polygons, respectively. Black bullets and black lines represent the points and the polygons obtained by the subdivision scheme (17).

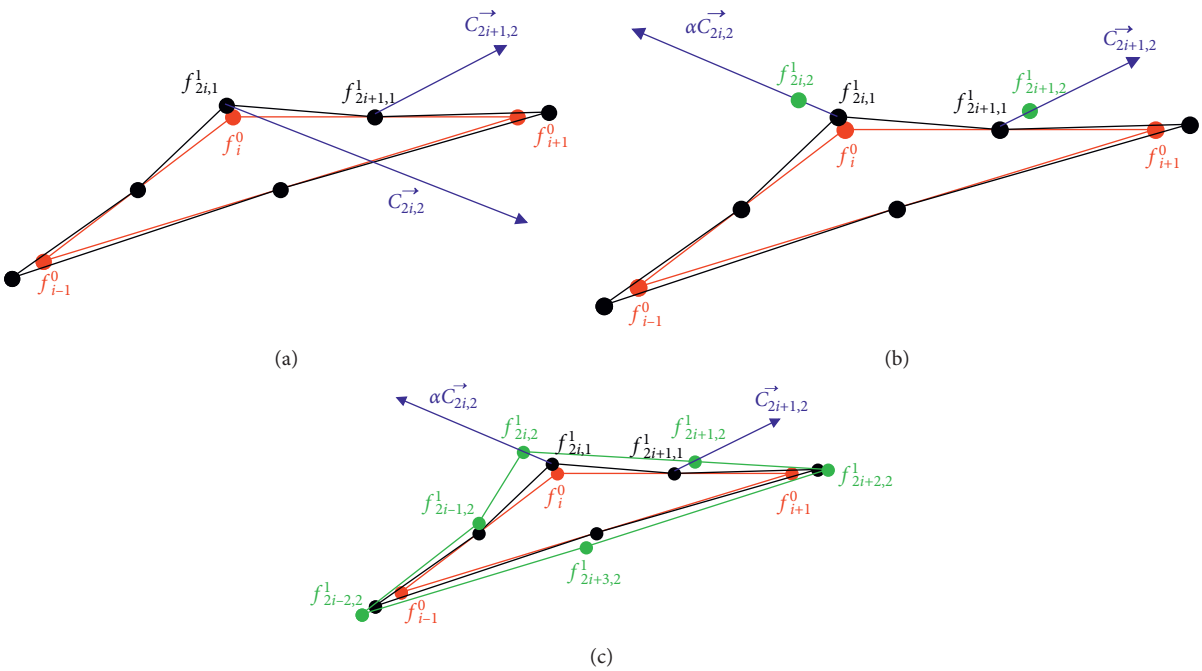


FIGURE 3: Geometrical interpretation of the proposed framework. Red bullets and red lines represent initial points and initial polygons, respectively. Black bullets and black lines represent the points and the polygons obtained by the subdivision scheme (17). Green bullets and green lines represent the points and the polygons obtained by the subdivision scheme (22).

$$\left[\beta(1-\alpha), -\alpha, -\frac{1}{16} - 3\beta(1-\alpha), 4\alpha, \frac{9}{16} + 2\beta(1-\alpha), 1 - 6\alpha, \frac{9}{16} + 2\beta(1-\alpha), 4\alpha, -\frac{1}{16} - 3\beta(1-\alpha), -\alpha, \beta(1-\alpha) \right]. \quad (28)$$

(iii) When $N = 2$, (25) gives the primal 7-point relaxed scheme with mask

$$\left[\begin{array}{c} \beta(1 - \alpha), \alpha, \frac{3}{256} - 5\beta(1 - \alpha), -6\alpha, -\frac{25}{256} + 9\beta(1 - \alpha), 15\alpha, \frac{150}{256} - 5\beta(1 - \alpha), 1 - 20\alpha, \frac{150}{256} - 5\beta(1 - \alpha), 15\alpha, -\frac{25}{256} + 9\beta(1 - \alpha), -6\alpha, \\ \frac{3}{256} - 5\beta(1 - \alpha), \alpha, \beta(1 - \alpha) \end{array} \right]. \tag{29}$$

3.4. Interpretation of Extended Form 3.3 for $N = 1$. When $N = 1$, (24) gives

$$\begin{aligned} & \sum_{j=-2}^1 (-1)^{j+2} \binom{2j+1}{2-j} \binom{4}{3+j} \beta(1 - \alpha) f_{i+j+1,2}^0 + \beta(1 - \alpha) (f_{i-2,2}^0 + f_{i+3,2}^0) \\ & = \beta(1 - \alpha) [f_{i-2,2}^0 - 3f_{i-1,2}^0 + 2f_{i,2}^0 + 2f_{i+1,2}^0 - 3f_{i+2,2}^0 + f_{i+3,2}^0]. \end{aligned} \tag{30}$$

Adding weights which are defined in (30) in the edge rule of (22), we get

$$\left\{ \begin{array}{l} f_{2i,2}^1 = -\alpha f_{i-2}^0 + 4\alpha f_{i-1}^0 + (1 - 6\alpha) f_i^0 + 4\alpha f_{i+1}^0 - \alpha f_{i+2}^0, \\ f_{2i+1,2}^1 = \beta(1 - \alpha) f_{i-2}^0 - \left(\frac{1}{16} + 3\beta(1 - \alpha)\right) f_{i-1}^0 + \left(\frac{9}{16} + 2\beta(1 - \alpha)\right) f_i^0 + \left(\frac{9}{16} + 2\beta(1 - \alpha)\right) f_{i+1}^0 \\ - \left(\frac{1}{16} + 3\beta(1 - \alpha)\right) f_{i+2}^0 + \beta(1 - \alpha) f_{i+3}^0. \end{array} \right. \tag{31}$$

Since the above scheme is stationary, the refinement rules of proposed 5-point relaxed scheme with two tension parameters are

$$\left\{ \begin{array}{l} f_{2i,2}^{k+1} = -\alpha f_{i-2}^k + 4\alpha f_{i-1}^k + (1 - 6\alpha) f_i^k + 4\alpha f_{i+1}^k - \alpha f_{i+2}^k, \\ f_{2i+1,2}^{k+1} = \beta(1 - \alpha) f_{i-2}^k - \left(\frac{1}{16} + 3\beta(1 - \alpha)\right) f_{i-1}^k + \left(\frac{9}{16} + 2\beta(1 - \alpha)\right) f_i^k + \left(\frac{9}{16} + 2\beta(1 - \alpha)\right) f_{i+1}^k \\ - \left(\frac{1}{16} + 3\beta(1 - \alpha)\right) f_{i+2}^k + \beta(1 - \alpha) f_{i+3}^k. \end{array} \right. \tag{32}$$

Remark 2.

(i) The schemes of [5] are the special cases of the proposed family of $(2N + 3)$ -point schemes.

(ii) The family of $(2N + 4)$ -point interpolatory schemes $S_{a_{2N+4}^I}$ with one tension parameter is obtained by putting $\alpha = 0$ in (25). The refinement rules of these schemes are given as follows:

$$\begin{cases} f_{2i,N+1}^{k+1} = f_{i,N+1}^k, \\ f_{2i+1,N+1}^{k+1} = \sum_{j=-N-2}^{N+1} b_{2j+1} f_{i+j+1,N+1}^k, \end{cases} \quad (33)$$

where b_{2j+1} is defined in (26).

4. Analysis of the Families of Schemes

In this section, we present properties of the proposed families of schemes. In Table 2, we present “ranges of tension parameter α ” for which the first six members of “the family of $(2N + 2)$ -point relaxed schemes” are C^n -continuous. The continuity of the proposed schemes is analyzed with a computer algebra system like Mathematica/Maple by using Theorems 1 and 2. Similarly, continuity of the first three members of $(2N + 3)$ -point relaxed schemes and $(2N + 4)$ -point interpolatory schemes is presented in Tables 3 and 4, respectively, for specific ranges of tension parameters.

In Tables 4–6, we tabulate the support widths, degrees of polynomial generation, and degrees of polynomial reproduction of the proposed families of $(2N + 2)$ -point relaxed, $(2N + 3)$ -point relaxed, and $(2N + 4)$ -point interpolatory schemes, respectively. The generation and reproduction degrees of the proposed schemes are analyzed by using Theorem 3, while the support widths of the proposed schemes are calculated by using Theorem 4. Properties of some special members of the family of schemes (11) are presented in Table 7.

Let $a_{2N+2}(z)$, $a_{2N+3}(z)$, and $a_{2N+4}^I(z)$ denote the symbols of schemes (11), (25), and (33), respectively. By Definition 1, the following theorem can be easily proved.

Theorem 5. *The families of subdivision schemes (11), (25), and (33) are the families of primal schemes.*

Proof. Since the symbols associated with schemes (11), (25), and (33) satisfy the relations $a_{2N+2}(z) = a_{2N+2}(z^{-1})$, $a_{2N+3}(z) = a_{2N+3}(z^{-1})$, and $a_{2N+4}^I(z) = a_{2N+4}^I(z^{-1})$, respectively, for all $N \in \mathbb{N}_0$, then by Definition 1, these schemes are primal. This completes the proof.

Now, we check the property of polynomial generation and reproduction of the families of schemes $S_{a_{2N+2}}$, $S_{a_{2N+3}}$, and $S_{a_{2N+4}^I}$ by using Theorem 3. We prove the following theorems for this purpose. \square

Theorem 6. *The families of subdivision schemes (11), (25), and (33) generate polynomials up to degree $2N + 1$ for all α and β and for all $N \in \mathbb{N}_0$.*

Proof. It is to be noted that for all α and β , the results $a_{2N+2}(1) = a_{2N+3}(1) = a_{2N+4}^I(1) = 2$ and $a_{2N+2}(-1) = a_{2N+3}(-1) = a_{2N+4}^I(-1) = 0$ are trivial for all $N \in \mathbb{N}_0$. Furthermore, $D^{(m)}a_{2N+2}(z)|_{z=-1} = D^{(m)}a_{2N+3}(z)|_{z=-1} = D^{(m)}a_{2N+4}^I(z)|_{z=-1} = 0$ for $m = 0, 1, \dots, 2N + 1$ and $N \in \mathbb{N}_0$. Therefore, by Theorem 3, the result proved. \square

Theorem 7. *The families of subdivision schemes (11), (25), and (33) reproduce polynomials up to degree $2N + 1$ for all α and β and $N \in \mathbb{N}_0$.*

Proof. Since by Theorem 5, the families of schemes (11), (25), and (33) are primal; hence, the parameter $\tau = 0$ for all α and β and $N \in \mathbb{N}_0$. Moreover, $D^{(m)}a_{2N+2}(z)|_{z=1} = D^{(m)}a_{2N+3}(z)|_{z=1} = D^{(m)}a_{2N+4}^I(z)|_{z=1} = 2 \prod_{h=0}^{m-1} (\tau - h)$ for $m = 0, 1, \dots, 2N + 1$ and $N \in \mathbb{N}_0$. Now, by combining these conditions with Theorem 6 and then by using Theorem 3, we get the required result. \square

Remark 3. Theorems 6 and 7 show that the schemes defined in (11), (25), and (33) generate and reproduce polynomials up to degree $2N + 1$ for all α and β . However, by choosing specific values of α and β , the polynomial generation and polynomial reproduction of these schemes can be increased. Tables 4, 6, and 7 summarize the generation and reproduction degrees of proposed schemes for special choices of tension parameters.

In the coming theorem, we give the support width of the proposed families of schemes.

Theorem 8. *The support width of the family of scheme (11) is $4N + 4$ where $N \in \mathbb{N}_0$. The support width of each family of subdivision schemes defined in (25) and (33) is $4N + 6$.*

Proof. By Theorem 4, the result is trivial.

We prove the following theorem by using Theorems 1 and 2. \square

Theorem 9. *The subdivision schemes S_{a_3} , S_{a_5} , and S_{a_7} are C^1 , C^3 , and C^5 , respectively, for some special conditions.*

Proof. The conditions for C^1 , ν , and C^5 continuities of the schemes S_{a_3} , S_{a_5} , and S_{a_7} , respectively, are given as follows:

The subdivision scheme S_{a_3} is C^1 if

$$\max\{\gamma_1, \gamma_2 + \gamma_3\} < 1, \quad (34)$$

where $\gamma_1 = 2|2\alpha - 4\beta(1 - \alpha)|$, $\gamma_2 = 2|2\beta(1 - \alpha)|$, and $\gamma_3 = |1 + 4\beta(1 - \alpha) - 4\alpha|$.

The scheme S_{a_5} is C^3 if

$$\max\{\eta_1 + \eta_2, \eta_3 + \eta_4\} < 1, \quad (35)$$

where $\eta_1 = 16|\beta(1 - \alpha)|$, $\eta_2 = 2|-56\beta(1 - \alpha) - 32\alpha + (1/2)|$, $\eta_3 = 2|-32\beta(1 - \alpha) - 8\alpha|$, and $\eta_4 = |-48\alpha - 64\beta(1 - \alpha) + 2|$.

Similarly, the subdivision scheme S_{a_7} is C^5 if

$$\max\{\chi_1 + \chi_2 + \chi_3, \chi_4 + \chi_5\} < 1, \quad (36)$$

where $\chi_1 = 64|\beta(1 - \alpha)|$, $\chi_2 = 2|-512\beta(1 - \alpha) + 192\alpha - (3/8)|$, $\chi_3 = |-19/4 - 960\beta(1 - \alpha) + 640\alpha|$, $\chi_4 = 2|-192\beta(1 - \alpha) + 32\alpha|$, and $\chi_5 = 2|480\alpha - (9/4) - 832\beta(1 - \alpha)|$. \square

Remark 4. Throughout the article, red bullets and red lines represent initial points and initial polygons/meshes, respectively.

TABLE 2: MC: the maximum continuity of the proposed schemes $S_{6_{4N^2}}$.

N	MC	C^0	C^1	C^2	C^3	C^4	C^5
0	1	$-(1/4) < \alpha < (3/4)$	$0 < \alpha < (1/4)$	$\alpha = (1/8)$			
1	2	$-(3/25) < \alpha < (6/25)$	$-(1/35) < \alpha < (27/200)$	$0 < \alpha < (1/16)$			
2	3	$-(1/21) < \alpha < (1/14)$	$-(1/64) < \alpha < (1/25)$	$-(1/80) < \alpha < (1/48)$	$(33/5000) < \alpha < (19/1250)$		
3	4	$-(1/256) < \alpha < (1/116)$	$-(1/151) < \alpha < (1/80)$	$-(1/384) < \alpha < (1/160)$	$-(1/21000) < \alpha < (1/246)$	$(29/50000) < \alpha < (41/50000)$	
4	5	$-(1/70) < \alpha < (1/129)$	$-(1/416) < \alpha < (1/255)$	$-(1/838) < \alpha < (1/501)$	$-(1/3560) < \alpha < (1/828)$	$-(1/200000) < \alpha < (1/1354)$	$(1/4099) < \alpha < (1/1717)$
5	5	$-(1/509) < \alpha < (1/400)$	$-(1/1208) < \alpha < (1/804)$	$-(1/2212) < \alpha < (1/1556)$	$-(1/7440) < \alpha < (1/2716)$	$-(1/26106) < \alpha < (1/4446)$	$(1/10160) < \alpha < (1/7240)$

TABLE 3: MC: the maximum continuity of the proposed scheme $S_{\alpha, \beta, \gamma}$.

N	(α/β)	MC	C^0	C^1	C^2	C^3	C^4
0	$\alpha = (1/8)(16\beta + 1/2\beta + 1)$ $\beta = -(1/16)(8\alpha - 1/\alpha - 1)$	4	$-(3/20) < \beta < (5/4)$ $-(1/4) < \alpha < (3/4)$	$-(1/16) < \beta < (3/8)$ $0 < \alpha < (1/2)$	$-(1/16) < \beta < (3/8)$ $0 < \alpha < (1/2)$	$0 < \beta < (1/12)$ $(1/8) < \alpha < (1/4)$	$\beta = (1/26)$ $\alpha = (3/16)$
1	$\alpha = (1/128)(256\beta - 3/2\beta - 1)$ $\beta = (1/256)(128\alpha - 3/\alpha - 1)$	4	$-(21/208) < \beta < (11/272)$ $-(1/16) < \alpha < (3/16)$	$-(13/224) < \beta < (3/256)$ $0 < \alpha < (1/8)$	$-(13/224) < \beta < (3/256)$ $0 < \alpha < (1/8)$	$-(2/121) < \beta < -(1/248)$ $(1/32) < \alpha < (7/128)$	$-(2/121) < \beta < -(1/248)$ $(1/32) < \alpha < (7/128)$
2	$\alpha = (1/1024)(2048\beta + 5/2\beta + 1)$ $\beta = -(1/2048)(1024\alpha - 5/\alpha - 1)$	4	$-(21/2080) < \beta < (113/5888)$ $-(1/64) < \alpha < (1/24)$	$-(5/2048) < \beta < (11/997)$ $0 < \alpha < (27/1024)$	$-(5/2048) < \beta < (11/997)$ $0 < \alpha < (27/1024)$	$(3/2032) < \beta < (8/3041)$ $(1/128) < \alpha < (31/3072)$	$(3/2032) < \beta < (8/3041)$ $(1/128) < \alpha < (31/3072)$

TABLE 4: GD and RD represent the degree of polynomial generation and degree of polynomial reproduction of the proposed schemes $S_{a_{2N4}}^d$.

N	0	1	2
C^0	$-(1/8) < \beta < 0$	$-(5/48) < \beta < (1/16)$	$-(39/2560) < \beta < (89/2560)$
C^1	$(2 - \sqrt{6}/8) < \beta < (1 - \sqrt{3}/8)$	$(15 - \sqrt{273}/96) < \beta < (-5 + 3\sqrt{37}/224)$	$(219 - \sqrt{661133}/31232) < \beta < (-171 + \sqrt{56713}/6144)$
C^2		$0 < \beta < (1/36)$	$(16 - \sqrt{286}/96) < \beta < (-675 + \sqrt{637161}/31744)$
C^3			$-(157/20000) < \beta < -(43/20000)$
GD	$1 \forall \beta$ 3 for $\beta = -(1/16)$	$3 \forall \beta$ 5 for $\beta = (3/256)$	$5 \forall \beta$ 7 for $\beta = -(5/2048)$
RD	$1 \forall \beta$ 3 for $\beta = -(1/16)$	$3 \forall \beta$ 5 for $\beta = (3/256)$	$5 \forall \beta$ 7 for $\beta = -(5/2048)$

TABLE 5: Properties of schemes $S_{a_{2N+2}}$ for $\forall \alpha$.

N	0	1	2	3	4	5
Support	4	8	12	16	20	24
Generation	1	3	5	7	9	11
Reproduction	1	3	5	7	9	11

TABLE 6: Properties of schemes $S_{a_{2N+3}}$.

N	0	1	2
Sp	6	10	14
GD	$1 \forall \alpha$ and β $3 \forall \alpha$ where $\beta = -(1/16)(8\alpha - 1/\alpha - 1)$ $3 \forall \beta$ where $\alpha = (1/8)(16\beta + 1/2\beta + 1)$ 5 for $\alpha = (3/16) \& \beta = -(1/16)(8\alpha - 1/\alpha - 1)$ 5 for $\beta = (1/26)$ where $\alpha = (1/8)(16\beta + 1/2\beta + 1)$	$3 \forall \alpha \& \beta$ $5 \forall \alpha$ where $\beta = (1/256)(128\alpha - 3/\alpha - 1)$ $5 \forall \beta$ where $\alpha = (1/128)(256\beta - 3/2\beta - 1)$ 7 for $\alpha = (5/128) \& \beta = (1/256)(128\alpha - 3/\alpha - 1)$ 7 for $\beta = -(1/123)$ where $\alpha = (1/128)(256\beta - 3/2\beta - 1)$	$5 \forall \alpha \& \beta$ $7 \forall \alpha$ where $\beta = -(1/2048)(1024\alpha - 5/\alpha - 1)$ $7 \forall \beta$ where $\alpha = (1/1024)(2048\beta + 5/2\beta + 1)$ 9 for $\alpha = (35/4096) \& \beta = -(1/2048)(1024\alpha - 5/\alpha - 1)$ 9 for $\beta = (15/8122)$ where $\alpha = (1/1024)(2048\beta + 5/2\beta + 1)$
RD	$1 \forall \alpha \& \beta$ 3 for $\alpha = 0 \& \beta = -(1/16)$ 3 for $\alpha = -(1/8) \& \beta = 0$	$3 \forall \alpha \& \beta$ 5 for $\alpha = 0 \& \beta = (3/256)$ 5 for $\alpha = -(3/128) \& \beta = 0$	$5 \forall \alpha \& \beta$ 7 for $\alpha = 0 \& \beta = -(5/2048)$ 7 for $\alpha = -(5/1024) \& \beta = 0$

Sp, GD, and RD represent support width, generation degree, and reproduction degree, respectively.

5. Numerical Examples and Comparisons

This section deals with the numerical examples of the proposed families of subdivision schemes. We also give some numerical and mathematical companions of the proposed schemes with the existing schemes. Numerical performance of 2-point, 3-point, 4-point, 5-point, 6-point, and 7-point relaxed subdivision schemes is shown in Figures 4(a), 4(b), 4(d), 4(e), 4(g), and 4(h), respectively. From these figures, it is easy to see that the tension parameters which are involved in the proposed schemes allow us to draw different models from same initial points. Similarly, geometrical behaviors of interpolatory 4-point, 6-point, and 8-point schemes for different values of tension parameters are shown in Figures 4(c), 4(f), and 4(i), respectively. An interesting geometrical behavior of 3-point, 5-point, and 7-point schemes is shown in Figures 5(a)–5(h) and 6(a)–6(d), respectively.

We apply these schemes to two different initial models with same values of the tension parameters. From these

figures, we observe that the artifacts in the limit curve can be removed either by changing values of the tension parameters or by changing the initial polygons. While schemes proposed by Deslauriers and Dubuc [1], which are also the special cases of the proposed schemes for specific values of tension parameters α and β , do not have this characteristic (see Figures 6(e)–6(h)). Figures 7–9 show that the surfaces produced by the tensor product schemes of proposed primal schemes also give better numerical results than those of the tensor product schemes of primal schemes [1]. Table 8 gives comparisons between proposed families of primal schemes and the family of primal interpolatory schemes of Deslauriers and Dubuc [1]. The parameters used in our families of subdivision schemes not only increase the choices of drawing different shapes but also increase the polynomial reproduction, polynomial generation, and smoothness of the proposed schemes. Moreover, we can draw interpolatory and approximating curves by using a single member of the family. Table 9 gives the comparisons of the proposed primal schemes with the primal approximating schemes of [6, 7].

TABLE 7: Properties of schemes $S_{a_{2N+2}}$ for specific values of α .

N	0	1	2	3	4	5
α	(1/8)	(3/128)	(5/1024)	(35/32768)	(63/262144)	(231/4194304)
Continuity	C^2	C^2	C^2	C^3	C^5	C^3
Generation	3	5	7	9	11	13
Reproduction	1	3	5	7	9	11

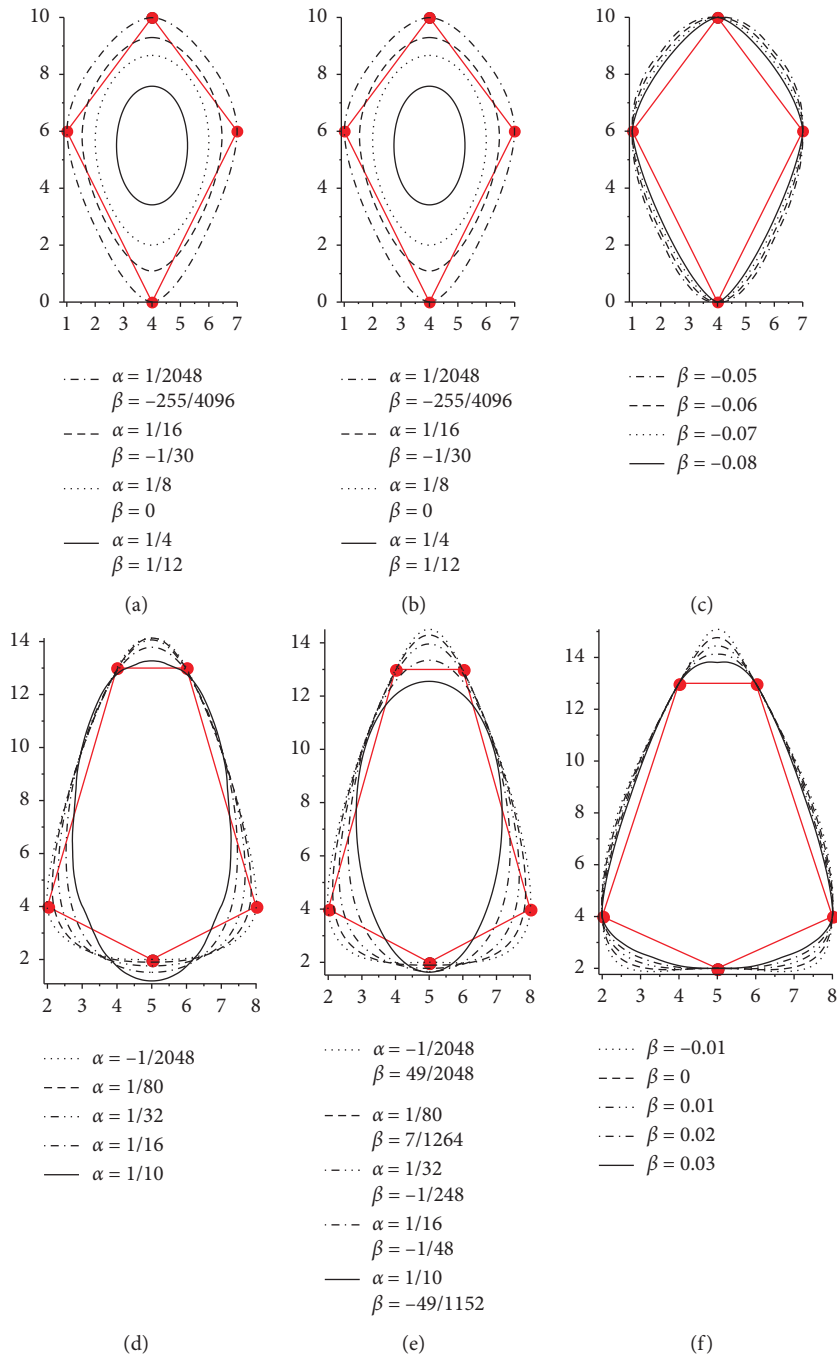


FIGURE 4: Continued.

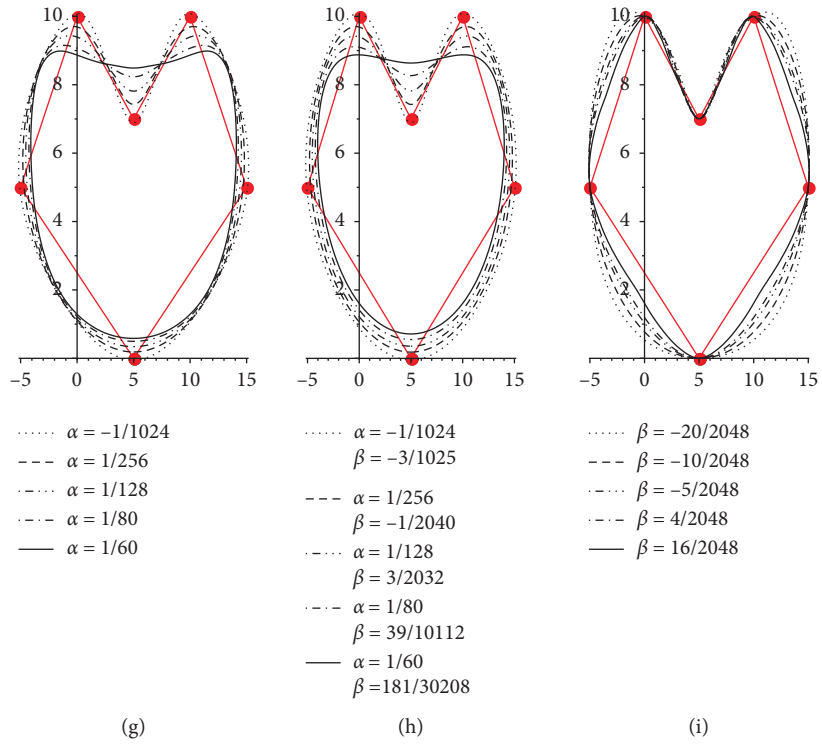


FIGURE 4: Black curves are the limit curves obtained by the subdivision schemes: (a) S_{a_2} ; (b) S_{a_3} ; (c) S_{a_4} ; (d) S_{a_4} ; (e) S_{a_5} ; (f) S_{a_6} ; (g) S_{a_6} ; (h) S_{a_7} ; (i) S_{a_8} , respectively.

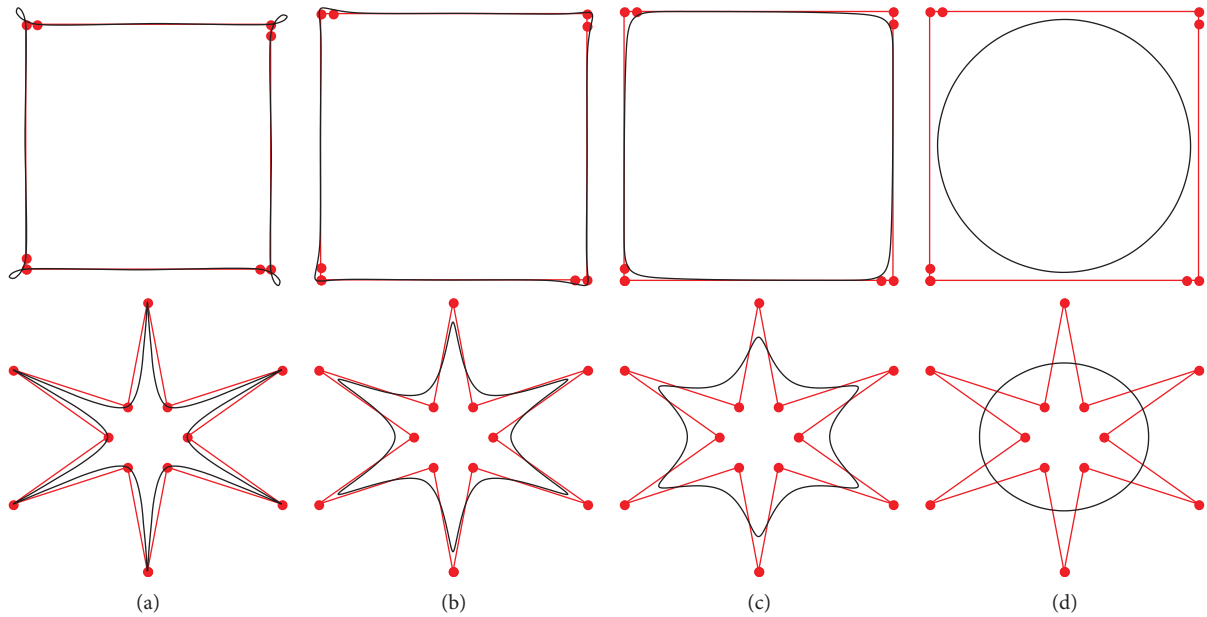


FIGURE 5: Continued.

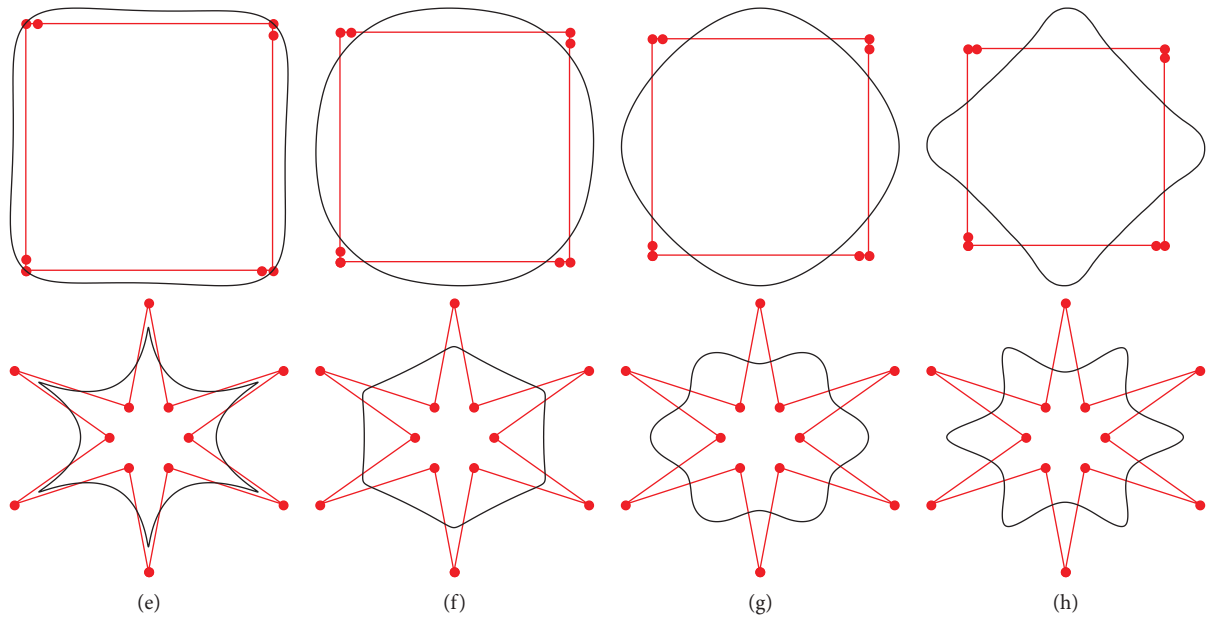


FIGURE 5: Black curves are the limit curves obtained by subdivision scheme S_{a_3} in (a–d) and by subdivision scheme S_{a_5} in (e–h), respectively: (a) $\alpha = 1/2048, \beta = 255/4096$; (b) $\alpha = 1/16, \beta = -(1/30)$; (c) $\alpha = 1/8, \beta = 0$; (d) $\alpha = 1/4, \beta = 1/4$; (e) $\alpha = 1/32, \beta = -3/62$; (f) $\alpha = 1/16, \beta = -1/48$; (g) $\alpha = 1/10, \beta = -49/1152$; (h) $\alpha = 1/8, \beta = -11/128$.

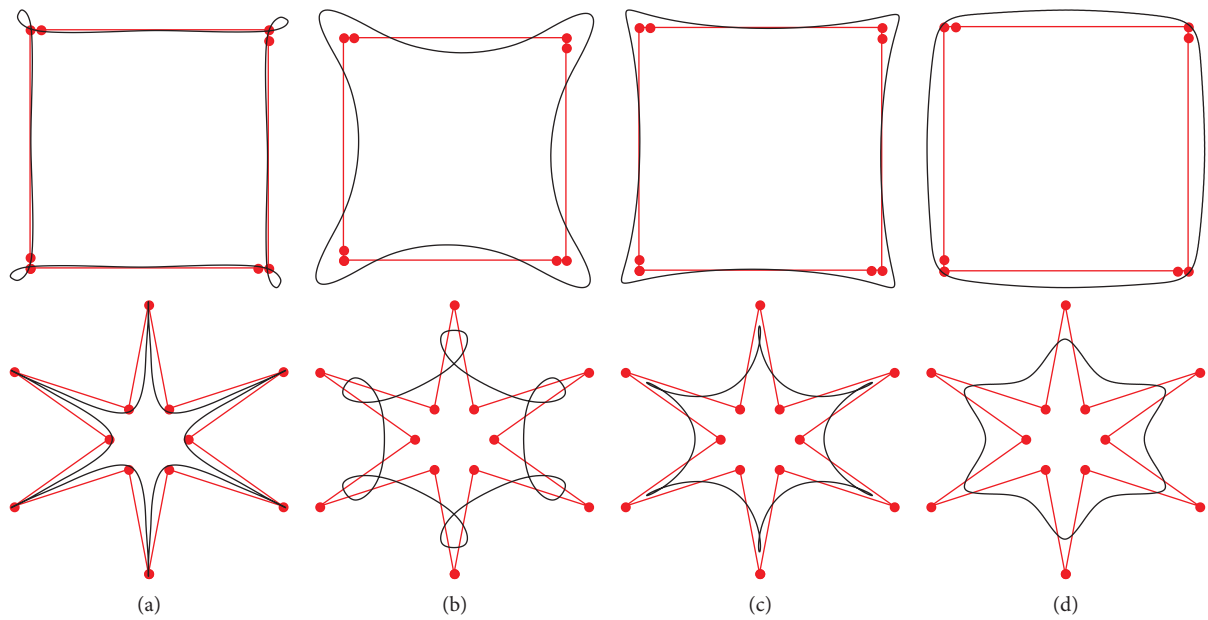


FIGURE 6: Continued.

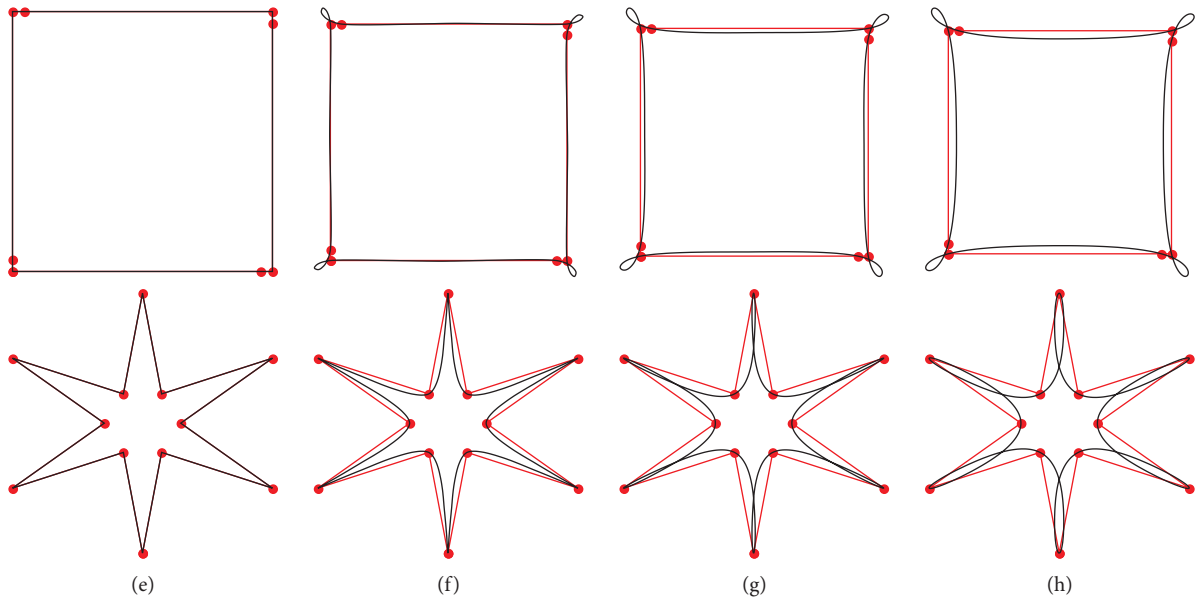


FIGURE 6: Black curves are the limit curves obtained by subdivision scheme S_{a_r} in (a–d) and by subdivision schemes of Deslauriers and Dubuc [1] in (e–h), respectively: (a) $\alpha = 1/2048, \beta = 1/512$; (b) $\alpha = 1/100, \beta = -1/128$; (c) $\alpha = 1/128, \beta = 1/512$; (d) $\alpha = 1/80, \beta = 1/80$; (e) 2-point scheme; (f) 4-point scheme; (g) 6-point scheme; (h) 8-point scheme.

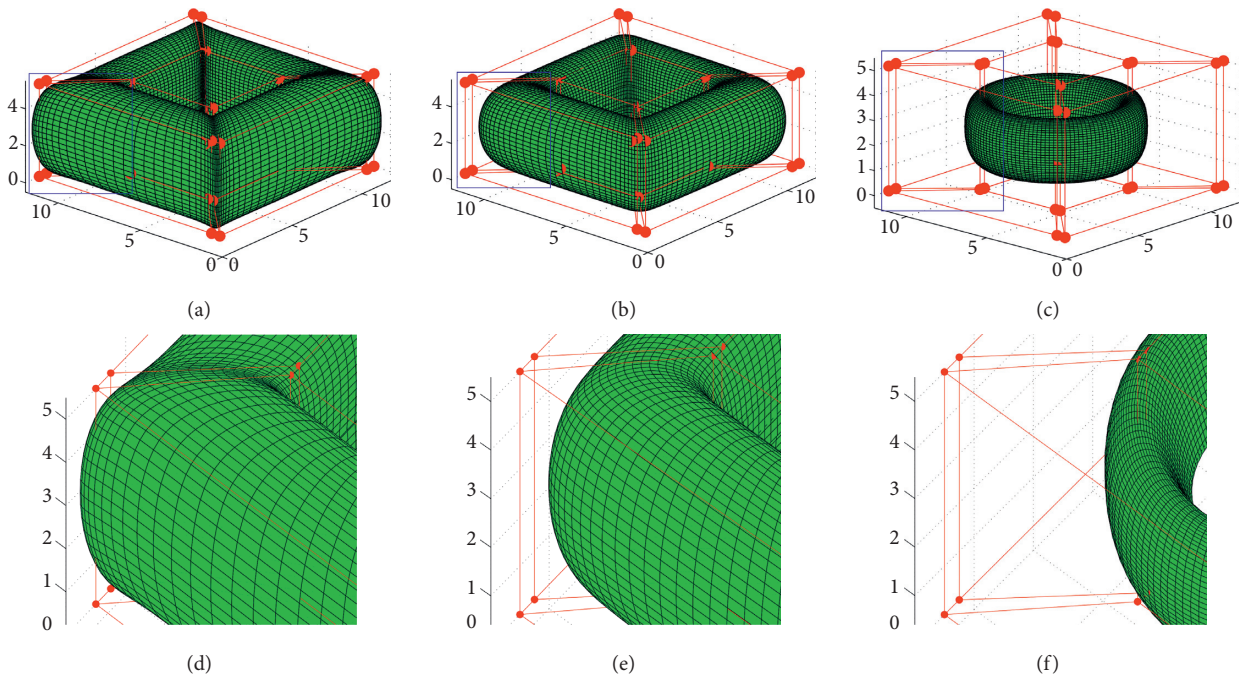


FIGURE 7: Continued.

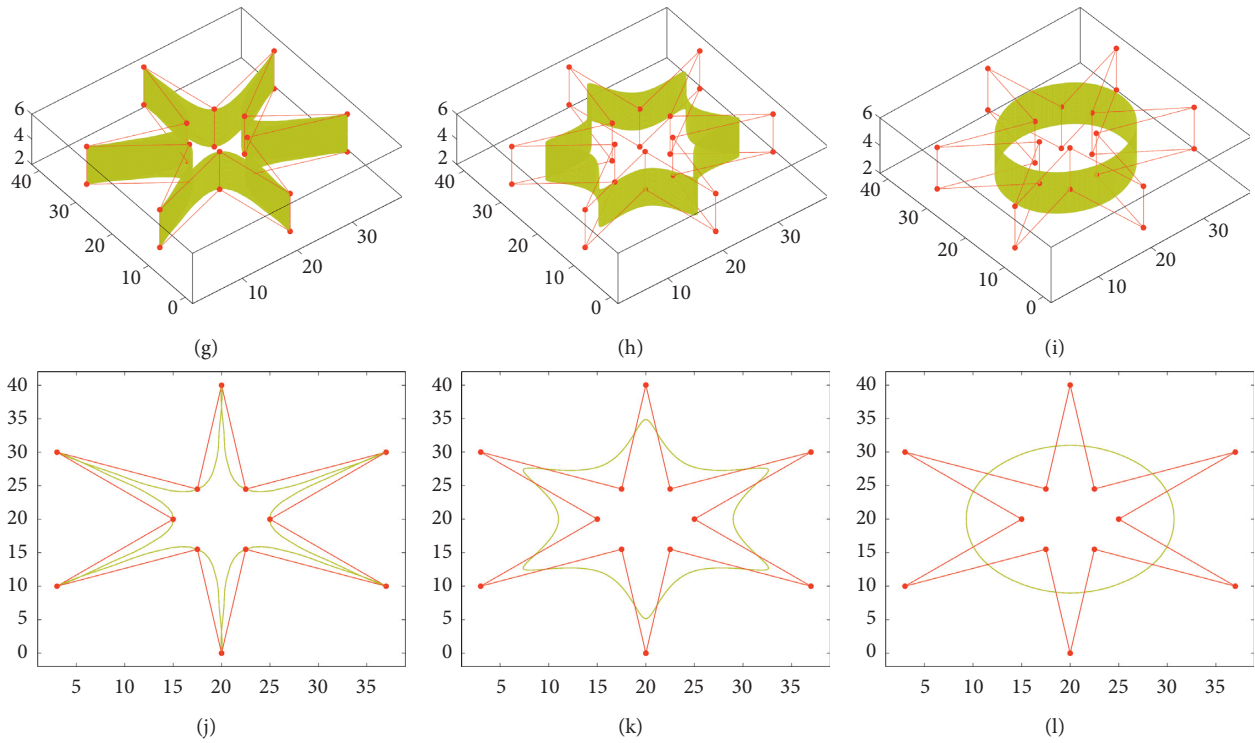


FIGURE 7: (a-c, g-i) The surfaces generated by the tensor product of scheme S_{d_3} . (d-f) The mirror images of the parts inside the blue rectangles of (a-c), respectively. (j-l) The 2-dimensional images in xy -planes of (g-i), respectively.

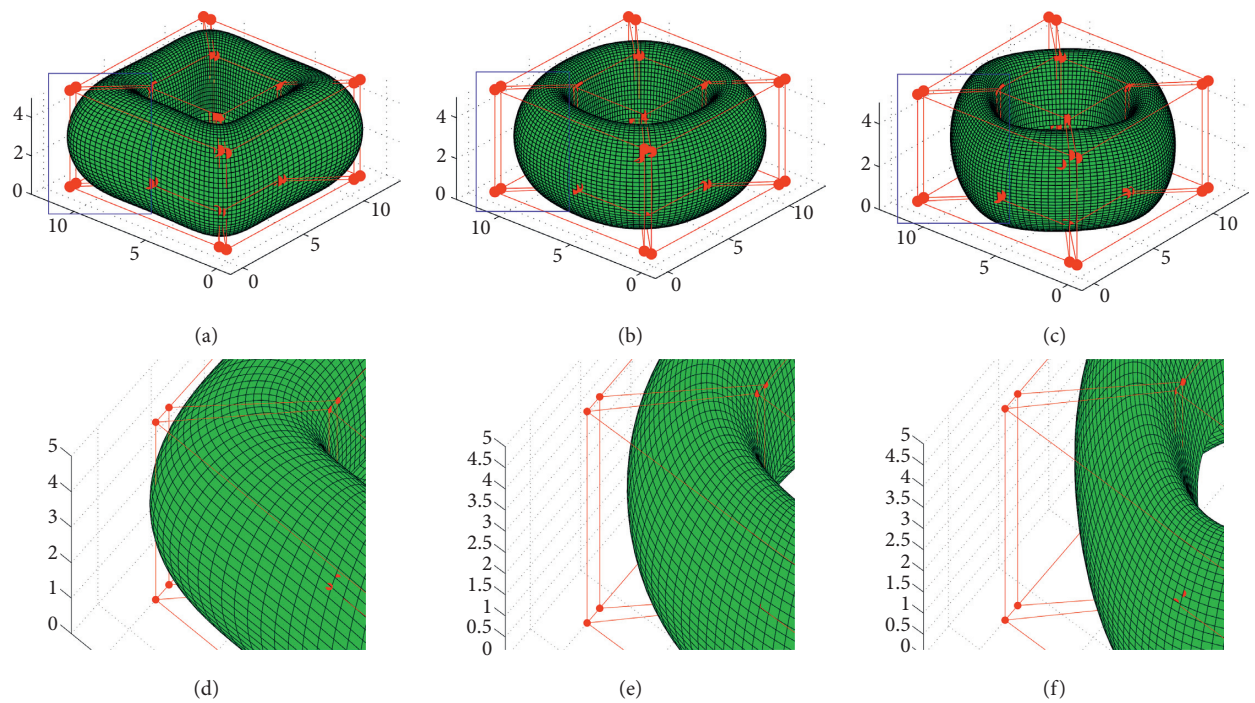


FIGURE 8: Continued.

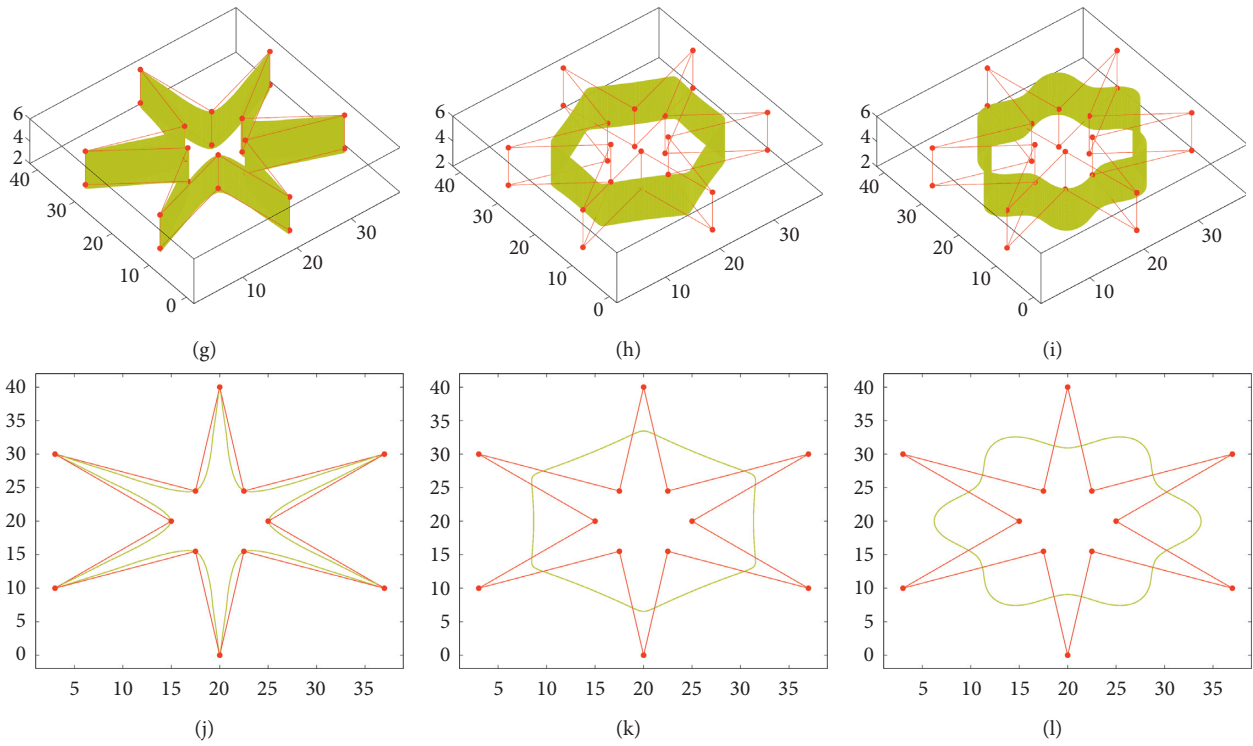


FIGURE 8: (a–c, g–i) The surfaces generated by the tensor product of scheme S_{a_2} . (d–f) The mirror images of the parts inside the blue rectangles of (a–c), respectively. (j–l) The 2-dimensional images in xy -planes of (g–i), respectively.

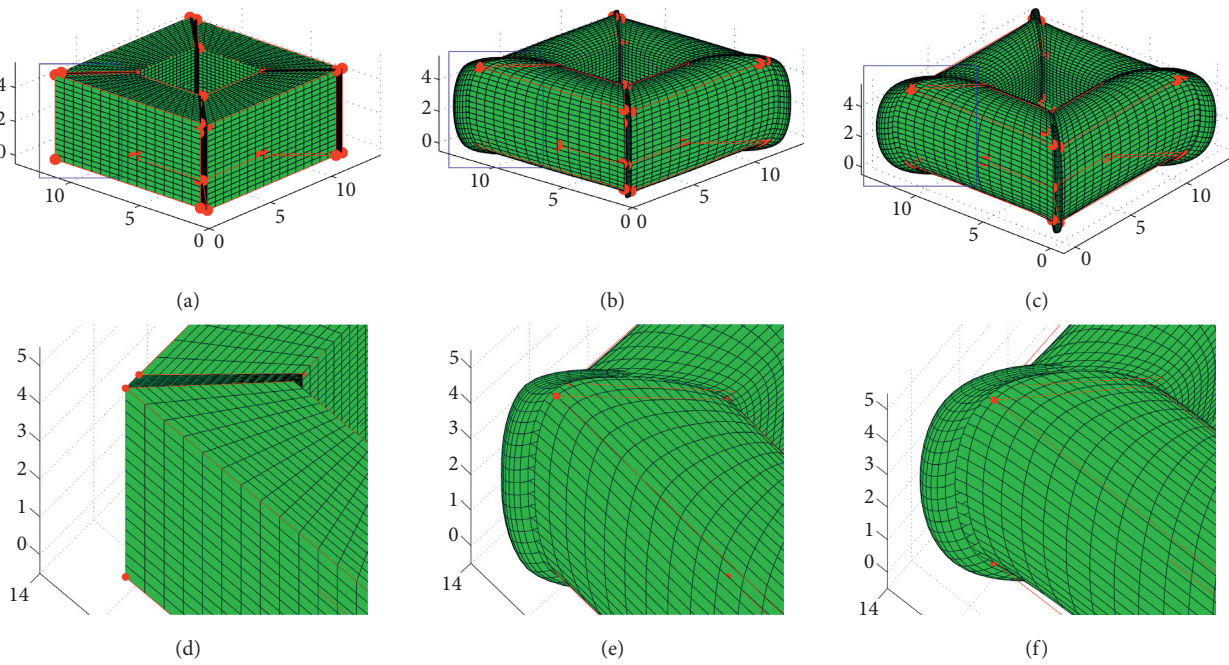


FIGURE 9: Continued.

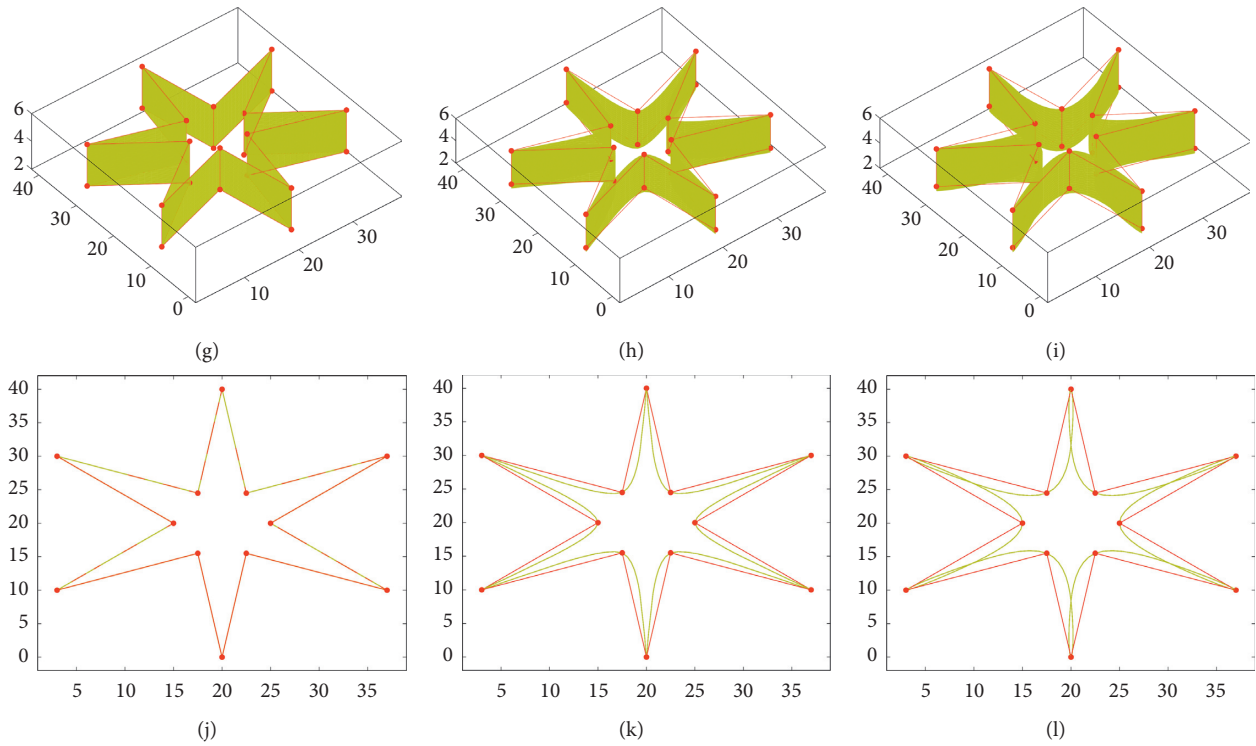


FIGURE 9: (a–c, g–i) The surfaces generated by the tensor product schemes of Deslauriers and Dubuc [1]. (d–f) The mirror images of the parts inside the blue rectangles of (a–c), respectively. (j–l) The 2-dimensional images in xy -planes of (g–i), respectively.

Since approximating subdivision schemes give more smoothness in limits curves as comparative to the interpolating and combined schemes, some of the proposed schemes give lower level of continuity than that of the schemes of [6, 7]. However, the degrees of polynomial reproduction of the proposed schemes are higher than those of these approximating primal schemes.

6. Interproximate Subdivision Schemes

In this section, we present a new family of subdivision schemes, that is, the family of interproximate subdivision schemes, for generating curves that interpolate certain given initial control points and approximate the other initial control points. By the interproximate subdivision scheme, only the initial control points specified to be interpolated are fixed and the other points are updated at each refinement step. The interproximate subdivision schemes can be defined by replacing α_i and β_i as the substitution of α and β in (25) and (26). In this interproximate subdivision process, the parameters α_i control the interpolating property of the subdivision schemes and parameters β_i control the approximating property of the subdivision schemes. Figures 10(a)–10(c) show the initial polygon and limit curves generated by the subdivision scheme S_{a_5} using initial control points $(1, 5), (1, 2), (13, 3.4), (14, 2.5), (14, 4.5), (13, 3.6),$ and $(1, 5)$. Figures 10(d)–10(f) demonstrate that this scheme interpolates the control points in a local manner and uses a different value of tension parameter for each edge of the control polygon. Values of the tension parameters at first

subdivision levels are shown in these figures. Whereas at the other subdivision levels, we use same interpolating values for the control points which are interpolated at the first subdivision levels and use the approximating values of the tension parameters for the modified and new inserted points. Figures 10(g)–10(l) show the limit curves generated by subdivision scheme S_{a_5} using initial control points $(0, 0), (4, 0), (5, 5), (4, 10), (0, 10), (0, 8), (1, 8), (2, 5), (1, 2),$ and $(0, 2)$. In this figure,

- (i) (g) represents the initial polygon with indexed initial control points.
- (ii) (h) shows the limit curve that interpolates all the control points with $(\alpha, \beta) = (0, -0.001)$.
- (iii) (i) represents the limit curve that approximates all the initial control points with $(\alpha, \beta) = ((1/16), -(1/48))$.
- (iv) (j) shows the interproximate limit curve with $(\alpha_i, \beta_i) = (1/10) - (49/1152), (1/10) - (49/1152), (1/10) - (49/1152), (1/10) - (49/1152), (1/10) - (49/1152), (0, (1/64)), (0, (1/64)), (0, (1/64)), (1/10) - (49/1152)$ at first subdivision level. Whereas at other subdivision levels, we use $(\alpha_i, \beta_i) = (0, (1/64))$ for the points $(1, 8), (2, 5),$ and $(1, 2)$ and $(\alpha_i, \beta_i) = (1/10), -(49/1152)$ for all the other points.
- (v) (k) shows the interproximate limit curve with $(\alpha_i, \beta_i) = [(1/14) - (43/1664), (0, -(2/125)), (0, -(2/125)), (0, -(2/125)), (1/14) - (43/1664), (1/14) - (43/1664), (1/14) - (43/1664), (1/14) - (43/1664), (1/14) - (43/1664), (1/14) - (43/1664)]$.

TABLE 8: NTP, RD, GD, MC, Pr, In, Cm, Re, and DD-schemes represent the number of tension parameter(s), degree of polynomial reproduction, degree of polynomial generation, maximum continuity, primal, interpolatory, combined, relaxed, and schemes of Deslauriers and Dubuc [1], respectively, where $N \in \mathbb{N}_0$ with $N < 5$.

Family of schemes	Type	NTP	RD	GD	MC
$(2N + 2)$ -point DD-schemes	Pr/In	0	$2N + 1$	$2N + 1$	C^N
$(2N + 2)$ -point schemes	Pr/Cm/Re	1	$2N + 1 \forall'$	$2N + 3 \forall'$	At least C^{N+1}
$(2N + 3)$ -point schemes	Pr/Cm/Re	2	$2N + 3 \forall'$	$2N + 5 \forall'$	At least C^4
$(2N + 4)$ -point schemes	Pr/In	1	$2N + 3 \forall'$	$2N + 3 \forall'$	C^{N+1}

Here, \forall and \forall' stand for “for all value(s) of parameter(s)” and “not for all value(s) of parameter(s) (at specific values of parameter(s)),” respectively.

TABLE 9: Comparison of the proposed schemes with existing primal relaxed schemes having the same support width.

Schemes	SW	NTP	Type	GD	GD1	RD	RD1	Continuity
Scheme S_{a_3}	6	2	Combined	1	5	1	3	C^4
Scheme [7]	6	1	Approximating	1	5	1	1	C^1
Scheme S_{a_4}	8	1	Combined	3	5	3	3	C^2
Scheme [7]	8	1	Approximating	3	7	1	1	C^3
Scheme [6]	8	1	Approximating	1	3	1	1	C^1
Scheme S_{a_5}	10	2	Combined	3	7	3	5	C^4
Scheme [7]	10	1	Approximating	5	9	1	1	C^5
Scheme S_{a_6}	12	1	Combined	5	7	5	5	C^3
Scheme [7]	12	1	Approximating	7	11	1	1	C^7
Scheme S_{a_7}	14	2	Combined	5	9	5	7	C^4
Scheme [6]	14	1	Approximating	3	5	1	3	C^3

SW, NTP, GD, GD1, RD, and RD1 represent the support width, number of tension parameter(s), degree of polynomial generation at all value(s) of tension parameter(s), degree of polynomial generation at specific value(s) of tension parameter(s), degree of polynomial reproduction for all value(s) of tension parameter(s), and degree of polynomial reproduction at specific value(s) of tension parameter(s).

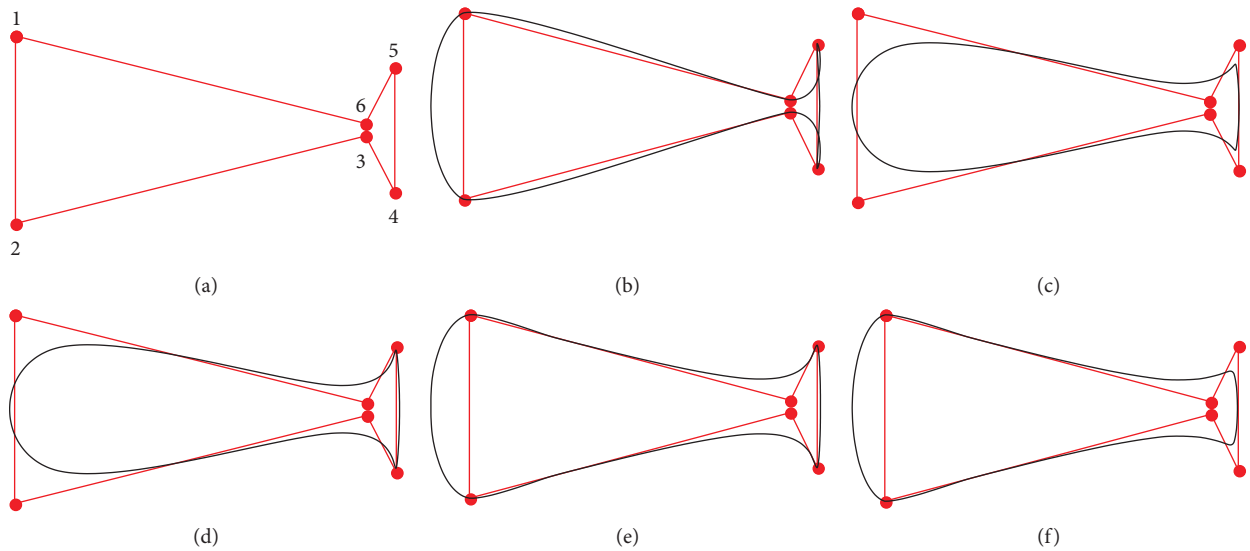


FIGURE 10: Continued.

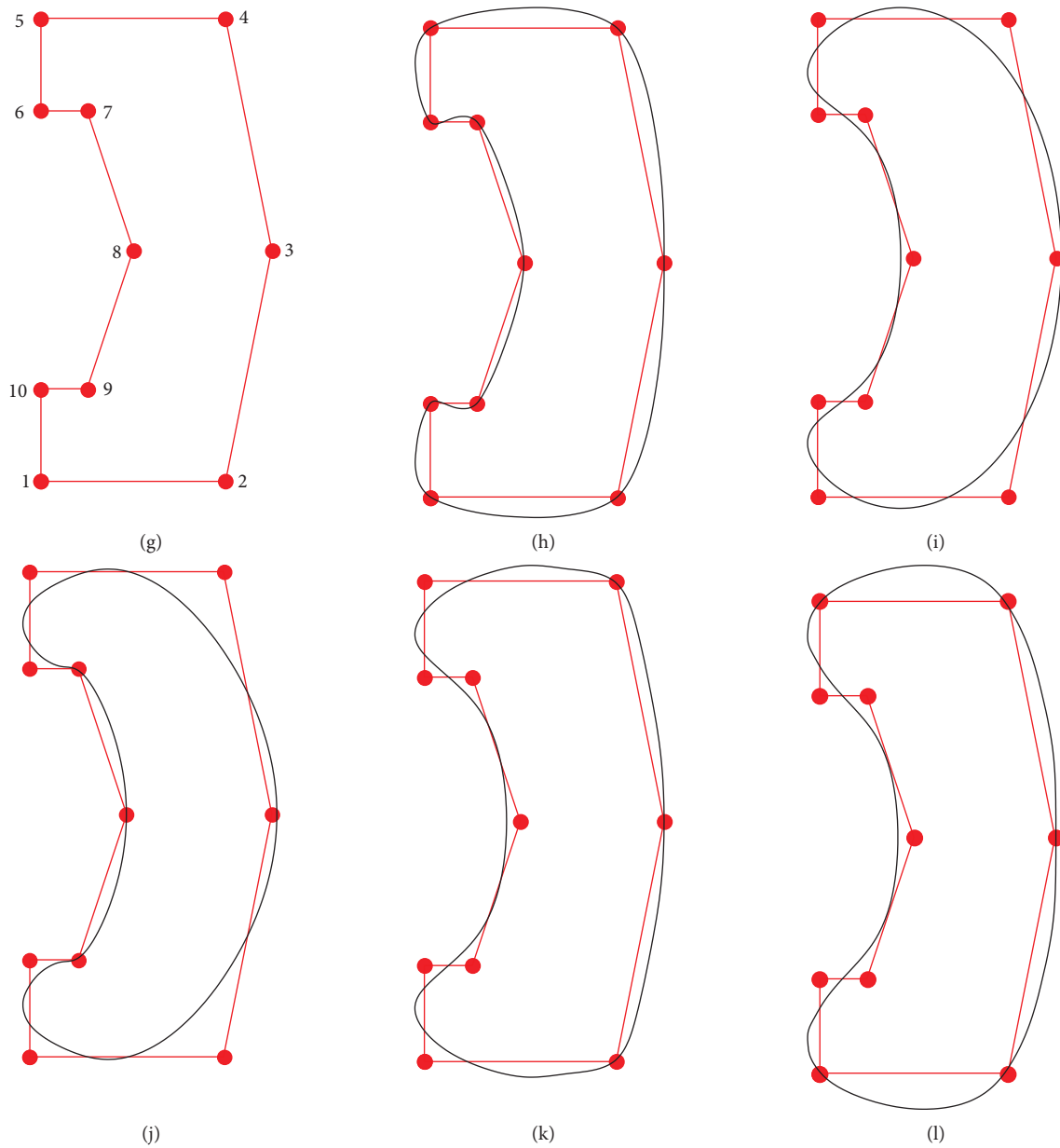


FIGURE 10: The effect of local interpolation by our combined subdivision scheme S_{a_3} with different α_i and β_i is shown in (a–f) and by our combined subdivision scheme S_{a_5} with different α_i and β_i is shown in (g–l), respectively.

$(43/1664), (1/14) - (43/1664), (1/14) - (43/1664)$ at first subdivision level. Whereas at other subdivision levels, we use $(\alpha_i, \beta_i) = (0, -(2/125))$ for the points $(4, 0), (5, 5),$ and $(4, 10)$ and $(\alpha_i, \beta_i) = (1/14), -(43/1664)$ for all the other points.

- (vi) (l) shows the interproximate limit curve with $(\alpha_i, \beta_i) = [(0, (1/30)), (0, (1/30)), (1/11), -(1/30), (0, (1/30)), (0, (1/30)), (1/11), -(1/30), (1/11), -(1/30), (1/11), -(1/30), (1/11) - (1/30)]$ at first subdivision level. Whereas at other subdivision levels, we use $(\alpha_i, \beta_i) = (0, (1/30))$ for the points $(0, 0), (4, 0), (4, 10),$ and $(0, 10)$ and $(\alpha_i, \beta_i) = (1/11), -(1/30)$ for all the other points.

These figures show that proposed schemes can interpolate the initial control points which are chosen by the programmers to be interpolated.

Figure 11 shows the limit surfaces generated by tensor product subdivision scheme of scheme S_{a_3} using initial control points $(0, 2, 0), (5, 0, 0), (10, 2, 0), (5, 15, 0), (0, 2, 0), (0, 2, 2), (5, 0, 2), (10, 2, 2), (5, 15, 2), (0, 2, 2), (0, 2, 4), (5, 0, 4), (10, 2, 4), (5, 15, 4), (0, 2, 4), (0, 2, 6), (5, 0, 6), (10, 2, 6), (5, 15, 6),$ and $(0, 2, 6)$, where Figure 11(a) shows the limit surface that interpolates all the initial control points with $(\alpha, \beta) = (0, -(1/40))$, Figure 11(b) shows the limit surface that approximates all the initial control points with $(\alpha, \beta) = (1/8, t_0)$, and Figure 11(c) shows the limit surface

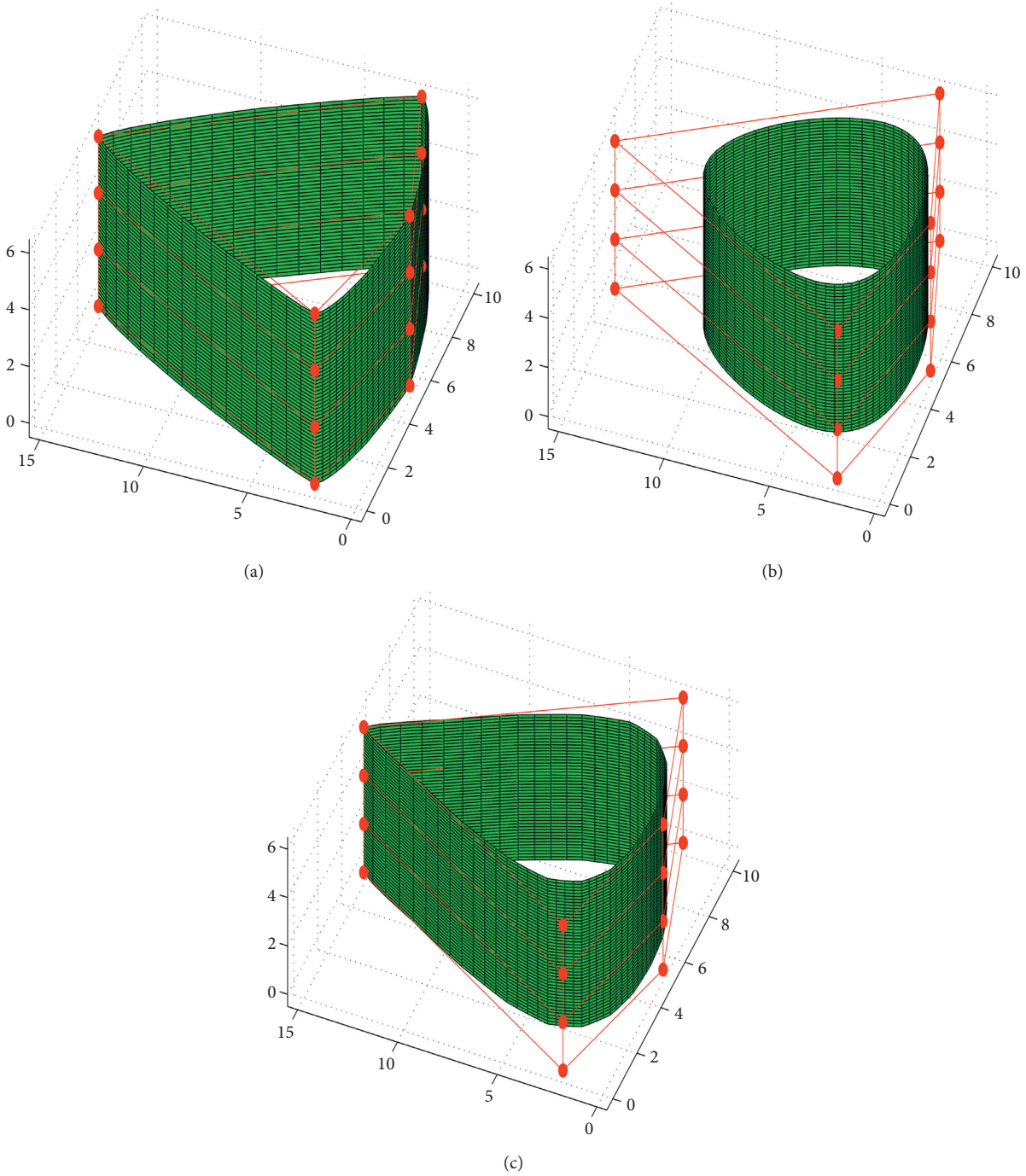


FIGURE 11: The effect of local interpolation by tensor product of our combined subdivision scheme S_{a_3} with different α_i and β_i .

that interpolates only the control points $(5, 15, 0)$, $(5, 15, 2)$, $(5, 15, 4)$, and $(5, 15, 6)$ at each level of subdivision with $(\alpha_i, \beta_i) = (0, -(1/40))$ and approximates all the other control points at each level of subdivision with $(\alpha_i, \beta_i) = ((1/8), 0)$. Similarly, a programmer can choose other control points of his choice to be interpolated by using the tensor product schemes of the proposed schemes. Moreover, the extension of these schemes to the more general schemes which can produce surfaces with arbitrary topology is a direction for future study.

7. Conclusion

In this article, we have proposed a recursive method to generate the refinement rules of combined subdivision schemes. On the basis of that recursive refinement rules, we have presented the family of $(2N + 2)$ -point relaxed primal combined schemes, the family of $(2N + 3)$ -point relaxed combined schemes, and the family of $(2N + 4)$ -point interpolatory subdivision schemes with reproduction degrees $2N + 1$, $2N + 3$, and $2N + 3$, respectively, at certain

values of the tension parameters. In fact, when value of N is increased by one, polynomial reproductions of the proposed families of schemes are increased by two. Similarly, polynomial generations of the proposed families of schemes are $2N + 3$, $2N + 5$, and $2N + 3$, respectively. N is also directly proportional to the polynomial generations of the schemes. The continuity of the proposed families may be increased by increasing N . Our families of schemes not only give the flexibility in fitting limit curves/surfaces because of the involvement of tension parameters but also give the optimal polynomial reproduction, polynomial generation, and continuity than the existing primal schemes. Moreover, we converted the proposed family of $(2N + 3)$ -point combined subdivision schemes to the family of interproximate subdivision schemes by defining local parameters. One of these parameters is defined to control the interpolating property of the subdivision schemes and other one is defined to control the approximating property of the subdivision schemes. The interproximate subdivision schemes have applications in situations where some of the initial data points cannot be measured exactly. Future work is to do a theoretical study that how to choose values of tension parameters in an interproximate algorithm automatically.

Data Availability

The data used to support the findings of the study are included within this paper.

Conflicts of Interest

The authors declare that they have no conflicts of interest regarding the publication of this paper.

Acknowledgments

This work was supported by the NRPU Project, no. 3183, Pakistan.

References

- [1] G. Deslauriers and S. Dubuc, "Symmetric iterative interpolation processes," *Constructive Approximation*, vol. 5, no. 1, pp. 49–68, 1989.
- [2] S. Amat, J. Ruiz, J. C. Trillo, and D. F. Yáñez, "Analysis of the Gibbs phenomenon in stationary subdivision schemes," *Applied Mathematics Letters*, vol. 76, pp. 157–163, 2018.
- [3] N. Dyn, M. S. Floater, and K. Hormann, "AC² four-point subdivision scheme with fourth order accuracy and its extensions," in *Modern Methods in Mathematics*, M. Dhlen, K. Mrken, and L. L. Schumaker, Eds., Nashboro Press, Brentwood, MA, USA, 2005.
- [4] R. Hameed and G. Mustafa, "Family of a b -point b -ary subdivision schemes with bell-shaped mask," *Applied Mathematics and Computation*, vol. 309, pp. 289–302, 2017.
- [5] S. W. Choi, B.-G. Lee, Y. J. Lee, and J. Yoon, "Stationary subdivision schemes reproducing polynomials," *Computer Aided Geometric Design*, vol. 23, no. 4, pp. 351–360, 2006.
- [6] R. Hameed and G. Mustafa, "Construction and analysis of binary subdivision schemes for curves and surfaces originated from Chaikin points," *International Journal of Analysis*, vol. 2016, p. 15, Article ID 1092476, 2016.
- [7] G. Mustafa and R. Hameed, "Families of univariate and bivariate subdivision schemes originated from quartic B-spline," *Advances in Computational Mathematics*, vol. 43, no. 5, pp. 1131–1161, 2017.
- [8] L. Romani, "A Chaikin-based variant of Lane-Riesenfeld algorithm and its non-tensor product extension," *Computer Aided Geometric Design*, vol. 32, pp. 22–49, 2015.
- [9] J. Pan, S. Lin, and X. Luo, "A combined approximating and interpolating subdivision scheme with C2 continuity," *Applied Mathematics Letters*, vol. 25, no. 12, pp. 2140–2146, 2012.
- [10] P. Novara and L. Romani, "Complete characterization of the regions of C2 and C3 convergence of combined ternary 4-point subdivision schemes," *Applied Mathematics Letters*, vol. 62, pp. 84–91, 2016.
- [11] X. Li and J. Zheng, "Interproximate curve subdivision," *Journal of Computational and Applied Mathematics*, vol. 244, pp. 36–48, 2013.
- [12] N. Dyn, D. Levin, and J. A. Gregory, "A 4-point interpolatory subdivision scheme for curve design," *Computer Aided Geometric Design*, vol. 4, no. 4, pp. 257–268, 1987.
- [13] J. Tan, G. Tong, L. Zhang, and J. Xie, "Four point interpolatory-corner cutting subdivision," *Applied Mathematics and Computation*, vol. 265, pp. 819–825, 2015.
- [14] Q. Pan, T. Rabczuk, C. Chen, G. Xu, and K. Pan, "Iso-geometric analysis of minimal surfaces on the basis of extended Catmull-Clark subdivision," *Computer Methods in Applied Mechanics and Engineering*, vol. 337, pp. 128–149, 2018.
- [15] N. Nguyen-Thanh, K. Zhou, X. Zhuang et al., "Iso-geometric analysis of large-deformation thin shells using RHT-splines for multiple-patch coupling," *Computer Methods in Applied Mechanics and Engineering*, vol. 316, pp. 1157–1178, 2017.
- [16] M. Charina and C. Conti, "Polynomial reproduction of multivariate scalar subdivision schemes," *Journal of Computational and Applied Mathematics*, vol. 240, pp. 51–61, 2013.
- [17] N. Dyn, "Subdivision schemes in computer-aided geometric design," *Advances in Numerical Analysis*, vol. 22, pp. 36–104, Oxford Science Publication, Oxford University Press, New York, NY, USA, 1992.
- [18] N. Dyn and D. Levin, "Subdivision schemes in geometric modelling," *Acta Numerica*, vol. 11, pp. 73–144, 2002.
- [19] L. Romani, "Interpolating m -refinable functions with compact support: the second generation class," *Applied Mathematics and Computation*, vol. 361, pp. 735–746, 2019.
- [20] L. Romani and A. Viscardi, "Dual univariate interpolatory subdivision of every arity: algebraic characterization and construction," *Journal of Mathematical Analysis and Applications*, vol. 484, no. 1, p. 123713, 2020.
- [21] C. Conti and K. Hormann, "Polynomial reproduction for univariate subdivision schemes of any arity," *Journal of Approximation Theory*, vol. 163, no. 4, pp. 413–437, 2011.
- [22] C. Beccari, G. Casciola, and L. Romani, "An interpolating 4-point ternary non-stationary subdivision scheme with tension control," *Computer Aided Geometric Design*, vol. 24, no. 4, pp. 210–219, 2007.

Research Article

On Distance-Based Topological Descriptors of Chemical Interconnection Networks

Min Hu,¹ Haidar Ali ,² Muhammad Ahsan Binyamin ,² Bilal Ali,² Jia-Bao Liu ,³ and Chengmei Fan⁴

¹School of Economics and Management, Anhui Normal University, Wuhu 241002, China

²Department of Mathematics, Government College University, Faisalabad, Pakistan

³School of Mathematics and Physics, Anhui Jianzhu University, Hefei 230601, China

⁴College of Modern Service Industry, Hefei College of Finance and Economics, Hefei 230601, China

Correspondence should be addressed to Muhammad Ahsan Binyamin; ahsanbinyamin@gmail.com

Received 8 January 2021; Revised 24 February 2021; Accepted 1 March 2021; Published 16 March 2021

Academic Editor: Ghulam Mustafa

Copyright © 2021 Min Hu et al. This is an open access article distributed under the Creative Commons Attribution License, which permits unrestricted use, distribution, and reproduction in any medium, provided the original work is properly cited.

Structure-based topological descriptors of chemical networks enable us the prediction of physico-chemical properties and the bioactivities of compounds through QSAR/QSPR methods. Topological indices are the numerical values to represent a graph which characterises the graph. One of the latest distance-based topological index is the Mostar index. In this paper, we study the Mostar index, Szeged index, PI index, ABC_{GG} index, and NGG index, for chain oxide network COX_n , chain silicate network CS_n , ortho chain S_n , and para chain Q_n , for the first time. Moreover, analytically closed formulae for these structures are determined.

1. Introduction and Preliminary Results

All the graphs G in this paper are considered to be finite, undirected, and loopless. Graph G is the set made up of vertices (also called the nodes) which are connected with the edges (also called links). It consists on two sets V and E , where V is called the vertex set and E is called the edge set. In order to understand the properties and information contained in the connectivity pattern of graphs, there are many numbers of numerical quantities, known as structure invariants, topological indices, or topological descriptors, which have been derived and studied over the past few decades. The topological indices have vast number of applications in the chemical graph theory which is the special branch of mathematical chemistry. Graph theory has a wide range of applications in engineering due to its diagrammatic nature. It is used in computer science to study the algorithms and flow of information. In engineering, it is used to model the graphics and designs of different networks by converting them in the form of graph.

The topological indices are very much used for characterizing the chemical graphs on the basis of their numerical values. They establish the relationship between the structure and properties of molecule. Topological indices are widely used in QSAR and QSPR research studies [1]. Till now, many topological indices have been derived. For any two graphs G and H which are isomorphic to each other, then $Top(G) = Top(H)$ [2]. Due to the success of simple topological indices, such as Wiener Index [3], Zagreb index [4], and Szeged index [5], motivated others, hundreds of topological indices are introduced. Wiener index is one of the first index which was introduced by Harold Wiener in 1947 [6], when he was working on the boiling point of paraffins. The Wiener index [7] of a graph G is defined as the sum of all the distances between pairs of vertices of G :

$$W(G) = \sum_{(u,v) \in V(G)} d(u,v), \quad (1)$$

where $d(u,v)$ denotes the shortest-path distance in G .

The Szeged index is defined as

$$S_z(G) = \sum_{e=uv \in E(G)} n_u n_v, \tag{2}$$

where n_u denotes the number of vertices of G closer to u than to v and n_v is defined as the number of vertices of G closer to v than to u . This was first studied by Gutman. Later, it is known as the Szeged index [8].

The PI index [9], of a graph G , is defined as

$$PI_v(G) = \sum_{e=uv \in E(G)} n_u + n_v. \tag{3}$$

The Graovac–Ghorbani index is defined as

$$ABC_{GG}(G) = \sum_{e=uv \in E(G)} \sqrt{\frac{n_u + n_v - 2}{n_u n_v}}, \tag{4}$$

and this index is introduced by Graovac and Ghorbani [10], and Furtula [11] used the name Graovac–Ghorbani index.

The normalized ABC_{GG} index is NGG index, first studied by Dimitrov et al. [12], and is defined as

$$NGG(G) = \sum_{e=uv \in E(G)} \frac{1}{\sqrt{n_u n_v}}. \tag{5}$$

A chemical graph is a simple graph in which atoms correspond to the vertices and edge denotes the bond between two atoms. A topological index, specially, the Mostar index is one of the latest topological index, derived in 2018 [13]. Previously, Arockiaraj [14] found the Mostar indices of carbon nanostructures, and Hayata and Zhou [15] calculated the large Mostar index on cacti. The Mostar index for a graph G is defined as the sum of all the absolute values of the difference between n_u and n_v , where u and v are the adjacent vertices of an edge:

$$Mo(G) = \sum_{e=uv \in E(G)} |n_u - n_v|. \tag{6}$$

2. Main Results

The main goal of this article is to compute the Mostar index of ortho chain and para chain using the edge cut method; also, we find the Mostar index, Szeged index, PI index, ABC_{GG} index, and NGG index of oxide chains, chain silicates, ortho chain, and para chain by using the technique of edge partition. The notations used in this paper are standard and taken from the book of west [16]. For the concepts and terms not defined here, we refer the reader to concern with the book of Harary [17] and also concern with [18–25].

2.1. Results for the Chain Oxide Network COX_n . In this section, we discuss COX_n and compute the exact results for Szeged, PI, ABC_{GG} , NGG, and Mostar index. If we remove the silicon atom from the silicate network, then the resulting

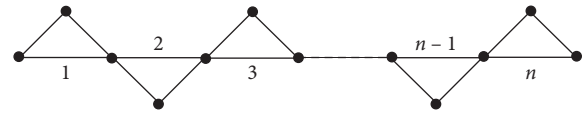


FIGURE 1: Oxide network.

network is an oxide network [26], which consists of three oxygen atoms. Oxide network has the triangular structure. If an oxide network shares its oxygen with other oxide network linearly, then the oxide chain is formed, as shown in Figure 1.

Theorem 1. *Let G_1 be the oxide network of n order, then its Szeged index is $2n^3 + 6n^2 + n/3$.*

Proof. Let $G_1 \cong OX(n)$, where $n \geq 2$; also, n is an integer.

$$Sz(G_1) = \sum_{e \in E(G_1)} n_u n_v, \tag{7}$$

$$Sz(G_1) = \sum_{e \in E(G_1)} n_2 n_2 + \sum_{e \in E(G_1)} n_2 n_4 + \sum_{e \in E(G_1)} n_4 n_4.$$

By using Table 1, we have

$$Sz(G_1) = 2 + 2n^2 + 4n - 4 + \frac{2n^3 - 11n + 6}{3}, \tag{8}$$

$$Sz(G_1) = \frac{2n^3 + 6n^2 + n}{3},$$

which is required. \square

Theorem 2. *Let G_1 be the oxide network of n order; then, its PI index is $4n^2 + 2n$.*

Proof. Let $G_1 \cong OX(n)$, where $n \geq 2$; also, n is an integer:

$$PI_v(G_1) = \sum_{e \in E(G_1)} n_u + n_v,$$

$$PI_v(G_1) = \sum_{e \in E(G_1)} n_2 + n_2 + \sum_{e \in E(G_1)} n_2 + n_4 + \sum_{e \in E(G_1)} n_4 + n_4. \tag{9}$$

By using Table 2, we have

$$PI_v(G_1) = 4 + 2n^2 + 6n - 4 + 2n^2 - 4n, \tag{10}$$

$$PI_v(G_1) = 4n^2 + 2n,$$

which is required. \square

Theorem 3. *Let G_1 be the oxide network of n order; then, its ABC_{GG} index is $1 + \sqrt{n^2 + 3n - 3/n^2 + 2n - 2} + \sqrt{6n^2 - 12n - 6/2n^3 - 11n + 6}$.*

TABLE 1: Edge partition of oxide network of n order.

Edge partition d_u, d_v	Number of edges	Szeged index
2, 2	2	2
2, 4	$2n$	$2n^2 + 4n - 4$
4, 4	$n - 2$	$2n^3 - 11n + 6/3$

TABLE 2: Edge partition of oxide network of n order.

Edge partition d_u, d_v	Number of edges	PI index
2, 2	2	4
2, 4	$2n$	$2n^2 + 6n - 4$
4, 4	$n - 2$	$2n^2 - 4n$

Proof. Let $G_1 \cong OX(n)$, where $n \geq 2$; also, n is an integer:

$$\begin{aligned}
 ABC_{GG}(G_1) &= \sum_{e \in E(G_1)} \sqrt{\frac{n_u + n_v - 2}{n_u n_v}}, \\
 ABC_{GG}(G_1) &= \sum_{e \in E(G_1)} \sqrt{\frac{n_2 + n_2 - 2}{n_2 n_2}} + \sum_{e \in E(G_1)} \sqrt{\frac{n_2 + n_4 - 2}{n_2 n_4}} + \sum_{e \in E(G_1)} \sqrt{\frac{n_4 + n_4 - 2}{n_4 n_4}}.
 \end{aligned}
 \tag{11}$$

By using Table 3, we have

$$ABC_{GG}(G_1) = 1 + \sqrt{\frac{n^2 + 3n - 3}{n^2 + 2n - 2}} + \sqrt{\frac{6n^2 - 12n - 6}{2n^3 - 11n + 6}}, \tag{12}$$

which is required. □

Theorem 4. Let G_1 be the oxide network of n order; then, its $NGG(G_1)$ index is $1/\sqrt{2} + 1/\sqrt{2n^2 + 4n - 4} + \sqrt{3/2n^3 - 11n + 6}$.

Proof. Let $G_1 \cong OX(n)$, where $n \geq 2$; also, n is an integer:

$$\begin{aligned}
 NGG(G_1) &= \sum_{e \in E(G_1)} \frac{1}{\sqrt{n_u n_v}}, \\
 NGG(G_1) &= \sum_{e \in E(G_1)} \frac{1}{\sqrt{n_2 n_2}} + \sum_{e \in E(G_1)} \frac{1}{\sqrt{n_2 n_4}} + \sum_{e \in E(G_1)} \frac{1}{\sqrt{n_4 n_4}}.
 \end{aligned}
 \tag{13}$$

By using Table 4, we have

$$NGG(G_1) = \frac{1}{\sqrt{2}} + \frac{1}{\sqrt{2n^2 + 4n - 4}} + \sqrt{\frac{3}{2n^3 - 11n + 6}}, \tag{14}$$

which is required. □

Theorem 5. Let G_1 be the oxide network of even order; then, its Mostar index is $3n^2 - 2n$.

Proof. Let $G_1 \cong OX(n)$, where $n \geq 2$; also, n is even:

TABLE 3: Edge partition of oxide network of n order.

Edge partition d_u, d_v	Number of edges	ABC_{GG} index
2,2	2	1
2,4	$2n$	$\sqrt{n^2 + 3n - 3/n^2 + 2n - 2}$
4,4	$n - 2$	$\sqrt{6n^2 - 12n - 6/2n^3 - 11n + 6}$

TABLE 4: Edge partition of oxide network of n order.

Edge partition d_u, d_v	Number of edges	NGG index
2, 2	2	$1/\sqrt{2}$
2, 4	$2n$	$1/\sqrt{2n^2 + 4n - 4}$
4, 4	$n - 2$	$\sqrt{3/2n^3 - 11n + 6}$

$$\begin{aligned}
 Mo(G_1) &= \sum_{uv \in E(G_1)} |n_u - n_v|, \\
 Mo(G_1) &= \sum_{uv \in E(G_1)} |n_2 - n_2| + \sum_{uv \in E(G_1)} |n_2 - n_4| + \sum_{uv \in E(G_1)} |n_4 - n_4|.
 \end{aligned}
 \tag{15}$$

By using Table 5, we have

$$\begin{aligned}
 Mo(G_1) &= 0 + 2n^2 + 2n - 4 + n^2 - 4n + 4, \\
 Mo(G_1) &= 3n^2 - 2n,
 \end{aligned}
 \tag{16}$$

which is required. □

Theorem 6. Let G_1 be the oxide network of odd order; then, its Mostar index is $3n^2 - 2n - 1$.

Proof. Let $G_1 \cong OX(n)$, where $n \geq 1$; also, n is odd:

$$\begin{aligned}
 Mo(G_1) &= \sum_{uv \in E(G_1)} |n_u - n_v|, \\
 Mo(G_1) &= \sum_{uv \in E(G_1)} |n_2 - n_2| + \sum_{uv \in E(G_1)} |n_2 - n_4| + \sum_{uv \in E(G_1)} |n_4 - n_4|.
 \end{aligned}
 \tag{17}$$

By using Table 6, we have

$$\begin{aligned}
 Mo(G_1) &= 0 + 2n^2 + 2n - 4 + n^2 - 4n + 3, \\
 Mo(G_1) &= 3n^2 - 2n - 1,
 \end{aligned}
 \tag{18}$$

which is required. □

2.2. Results for the Chain Silicate Network CS_n . In this section, we discuss CS_n and compute the exact results for Szeged, PI, ABC_{GG} , NGG, and Mostar index. Silicates are the

TABLE 5: Edge partition of oxide network of even order.

Edge partition d_u, d_v	Number of edges	Mostar index
2, 2	2	0
2, 4	$2n$	$2n^2 + 2n - 4$
4, 4	$n - 2$	$n^2 - 4n + 4$

TABLE 6: Edge partition of oxide network of odd order.

Edge partition d_u, d_v	Number of edges	Mostar index
2, 2	2	0
2, 4	$2n$	$2n^2 + 2n - 4$
4, 4	$n - 2$	$n^2 - 4n + 3$

compounds which consist of silicon and oxygen, having the tetrahedron structure with bond angle of 109.5° . SiO_4 is found in almost all of the silicates. A single tetrahedron has a shape like a pyramid with triangular base. It has four oxygen atoms at its corners, and silicon atom is bounded equally with oxygen atoms with bond length of 162 pm. A single tetrahedron is shown in Figure 2(a). If a single tetrahedron shares its oxygen with other tetrahedrons; then, a linear silicate chain [27] is formed, as shown in Figure 2(b).

Theorem 7. Let G_2 be the chain silicate network of n order; then, its Szeged index is $3n^3 + 9n^2/2$.

Proof. Let $G_2 \cong \text{CS}_n$, where $n \geq 2$; also, n is an integer:

$$\begin{aligned} \text{Sz}(G_2) &= \sum_{e \in E(G_2)} n_u n_v, \\ \text{Sz}(G_2) &= \sum_{e \in E(G_2)} n_3 n_3 + \sum_{e \in E(G_2)} n_3 n_6 + \sum_{e \in E(G_2)} n_6 n_6. \end{aligned} \tag{19}$$

$$\begin{aligned} \text{ABC}_{\text{GG}}(G_2) &= \sum_{e \in E(G_2)} \sqrt{\frac{n_u + n_v - 2}{n_u n_v}}, \\ \text{ABC}_{\text{GG}}(G_2) &= \sum_{e \in E(G_2)} \sqrt{\frac{n_3 + n_3 - 2}{n_3 n_3}} + \sum_{e \in E(G_2)} \sqrt{\frac{n_3 + n_6 - 2}{n_3 n_6}} + \sum_{e \in E(G_2)} \sqrt{\frac{n_6 + n_6 - 2}{n_6 n_6}}. \end{aligned} \tag{23}$$

By using Table 9, we have

$$\text{ABC}_{\text{GG}}(G_2) = \sqrt{\frac{2n+6}{n+4}} + \sqrt{\frac{3n^2+4n-6}{3n^2+2n-4}} + \sqrt{\frac{6n^2-14n}{3n^3-3n^2-10n+8}}, \tag{24}$$

which is required. □

Theorem 10. Let G_2 be the chain silicate network of n order; then, its NGG index is $1/\sqrt{n+4} + 1/\sqrt{6n^2+4n-8} + \sqrt{2/3n^3-3n^2-10n+8}$.

Proof. Let $G_2 \cong \text{CS}_n$, where $n \geq 2$; also, n is an integer:

By using Table 7, we have

$$\begin{aligned} \text{Sz}(G_2) &= n + 4 + 6n^2 + 4n - 8 + \frac{3n^3 - 3n^2 - 10n + 8}{2}, \\ \text{Sz}(G_2) &= \frac{3n^3 + 9n^2}{2}, \end{aligned} \tag{20}$$

which is required. □

Theorem 8. Let G_2 be the chain silicate network of n order; then, its PI index is $9n^2 + 3n$.

Proof. Let $G_2 \cong \text{CS}_n$, where $n \geq 2$; also, n is an integer:

$$\begin{aligned} \text{PI}_v(G_2) &= \sum_{e \in E(G_2)} n_u + n_v, \\ \text{PI}_v(G_2) &= \sum_{e \in E(G_2)} n_3 + n_3 + \sum_{e \in E(G_2)} n_3 + n_6 + \sum_{e \in E(G_2)} n_6 + n_6. \end{aligned} \tag{21}$$

By using Table 8, we have

$$\begin{aligned} \text{PI}_v(G_2) &= 2n + 8 + 6n^2 + 8n - 10 + 3n^2 - 7n + 2, \\ \text{PI}_v(G_2) &= 9n^2 + 3n, \end{aligned} \tag{22}$$

which is required. □

Theorem 9. Let G_2 be the chain silicate network of n order then its ABC_{GG} index is $\frac{\sqrt{2n+6/n+4} + \sqrt{3n^2+4n-6/3n^2+2n-4} + \sqrt{6n^2-14n/3n^3-3n^2-10n+8}}$.

Proof. Let $G_2 \cong \text{CS}_n$, where $n \geq 2$; also, n is an integer:

$$\begin{aligned} \text{NGG}(G_2) &= \sum_{e \in E(G_2)} \frac{1}{\sqrt{n_u n_v}}, \\ \text{NGG}(G_2) &= \sum_{e \in E(G_2)} \frac{1}{\sqrt{n_3 n_3}} + \sum_{e \in E(G_2)} \frac{1}{\sqrt{n_3 n_6}} + \sum_{e \in E(G_2)} \frac{1}{\sqrt{n_6 n_6}}. \end{aligned} \tag{25}$$

By using Table 10, we have

$$\text{NGG}(G_2) = \frac{1}{\sqrt{n+4}} + \frac{1}{\sqrt{6n^2+4n-8}} + \sqrt{\frac{2}{3n^3-3n^2-10n+8}}, \tag{26}$$

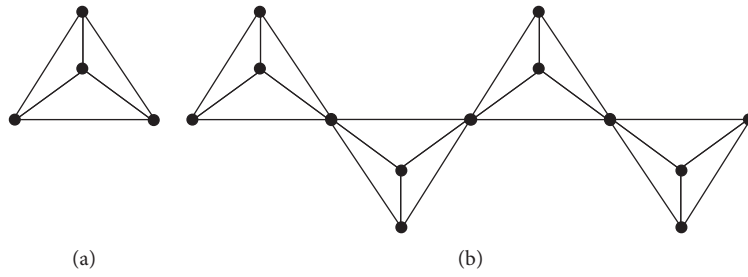


FIGURE 2: (a) Single silicate and (b) chain silicate.

TABLE 7: Edge partition of chain silicate network of n order.

Edge partition d_u, d_v	Number of edges	Szeged index
3, 3	$n + 4$	$n+4$
3, 6	$2(2n - 1)$	$6n^2 + 4n - 8$
6, 6	$n - 2$	$3n^3 - 3n^2 - 10n + 8/2$

TABLE 8: Edge partition of chain silicate network of n order.

Edge partition d_u, d_v	Number of edges	PI index
3, 3	$n + 4$	$2n+8$
3, 6	$2(2n - 1)$	$6n^2 + 8n - 10$
6, 6	$n - 2$	$3n^2 - 7n + 2$

TABLE 9: Edge partition of chain silicate network of n order.

Edge partition d_u, d_v	Number of edges	ABC_{GG} index
3, 3	$n + 4$	$\sqrt{2n + 6/n + 4}$
3, 6	$2(2n - 1)$	$\sqrt{3n^2 + 4n - 6/3n^2 + 2n - 4}$
6, 6	$n - 2$	$\sqrt{6n^2 - 14n/3n^3 - 3n^2 - 10n + 8}$

TABLE 10: Edge partition of chain silicate network of n order.

Edge partition d_u, d_v	Number of edges	ABC_{GG} index
3, 3	$n + 4$	$1/\sqrt{n + 4}$
3, 6	$2(2n - 1)$	$1/\sqrt{6n^2 + 4n - 8}$
6, 6	$n - 2$	$\sqrt{2/3n^3 - 3n^2 - 10n + 8}$

TABLE 11: Edge partition of chain silicate network of even order.

Edge partition d_u, d_v	Number of edges	Mostar index
3, 3	$n + 4$	0
3, 6	$2(2n - 1)$	$6n^2 - 6$
6, 6	$n - 2$	$3n^2 - 12n + 12/2$

which is required. \square

Theorem 11. Let G_2 be the chain silicate network of even order; then, its Mostar index is $15n^2 - 12n/2$.

Proof. Let $G_2 \cong CS_n$, where $n \geq 2$; also, n is even.

$$\begin{aligned}
 Mo(G_2) &= \sum_{uv \in E(G_2)} |n_u - n_v|, \\
 Mo(G_2) &= \sum_{uv \in E(G_2)} |n_3 - n_3| + \sum_{uv \in E(G_2)} |n_3 - n_6| + \sum_{uv \in E(G_2)} |n_6 - n_6|.
 \end{aligned}
 \tag{27}$$

By using Table 11, we have

$$\begin{aligned}
 Mo(G_2) &= 0 + 6n^2 - 6 + \frac{3n^2 - 12n + 12}{2}, \\
 Mo(G_2) &= \frac{15n^2 - 12n}{2},
 \end{aligned}
 \tag{28}$$

which is required. \square

Theorem 12. Let G_2 be the chain silicate network of odd order; then, its Mostar index is $15n^2 - 12n - 3/2$.

Proof. Let $G_2 \cong CS_n$, where $n \geq 1$; also, n is odd:

$$\begin{aligned}
 Mo(G_2) &= \sum_{uv \in E(G_2)} |n_u - n_v|, \\
 Mo(G_2) &= \sum_{uv \in E(G_2)} |n_3 - n_3| + \sum_{uv \in E(G_2)} |n_3 - n_6| + \sum_{uv \in E(G_2)} |n_6 - n_6|.
 \end{aligned}
 \tag{29}$$

By using Table 12, we have

$$\begin{aligned}
 Mo(G_2) &= 0 + 6n^2 - 6 + \frac{3n^2 - 12n + 9}{2}, \\
 Mo(G_2) &= \frac{15n^2 - 12n - 3}{2},
 \end{aligned}
 \tag{30}$$

TABLE 12: Edge partition of chain silicate network of odd order.

Edge partition d_u, d_v	Number of edges	Mostar index
3, 3	$n + 4$	0
3, 6	$2(2n - 1)$	$6n^2 - 6$
6, 6	$n - 2$	$3n^2 - 12n + 9/2$

which is required. □

2.3. *Results for the Ortho Chain S_n .* In this section, we discuss S_n and compute the exact results for Szeged, PI, ABC_{GG} , NGG, and Mostar index. The single molecule of para and ortho chain has the same structure. Basically, it is a cycle graph having 4 sides denoted as C_4 and represented as a four-sided regular polygon. The ortho chain has a zig-zag structure where each corner of C_4 is attached linearly, as shown in Figure 3. The para chain has a structure in which each C_4 is attached at corner to corner with other C_4 but not linearly, as shown in Figure 4 [28].

Theorem 13. *Let G_3 be the ortho chain of n order; then, its Szeged index is $3n^3 + 15n^2 - 2n$.*

Proof. Let $G_3 \cong S_n$, where $n \geq 2$; also, n is an integer.

$$Sz(G_3) = \sum_{e \in E(G_3)} n_u n_v, \tag{31}$$

$$Sz(G_3) = \sum_{e \in E(G_3)} n_2 n_2 + \sum_{e \in E(G_3)} n_2 n_4 + \sum_{e \in E(G_3)} n_4 n_4.$$

By using Table 13, we have

$$Sz(G_3) = \frac{3n^3 + 3n^2 + 26n - 8}{2} + 12n^2 - 4n + \frac{3n^3 + 3n^2 - 22n + 8}{2},$$

$$Sz(G_3) = 3n^3 + 15n^2 - 2n, \tag{32}$$

which is required. □

Theorem 14. *Let G_3 be the ortho chain of n order; then, its PI index is $12n^2 + 4n$.*

Proof. Let $G_3 \cong S_n$, where $n \geq 2$; also, n is an integer:

$$PI_v(G_3) = \sum_{e \in E(G_3)} n_u + n_v,$$

$$PI_v(G_3) = \sum_{e \in E(G_3)} n_2 + n_2 + \sum_{e \in E(G_3)} n_2 + n_4 + \sum_{e \in E(G_3)} n_4 + n_4. \tag{33}$$

By using Table 14, we have

$$PI_v(G_3) = 3n^2 + 7n + 2 + 6n^2 + 2n + 3n^2 - 5n - 2, \tag{34}$$

$$PI_v(G_3) = 12n^2 + 4n,$$

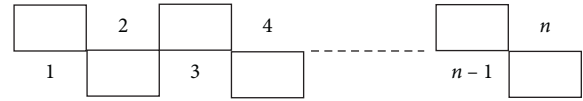


FIGURE 3: Ortho chain of n vertices.

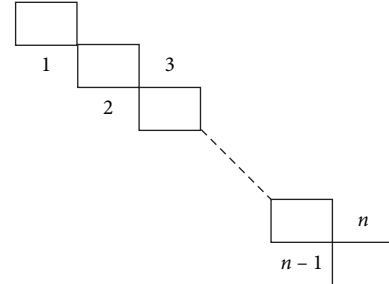


FIGURE 4: Para chain of n order.

TABLE 13: Edge partition of ortho chain of n order.

Edge partition d_u, d_v	Number of edges	Szeged index
2, 2	$n + 2$	$3n^3 + 3n^2 + 26n - 8/2$
2, 4	$2n$	$12n^2 - 4n$
4, 4	$n - 2$	$3n^3 + 3n^2 - 22n + 8/2$

TABLE 14: Edge partition of ortho chain of n order.

Edge partition d_u, d_v	Number of edges	PI index
2, 2	$n + 2$	$3n^2 + 7n + 2$
2, 4	$2n$	$6n^2 + 2n$
4, 4	$n - 2$	$3n^2 - 5n - 2$

which is required. □

Theorem 15. *Let G_3 be the ortho chain of n order; then, its ABC_{GG} index is $\frac{\sqrt{6n^2 + 14n/3n^3 + 3n^2 + 26n - 8}}{+ \sqrt{3n^2 + n - 1/6n^2 - 2n}} + \frac{\sqrt{6n^2 - 10n - 8/3n^3 + 3n^2 - 22n}}{+ 8}$.*

Proof. Let $G_3 \cong S_n$, where $n \geq 2$; also, n is an integer:

$$ABC_{GG}(G_3) = \sum_{e \in E(G_3)} \sqrt{\frac{n_u + n_v - 2}{n_u n_v}},$$

$$ABC_{GG}(G_3) = \sum_{e \in E(G_3)} \sqrt{\frac{n_2 + n_2 - 2}{n_2 n_2}} + \sum_{e \in E(G_3)} \sqrt{\frac{n_2 + n_4 - 2}{n_2 n_4}}$$

$$+ \sum_{e \in E(G_3)} \sqrt{\frac{n_4 + n_4 - 2}{n_4 n_4}}. \tag{35}$$

By using Table 15, we have

TABLE 15: Edge partition of ortho chain of n order.

Edge partition d_u, d_v	Number of edges	ABC_{GG} index
2, 2	$n + 2$	$\sqrt{6n^2 + 14n/3n^3 + 3n^2 + 26n - 8}$
2, 4	$2n$	$\sqrt{3n^2 + n - 1/6n^2 - 2n}$
4, 4	$n - 2$	$\sqrt{6n^2 - 10n - 8/3n^3 + 3n^2 - 22n + 8}$

$$\begin{aligned}
 ABC_{GG}(G_3) &= \sqrt{\frac{6n^2 + 14n}{3n^3 + 3n^2 + 26n - 8}} + \sqrt{\frac{3n^2 + n - 1}{6n^2 - 2n}} \\
 &\quad + \sqrt{\frac{6n^2 - 10n - 8}{3n^3 + 3n^2 - 22n + 8}},
 \end{aligned}
 \tag{36}$$

which is required. □

Theorem 16. Let G_3 be the ortho chain of n order; then, its $NGG(G_3)$ index is $\sqrt{2/3n^3 + 3n^2 + 26n - 8} + 1/2\sqrt{3n^2 - n} + \sqrt{2/3n^3 + 3n^2 - 22n + 8}$.

Proof. Let $G_3 \cong S_n$, where $n \geq 2$; also, n is an integer:

$$\begin{aligned}
 NGG(G_3) &= \sum_{e \in E(G_3)} \frac{1}{\sqrt{n_u n_v}}, \\
 NGG(G_3) &= \sum_{e \in E(G_3)} \frac{1}{\sqrt{n_2 n_2}} + \sum_{e \in E(G_3)} \frac{1}{\sqrt{n_2 n_4}} + \sum_{e \in E(G_3)} \frac{1}{\sqrt{n_4 n_4}}.
 \end{aligned}
 \tag{37}$$

By using Table 16, we have

$$\begin{aligned}
 NGG(G_3) &= \sqrt{\frac{2}{3n^3 + 3n^2 + 26n - 8}} + \frac{1}{2\sqrt{3n^2 - n}} \\
 &\quad + \sqrt{\frac{2}{3n^3 + 3n^2 - 22n + 8}},
 \end{aligned}
 \tag{38}$$

which is required. □

Theorem 17. Let G_3 be the ortho chain of even order; then, its Mostar index is $9n^2 - 6n$.

Proof. Let $G_3 \cong S_n$, where $n \geq 2$; also, n is even:

$$\begin{aligned}
 Mo(G_3) &= \sum_{uv \in E(G_3)} |n_u - n_v|, \\
 Mo(G_3) &= \sum_{uv \in E(G_3)} |n_2 - n_2| + \sum_{uv \in E(G_3)} |n_2 - n_4| \\
 &\quad + \sum_{uv \in E(G_3)} |n_4 - n_4|.
 \end{aligned}
 \tag{39}$$

By using Table 17, we have

TABLE 16: Edge partition of oxide network of n order.

Edge partition d_u, d_v	Number of edges	NGG index
2, 2	$n + 2$	$\sqrt{2/3n^3 + 3n^2 + 26n - 8}$
2, 4	$2n$	$1/2\sqrt{3n^2 - n}$
4, 4	$n - 2$	$\sqrt{2/3n^3 + 3n^2 - 22n + 8}$

TABLE 17: Edge partition of ortho chain of even order.

Edge partition d_u, d_v	Number of edges	Mostar index
2, 2	$n + 2$	$3n^2 + 12n - 12/2$
2, 4	$2n$	$6n^2 - 6n$
4, 4	$n - 2$	$3n^2 - 12n + 12/2$

$$Mo(G_3) = \frac{3n^2 + 12n - 12}{2} + 6n^2 - 6n + \frac{3n^2 - 12n + 12}{2},$$

$$Mo(G_3) = 9n^2 - 6n,
 \tag{40}$$

which is required. □

Theorem 18. Let G_3 be the ortho chain of odd order; then, its Mostar index is $9n^2 - 6n - 3$.

Proof. Let $G_3 \cong S_n$, where $n \geq 1$; also, n is odd:

$$\begin{aligned}
 Mo(G_3) &= \sum_{uv \in E(G_3)} |n_u - n_v|, \\
 Mo(G_3) &= \sum_{uv \in E(G_3)} |n_2 - n_2| + \sum_{uv \in E(G_3)} |n_2 - n_4| \\
 &\quad + \sum_{uv \in E(G_3)} |n_4 - n_4|.
 \end{aligned}
 \tag{41}$$

By using Table 18, we have

$$Mo(G_3) = \frac{3n^2 + 12n - 15}{2} + 6n^2 - 6n + \frac{3n^2 - 12n + 9}{2},$$

$$Mo(G_3) = 9n^2 - 6n - 3,
 \tag{42}$$

which is required. □

2.4. Results for the Para Chain Q_n . In this section, we discuss Q_n and compute the exact results for Szeged, PI, ABC_{GG} , NGG , and Mostar index.

Theorem 19. Let G_4 be the para chain of n order; then, its Szeged index is $6n^3 + 6n^2 + 4n$.

Proof. Let $G_4 \cong Q_n$, where $n \geq 2$; also, n is an integer.

TABLE 18: Edge partition of ortho chain of odd order.

Edge partition d_u, d_v	Number of edges	Mostar index
2, 2	$n + 2$	$3n^2 + 12n - 15/2$
2, 4	$2n$	$6n^2 - 6n$
4, 4	$n - 2$	$3n^2 - 12n + 9/2$

$$\begin{aligned}
 Sz(G_4) &= \sum_{e \in E(G_4)} n_u n_v, \\
 Sz(G_4) &= \sum_{e \in E(G_4)} n_2 n_2 + \sum_{e \in E(G_4)} n_2 n_4.
 \end{aligned}
 \tag{43}$$

By using Table 19, we have

$$\begin{aligned}
 Sz(G_4) &= 24n - 8 + 6n^3 + 6n^2 - 20n + 8, \\
 Sz(G_4) &= 6n^3 + 6n^2 + 4n,
 \end{aligned}
 \tag{44}$$

which is required. □

Theorem 20. Let G_4 be the para chain of n order; then, its PI index is $12n^2 + 4n$.

Proof. Let $G_4 \cong Q_n$, where $n \geq 2$; also, n is an integer:

$$\begin{aligned}
 PI_v(G_4) &= \sum_{e \in E(G_4)} n_u + n_v, \\
 PI_v(G_4) &= \sum_{e \in E(G_4)} n_2 + n_2 + \sum_{e \in E(G_4)} n_2 + n_4.
 \end{aligned}
 \tag{45}$$

By using Table 20, we have

$$\begin{aligned}
 PI_v(G_4) &= 12n + 4 + 12n^2 - 8n - 4, \\
 PI_v(G_4) &= 12n^2 + 4n,
 \end{aligned}
 \tag{46}$$

which is required. □

Theorem 21. Let G_4 be the para chain of n order; then, its ABC_{GG} index is $\frac{\sqrt{6n + 1/12n - 4} + \sqrt{6n^2 - 4n - 3/3n^3 + 3n^2 - 10n + 4}}$.

Proof. Let $G_4 \cong OX(n)$, where $n \geq 2$; also, n is an integer:

$$\begin{aligned}
 ABC_{GG}(G_4) &= \sum_{e \in E(G_4)} \sqrt{\frac{n_u + n_v - 2}{n_u n_v}}, \\
 ABC_{GG}(G_4) &= \sum_{e \in E(G_4)} \sqrt{\frac{n_2 + n_2 - 2}{n_2 n_2}} + \sum_{e \in E(G_4)} \sqrt{\frac{n_2 + n_4 - 2}{n_2 n_4}}.
 \end{aligned}
 \tag{47}$$

By using Table 21, we have

$$ABC_{GG}(G_4) = \sqrt{\frac{6n + 1}{12n - 4}} + \sqrt{\frac{6n^2 - 4n - 3}{3n^3 + 3n^2 - 10n + 4}},
 \tag{48}$$

which is required. □

TABLE 19: Edge partition of para chain of n order.

Edge partition d_u, d_v	Number of edges	Szeged index
2, 2	4	$24n - 8$
2, 4	$4n - 4$	$6n^3 + 6n^2 - 20n + 8$

TABLE 20: Edge partition of para chain of n order.

Edge partition d_u, d_v	Number of edges	PI index
2, 2	4	$12n + 4$
2, 4	$4n - 4$	$12n^2 - 8n - 4$

TABLE 21: Edge partition of para chain of n order.

Edge partition d_u, d_v	Number of edges	ABC_{GG} index
2, 2	4	$\sqrt{6n + 1/12n - 4}$
2, 4	$4n - 4$	$\sqrt{6n^2 - 4n - 3/3n^3 + 3n^2 - 10n + 4}$

Theorem 22. Let G_4 be the para chain of n order; then, its $NGG(G_4)$ index is $1/2\sqrt{6n - 2} + 1/\sqrt{6n^3 + 6n^2 - 20n + 8}$.

Proof. Let $G_4 \cong Q_n$, where $n \geq 2$ also n is an integer:

$$\begin{aligned}
 NGG(G_4) &= \sum_{e \in E(G_4)} \frac{1}{\sqrt{n_u n_v}}, \\
 NGG(G_4) &= \sum_{e \in E(G_4)} \frac{1}{\sqrt{n_2 n_2}} + \sum_{e \in E(G_4)} \frac{1}{\sqrt{n_2 n_4}}.
 \end{aligned}
 \tag{49}$$

By using Table 22, we have

$$NGG(G_4) = \frac{1}{2\sqrt{6n - 2}} + \frac{1}{\sqrt{6n^3 + 6n^2 - 20n + 8}},
 \tag{50}$$

which is required. □

Theorem 23. Let G_4 be the para chain of even order; then, its Mostar index is $6n^2$.

Proof. Let $G_4 \cong Q_n$, where $n \geq 2$; also, n is even:

$$\begin{aligned}
 Mo(G_4) &= \sum_{uv \in E(G_4)} |n_u - n_v|, \\
 Mo(G_4) &= \sum_{uv \in E(G_4)} |n_2 - n_2| + \sum_{uv \in E(G_4)} |n_2 - n_4|.
 \end{aligned}
 \tag{51}$$

By using Table 23, we have

$$\begin{aligned}
 Mo(G_4) &= 12n - 12 + 6n^2 - 12n + 12, \\
 Mo(G_4) &= 6n^2,
 \end{aligned}
 \tag{52}$$

which is required. □

Theorem 24. Let G_4 be the para chain of odd order; then, its Mostar index is $6n^2 - 6$.

TABLE 22: Edge partition of para chain of n order.

Edge partition d_u, d_v	Number of edges	NGG index
2, 2	4	$1/2\sqrt{6n-2}$
2, 4	$4n-4$	$1/\sqrt{6n^3+6n^2-20n+8}$

TABLE 23: Edge partition of para chain of even order.

Edge partition d_u, d_v	Number of edges	Mostar index
2, 2	4	$12n-12$
2, 4	$4n-4$	$6n^2-12n+12$

TABLE 24: Edge partition of para chain of odd order.

Edge partition d_u, d_v	Number of edges	Mostar index
2, 2	4	$12n-12$
2, 4	$4n-4$	$6n^2+12n+6$

TABLE 25: Comparison table for chain oxide network.

OX(n)	Sz(G)	PI	ABC	NGG
1	3	6	—	—
2	14	20	—	—
3	37	42	—	—
4	76	72	2.75	1.04
5	135	110	2.71	0.95
6	218	156	2.66	0.90
7	329	210	2.62	0.86
8	472	272	2.59	0.84
9	651	342	2.56	0.83
10	870	420	2.53	0.81

TABLE 26: Comparison table for chain silicate.

CS $_n$	Sz(G)	PI	ABC	NGG
1	6	12	—	—
2	30	42	—	—
3	81	90	—	—
4	168	156	2.91	0.58
5	300	240	2.89	0.49
6	486	342	2.88	0.45
7	735	462	2.86	0.41
8	1056	600	2.83	0.38
9	1458	756	2.81	0.35
10	1950	930	2.80	0.33

Proof. Let $G_4 \cong Q_n$, where $n \geq 1$; also, n is odd:

$$\begin{aligned}
 \text{Mo}(G_4) &= \sum_{uv \in E(G_4)} |n_u - n_v|, \\
 \text{Mo}(G_4) &= \sum_{uv \in E(G_4)} |n_2 - n_2| + \sum_{uv \in E(G_4)} |n_2 - n_4|.
 \end{aligned}
 \tag{53}$$

By using Table 24, we have

$$\begin{aligned}
 \text{Mo}(G_4) &= 12n - 12 + 6n^2 + 12n + 6, \\
 \text{Mo}(G_4) &= 6n^2 - 6,
 \end{aligned}
 \tag{54}$$

which is required.

TABLE 27: Comparison table for ortho chain.

S $_n$	Sz(G)	PI	ABC	NGG
1	16	16	—	—
2	80	56	—	—
3	210	120	—	—
4	424	208	1.98	0.26
5	740	320	1.88	0.19
6	1176	456	1.80	0.15
7	1750	616	1.74	0.12
8	2480	800	1.68	0.10
9	3384	1006	1.63	0.09
10	4480	1240	1.58	0.08

TABLE 28: Comparison table for para chain.

Q $_n$	Sz(G)	PI	ABC	NGG
1	16	16	—	—
2	80	56	1.61	0.32
3	228	120	1.46	0.20
4	496	208	1.37	0.16
5	920	320	1.30	0.13
6	1536	456	1.26	0.11
7	2380	616	1.22	0.10
8	3488	800	1.19	0.09
9	4896	1008	1.16	0.08
10	6640	1240	1.14	0.07

For the comparison of Szeged, PI, ABC $_{GG}$, and NGG index of COX $_n$, we computed the indices for different values of n . By increasing the values of n , we can clearly check from Table 25 that the order of Szeged and PI index is increasing while that of ABC $_{GG}$ and NGG is decreasing.

For the comparison of Szeged, PI, ABC $_{GG}$, and NGG index of CS $_n$, we computed the indices for different values of n . By increasing the values of n , we can clearly check from Table 26 that the order of Szeged and PI index is increasing while that of ABC $_{GG}$ and NGG is decreasing.

For the comparison of Szeged, PI, ABC $_{GG}$, and NGG index of S $_n$, we computed the indices for different values of n . By increasing the values of n , we can clearly check from Table 27 that the order of Szeged and PI index is increasing while that of ABC $_{GG}$ and NGG is decreasing.

For the comparison of Szeged, PI, ABC $_{GG}$, and NGG index of Q $_n$, we computed the indices for different values of n . By increasing the values of n , we can clearly check from Table 28 that the order of Szeged and PI index is increasing while that of ABC $_{GG}$ and NGG is decreasing. \square

3. Conclusion

In this article, we have figured out several bond-additive TIs such as Szeged, PI, ABC, NGG, and Mostar index. We calculated the closed formulae for abovementioned TIs of chain silicate, oxide network, para, and ortho chain. The above outcomes contribute in the field of natural sciences

and pharmaceutical science. Our exploration kept on determining new consequences of these graphs.

Data Availability

No data were used to support this study.

Conflicts of Interest

The authors declare that they have no conflicts of interest.

References

- [1] K. Nandan, K. Ranjan, M. B. Ahmad, and B. Sah, "QSAR Studies on polychlorinated aromatic compounds using topological descriptors," *International Journal of Pharmaceutical Sciences and Research*, vol. 4, no. 7, p. 2691, 2013.
- [2] P. J. Hansen and P. C. Jurs, "Chemical applications of graph theory. Part I. Fundamentals and topological indices," *Journal of Chemical Education*, vol. 65, no. 7, p. 574, 1988.
- [3] I. Gutman, "A formula for the Wiener number of trees and its extension to graphs containing cycles," *Graph Theory Notes New York*, vol. 27, no. 9, pp. 9–15, 1994.
- [4] H. Lin, "On segments, vertices of degree two and the first Zagreb index of trees," *Match Communications in Mathematical and in Computer Chemistry*, vol. 72, no. 3, pp. 825–834, 2014.
- [5] M. Črepnjak and N. Tratnik, "The szeged index and the wiener index of partial cubes with applications to chemical graphs," *Applied Mathematics and Computation*, vol. 309, pp. 324–333, 2017.
- [6] H. Wiener, "Structural determination of paraffin boiling points," *Journal of the American Chemical Society*, vol. 69, no. 1, pp. 17–20, 1947.
- [7] S. Nikolić and N. Trinajstić, "The Wiener index: development and applications," *Croatica Chemica Acta*, vol. 68, no. 1, pp. 105–129, 1995.
- [8] I. Gutman and A. A. Dobrynin, "The Szeged index a success story," *Graph Theory Notes New York*, vol. 34, pp. 37–44, 1998.
- [9] M. H. Khalifeh, H. Yousefi-Azari, and A. R. Ashrafi, "Vertex and edge PI indices of Cartesian product graphs," *Discrete Applied Mathematics*, vol. 156, no. 10, pp. 1780–1789, 2008.
- [10] A. Graovac and M. Ghorbani, "A new version of atom-bond connectivity index," *Acta Chimica Slovenica*, vol. 57, no. 3, p. 609, 2010.
- [11] B. Furtula, "Atom-bond connectivity index versus Graovac Ghorbani analog," *Match Communications in Mathematical and in Computer Chemistry*, vol. 75, pp. 233–242, 2016.
- [12] D. Dimitrov, B. Ikić, and R. Škrekovski, "Remarks on the Graovac-Ghorbani index of bipartite graphs," *Applied Mathematics and Computation*, vol. 293, pp. 370–376, 2017.
- [13] T. Došlić, I. Martinjak, R. Škrekovski, S. T. Spužević, and I. Zubac, "Mostar index," *Journal of Mathematical Chemistry*, vol. 56, no. 10, pp. 2995–3013, 2018.
- [14] M. Arockiaraj, J. Clement, and N. Tratnik, "Mostar indices of carbon nanostructures and circumscribed donut benzenoid systems," *International Journal of Quantum Chemistry*, vol. 119, no. 1, p. 26043, 2019.
- [15] F. Hayat and B. Zhou, "On cacti with large Mostar index," *Filomat*, vol. 33, no. 15, pp. 4865–4873, 2019.
- [16] D. B. West, *Introduction to Graph Theory*, Prentice-Hall, Upper Saddle River, Bergen, 2001.
- [17] F. Harary, *Graph Theory*, Addison-Wesley, Reading, MA, USA, 1969.
- [18] H. Ali, M. K. Shafiq, M. R. Farahani, M. Cancan, and M. S. Aldemir, "Degree-based topological descriptors of star of david and hexagonal cage networks," *Eurasian Chemical Communications*, vol. 2, no. 11, pp. 1093–1100, 2020.
- [19] G. Dustigeer, H. Ali, M. Imran Khan, and Y.-M. Chu, "On multiplicative degree based topological indices for planar octahedron networks," *Main Group Metal Chemistry*, vol. 43, no. 1, pp. 219–228, 2020.
- [20] Y. Huo, H. Ali, M. A. Binyamin, S. S. Asghar, U. Babar, and J. B. Liu, "On topological indices of m-th chain hex-derived network of third type," *Frontiers of Physics*, vol. 8, Article ID 593275, 2020.
- [21] J. B. Liu, S. Wang, C. Wang, and S. Hayat, "Further results on computation of topological indices of certain networks," *IET Control Theory & Applications*, vol. 11, no. 13, pp. 2065–2071, 2017.
- [22] J.-B. Liu, M. Siddiqui, M. Zahid, M. Naeem, and A. Baig, "Topological properties of crystallographic structure of molecules," *Symmetry*, vol. 10, no. 7, p. 265, 2018.
- [23] J.-B. Liu, J. Zhao, S. Wang, M. Javaid, and J. Cao, "On the topological properties of the certain neural networks," *Journal of Artificial Intelligence and Soft Computing Research*, vol. 8, no. 4, pp. 257–268, 2018.
- [24] J.-B. Liu, S. Javed, M. Javaid, and K. Shabbir, "Computing first general Zagreb index of operations on graphs," *IEEE Access*, vol. 7, pp. 47494–47502, 2019.
- [25] J.-B. Liu, M. Younas, M. Habib, M. Yousaf, and W. Nazeer, "M-Polynomials and Degree-Based Topological Indices of VC5C7 [p, q] and HC5C7 [p, q] Nanotubes," *IEEE Access*, vol. 7, pp. 41125–41132, 2019.
- [26] P. Manuel and I. Rajasingh, "Topological properties of silicate networks," in *Proceedings of the 2009 5th IEEE GCC Conference & Exhibition*, pp. 1–5, IEEE, Kuwait City, Kuwait, 2009 March.
- [27] H. Ali, H. M. A. Siddiqui, and M. K. Shafiq, "On degree-based topological descriptors of oxide and silicate molecular structures," *Magnet Research Report*, vol. 4, pp. 135–142, 2016.
- [28] A. Sadeghieh, S. Alikhani, N. Ghanbari, and A. J. M. Khalaf, "Hosoya polynomial of some cactus chains," *Cogent Mathematics*, vol. 4, no. 1, Article ID 1305638, 2017.

Research Article

A Family of Optimal Eighth Order Iteration Functions for Multiple Roots and Its Dynamics

Saima Akram ¹, Faiza Akram ¹, Moin-ud-Din Junjua ², Misbah Arshad ³,
and Tariq Afzal ²

¹Centre for Advanced Studies in Pure & Applied Mathematics, Bahauddin Zakariya University Multan, Multan 60000, Pakistan

²Department of Mathematics and Statistics, Institute of Southern Punjab Multan, Multan 60000, Pakistan

³Department of Mathematics, COMSATS University Islamabad, Sahiwal Campus, Punjab 57000, Pakistan

Correspondence should be addressed to Saima Akram; saimaakram@bzu.edu.pk

Received 29 January 2021; Revised 17 February 2021; Accepted 27 February 2021; Published 15 March 2021

Academic Editor: Ghulam Mustafa

Copyright © 2021 Saima Akram et al. This is an open access article distributed under the Creative Commons Attribution License, which permits unrestricted use, distribution, and reproduction in any medium, provided the original work is properly cited.

In this manuscript, we present a new general family of optimal iterative methods for finding multiple roots of nonlinear equations with known multiplicity using weight functions. An extensive convergence analysis is presented to verify the optimal eighth order convergence of the new family. Some special cases of the family are also presented which require only three functions and one derivative evaluation at each iteration to reach optimal eighth order convergence. A variety of numerical test functions along with some real-world problems such as beam designing model and Van der Waals' equation of state are presented to ensure that the newly developed family efficiently competes with the other existing methods. The dynamical analysis of the proposed methods is also presented to validate the theoretical results by using graphical tools, termed as the basins of attraction.

1. Introduction

The solution of a nonlinear equation of the type, $g(x) = 0$, is one of the important problems and is a demanding task in computational mathematics. This problem becomes more complex when we deal with multiple roots of nonlinear equations. Many problems arise in the areas of engineering and mathematical modeling with the need to determine roots of the nonlinear equations as an intermediate problem for their solution. We have a large number of one-point and multipoint methods in the literature which are used to find roots of nonlinear equations, see [1–4]. A natural question arises that, is there any need of these variants? This question is pinching and alarming. So, we decided to investigate for its answer. We have tested iterative schemes having the same order of convergence for different test functions. We have also chosen test functions from real-world problems such as Van der Waals' equation of state and beam positioning problem. It is observed that every variant behaves differently for different test functions, so the need for more and more variants is justified. It is almost fictitious to find solutions of

such problems in analytical form. In practice, to obtain approximated and effective solution up to a specific degree of accuracy, we use an iterative procedure. In the past years, many researchers have been worked to formulate iterative multiple root finding schemes with higher order of convergence, by knowing the practical, challenging, and demanding nature of multiple zeros. The behavior of iterative schemes for multiple roots is not similar to that of simple ones of nonlinear equations.

The well-known classical Newton's method with quadratic order of convergence is given as [5]

$$x_{\zeta+1} = x_{\zeta} - \frac{g(x_{\zeta})}{g'(x_{\zeta})}. \quad (1)$$

In case of multiple roots of nonlinear equations, this classical Newton's method fails to keep the quadratic convergence and drops to linear convergence, when provided a good initial guess x_0 near the exact root α . Classical Newton's method with a prior knowledge of multiplicity ($k > 1$) yields a modified Newton's method also known as Rall's

method [6] which converges quadratically to the desired multiple root, given as

$$x_{\zeta+1} = x_{\zeta} - k \cdot \frac{g(x_{\zeta})}{g'(x_{\zeta})}, \quad \zeta \geq 0. \quad (2)$$

In recent years, many researchers have presented optimal fourth order convergent schemes for multiple roots when multiplicity is known in advance [7–11]. Thukral [12], Geum et al. [13, 14], and Sharma et al. [15] presented nonoptimal sixth and seventh order multiple root finding methods. The optimal convergence order is defined by Kung and Traub [16] that a without memory method can accomplish the order of convergence at most 2^{n-1} consuming n function or derivative evaluations. Efficiency index is defined by Ostrowski [17] as, if the order of convergence of an iterative family is r and the total number of function or derivative evaluations per iteration is n , then the efficiency index of an iterative scheme is $r^{1/n}$.

In 2018, Behl et al. [18] presented a class of optimal eighth order methods for approximating multiple roots of nonlinear equations with known multiplicity k , given as follows:

$$\begin{aligned} y_{\zeta} &= x_{\zeta} - k \cdot \frac{g(x_{\zeta})}{g'(x_{\zeta})}, \quad \zeta \geq 0, \\ z_{\zeta} &= y_{\zeta} - G(t_{\zeta}) \cdot s_{\zeta} \cdot \frac{g(x_{\zeta})}{g'(x_{\zeta})}, \\ x_{\zeta+1} &= z_{\zeta} - H(s_{\zeta}, w_{\zeta}) \cdot s_{\zeta} \cdot w_{\zeta} \cdot \frac{g(x_{\zeta})}{g'(x_{\zeta})}, \end{aligned} \quad (3)$$

where $s_{\zeta} = [(g(y_{\zeta})/g(x_{\zeta}))]^{(1/k)}$, $t_{\zeta} = (s_{\zeta}/\beta_1 + \beta_2 s_{\zeta})$, $w_{\zeta} = [(g(z_{\zeta})/g(y_{\zeta}))]^{(1/k)}$, β_1 and β_2 are parameters. The univariate weight function $G: \mathbb{C} \rightarrow \mathbb{C}$ and bivariate weight function $H: \mathbb{C}^2 \rightarrow \mathbb{C}$ are analytic in a neighborhood of (0) and (0, 0), respectively.

In 2019, Akram et al. [19] proposed an optimal eighth order multiple root finding scheme based on weight function approach with known multiplicity ($k \geq 1$), which is given as follows:

$$\begin{aligned} y_{\zeta} &= x_{\zeta} - k \cdot \frac{g(x_{\zeta})}{g'(x_{\zeta})}, \quad \zeta \geq 0, \\ z_{\zeta} &= y_{\zeta} - k \cdot G(s_{\zeta}) \cdot s_{\zeta} \cdot \frac{g(x_{\zeta})}{g'(x_{\zeta})}, \\ x_{\zeta+1} &= z_{\zeta} - k \cdot H(t_{\zeta}, w_{\zeta}) \cdot s_{\zeta} \cdot \frac{g(x_{\zeta})}{g'(x_{\zeta})}, \end{aligned} \quad (4)$$

where $s_{\zeta} = [(g(y_{\zeta})/g(x_{\zeta}))]^{(1/k)}$, $t_{\zeta} = [(g(z_{\zeta})/g(y_{\zeta}))]^{(1/k)}$, $w_{\zeta} = [(g(z_{\zeta})/g(x_{\zeta}))]^{(1/k)}$. The univariate weight function $G: \mathbb{C} \rightarrow \mathbb{C}$ is analytic and bivariate weight function

$H: \mathbb{C}^2 \rightarrow \mathbb{C}$ is holomorphic in a neighborhood of (0) and (0, 0), respectively.

Zafar et al. [20] presented another family of optimal eighth order multiple root finders with known multiplicity by using free parameters $\lambda_1, \lambda_2 \in \mathbb{R}$, given as follows:

$$\begin{aligned} y_{\zeta} &= x_{\zeta} - k \cdot \frac{g(x_{\zeta})}{g'(x_{\zeta})}, \quad \zeta \geq 0, \\ z_{\zeta} &= y_{\zeta} - k \cdot G(s_{\zeta}) \cdot s_{\zeta} \cdot \frac{g(x_{\zeta})}{g'(x_{\zeta})}, \\ x_{\zeta+1} &= z_{\zeta} - k \cdot H(t_{\zeta}) \cdot P(w_{\zeta}) \cdot (\lambda_1 + \lambda_2 s_{\zeta}) \cdot s_{\zeta} \cdot w_{\zeta} \cdot \frac{g(x_{\zeta})}{g'(x_{\zeta})}, \end{aligned} \quad (5)$$

where $s_{\zeta} = [(g(y_{\zeta})/g(x_{\zeta}))]^{(1/k)}$, $w_{\zeta} = [(g(z_{\zeta})/g(y_{\zeta}))]^{(1/k)}$, $t_{\zeta} = [(g(z_{\zeta})/g(x_{\zeta}))]^{(1/k)}$. The univariate weight functions $G: \mathbb{C} \rightarrow \mathbb{C}$, $H: \mathbb{C} \rightarrow \mathbb{C}$, and $P: \mathbb{C} \rightarrow \mathbb{C}$ are analytic in a neighborhood of (0). The above-presented schemes (3), (4), and (5) require only four-function or derivative evaluations and their efficiency index is $8^{(1/4)} = 1.6818$.

There is very limited literature about the higher order optimal multiple root finding iterative schemes that can handle multiple roots with known multiplicity ($k \geq 1$). The main reason is that it is a more challenging and time taking task with tough and lengthy computations to develop iterative methods for finding multiple roots. In the literature, most of the iterative procedures for multiple roots are the extensions of modified Newton's method with complex body structures.

Our aim for the presented work is to develop a general family of multiple root finding methods with simple and compact body structures. Therefore, with the demand to construct simple and more effective optimal higher order methods for multiple roots, we present a family of optimal eighth order convergent iterative methods. The proposed scheme requires only four-function evaluations per iterative step which satisfies the classical conjecture given by Kung and Traub [16] and thus falls in the category of optimal methods. The new simple structured scheme is based on univariate and trivariate weight functions in each iterative step. Our scheme provides faster convergence and wider regions of convergence as compared to the results obtained by the earlier methods of similar kind.

The rest of the manuscript is organized as follows: in Section 2, we present the development of the new family based on weight function approach for finding multiple roots with known multiplicity ($k \geq 1$), followed by the analysis of its convergence to achieve the optimal eighth order of convergence. In Section 3, some simple special cases of weight functions and proposed family are presented. These special cases are used to perform the numerical tests and comparison of the performance of newly developed methods with the existing schemes is presented in Section 4. In Section 5, an extensive dynamical analysis of the presented methods in complex plane is shown by using a

graphical tool, namely, basins of attraction. Finally, the concluding remarks are given in Section 6.

2. Methodology of Iterative Scheme

In this section, we define a general and simple iterative family in order to approximate multiple roots of nonlinear equations. Let α be a multiple root with known multiplicity ($k \geq 1$) of the function $g: \mathbb{C} \rightarrow \mathbb{C}$. We consider the following iterative scheme by employing weight functions at each iterative step:

$$\begin{aligned} y_\zeta &= x_\zeta - G(v_\zeta), \quad \zeta \geq 0, \\ z_\zeta &= y_\zeta - H(t_\zeta) \cdot G(v_\zeta), \\ x_{\zeta+1} &= z_\zeta - H(t_\zeta)(v_\zeta) \cdot D(t_\zeta, s_\zeta, w_\zeta)G, \end{aligned} \tag{6}$$

where $v_\zeta = (g(x_\zeta)/g'(x_\zeta))$, $t_\zeta = [(g(y_\zeta)/g(x_\zeta))]^{(1/k)}$, $s_\zeta = [(g(z_\zeta)/g(y_\zeta))]^{(1/k)}$, $w_\zeta = [(g(z_\zeta)/g(x_\zeta))]^{(1/k)}$.

The weight functions G , H , and D involved in the above iterative scheme (6) play an eminent role to obtain optimal eighth order convergence. The univariate weight functions

$G: \mathbb{C} \rightarrow \mathbb{C}$ and $H: \mathbb{C} \rightarrow \mathbb{C}$ are analytic in the neighborhood of (0) and the trivariate weight function $D: \mathbb{C}^3 \rightarrow \mathbb{C}$ is analytic in the neighborhood of (0, 0, 0). Note that the schemes given by (3), (4), and (5) are the special cases of our proposed family (6).

In the next theorem, we find the conditions on univariate and trivariate weight functions and investigate the optimal eighth order of convergence of presented scheme (6).

Theorem 1. *Let α be a multiple root with multiplicity ($k \geq 1$) of the involved function g and $g: \mathbb{C} \rightarrow \mathbb{C}$ is analytic in the region enclosing a multiple zero α of g . Further, we also suppose that $D: \mathbb{C}^3 \rightarrow \mathbb{C}$, $G: \mathbb{C} \rightarrow \mathbb{C}$, and $H: \mathbb{C} \rightarrow \mathbb{C}$ are analytic in neighborhood of their respected origins. Then, for an initial guess x_0 provided sufficiently close to α of g , the iterative method defined by (6) has an optimal eighth order of convergence when the following conditions hold: $A_0 = 0$; $A_1 = k$; $A_2 = 0$; $B_0 = 0$; $B_1 = 1$; $B_2 = 4$; $B_3 = 18$; $D_{000} = 0$; $D_{100} = 0$; $D_{010} = 1$; $D_{200} = 0$; $D_{001} = -1$; $D_{110} = 1$; $D_{020} = 2$; $D_{101} = 1$; $D_{011} = 2$, with the following error equation:*

$$e_{\zeta+1} = \frac{1}{24k^7} \{C_1((3+k)C_1^2 - 2kC_2)((-163 + 7k^2)C_1^4 - 24k^2C_1^2C_2 - 12k^2C_2^2 + 12k^2C_1C_3)e_\zeta^8\} + O(e_\zeta^9), \tag{7}$$

where $e_\zeta = x_\zeta - \alpha$ and $C_t = (k!/(k+t)!) (g^{(k+t)}(\alpha)/g^{(k)}(\alpha))$, for $t \in \mathbb{N}$.

Proof. Let α be the multiple zero of g and $e_\zeta = x_\zeta - \alpha$ be the error at ζ^{th} iteration, where k is the known multiplicity and $k \geq 1$. Now, we adopt the Taylor series expansion of $g(x_\zeta)$ and $g'(x_\zeta)$ around α ; we have

$$g(x_\zeta) = \frac{g^{(k)}(\alpha)}{k!} e_\zeta^k (1 + C_1 e_\zeta + C_2 e_\zeta^2 + C_3 e_\zeta^3 + C_4 e_\zeta^4 + C_5 e_\zeta^5 + C_6 e_\zeta^6 + C_7 e_\zeta^7 + C_8 e_\zeta^8 + O(e_\zeta^9)), \tag{8}$$

$$g'(x_\zeta) = \frac{g^{(k)}(\alpha)}{k!} e_\zeta^{k-1} (k + (k+1)C_1 e_\zeta + (k+2)C_2 e_\zeta^2 + (k+3)C_3 e_\zeta^3 + (k+4)C_4 e_\zeta^4 + \dots + O(e_\zeta^9)), \tag{9}$$

respectively.

By using expressions (8) and (9), we get

$$v_\zeta = \frac{1}{k} e_\zeta - \frac{C_1}{k} e_\zeta^2 + \frac{(1+k) - 2kC_1}{k^3} e_\zeta^3 + O(e_\zeta^4). \tag{10}$$

We expand the weight function $G(v_\zeta)$ by using Taylor series, which leads us to the following expression:

$$G(v_\zeta) = A_0 + A_1 v_\zeta + \frac{1}{2} A_2 v_\zeta^2, \tag{11}$$

where $A_j = (A^j(0)/j!)$ for $0 \leq j \leq 2$.

By employing expression (11) in the first step of scheme (6), we have

$$y_\zeta = -A_0 + \left(1 - \frac{A_1}{k}\right) e_\zeta - \left(\frac{-2C_1 A_1 + A_2}{2k^2}\right) e_\zeta^2 + O(e_\zeta^3). \tag{12}$$

To achieve the second order of convergence, we select $A_0 = 0$ and $A_1 = k$ and obtain

$$y_\zeta = \left(\frac{2kC_1 - A_2}{2k^2}\right) e_\zeta^2 + O(e_\zeta^3). \tag{13}$$

By using expression (13) and Taylor series expansion of y_ζ , we get the following expression:

$$g(y_\zeta) = g^{(k)}(\alpha)e^{2k} \left(\frac{2^{-k}(- (A_2 - 2kC_1/k^2))^k}{k!} - \frac{2^{1-k}(A_2 - 2kC_1/k^2)^{k-1}(-A_2C_1 + k(1+k)C_1^2 - 2k^2C_2)}{k^2k!} \right) e_\zeta + g^{(k)}(\alpha)e^{2k} \left(\sum_{x=0}^2 F_x e_\zeta^{x+2} \right) + O(e_\zeta^5), \tag{14}$$

where $F_x = F_x(k, C_1, C_2, \dots, C_8)$ are given in terms of k, C_1, C_2, \dots, C_8 . For example, the expressions for coefficients F_0 and F_1 are as follows:

$$F_0 = \frac{1}{k^2k!(- (A_2 - 2kC_1/k^2))^k} 2^{-1-k} \left(\frac{A_2 - 2kC_1}{k^2} \right)^k (-4A_2k^2(5 + 4k + 3k^2)C_1^3 + 4k^3(3 + 3k + 3k^2 + k^3)C_1^4 + 8kC_1^2(A_2(1+k) - k^3(2 + 3k + 2k^2)C_2) - 4(2A_2k^2C_2 - 4(-1+k)k^5C_2^2 + 3A_2k^4C_3) + C_1(-A_2^3 + 4A_2k^3(4 + 7k)C_2 + 24k^5C_3)),$$

$$F_1 = \frac{1}{3k^3k!} 2^{-k} \left(\frac{A_2 - 2kC_1}{k^2} \right)^k (3C_1(A_2C_1 - k(k+1)C_1^2 + 2k^2C_2) + 3kC_1(A_2C_1 - k(1+k)C_1^2 + 2k^2C_2) - \frac{4(-2+k)(-1+k)k(A_2C_1 - k(1+k)C_1^2 + 2k^2C_2)^3}{(A_2 - 2kC_1)^3} + \frac{6(-1+k)k(A_2C_1 - k(1+k)C_1^2 + 2k^2C_2)(-A_2(3-2k)C_1^2 + 2k(1+k)^2C_1^3 - 4A_2kC_2 - 2k^2(4+3k)C_1C_2 - 6k^3C_3)}{(A_2 - 2kC_1)^2})$$

(15)

From expressions (8) and (14), we obtain

$$t_\zeta = -\frac{(A_2 - 2kC_1)}{2k^2} e_\zeta + \frac{(3A_2C_1 - 2k(2+k)C_1^2 + 4k^2C_2)}{2k^3} e_\zeta^2 + \phi_1 e_\zeta^3 + \phi_2 e_\zeta^4 + O(e_\zeta^5), \tag{16}$$

where $\phi_1 = (1/4k^5)(-5A_2k(3+k)C_1^2 + 2k^2(7+7k+2k^2)C_1^3 + C_1(A_2^2 - 4k^3(7+3k)C_2) + 2k^2(5A_2C_2 + 6k^2C_3))$, $\phi_2 = (1/12k^6)(A_2k(97 - 69k - 14k^2)C_1^3 - 2k^2(34 + 51k + 29k^2 + 6k^3)C_1^4 + 3C_1^2(-5A_2^2 - 4k^3(17 + 16k + 4k^2)C_2) - 6k^2C_1(A_2$

$$(23 + 7k)C_2 + 4k^2(5 + 2k)C_3) + 6k^3(-4k(3+k)C_2^2 - 7A_2C_3 + 8k^2C_4)).$$

Expansion of the weight function $H(t_\zeta)$ by using Taylor series is given as follows:

$$H(t_\zeta) = B_0 + B_1 t_\zeta + \frac{1}{2} B_2 t_\zeta^2 + \frac{1}{6} B_3 t_\zeta^3, \tag{17}$$

where $B_j = (B^j(0)/j!)$ for $0 \leq j \leq 3$.

By inserting (11) and (17) in the second step of scheme (6), we attain

$$z_\zeta = -B_0 e_\zeta - \frac{1}{2k^2} ((1 + B_0 - B_1)(A_2 - 2kC_1))e_\zeta^2 + \frac{1}{8k^4} \left(\begin{array}{c} A_2^2(2B_1 - B_2) + 4A_2(2 + 2B_0 - 5B_1 + B_2)kC_1 \\ -4k^2(2 + B_2 + 2k + 2B_0(1 + k) - 2B_1(3 + k))C_1^2 + 16(1 + B_0 - B_1)k^3C_2 \end{array} \right) e_\zeta^3 + \frac{1}{48k^6} \left(\begin{array}{c} -3A_2^3B_2 - A_2^3B_3 - 12A_2k^2(6 + 13B_2 - B_3 + 4k + 2B_2k + B_0(6 + 4k) - B_1(31 + 9k)) \\ C_1^2 + 8k^3(6 - 15B_2 - B_3 - 6B_2k + 6k^2 + 6B_0(1 + k)^2 - 3B_1(13 + 11k - 2k^2)) \\ C_1^3 + 24A_2(4 + 4B_0 - 9B_1 - 2B_2)k^3C_2 - 6kC_1 \\ (A_2^2(12B_1 - 9B_2 + B_3) + 8k^3(4 - 11B_1 - 2B_2 + 3k - 3B_1k + H(4 + 3k))C_2) \\ + 144k^5C_3 - 144B_0k^5C_3 - 144B_1k^5C_3 \end{array} \right) e_\zeta^4 + O(e_\zeta^5). \tag{18}$$

By selecting $B_0 = 0, B_1 = 1, B_2 = 4,$ and $A_2 = 0,$ we get

$$z_\zeta = \frac{1}{6k^3} ((-B_3 - 3(9 + k))C_1^3 - 6kC_1C_2)e_\zeta^4 + O(e_\zeta^5). \tag{19}$$

Hence, scheme (6) reaches at fourth order of convergence by using its first two steps.

Now, again by using the Taylor series expansion of $z_\zeta,$ we obtain

$$g(z_\zeta) = g^{(k)}(\alpha)e^{4k} \left(\frac{6^{-k}((-B_3 + 3(9 + k))C_1^3 - 6kC_1C_2/k^3)^k}{k!} + \frac{6^{-k}((-B_3 + 3(9 + k))C_1^3 - 6kC_1C_2/k^3)^{-1+k}\psi_0}{k^3k!} \right) + g^{(k)}(\alpha)e^{4k} \left(\sum_{x=0}^7 L_x e_\zeta^{x+1} \right) + O(e_\zeta^9), \tag{20}$$

where $\psi_0 = (-125 - 84k - 7k^2 + B_3(7 + 3k))C_1^4 + 6k(-B_3 + 4(7 + k))C_1^2C_2 - 12k^2C_2^2 - 12k^2C_1C_3.$

With the help of expressions (14) and (20), we have

$$s_\zeta = \frac{((-B_3 + 3(9 + k))C_1^2 - 6kC_2)}{6k^2} e_\zeta^2 + \psi_1 e_\zeta^3 + \psi_2 e_\zeta^4 + O(e_\zeta^5), \tag{21}$$

where $\psi_1 = \frac{(-49 - 27k - 2k^2 + B_3(3 + k))C_1^3 + 2k(-B_3 + 3(9 + k))C_1C_2 - 6k^2C_3}{6k^2C_3},$ $\psi_2 = \frac{(1/24k^4) \left(\begin{array}{c} (899 + 1002k + 313k^2 + 18k^3 - 2B_3(43 + 33k + 6k^2))C_1^4 \\ -4k(501 - 33B_3 + 261k - 10B_3k + 18k^2)C_1^2C_2 + 24k^2(26 - B_3 - 3k)C_1C_3 \\ + 4k^2((105 - 4B_3 - 9k)C_2^2 - 18kC_4) \end{array} \right)}{6k^2C_3}.$

With the help of expressions (8) and (20), we obtain

$$w_\zeta = \frac{1}{6k^3} ((-B_3 + 3(9 + k))C_1^2 - 6kC_1C_2)e_\zeta^3 + \psi_3 e_\zeta^4 + O(e_\zeta^5), \tag{22}$$

where $\psi_3 = (1/6k^4)((-152 - 87k - 7k^2 + B_3(8 + 3k))C_1^4 + 6k(29 - B_3 + 4k)C_1^2C_2 - 12k^2C_2^2 - 12k^2C_1C_3).$

Now, we expand the trivariate weight function $D(t_\zeta, s_\zeta, w_\zeta)$ in the neighborhood of $(0, 0, 0)$ by using the Taylor series expansion as follows:

$$D(t_\zeta, s_\zeta, w_\zeta) = D_{000} + D_{100}t_\zeta + D_{010}s_\zeta + D_{001}w_\zeta + D_{101}t_\zeta w_\zeta + D_{011}s_\zeta w_\zeta + D_{111}t_\zeta s_\zeta w_\zeta + \frac{1}{2}D_{200}t_\zeta^2 + \frac{1}{2}D_{020}s_\zeta^2 + \frac{1}{2}D_{002}w_\zeta^2, \tag{23}$$

where $D_{ijk} = (1/i!j!k!)(\partial^{i+j+k}/\partial t_\zeta^i \partial s_\zeta^j \partial w_\zeta^k)D(t_\zeta, s_\zeta, w_\zeta),$ for $i, j, k \in \mathbb{N}.$

We obtain the asymptotic error constant term by employing expressions (11), (17), and (23) in the third step of scheme (6), as follows:

$$e_{\zeta+1} = \frac{D_{000}C_1}{k}e_{\zeta}^2 + \frac{((D_{000} + kD_{000} - D_{100})C_1^2 - 2kD_{000}C_2)}{k^2}e_{\zeta}^3 + D_4e_{\zeta}^4 + D_5e_{\zeta}^5 + D_6e_{\zeta}^6 + D_7e_{\zeta}^7 + O(e_{\zeta}^8). \tag{24}$$

The coefficients $D_i (4 \leq i \leq 7)$ simultaneously depend generally upon the weights D_{ijk} and multiplicity k . To obtain the eighth order convergence of scheme (6), we have to select the following conditions of the weights such as $D_{000} = 0$; $D_{100} = 0$; $D_{010} = 1$; $D_{200} = 0$; $D_{001} = -1$; $D_{110} = 1$; $D_{020} = 2$; $D_{101} = 1$; $D_{011} = 2$; and $B_3 = 18$.

By using the above conditions, we get the required asymptotic error constant equation as follows:

$$e_{\zeta+1} = \frac{1}{24k^7} \{C_1((3+k)C_1^2 - 2kC_2)((-163 + 7k^2)C_1^4 - 24k^2C_1^2C_2 - 12k^2C_2^2 + 12k^2C_1C_3)e_{\zeta}^8\} + O(e_{\zeta}^9). \tag{25}$$

The above equation (25) confirms that the proposed scheme (6) has optimal eighth order of convergence consuming only one-derivative and three-function evaluations per full iteration (i.e., $g'(x_{\zeta}), g(x_{\zeta}), g(y_{\zeta})$ and $g(z_{\zeta})$). \square

3. Some Special Cases of Weight Functions

We consider some special choices of weight functions employed in our new scheme (6) satisfying the conditions of Theorem 1. The considered weight functions are simple.

First, we consider the polynomial weight function $G(v_{\zeta})$, satisfying the conditions given in Theorem 1 and can be represented as

$$G(v_{\zeta}) = k \cdot v_{\zeta}, \quad \zeta \geq 0. \tag{26}$$

The trivariate weight function $D(t_{\zeta}, s_{\zeta}, w_{\zeta})$ is also chosen as a polynomial and is given as

$$D(t_{\zeta}, s_{\zeta}, w_{\zeta}) = s_{\zeta} \cdot (1 + s_{\zeta} + 2s_{\zeta}t_{\zeta} + t_{\zeta}^2) + D_{201} \cdot w_{\zeta}t_{\zeta}^2, \tag{27}$$

where D_{201} is a free parameter. By taking different choices for D_{201} , we have three cases described as follows.

3.1. Case 1. We take the polynomial weight function $H(t_{\zeta})$ directly from Theorem 1 as follows:

$$H(t_{\zeta}) = t_{\zeta} + 2t_{\zeta}^2. \tag{28}$$

We select the parameter $D_{201} = -6$ in (28), and also by using the weight functions given in equations (26), (28), and (27), respectively, we prevail the special case of our newly developed optimal eighth order family (6), named as SFM1 given by

$$\begin{aligned} y_{\zeta} &= e_{\zeta} - (k \cdot v_{\zeta}), \quad \zeta \geq 0, \\ z_{\zeta} &= y_{\zeta} - (t_{\zeta} + 2t_{\zeta}^2) \times (k \cdot v_{\zeta}), \\ x_{\zeta+1} &= z_{\zeta} - (t_{\zeta} + 2t_{\zeta}^2) \times (s_{\zeta} \cdot (1 + s_{\zeta} + 2s_{\zeta}t_{\zeta} + t_{\zeta}^2) - 6w_{\zeta}t_{\zeta}^2) \times (k \cdot v_{\zeta}), \end{aligned} \tag{29}$$

where $v_{\zeta} = (g(x_{\zeta})/g'(x_{\zeta}))$, $t_{\zeta} = [(g(y_{\zeta})/g(x_{\zeta}))]^{(1/k)}$, $s_{\zeta} = [(g(z_{\zeta})/g(y_{\zeta}))]^{(1/k)}$, $w_{\zeta} = [(g(z_{\zeta})/g(x_{\zeta}))]^{(1/k)}$.

$$H(t_{\zeta}) = \frac{t_{\zeta}}{1 - 2t_{\zeta}}. \tag{30}$$

3.2. Case 2. By keeping the fact in our mind that the rational functions show more stable behavior by using the same degree polynomial in contrast to simple polynomial of the same degree, we take the rational weight function $H(t_{\zeta})$ from the hypothesis of Theorem 1 as follows:

For this special choice of weight function given in (30), we choose the parameter $D_{201} = 2$, involved in expression (27). By using the weight functions given in equations (26), (30), and (27), respectively, we obtain another special case of our newly developed optimal eighth order family (6) denoted by SFM2 as follows:

$$\begin{aligned}
 y_\zeta &= e_\zeta - (k \cdot v_\zeta), \quad \zeta \geq 0, \\
 z_\zeta &= y_\zeta - \left(\frac{t_\zeta}{1 - 2t_\zeta} \right) \times (k \cdot v_\zeta), \\
 x_{\zeta+1} &= z_\zeta - \left(\frac{t_\zeta}{1 - 2t_\zeta} \right) \times (s_\zeta \cdot (1 + s_\zeta + 2s_\zeta t_\zeta + t_\zeta^2) + 2w_\zeta t_\zeta^2) \times (k \cdot v_\zeta),
 \end{aligned}
 \tag{31}$$

where $v_\zeta = (g(x_\zeta)/g'(x_\zeta))$, $t_\zeta = [(g(y_\zeta)/g(x_\zeta))]^{(1/k)}$, $s_\zeta = [(g(z_\zeta)/g(y_\zeta))]^{(1/k)}$, $w_\zeta = [(g(z_\zeta)/g(x_\zeta))]^{(1/k)}$.

3.3. Case 3. We consider the logarithmic weight function $H(t_\zeta)$ as follows:

$$H(t_\zeta) = \frac{5}{2}t_\zeta^2 + \log(t_\zeta + 1). \tag{32}$$

By using $D_{201} = -(16/3)$ in (27) and the weight functions given in equations (26), (32), and (27), respectively, we prevail the special case of the family (6), named as SFM3, given as

$$\begin{aligned}
 y_\zeta &= e_\zeta - (k \cdot v_\zeta), \quad \zeta \geq 0, \\
 z_\zeta &= y_\zeta - \left(\frac{5}{2}t_\zeta^2 + \log(t_\zeta + 1) \right) \times (k \cdot v_\zeta), \\
 x_{\zeta+1} &= z_\zeta - \left(\frac{5}{2}t_\zeta^2 + \log(t_\zeta + 1) \right) \times \left(s_\zeta \cdot (1 + s_\zeta + 2s_\zeta t_\zeta + t_\zeta^2) - \frac{16}{3}w_\zeta t_\zeta^2 \right) \times (k \cdot v_\zeta),
 \end{aligned}
 \tag{33}$$

where $v_\zeta = (g(x_\zeta)/g'(x_\zeta))$, $t_\zeta = [(g(y_\zeta)/g(x_\zeta))]^{(1/k)}$, $s_\zeta = [(g(z_\zeta)/g(y_\zeta))]^{(1/k)}$, $w_\zeta = [(g(z_\zeta)/g(x_\zeta))]^{(1/k)}$.

4. Computational Results

In this section, we examine the convergence behavior, strength, and effectiveness of the proposed multiple root finding scheme (6). We consider some numerical test

functions including two real-life problems and some standard nonlinear functions. We take the special cases of our newly proposed scheme given in (29), (31), and (33) denoted by SFM1, SFM2, and SFM3, respectively. We compare them with the eighth order optimal scheme by Behl et al. [18], given in (3). We choose a special case of their scheme with the parametric values ($\beta_1 = 1$ and $\beta_2 = 1$) given below, denoted by BM1:

$$\begin{aligned}
 y_\zeta &= x_\zeta - k \cdot \frac{g(x_\zeta)}{g'(x_\zeta)}, \quad \zeta \geq 0, \\
 z_\zeta &= y_\zeta - \left(k + 2t_\zeta k \beta_1 + \frac{1}{2}t_\zeta^2 (4k\beta_1^2 + 2k\beta_1\beta_2) \right) \cdot s_\zeta \cdot \frac{g(x_\zeta)}{g'(x_\zeta)}, \\
 x_{\zeta+1} &= z_\zeta - \left(\frac{k(1 + 2w_\zeta + 3t_\zeta^2\beta_1^2 + t_\zeta\beta_1(2 + 6w_\zeta + t_\zeta\beta_2))}{1 + w_\zeta} \right) \cdot s_\zeta \cdot w_\zeta \cdot \frac{g(x_\zeta)}{g'(x_\zeta)},
 \end{aligned}
 \tag{34}$$

where $s_\zeta = [(g(y_\zeta)/g(x_\zeta))]^{(1/k)}$, $t_\zeta = (s_\zeta/\beta_1 + \beta_2 s_\zeta)$, $w_\zeta = [(g(z_\zeta)/g(y_\zeta))]^{(1/k)}$.

We also compare the results of our methods with the three-step optimal eighth order family by Akram et al. [19], given in (4). We choose the following special case of their scheme denoted by AM2:

$$y_\zeta = x_\zeta - k \cdot \frac{g(x_\zeta)}{g'(x_\zeta)}, \quad \zeta \geq 0,$$

$$z_\zeta = y_\zeta - k \cdot (6s_\zeta^3 - s_\zeta^2 + 2s_\zeta + 1) \cdot s_\zeta \cdot \frac{g(x_\zeta)}{g'(x_\zeta)}, \quad (35)$$

$$x_{\zeta+1} = z_\zeta - k \cdot (2w_\zeta + 4t_\zeta w_\zeta + t_\zeta + t_\zeta^2) \cdot s_\zeta \cdot \frac{g(x_\zeta)}{g'(x_\zeta)},$$

where $s_\zeta = [(g(y_\zeta)/g(x_\zeta))]^{(1/k)}$, $t_\zeta = [(g(z_\zeta)/g(y_\zeta))]^{(1/k)}$, $w_\zeta = [(g(z_\zeta)/g(x_\zeta))]^{(1/k)}$.

We compare our methods with another three-step optimal eighth order family presented by Zafar et al. [20], given in (5). We select the following special case of their scheme denoted by ZM3:

$$y_\zeta = x_\zeta - k \cdot \frac{g(x_\zeta)}{g'(x_\zeta)}, \quad \zeta \geq 0,$$

$$z_\zeta = y_\zeta - k \cdot (1 + 6s_\zeta^3 - s_\zeta^2 + 2s_\zeta) \cdot s_\zeta \cdot \frac{g(x_\zeta)}{g'(x_\zeta)},$$

$$x_{\zeta+1} = z_\zeta - k \cdot (2t_\zeta + 1) \cdot (w_\zeta + 1) \cdot (2s_\zeta + 1) \cdot s_\zeta \cdot \frac{g(x_\zeta)}{g'(x_\zeta)}, \quad (36)$$

where $s_\zeta = [(g(y_\zeta)/g(x_\zeta))]^{(1/k)}$, $w_\zeta = [(g(z_\zeta)/g(y_\zeta))]^{(1/k)}$, $t_\zeta = [(g(z_\zeta)/g(x_\zeta))]^{(1/k)}$.

Comparison has been made on the basis of $|g(x_\zeta)|$, that is, function value at x_ζ or also known as the absolute residual error, $|x_\zeta - \alpha|$, that is, the absolute error approximation to the sought zero at each iteration, $AEC = |(x_{\zeta+1} - x_\zeta)/(x_\zeta - x_{\zeta-1})^r|$ (r represents the order of convergence), that is, the asymptotic error constant and COC $\approx (\log(|x_{\zeta+1} - \alpha|/|x_\zeta - \alpha|)/\log(|x_\zeta - \alpha|/|x_{\zeta-1} - \alpha|))$ (formula given by Jay [21]), that is, the computational order of convergence. Tables 1–7 show the comparison of the methods BM1, AM2, and ZM3, given in (34), (35), and (36), with our newly developed methods SFM1, SFM2, and SFM3. The programming packages Maple 18 and Wolfram Mathematica 8 have been used to perform all the computational works for the numerical and theoretical results. The calculations for numerical results have been made by using several (minimum 1000) number of significant digits of precision. Due to limited space of paper, numerical results are displayed up to only four decimal places.

Example 1. Van der Waals' equation of state

Van der Waals' equation is particularly useful in our effort to understand the behavior of real gases, because it embodies a simple physical picture for the difference between a real and an ideal gas. We know the ideal gas law as

$$PV = nRT. \quad (37)$$

The relationship between the pressure P , the volume V , and the temperature T for real gases is the Van der Waals' equation expressed as

$$\left(P + \frac{\beta_1 n^2}{V^2}\right)(V - n\beta_2) = nRT. \quad (38)$$

This expression explains the behavior of real gas by taking in the ideal gas equation. The involving two parameters β_1 and β_2 are specific for each gas. We require the solution of the following nonlinear function in V to determine the volume V of the gas in terms of the remaining parameters:

$$PV^3 - (n\beta_2 P + nRT)V^2 + \beta_1 n^2 V - \beta_1 \beta_2 n^3 = 0. \quad (39)$$

Considering the involving parameters β_1 and β_2 of a particular gas, one can find values for n , P , and T . By the implementation of particular values, we have the below given nonlinear function:

$$g_1(x) = x^3 - 5.22x^2 + 9.0825x - 5.2675, \quad (40)$$

where $g_1(x)$ has three roots. One is simple root $\alpha = 1.72$ and the other is a multiple zero $\alpha = 1.75$ of multiplicity 2. We considered the initial approximation $x_0 = 1.8$ for this test problem. The computational results are mentioned in Table 1.

Regarding the results shown in Table 1, the convergence behavior of newly developed methods SFM1, SFM2, and SFM3 is far better than the earlier known methods BM1, AM2, and ZM3 for the test problem $g_1(x)$. The comparison of function value at x_ζ and absolute error shows that SFM2 and SFM3 have smaller error values than the existing known methods.

Example 2. Beam designing model.

We consider a beam positioning problem [22] where a beam of p unit length is straight towards the edge of the cubical box having 1 unit length of each side. One end of the beam touches the wall and the other end touches with the floor, as depicted in Figure 1.

We have problem here to measure the distance alongside the floor from the base of the wall to the bottom of the beam. Assume that x is the distance in units from the bottom of the beam at floor to the bottom of the box and let y be the distance in units from the bottom of the beam at floor to the edge of the box, along the beam. Then, by employing a specific value of p , we have the following nonlinear equation:

$$g_2(x) = x^4 + 4x^3 - 24x^2 + 16x + 16 = 0, \quad (41)$$

having a multiple zero $\alpha = 2.0$ of multiplicity 2. We considered the initial approximation $x_0 = 2.5$ for this test function. The comparison results are depicted in Table 2.

TABLE 1: Convergence behavior of different iterative methods for $g_1(x)$.

$g_1(x) = x^3 - 5.22x^2 + 9.0825x - 5.2675, x_0 = 1.8$						
	ζ	x_ζ	$ g(x_\zeta) $	$ x_\zeta - \alpha $	AEC	COC
BM1	1	1.75	9.9347×10^{-9}	5.7007×10^{-4}		
	2	1.75	5.5189×10^{-32}	1.3563×10^{-15}	7.9067×10^5	
	3	1.75	8.4215×10^{-218}	1.6754×10^{-108}	6.9320×10^7	7.990
AM2	1	1.75	6.6085×10^{-9}	4.6574×10^{-4}		
	2	1.75	3.1520×10^{-33}	3.2414×10^{-16}	1.2849×10^7	
	3	1.75	1.4151×10^{-227}	2.1718×10^{-113}	1.464×10^{11}	7.990
ZM3	1	1.75	4.5788×10^{-9}	3.8817×10^{-4}		
	2	1.75	7.9903×10^{-35}	5.1608×10^{-17}	1.057×10^7	
	3	1.75	1.0549×10^{-240}	5.9301×10^{-120}	1.001×10^{11}	7.992
SFM1	1	1.75	5.5235×10^{-9}	4.2607×10^{-4}		
	2	1.75	2.0673×10^{-34}	8.3013×10^{-17}	1.1680×10^7	
	3	1.75	1.2060×10^{-237}	2.0050×10^{-118}	7.6431×10^{10}	7.992
SFM2	1	1.75	1.0796×10^{-9}	1.8910×10^{-4}		
	2	1.75	3.6782×10^{-42}	1.1072×10^{-20}	4.990×10^6	
	3	1.75	7.7223×10^{-302}	1.6044×10^{-150}	6.7693×10^9	7.998
SFM3	1	1.75	5.0786×10^{-9}	4.0867×10^{-4}		
	2	1.75	7.3241×10^{-35}	4.9410×10^{-17}	1.117×10^7	
	3	1.75	2.0151×10^{-241}	2.5917×10^{-120}	6.350×10^{10}	7.993

TABLE 2: Convergence behavior of different iterative methods for $g_2(x)$.

$g_2(x) = x^4 + 4x^3 - 24x^2 + 16x + 16, x_0 = 2.5$						
	ζ	x_ζ	$ g(x_\zeta) $	$ x_\zeta - \alpha $	AEC	COC
BM1	1	2.0	3.2691×10^{-9}	1.1671×10^{-5}		
	2	2.0	1.1447×10^{-81}	6.9063×10^{-42}	1.494×10^{-3}	
	3	2.0	2.5882×10^{-661}	1.0384×10^{-331}	2.341×10^{-7}	7.99
AM2	1	2.0	2.4815×10^{-9}	1.0168×10^{-5}		
	2	2.0	2.1471×10^{-82}	2.9910×10^{-42}	2.603×10^{-3}	
	3	2.0	6.7449×10^{-667}	1.6764×10^{-334}	2.616×10^{-2}	7.99
ZM3	1	2.0	1.1173×10^{-9}	6.8232×10^{-6}		
	2	2.0	1.5102×10^{-85}	7.9327×10^{-44}	1.746×10^{-3}	
	3	2.0	1.6824×10^{-692}	2.6477×10^{-347}	1.688×10^{-2}	7.99
SFM1	1	2.0	1.1137×10^{-9}	6.8121×10^{-6}		
	2	2.0	8.0859×10^{-86}	5.8044×10^{-44}	1.744×10^{-3}	
	3	2.0	6.2434×10^{-695}	1.6128×10^{-348}	1.251×10^{-2}	7.99
SFM2	1	2.0	1.2487×10^{-11}	7.2132×10^{-7}		
	2	2.0	7.0178×10^{-104}	5.4074×10^{-53}	1.846×10^{-4}	
	3	2.0	6.9822×10^{-842}	5.3937×10^{-422}	7.377×10^{-4}	7.99
SFM3	1	2.0	8.4488×10^{-10}	5.9332×10^{-6}		
	2	2.0	5.7599×10^{-87}	1.5491×10^{-44}	1.519×10^{-3}	
	3	2.0	2.6878×10^{-704}	3.3465×10^{-353}	1.008×10^{-2}	7.99

The comparison results of the model presented in Table 2 show the newly developed schemes SFM1, SFM2, and SFM3 are not only convergent but also their speed of convergence is better than BM1, AM2, and ZM3.

Example 3. Further, we consider the standard test problem involving trigonometric function is as follows:

$$g_3(x) = (\sin^2 x + x)^5, \quad (42)$$

having a root $\alpha = 0.0$ of multiplicity 5. We considered the initial approximation $x_0 = 0.2$ for this test problem. The numerical results are shown in Table 3.

In Table 3, it can be seen that the newly proposed methods SFM2 and SFM3 are computationally more efficient than all other methods BM1, AM2, and ZM3 for the test function $g_3(x)$. Among all the methods, convergence behavior of SFM2 is very efficient and results of SFM1 are comparable with ZM3.

TABLE 3: Convergence behavior of different iterative methods for $g_3(x)$.

$g_3(x) = (\sin^2 x + x)^5, x_0 = 0.2$						
	ζ	x_ζ	$ g(x_\zeta) $	$ x_\zeta - \alpha $	AEC	COC
BM1	1	0.0	2.7742×10^{-22}	4.8821×10^{-5}		
	2	0.0	7.2420×10^{-161}	9.3750×10^{-33}	3.820	
	3	0.0	1.5699×10^{-1269}	1.7345×10^{-254}	0.014	7.99
AM2	1	0.0	9.2496×10^{-23}	3.9192×10^{-5}		
	2	0.0	5.0593×10^{-164}	2.1918×10^{-33}	15.333	
	3	0.0	4.0762×10^{-1294}	2.0991×10^{-259}	393.69	7.99
ZM3	1	0.0	1.4220×10^{-23}	2.6950×10^{-5}		
	2	0.0	1.6273×10^{-171}	6.9550×10^{-35}	10.539	
	3	0.0	4.8042×10^{-1355}	1.3687×10^{-271}	249.86	7.99
SFM1	1	0.0	2.04471×10^{-23}	2.8981×10^{-5}		
	2	0.0	6.3062×10^{-171}	9.1191×10^{-35}	11.333	
	3	0.0	5.1803×10^{-1351}	8.7674×10^{-271}	183.24	7.99
SFM2	1	0.0	9.0702×10^{-28}	3.9041×10^{-6}		
	2	0.0	2.2390×10^{-212}	4.6775×10^{-43}	1.5252	
	3	0.0	3.0889×10^{-1689}	1.9859×10^{-338}	8.6663	7.99
SFM3	1	0.0	1.1580×10^{-23}	2.5866×10^{-5}		
	2	0.0	2.1367×10^{-173}	2.9238×10^{-35}	10.114	
	3	0.0	2.8788×10^{-1371}	7.7954×10^{-275}	145.90	7.99

TABLE 4: Convergence behavior of different iterative methods for $g_4(x)$.

$g_4(x) = (x - 1)(x \ln(x) - \sqrt{x} + x^4)^2, x_0 = 1.2$						
	ζ	x_ζ	$ g(x_\zeta) $	$ x_\zeta - \alpha $	AEC	COC
BM1	1	1.0	5.0023×10^{-12}	6.2741×10^{-5}		
	2	1.0	2.2328×10^{-93}	4.7952×10^{-32}	4.9124	
	3	1.0	3.5294×10^{-744}	3.5294×10^{-249}	0.0125	7.99
AM2	1	1.0	2.8876×10^{-12}	5.2241×10^{-5}		
	2	1.0	8.9735×10^{-95}	1.6425×10^{-32}	20.449	
	3	1.0	7.8338×10^{-755}	1.5698×10^{-252}	296.052	7.99
ZM3	1	1.0	8.1638×10^{-13}	3.4287×10^{-5}		
	2	1.0	8.7066×10^{-100}	3.5032×10^{-34}	13.412	
	3	1.0	1.4607×10^{-795}	4.1628×10^{-266}	183.375	7.99
SFM1	1	1.0	1.0911×10^{-12}	3.7768×10^{-5}		
	2	1.0	3.3006×10^{-99}	5.4625×10^{-34}	14.775	
	3	1.0	2.3195×10^{-791}	1.0463×10^{-264}	131.923	7.99
SFM2	1	1.0	3.7040×10^{-16}	2.6348×10^{-6}		
	2	1.0	1.6585×10^{-131}	9.3563×10^{-45}	1.0293	
	3	1.0	2.6810×10^{-1054}	2.3656×10^{-352}	4.0281	7.99
SFM3	1	1.0	7.2300×10^{-13}	3.2927×10^{-5}		
	2	1.0	5.8147×10^{-101}	1.4213×10^{-34}	12.879	
	3	1.0	1.0197×10^{-805}	1.7140×10^{-269}	102.858	7.99

Example 4. Now, we choose standard nonlinear problem involving logarithmic function, which is given as

$$g_4(x) = (x - 1)(x \ln(x) - \sqrt{x} + x^4)^2, \quad (43)$$

having a root $\alpha = 1.0$ of multiplicity 3. We considered the initial approximation $x_0 = 1.2$ for this test problem. The comparison results are depicted in Table 4.

In Table 4, we can see that the newly developed method performs better than the existing presented schemes BM1, AM2, and ZM3. However, ZM3 performs slightly better than

SFM1, for the test function $g_4(x)$. SFM2 performs very well among all the presented methods.

Example 5. We consider one more standard nonlinear test problem, which is as follows:

$$g_5(x) = (x^3 - 2x^2 + 1)^3. \quad (44)$$

We select $\alpha = 1.0$ multiple zero of multiplicity 6 for the computational point of view. The comparison results are shown in Table 5 corresponding to initial approximation $x_0 = 1.2$.

TABLE 5: Convergence behavior of different iterative methods for $g_5(x)$.

$g_5(x) = (x^3 - 2x^2 + 1)^3, x_0 = 1.2$						
	ζ	x_ζ	$ g(x_\zeta) $	$ x_\zeta - \alpha $	AEC	COC
BM1	1	1.0	6.0797×10^{-34}	1.4552×10^{-6}		
	2	1.0	5.9820×10^{-271}	4.5896×10^{-47}	0.113	
	3	1.0	5.2548×10^{-2221}	4.4915×10^{-371}	0.003	7.99
AM2	1	1.0	3.7688×10^{-34}	1.3438×10^{-6}		
	2	1.0	8.1145×10^{-278}	3.2898×10^{-47}	0.524	
	3	1.0	3.7475×10^{-2227}	4.2454×10^{-372}	3.093	7.99
ZM3	1	1.0	2.9165×10^{-35}	8.7723×10^{-7}		
	2	1.0	6.9307×10^{-288}	6.9039×10^{-49}	0.342	
	3	1.0	7.0488×10^{-2309}	1.0162×10^{-385}	1.968	7.99
SFM1	1	1.0	2.3448×10^{-35}	8.4590×10^{-7}		
	2	1.0	1.8939×10^{-289}	3.7890×10^{-49}	0.330	
	3	1.0	3.4308×10^{-2322}	6.1405×10^{-388}	1.445	7.99
SFM2	1	1.0	5.8129×10^{-42}	6.7045×10^{-8}		
	2	1.0	3.5820×10^{-350}	2.8707×10^{-59}	0.026	
	3	1.0	7.4467×10^{-2816}	3.2431×10^{-470}	0.070	7.99
SFM3	1	1.0	9.0965×10^{-36}	7.2240×10^{-7}		
	2	1.0	2.4977×10^{-293}	8.5486×10^{-50}	0.282	
	3	1.0	8.0724×10^{-2354}	3.2870×10^{-393}	1.152	7.99

TABLE 6: Convergence behavior of different iterative methods for $g_6(x)$.

$g_6(x) = ((x - 1)^3 - 1)^{50}, x_0 = 2.9$						
	ζ	x_ζ	$ g(x_\zeta) $	$ x_\zeta - \alpha $	AEC	COC
BM1	1	2.0	1.5168×10^{-39}	5.2931×10^{-2}		
	2	2.0	1.8108×10^{-381}	8.0916×10^{-9}	0.169	
	3	2.0	7.3247×10^{-3096}	4.1703×10^{-63}	6.951	7.93
AM2	1	2.0	7.2090×10^{-44}	4.3768×10^{-2}		
	2	2.0	4.8078×10^{-409}	2.2725×10^{-9}	0.1515	
	3	2.0	6.8409×10^{-3308}	2.3965×10^{-67}	168.72	7.93
ZM3	1	2.0	3.1076×10^{-48}	3.6070×10^{-2}		
	2	2.0	1.6232×10^{-450}	3.3657×10^{-10}	0.1162	
	3	2.0	4.3287×10^{-3650}	3.4324×10^{-74}	117.44	7.95
SFM1	1	2.0	7.4516×10^{-45}	4.1903×10^{-2}		
	2	2.0	2.8683×10^{-430}	8.5512×10^{-10}	0.1425	
	3	2.0	2.8294×10^{-3495}	4.2846×10^{-71}	89.952	7.95
SFM2	1	2.0	9.7376×10^{-71}	1.3091×10^{-2}		
	2	2.0	1.8913×10^{-699}	3.5352×10^{-15}	0.0341	
	3	2.0	9.3674×10^{-5725}	1.1023×10^{-115}	4.0984	7.99
SFM3	1	2.0	7.2719×10^{-46}	4.0070×10^{-2}		
	2	2.0	2.9188×10^{-442}	4.9224×10^{-10}	0.1340	
	3	2.0	1.2411×10^{-3596}	4.0249×10^{-73}	74.059	7.95

In Table 5, we observe that our new iterative schemes SFM1, SFM2, and SFM3 perform better than the existing schemes BM1, AM2, and ZM3 for test function $g_5(x)$.

Example 6. In addition, we select the below given standard nonlinear test function:

$$g_6(x) = ((x - 1)^3 - 1)^{50}. \tag{45}$$

This expression has a multiple zero at $\alpha = 2$ of multiplicity $k = 50$. The computational results with the initial approximation $x_0 = 2.9$ are mentioned in Table 6.

From Table 6, it is observed that computational efficiency of newly developed methods SFM1, SFM2, and SFM3 is better than the earlier known methods BM1 and AM2, whereas our scheme SFM2 is more efficient as compared to ZM3. However, performance of ZM3 is comparable with the new method SFM1 for function $g_6(x)$.

Example 7. We use the following standard test problem involving logarithmic function:

TABLE 7: Convergence behavior of different iterative methods for $g_7(x)$.

$g_7(x) = x^2(x^3 - \log(x^2 + 1))^2, x_0 = -0.9$						
	ζ	x_ζ	$ g(x_\zeta) $	$ x_\zeta - \alpha $	AEC	COC
BM1	1	-0.0	2.1027×10^{-23}	1.6612×10^{-4}		
	2	-0.0	7.4964×10^{-184}	3.0139×10^{-31}	3.4×10^{-4}	
	3	-0.0	1.9858×10^{-1467}	3.5453×10^{-245}	8.6×10^{-5}	7.99
AM2	1	-0.0	7.1551×10^{-24}	1.3880×10^{-4}		
	2	-0.0	9.7548×10^{-188}	6.7847×10^{-32}	3.2×10^{-4}	
	3	-0.0	1.1811×10^{-1498}	2.2150×10^{-250}	0.4922	7.99
ZM3	1	-0.0	2.8275×10^{-24}	1.1890×10^{-4}		
	2	-0.0	8.9533×10^{-192}	1.4410×10^{-32}	2.7×10^{-4}	
	3	-0.0	9.1591×10^{-1532}	6.7139×10^{-256}	0.3605	7.99
SFM1	1	-0.0	2.9473×10^{-24}	1.1973×10^{-4}		
	2	-0.0	3.5576×10^{-192}	1.2355×10^{-32}	2.7×10^{-4}	
	3	-0.0	1.6211×10^{-1535}	1.5908×10^{-256}	0.2924	7.99
SFM2	1	-0.0	3.7297×10^{-26}	5.7801×10^{-5}		
	2	-0.0	1.7193×10^{-211}	7.4569×10^{-36}	1.3×10^{-4}	
	3	-0.0	3.5209×10^{-1694}	5.7250×10^{-283}	5.9×10^{-2}	7.99
SFM3	1	-0.0	2.2186×10^{-24}	1.1419×10^{-4}		
	2	-0.0	1.6657×10^{-193}	7.4176×10^{-33}	2.6×10^{-4}	
	3	-0.0	1.6993×10^{-1546}	2.3534×10^{-258}	0.2564	7.99

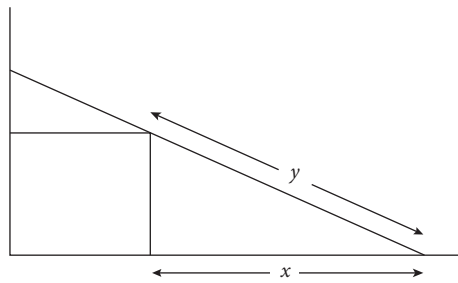


FIGURE 1: Beam positioning problem.

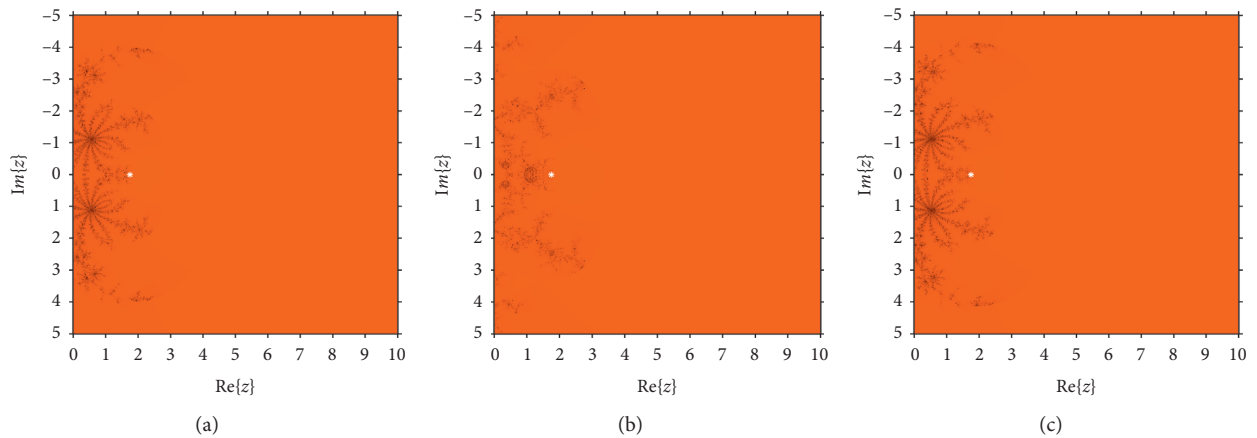


FIGURE 2: Basins of attraction of (a) SFM1, (b) SFM2, and (c) SFM3 for $g_1(x)$.

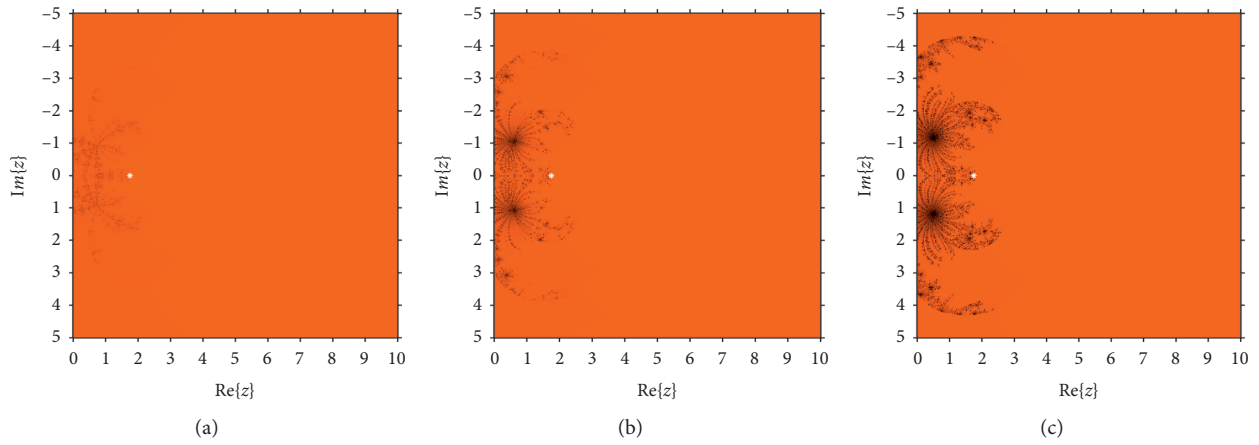


FIGURE 3: Basins of attraction of (a) BM1, (b) AM2, and (c) ZM3 for $g_1(x)$.

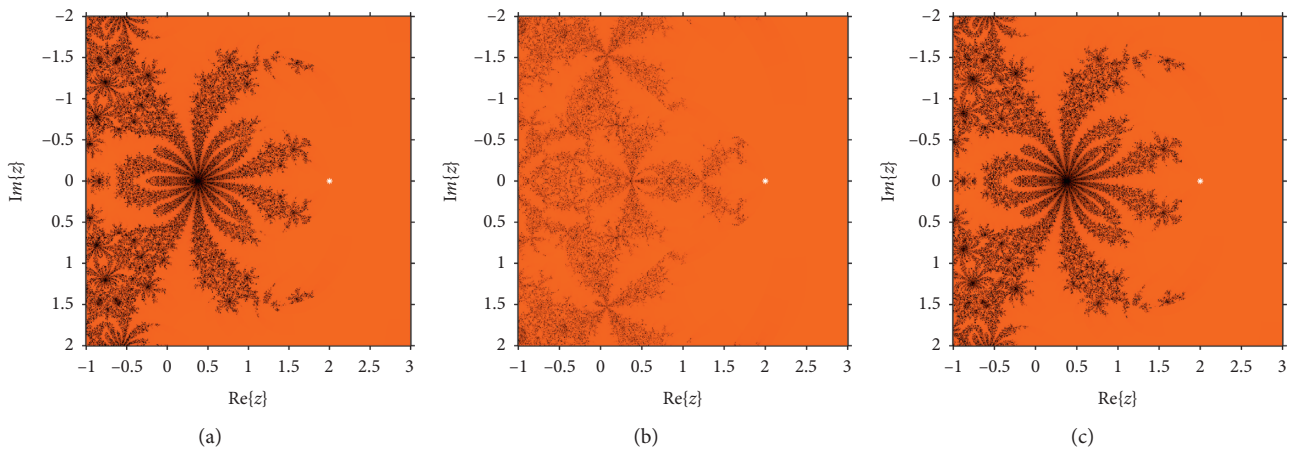


FIGURE 4: Basins of attraction of (a) SFM1, (b) SFM2, and (c) SFM3 for $g_2(x)$.

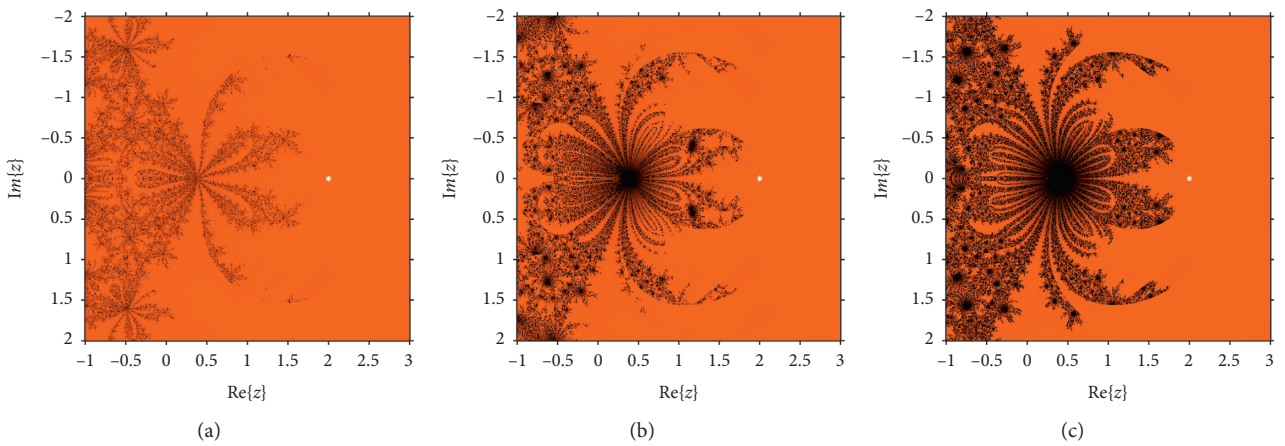


FIGURE 5: Basins of attraction of (a) BM1, (b) AM2, and (c) ZM3 for $g_2(x)$.

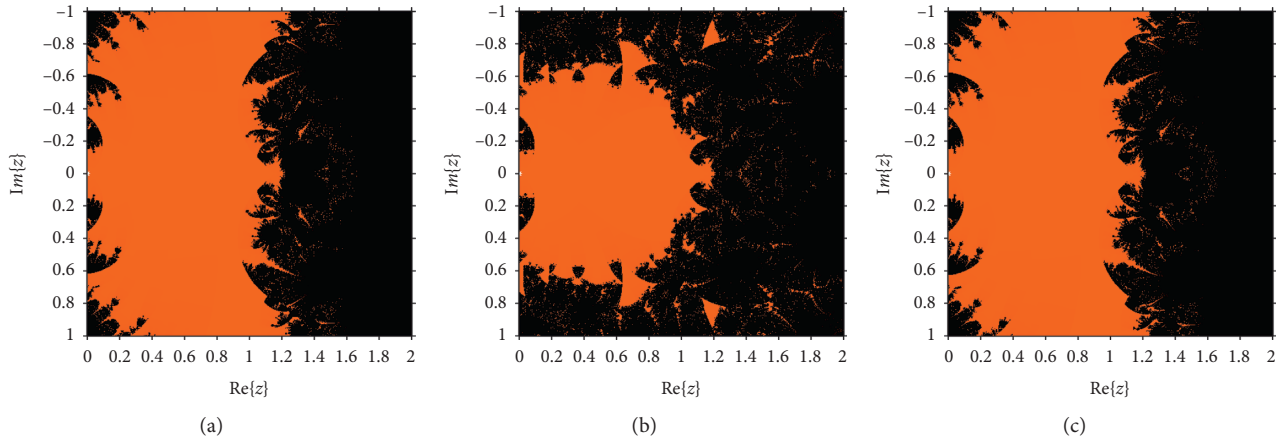


FIGURE 6: Basins of attraction of (a) SFM1, (b) SFM2, and (c) SFM3 for $g_3(x)$.

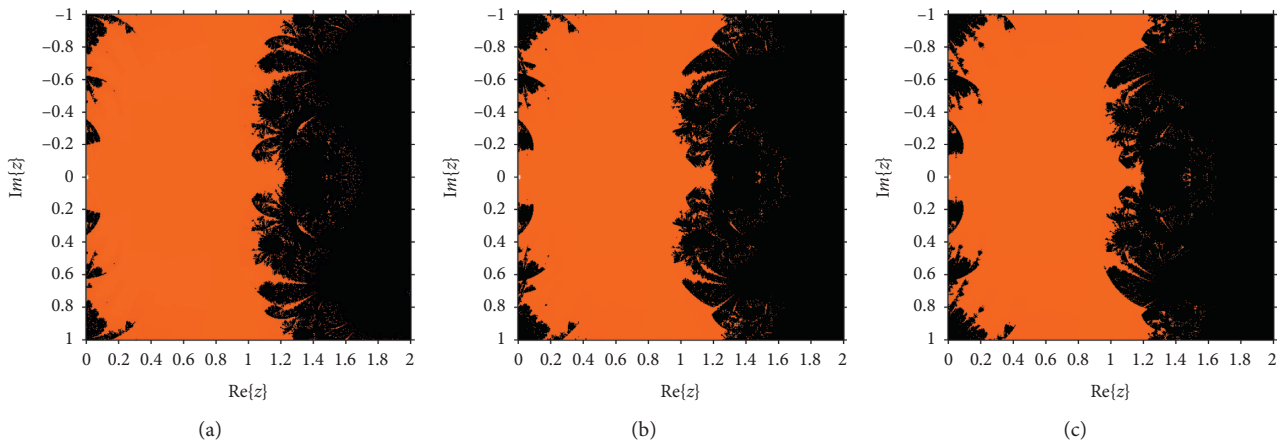


FIGURE 7: Basins of attraction of (a) BM1, (b) AM2, and (c) ZM3 for $g_3(x)$.

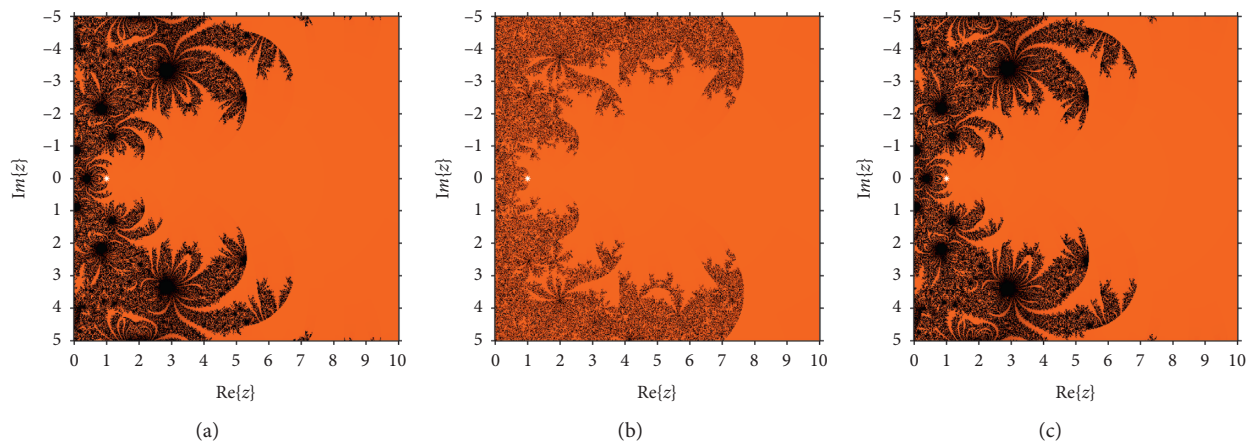


FIGURE 8: Basins of attraction of (a) SFM1, (b) SFM2, and (c) SFM3 for $g_4(x)$.

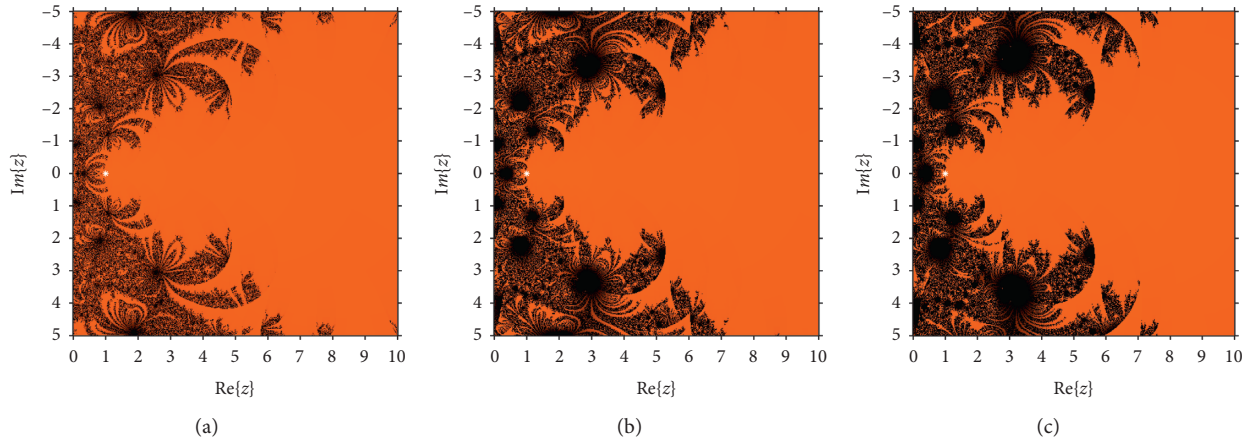


FIGURE 9: Basins of attraction of (a) BM1, (b) AM2, and (c) ZM3 for $g_4(x)$.

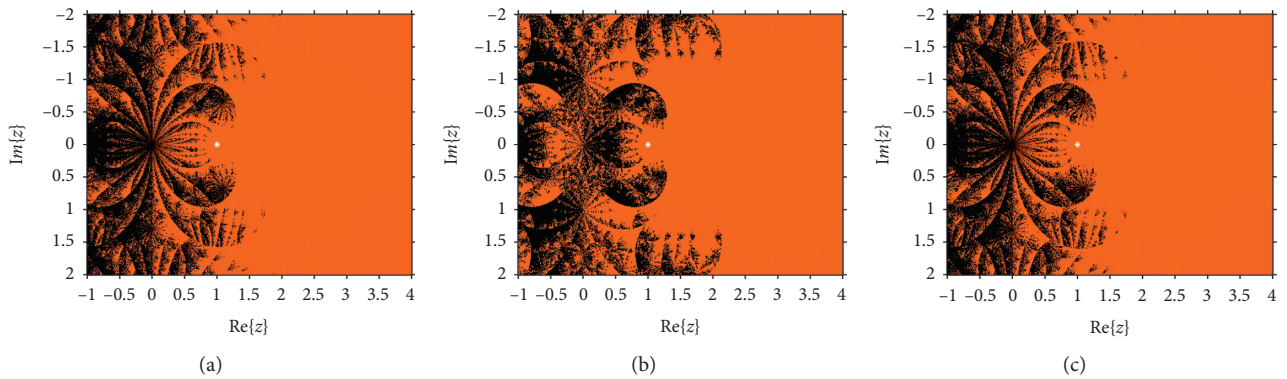


FIGURE 10: Basins of attraction of (a) SFM1, (b) SFM2, and (c) SFM3 for $g_5(x)$.

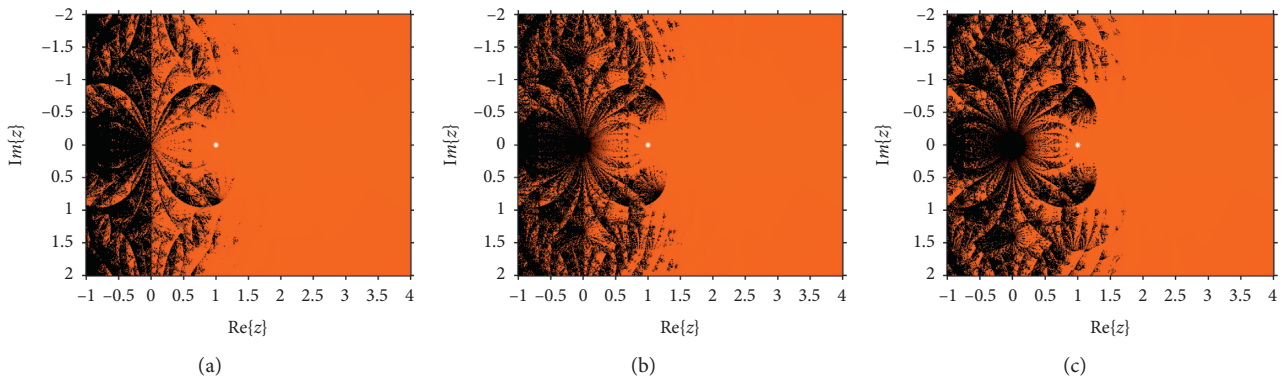


FIGURE 11: Basins of attraction of (a) BM1, (b) AM2, and (c) ZM3 for $g_5(x)$.

$$g_7(x) = x^2(x^3 - \log(x^2 + 1))^2, \quad (46)$$

having multiple zero $\alpha = 0.0$ of multiplicity 6. We choose the initial guess $x_0 = -0.9$ for the comparison results shown in Table 7.

From Table 7, it can be observed that the newly developed schemes SFM1, SFM2, and SFM3 give the faster

convergence and smaller errors than the earlier known methods for test function $g_7(x)$ and these numerical results confirm the robust nature of our presented iterative method.

It can be seen from the results depicted in Tables 1–7 that the special cases of our newly developed methods SFM1, SFM2, and SFM3 are faster, efficient, and reliable than the existing known methods BM1, AM2, and ZM3 in terms of absolute error and computational order of convergence, etc.

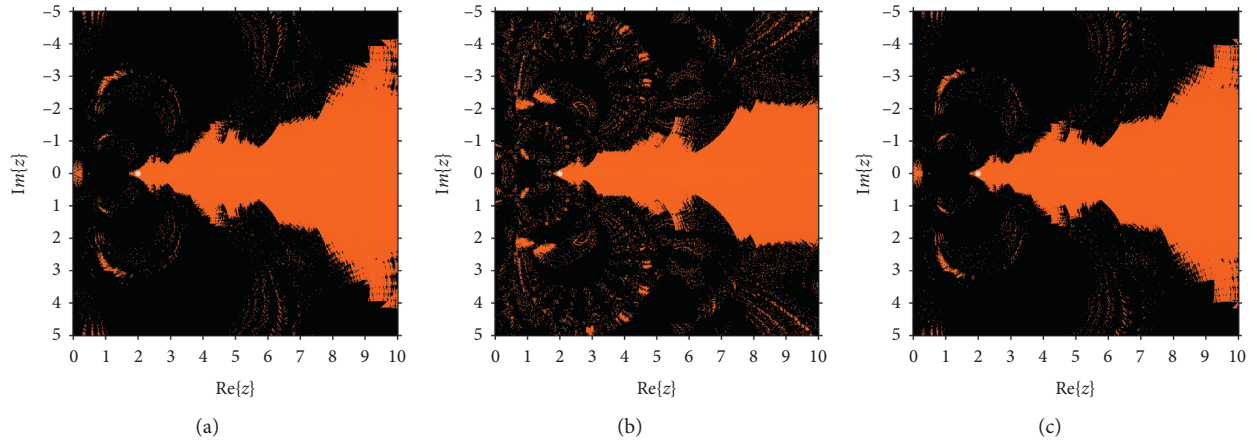


FIGURE 12: Basins of attraction of (a) SFM1, (b) SFM2, and (c) SFM3 for $g_6(x)$.

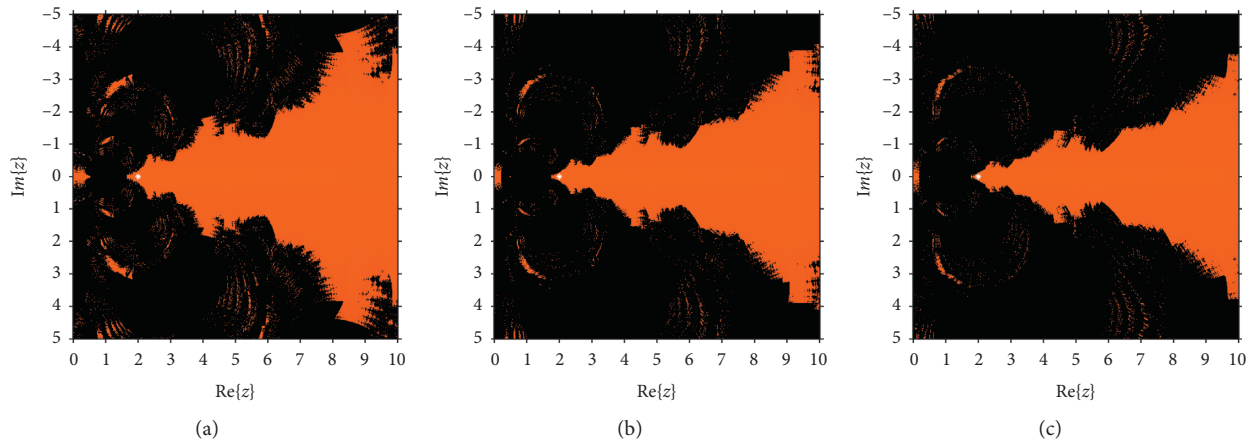


FIGURE 13: Basins of attraction of (a) BM1, (b) AM2, and (c) ZM3 for $g_6(x)$.

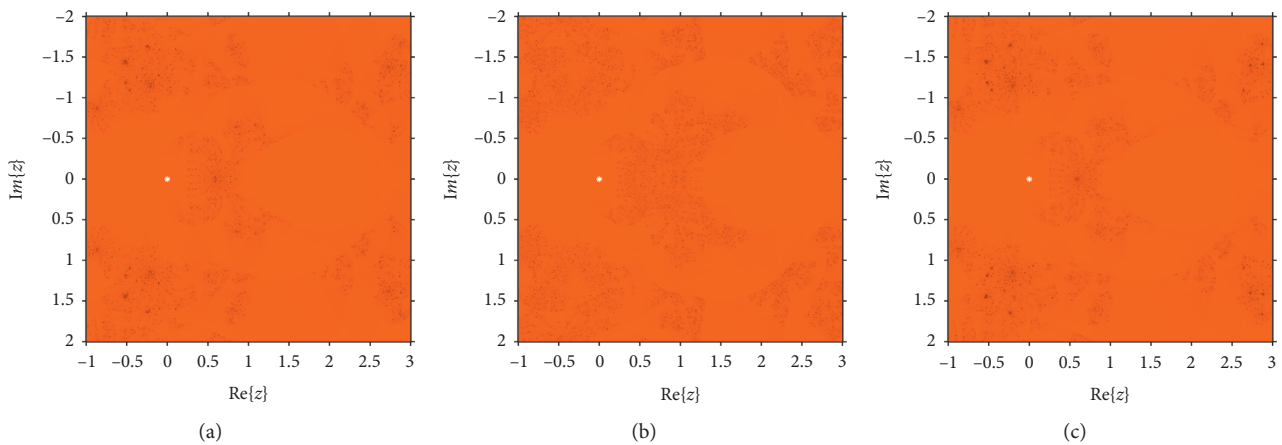


FIGURE 14: Basins of attraction of (a) SFM1, (b) SFM2, and (c) SFM3 for $g_7(x)$.

We conclude that the newly developed family gives the faster convergence, small absolute, and residual error corresponding to the involved function. It is also observed

that, in most cases, SFM2 is faster among all schemes. Therefore, the new presented schemes are better alternatives to the present schemes.

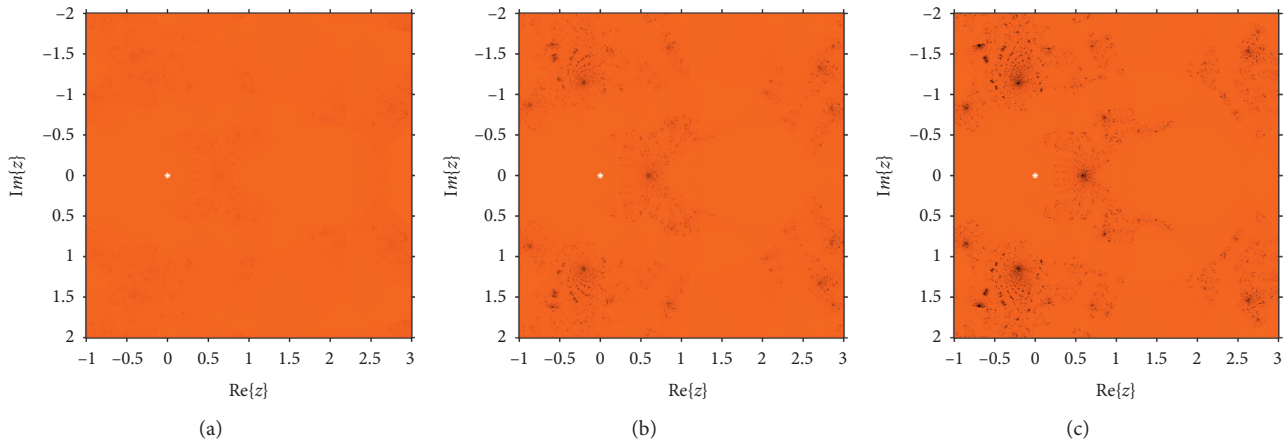


FIGURE 15: Basins of attraction of (a) BM1, (b) AM2, and (c) ZM3 for $g_7(x)$.

5. Complex Dynamics

Regarding the dynamical behavior, our goal is to observe and compare the performance of proposed methods by means of a graphical tool, named as the basins of attraction. Initially, Vrscay and Gilbert [23] suggest this idea to investigate the convergence and dynamical behavior of iterative schemes. For the sake of stability comparison, we plot the dynamical planes corresponding to each scheme, SFM1, SFM2, SFM3, BM1, AM2, and ZM3, for the nonlinear functions $g_1(x)$, $g_2(x)$, $g_3(x)$, $g_4(x)$, $g_5(x)$, $g_6(x)$, and $g_7(x)$ used for numerical comparison in Section 4. The complex dynamical planes presented in Figures 2–15 have been generating by using the procedure defined in [1]. Regarding the stability comparison, a mesh of $[500 \times 500]$ points is defined in the region of the complex plane to check how wide the set of initial guess leads us to the desired repeated root. We used to work out up to a total number of 80 iterations with the stopping criterion 10^{-3} . If the iteration sequence converges to the multiple root, then the convergence region is painted in orange colour. The divergence region is painted in black colour, when the iteration sequence does not converge to the multiple root or converge to strange fixed points (which are not roots of nonlinear function). A white star represents the multiple zero in Figures 2–15.

Figures 2–15 show the study of the convergence and divergence regions of the new schemes SFM1, SFM2, and SFM3 in comparison with the other schemes of the same order. It is observed that our methods SFM1, SFM2, and SFM3 have more wider convergence region than the earlier ones BM1, AM2, and ZM3. In the case of $g_1(x)$, $g_2(x)$, and $g_6(x)$, we observed that the new schemes SFM1, SFM2, and SFM3 are more stable than BM1, AM2, and ZM3 as they are almost divergence-free and converge faster than BM1, AM2, and ZM3 in their common regions of convergence. So, the stable and consistent nature of newly developed scheme is clear from the graphics.

6. Conclusion

In this paper, we have presented a new general family of optimal iterative methods for finding multiple roots of

nonlinear equations with known multiplicity using weight functions. An extensive convergence analysis is presented to verify the optimal convergence of the new family. Some special cases of the family are also presented which require only three-function and one-derivative evaluations at each iteration to reach optimal eighth order convergence. A variety of numerical test functions along with some real-world problems such as beam positioning model and Van der Waals' equation of state are used to ensure that the newly developed family efficiently competes with the other existing methods. The dynamical analysis of the proposed methods is also presented to validate the theoretical results by using graphical tool, termed as the basins of attraction. As the proposed methods are sensitive towards initial guess, so for the safe selection of initial guess, convergence regions are presented. Figures 2–15 show that our newly developed schemes have wider regions of convergence. Hence, we have more choices for initial guess to choose from. Finally, our newly presented scheme shows stable behavior in complex plane and validates the theoretical results. By considering the above stated facts, it is concluded that the new methods SFM1, SFM2, and SFM3 are efficient, stable, and robust among the existing schemes of their domain.

Data Availability

No data were used to support this study.

Conflicts of Interest

The authors declare that they have no conflicts of interest.

References

- [1] N. A. Mir, M. Shams, N. Rafiq, S. Akram, and R. Ahmed, "On family of simultaneous method for finding distinct as well as multiple roots of Non-Linear polynomial equation," *PUJM*, vol. 52, no. 6, pp. 31–44, 2020.
- [2] M. S. Petkovi'c, B. Neta, L. D. Petkovic, and J. D. zunic, *Multipoint Methods for Solving Non-Linear Equations*, Academic Press, New York, NY, USA, pp. 635–660, 2014.

- [3] N. Rafiq, S. Akram, N. A. Mir, and M. Shams, "Study of dynamical behavior and stability of iterative methods for nonlinear equation with applications in engineering," *Mathematical Problems in Engineering*, vol. 2020, Article ID 3524324, 2020.
- [4] M. Shams, N. A. Mir, N. Rafiq, A. O. Almatroud, and S. Akram, "On dynamics of iterative techniques for nonlinear equation with applications in engineering," *Mathematical Problems in Engineering*, vol. 2020, Article ID 5853296, 2020.
- [5] J. F. Traub, *Iterative Methods for the Solution of Equations*, Prentice-Hall, Englewood Cliffs, NJ, USA, 1964.
- [6] L. B. Rall, "Convergence of the Newton process to multiple solutions," *Numerische Mathematik*, vol. 9, no. 1, pp. 23–37, 1966.
- [7] R. Behl, A. Cordero, S. S. Motsa, and J. R. Torregrosa, "On developing fourth-order optimal families of methods for multiple roots and their dynamics," *Applied Mathematics and Computation*, vol. 265, no. 15, pp. 520–532, 2015.
- [8] R. Behl, A. Cordero, S. S. Motsa, J. R. Torregrosa, and V. Kanwar, "An optimal fourth-order family of methods for multiple roots and its dynamics," *Numerical Algorithms*, vol. 71, no. 4, pp. 775–796, 2016.
- [9] F. Soleymani, D. K. R. Babajee, and T. Lotfi, "On a numerical technique for finding multiple zeros and its dynamic," *Journal of the Egyptian Mathematical Society*, vol. 21, no. 3, pp. 346–353, 2013.
- [10] R. Thukral, "A new family of fourth-order iterative methods for solving non-linear equations with multiple roots," *Journal of Numerical Mathematics and Stochastics*, vol. 6, no. 1, pp. 37–44, 2014.
- [11] X. Zhou, X. Chen, and Y. Song, "Constructing higher-order methods for obtaining the multiple roots of nonlinear equations," *Journal of Computational and Applied Mathematics*, vol. 235, no. 14, pp. 4199–4206, 2011.
- [12] R. Thukral, "Introduction to higher-order iterative methods for finding multiple roots of nonlinear equations," *Journal of Mathematics*, vol. 2013, Article ID 404635, 2013.
- [13] Y. H. Geum, Y. I. Kim, and B. Neta, "A class of two-point sixth-order multiple-zero finders of modified double-Newton type and their dynamics," *Applied Mathematics and Computation*, vol. 270, pp. 387–400, 2015.
- [14] Y. H. Geum, Y. I. Kim, and B. Neta, "A sixth-order family of three-point modified Newton-like multiple-root finders and the dynamics behind their extraneous fixed points," *Applied Mathematics and Computation*, vol. 283, pp. 120–140, 2016.
- [15] J. R. Sharma, D. Kumar, and C. Cattani, "An efficient class of weighted-Newton multiple root solvers with seventh order convergence," *Symmetry*, vol. 11, no. 8, p. 1054, 2019.
- [16] H. T. Kung and J. F. Traub, "Optimal order of one-point and multipoint iteration," *Journal of the ACM*, vol. 21, no. 4, pp. 643–651, 1974.
- [17] A. M. Ostrowski, *Solution of Equations and Systems of Equations*, Academic Press, Cambridge, MA, USA, 1960.
- [18] R. Behl, A. Cordero, S. S. Motsa, and J. R. Torregrosa, "An eighth-order family of optimal multiple root finders and its dynamics," *Numerical Algorithms*, vol. 77, no. 4, pp. 1249–1272, 2018.
- [19] S. Akram, F. Zafar, and N. Yasmin, "An optimal eighth-order family of iterative methods for multiple roots," *Mathematics*, vol. 7, no. 8, p. 672, 2019.
- [20] F. Zafar, A. Cordero, R. Quratulain, and J. R. Torregrosa, "Optimal iterative methods for finding multiple roots of nonlinear equations using free parameters," *Journal of Mathematical Chemistry*, vol. 56, no. 7, pp. 1884–1901, 2017.
- [21] L. O. Jay, "A note on Q-order of convergence," *Bit Numerical Mathematics*, vol. 41, no. 2, pp. 422–429, 2001.
- [22] J. L. Zachary, *Introduction to Scientific Programming, Computational Problem Solving Using Maple and C*, Springer, New York, NY, USA, 2012.
- [23] E. R. Vrscay and W. J. Gilbert, "Extraneous fixed points, basin boundaries and chaotic dynamics for Schröder and König rational iteration functions," *Numerische Mathematik*, vol. 52, no. 1, pp. 1–16, 1987.

Retraction

Retracted: Evaluation of SMEs' Credit Decision Based on Support Vector Machine-Logistics Regression

Journal of Mathematics

Received 15 August 2023; Accepted 15 August 2023; Published 16 August 2023

Copyright © 2023 Journal of Mathematics. This is an open access article distributed under the Creative Commons Attribution License, which permits unrestricted use, distribution, and reproduction in any medium, provided the original work is properly cited.

This article has been retracted by Hindawi following an investigation undertaken by the publisher [1]. This investigation has uncovered evidence of one or more of the following indicators of systematic manipulation of the publication process:

- (1) Discrepancies in scope
- (2) Discrepancies in the description of the research reported
- (3) Discrepancies between the availability of data and the research described
- (4) Inappropriate citations
- (5) Incoherent, meaningless and/or irrelevant content included in the article
- (6) Peer-review manipulation

The presence of these indicators undermines our confidence in the integrity of the article's content and we cannot, therefore, vouch for its reliability. Please note that this notice is intended solely to alert readers that the content of this article is unreliable. We have not investigated whether authors were aware of or involved in the systematic manipulation of the publication process.

Wiley and Hindawi regrets that the usual quality checks did not identify these issues before publication and have since put additional measures in place to safeguard research integrity.

We wish to credit our own Research Integrity and Research Publishing teams and anonymous and named external researchers and research integrity experts for contributing to this investigation.

The corresponding author, as the representative of all authors, has been given the opportunity to register their agreement or disagreement to this retraction. We have kept a record of any response received.

References

- [1] R. Xie, R. Liu, X. Liu, and J. Zhu, "Evaluation of SMEs' Credit Decision Based on Support Vector Machine-Logistics Regression," *Journal of Mathematics*, vol. 2021, Article ID 5541436, 10 pages, 2021.

Research Article

Evaluation of SMEs' Credit Decision Based on Support Vector Machine-Logistics Regression

Rui Xie ¹, Rui Liu ¹, Xian-Bei Liu ², and Jia-Ming Zhu ²

¹School of Accounting, Anhui University of Finance and Economics, Bengbu 233030, China

²School of Statistics and Applied Mathematics, Anhui University of Finance & Economics, Bengbu 233030, China

Correspondence should be addressed to Jia-Ming Zhu; zhujm1973@163.com

Received 26 January 2021; Revised 12 February 2021; Accepted 23 February 2021; Published 4 March 2021

Academic Editor: Ghulam Mustafa

Copyright © 2021 Rui Xie et al. This is an open access article distributed under the Creative Commons Attribution License, which permits unrestricted use, distribution, and reproduction in any medium, provided the original work is properly cited.

This article uses support vector machines, logistics regression, and other methods for the comprehensive evaluation of credit decision-making of small, medium, and microenterprises and comprehensively uses software programming such as MATLAB and SPSS Modeler to solve the problem. The results, such as credit risk evaluation index system, credit risk classification model, and credit decision-making comprehensive evaluation model, are obtained. Finally, this article starts from the credit decision of small, medium, and microenterprises and provides theoretical and practical suggestions for banks to control the risks of small, medium, and microenterprises and their own development.

1. Introduction

In the context of economic globalization, our country's economy is booming. Small- and medium-sized enterprises, known as the "new economic turning point," have sprung up. They have played a huge role in the country's industrial upgrading and economic construction and have gradually become the economic pillars of various regions. However, under negative conditions such as inadequate economic volume, loose economic system, and high financing costs, small, medium, and microenterprises are gradually in a disadvantaged position under the background of environmental competition and face the risk of being merged by companies in the same industry. They urgently need to "make blood" for enterprises through direct financing and indirect financing and solve the problem of financing difficulties, which is a stumbling block on the development of small, medium, and microenterprises.

The main reasons are the following two aspects: on the one hand, due to the pressure of the competitive environment in the same industry, small, medium, and microenterprises cannot provide the same accurate and reliable assessment

information as mature enterprises, which causes commercial banks to face the challenge of credit risk management; on the one hand, due to a loose management system and insufficient managerial experience, legal loopholes and moral hazards appear, which affect the order of the credit market and disrupt the market balance. Nowadays, encouraging and protecting the active development of small- and medium-sized enterprises have become a new economic trend. Banks urgently need to solve the problems of whether to lend to enterprises and how much to allocate to enterprises.

The data in this article come from the 2020 China National College Students Mathematical Modeling Contest Question C: A bank's loan amount to companies determined to lend is 100,000 to 1 million yuan; the annual interest rate is 4% to 15%; the loan period is 1 year, which is known statistics on the relationship between 123 companies with credit records and 302 companies without credit records and the relationship between loan interest rates and customer churn rates in 2019. Through the establishment of a mathematical model, the bank's credit strategy for small, medium, and microenterprises is studied under certain conditions.

2. Literature Review

Regarding the evaluation of credit decision-making for small, medium, and microenterprises, Gen [1] took Shandong Province as an example to analyze the causes of credit rationing misbehavior and ways to correct them and provide a way to improve the efficiency of credit rationing and realize the Pareto improvement of credit resource allocation. Wang and Tang [2] compared the allocation of bank financing opportunities and the expected loans of enterprises and found that banks' credit decisions are based on rational risk control decisions, while the discrimination against SMEs in lending is due to the recognition of both banks and enterprises, caused by gaps in knowledge and lag in cognition. Wu [3] combined the actual characteristics of SMEs and used fuzzy analytic hierarchy process to determine the weight of SME credit risk evaluation indicators and constructed a scientific and reasonable credit risk evaluation indicator system for SMEs. Li [4] believes that our country's banking industry's credit decisions on SMEs have problems such as low quality of preloan review, long loan approval cycles, and difficulty in implementing postloan management. Commercial banks should control the production and financial status of SMEs. Reasonable evaluation of its guarantee capacity will improve the quality of credit support decision-making for SMEs.

The abovementioned documents all give relevant opinions on banks' credit for small- and medium-sized enterprises, but most of them are based on theoretical research in a specific situation and do not give a more universal model that includes dynamic factors. Aiming at the abovementioned shortcomings, this paper attempts to establish a relatively general credit model by establishing a related mathematical model.

3. Basic Assumptions

In order to facilitate the handling of the problem, the following assumptions are proposed: (i) assuming that when banks make loan decisions to SMEs, there is no corporate loan failure; (ii) assuming that there are no changes in macropolicy when banks make loan decisions to SMEs; (iii) assumptions: the average supply and demand of available companies can represent the stable value of supply and demand; (iv) assuming that the impact of unexpected factors on the enterprise is mainly the impact on the amount of sales invoices of the enterprise; (v) assuming that the reputation of small, medium, and microenterprises is only determined by the research variables in this article.

4. Based on Multiobjective Optimization, the Credit Risk and Strategy Research of SMEs when the Bank's Annual Total Credit Is Fixed

4.1. Research Thought. It is required to quantitatively analyze the credit risk of 123 companies in the data source when the loan period is one year and when the bank's annual total credit is fixed, and for companies that are determined to lend, the loan line of each company is

100,000 to 1 million yuan, and the annual interest rate is 4%–15%; give credit strategies to these companies. Based on the existing research literature, this article assumes that the credit strategy consists of four parts: whether to lend, loan amount, loan interest, and loan period. In principle, companies with a credit rating of D will not lend. First, based on relevant data, calculate the relevant index values of the upstream and downstream corporate influence, strength, supply and demand relationship stability, and customer churn rate of each enterprise; then construct a bank profit maximization model based on nonlinear regression, a credit risk minimization model based on Logistics regression, and a comprehensive evaluation system based on principal component analysis. Finally the abovementioned three optimization models are transformed into a multiobjective optimization model to obtain the bank's credit strategy [5].

4.2. Analysis Procedure

4.2.1. Bank Income Maximization Model Based on Nonlinear Regression

(1) Research Steps. First, process the corresponding original data in the data source. After referring to related books, this article believes that the formula for the upstream and downstream corporate influence of each company is as follows:

$$P_{i,j} = \frac{(|\alpha_0 S_{i,j}| - |\alpha_1 C_{i,j}|)}{(|S_{i,j}| - |C_{i,j}|)} \quad (i = 1, 2, \dots, n; j = 1, 2, \dots, 12), \quad (1)$$

where $P_{i,j}$ represents the upstream and downstream influence of the i -th company in the j -th month, $S_{i,j}$ represents the sum of the output bills of the i -th company in the j -th month, $C_{i,j}$ represents the sum of the input bills of the i -th company in the j -th month, and α_i ($i = 1, 2$) indicates that different companies place different emphases on output and input.

In order to comprehensively evaluate the comprehensive strength of each enterprise, this article considers the actual income, expenditure, tax amount, and monthly sales volume of the enterprise. On the basis of the existing literature research in the reference part, the average monthly tax payment of each company is obtained as an index to evaluate the comprehensive strength of the company, and the following formula is obtained:

$$\Delta T_{i,j} = \text{Log} \left(\frac{|TI_{i,j}/S_{i,j}| + |TO_{i,j}/C_{i,j}|}{N_{i,j}} \right) \quad (2)$$

$$(i = 1, 2, \dots, n; j = 1, 2, \dots, 12),$$

where $\Delta T_{i,j}$ represents the average tax payment of the i -th company in the j -th month, $TI_{i,j}$ represents the tax payment of the i -th company's output bill in the j -th month, $TO_{i,j}$

represents the tax payment of the i -th company's input bill in the j -th month, and $N_{i,j}$ represents the number of sales of the i -th company in the j -th month.

According to the checked literature and actual life experience, the stability of the supply-demand relationship of an enterprise will greatly affect the income of the enterprise, which will also affect the evaluation of the enterprise by the bank, so the supply stability value coefficient G and the demand stability value are constructed. The coefficient Q is used to quantify the degree of stability, and the specific formula is as follows [6–8]:

$$\begin{aligned} G_{i,j} &= \beta_1 \log \left(\frac{|C_{i,j}|}{N_{i,j}^1} \right), \quad i = 1, 2, \dots, n; j = 1, 2, \dots, 12, \\ Q_{i,j} &= \beta_2 \log \left(\frac{|S_{i,j}|}{N_{i,j}^2} \right), \quad i = 1, 2, \dots, n; j = 1, 2, \dots, 12, \end{aligned} \quad (3)$$

where $G_{i,j}$ represents the supply stability of the i -th company in the j -th month, $N_{i,j}^1$ represents the demand of the i -th company in the j -th month, $Q_{i,j}$ represents the demand stability of the i -th company in the j -th month, $N_{i,j}^2$ represents the supply of the i -th company in the j -th month, and β_1, β_2 is a balance parameter.

The monthly comprehensive supply stability degree and demand stability degree of each company are as follows:

$$\begin{aligned} G_i &= \frac{G_{i,j}}{\sum_{j=1}^{12} G_{i,j}}, \\ Q_i &= \frac{Q_{i,j}}{\sum_{j=1}^{12} Q_{i,j}}. \end{aligned} \quad (4)$$

The formula for a company's customer churn rate is

$$M = \frac{R}{Z} \quad (5)$$

Among them, M represents the customer churn rate of the company, R represents the number of voided output bills of the company, and Z represents the total number of sales bills of the company.

(2) *Result Analysis.* First of all, from the meaning of the question, companies with a credit rating of D do not grant loans in principle, so this type of corporate data is excluded when allocating the total amount of loans. Then, use the above formula to calculate the customer churn rate, upstream and downstream enterprise influence, strength, stability of supply and demand relationship, customer churn rate index value, and other data of each company with reputation ratings of A , B , and C . At this time, the desire to maximize the bank's profit is to ask the bank to deduct the amount of loan income from the profitable income from deposits in the same period. The expression for maximizing bank profit based on known conditions is as follows:

$$\begin{aligned} f(x) &= \max \sum_1^{99} A_i (r_i - r_0) (1 - z_i), \\ \text{s.t.} &\begin{cases} 10 \leq A_i \leq 100, \\ 4\% \leq r_i \leq 15\%, \\ \sum_1^{99} A_i \leq a. \end{cases} \end{aligned} \quad (6)$$

Among them, A_i represents the loan amount to each company, r_i represents the interest rate of the loan to each company, r_0 represents the bank deposit interest rate over the same period, z_0 means customer churn rate, and a represents the annual bank credit value of a fixed total amount.

4.2.2. Bank Credit Risk Quantification Model Based on Logistics Regression

(1) *Research Steps.* According to Section 4.2.1, the company's reputation rating is divided into A – D , and when the risk is low, the reputation rating is A , and when the risk is high, the reputation rating is D . This article uses default as the dependent variable. Default is recorded as 1, and nondefault is recorded as 0. Therefore, a company with a reputation rating of A can be assigned a risk of 0.2, a company with a reputation of B can be assigned a risk of 0.4, a company with a reputation of C can be assigned a risk of 0.6, and a company with a reputation of D can be assigned a risk of 0.8, with different quantifications credit risk of credit-rated companies [9].

At this point, the solving steps based on logistics regression are as follows:

- Step1: Collect relevant data according to business goals;
- Step2: Standardized data;
- Step3: Analyze the data and preprocess the data;
- Step4: Train the algorithm to find the best classification coefficient, ① Find the h function (namely, hypothesis). ② Construct J function (loss function). ③ Minimize the J function and obtain the regression parameters (θ);
- Step5: Test algorithm and model evaluation;
- Step6: Get new data and convert it into corresponding structured values. Based on the trained regression coefficients, you can perform simple regression calculations on these values to determine which category the new data belongs to.

(2) *Result Analysis.* Suppose the risk of bank loans is R , and the value is $0 < R < 1$. The closer the R value is to 0, the lower the credit risk of the company and the better the credit rating of the company; the closer the R value is to 1, the higher the financial risk of the company and the worse the credit rating of the company. The influencing factors are the influence of upstream and downstream enterprises' influence, strength,

stability of supply-demand relationship, customer churn rate index value, and other indicators. Banks should minimize the total risk of loans [10–12].

The quantified data and the original enterprise data were imported into SPSS, and the normality test and significance test passed. Then, proceed to principal component analysis, and the results are shown in Table 1.

According to the screening results of the above component score coefficient matrix, redefine the name of the principal component: N_1 is the amount of tax contribution, and N_2 is the relative fluctuation of sales.

At this time, two principal component factors N_1 and N_2 are used as research variables, and SPSS is used to do forward stepwise logistic regression on these two variables. The final model statistics are shown in Table 2.

The logistic reputation risk quantification model that can be established based on the above results is as follows:

$$R = \frac{I^{-1.274-0.107N_1-0.087N_2}}{1 + I^{-1.274-0.107N_1-0.087N_2}}, \tag{7}$$

$$= \frac{1}{1 + e^{1.274+0.107N_1+0.087N_2}}.$$

4.2.3. Quantification Model of Corporate Reputation Risk Based on Analytic Hierarchy Process.

(1) Principal component analysis method

- Step 1: Standardize the original data and calculate the correlation matrix;
- Step 2: Calculate the eigenvalues and eigenvectors of the correlation matrix;
- Step 3: Take the first 2–3 principal components based on the cumulative contribution rate reaching 85%;
- Step 4: Explain the principal components;
- Step 5: Calculate the principal component score. That is, standardize each sample data and bring it into the principal component formula of the third step to calculate the first principal component score and the second principal component score;
- Step 6: Regard the principal component score as a new dependent variable that can be linearly regressed.

(2) Establish an indicator system. This article summarizes the corporate reputation risk into three dimensions, namely, debt service capacity, credit guarantee situation, and macropolicy. Based on this, it is preliminarily subdivided into 10 specific corporate reputation risk indicator systems, as shown in Figure 1.

The quantified enterprise credit risk and original enterprise index data are imported into SPSS, and its normality test and significance test are passed. According to the screening results of the component score coefficient matrix, redefine the names of the

first three principal components: N_1 is the debt service capacity, N_2 is the credit guarantee situation, and N_3 is the macropolicy.

(3) Model Construction. At this time, three principal component factors are used as research variables, and O_i is used as the size of corporate reputation risk, and SPSS is used to perform forward stepwise logistic regression on these two variables. Based on the above results, a logistic corporate reputation risk prediction model can be established:

$$O_i = e^{[(1+(1/\ln N_1))/(N_2+(e/\ln N_3))]} \tag{8}$$

4.2.4. A Model for Maximizing Bank Revenue and Minimizing Credit Risk Based on Multiobjective Optimization. According to the relationship between the interest rate and the customer churn rate in the data source, the relationship between the loan interest rate and the customer churn rate of three types of credit risk companies A, B, and C is constructed. The images are established in the order of A, B, and C companies from top to bottom, and the result is shown in Figure 2.

The specific equation results are as follows:

$$z_i = \begin{cases} 7.524r_A - 0.09793 \dots \dots (A), \\ 7.351r_B - 0.1178 \dots \dots (B), \\ 7.468r_C - 0.1379 \dots \dots (C). \end{cases} \tag{9}$$

Combining the two optimization models of bank profit maximization and enterprise credit risk minimization, the optimized objective function and its limiting conditions are as follows:

$$Y = \min \sum_1^{99} R_i + \sum_1^{99} A_i(r_i - r_0)(1 - z_i) + \sum_1^{99} O_i,$$

$$\text{s.t.} \begin{cases} O_i = e^{(1+(1/\ln N_1)/N_2+(N_3/\ln N_4))}, \\ 10 \leq A_i \leq 100, \\ 4\% \leq r_i \leq 15\%, \\ \sum_1^{99} A_i \leq a, \\ Z_0 = a^* p_a + b^* p_b + c^* p_c (a^*, b^*, c^* = \{0, 1\}), \\ (i = 1, 2, \dots, 99). \end{cases} \tag{10}$$

At this time, a^* , b^* , and c^* represent the total amount of loans that can be allocated to companies A, B, and C, respectively. The value of the overall function should be as small as possible. Introducing the index value of each enterprise into the model, the loan interest rate and total loan amount of each enterprise are obtained.

TABLE 1: Component score coefficient matrix.

Variable Zscore	Profit	Contribution tax	Relative sales fluctuation	Purchase fluctuation size	Customer churn rate
1	0.871	0.876	0.198	0.426	0.525
2	-0.107	-0.018	0.849	0.406	-0.441

TABLE 2: Variable coefficients in the equation.

Variable name	B	S. E.	Wals	Df	Sig.	Exp (B)	95% of EXP (B) C. I.	
							Lower limit	Upper limit
Z (size of contribution tax)	-0.107	0.223	0.23	1	0.631	0.898	0.58	1.392
Z (relative sales fluctuation size)	-0.087	0.26	0.113	1	0.737	0.916	0.55	1.526
Constant	-1.274	0.219	33.868	1	0	0.28	—	—

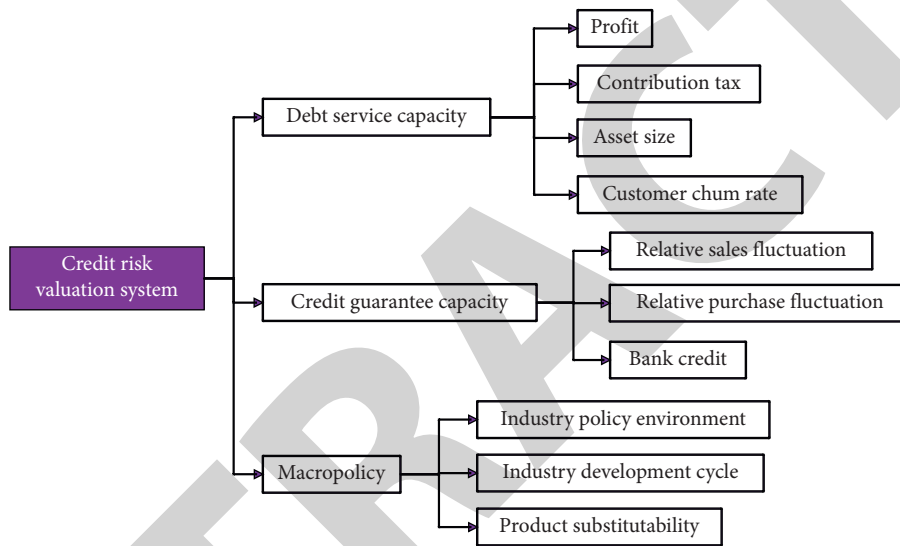


FIGURE 1: Corporate reputation risk evaluation index system.

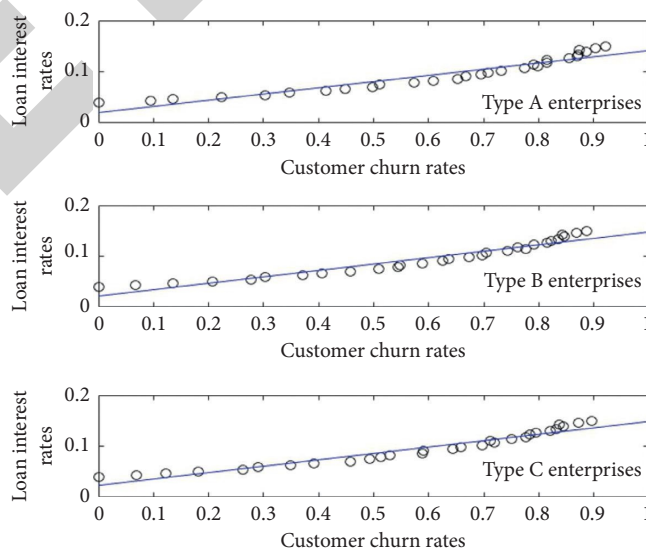


FIGURE 2: The relationship between loan interest rates and customer churn rates of three types of credit risk.

5. Research on the Classification of Credit Ratings of SMEs Based on Support Vector Machines and the Credit Risk and Strategy of Banks

5.1. Research Thought. It is required to quantify the credit risk of 302 companies in the data source and give the bank's credit strategy for these companies when the total annual credit is 100 million yuan. This paper first constructs a support vector machine training set to classify the reputation ratings of each company in the data source; then, according to the risk level of each company, after removing the company with a risk level of *D*, it is substituted into the model constructed in Section 4, and calculate the bank's credit strategy for 302 companies when the total annual credit is 100 million yuan.

5.2. Research Methods

5.2.1. Research Steps.

Step 1: Further process the relevant data according to the indicators in the previous section to obtain the corresponding indicator values;

Step 2: Perform normalization and cluster analysis on all data;

Step 3: Split the processed data into the training set and test set, and use support vector machine clustering analysis results to verify [13].

5.2.2. Model Construction. Perform cluster analysis on standardized data to obtain the proportions of all types of companies with loan records, as shown in Figure 3, and the proportion of all types of companies with no loan records, as shown in Figure 4.

Then, import the relevant data and classification results into MATLAB and perform support vector machine analysis on the accuracy of the classification results. The accuracy of the cluster analysis test set is close to 70%, and the classification results are acceptable. The classification and prediction results are shown in Figure 5 [14–16].

Based on the results of reputation risk classification, substituting into the multiobjective optimized bank revenue maximization and credit risk minimization models in the previous section [15], the partial results of the loans to enterprises and interest rates are shown in Table 3.

6. Credit Adjustment Strategy Model under the Influence of Emergencies Based on Analytic Hierarchy Process

6.1. Research Thought. This question requires comprehensive consideration of the credit risk of each enterprise in the previous section and the impact of possible emergent factors such as the new crown virus epidemic on each enterprise and gives the bank's credit adjustment strategy when the total annual credit is 100 million yuan. In response to this problem, this article treats emergencies as a single overall influencing factor, considering how it affects the first-level indicators

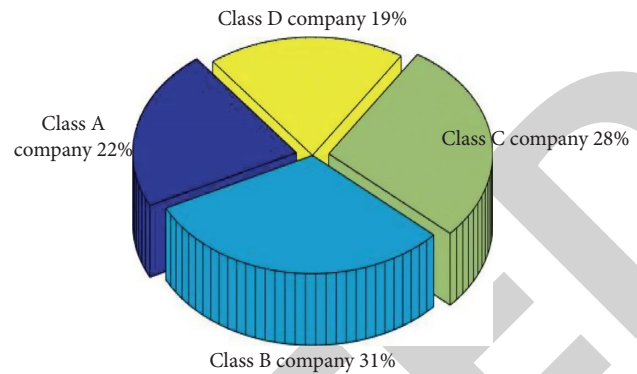


FIGURE 3: Visual pie chart of business classification with loan records.

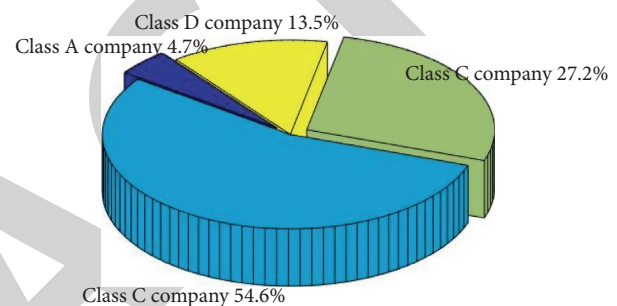


FIGURE 4: Visual pie chart of business classification with no loan records.

selected in Section 4 and then affects the second-level indicators. Therefore, the analytic hierarchy process is used to give different adjustment plans for different industries in emergencies. The processed values are respectively calculated on the relevant index values and brought into the existing model for calculation, and the bank's credit adjustment strategy when the total annual credit is 100 million yuan under the influence of unexpected factors can be obtained [17–20].

6.2. Research Methods

6.2.1. Analytic Hierarchy Process. Analytic hierarchy process is abbreviated as AHP, which refers to a decision-making method that decomposes elements that are always related to decision-making into goals, guidelines, and plans, and then conducts qualitative and quantitative analysis on this basis. The steps of the analytic hierarchy process are as follows:

- Step 1: Establish a hierarchical structure model;
- Step 2: Construct a pair of comparison matrix;
- Step 3: Calculate the weight vector and do the consistency check;
- Step 4: Calculate the combination weight vector and do the combination consistency test.

6.2.2. Model Construction. Based on the indicator system constructed in Section 5, and the impact of unexpected factors (such as the epidemic) on each company, according

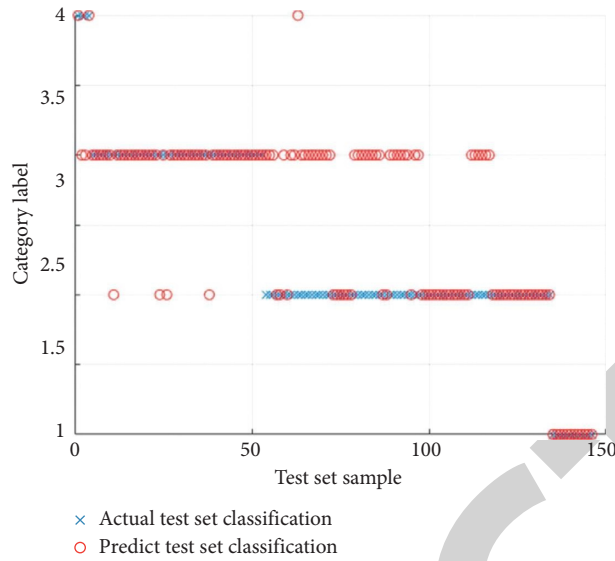


FIGURE 5: Results of corporate reputation risk classification.

TABLE 3: Screenshot of loan interest and loan limit of some of the 302 companies.

Enterprise code	Reputation	Loan interest rate (%)	Loan limit (yuan)
E124	A	15.000	2896690.49
E125	A	14.337	2910374.58
E126	A	10.823	1753908.32
E127	A	4.000	731860.94
E128	A	15.000	861454.12
E129	A	15.000	267664.16
E130	A	12.481	352527.12
E131	A	11.736	290436.29
E132	A	8.650	525292.91
E133	A	9.033	3486055.36
E134	A	10.005	181575.50
E135	A	9.502	1605406.61

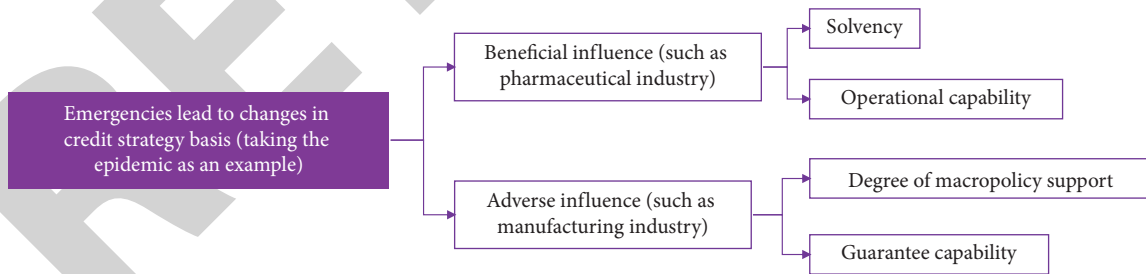


FIGURE 6: Credit adjustment strategy model under the influence of emergencies.

to the industry characteristics of each company, build a reputation risk evaluation system and bank loan strategy for companies in different industries. Taking the epidemic as an emergency factor as an example, for the pharmaceutical industry, the increase in the amount of its sales will increase its profits. At this time, it is more appropriate to use the company's debt servicing capacity as the main indicator to evaluate the loan strategy of the industry's enterprises; but for the manufacturing industry, due to the epidemic, it will

not be possible to resume work and production. At this time, it is more appropriate to evaluate the company's guarantee capacity and the favorable situation of the macropolicy. The specific model is shown in Figure 6 [21–24].

Bring the processed index values into the final multi-objective optimization model in Section 4, and recalculate the results of the credit adjustment strategy of each enterprise when the total annual credit is 100 million yuan, as shown in Table 4.

TABLE 4: Loan lines and interest rates of adjusted enterprises.

Enterprise code	E124	E126	E127	E128	E129	E130	E131	E132	E133	E134	E135	E136	E137	E138
Loan interest	2.37%	3.28%	2.13%	2.28%	3.42%	4.13%	2.90%	3.12%	2.16%	2.57%	2.32%	2.14%	1.32%	3.08%
Loan limit	60836.357	371862.11	420713.59	399685.57	370961.49	366222.64	353626.29	375173.62	382690.82	397228.21	389641.77	352743.14	353712.4	389603.55

7. Conclusion

In Section 4, the analytic hierarchy process is used to quantify the corporate reputation risk. This method can be extended to the quantitative analysis of an unknown risk affected by multiple factors, such as the financial risk of the enterprise and the risk of stock trading; the method of using nonlinear regression to maximize bank returns can be extended to any conditional constraint solution. The method of using nonlinear regression to maximize bank revenue can be extended to any conditional constraint to solve the maximum value, such as finding the maximum value of production capacity under resource constraints. In Section 5, since the support vector machine is a small sample learning method, the category prediction of 302 companies without loan records has a natural advantage different from other machine learning algorithms. From the perspective of algorithm principles, the novel nonlinear mapping and optimal hyperplane ideas greatly simplify many traditional classification and regression problems. In addition, the method of using support vector machines to classify the credit risk of SMEs can be extended to classify any item according to specific attributes, such as classifying wine quality and classifying food quality [25–29].

However, it should be noted that in the data processing, this article uses the average value to represent the stable supply and marketing status of the enterprise. If the supply and marketing data of the company have a large extreme value, the average value will not represent the stable supply and marketing status. In addition, when calculating the customer churn rate in the analysis in Section 4, the absolute customer churn rate is used because the relative purchase amount of the churn customer is lacking in the data source. In view of these two shortcomings, when calculating the fluctuation value of supply and demand of small, medium, and microenterprises, the median can be used instead of the average to represent the stable supply and demand status, thereby reducing the influence of extreme values to assess the reputation risk of SMEs; at that time, the customer churn rate can be calculated using the relative customer churn rate, and the relative purchase volume of the relative customer churn is included in the calculation, so that the result is more objective and reliable.

Data Availability

The data in this article come from Question C of the 2020 China National College Students Mathematical Contest in Modeling.

Conflicts of Interest

Authors declare that they have no conflicts of interest.

Acknowledgments

This study was funded by the Natural Science Foundation of Anhui Province (1808085MC88), the Teaching and Research Fund Project of the Education Department of Anhui

Province (2020jyxm0017 and 2018jyxm1305), “First-Class Course” of Anhui University of Finance and Economics (acylkc202008), and the Teaching and Research Fund Project of the Anhui University of Finance and Economics (acjyyb2020011 and acjyyb2020014).

References

- [1] X. Gen, “Correction of misappropriation of credit for small and medium-sized enterprises: theory and practice,” *Shandong Social Sciences*, vol. 11, pp. 123–126, 2011.
- [2] X. Q. Wang and Z.-B. Tang, “SME credit decision: discrimination, rationality or cognitive gap?” *Financial Research*, vol. 39, no. 8, pp. 99–109, 2013.
- [3] J. R. Wu, “Construction of credit risk evaluation index system for small and medium-sized enterprises,” *Finance and Accounting Newsletter*, vol. 26, pp. 102–104, 2016.
- [4] X. Li, “A case study on optimization of credit decision-making process for small and medium-sized commercial banks,” *Journal of Henan University (Social Science Edition)*, vol. 56, no. 1, pp. 54–61, 2016.
- [5] B. S. Yan, X. Zheng, and W. Y. Chen, “Loan migration and “crowding effect” in the small and micro credit market based on the audit survey of small and micro enterprise financial services,” *Financial Theory and Practice*, vol. 10, pp. 54–62, 2020.
- [6] L. H. Xu and Q. Li, “The influence of the structure of credit sources on the multi-dimensional innovation activities of SMEs,” *Financial Research*, vol. 46, no. 7, pp. 19–34, 2020.
- [7] H. Li, “Analysis of the fit and implementation path of open banking to crack the “Macmillan gap”” *Financial Theory and Practice*, vol. 7, pp. 67–75, 2020.
- [8] T. X. Sheng and C. Fan, “Review of fintech and small and micro enterprise credit supply: mechanism, practice and problems,” *Modern Economic Research*, vol. 46, pp. 39–44, 2020.
- [9] Q. L. Zhang, H. X. Lu, and Y. Zhang, “Optimal control strategy of *Hyphantria cunea* based on generalized Logistic model,” *Journal of Yangzhou University (Natural Science Edition)*, vol. 23, no. 4, pp. 19–21, 2020.
- [10] J. W. Jiao and C. Yu, “Robust logistic regression model based on non-convex penalty regression and its empirical evidence”” *Statistics and Decision*, vol. 36, no. 16, pp. 23–27, 2020.
- [11] B. Liu, T. S. Zhao, and R. X. Zhang, “Prediction of personal car ownership based on improved PCA-Logistic model,” *Highway and Transportation Science and Technology*, vol. 37, no. 8, pp. 136–143, 2020.
- [12] Z. S. Kuang, “What is the logic of the adjustment of administrative divisions in China in recent years?—an empirical analysis based on the EHA-Logistic model,” *Public Administration Review*, vol. 13, no. 4, pp. 22–40+205, 2020.
- [13] Y. Wu, J. M. Zhu, Y. Y. Wu et al., “Comprehensive evaluation of Anhui logistics development level based on factor analysis and cluster analysis,” *Journal of Wuhan University of Light Industry*, vol. 38, no. 6, pp. 74–80, 2019.
- [14] D. Li and J. M. Zhu, “Research on financial early warning of chemical products industry based on factor analysis and SVM model,” *Journal of Qiqihar University (Natural Science Edition)*, vol. 35, no. 4, pp. 90–94, 2018.
- [15] H. Y. Huang, L. B. Wu, S. Z. LI et al., “Application of support vector machine optimized by an improved simulated annealing algorithm in the research and judgment of trading

Research Article

A Modified Hybrid Conjugate Gradient Method for Unconstrained Optimization

Minglei Fang , Min Wang, Min Sun, and Rong Chen

School of Mathematics and Big Data, Anhui University of Science and Technology, Huainan 232001, China

Correspondence should be addressed to Minglei Fang; fmlmath@sina.com

Received 14 January 2021; Revised 3 February 2021; Accepted 5 February 2021; Published 23 February 2021

Academic Editor: Ghulam Mustafa

Copyright © 2021 Minglei Fang et al. This is an open access article distributed under the Creative Commons Attribution License, which permits unrestricted use, distribution, and reproduction in any medium, provided the original work is properly cited.

The nonlinear conjugate gradient algorithms are a very effective way in solving large-scale unconstrained optimization problems. Based on some famous previous conjugate gradient methods, a modified hybrid conjugate gradient method was proposed. The proposed method can generate decent directions at every iteration independent of any line search. Under the Wolfe line search, the proposed method possesses global convergence. Numerical results show that the modified method is efficient and robust.

1. Introduction

Consider the following unconstrained optimization problem:

$$\min_{x \in R^n} f(x), \quad (1)$$

where $x \in R^n$ is a real vector with $n \geq 1$ component and $f: R^n \rightarrow R$ is a smooth function and its gradient $g(x) \triangleq \nabla f(x)$ is available. Unconstrained problem is an important problem with a broad range of scientific and operational applications.

During the last decade, the conjugate gradient methods constitute an active choice for efficiently solving the above optimization problem, especially when the dimension n is large, characterized by the simplicity of their iteration, their low memory requirement, and their excellent numerical performance. The general procedure of the iterative computational scheme is as follows.

When applied to solve problem (1), starting from an initial guess $x_1 \in R^n$, the conjugate gradient method usually generates a sequence $\{x_k\}$ as

$$x_{k+1} = x_k + \alpha_k d_k, \quad (2)$$

where x_k is the current iterate, $\alpha_k > 0$ is called a step size determined by some suitable line search, and d_k is the search direction defined by

$$d_k = \begin{cases} -g_k, & k = 1, \\ -g_k + \beta_k d_{k-1}, & k \geq 2, \end{cases} \quad (3)$$

where $g_k = \nabla f(x_k)$ and β_k is an important scalar parameter.

Generally inexact line search is used in order to get the global convergence of conjugate gradient method, such as the Wolfe line search or the strong Wolfe line search. That is, the step length α_k is usually computed by the Wolfe line search:

$$\begin{aligned} f(x_k) - f(x_k + \alpha_k d_k) &\geq -\delta \alpha_k g_k^T d_k, \\ g(x_k + \alpha_k d_k)^T d_k &\geq \sigma g_k^T d_k, \end{aligned} \quad (4)$$

or the strong Wolfe line search:

$$\begin{aligned} f(x_k) - f(x_k + \alpha_k d_k) &\geq -\delta \alpha_k g_k^T d_k, \\ |g(x_k + \alpha_k d_k)^T d_k| &\leq \sigma |g_k^T d_k|, \end{aligned} \quad (5)$$

where $0 < \delta < \sigma < 1$ are some fixed parameters.

Different conjugate gradient methods correspond to different values of the scalar parameter β_k . The well-known conjugate gradient methods include the Fletcher-Reeves (FR) method [1], the Polak-Ribière-Polyak (PRP) method [2, 3], the Hestenes-Stiefel (HS) method [4], the Dai-Yuan (DY) method [5], the conjugate-descent method (CD) [6], and the Liu-Storey method (LS) [7]. The parameters β_k in these conjugate gradient methods are specified as follows:

$$\begin{aligned}
\beta_k^{\text{FR}} &= \frac{\|g_k\|^2}{\|g_{k-1}\|^2}, \\
\beta_k^{\text{PRP}} &= \frac{g_k^T (g_k - g_{k-1})}{\|g_{k-1}\|^2}, \\
\beta_k^{\text{HS}} &= \frac{g_k^T (g_k - g_{k-1})}{d_{k-1}^T (g_k - g_{k-1})}, \\
\beta_k^{\text{DY}} &= \frac{\|g_k\|^2}{d_{k-1}^T (g_k - g_{k-1})}, \\
\beta_k^{\text{CD}} &= -\frac{\|g_k\|^2}{g_{k-1}^T d_{k-1}}, \\
\beta_k^{\text{LS}} &= \frac{g_k^T (g_k - g_{k-1})}{d_{k-1}^T g_{k-1}},
\end{aligned} \tag{6}$$

where $\|\cdot\|$ stands for the Euclidean norm. These methods are identical when $f(x)$ is a strongly convex quadratic function and the line search is exact, since the gradients are mutually orthogonal, and the parameters β_k in these methods are equal. When applied to general nonlinear functions with inexact line searches, the behavior of these methods is marked different.

It is well known that FR, DY, and CD methods have strong convergent properties, but they may not perform well in practice due to jamming. Moreover, although PRP, HS, and LS methods may not converge in general, they often perform better. Naturally, people try to devise some new methods, which have the advantages of these two kinds of methods. So far, various hybrid methods have been proposed (see [8–20]).

In [14], Wei et al. gave a variant of the PRP method, WYL method for short, where the parameter β_k is yielded by

$$\beta_k^{\text{WYL}} = \frac{\|g_k\|^2 - (\|g_k\|/\|g_{k-1}\|)g_k^T g_{k-1}}{\|g_{k-1}\|^2}. \tag{7}$$

The above WYL method can be considered as the modification of the PRP method. It inherits the good properties of the PRP method, such as excellent numerical effect. Furthermore, Huang et al. [15] proved that the WYL method satisfies the sufficient descent condition and converges globally under the strong Wolfe line search (5) if the parameter satisfies $\sigma < (1/4)$.

Yao et al. [16] gave a modification of the HS conjugate gradient method as follows:

$$\beta_k^{\text{MHS}} = \frac{\|g_k\|^2 - (\|g_k\|/\|g_{k-1}\|)g_k^T g_{k-1}}{d_{k-1}^T (g_k - g_{k-1})}. \tag{8}$$

Under the strong Wolfe line search (5) with the parameter $\sigma < (1/3)$, it has been shown that the MHS method can generate sufficient descent directions and converges globally for general objective functions.

Jiang et al. [17] proposed a hybrid conjugate gradient method with

$$\beta_k^{\text{JHJ}} = \frac{\|g_k\|^2 - \max\{0, (\|g_k\|/\|d_{k-1}\|)g_k^T d_{k-1}, (\|g_k\|/\|g_{k-1}\|)g_k^T g_{k-1}\}}{d_{k-1}^T (g_k - g_{k-1})}. \tag{9}$$

Under the Wolfe line search (4), the method possesses global convergence and efficient numerical performance.

In [18], Jiang et al. proposed a hybrid conjugate gradient method with

$$\beta_k^{\text{MDY}} = \frac{\|g_k\|^2}{\max\{\mu|g_k^T d_{k-1}|, d_{k-1}^T (g_k - g_{k-1})\}}. \tag{10}$$

Under the parameter $\mu > 1$, it has been shown that the MDY method can generate sufficient descent directions and converges globally for general objective functions.

In [19], Jiang et al. proposed a hybrid conjugate gradient method, denote it by JHS with

$$\beta_k^{\text{JHS}} = \frac{\|g_k\|^2 - (\|g_k\|/\|g_{k-1}\|)g_k^T g_{k-1}}{\max\{\mu|g_k^T d_{k-1}|, d_{k-1}^T (g_k - g_{k-1})\}}. \tag{11}$$

Under the parameter $\mu > 2$, it has been shown that the JHS method can generate sufficient descent directions and converges globally for general objective functions.

In this paper, we introduce a new hybrid choice for parameter β_k . This motivation mainly comes from [18, 19]. For convenience, we call the iteration method a FW method as follows:

$$\beta_k^{\text{FW}} = \frac{\|g_k\|^2 - \max\{0, (\|g_k\|/\|g_{k-1}\|)g_k^T g_{k-1}\}}{\max\{\mu|g_k^T d_{k-1}|, d_{k-1}^T (g_k - g_{k-1})\}}, \tag{12}$$

where $\mu > 1$.

It is easy to know that $\beta_k^{\text{FW}} = \beta_k^{\text{DY}}$ or $\beta_k^{\text{FW}} = \beta_k^{\text{MDY}}$ or $\beta_k^{\text{FW}} = \beta_k^{\text{JHS}}$ or $\beta_k^{\text{FW}} = \beta_k^{\text{MHS}}$, so β_k^{FW} is one of the hybrids of β_k^{DY} , β_k^{MDY} , β_k^{JHS} , and β_k^{MHS} . The proposed method has attractive property of satisfying the sufficient descent condition independent of any line search and attains global convergence if the step length is yielded by the Wolfe line search (4).

This paper is organized as follows. In Section 2, we give the details of our algorithm and discuss its sufficient descent property. In Section 3, we prove the global convergence of the proposed method with Wolfe line search (4). A number of numerical experiments comparing the proposed method with other conjugate gradient methods are given in Section 4. Finally, conclusion is given in Section 5.

2. Algorithm and Its Property

In this section, first, based on the discussed above, we describe our algorithm framework (Algorithm 1) without fixed line search as follows.

Initialization. Given constants $\varepsilon \geq 0, \delta \in (0, 1), \sigma \in (\delta, 1), \mu > 1$ and $x_1 \in R^n$. Let $d_1 = -g_1, k = 1$.
Step 1. If $\|g_k\| < \varepsilon$, then stop. Otherwise, go to Step 2.
Step 2. Determine a step length α_k by a suitable line search.
Step 3. Let $x_{k+1} = x_k + \alpha_k d_k$ and compute $g_{k+1} = g(x_{k+1})$ and β_{k+1}^{FW} by (12).
Step 4. Let $d_{k+1} = -g_{k+1} + \beta_{k+1}^{\text{FW}} d_k$. Set $k = k + 1$; go to Step 1.

ALGORITHM 1: FW

The following lemma states that the search direction in Algorithm 1 is always sufficient descent depending on no line search.

Lemma 1. *If the objective function $f(x)$ is continuously differentiable, let d_k be generated by Algorithm 1. Then, $g_k^T d_k < 0$ holds for each $k \geq 1$.*

Proof. We prove this lemma by induction. For $k = 1$, it is easy to know that $g_1^T d_1 = g_1^T (-g_1) = -\|g_1\|^2 < 0$. Assume that $g_{k-1}^T d_{k-1} < 0$ holds for $k - 1$ and $k > 2$. Now we prove that $g_k^T d_k < 0$ holds for k .

If $g_k^T d_{k-1} = 0$, then $\beta_k^{\text{FW}} = (\|g_k\|^2 - \max\{0, (\|g_k\|/\|g_{k-1}\|)g_k^T g_{k-1}\})/(-d_{k-1}^T g_{k-1})$; furthermore, we have

$$g_k^T d_k = g_k^T (-g_k + \beta_k^{\text{FW}} d_{k-1}) = -\|g_k\|^2 + \beta_k^{\text{FW}} g_k^T d_{k-1} = -\|g_k\|^2 < 0. \quad (13)$$

If $g_k^T d_{k-1} \neq 0$, we divide the proof into four following cases.

- (i) If $g_k^T g_{k-1} \leq 0$ and $\mu|g_k^T d_{k-1}| \leq d_{k-1}^T (g_k - g_{k-1})$, then $\beta_k^{\text{FW}} = (\|g_k\|^2/d_{k-1}^T (g_k - g_{k-1})) = \beta_k^{\text{DYS}}$ by the definition of β_k^{FW} . Noticing that $\mu|g_k^T d_{k-1}| > 0, d_{k-1}^T (g_k - g_{k-1}) > 0$ holds.

From (3) and (12), we have

$$\begin{aligned} g_k^T d_k &= g_k^T (-g_k + \beta_k^{\text{FW}} d_{k-1}) = -\|g_k\|^2 + \frac{\|g_k\|^2}{d_{k-1}^T (g_k - g_{k-1})} g_k^T d_{k-1} \\ &= \frac{\|g_k\|^2}{d_{k-1}^T (g_k - g_{k-1})} g_{k-1}^T d_{k-1} < 0. \end{aligned} \quad (14)$$

- (ii) If $g_k^T g_{k-1} \leq 0, \mu|g_k^T d_{k-1}| > d_{k-1}^T (g_k - g_{k-1})$, then from (12), one has $\beta_k^{\text{FW}} = (\|g_k\|^2/\mu|g_k^T d_{k-1}|)$.

Therefore, we obtain

$$\begin{aligned} g_k^T d_k &= g_k^T (-g_k + \beta_k^{\text{FW}} d_{k-1}) = -\|g_k\|^2 + \frac{\|g_k\|^2}{\mu|g_k^T d_{k-1}|} g_k^T d_{k-1} \\ &\leq -\|g_k\|^2 + \frac{\|g_k\|^2}{\mu|g_k^T d_{k-1}|} |g_k^T d_{k-1}| = -\left(1 - \frac{1}{\mu}\right) \|g_k\|^2 < 0. \end{aligned} \quad (15)$$

- (iii) If $g_k^T g_{k-1} > 0$ and $\mu|g_k^T d_{k-1}| \leq d_{k-1}^T (g_k - g_{k-1})$, then from (12), one knows

$$\beta_k^{\text{FW}} = \frac{\|g_k\|^2 - (\|g_k\|/\|g_{k-1}\|)g_k^T g_{k-1}}{d_{k-1}^T (g_k - g_{k-1})} = \beta_k^{\text{MHS}}. \quad (16)$$

Noticing $g_k^T g_{k-1} > 0$, we have $0 < \cos \theta_k < 1$, where θ_k is the angle between g_k and g_{k-1} .

Furthermore, we obtain

$$\begin{aligned} g_k^T d_k &= g_k^T (-g_k + \beta_k^{\text{FW}} d_{k-1}) = -\|g_k\|^2 \\ &\quad + \frac{\|g_k\|^2 - (\|g_k\|/\|g_{k-1}\|)g_k^T g_{k-1}}{d_{k-1}^T (g_k - g_{k-1})} g_k^T d_{k-1} \\ &= -\|g_k\|^2 + \frac{\|g_k\|^2 g_k^T d_{k-1} - \|g_k\|^2 \cos \theta_k g_k^T d_{k-1}}{d_{k-1}^T (g_k - g_{k-1})} \\ &= \frac{\|g_k\|^2 g_{k-1}^T d_{k-1} - \|g_k\|^2 \cos \theta_k g_k^T d_{k-1}}{d_{k-1}^T (g_k - g_{k-1})} \\ &< \frac{\|g_k\|^2 g_{k-1}^T d_{k-1} - \|g_k\|^2 \cos \theta_k g_{k-1}^T d_{k-1}}{d_{k-1}^T (g_k - g_{k-1})} \\ &= \frac{\|g_k\|^2 (1 - \cos \theta_k) g_{k-1}^T d_{k-1}}{d_{k-1}^T (g_k - g_{k-1})} < 0. \end{aligned} \quad (17)$$

- (iv) If $g_k^T g_{k-1} > 0$ and $\mu|g_k^T d_{k-1}| > d_{k-1}^T (g_k - g_{k-1})$, then from (12), one gets

$$\beta_k^{\text{FW}} = \frac{\|g_k\|^2 - (\|g_k\|/\|g_{k-1}\|)g_k^T g_{k-1}}{\mu|g_k^T d_{k-1}|}. \quad (18)$$

As in the case of (iii), we have

$$\begin{aligned}
g_k^T d_k &= g_k^T (-g_k + \beta_k^{\text{FW}} d_{k-1}) \\
&= -\|g_k\|^2 + \frac{\|g_k\|^2 - (\|g_k\|/\|g_{k-1}\|)g_k^T g_{k-1}}{\mu|g_k^T d_{k-1}|} g_k^T d_{k-1} \\
&= -\|g_k\|^2 + \frac{\|g_k\|^2 - \|g_k\|^2 \cos \theta_k}{\mu|g_k^T d_{k-1}|} g_k^T d_{k-1} \\
&\leq -\|g_k\|^2 + \frac{\|g_k\|^2 (1 - \cos \theta_k)}{\mu|g_k^T d_{k-1}|} \|g_k^T d_{k-1}\| \\
&= -\left(1 - \frac{1 - \cos \theta_k}{\mu}\right) \|g_k\|^2 < 0.
\end{aligned} \tag{19}$$

Therefore, $g_k^T d_k < 0$ holds for all $k \geq 1$. \square

Lemma 2. Let $\{x_k\}$ be generated by Algorithm 1. Then, for any $k \geq 1$, we can obtain the following relations:

$$0 \leq \beta_k^{\text{FW}} \leq \frac{g_k^T d_k}{g_{k-1}^T d_{k-1}}. \tag{20}$$

Proof. From formula (12), it is easy to see that

$$\beta_k^{\text{FW}} = \frac{\|g_k\|^2 - \max\{0, (\|g_k\|/\|g_{k-1}\|)g_k^T g_{k-1}\}}{\max\{\mu|g_k^T d_{k-1}|, d_{k-1}^T (g_k - g_{k-1})\}} \geq 0. \tag{21}$$

Now we are ready to prove $\beta_k^{\text{FW}} \leq (g_k^T d_k / g_{k-1}^T d_{k-1})$ by considering the following four cases.

(i) If $g_k^T g_{k-1} \leq 0$ and $\mu|g_k^T d_{k-1}| \leq d_{k-1}^T (g_k - g_{k-1})$, then $\beta_k^{\text{FW}} = (\|g_k\|^2 / d_{k-1}^T (g_k - g_{k-1})) = \beta_k^{\text{D}^Y}$.

In view of Lemma 1 and (14), we have

$$\beta_k^{\text{FW}} = \frac{\|g_k\|^2}{d_{k-1}^T (g_k - g_{k-1})} = \frac{g_k^T d_k}{g_{k-1}^T d_{k-1}}. \tag{22}$$

(ii) If $g_k^T g_{k-1} \leq 0$, $\mu|g_k^T d_{k-1}| > d_{k-1}^T (g_k - g_{k-1})$, then $\beta_k^{\text{FW}} = (\|g_k\|^2 / \mu|g_k^T d_{k-1}|)$.

If $g_k^T d_{k-1} > 0$, by the recurrence formula, we have

$$\beta_k^{\text{FW}} = \frac{\|g_k\|^2}{\mu g_k^T d_{k-1}}, \quad (1 - \mu)g_k^T d_{k-1} < g_{k-1}^T d_{k-1}. \tag{23}$$

Therefore, one gets

$$\begin{aligned}
g_k^T d_k &= g_k^T (-g_k + \beta_k^{\text{FW}} d_{k-1}) \\
&= -\|g_k\|^2 + \frac{\|g_k\|^2}{\mu g_k^T d_{k-1}} g_k^T d_{k-1} \\
&= \frac{(1 - \mu)\|g_k\|^2}{\mu g_k^T d_{k-1}} g_k^T d_{k-1} < \frac{\|g_k\|^2}{\mu g_k^T d_{k-1}} g_k^T d_{k-1} \\
&= \beta_k^{\text{FW}} g_{k-1}^T d_{k-1}.
\end{aligned} \tag{24}$$

Dividing both sides of (24) by $g_{k-1}^T d_{k-1}$, it follows that

$$\beta_k^{\text{FW}} \leq \frac{g_k^T d_k}{g_{k-1}^T d_{k-1}}. \tag{25}$$

If $g_k^T d_{k-1} < 0$, similarly, we can get that

$$\begin{aligned}
\beta_k^{\text{FW}} &= \frac{\|g_k\|^2}{-\mu g_k^T d_{k-1}}, \quad (1 + \mu)g_k^T d_{k-1} < g_{k-1}^T d_{k-1}, \\
g_k^T d_k &= g_k^T (-g_k + \beta_k^{\text{FW}} d_{k-1}) = -\|g_k\|^2 + \frac{\|g_k\|^2}{-\mu g_k^T d_{k-1}} g_k^T d_{k-1} \\
&= \frac{(1 + \mu)\|g_k\|^2}{-\mu g_k^T d_{k-1}} g_k^T d_{k-1} < \frac{\|g_k\|^2}{-\mu g_k^T d_{k-1}} g_k^T d_{k-1} = \beta_k^{\text{FW}} g_{k-1}^T d_{k-1}.
\end{aligned} \tag{26}$$

Dividing both sides of (26) by $g_{k-1}^T d_{k-1}$, one has

$$\beta_k^{\text{FW}} \leq \frac{g_k^T d_k}{g_{k-1}^T d_{k-1}}. \tag{27}$$

(iii) If $g_k^T g_{k-1} > 0$ and $\mu|g_k^T d_{k-1}| \leq d_{k-1}^T (g_k - g_{k-1})$, then $\beta_k^{\text{FW}} = (\|g_k\|^2 - (\|g_k\|/\|g_{k-1}\|)g_k^T g_{k-1}) / d_{k-1}^T (g_k - g_{k-1}) = \beta_k^{\text{MHS}}$.

From the above formula, we have

$$\beta_k^{\text{FW}} = \frac{\|g_k\|^2 - (\|g_k\|/\|g_{k-1}\|)g_k^T g_{k-1}}{d_{k-1}^T (g_k - g_{k-1})} = \frac{\|g_k\|^2 (1 - \cos \theta_k)}{d_{k-1}^T (g_k - g_{k-1})}. \tag{28}$$

Combining with (17), we get

$$\beta_k^{\text{FW}} \leq \frac{g_k^T d_k}{g_{k-1}^T d_{k-1}}. \tag{29}$$

(iv) If $g_k^T g_{k-1} > 0$ and $\mu|g_k^T d_{k-1}| > d_{k-1}^T (g_k - g_{k-1})$, then $\beta_k^{\text{FW}} = (\|g_k\|^2 - (\|g_k\|/\|g_{k-1}\|)g_k^T g_{k-1}) / \mu|g_k^T d_{k-1}|$.

Noticing that $g_k^T d_{k-1} < \mu |g_k^T d_{k-1}| + g_{k-1}^T d_{k-1}$, we have from the above formula that

$$\beta_k^{\text{FW}} = \frac{\|g_k\|^2 (1 - \cos \theta_k)}{\mu |g_k^T d_{k-1}|}. \quad (30)$$

So,

$$\begin{aligned} g_k^T d_k &= g_k^T (-g_k + \beta_k^{\text{FW}} d_{k-1}) \\ &= -\|g_k\|^2 + \frac{\|g_k\|^2 (1 - \cos \theta_k)}{\mu |g_k^T d_{k-1}|} g_k^T d_{k-1} \\ &< -\|g_k\|^2 + \frac{\|g_k\|^2 (1 - \cos \theta_k)}{\mu |g_k^T d_{k-1}|} (\mu |g_k^T d_{k-1}| + g_{k-1}^T d_{k-1}) \\ &= -\cos \theta_k \|g_k\|^2 + \frac{\|g_k\|^2 (1 - \cos \theta_k)}{\mu |g_k^T d_{k-1}|} g_{k-1}^T d_{k-1} \\ &< \frac{\|g_k\|^2 (1 - \cos \theta_k)}{\mu |g_{k-1}^T d_{k-1}|} g_{k-1}^T d_{k-1} = \beta_k^{\text{FW}} g_{k-1}^T d_{k-1}. \end{aligned} \quad (31)$$

Dividing both sides of (31) by $g_{k-1}^T d_{k-1}$, we have

$$\beta_k^{\text{FW}} \leq \frac{g_k^T d_k}{g_{k-1}^T d_{k-1}}. \quad (32)$$

The proof is complete. \square

3. Global Convergence of Algorithm

This section is devoted to the global convergence of algorithm framework under the Wolfe line search condition, i.e., the step length α_k is yielded by condition (4). For this goal, we make the following basic assumptions in subsequent discussions.

H 3.1 $f(x)$ is bounded from below on the level set $\Omega = \{x \in R^n | f(x) \leq f(x_1)\}$, where x_1 is the initial point.

H 3.2 In some neighborhood Ω_1 of the level set Ω , $f(x)$ is continuous differentiable, and its gradient $g(x)$ is Lipschitz continuous, that is to say, for all $x, y \in \Omega_1$, there exists a constant $L > 0$ such that

$$\|g(x) - g(y)\| \leq L \|x - y\|. \quad (33)$$

Lemma 3. Suppose that assumptions (H 3.1) and (H 3.2) hold. Let $\{x_k\}$ be generated by Algorithm 1, where the step length α_k satisfies the Wolfe line search (4). Then, $\sum_{k \geq 1} ((g_k^T d_k)^2 / \|d_k\|^2) < +\infty$.

Proof. In view of (4) and (33), we have

$$(\sigma - 1) g_k^T d_k \leq d_k^T (g_{k+1} - g_k) \leq \alpha_k L \|d_k\|^2. \quad (34)$$

Therefore, we get

$$\alpha_k \geq \frac{\sigma - 1}{L} \frac{g_k^T d_k}{\|d_k\|^2}. \quad (35)$$

Combining (4) and (20), we can get that

$$f_k - f_{k+1} \geq -\delta \alpha_k g_k^T d_k \geq -\frac{\delta(\sigma - 1)}{L} \frac{(g_k^T d_k)^2}{\|d_k\|^2} = \frac{\delta(1 - \sigma)}{L} \frac{(g_k^T d_k)^2}{\|d_k\|^2}. \quad (36)$$

Let us sum up the inequalities (36) for $k = 1, \dots$. We obtain

$$\sum_{k \geq 1} (f_k - f_{k+1}) = f_1 - \lim_{k \rightarrow \infty} f_k \geq \sum_{k \geq 1} \frac{\delta(1 - \sigma)}{L} \frac{(g_k^T d_k)^2}{\|d_k\|^2}. \quad (37)$$

This inequality along with the assumption (H3.1) results in

$$\sum_{k \geq 1} \frac{(g_k^T d_k)^2}{\|d_k\|^2} < +\infty. \quad (38)$$

Therefore, Lemma 3 holds. \square

Theorem 1. Suppose that Assumptions (H 3.1) and (H 3.2) hold. Consider iterate $x_{k+1} = x_k + \alpha_k d_k$ by Algorithm 1; if the direction d_k is a descent direction and the step length α_k satisfies the Wolfe line search (4), then $\lim_{k \rightarrow \infty} \inf \|g_k\| = 0$.

Proof. We prove this theorem by contradiction. If $\lim_{k \rightarrow \infty} \inf \|g_k\| \neq 0$, in view of $\|g_k\| > 0$, there exists a constant $c > 0$ such that $\|g_k\| \geq c, \forall k \geq 1$. Again, from (3), it follows that $d_k + g_k = \beta_k^{\text{FW}} d_{k-1}$. Squaring both sides of above equality, we have

$$\|d_k\|^2 = (\beta_k^{\text{FW}})^2 \|d_{k-1}\|^2 - 2g_k^T d_k - \|g_k\|^2. \quad (39)$$

Dividing both sides of (39) by $(g_k^T d_k)^2$ and in view of (20), it follows that

$$\begin{aligned} \frac{\|d_k\|^2}{(g_k^T d_k)^2} &= \frac{(\beta_k^{\text{FW}})^2 \|d_{k-1}\|^2}{(g_k^T d_k)^2} - \frac{2}{g_k^T d_k} - \frac{\|g_k\|^2}{(g_k^T d_k)^2} \\ &\leq \frac{\|d_{k-1}\|^2}{(g_{k-1}^T d_{k-1})^2} - \frac{2}{g_k^T d_k} - \frac{\|g_k\|^2}{(g_k^T d_k)^2} \\ &= \frac{\|d_{k-1}\|^2}{(g_{k-1}^T d_{k-1})^2} + \frac{1}{\|g_k\|^2} - \left(\frac{1}{\|g_k\|^2} + \frac{\|g_k\|^2}{(g_k^T d_k)^2} \right) \\ &\leq \frac{\|d_{k-1}\|^2}{(g_{k-1}^T d_{k-1})^2} + \frac{1}{\|g_k\|^2}. \end{aligned} \quad (40)$$

Combining with (40), by a recurrence of relation $\|g_k\| \geq c$ and $d_1 = -g_1$, we have

TABLE 1: Test results of the FW method, MDY method, JHS method, and MHS method.

p	n	FW				MDY				JHS				MHS			
		I	NF	NG	TCpu	I	NF	NG	TCpu	I	NF	NG	TCpu	I	NF	NG	TCpu
badscp	2	3	58	5	0.0189	3	58	5	0.0144	3	58	5	0.1081	3	58	5	0.0116
beale	2	17	57	29	0.0290	21	62	34	0.0094	23	79	40	0.0140	19	60	31	0.0239
jensam	2	2	52	3	0.0054	2	52	3	0.0079	2	52	3	0.0091	2	52	3	0.0098
helix	3	63	465	245	0.0855	79	648	339	0.1265	113	756	401	0.2044	70	467	226	0.1752
bard	3	37	99	58	0.0214	86	199	122	0.0909	49	161	71	0.0538	47	94	61	0.0454
gauss	3	4	9	5	0.0144	4	9	5	0.0388	4	9	5	0.0154	4	9	5	0.0138
meyer	3	3	56	5	0.0187	3	56	5	0.0156	3	56	5	0.0176	3	56	5	0.0230
gulf	3	2	52	4	0.0115	2	52	4	0.0138	2	52	4	0.0162	2	52	4	0.0188
box	3	1	51	2	0.0166	1	51	2	0.0147	1	51	2	0.0168	1	51	2	0.0214
wood	4	111	335	166	0.0865	85	245	136	0.0774	14	146	90	0.0657	85	250	135	0.0567
kowosb	4	153	332	212	0.0452	15	180	126	0.0821	15	147	95	0.0556	105	317	182	0.0747
osb1	5	1	51	2	0.0102	1	51	2	0.0110	1	51	2	0.0142	1	51	2	0.0188
biggs	6	8	65	10	0.0210	8	69	12	0.0066	12	95	22	0.0087	11	89	20	0.0075
osb2	11	17	89	23	0.0147	28	117	40	0.0178	16	93	24	0.0136	7	66	10	0.0143
pen1	10	2	58	7	0.0156	2	58	7	0.0149	2	58	7	0.0211	2	58	7	0.0194
pen1	100	2	101	3	0.0132	2	101	3	0.0216	7	351	8	0.1244	5	251	6	0.0487
pen1	200	1	51	2	0.0119	1	51	2	0.0256	1	51	2	0.0213	1	51	2	0.0244
pen1	1000	1	51	2	0.9192	1	51	2	0.9964	1	51	2	0.9902	1	51	2	0.9578
pen1	1500	1	51	2	2.0667	1	51	2	2.2766	1	51	2	2.0790	1	51	2	2.1576
pen1	2000	1	51	2	3.6421	1	51	2	4.0836	1	51	2	3.7250	1	51	2	3.7133
pen1	3000	1	51	2	8.2712	1	51	2	9.2095	1	51	2	8.1979	1	51	2	8.5341
pen1	5000	1	51	2	23.0663	1	51	2	25.5505	1	51	2	22.1556	1	51	2	23.6629
pen2	10	2	52	3	0.0160	2	52	3	0.0171	2	52	3	0.0156	2	52	3	0.0180
pen2	50	1	51	2	0.0165	2	52	3	0.0266	1	51	2	0.0210	1	51	2	0.0197
vardim	2	4	27	10	0.0024	4	30	11	0.0035	5	25	10	0.0034	5	25	10	0.0033
vardim	100	1	51	2	0.0119	1	51	2	0.0218	1	51	2	0.0131	1	51	2	0.0116
vardim	500	1	51	2	0.0776	1	51	2	0.1024	1	51	2	0.0982	1	51	2	0.1105
vardim	1000	1	51	2	0.2908	1	51	2	0.3441	1	51	2	0.3951	1	51	2	0.3326
vardim	2000	1	51	2	0.9955	1	51	2	1.0401	1	51	2	1.0591	1	51	2	1.0676
vardim	3000	1	51	2	1.9162	1	51	2	2.1069	1	51	2	1.9204	1	51	2	2.0107
vardim	4000	1	51	2	3.1114	1	51	2	3.4843	1	51	2	3.3016	1	51	2	3.3019
vardim	5000	1	51	2	4.6175	1	51	2	5.2175	1	51	2	4.8257	1	51	2	4.9972
trig	10	42	80	50	0.0130	40	70	45	0.0169	41	73	46	0.0182	48	94	60	0.0153
trig	50	56	101	64	0.0294	49	108	65	0.0538	51	112	67	0.0436	52	114	68	0.0482
trig	150	62	110	71	0.1451	54	112	69	0.1962	61	113	73	0.1620	81	185	113	0.2364
trig	200	54	103	65	0.2280	60	124	77	0.3072	67	176	85	0.3789	68	230	102	0.3682
ie	10	7	15	8	0.0231	6	13	7	0.0398	7	15	8	0.0314	7	15	8	0.0287
ie	100	9	18	10	0.1928	7	16	9	0.2051	7	14	8	0.1332	11	21	12	0.2035
ie	500	8	18	10	2.8779	8	18	10	3.2010	8	18	10	2.9477	8	18	10	2.9802
ie	1000	8	18	10	11.3304	7	16	9	11.2570	8	18	10	12.0797	8	18	10	11.9909
ie	2000	8	18	10	45.4075	8	18	10	50.2927	7	16	9	40.4006	7	16	9	42.0180
ie	4000	8	21	11	200.1344	8	21	11	216.9107	7	19	10	179.2517	7	19	10	195.2297
trid	100	36	74	40	0.0350	32	69	36	0.0562	33	69	37	0.0544	38	78	43	0.0438
trid	500	33	74	39	0.3026	32	70	38	0.3045	32	71	38	0.3125	35	90	47	0.3451
band	10	21	58	26	0.0229	25	66	31	0.0072	18	56	23	0.0084	20	63	27	0.0074
band	500	1	51	2	0.3930	1	51	2	0.4692	1	51	2	0.4523	1	51	2	0.4562
band	5000	1	51	2	32.4417	1	51	2	37.1887	1	51	2	32.5321	1	51	2	33.9574
lin	2	1	4	3	0.0061	1	4	3	0.0091	1	4	3	0.0047	1	4	3	0.0046
lin	50	1	4	3	0.0058	1	4	3	0.0047	1	4	3	0.0053	1	4	3	0.0084
lin	500	1	4	3	0.0432	1	4	3	0.0646	1	4	3	0.0522	1	4	3	0.0632
lin	1000	1	4	3	0.2213	1	4	3	0.2170	1	4	3	0.1997	1	4	3	0.1960
lin	1500	1	4	3	0.4253	1	4	3	0.4649	1	4	3	0.3651	1	4	3	0.3824
lin	2000	1	4	3	0.6977	1	4	3	0.8611	1	4	3	0.7180	1	4	3	0.8242
lin	3000	1	4	3	1.6127	1	4	3	1.9749	1	4	3	1.6681	1	4	3	1.6817
lin	5000	1	4	3	4.7730	1	4	3	5.3896	1	4	3	4.8142	1	4	3	4.8166
lin1	2	2	4	3	0.0086	2	4	3	0.0018	2	4	3	0.0134	2	4	3	0.0096
lin1	10	1	4	3	0.0029	1	4	3	0.0034	1	4	3	0.0042	1	4	3	0.0065
lin1	100	6	62	9	0.0580	6	62	9	0.0408	6	62	9	0.0530	6	62	9	0.0598
lin1	500	3	56	7	0.5768	3	56	7	0.6440	3	56	7	0.5921	3	56	7	0.6223

TABLE 1: Continued.

p	n	FW				MDY				JHS				MHS			
		I	NF	NG	TCpu	I	NF	NG	TCpu	I	NF	NG	TCpu	I	NF	NG	TCpu
lin1	1000	3	56	5	2.1466	3	56	5	2.5596	3	56	5	2.1943	3	56	5	2.3149
lin1	2000	3	56	5	9.0047	3	56	5	10.9094	3	56	5	9.0499	3	56	5	9.8109
lin1	3000	3	56	5	25.2678	5	63	8	30.5328	5	63	8	25.2772	5	63	8	27.4500
lin0	4	2	4	3	0.0111	2	4	3	0.0096	2	4	3	0.0142	2	4	3	0.0138
lin0	500	3	58	6	0.7479	3	58	6	0.7779	3	58	6	0.7604	3	58	6	0.6715
lin0	800	3	56	5	1.8232	3	56	5	2.1614	3	56	5	1.9628	3	56	5	1.8111
lin0	1000	7	62	9	3.3620	7	62	9	3.6958	7	62	9	3.6405	7	64	9	3.3911
lin0	2000	3	56	5	11.8533	3	56	5	14.5539	3	56	5	12.0432	3	56	5	12.2544
lin0	2500	3	56	5	19.5770	3	56	5	23.3801	3	56	5	19.6448	3	56	5	22.1141
lin0	3000	3	57	5	28.9680	3	57	5	33.4278	3	57	5	28.9657	3	57	5	30.2009

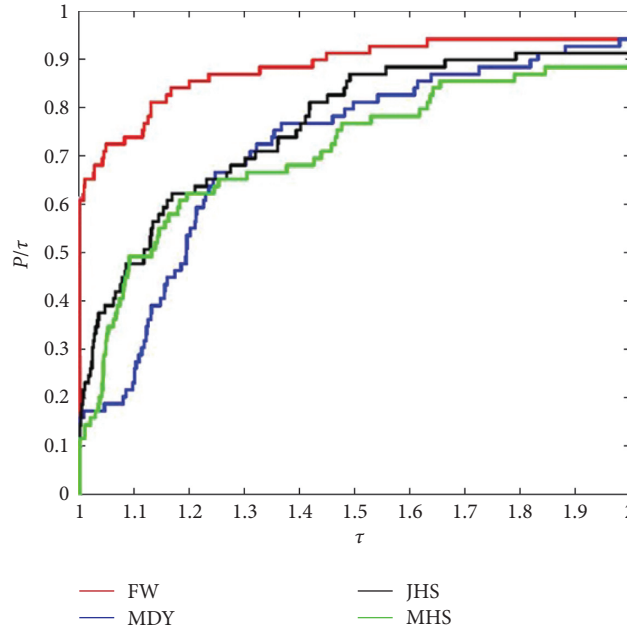


FIGURE 1: Performance profiles with respect to CPU time (FW versus MDY, JHS, and MHS).

$$\frac{\|d_k\|^2}{(g_k^T d_k)^2} \leq \frac{\|d_1\|^2}{(g_1^T d_1)^2} + \sum_{i=2}^k \frac{1}{\|g_i\|^2} = \sum_{i=1}^k \frac{1}{\|g_i\|^2}. \quad (41)$$

Therefore, we have

$$\frac{(g_k^T d_k)^2}{\|d_k\|^2} \geq \frac{c^2}{k}. \quad (42)$$

Hence, by recurrence formula (42), we obtain

$$\sum_{k \geq 1} \frac{(g_k^T d_k)^2}{\|d_k\|^2} \geq \sum_{k \geq 1} \frac{c^2}{k} = +\infty. \quad (43)$$

This is a contradiction to Lemma 3. The proof is completed. \square

4. Numerical Results

In this part of the paper, we report some numerical experiments that indicate the efficiency of the proposed

algorithm. To test and compare the computation effect of the proposed FW, a large number of testing problems from Morè et al. [21] are solved by the FW, MHS [16], MDY [18], and JHS [19]. In all conjugate gradient methods, the step length α_k is yielded by the Wolfe line search (4). All codes were written in Matlab 7.5 and run on Dell with 2.90 GHz CPU processor, 8 GB RAM memory, and Windows 10 operating system. The parameters are set as follows: $\sigma = 0.2$, $\delta = 0.02$, $\mu = 10.75$, and $\varepsilon = 10^{-6}$. We stop the iteration if one of the following conditions is satisfied: (1) $\|g_k\| \leq \varepsilon = 10^{-6}$; (2) the number of iteration $Itr > 1000$. If condition (2) occurs, the method is deemed to fail for solving the corresponding test problem and denote it by F . The simulation results of the proposed method were efficient and robust as compared with hybrid conjugate gradient methods (FW, MHS, MDY, and JHS). The hybrid conjugate gradient methods are listed in Table 1. Here P denotes the abbreviation of the test problems, n denotes the dimension of the test problems, and Itr , NF , and NG denote the number of iteration, function evaluations, and gradient evaluations, respectively. $TCpu$ denotes the computing time of CPU for

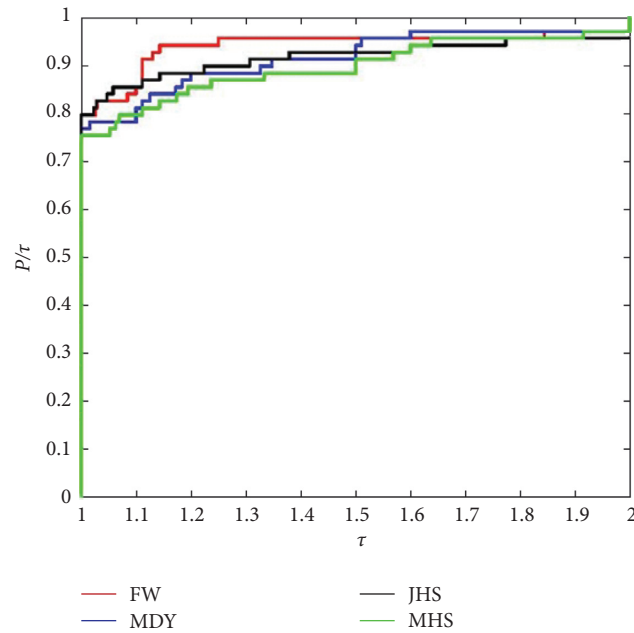


FIGURE 2: Performance profile on the number of gradient evaluation (FW versus MDY, JHS, and MHS).

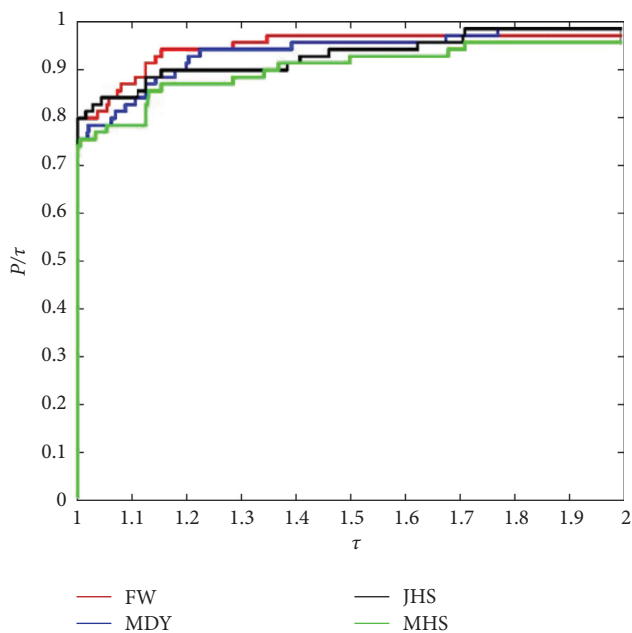


FIGURE 3: Performance profile on the number of function evaluation (FW versus MDY, JHS, and MHS).

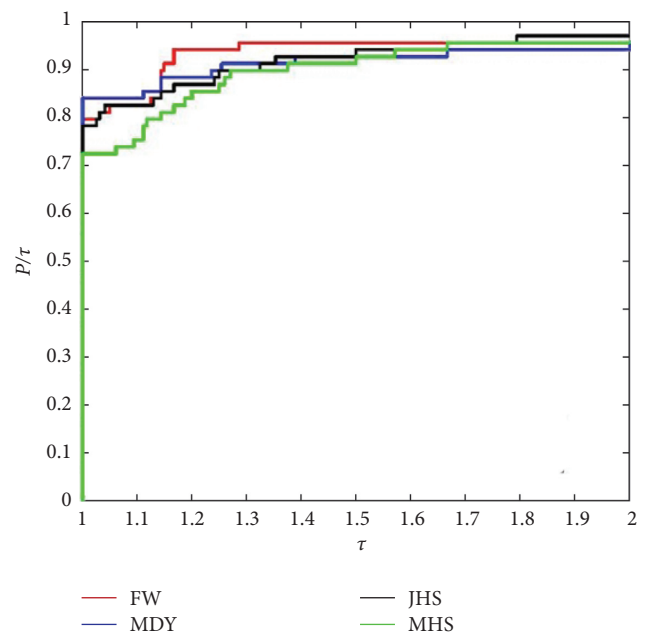


FIGURE 4: Performance profile on the number of iteration (FW versus MDY, JHS, and MHS).

computing the corresponding test problem (unit: seconds). To visualize the whole behaviour of the algorithms, we use the performance profiles proposed by Dolan and Morè [22] to compare the performance based on the CPU time, the number of function evaluation, the number of gradient evaluation, and the number of iteration, respectively. For each method, we plot the fraction P/τ of the problems for which the method is within a factor τ of the best time. The left side of the figure gives the percentage of the test problems for which a method is the fastest. Based on the

theory of the performance profile above, four performance figures, i.e., Figures 1–4, can be generated according to Table 1. From the four figures, we can see that our methods perform effectively on the testing problems.

5. Conclusion

In this paper, we proposed a new hybrid conjugate gradient method for solving unconstrained optimization problems. The proposed method satisfied sufficient descent condition

irrespective of the line searches condition. Moreover, the global convergence of the proposed method has been established under the Wolfe line search (4). Numerical experiments show the efficiency and robustness of the new algorithm in solving a collection of unconstrained optimization problems from [21].

Data Availability

Data will be available upon request.

Conflicts of Interest

The authors declare that they have no conflicts of interest.

Acknowledgments

This study was supported in part by the National Natural Science Foundation of China (nos. 61967004 and 11601007) and Anhui Provincial Natural Science Foundation (no. 2008085MA01).

References

- [1] R. Fletcher and C. M. Reeves, "Function minimization by conjugate gradients," *The Computer Journal*, vol. 7, no. 2, pp. 149–154, 1964.
- [2] E. Polak and G. Ribière, "Note sur la convergence de méthodes de directions conjuguées," *Revue Française D'informatique et de Recherche Opérationnelle. Série Rouge*, vol. 3, no. 16, pp. 35–43, 1969.
- [3] B. T. Polyak, "The conjugate gradient method in extremal problems," *USSR Computational Mathematics and Mathematical Physics*, vol. 9, no. 4, pp. 94–112, 1969.
- [4] M. R. Hestenes and E. Stiefel, "Method of conjugate gradient for solving linear equations," *Journal of Research of the National Institute of Standards*, vol. 5, no. 49, pp. 409–436, 1952.
- [5] Y. H. Dai and Y. Yuan, "A nonlinear conjugate gradient method with a strong global convergence property," *SIAM Journal on Optimization*, vol. 10, no. 1, pp. 177–182, 1999.
- [6] R. Fletcher, *Practical Methods of Optimization Vol 1: Unconstrained Optimization*, Wiley and Sons, New York, NY, USA, 1987.
- [7] Y. Liu and C. Storey, "Efficient generalized conjugate gradient algorithms," *Journal of Optimization Theory and Applications*, vol. 69, pp. 129–137, 1991.
- [8] S. Djordjevic, "New hybrid conjugate gradient method as a convex combination of Ls and Fr methods," *Acta Mathematica Scientia*, vol. 39, no. 1, pp. 214–228, 2019.
- [9] J. Jian, L. Han, and X. Jiang, "A hybrid conjugate gradient method with descent property for unconstrained optimization," *Applied Mathematical Modelling*, vol. 39, no. 3-4, pp. 1281–1290, 2015.
- [10] Y.-H. Dai and C.-X. Kou, "A nonlinear conjugate gradient algorithm with an optimal property and an improved Wolfe line search," *SIAM Journal on Optimization*, vol. 23, no. 1, pp. 296–320, 2013.
- [11] K. Wang and P. Gao, "Two mixed conjugate gradient methods based on DY," *Journal of Shandong University (Natural Science)*, vol. 51, no. 6, pp. 16–23, 2016.
- [12] X. Zheng, Z. Tian, and L. Song, "The global convergence of a mixed conjugate gradient method with the Wolfe line search," *Operations Research Transactions*, vol. 13, no. 2, pp. 18–24, 2009.
- [13] X. Jiang and J. Jian, "Two modified nonlinear conjugate gradient methods with disturbance factors for unconstrained optimization," *Nonlinear Dynamics*, vol. 77, no. 1-2, pp. 387–394, 2014.
- [14] Z. Wei, S. Yao, and L. Liu, "The convergence properties of some new conjugate gradient methods," *Applied Mathematics and Computation*, vol. 183, no. 2, pp. 1341–1350, 2006.
- [15] H. Huang, Z. Wei, and Y. Shengwei, "The proof of the sufficient descent condition of the Wei-Yao-Liu conjugate gradient method under the strong Wolfe-Powell line search," *Applied Mathematics and Computation*, vol. 189, no. 2, pp. 1241–1245, 2007.
- [16] S. W. Yao, Z. X. Wei, and H. Huang, "A note about WYLS conjugate gradient method and its application," *Applied Mathematics and Computation*, vol. 191, pp. 381–388, 2007.
- [17] X. Z. Jiang, L. Han, and J. B. Jian, "A globally convergent mixed conjugate gradient method with Wolfe line search," *Mathematica Numerica Sinica*, vol. 34, pp. 103–112, 2012.
- [18] X.-Z. Jiang and J.-B. Jian, "A sufficient descent Dai-Yuan type nonlinear conjugate gradient method for unconstrained optimization problems," *Nonlinear Dynamics*, vol. 72, no. 1-2, pp. 101–112, 2013.
- [19] X. Jiang, J. Jian, and G. Ma, "Two conjugate gradient methods with sufficient descent property," *Acta Mathematica Sinica, Chinese Series*, vol. 57, no. 2, pp. 365–372, 2014.
- [20] P. Mtagulwa and P. Kaelo, "An efficient modified PRP-FR hybrid conjugate gradient method for solving unconstrained optimization problems," *Applied Numerical Mathematics*, vol. 145, pp. 111–120, 2019.
- [21] J. J. Moré, B. S. Garbow, and K. E. Hillstom, "Testing unconstrained optimization software," *ACM Transactions on Mathematical Software*, vol. 7, no. 1, pp. 17–41, 1981.
- [22] E. D. Dolan and J. J. Moré, "Benchmarking optimization software with performance profiles," *Mathematical Programming*, vol. 91, no. 2, pp. 201–213, 2002.

Research Article

Some Graph-Based Encryption Schemes

Baizhu Ni,¹ Rabiha Qazi,² Shafiq Ur Rehman ² and Ghulam Farid ²

¹Mathematics Science Department, Normal University of Mudanjiang, Mudanjiang, Heilongjiang, China

²Department of Mathematics, COMSATS University, Islamabad, Attock Campus, Pakistan

Correspondence should be addressed to Shafiq Ur Rehman; shafiq@cuiatk.edu.pk

Received 9 November 2020; Revised 21 December 2020; Accepted 28 December 2020; Published 19 February 2021

Academic Editor: Ghulam Mustafa

Copyright © 2021 Baizhu Ni et al. This is an open access article distributed under the Creative Commons Attribution License, which permits unrestricted use, distribution, and reproduction in any medium, provided the original work is properly cited.

In today's technological world, confidentiality is an important issue to deal with, and it is carried out through different proficiencies. Cryptography is a scientific technique of securing a communication from unauthenticated approach. There exist many encryption algorithms in cryptography for data security. The need of new nonstandard encryption algorithms has been raised to prevent the communication from traditional attacks. This paper proposes some new encryption algorithms for secure transmission of messages using some special corona graphs and bipartite graph along with some algebraic properties. These proposed encryption schemes will lead to more secure communication of secret messages.

1. Introduction

Secret communications have been needed by military officers and diplomats since ancient times. In today's advanced age, where the internet, mobile phones, and computer technology are widely used in almost every sphere of life, the need to keep important information secure and confidential is also increasing day by day. Overtime, as data security continues to evolve, new ways to break the confidential communication are being discovered.

Cryptography is the science of transforming the secret data into coded information with the goal that it can safely reach its end without leakage. It was basically utilized for war time plans. Classical cryptography goes back over two thousand years. Modern cryptography was established by Shannon in 1949 [1]. After the development of digital communications, new forms of cryptography have come. It addresses the problems of secrecy, privacy, authentication, passwords, digital signatures, identification, and digital money. It is now an integral part of a modern society.

The process to transform the original message into a code format is called the encryption, and the reverse process is known as decryption [2]. Encryption prevents the original contents from interception. Uncovered message is known as plaintext. In any encryption scheme, the information which

is referred as plaintext is encoded or encrypted to generate a cipher text with the help of a specified key. This cipher text is then converted into readable message through decryption. Key is such a piece of information that is used to put the original data in code shape and then decrypt to get real text. Through a provided key, the authorized recipient can open up the hidden message with full ease, but it is not possible for an interceptor. Mainly, three types of schemes are used in modern cryptography, i.e., symmetric key cryptography, public key cryptography, and hash functions [3]. Symmetric key cryptography uses one key for both encryption and decryption, while the public key cryptography uses one key for encryption and another key for decryption. The hash functions use a transformation to irreversibly encrypt information.

We are interested in developing encryption by using graph theory and some algebraic concepts. Firstly, some useful concepts of graph theory are recalled [4]. A graph $G = G(V, E)$ consists of two sets: the set of vertices $V(G)$ and the set of edges $E(G)$. If the vertex set $V(G)$ can be partitioned into two disjoint nonempty subsets such that each edge has one vertex in each partition, then the graph G is said to be a bipartite graph. A bipartite graph is said to be complete-bipartite if every vertex in one partition is joined to all vertices of other partition. A complete-bipartite graph, in

which only one vertex is in one partition while all other vertices are in second partition, is termed as star graph. A vertex of degree one is named a pendent vertex, and the edge incident to it is pendent edge. The corona of two graphs G and H is the graph $G \odot H$ formed by one copy of G and $|V(G)|$ copies of H , where the i th vertex of G is joined to each vertex in the i th copy of H . This product is an important operation between graphs, introduced by Frucht and Harary [5]. The star graph S_{n+1} on $n + 1$ vertices can be seen as a corona graph $K_1 \odot \overline{K}_n$. The corona graph of the cycle C_n with K_1 , i.e., $C_n \odot K_1$, is a graph on $2n$ vertices obtained by attaching n pendant edges in a cycle graph C_n .

Graphs can be used for designing different encryption algorithms. The interaction between graph theory and cryptography is quite interesting. For applications of graph theory in cryptography, refer to [6–9]. The recent past has seen a growing interest in exploring graphs as a tool to propose new methodologies in different areas of cryptography (see [10–20]). In [10], Selvakumar and Gupta proposed an innovative algorithm for encryption and decryption using connected graphs. In [11], Kedia and Agrawal discussed a new encryption algorithm, in which data are secured through numeric representation and letters, using basic concepts of mathematics like Venn diagram. In [12], the authors have proposed a graph-based algorithm for encryption in which fundamental circuits are chosen with respect to corresponding weights of edges. In [13], Yamuna and Karthika describe a unique method of transferring data by using bipartite graph. They constructed a numeric table for the representation of alphabets. In [14], Al Etaiwi presented a new symmetric encryption algorithm using cycle graph, complete graph, and minimum spanning tree. It is reflected in paper [15] that the authors highlight some vast applications of bipartite graph in computation. In [16], the authors presented a scheme for securing a data by giving a new concept of line sigraph. Sigraph consists of graphs with sign of edges and belongs to $\{-1, +1\}$ as their labeled number. In [17], the authors proposed a novel bipartite graph-based propagation approach to overcome fraud detection in large advertising system. In [18], Razaq et al. used coset diagram for the action of $PSL(2, \mathbb{Z})$ on projective line over the finite field \mathbb{F}_{2^9} to construct proposed substitution box (S-box). The strong S-box is an important area of research in cryptography. In [19], Razaq et al. generated a strong S-box using orbits of coset graphs and the action of the symmetric group S_{256} . In [20], Selim G. Akl described an algorithm for encrypting a graph for its secure transmission from a sender to a receiver.

Our aim in this work is to describe new encryption algorithms based on some types of graphs, particularly, the corona graph $C_n \odot K_1$, $K_1 \odot \overline{K}_n$ (also called star graph), and the bipartite graph. The proposed algorithms send and receive secure messages consisting of words of any length by using graphs and certain algebraic properties. After applying prescribed algorithmic steps, data could be fully protected. The recipient then gets the labeled graph and eventually approaches to the original message.

In Section 2, an encryption scheme is described by using the corona graph $C_n \odot K_1$. Afterwards, an algorithm of this scheme is formulated. Application of this algorithm is studied

through an example. However, in Section 3, bipartite graphs are used to construct a secure encryption scheme with described algorithm. This scheme is applicable on important information, shown by an example. In Section 4, a secured encryption scheme is described by using a special corona graph $K_1 \odot \overline{K}_n$, also named as a star graph. Its algorithm is mentioned, and application is viewed through an example.

2. Secure Data Transfer Using Corona Graph $C_n \odot K_1$

To initiate the described algorithm, the first step is to take a simple text which is to be transferred and is to be encrypted before sending. Every letter in data has its unique numeric representation, mentioned in encoding table, which is used to encode each alphabetic character. Then, each digit is transmuted up to n -place, through shift type of cipher. Now, new numeric values a_i are obtained. Randomly, some positive integers b_i are selected which are relatively prime with a_i . By taking inverse of that a_i in the modulus of b_i , corona graph $C_n \odot K_1$ is considered according to length of simple text with specified outward vertices and allocates the resulting inverses to suspended outward vertices, while main vertices are labeled with b_i . The final labeled corona graph $C_n \odot K_1$ is the encrypted data, in which the recipient receives to get required information. Figure 1 replicates the schematic diagram of the proposed algorithm.

Algorithm for encryption is as follows:

Give a plain-text word of length n .

Give the numerical values to the alphabets of plain-text word and apply shift cipher; $e_n(x) = x + n \pmod{26}$, to each numerical value obtained before and get new numerical values, say $a_1, a_2, a_3, \dots, a_n$.

Find a sequence; $b_1, b_2, b_3, \dots, b_n$ of positive integers in increasing order such that $\gcd(b_i, a_i) = 1$ and $b_i > 26$.

Consider a corona graph $C_n \odot K_1$ with $2n$ vertices and allot weights $b_1, b_2, b_3, \dots, b_n$ to the vertices, adjacent to pendent vertices randomly.

Find the inverse of $a_i \pmod{b_i}$ for all i and denote them by c_i , i.e., $c_i = (a_i)^{-1} \pmod{b_i} \forall i$.

Give numeric values $c_1, c_2, c_3, \dots, c_n$ to pendent vertices.

Send this corona graph $C_n \odot K_1$ to the receiver.

Algorithm for decryption is as follows.

The receiver receives the graph, and following steps are applied to transform the information and get original data:

Arrange those vertices which are adjacent to the pendent vertices, in increasing order as $b_1 < b_2 < b_3 < \dots < b_n$.

Find the inverse of the weights of pendent vertices c_i modulus their adjacent vertices b_i and denote them by a_i for each i .

Compute $w_i = a_i - (\text{order of graph}/2) \pmod{26}, \forall i$.

Convert the numeric values w_i for each i , to relate specific alphabets.

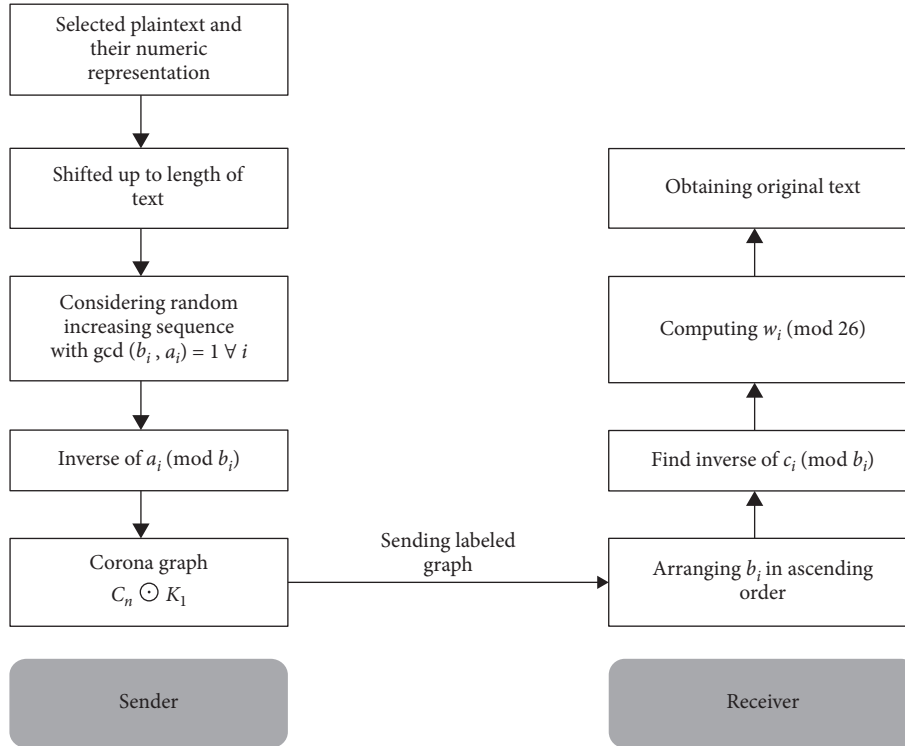


FIGURE 1: Schematic diagram.

Example 1. Let us suppose we have to transfer information, i.e., EDGE, encrypting it and then sending it to the recipient.

The starting point is to convert the alphabetic letters into numbers of their respective positions through the encoding table, as shown in Figure 2:

$$\begin{matrix} E & D & G & E \\ 5 & 4 & 7 & 5 \end{matrix} \quad (1)$$

Here, length of word is $n = 4$. Applying shift cipher $e_n = x + n \pmod{26}$, we get

$$\begin{aligned} 5 + 4 &= 9 = a_1, \\ 4 + 4 &= 8 = a_2, \\ 7 + 4 &= 11 = a_3, \\ 5 + 4 &= 9 = a_4. \end{aligned} \quad (2)$$

Given word is encrypted in the form

$$I \ H \ K \ I. \quad (3)$$

Selecting random increasing integers b_i such that value of $b_i > 26$:

$$\begin{aligned} \gcd(b_1, a_1) &= \gcd(28, 9) = 1, \\ \gcd(b_2, a_2) &= \gcd(31, 8) = 1, \\ \gcd(b_3, a_3) &= \gcd(35, 11) = 1, \\ \gcd(b_4, a_4) &= \gcd(47, 9) = 1. \end{aligned} \quad (4)$$

Construct corona graph $C_n \odot K_1$ and put value of b_i to main vertices randomly, as shown in Figure 3.

Now, through the below-mentioned step,

$$c_i = (a_i)^{-1} \pmod{b_i}, \quad (5)$$

we get

$$\begin{aligned} c_1 &= (a_1)^{-1} \pmod{b_1} = (9)^{-1} \pmod{28} = 25, \\ c_2 &= (a_2)^{-1} \pmod{b_2} = (8)^{-1} \pmod{31} = 4, \\ c_3 &= (a_3)^{-1} \pmod{b_3} = (11)^{-1} \pmod{35} = 16, \\ c_4 &= (a_4)^{-1} \pmod{b_4} = (9)^{-1} \pmod{47} = 21. \end{aligned} \quad (6)$$

These inverse values are given to the adjacent pendant vertices of Figure 3, as shown in Figure 4.

Send this labeled graph (Figure 4) to the receiver.

The recipient, after receiving that labeled graph, arranges the main vertices in ascending order such that

$$28 < 31 < 35 < 47, \quad (7)$$

and considers these numbers as values of b_i such that

$$b_1 < b_2 < b_3 < b_4. \quad (8)$$

Taking inverses of corresponding pendent vertices with respect to the value of each b_i , as shown in Figure 4, we get

$$\begin{aligned} 25^{-1} \pmod{28} &= 9 = a_1, \\ 4^{-1} \pmod{31} &= 8 = a_2, \\ 16^{-1} \pmod{35} &= 11 = a_3, \\ 21^{-1} \pmod{47} &= 9 = a_4. \end{aligned} \quad (9)$$

A	B	C	D	E	F	G	H	I	J	K	L	M
1	2	3	4	5	6	7	8	9	10	11	12	13
N	O	P	Q	R	S	T	U	V	W	X	Y	Z
14	15	16	17	18	19	20	21	22	23	24	25	26

FIGURE 2: Numeric representation.

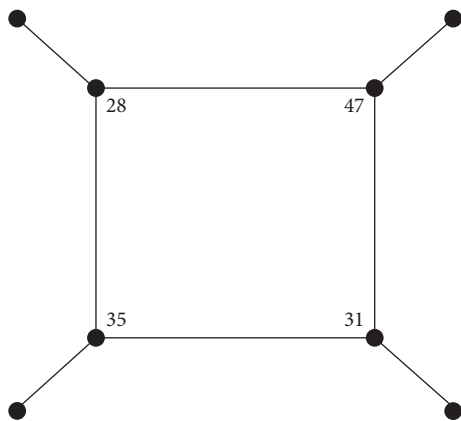


FIGURE 3

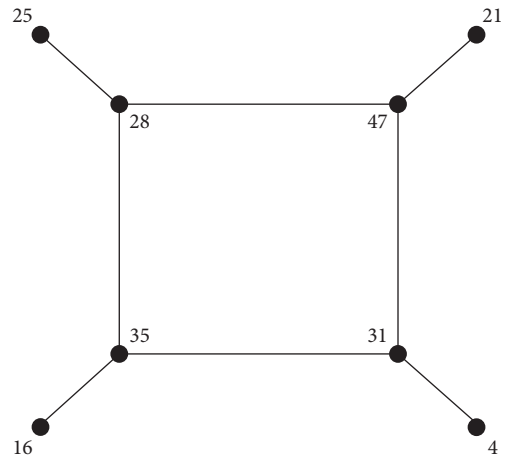


FIGURE 4

Now, for w_i ,

$$w_i = a_i - \left(\frac{2n}{2}\right) \text{mod} 26. \tag{10}$$

Find values of $a_1, a_2, a_3,$ and a_4 :

$$\begin{aligned} w_1 &= a_1 - \left[\frac{2(4)}{2}\right] \text{mod} 26 = 5 = E, \\ w_2 &= a_2 - \left[\frac{2(4)}{2}\right] \text{mod} 26 = 4 = D, \\ w_3 &= a_3 - \left[\frac{2(4)}{2}\right] \text{mod} 26 = 7 = G, \\ w_4 &= a_4 - \left[\frac{2(4)}{2}\right] \text{mod} 26 = 5 = E. \end{aligned} \tag{11}$$

Finally, we get the original text.

3. Secure Data Transfer Using Bipartite Graphs

In this section, we propose an encryption algorithm for the secure and confidential communication of messages between two communicating parties. The construction of this encryption algorithm is based on bipartite graph and the concept of unique factorization domain (UFD). The following are the steps of algorithm.

Algorithm for encryption is as follows:

Take a UFD with infinite primes. For example, \mathbb{Z} .

Take a set P_n of first “ n ” primes, where $n = \lceil (26/k) + k \rceil, 2 < k < 13,$ and $k = \text{key}$ (which is fixed according to length of a word).

Consider a message, for encryption with length S .

Then, make a table $(n - k) \times k$ such that the first value shows number of rows and second value shows the number of columns.

After that, alphabets are partitioned as

1 st, 2 nd, 3 rd, . . . , k th position primes. (horizontally) while;

$(k + 1)$ th, $(k + 2)$ th, $(k + 3)$ th, . . . , n th position primes. (vertically)

Now, label the alphabets with the integers $r_i c_i$; $r_i = \text{row position}, c_i = \text{column position}$.

Label the entry ij with $r_i c_j$, where $k + 1 \leq i \leq n, 1 \leq j \leq k$ Forming each number as vertex of path graph (according to sequence of letters).

Multiplying i, j and then label each vertex with that number (say, a_p where $1 \leq p \leq k$). Keeping in view that, one place digits are not taken in column position. In other words, we say that column position has just 2-digit primes.

Construct a path graph by giving consecutive i, j numbers to each vertex.

Separate the graph labels as row and column numbers;

$V_1 = \{\text{first place numbers from } i\}$
 $V_2 = \{\text{second place numbers from } j\}$
 Edge set of G becomes $(r_1, c_1), (r_2, c_2), \dots, (r_n, c_n)$.
 Now construct a bipartite graph with mentioned edge set. Edges move from r_i to c_i .
 Assign random numbers to the edges as weight in increasing order.
 Send that labeled graph.

Algorithm for decryption is as follows.
 The recipient receives the labeled bipartite graph.
 Arrange the weight of edges in increasing order.
 Then, arrange edges with respect to weights in a set of order pair such that number of rows at first and number of columns at second position.
 Construct path graph with the help of order pair information.
 Find prime factorization of each vertex label.
 Resultantly, required alphabets are taken through factorization, by using table (described).

	2	3	5	7	11
13	A	B	C	D	E
17	F	G	H	I	J
19	K	L	M	N	O
23	P	Q	R	S	T
29	U	V	W	X	Y
31	Z				

FIGURE 5

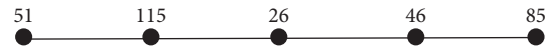


FIGURE 6

Example 2. For defining the scheme, we have to explain an example. Take a word, **GRAPH**. Numerically, corresponding digits are 7, 18, 1, 16, and 8, respectively. Here, length of word is $k = 5$.

Step 1: take a UFD with infinite primes, i.e., \mathbb{Z} .
 Step 2: in this example, $n = \lceil (26/5) + 5 \rceil$; $2 < k < 13$. So, $n = 11$. Take a set P_{11} of first 11 primes. As, $P_{11} = \{2, 3, 5, 7, 11, 13, 17, 19, 23, 29, 31\}$.
 Step 3: Figure 5 shows a table. For making a table, $(n - k) \times k = 6 \times 5$. First value, i.e., 6 shows the number of rows and 5 the number of columns.
 Step 4: message becomes $G = 173, R = 235, A = 132, P = 232, H = 175$; $6 \leq i \leq 11, 1 \leq j \leq 5$.
 Step 5: corresponding values are

$$\begin{aligned}
 a_1 &= 17 \times 3 = 51, \\
 a_2 &= 23 \times 5 = 115, \\
 a_3 &= 13 \times 2 = 26, \\
 a_4 &= 23 \times 2 = 46, \\
 a_5 &= 17 \times 5 = 85.
 \end{aligned} \tag{12}$$

Next, we construct a path graph by labelling the vertices, as shown in Figure 6
 Here, $V_1 = \{5, 11, 2, 4, 8\}$ and $V_2 = \{1, 5, 6\}$.
 The vertex set of bipartite graph becomes
 $G(V_1, V_2) = \{(5, 1), (11, 5), (2, 6), (4, 6), (8, 5)\}$. (13)
 Graph is obtained as shown in Figure 7.
 Now, apply arbitrary weights to the adjacent edges of the bipartite graph in Figure 7, as shown in Figure 8.
 Send the labeled graph in Figure 8 to the receiving authority. Then, apply the steps for decryption:

Step 1: at first, arrange the weight of the edges in ascending order:

$$W = \{10, 18, 21, 36, 41\}. \tag{14}$$

Step 2: now, arrange edges $\{(5,1), (11,5), (2,6), (4,6), (8,5)\}$.

The corresponding path graph is shown in Figure 9.

Step 3: prime factorization of each vertex label. As, $51 = 3 \times 17, \dots, 85 = 5 \times 17$. Numerical values are 173, 235, 132, 232, and 175, respectively.

Step 4: we finally get the alphabets **GRAPH** according to values in the described table. Keep in view that one place digits are not in column position.

The examples prove the security of described algorithm. This tells a simple bipartite graph can make secrecy of information very strong, that is, the major output of any encryption scheme.

4. Secure Data Transfer Using Star Graphs

Many schemes are introduced to protect data. The mentioned scheme is based on star graphs. Information is transferred with full secrecy of main idea. These steps are followed to encrypt data and then decrypt it by applying decryption steps.

Algorithm for encryption is as follows:

Let M be the message which is to be encrypted. Length is $l(\text{say})$.

Here, we have to use shift cipher with formulation:

$$e_k(x) = x + k \pmod{26}. \tag{15}$$

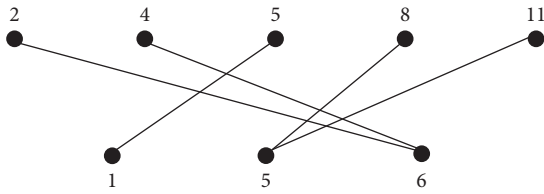


FIGURE 7

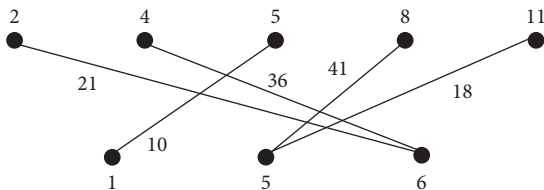


FIGURE 8

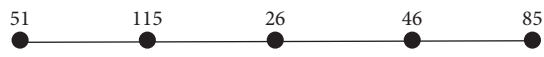


FIGURE 9

Keeping $k = l$ (fixed).

Converting the plaintext message to a sequence of integers by adding k into every value, by reducing every sum into modulo 26.

Now, take a star graph $S_{n+1} = K_1 \odot \overline{K_n}$, corresponding to the length of message, by fixing center vertex with the numeric value zero, such that number of vertices of star graph = 1 + number of alphabetic characters in the text.

Representing data as vertices of a graph, each vertex is represented by a letter. However, all adjacent vertices of a graph will be represented as adjacent letters.

Now label each vertex with respect to their numeric representation in shift cipher.

Next, give weights $w_1, w_2, w_3, \dots, w_n$ to each edge $e_1, e_2, e_3, \dots, e_n$ in such a way that

$$w_1(e_1) < w_2(e_2) < w_3(e_3) < \dots < w_n(e_n). \quad (16)$$

Method for finding weights of edges.

Subtract increasing power of 10 from each vertex label, adjacently with respect to edges, such that

$$V_1 - 10, V_2 - 10^2, V_3 - 10^3, \dots, V_n - 10^n, \quad (17)$$

where $V_i \in$ vertex tex $i = \{1, 2, 3, \dots, n\}$.

These resulting values become weight of corresponding edges e_i .

Now, the final graph is the star graph with edge's weights (hiding the vertex label).

Send this graph to the receiver.

After explaining the encryption procedure, we have to explain the decryption scheme as well.

Algorithm for decryption is as follows:

Arrange the weight of edges in ascending order.

Now add up the increasing power of 10, respectively.

Apply the decryption formulation for shift cipher in the resulting number.

Decode the characters from encoding table, and eventually, we get the required text.

Example 3. For explaining the described scheme, we have to take an example for satisfying the steps. Let us take a word **CODE**. We have to send this word by encrypting it with the help of such scheme.

Replace the alphabetic characters with their numeric representation. Length of message is $k = 4$:

$$\begin{matrix} C & O & D & E \\ 3 & 15 & 4 & 5 \end{matrix} \quad (18)$$

Now, consider a star graph $S_5 = K_1 \odot \overline{K_4}$, such that the number of its corner vertices is equal to the length of message. Figure 10 shows the respective star graph in such a way that edges are labeled as $e_1, e_2, e_3,$ and e_4 .

Apply the shift type of cipher as shifting up to the length k of the message. In this example, translated through formula,

$$e_4(x) = x + 4 \pmod{6}. \quad (19)$$

New shifted numeric values are 7, 19, 8, and 9, respectively. The related graph becomes as shown in Figure 11.

After that, apply weights $w_i, \forall i \in \{1, 2, 3, 4\}$ to the corresponding edges of the vertices:

$$w_1(7) < w_2(19) < w_3(8) < w_4(9). \quad (20)$$

Weights are given by subtracting the increasing power of 10 from each adjacent numeric value in Figure 11:

$$\begin{aligned} \text{weight of edge } e_1 &= w_1 = 7 - 10, \\ \text{weight of edge } e_2 &= w_2 = 19 - 10^2, \\ \text{weight of edge } e_3 &= w_3 = 8 - 10^3, \\ \text{weight of edge } e_4 &= w_4 = 9 - 10^4. \end{aligned} \quad (21)$$

Resulting star graph is shown in Figure 12.

This is the final labeled graph, which is to be send to the second authority. Now, describe the decryption process. Firstly, the recipient receives the labeled graph, as shown in Figure 12.

The initial step is arranging the weights of edges (Figure 13) in ascending order of mod values, i.e.,

$$|-3| < |-81| < |-992| < |-9991|. \quad (22)$$

Add the increasing power of 10 to each adjacent value such that

$$|-3 + 10| < |-81 + 100| < |-992 + 1000| < |-9991 + 10000|. \quad (23)$$

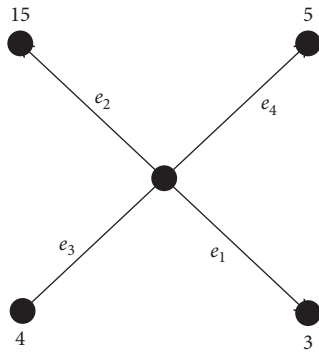


FIGURE 10

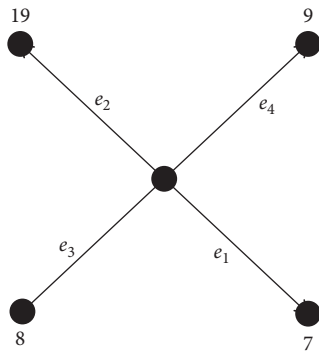


FIGURE 11

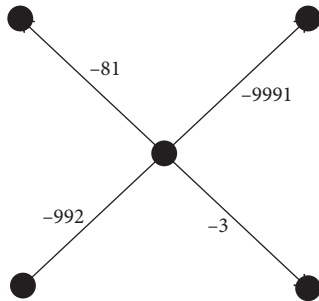


FIGURE 12

Through this mod operation, we get the values:

$$7, 19, 8, 9. \tag{24}$$

Apply inverse shifting by guessing the number of edges of the star graph, which is 4. So, the values become as follows:

$$\begin{aligned} 7 - 4 &= 3, \\ 19 - 4 &= 15, \\ 8 - 4 &= 4, \\ 9 - 4 &= 5. \end{aligned} \tag{25}$$

Finally, we get the values 3, 15, 4, 5. Through the encoding table, we get their respective letters as **C O D E**. Get the required hidden text.

This example explains that any type of data is hidden and is kept secure until it approaches to the receiver. The

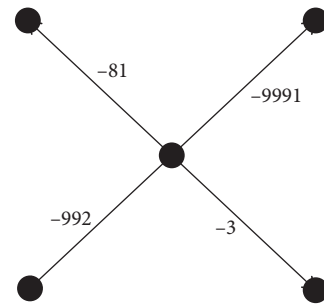


FIGURE 13

algorithm depends on star graphs. Labeled graphs are sent to the recipient. It is a best possible way to secure the data.

5. Conclusion

This work presents graph theoretic-based schemes to improve encryption quality. Three new encryption algorithms are proposed which are very helpful for secure communication of secret messages. In the first algorithm, encryption and decryption is performed by using a specific corona graph $C_n \odot K_1$ along with some basic algebraic properties. The second algorithm is based on encoding table, bipartite graph, and the concept of unique factorization domain (UFD). In third algorithm, we used a certain labeling of vertices and edges of the star graph $K_1 \odot \overline{K}_n$. These symmetric algorithms use the concept of shared key that must be predefined and shared between two communicating parties. We can modify the proposed algorithms, to be applicable for the communication of sentences or the set of sentences. Furthermore, for more complexity, these algorithms could be improved by using the public key cryptography. Moreover, we can try to implement these algorithms using any programming language like C++, JAVA, or Microsoft.Net.

Data Availability

There are no additional data required.

Conflicts of Interest

The authors declare that there are no conflicts of interest.

Acknowledgments

The study was supported by the Heilongjiang Education Department Project (project number: 1355MSYQN001) and Research Project of Mudanjiang Normal University (project number: QN2020008). Also, the authors are thankful to the referees for many useful suggestions.

References

- [1] C. E. Shannon, "Communication theory of secrecy systems*," *Bell System Technical Journal*, vol. 28, no. 4, pp. 656–715, 1949.
- [2] K. H. Rosen, *Elementary Number Theory and its Applications*, Addison-Wesley, Boston, MA, USA, 5th edition, 2005.

- [3] D. R. Stinson, *Cryptography: Theory and Practice*, Chapman and Hall/CRC, Boca Raton, FL, USA, 4th edition, 2018.
- [4] D. B. West, *Introduction to Graph Theory*, Pearson, London, UK, 2nd edition, 2001.
- [5] R. Frucht and F. Harary, "On the corona of two graphs," *Aequationes Math*, vol. 4, pp. 322–325, 1970.
- [6] R. L. Rivest, A. Shamir, and L. Adleman, "A method for obtaining digital signatures and public-key cryptosystems," *Communications of the ACM*, vol. 21, no. 2, pp. 120–126, 1978.
- [7] V. A. Ustimenko, "On graph-based cryptography and symbolic computations," *Serdica Journal of Computing*, vol. 1, pp. 131–156, 2007.
- [8] D. X. Charles, K. E. Lauter, and E. Z. Goren, "Cryptographic hash functions from expander graphs," *Journal of Cryptology*, vol. 22, no. 1, pp. 93–113, 2009.
- [9] P. L. K. Priyadarsini, "A survey on some applications of graph theory in cryptography," *Journal of Discrete Mathematical Sciences and Cryptography*, vol. 18, no. 3, pp. 209–217, 2015.
- [10] R. Selvakumar and N. Gupta, "Fundamental circuits and cut-sets used in cryptography," *Journal of Discrete Mathematical Sciences and Cryptography*, vol. 15, no. 4-5, pp. 287–301, 2012.
- [11] P. Kedia and S. Agrawal, "Encryption using Venn-diagrams and graph," *International Journal of Advanced Computer Technology*, vol. 4, no. 01, pp. 94–99, 2015.
- [12] M. Yamuna and A. Elakkiya, "Data transfer using fundamental circuits," *International Journal of Computer and Modern Technology*, vol. 2, no. 01, 2015.
- [13] M. Yamuna and K. Karthika, "Data transfer using bipartite graphs," *International Journal of Advance Research in Science and Engineering*, vol. 4, no. 02, pp. 128–131, 2015.
- [14] W. Mahmoud and A. Etaiwi, "Encryption algorithm using graph theory," *Journal of Scientific Research and Reports*, vol. 3, no. 19, pp. 2519–2527, 2014.
- [15] B. R. Arunkumar, "Applications of Bipartite Graph in diverse fields including cloud computing," *International Journal of Modern Engineering Research*, vol. 5, no. 7, p. 7, 2015.
- [16] D. Sinha and A. Sethi, "Encryption using network and matrices through signed graphs," *International Journal of Computer Applications (0975-8887)*, vol. 138, no. 4, pp. 6–13, 2016.
- [17] J. Hu, J. Liang, and S. Dong, "A bipartite graph propagation approach for mobile advertising fraud detection," *Mobile Information Systems*, vol. 2017, p. 12, Article ID 6412521, 2017.
- [18] A. Razaq, M. Awais Yousaf, U. Shuaib, N. Siddiqui, A. Ullah, and A. Waheed, "A novel construction of substitution box involving coset diagram and a bijective map," *Security and Communication Networks*, vol. 2017, p. 16, Article ID 5101934, 2017.
- [19] A. Razaq, H. Alolaiyan, M. Ahmad et al., "A novel method for generation of strong substitution-boxes based on coset graphs and symmetric groups," *IEEE Access*, vol. 8, pp. 75473–75490, 2020.
- [20] G. A. Selim, "How to encrypt a graph," *International Journal of Parallel, Emergent and Distributed Systems*, vol. 35, no. 6, pp. 668–681, 2020.

Research Article

Some Algebraic Properties of a Class of Integral Graphs Determined by Their Spectrum

Jia-Bao Liu ¹, S. Morteza Mirafzal ², and Ali Zafari ³

¹School of Mathematics and Physics, Anhui Jianzhu University, Hefei 230601, China

²Lorestan University, Department of Mathematics, Faculty of Science, Khorramabad, Iran

³Department of Mathematics, Faculty of Science, Payame Noor University, P.O. Box 19395-4697, Tehran, Iran

Correspondence should be addressed to Ali Zafari; zafari.math.pu@gmail.com

Received 28 December 2020; Revised 27 January 2021; Accepted 5 February 2021; Published 17 February 2021

Academic Editor: Ghulam Mustafa

Copyright © 2021 Jia-Bao Liu et al. This is an open access article distributed under the Creative Commons Attribution License, which permits unrestricted use, distribution, and reproduction in any medium, provided the original work is properly cited.

Let $\Gamma = (V, E)$ be a graph. If all the eigenvalues of the adjacency matrix of the graph Γ are integers, then we say that Γ is an integral graph. A graph Γ is determined by its spectrum if every graph cospectral to it is in fact isomorphic to it. In this paper, we investigate some algebraic properties of the Cayley graph $\Gamma = \text{Cay}(\mathbb{Z}_n, S)$, where $n = p^m$ (p is a prime integer and $m \in \mathbb{N}$) and $S = \{a \in \mathbb{Z}_n \mid (a, n) = 1\}$. First, we show that Γ is an integral graph. Also, we determine the automorphism group of Γ . Moreover, we show that Γ and $K_\nu \nabla \Gamma$ are determined by their spectrum.

1. Introduction

The graphs in this paper are simple, undirected, and connected. We always assume that $\bar{\Gamma}$ denotes the complement graph of Γ . The eigenvalues of a graph Γ are the eigenvalues of the adjacency matrix of Γ . The spectrum of Γ is the list of the eigenvalues of the adjacency matrix of Γ together with their multiplicities, and it is denoted by $\text{Spec}(\Gamma)$; see [1]. If all the eigenvalues of the adjacency matrix of the graph Γ are integers, then we say that Γ is an integral graph. The notion of integral graphs was first introduced by Harary and Schwenk in 1974; see [2]. In general, the problem of characterizing integral graphs seems to be very difficult. There are good surveys in this area; see [3]. For more results depending on the integral graphs and their applications in engineering networks, see [4–6]. For any vertex v of a connected graph Γ , we denote the set of vertices of Γ at distance r from v by $\Gamma_r(v)$. Then, we have

$$\Gamma_r(v) = \{u \in V(\Gamma) \mid d(u, v) = r\}, \quad (1)$$

where $d(u, v)$ denotes the distance in Γ between the vertices u and v and r is a nonnegative integer not exceeding d , the diameter of Γ . It is clear that $\Gamma_0(v) = \{v\}$, and $V(\Gamma)$ is

partitioned into the disjoint subsets $\Gamma_0(v), \dots, \Gamma_d(v)$, for each v in $V(\Gamma)$. The graph Γ is called distance regular with diameter d and intersection array $\{b_0, \dots, b_{d-1}; c_1, \dots, c_d\}$ if it is regular of valency k and, for any two vertices u and v in Γ at distance r , we have $|\Gamma_{r+1}(v) \cap \Gamma_1(u)| = b_r$, ($0 \leq r \leq d-1$), and $|\Gamma_{r-1}(v) \cap \Gamma_1(u)| = c_r$ ($1 \leq r \leq d$). The intersection numbers c_r, b_r , and a_r satisfy $a_r = k - b_r - c_r$ ($0 \leq r \leq d$), where a_r is the number of neighbours of u in $\Gamma_r(v)$. Let G be a finite group and let H be a subset of G such that it is closed under taking inverses and does not contain the identity. A Cayley graph $\Gamma = \text{Cay}(G, H)$ is the graph whose vertex set and edge set are defined as follows:

$$\begin{aligned} V(\Gamma) &= G; \\ E(\Gamma) &= \{\{x, y\} \mid x^{-1}y \in H\}. \end{aligned} \quad (2)$$

It is well known that if Γ is a distance regular graph with valency k , diameter d , adjacency matrix A , and intersection array

$$\{b_0, b_1, \dots, b_{d-1}; c_1, c_2, \dots, c_d\}, \quad (3)$$

then the tridiagonal $(d+1) \times (d+1)$ matrix,

$$B = \begin{bmatrix} a_0 & b_0 & 0 & 0 & \dots \\ c_1 & a_1 & b_1 & 0 & \dots \\ 0 & c_2 & a_2 & b_2 & \\ & & & \dots & \\ & & & & c_{d-2} & a_{d-2} & b_{d-2} & 0 \\ & & & & \dots & 0 & c_{d-1} & a_{d-1} & b_{d-1} \\ & & & & \dots & 0 & 0 & c_d & a_d \end{bmatrix}, \quad (4)$$

determines all the eigenvalues of Γ [7]. Note that the concept of distance regular graphs dates back to the 1960s. They were defined by Biggs; see [8]; and their basic theory was developed by him and others. Distance regular graphs of diameter 2 are just the connected strongly regular graphs. The theory of distance regular graphs has connections to many parts of graph theory such as design theory, coding theory, geometry, and group theory. Two graphs with the same spectrum are called cospectral. It is not hard to see that the spectrum of a graph does not determine its isomorphism class. The authors in [9] proposed the following question: which graphs are determined by their spectrum? It seems hard to prove a graph to be determined by its spectrum. Up to now, only a few classes of graphs are proved to be determined by their spectrum, such as the path P_n , the complete graph K_n and the cycle C_n , graph Z_n , and their complements; see [10–12]. For a graph Γ , let $A(\Gamma)$ and $L(\Gamma) = D(\Gamma) - A(\Gamma)$ be, respectively, the adjacency matrix and Laplacian matrix of Γ , where $D(\Gamma)$ is the diagonal matrix of vertex degrees with $\{d_1, d_2, \dots, d_n\}$ as diagonal entries. Laplacian spectra and their applications are involved in diverse theoretical problems on complex networks [13, 14]. Many results have been devoted to studying Laplacian spectrum for complex networks [15, 16]. Calculating the Laplacian spectrum of networks has many applications in lots of aspects, such as the topological structures and dynamical processes [17]. Algebraic properties of various classes of Cayley graphs have been studied by various authors; see [18, 19]. In this paper, we want to study some algebraic properties of a class of Cayley graphs constructed on the cyclic additive group \mathbb{Z}_n , denoted by $\Gamma = \text{Cay}(\mathbb{Z}_n, S)$, where $n = p^m$ (p is a prime integer and $m \in \mathbb{N}$) and $S = \{a \in \mathbb{Z}_n \mid (a, n) = 1\}$. It is easy to check that S is an inverse closed subset in the group \mathbb{Z}_n and $0 \notin S$. Thus, Γ is a simple graph. This class of graphs is a special subclass of graphs, which are investigated from some other aspects by Basić and Ilić [20]. Using the theory of distance regular graphs, we show that the adjacency spectrum of Γ is $\{n - p^{m-1}, 0^{(n-p)}, (-p^{m-1})^{(p-1)}\}$, where the superscripts give the multiplicities of eigenvalues with multiplicity greater than one. Finally, we show that any graph cospectral with the multicone graph $K_v \nabla \Gamma$ is determined by its adjacency spectrum as well as its Laplacian spectrum, where K_v is the complete graph on v vertices.

2. Definitions and Preliminaries

Definition 1 (see [7, 21]). Let Γ be a graph with automorphism group $\text{Aut}(\Gamma)$. We say that Γ is a vertex transitive graph if, for all vertices x, y of Γ , there is an automorphism θ in $\text{Aut}(\Gamma)$ satisfying $\theta(x) = y$. Also, we say that Γ is distance transitive graph if, for all vertices u, v, x, y of Γ such that $d(u, v) = d(x, y)$, there is an automorphism θ in $\text{Aut}(\Gamma)$ satisfying $\theta(u) = x$ and $\theta(v) = y$.

Theorem 1 (see [22]). Let Γ be a graph such that it contains k components $\Gamma_1, \dots, \Gamma_k$. If, for any $i \in I = \{1, \dots, k\}$, we have $\Gamma_i \cong \Gamma_1$, then $\text{Aut}(\Gamma) \cong \text{Aut}(\Gamma_1) \text{wr}_1 \text{Sym}(k)$, where the wreath product is defined.

Definition 2 (see [23]). Let $\Gamma_1 \cup \Gamma_2$ denote the disjoint union of graphs Γ_1 and Γ_2 . The join $\Gamma_1 \nabla \Gamma_2$ is the graph obtained from $\Gamma_1 \cup \Gamma_2$ by joining every vertex of Γ_1 with every vertex of Γ_2 . A multicone graph is defined to be the join of a clique and a regular graph.

Theorem 2 (see [9]). If Γ is a distance regular graph with diameter d and girth g satisfying one of the following properties, then every graph cospectral with Γ is also distance regular, with the same parameters as Γ :

- (i) $g \geq 2d - 1$
- (ii) $g \geq 2d - 2$ and Γ is bipartite

Proposition 1 (see [9]). For regular graphs, being DS (or not DS) is equivalent for the adjacency matrix, the adjacency matrix of the complement, and the Laplacian matrix.

Proposition 2 (see [9]). The following graph and its complement, which have at most four eigenvalues, are regular DS graphs:

- (i) The disjoint union of k copies of a strongly regular DS graph.

Theorem 3 (see [24]). Let Γ_1 and Γ_2 be two graphs with the Laplacian spectrum $\lambda_1 \geq \lambda_2 \geq \dots \geq \lambda_n$ and $\mu_1 \geq \mu_2 \geq \dots \geq \mu_m$, respectively. Then, the Laplacian spectrum of $\Gamma_1 \nabla \Gamma_2$ is $n + m, m + \lambda_1, m + \lambda_2, \dots, m + \lambda_{n-1}, n + \mu_1, n + \mu_2, \dots, n + \mu_{m-1}, 0$.

Theorem 4 (see [1]). Let Γ be a graph on n vertices. Then, n is a Laplacian eigenvalue of Γ if and only if Γ is the join of two graphs.

Lemma 1 (see [1]). A connected graph Γ has exactly one positive eigenvalue if and only if it is a complete multipartite graph.

3. Main Results

Theorem 5. Let $\Gamma = \text{Cay}(\mathbb{Z}_n, S)$ be the Cayley graph on the cyclic group \mathbb{Z}_n , where $n = p^m$ (p is a prime integer and $m \in \mathbb{N}$) and $S = \{a \in \mathbb{Z}_n \mid (a, n) = 1\}$. Then,

$$\text{Aut}(\Gamma) \cong \text{Sym}(p^{m-1})wr_I \text{Sym}(p), \quad (5)$$

where $I = \{1, 2, \dots, p\}$.

Proof. Let $V(\Gamma) = \{1, \dots, n\}$ be the vertex set of Γ . Note that if $m = 1$, then the result immediately follows. Because, in this case, $\Gamma \cong K_p$, where K_p is the complete graph on p vertices, in the sequel, we assume that $m \geq 2$. Let $T = \langle p \rangle = \{kp \mid 0 \leq k \leq p^{m-1} - 1\}$ be the subgroup of the group \mathbb{Z}_n of order p^{m-1} . It is clear that T and every coset of T represent an independent set in the graph Γ . In fact, if $T + a$ is a coset of T in the group \mathbb{Z}_n such that $T \cap T + a = \emptyset$, then a and p are coprime and hence we have $a \in S$. It follows that every coset of T is a clique of order p^{m-1} in the complement of the graph Γ . Thus, $\bar{\Gamma}$ contains p disjoint components $\Gamma_1, \Gamma_2, \dots, \Gamma_p$ such that $\Gamma_i \cong K_{p^{m-1}}$ ($1 \leq i \leq p$), where $K_{p^{m-1}}$ is the complete graph on p^{m-1} vertices. It follows that $\bar{\Gamma} \cong pK_{p^{m-1}}$. Hence, by Theorem 1, $\text{Aut}(\bar{\Gamma}) \cong \text{Aut}(K_{p^{m-1}})wr_I \text{Sym}(p) = \text{Sym}(p^{m-1})wr_I \text{Sym}(p)$. On the other hand, it is well known that, for any graph Γ , $\text{Aut}(\Gamma) = \text{Aut}(\bar{\Gamma})$; see [1]. \square

Proposition 3. Let $\Gamma = \text{Cay}(\mathbb{Z}_n, S)$ be the Cayley graph on the cyclic group \mathbb{Z}_n , where $n = p^m$ (p is a prime integer and $m \in \mathbb{N}$) and $S = \{a \in \mathbb{Z}_n \mid (a, n) = 1\}$. Then Γ is a distance transitive graph.

Proof. Suppose that u, v, x, y are vertices of Γ such that $d(u, v) = d(x, y) = r$, where r is a nonnegative integer not exceeding d , the diameter of Γ . So $d(u, v) = d(x, y) = 1$ or 2 , since we now have the diameter of Γ as $d = 2$. In the following cases, we show that Γ is a distance transitive graph.

Case 1. If $d(u, v) = d(x, y) = 2$, then $u^{-1}v \notin S$ and $x^{-1}y \notin S$. Therefore, two vertices u and v are adjacent in the complement $\bar{\Gamma}$ of Γ ; also two vertices x and y are adjacent in the complement $\bar{\Gamma}$ of Γ . By Theorem 5, we know that $\bar{\Gamma}$ contains p components $\Gamma_1, \Gamma_2, \dots, \Gamma_p$ such that, for any $i \in \{1, 2, \dots, p\}$, $\Gamma_i \cong K_{p^{m-1}}$. Therefore, $\bar{\Gamma} \cong pK_{p^{m-1}}$. If $u = x$, then u, v, y lie in a clique of graph $\bar{\Gamma}$, and hence we may assume that $\theta = (vy) \in \text{Aut}(\bar{\Gamma}) = \text{Aut}(\Gamma)$, so $\theta(u) = x$ and $\theta(v) = y$. If $u \neq x$ and $v \neq y$, then u, v lie in a clique of graph $\bar{\Gamma}$, say Γ_i ; also x, y lie in a clique of graph $\bar{\Gamma}$, say Γ_j , where $\Gamma_i \neq \Gamma_j$ or $\Gamma_i = \Gamma_j$. Hence, we may assume that $\theta = (ux)(vy) \in \text{Aut}(\bar{\Gamma}) = \text{Aut}(\Gamma)$. Thus, $\theta(u) = x$ and $\theta(v) = y$.

Case 2. If $d(u, v) = d(x, y) = 1$, then we can show that there is an automorphism θ in $\text{Aut}(\Gamma)$ such that $\theta(u) = x$ and $\theta(v) = y$. \square

Proposition 4. Let $\Gamma = \text{Cay}(\mathbb{Z}_n, S)$ be the Cayley graph on the cyclic group \mathbb{Z}_n , where $n = p^m$ (p is a prime integer and

$m \in \mathbb{N}$) and $S = \{a \in \mathbb{Z}_n \mid (a, n) = 1\}$. Then Γ is an integral graph.

Proof. It is well known that if Γ is a distance transitive graph, then Γ is also distance regular; see [21]. Now, let $V(\Gamma) = \{1, 2, \dots, n\}$ be the vertex set of Γ . Consider the vertex $v = n$ in $V(\Gamma)$; then $\Gamma_0(v) = \{n\}$, $\Gamma_1(v) = \{a \in V(\Gamma) \mid (a, n) = 1\}$, and $\Gamma_2(v) = \{a \in V(\Gamma) \mid (a, n) \neq 1\}$. Let u be the vertex in $V(\Gamma)$ such that $d(u, v) = 0$; then $u = v = n$ and $|\Gamma_1(v) \cap \Gamma_1(u)| = n - p^{m-1}$. Hence, $b_0 = n - p^{m-1}$, and, by definition of distance regularity of graph, we have $a_0 = (n - p^{m-1}) - b_0 = 0$. Also, if u in $V(\Gamma)$ and $d(u, v) = 1$, then two vertices u, v are adjacent in Γ , so $|\Gamma_0(v) \cap \Gamma_1(u)| = 1$, and $|\Gamma_2(v) \cap \Gamma_1(u)| = p^{m-1} - 1$. Hence, $c_1 = 1$, $b_1 = p^{m-1} - 1$, and $a_1 = (n - p^{m-1}) - b_1 - c_1 = n - 2p^{m-1}$. Finally, if u in $V(\Gamma)$ and $d(u, v) = 2$, then two vertices u, v are not adjacent in Γ , so $|\Gamma_1(v) \cap \Gamma_1(u)| = n - p^{m-1}$; hence, $c_2 = n - p^{m-1}$ and $a_2 = (n - p^{m-1}) - (n - p^{m-1}) = 0$. Thus, the intersection array of Γ is $\{n - p^{m-1}, p^{m-1} - 1; 1, n - p^{m-1}\}$. Therefore, the tridiagonal $(3) \times (3)$ matrix,

$$\begin{bmatrix} a_0 & b_0 & 0 \\ c_1 & a_1 & b_1 \\ 0 & c_2 & a_2 \end{bmatrix} = \begin{bmatrix} 0 & n - p^{m-1} & 0 \\ 1 & n - 2p^{m-1} & p^{m-1} - 1 \\ 0 & n - p^{m-1} & 0 \end{bmatrix}, \quad (6)$$

determines all the eigenvalues of Γ . It is clear that all the eigenvalues of Γ are $n - p^{m-1}, 0, -p^{m-1}$, and their multiplicities are $1, n - p, p - 1$, respectively. Thus, Γ is an integral graph. \square

Corollary 1. Let $\Gamma = \text{Cay}(\mathbb{Z}_n, S)$ be the Cayley graph on the cyclic group \mathbb{Z}_n , where $n = p^m$ (p is a prime integer and $m \in \mathbb{N}$) and $S = \{a \in \mathbb{Z}_n \mid (a, n) = 1\}$. Then the adjacency spectrum of Γ is $\{n - p^{m-1}, 0^{(n-p)}, (-p^{m-1})^{(p-1)}\}$.

Theorem 6. Let $\Gamma = \text{Cay}(\mathbb{Z}_n, S)$ be the Cayley graph on the cyclic group \mathbb{Z}_n , where $n = p^m$ (p is a prime integer and $m \in \mathbb{N}$) and $S = \{a \in \mathbb{Z}_n \mid (a, n) = 1\}$. Then Γ is a DS graph with respect to its adjacency spectrum.

Proof. We know that if p is even prime integer, then Γ is isomorphic to the bipartite graph $K_{p^{m-1}, p^{m-1}}$, and hence the result immediately follows.

Now, let p be an odd prime integer; then, Γ is not bipartite graph. In particular, $g \geq 2d - 1$, because the diameter of Γ is 2 and the girth of Γ is 3. Hence, by Theorem 2, every graph cospectral with Γ is also distance regular, with the same parameters as Γ . Because by Proposition 3 we know that Γ is a distance regular graph, Γ is a DS graph with respect to its adjacency spectra. Because, by Proposition 2, $\bar{\Gamma}$ contains disjoint union of p copies of the strongly regular DS graph $K_{p^{m-1}}$ in addition to the graph Γ and its complement, which have at most four eigenvalues. \square

Proposition 5. Let Π be a graph cospectral with the multicone graph $K_v \nabla \Gamma$ with respect to its adjacency matrix

spectrum, where $\Gamma = \text{Cay}(\mathbb{Z}_n, S)$, which is defined as before. Then Π is a bidegreed graph. Also,

$$\text{Spec}(\Pi) = \left\{ 0^{(n-p)}, (-p^{m-1})^{(p-1)}, -1^{(v-1)}, \left(\frac{M + \sqrt{M^2 + 4N}}{2} \right), \left(\frac{M - \sqrt{M^2 + 4N}}{2} \right) \right\}, \quad (7)$$

where $M = v - 1 + p^m - p^{m-1}$ and $N = p^m + p^{m-1}v - p^{m-1}$.

Proof. We can deduce the following from Theorem 2.1.8 in [25] and Theorem 2.1 in [26]. \square

Theorem 7. Consider the multicone graph $K_v \nabla \Gamma$, where $\Gamma = \text{Cay}(\mathbb{Z}_n, S)$, which is defined as before. Then $K_v \nabla \Gamma$ is DS with respect to its adjacency matrix spectrum.

Proof. In the following, we proceed by induction on the number of vertices in K_v . Let K_v have one vertex and let Π be a graph cospectral with the multicone graph $K_1 \nabla \Gamma$ with respect to its adjacency matrix spectrum. By Proposition 5, it is easy to see that Π has one vertex of degree p^m , say j . Hence, if $\text{Spec}(\Pi - j) = \text{Spec}(\Gamma)$, then $\Pi - j \cong \Gamma$. Because, by Theorem 6, we know that Γ is DS graph with respect to its adjacency matrix spectrum, $\Pi \cong K_1 \nabla \Gamma$. We assume inductively that this claim holds for K_v ; that is, if Π_1 is a graph cospectral with the multicone graph $K_v \nabla \Gamma$ with respect to its adjacency matrix spectrum, then $\Pi_1 \cong K_v \nabla \Gamma$. We show that the claim is true for K_{v+1} ; that is, if Π is a graph cospectral with the multicone graph $K_{v+1} \nabla \Gamma$ with respect to its adjacency matrix spectrum, then $\Pi \cong K_{v+1} \nabla \Gamma$. It is obvious that Π has one vertex and $p^m + v$ edges more than Π_1 . On the other hand, by Proposition 5, we know that Π_1 has v vertices of degree $p^m + v - 1$ and p^m vertices of degree $p^m - p^{m-1} + v$, and also Π has $v + 1$ vertices of degree $p^m + v$ and p^m vertices of degree $p^m - p^{m-1} + v + 1$. So, we must have $\Pi \cong K_1 \nabla \Pi_1$. Now, by assuming induction, we conclude that $\Pi \cong K_{v+1} \nabla \Gamma$ and complete the proof. \square

Theorem 8. Consider the complement $\overline{K_v \nabla \Gamma}$ of multicone graph $K_v \nabla \Gamma$ with respect to its adjacency spectrum, where $\Gamma = \text{Cay}(\mathbb{Z}_n, S)$, which is defined as before. Then, $\overline{K_v \nabla \Gamma}$ is a DS graph.

Proof. By Theorem 5, we know that $\overline{\Gamma}$ contains p components $\Gamma_1, \Gamma_2, \dots, \Gamma_p$ such that $\Gamma_i \cong K_{p^{m-1}}$ ($1 \leq i \leq p$). So $\overline{\Gamma} \cong pK_{p^{m-1}}$. In addition, the adjacency matrix spectrum of $\overline{\Gamma}$ is

$$\left\{ (p^{m-1} - 1)^{(p)}, -1^{(p^{m-p})} \right\}. \quad (8)$$

Also, the adjacency matrix spectrum of $\overline{K_v}$ is $\{0^{(v)}\}$. Thus, the adjacency matrix spectrum of $\overline{\Gamma \cup \overline{K_v}}$ is

$$\left\{ (p^{m-1} - 1)^{(p)}, -1^{(p^{m-p})}, 0^{(v)} \right\}. \quad (9)$$

On the other hand, it is not hard to see that $\overline{\Gamma \cup \overline{K_v}} \cong \overline{K_v \nabla \Gamma}$. Let Π be a graph cospectral with the complement $\overline{K_v \nabla \Gamma}$ of multicone graph $K_v \nabla \Gamma$ with respect to its adjacency spectrum; then,

$$\text{Spec}(\Pi) = \text{Spec}(\overline{K_v \nabla \Gamma}) = \left\{ (p^{m-1} - 1)^{(p)}, -1^{(p^{m-p})}, 0^{(v)} \right\}. \quad (10)$$

It is easy to prove that Π cannot be regular, since regularity of a graph can be determined by its spectrum. Also, we show that Π is disconnected graph. Suppose to the contrary that Π is connected; hence, by Lemma 1, Π is complete multipartite graph, contradicting the adjacency spectrum of Π . Thus, Π is disconnected graph. Therefore, we conclude that $\overline{K_v \nabla \Gamma}$ is DS with respect to its adjacency spectrum. \square

Proposition 6. Consider the multicone graph $K_v \nabla \Gamma$, where $\Gamma = \text{Cay}(\mathbb{Z}_n, S)$, which is defined as before. Then $K_v \nabla \Gamma$ is DS with respect to its Laplacian spectrum.

Proof. By Theorem 3, the Laplacian matrix spectrum of $K_v \nabla \Gamma$ is

$$\left\{ (n + v)^{(p+v-1)}, (n + v - p^{m-1})^{(n-p)}, 0 \right\}. \quad (11)$$

We proceed by induction on the number of vertices in K_v . If $v = 1$, there is nothing to prove. We assume inductively that this claim holds for K_v ; that is, if $\text{Spec}(L(\Pi_1)) = \text{Spec}(L(K_v \nabla \Gamma))$, then $\Pi_1 \cong K_v \nabla \Gamma$, where Π_1 is a graph cospectral with the multicone graph $K_v \nabla \Gamma$ with respect to its Laplacian spectrum. We show that the claim is true for K_{v+1} ; that is, if

$$\begin{aligned} \text{Spec}(L(\Pi)) &= \text{Spec}(L(K_{v+1} \nabla \Gamma)) \\ &= \left\{ (n + v + 1)^{(p+v)}, (n + v + 1 - p^{m-1})^{(n-p)}, 0 \right\}, \end{aligned} \quad (12)$$

then $\Pi \cong K_{v+1} \nabla \Gamma$, where Π is a graph cospectral with the multicone graph $K_{v+1} \nabla \Gamma$ with respect to its Laplacian spectrum. By Theorem 4, we know that Π_1 and Π are join of two graphs, because $n + v$ and $n + v + 1$ are eigenvalues of Π_1 and Π , respectively. In addition, Π has one vertex of degree $n + v$ more than Π_1 , say j ; hence, $\text{Spec}(L(\Pi - j)) \cong \text{Spec}(L(K_v \nabla \Gamma))$, and, by assuming induction, $\Pi - j \cong K_v \nabla \Gamma$. Thus, it can be concluded that $\Pi \cong K_{v+1} \nabla \Gamma$. \square

4. Conclusion

In this paper, we computed the adjacency spectrum of a class of integral graphs, denoted by $\Gamma = \text{Cay}(\mathbb{Z}_n, S)$, where $n = p^m$ (p is a prime integer and $m \in \mathbb{N}$) and $S = \{a \in \mathbb{Z}_n \mid (a, n) = 1\}$. Indeed, by using the theory of distance regular graphs, it is shown that the adjacency spectrum of Γ is $\{n - p^{m-1}, 0^{(n-p)}, (-p^{m-1})^{(p-1)}\}$, where the superscripts give the multiplicities of eigenvalues with multiplicity greater than one. Moreover, it is shown that the Cayley graph Γ and $K_\nu \nabla \Gamma$ are determined by their spectrum. Note that this class of graphs is a special subclass of integral circulants, and hence clearly not only is this class of graphs mathematically applicable, but also it is used in the design of engineering networks.

Data Availability

No data were used to support this study.

Conflicts of Interest

The authors declare that there are no conflicts of interest regarding the publication of this paper.

Acknowledgments

This work was supported in part by Anhui Provincial Natural Science Foundation under Grant 2008085J01 and Natural Science Fund of Education Department of Anhui Province under Grant KJ2020A0478.

References

- [1] C. Godsil and G. Royle, "Algebraic graph theory," *Graduate Texts in Mathematics*, vol. 207, Springer, New York, NY, USA, 2001.
- [2] F. Harary and A. Schwenk, "Which graphs have integral spectra?" in *Graphs and Combinatorics, Lecture Notes in Mathematics*, vol. 406, pp. 45–51, Springer, Berlin, Germany, 1974.
- [3] K. Balinska, D. Cvetkovic, Z. Radosavljevic, S. Simic, and D. Stevanovic, "A survey on integral graphs," *Publikacije Elektrotehnickog Fakulteta—Serija: Matematika*, vol. 13, no. 13, pp. 42–65, 2002.
- [4] S. R. Blackburn and I. E. Shparlinski, "On the average energy of circulant graphs," *Linear Algebra and Its Applications*, vol. 428, no. 8–9, pp. 1956–1963, 2008.
- [5] A. Ilić and M. Basić, "New results on the energy of integral circulant graphs," *Applied Mathematics and Computation*, vol. 218, no. 7, pp. 3470–3482, 2011.
- [6] S. M. Mirafzal, "A new class of integral graphs constructed from the hypercube," *Linear Algebra and Its Applications*, vol. 558, pp. 186–194, 2018.
- [7] A. E. Brower, A. M. Cohen, and A. Neumaier, *Distance-regular Graphs*, vol. 18, Springer, Berlin, Germany, 1989.
- [8] N. L. Biggs, *Intersection Matrices for Linear Graphs, Combinatorial Mathematics and Its Applications*, Academic Press, Oxford, UK, 1969.
- [9] E. R. van Dam and W. H. Haemers, "Which graphs are determined by their spectrum?" *Linear Algebra and Its Applications*, vol. 373, pp. 241–272, 2003.
- [10] X. Liu, Y. Zhang, and X. Gui, "The multi-fan graphs are determined by their Laplacian spectra," *Discrete Mathematics*, vol. 308, no. 18, pp. 4267–4271, 2008.
- [11] X. Shen, Y. Hou, and Y. Zhang, "Graph Z_n and some graphs related to Z_n are determined by their spectrum," *Linear Algebra and Its Applications*, vol. 404, pp. 58–68, 2005.
- [12] W. Wang and C.-X. Xu, "Note the T-shape tree is determined by its Laplacian spectrum," *Linear Algebra and Its Applications*, vol. 419, no. 1, pp. 78–81, 2006.
- [13] B. Y. Hou, H. J. Zhang, and L. Liu, "Applications of Laplacian spectra for extended Koch networks," *The European Physical Journal B*, vol. 85, p. 30373, 2012.
- [14] Z. Zhang, H. Liu, B. Wu, and T. Zou, "Spanning trees in a fractal scale-free lattice," *Phys.Rev.E*, vol. 83, Article ID 016116, 8 pages, 2011.
- [15] J.-B. Liu and X.-F. Pan, "Asymptotic incidence energy of lattices," *Physica A: Statistical Mechanics and Its Applications*, vol. 422, pp. 193–202, 2015.
- [16] J. B. Liu, Z. Y. Shi, Y. H. Pan, J. Cao, M. A. Aty, and U. A. Juboori, *Computing the Laplacian Spectrum of Linear Octagonal-Quadrilateral Networks and its Applications, Polycyclic Aromatic Compounds*, Taylor and Francis Group, Oxfordshire, UK, 2020.
- [17] Z. Cheng, J. Cao, and T. Hayat, "Cascade of failures in interdependent networks with different average degree," *International Journal of Modern Physics C*, vol. 25, no. 5, Article ID 1440006, 2014.
- [18] S. M. Mirafzal, A. Zafari, and A. Zafari, "On the spectrum of a class of distance-transitive graphs," *Electronic Journal of Graph Theory and Applications*, vol. 5, no. 1, pp. 63–69, 2017.
- [19] S. M. Mirafzal and A. Zafari, "An interesting property of a class of circulant graphs," *Journal of Mathematics*, vol. 2017, Article ID 6454736, 4 pages, 2017.
- [20] M. Basić and A. Ilić, "On the automorphism group of integral circulant graphs," *The Electronic Journal of Combinatorics*, vol. 18, pp. 1–21, 2011.
- [21] N. L. Biggs, *Algebraic Graph Theory*, Cambridge University Press, New York, NY, USA, 1993.
- [22] L. Beineke and R. J. Wilson, *Topics in Algebraic Graph Theory*, Mathematical Sciences Faculty Publications, Cambridge University Press, Cambridge, UK, 2004.
- [23] J. Wang, H. Zhao, and Q. Huang, "Spectral characterization of multicone graphs," *Czechoslovak Mathematical Journal*, vol. 62, no. 1, pp. 117–126, 2012.
- [24] R. Merris, "Laplacian graph eigenvectors," *Linear Algebra and Its Applications*, vol. 278, no. 1–3, pp. 221–236, 1998.
- [25] D. Cvetković, P. Rowlinson, and S. Simić, "An introduction to the theory of graph spectra," *London Mathematical Society Student Texts*, vol. 75, Cambridge University Press, Cambridge, UK, 2010.
- [26] Y. Hong, J.-L. Shu, and K. Fang, "A sharp upper bound of the spectral radius of graphs," *Journal of Combinatorial Theory, Series B*, vol. 81, no. 2, pp. 177–183, 2001.

Research Article

A New Paradigm to Design a Class of Combined Ternary Subdivision Schemes

Humaira Mustanira Tariq ¹, Rabia Hameed ² and Ghulam Mustafa ¹

¹Department of Mathematics, The Islamia University of Bahawalpur, Bahawalpur 63100, Pakistan

²Department of Mathematics, The Government Sadiq College Women University Bahawalpur, Bahawalpur 63100, Pakistan

Correspondence should be addressed to Ghulam Mustafa; ghulam.mustafa@iub.edu.pk

Received 23 November 2020; Revised 8 January 2021; Accepted 2 February 2021; Published 16 February 2021

Academic Editor: Jia-Bao Liu

Copyright © 2021 Humaira Mustanira Tariq et al. This is an open access article distributed under the Creative Commons Attribution License, which permits unrestricted use, distribution, and reproduction in any medium, provided the original work is properly cited.

Subdivision schemes play a vital role in curve modeling. The curves produced by the class of $(2n + 2)$ -point ternary scheme (Deslauriers and Dubuc (1989)) interpolate the given data while the curves produced by a class of $(2n + 2)$ -point ternary B-spline schemes approximate the given data. In this research, we merge these two classes to introduce a consolidated and unified class of combined subdivision schemes with two shape control parameters in order to grow versatility for overseeing valuable necessities. However, the proposed class of subdivision schemes gives optimal smoothness in the final shapes, yet we can increase its smoothness by using a proposed general formula in form of its Laurent polynomial. The theoretical analysis of the class of subdivision schemes is done by using various mathematical tools and using their coding in the Maple environment. The graphical analysis of the class of schemes is done in the Maple environment by writing the codes based on the recursive mathematical expressions of the class of subdivision schemes.

1. Introduction

Nowadays, subdivision schemes have got great importance in the field of geometric modeling. It is an innovation which creates smooth shapes. This technique produces a sequence of refined polygons which converge to a limiting shape. New points are added at each refinement level in order to get a smooth final shape. The number of points which are inserted at each refinement level is known as the arity of the curve subdivision scheme. Binary schemes insert two new points at each refinement level between every old consecutive pair of points of the previous refinement level [1]. Similarly, ternary subdivision schemes insert three new points at each refinement level between every old consecutive pair of points of the previous refinement level. Hence, ternary schemes smooth the given sketch in fewer subdivision steps as compared to the binary subdivision schemes. If we move the single point of the control polygon, then the shape of the curve changes over the specific region. This region is known as the support of the scheme. Subdivision schemes give us

local control on the shapes. Schemes with small support give better local control on shapes as compared to the schemes with large support size. Ternary schemes give us small support as compared to the binary subdivision scheme and hence give better local control on the shapes. Because of these two main characteristics of ternary schemes, we consider them superior to the binary subdivision schemes.

Subdivision schemes can also produce the shapes which pass through the initial data. These types of subdivision schemes are known as interpolatory subdivision schemes. These schemes have been introduced by [2–6]. The other types of subdivision schemes produce shapes which do not pass through the initial data. This type of subdivision schemes is known as approximating subdivision schemes and was introduced by [7–10]. The analysis of both types of schemes is done by [11, 12]. In [13–16], the subdivision schemes are introduced with parameters which can produce both the interpolatory and approximating shapes. The combined behaviour of these combined subdivision schemes got more attention in curve modeling.

In this paper, we present a class of ternary combined schemes which is obtained from the well-known classes of interpolatory and approximating subdivision schemes. We unify interpolatory and approximating classes of subdivision schemes into a single class of combined schemes by applying certain mathematical operations on their refinement rules. Consequently, we get a class of $(2n+2)$ -point ternary combined subdivision schemes. Two shape parameters are also inserted in the refinement rules to control the appearance of the limiting shapes. A sketch of our construction procedure is shown in Figure 1.

The remaining layout of the paper is as follows: in Section 2, basic definitions, notations, and established tools are introduced. In Section 3, we construct a parametric class of $(2n+2)$ -point ternary relaxed subdivision schemes. This class depends on two parameters. In Section 4, we discuss several features of this class. In Section 5, we present the geometrical influence of the schemes on the shapes. The conclusion of this research is presented in Section 6.

2. Preliminaries

In this section, we review some fundamental definitions and known realities about subdivision schemes, which structure the basis of the remainder of this paper. If $q^k = \{q_i^k\}_{i \in \mathbb{Z}}$ and $q^{k+1} = \{q_i^{k+1}\}_{i \in \mathbb{Z}}$ are two polygons at k th and $(k+1)$ level, then the ternary subdivision scheme $(SS)_a$ which produces q^{k+1} from q^k is defined as

$$((SS)_a q^k)_i = q_i^{k+1} = \sum_{j \in \mathbb{Z}} a_{i-3j} q_j^k, \quad i \in \mathbb{Z}, \quad (1)$$

where the set $a = \{a_i: i \in \mathbb{Z}\}$ of coefficients is called the mask of the subdivision scheme.

For the ternary subdivision scheme $(SS)_a$, a point at $(k+1)$ -th level is calculated by

$$((SS)_a q^k)_{3i+l} = q_{3i+l}^{k+1} = \sum_{\gamma \in \mathbb{Z}} a_{3\gamma+l} q_{i-\gamma}^k, \quad i \in \mathbb{Z}, 0 \leq l \leq 2. \quad (2)$$

A necessary condition of the subdivision scheme for uniform convergence is that

$$\sum_{j \in \mathbb{Z}} a_{3j} = \sum_{j \in \mathbb{Z}} a_{3j+1} = \sum_{j \in \mathbb{Z}} a_{3j+2} = 1. \quad (3)$$

In order to analyze the characteristics of the subdivision scheme, the z -transform of the mask is

$$a(z) = \sum_{i \in \mathbb{Z}} a_i z^i, \quad z \in \mathbb{C} \setminus \{0\}, \quad (4)$$

which is also known as the Laurent polynomial of the scheme.

Definition 1. A subdivision scheme is uniformly convergent if, for any initial data $q^0 = \{q_i^0: i \in \mathbb{Z}\}$, there exists a continuous function f , such that for any closed interval $I \subset \mathbb{R}$ that satisfies

$$\lim_{k \rightarrow \infty} \sup_{j \in 3^k I} \left| f\left(\frac{j}{3^k}\right) - q_j^k \right| = 0, \quad (5)$$

where $f = S^\infty q^0$.

Definition 2. If we rewrite the Laurent polynomial of $(SS)_a$ as $a(z) = (1+z+z^2/3)^k \delta(z)$, where $\delta(z)$ has no factor of the form $(1+z+z^2)$ and $\bar{m}_0, \dots, \bar{m}_l$ are nonzero coefficients of $\delta(z)$. Let F_0, F_1, \dots, F_l be $l \times l$ matrices with the elements given by $(F_h)_{i,j} = \bar{m}_{\ell+i-3j+h}$, where $h = 0, 1, \dots, l$ while $i, j = 1, \dots, l$. Hölder's regularity/continuity is defined as $r = k - \log_n(\mu)$, whereas the parameter μ is known as a joint spectral radius of F_0, F_1, \dots, F_l . It is bounded below by spectral radii and from above by the norm of matrices F_0, F_1, \dots, F_l . If lower and upper bounds coincide, an explicit formula for the joint spectral radius is obtained:

$$\begin{aligned} & \max\{\rho(F_0), \rho(F_1), \dots, \rho(F_l)\} \\ & \leq \mu \leq \max\{\|F_0\|_\infty, \|F_1\|_\infty, \dots, \|F_l\|_\infty\}. \end{aligned} \quad (6)$$

Theorem 1 (see [17]). *If S_a is the subdivision scheme with Laurent polynomial $a(z)$, then S_a is said to be C^j -continuous if the subdivision scheme $(1/3)S_n$ is contractive. That is,*

$$\left\| \left(\frac{1}{3} S_n \right)^L \right\|_\infty = \frac{1}{3^L} \max \left\{ \sum_{j \in \mathbb{Z}} \left| a_{i+3^L j}^{[n,L]} \right|; i = 0, 1, 2, \dots, 3^L - 1 \right\} < 1, \quad (7)$$

where

$$a^{[n,L]} = \prod_{j=1}^L a(z^{3^{j-1}}), \quad (8)$$

$$a^{(n)}(z) = \left(\frac{3z^2}{1+z+z^2} \right) a^{(n-1)}(z).$$

3. Formulation of the Class of Combined Schemes

Here, we construct and unify the generalized form of the refinement rules of the class of interpolating and approximating schemes. The construction of the class of combined subdivision schemes is based on two classes of subdivision schemes. One of which is the class of $(2n+2)$ -point ternary interpolatory subdivision schemes (CETISS), which is constructed by the Lagrange interpolating polynomial, and the other one is the class of $(2n+2)$ -point relaxed ternary approximating subdivision schemes (CETASS), which is constructed by the B-spline basis function. We merge these classes of schemes in a specific manner such that we get a single class of $(2n+2)$ -point combined schemes from them.

3.1. Mathematical Representation of the Construction Procedure. In this subsection, we present the stepwise procedure to construct the class of combined ternary

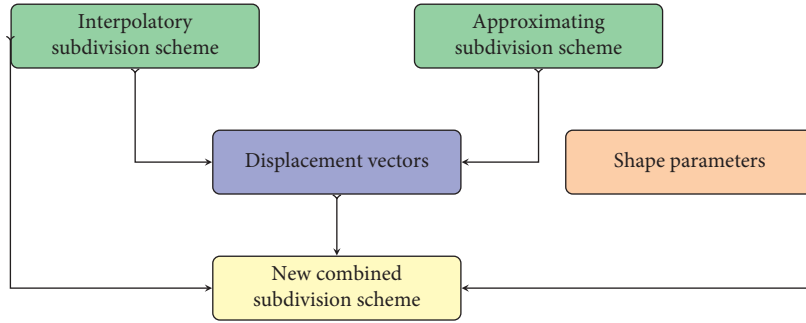


FIGURE 1: Flowchart for the construction of combined subdivision schemes.

subdivision schemes. The construction procedure of the class of combined subdivision schemes is given below.

Step 1. We define the generalized form of the refinement rules of the CETISS; that is, if we have a shape which is

obtained by joining the 2D points $q_{i,2n+2}^k: i \in \mathbb{Z}$, then, to refine this shape by CETISS, we use the following refinement rules:

$$\left\{ \begin{aligned} L_{3i,2n+2}^{k+1} &= q_{i,2n+2}^k, \\ L_{3i+1,2n+2}^{k+1} &= \frac{1}{3^{3n+1}} \sum_{j=-n}^{n+1} \frac{(-1)^j (n-j+2)}{(1-3j)} \binom{3n+2}{n} \binom{2n+2}{n+j} q_{i+j,2n+2}^k, \\ L_{3i+2,2n+2}^{k+1} &= \frac{1}{3^{3n+1}} \sum_{j=-n-1}^{n+1} \frac{(-1)^{j+1} (n+j+1)}{(3j-2)} \binom{3n+2}{n} \binom{2n+2}{n+j+1} q_{i+j,2n+2}^k, \end{aligned} \right. \quad (9)$$

and, hence, we get a refined shape by joining the 2D refined points $L_{i,2n+2}^{k+1}: i \in \mathbb{Z}$, where $\binom{n}{r} = (n!/r!(n-r)!)$.

Step 2. By Pitolli [18], ternary B-spline schemes of degree- M can be written as

$$B_{\delta,M}^{k+1} = \frac{1}{3^M} \sum_{\eta=\lfloor(\delta+1/2)\rfloor}^{\delta} \binom{M+1}{\eta} \binom{\eta}{\delta-\eta}, \quad 0 \leq \delta \leq 2(M+1). \quad (10)$$

By using (10), we can generalize the refinement rules of the CETASS; that is, if we have a shape which is obtained by joining the 2D points $q_{i,2n+2}^k: i \in \mathbb{Z}$, then to refine this shape by CETASS, we use the following refinement rules:

$$\left\{ \begin{aligned} S_{3i,2n+2}^{k+1} &= \frac{1}{3^{3m+1}} \sum_{\eta=0}^{2m} \sum_{\gamma=\lfloor(3\eta+3/2)\rfloor}^{3\eta+2} \binom{3m+2}{\gamma} \binom{\gamma}{3\eta+2-\gamma} q_{i+\eta-m,2n+2}^k, \\ S_{3i+1,2n+2}^{k+1} &= \frac{1}{3^{3m+1}} \sum_{\eta=0}^{2m+1} \sum_{\gamma=\lfloor(3\eta+2/2)\rfloor}^{3\eta+2} \binom{3m+2}{\gamma} \binom{\gamma}{3\eta+1-\gamma} q_{i+\eta-m,2n+2}^k, \\ S_{3i+2,2n+2}^{k+1} &= \frac{1}{3^{3m+1}} \sum_{\eta=0}^{2m+1} \sum_{\gamma=\lfloor(3\eta+1/2)\rfloor}^{3\eta+2} \binom{3m+2}{\gamma} \binom{\gamma}{3\eta-\gamma} q_{i+\eta-m,2n+2}^k, \end{aligned} \right. \quad (11)$$

and thus we get a refined shape by joining the 2D refined points $S_{i,2n+2}^{k+1}$: $i \in \mathbb{Z}$.

Step 3. Now we calculate the displacement vectors from the refined points of CETISS, that is, $L_{3i+\alpha,2n+2}^{k+1}$: $\alpha = 0, 1, 2$ to the refined points of CETASS, that is, $S_{3i+\alpha,2n+2}^{k+1}$: $\alpha = 0, 1, 2$. We denote these displacement vectors by $\Delta_{3i+\alpha,2n+2}^{k+1}$ where $\alpha = 0, 1, 2$, respectively. Hence the displacement vectors are

$$\Delta_{3i+\alpha,2n+2}^{k+1} = L_{3i+\alpha,2n+2}^{k+1} - S_{3i+\alpha,2n+2}^{k+1}, \quad (12)$$

where $\alpha = 0, 1, 2$.

Step 4. Now we find the new refinement point $q_{3i+\alpha,2n+2}^{k+1}$: $\alpha = 0, 1, 2$ by using the displacement vectors $\Delta_{3i+\alpha,2n+2}^{k+1}$: $\alpha = 0, 1, 2$ and the refined points $L_{3i+\alpha,2n+2}^{k+1}$: $\alpha = 0, 1, 2$, respectively. We

control the position of the refinement points $q_{3i+\alpha,2n+2}^{k+1}$: $\alpha = 0, 1, 2$ by controlling the direction and size of these displacement vectors. The shape parameters μ and ν control the direction and size of the displacements vectors. The proposed refined points are given below:

$$\begin{cases} q_{3i,2n+2}^{k+1} = L_{3i,2n+2}^{k+1} - (\mu + \nu)\Delta_{3i,2n+2}^{k+1}, \\ q_{3i+1,2n+2}^{k+1} = L_{3i+1,2n+2}^{k+1} - \mu\Delta_{3i+1,2n+2}^{k+1} - \nu\Delta_{3i+2,2n+2}^{k+1}, \\ q_{3i+2,2n+2}^{k+1} = L_{3i+2,2n+2}^{k+1} - \nu\Delta_{3i+1,2n+2}^{k+1} - \mu\Delta_{3i+2,2n+2}^{k+1}. \end{cases} \quad (13)$$

Step 5. Hence we get the refinement rules $q_{3i+\alpha,2n+2}^{k+1}$: $\alpha = 0, 1, 2$ by using (9), (12), and (13). That is,

$$\left\{ \begin{aligned} q_{3i,2n+2}^{k+1} &= (1 - \mu - \nu)q_{i,2n+2}^k + (\mu + \nu) \times \left[\frac{1}{3^{3m+1}} \sum_{\eta=0}^{2m} \sum_{\gamma=\lfloor(3\eta+3/2)\rfloor}^{3\eta+2} \binom{3m+2}{\gamma} \binom{\gamma}{3\eta+2-\gamma} \right] q_{i+\eta-m,2n+2}^k, \\ q_{3i+1,2n+2}^{k+1} &= \frac{1}{3^{3n+1}} \sum_{j=-n}^{n+1} \frac{(-1)^j (n-j+2)}{(1-3j)} \binom{3n+2}{n} \binom{2n+2}{n+j} q_{i+j,2n+2}^k \\ &\quad - \mu \left[\frac{1}{3^{3n+1}} \sum_{j=-n}^{n+1} \frac{(-1)^j (n-j+2)}{(1-3j)} \binom{3n+2}{n} \binom{2n+2}{n+j} q_{i+j,2n+2}^k - \frac{1}{3^{3m+1}} \sum_{\eta=0}^{2m+1} \sum_{\gamma=\lfloor(3\eta+2/2)\rfloor}^{3\eta+2} \binom{3m+2}{\gamma} \binom{\gamma}{3\eta+1-\gamma} q_{i+\eta-m,2n+2}^k \right] \\ &\quad - \nu \left[\frac{1}{3^{3n+1}} \sum_{j=-n-1}^{n+1} \frac{(-1)^{j+1} (n+j+1)}{(3j-2)} \binom{3n+2}{n} \binom{2n+2}{n+j+1} q_{i+j,2n+2}^k - \frac{1}{3^{3m+1}} \sum_{\eta=0}^{2m+1} \sum_{\gamma=\lfloor(3\eta+1/2)\rfloor}^{3\eta+2} \binom{3m+2}{\gamma} \binom{\gamma}{3\eta-\gamma} q_{i+\eta-m,2n+2}^k \right], \\ q_{3i+2,2n+2}^{k+1} &= \frac{1}{3^{3n+1}} \sum_{j=-n-1}^{n+1} \frac{(-1)^{j+1} (n+j+1)}{(3j-2)} \binom{3n+2}{n} \binom{2n+2}{n+j+1} q_{i+j,2n+2}^k \\ &\quad - \nu \left[\frac{1}{3^{3n+1}} \sum_{j=-n}^{n+1} \frac{(-1)^j (n-j+2)}{(1-3j)} \binom{3n+2}{n} \binom{2n+2}{n+j} q_{i+j,2n+2}^k - \frac{1}{3^{3m+1}} \sum_{\eta=0}^{2m+1} \sum_{\gamma=\lfloor(3\eta+2/2)\rfloor}^{3\eta+2} \binom{3m+2}{\gamma} \binom{\gamma}{3\eta+1-\gamma} q_{i+\eta-m,2n+2}^k \right] \\ &\quad - \mu \left[\frac{1}{3^{3n+1}} \sum_{j=-n-1}^{n+1} \frac{(-1)^{j+1} (n+j+1)}{(3j-2)} \binom{3n+2}{n} \binom{2n+2}{n+j+1} q_{i+j,2n+2}^k - \frac{1}{3^{3m+1}} \sum_{\eta=0}^{2m+1} \sum_{\gamma=\lfloor(3\eta+1/2)\rfloor}^{3\eta+2} \binom{3m+2}{\gamma} \binom{\gamma}{3\eta-\gamma} q_{i+\eta-m,2n+2}^k \right]. \end{aligned} \right. \quad (14)$$

where $\lfloor \cdot \rfloor$ denotes the floor function. In this article, we denote the class of combined subdivision schemes (14) by $(CSS)_{a_{2n+2}}$.

3.2. The Graphical Clarification of the Parameters and the Refinement Rules. In this subsection, we graphically explain the construction of the class of subdivision schemes. For this,

we restrict the value of n to be 1. Let $q_{i+\alpha,4}^k = q_{i+\alpha}^k$; $\alpha = -1, 0, 1, 2$ be the control points of the polygon $q^k q^k$; then, for $n = 1$, the class of subdivision schemes (9) gives the following 4-point ternary interpolatory subdivision scheme:

$$\begin{cases} L_{3i}^{k+1} = L_{3i,4}^{k+1} = q_i^k, \\ L_{3i+1}^{k+1} = L_{3i+1,4}^{k+1} = \frac{-5}{81}q_{i-1}^k + \frac{60}{81}q_i^k + \frac{30}{81}q_{i+1}^k - \frac{4}{81}q_{i+2}^k, \\ L_{3i+2}^{k+1} = L_{3i+2,4}^{k+1} = \frac{-4}{81}q_{i-1}^k + \frac{30}{81}q_i^k + \frac{60}{81}q_{i+1}^k - \frac{5}{81}q_{i+2}^k. \end{cases} \quad (15)$$

Similarly, for $n = 1$, the class of scheme (11) gives the following 4-point relaxed approximating subdivision scheme:

$$\begin{cases} S_{3i}^{k+1} = S_{3i,4}^{k+1} = \frac{5}{27}q_{i-1}^k + \frac{17}{27}q_i^k + \frac{5}{27}q_{i+1}^k, \\ S_{3i+1}^{k+1} = S_{3i+1,4}^{k+1} = \frac{5}{81}q_{i-1}^k + \frac{5}{9}q_i^k + \frac{10}{27}q_{i+1}^k + \frac{1}{81}q_{i+2}^k, \\ S_{3i+2}^{k+1} = S_{3i+2,4}^{k+1} = \frac{1}{81}q_{i-1}^k + \frac{10}{27}q_i^k + \frac{5}{9}q_{i+1}^k + \frac{5}{81}q_{i+2}^k. \end{cases} \quad (16)$$

Now, we find the displacement vectors from the refined points defined in (15) to the refined points defined in (16); thus, we have

$$\begin{aligned} \Delta_{3i}^{k+1} &= \Delta_{3i,4}^{k+1} = L_{3i}^{k+1} - S_{3i}^{k+1} = \frac{10}{27}q_i^k - \frac{5}{27}q_{i-1}^k - \frac{5}{27}q_{i+1}^k, \\ \Delta_{3i+1}^{k+1} &= \Delta_{3i+1,4}^{k+1} = L_{3i+1}^{k+1} - S_{3i+1}^{k+1} = -\frac{10}{81}q_{i-1}^k + \frac{5}{27}q_i^k - \frac{5}{81}q_{i+2}^k, \\ \Delta_{3i+2}^{k+1} &= \Delta_{3i+2,4}^{k+1} = L_{3i+2}^{k+1} - S_{3i+2}^{k+1} = -\frac{5}{81}q_{i-1}^k + \frac{5}{27}q_{i+1}^k - \frac{10}{81}q_{i+2}^k. \end{aligned} \quad (17)$$

Now, we find the refined points by applying operations on vectors $-(\mu + \nu)\Delta_{3i}^{k+1}$, $-\mu\Delta_{3i+1}^{k+1}$, $-\nu\Delta_{3i+2}^{k+1}$ and refined points $L_{3i+\alpha}^{k+1}$; $\alpha = 0, 1, 2$, where μ and ν are real numbers. Hence, we get

$$\begin{cases} q_{3i}^{k+1} = q_{3i,4}^{k+1} = L_{3i}^{k+1} - (\mu + \nu)\Delta_{3i}^{k+1}, \\ q_{3i+1}^{k+1} = q_{3i+1,4}^{k+1} = L_{3i+1}^{k+1} - \mu\Delta_{3i+1}^{k+1} - \nu\Delta_{3i+2}^{k+1}, \\ q_{3i+2}^{k+1} = q_{3i+2,4}^{k+1} = L_{3i+2}^{k+1} - \nu\Delta_{3i+1}^{k+1} - \mu\Delta_{3i+2}^{k+1}. \end{cases} \quad (18)$$

By simplifying (18), we get

$$\begin{cases} q_{3i}^{k+1} = \left(\frac{5\mu}{27} + \frac{5\nu}{27}\right)q_{i-1}^k + \left(1 - \frac{10\mu}{27} - \frac{10\nu}{27}\right)q_i^k + \left(\frac{5\mu}{27} + \frac{5\nu}{27}\right)q_{i+1}^k, \\ q_{3i+1}^{k+1} = \left(\frac{-5}{81} + \frac{5\nu}{81} + \frac{10\mu}{81}\right)q_{i-1}^k + \left(\frac{20}{27} - \frac{5\mu}{27}\right)q_i^k + \left(\frac{10}{27} - \frac{5\nu}{27}\right)q_{i+1}^k + \left(\frac{-4}{81} + \frac{5\mu}{81} + \frac{10\nu}{81}\right)q_{i+2}^k, \\ q_{3i+2}^{k+1} = \left(\frac{-4}{81} + \frac{5\mu}{81} + \frac{10\nu}{81}\right)q_{i-1}^k + \left(\frac{10}{27} - \frac{5\nu}{27}\right)q_i^k + \left(\frac{20}{27} - \frac{5\mu}{27}\right)q_{i+1}^k + \left(\frac{-5}{81} + \frac{5\nu}{81} + \frac{10\mu}{81}\right)q_{i+2}^k. \end{cases} \quad (19)$$

Scheme (19) is the first member of the class of combined subdivision schemes, that is, 4-point combined subdivision scheme. The graphical sketch of the refined points of (19) is shown in Figure 2. In this figure, green bullets show the points q_i^k ; $i \in \mathbb{Z}$, green lines show the polygon q^k , red squares show the refined points $L_{3i+\alpha}^{k+1}$; $\alpha \in \mathbb{R}$, red lines show the refined polygon L^{k+1} , blue squares show the refined points $S_{3i+\alpha}^{k+1}$; $\alpha \in \mathbb{R}$, blue lines show the refined polygon S^{k+1} , black arrows show the displacement vectors, and black solid circles show the refined points $q_{i,2n+2}^{k+1} = q_i^{k+1}$; $i \in \mathbb{Z}$.

Remark 1. When $\mu = \nu = 0$, the first member of the class of combined subdivision schemes which is defined in (19) reduces to the first member of the CETISS. And when $\mu = 1$ and $\nu = 0$, the first member of the class of combined subdivision schemes which is defined in (19) reduces to the first member of the CETASS.

4. Analysis of the Class of Combined Subdivision Schemes by Using Mathematical Tools

In this section, we present the characteristics of the class of combined subdivision schemes. We use the mathematical tools to analyze the class of schemes.

4.1. Affine Combination of Control Points. A linear combination in which the sum of coefficients is equal to one is called the affine combination. The necessary condition for the convergence of a subdivision scheme is that each refinement rule of it must be the affine combination of the control points in the previous subdivision step. To check this property for $(CSS)_{a_{2n+2}}$, we prove the following theorem.

Theorem 2. *Each refined point of the $(CSS)_{a_{2n+2}}$ at $(k + 1)$ -th subdivision step which is defined in (14) is the affine combination of control points of k -th subdivision step.*

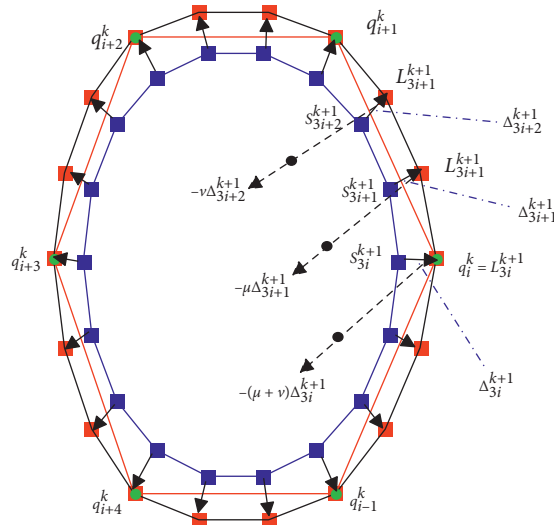


FIGURE 2: Graphical sketch of the construction of the refinement points of scheme (19).

Proof. To prove this theorem, we have to prove that the mask $\{a_{i,2n+2}; i \in \mathbb{Z}\}$ of $(\text{CSS})_{a_{2n+2}}$ satisfies the relation $\sum_{i \in \mathbb{Z}} a_{3i+\alpha,2n+2} = 1$, where $\alpha = 0, 1, 2$.

Let us simplify the expressions:

$$\left\{ \begin{aligned} \sum_{\eta=0}^{2m} \sum_{\gamma=\lfloor(3\eta+3/2)\rfloor}^{3\eta+2} \binom{3m+2}{\gamma} \binom{\gamma}{3\eta+2-\gamma} &= 3^{3m+1}, \\ \sum_{\eta=0}^{2m+1} \sum_{\gamma=\lfloor(3\eta+2/2)\rfloor}^{3\eta+2} \binom{3m+2}{\gamma} \binom{\gamma}{3\eta+1-\gamma} &= 3^{3m+1}, \\ \sum_{\eta=0}^{2m+1} \sum_{\gamma=\lfloor(3\eta+1/2)\rfloor}^{3\eta+2} \binom{3m+2}{\gamma} \binom{\gamma}{3\eta-\gamma} &= 3^{3m+1}. \end{aligned} \right. \quad (20)$$

We also calculate

$$\left\{ \begin{aligned} \sum_{j=-n}^{n+1} \frac{(-1)^j (n-j+2)}{(1-3j)} \binom{3n+2}{n} \binom{2n+2}{n+j} &= 3^{3n+1}, \\ \sum_{j=-n-1}^{n+1} \frac{(-1)^{j+1} (n+j+1)}{(3j-2)} \binom{3n+2}{n} \binom{2n+2}{n+j+1} &= 3^{3n+1}. \end{aligned} \right. \quad (21)$$

Hence, to prove that each of the refined points $q_{3i,2n+2}^{k+1}$, $q_{3i+1,2n+2}^{k+1}$, and $q_{3i+2,2n+2}^{k+1}$ is the affine combinations of $\{q_i^k; i \in \mathbb{Z}\}$, we use (20) and (21). Thus,

$$\left\{ \begin{aligned} \sum_{i \in \mathbb{Z}} a_{3i,2n+2} &= (1 - \mu - \nu) + (\mu + \nu) \left[\frac{1}{3^{3m+1}} 3^{3m+1} \right] = 1, \\ \sum_{i \in \mathbb{Z}} a_{3i+1,2n+2} &= \frac{1}{3^{3n+1}} 3^{3n+1} - \mu \left[\frac{1}{3^{3n+1}} 3^{3n+1} - \frac{1}{3^{3m+1}} 3^{3m+1} \right] - \nu \left[\frac{1}{3^{3n+1}} 3^{3n+1} - \frac{1}{3^{3m+1}} 3^{3m+1} \right] = 1, \\ \sum_{i \in \mathbb{Z}} a_{3i+2,2n+2} &= \frac{1}{3^{3n+1}} 3^{3n+1} - \nu \left[\frac{1}{3^{3n+1}} 3^{3n+1} - \frac{1}{3^{3m+1}} 3^{3m+1} \right] - \mu \left[\frac{1}{3^{3n+1}} 3^{3n+1} - \frac{1}{3^{3m+1}} 3^{3m+1} \right] = 1, \end{aligned} \right. \quad (22)$$

which completes the proof. \square

Theorem 3. The support of the class of subdivision schemes $(\text{CSS})_{a_{2n+2}}$ is $[-((3n+2)/2), ((3n+2)/2)]$.

4.2. Support of the Class of Combined Schemes. In this subsection, we present the support size of the class of combined schemes. The support of a subdivision scheme represents how far one vertex is affected by its neighboring points. Its size represents the local support property of the subdivision curve.

Proof. Let $\{q_{i,2n+2}^0 = q_i^0 \in \mathbb{R}\}_{i \in \mathbb{Z}}$ be the initial data such that $q_0^0 = 1$ and $q_\alpha^0 \neq 0$ for $\alpha \in \mathbb{Z} \setminus \{0\}$; that is,

$$q_{\alpha,2n+2}^0 = \begin{cases} 1, & \text{for } \alpha = 0, \\ 0, & \text{otherwise.} \end{cases} \quad (23)$$

In order to calculate the support size of $(\text{CSS})_{a_{2n+2}}$, we have to calculate the distance between two corresponding subscripts belonging to the leftmost vertex and rightmost vertex after k -steps of subdivision.

If we operate on initial data $\{q_{i,2n+2}^0 = q_i^0 \in \mathbb{R}\}_{i \in \mathbb{Z}}$ by $(\text{CSS})_{a_{2n+2}}$ one time, then we get

$$q_{\alpha,2n+2}^1 = \begin{cases} \neq 0, & \text{for } \alpha = -3^0(3n+2), -3^0(3n+2)+1, \dots, 3^0(3n+2)-1, 3^0(3n+2), \\ 0, & \text{otherwise.} \end{cases} \tag{24}$$

If we operate on the data $\{q_{i,2n+2}^1 \in \mathbb{R}\}_{i \in \mathbb{Z}}$ which is defined in (24) by $(\text{CSS})_{a_{2n+2}}$ one time, that is, we operate on

initial data $\{q_{i,2n+2}^0 = q_i^0 \in \mathbb{R}\}_{i \in \mathbb{Z}}$ by $(\text{CSS})_{a_{2n+2}}$ two times, then we get

$$q_{\alpha,2n+2}^2 = \begin{cases} \neq 0, & \text{for } \alpha = -\sum_{j=0}^1 3^j(3n+2), -\sum_{j=0}^1 3^j(3n+2)+1, \dots, \sum_{j=0}^1 3^j(3n+2)-1, \sum_{j=0}^1 3^j(3n+2), \\ 0, & \text{otherwise.} \end{cases} \tag{25}$$

Similarly, if we operate on initial data $\{q_{i,2n+2}^0 = q_i^0 \in \mathbb{R}\}_{i \in \mathbb{Z}}$ which is defined in (23) by $(\text{CSS})_{a_{2n+2}}$ k -times, then we get

$$q_{\alpha,2n+2}^k = \begin{cases} \neq 0, & \text{for } \alpha = -\sum_{j=0}^{k-1} 3^j(3n+2), -\sum_{j=0}^{k-1} 3^j(3n+2)+1, \dots, \sum_{j=0}^{k-1} 3^j(3n+2)-1, \sum_{j=0}^{k-1} 3^j(3n+2), \\ 0, & \text{otherwise.} \end{cases} \tag{26}$$

Hence, after k -steps of subdivision, the leftmost nonzero vertex is $q_{-(3n+2)\sum_{j=0}^{k-1} 3^j, 2n+2}^k$ and the rightmost nonzero vertex is $q_{(3n+2)\sum_{j=0}^{k-1} 3^j, 2n+2}^k$. Since k -times, the subdivision process is applied and, at each step, we have relabeled the subscripts of

the vertices; thus, $q_{(i/3^k), 2n+2}^k = q_{(i/3^{k-1}), 2n+2}^{k-1} = \dots = q_{(i/3), 2n+2}^1 = q_{i, 2n+2}^0$. Hence, after k -steps, the distance between leftmost and rightmost nonzero vertices is equal to the support of $(\text{CSS})_{a_{2n+2}}$; that is,

$$\begin{aligned} \text{support} &= \left[\frac{(3n+2)(1+3+3^2+\dots+3^{k-1})}{3^k} - \frac{-(3n+2)(1+3+3^2+\dots+3^{k-1})}{3^k} \right] \\ &= 2(3n+2) \left(\frac{1}{3} + \frac{1}{3^2} + \dots + \frac{1}{3^k} \right) \\ &= 2(3n+2) \left(\frac{(1/3)}{1-(1/3)} \right) \\ &= (3n+2). \end{aligned} \tag{27}$$

Since the class of subdivision schemes is symmetric, then obviously the support region is $[(-(3n+2)/2), ((3n+2)/2)]$. \square

4.3. Generation Degree. One of the necessary conditions for generating C^n -continuous limit curves is the order of polynomial generation of the subdivision scheme. A ternary

subdivision scheme can generate polynomials up to degree d if and only if its Laurent polynomial can be written in the following form:

$$a(z) = \left(\frac{1+z+z^2}{3}\right)^{d+1} \varphi(z), \quad z \in \mathbb{C} \setminus \{0\}. \quad (28)$$

Here, $\varphi(z)$ is the Laurent polynomial with $\varphi(1) = 3$ and it does not have the factor $(1+z+z^2)$.

Theorem 4. *The class of combined schemes $(CSS)_{a_{2n+2}}$ generates polynomials of degree up to 2 for all μ and ν .*

Proof. The Laurent polynomial of $(CSS)_{a_{2n+2}}$ is

$$a_4(z) = \frac{1}{81z^5} (1+z+z^2)^3 \left[(10\nu - 4 + 5\mu)z^4 + (-25\nu + 7 - 5\mu)z^3 + (30\nu + 3)z^2 + (-25\nu + 7 - 5\mu)z + (10\nu - 4 + 5\mu) \right]. \quad (30)$$

By using Laurent polynomial of $(CSS)_{a_4}$, we prove the following theorem.

Theorem 5. *Let $\{q_i^0\}_{i \in \mathbb{Z}}$ be the initial data; then, the refinement rules defined in (19) of $(CSS)_{a_4}$ produce the C^2 -continuous shapes if $\nu \in ((-2/5), (1/5))$ and its corresponding $\mu \in ((1/5) - (7\nu/2), 2 - (7\nu/2))$.*

Proof. To prove that $(CSS)_{a_4}$ produces the C^2 -continuous shapes, first, we have to prove that this scheme produces

$$\begin{aligned} a_4^{(1)}(z) &= \frac{1}{27z^2} \left[\begin{aligned} &(-4 + 5\mu + 10\nu)z^5 + (-1 + 5\mu - 5\nu)z^4 + \\ &(10\nu + 5\mu + 5)z^3 + (26 - 10\mu - 20\nu)z^2 + (29 + 10\nu - 10\mu)z^1 + (26 - 10\mu - 20\nu)z^0 \end{aligned} \right] \\ &= \sum_{j=-2}^3 a_{j,4} z^j, \end{aligned} \quad (32)$$

where the subdivision scheme corresponding to the Laurent polynomial $a_4^{(1)}(z)$ is denoted by $(CSS)_{a_4^{(1)}}$; then, by Theorem 1, we have

$$\left\| \left(\frac{1}{3}(CSS)_{a_4^{(1)}}\right)^1 \right\|_{\infty} = \frac{1}{3} \max \left\{ \sum_{j \in \mathbb{Z}} |a_{i+3j,4}^{[1,1]}|; i = 0, 1, 2 \right\}. \quad (33)$$

$$\left\| \left(\frac{1}{3}(CSS)_{a_4^{(1)}}\right)^1 \right\|_{\infty} = \max \frac{1}{81} \quad (35)$$

$$\{ |-4 + 5\mu + 10\nu| + |26 - 10\mu - 20\nu| + |10\nu + 5\mu + 5|, |-1 + 5\mu - 5\nu| + |29 + 10\nu - 10\mu| + |-1 + 5\mu - 5\nu| \}.$$

$$a_{2n+2}(z) = \left(\frac{1+z+z^2}{3}\right)^3 b_{2n+2}(z), \quad (29)$$

where $b_{2n+2}(z)$ is a Laurent polynomial obtained by $b_{2n+2}(z) = (3a_{2n+2}(z)/1+z+z^2)$. Hence, the degree of polynomial generation of $(CSS)_{a_{2n+2}}$ is 2. \square

4.4. Properties of the 4-Point Subdivision Scheme (19).

From Theorem 2, the subdivision scheme which is defined in (14) and denoted by $(CSS)_{a_4}$ satisfies the necessary conditions for convergence. Moreover, the Laurent polynomial of $(CSS)_{a_4}$ is

C^0 -continuous and C^1 -continuous shapes in the given intervals of μ and ν .

Thus, by using (30), we calculate

$$a_4^{(1)}(z) = \left(\frac{3z^2}{1+z+z^2}\right) a_4^{(0)}(z). \quad (31)$$

Hence, from the above equation, we have

This implies that

$$\left\| \left(\frac{1}{3}(CSS)_{a_4^{(1)}}\right)^1 \right\|_{\infty} = \frac{1}{3} \max \left\{ \sum_{j \in \mathbb{Z}} |a_{3j,4}^{[1,1]}|, \sum_{j \in \mathbb{Z}} |a_{1+3j,4}^{[1,1]}|, \sum_{j \in \mathbb{Z}} |a_{2+3j,4}^{[1,1]}| \right\}. \quad (34)$$

By substituting values, we get

Hence, $\|((1/3)(\text{CSS})_{a_4^{(1)}})^1\|_\infty < 1$ for $\mu + 2\nu \in ((-14/5), (53/10))$ and $\mu - \nu \in ((5/2), (28/5))$.

This implies that $(\text{CSS})_{a_4^{(1)}}$ is contractive and the scheme $(\text{CSS})_{a_4}$ produces C^0 -continuous shapes.

Now, we again calculate

$$a_4^{(2)}(z) = \left(\frac{3z^2}{1+z+z^2} \right) a_4^{(1)}(z), \tag{36}$$

which implies

$$a_4^{(1)}(z) = \frac{1}{9z^2} [(10\nu - 4 + 5\mu)z^5 + (3 - 15\nu)z^4 + (6 + 15\nu)z^3 + (-10\mu + 17 - 20\nu)z^2 + (6 + 15\nu)z^1 + (3 - 15\nu)z^0 + (10\nu - 4 + 5\mu)z^{-1}], \tag{37}$$

where the subdivision scheme corresponding to the Laurent polynomial $a_4^{(2)}(z)$ is denoted by $(\text{CSS})_{a_4^{(2)}}$; then, by Theorem 1, we have

$$\left\| \left(\frac{1}{3} (\text{CSS})_{a_4^{(2)}} \right)^1 \right\|_\infty = \max \frac{1}{27} \{ | -4 + 5\mu + 10\nu | + | 17 - 10\mu - 20\nu | + | 10\nu + 5\mu - 4 |, | 3 - 15\nu | + | 6 + 15\nu | \}. \tag{38}$$

Thus, $\|((1/3)(\text{CSS})_{a_4^{(2)}})^1\|_\infty < 1$ for $\nu \in (-1, (4/5))$ and $\mu \in ((-1/10) - 2\nu, -2\nu + (13/5))$.

Therefore, $(\text{CSS})_{a_4^{(2)}}$ is contractive and hence $(\text{CSS})_{a_4}$ produces C^1 -continuous shapes.

Now, we find the following Laurent polynomial by using $a_4^{(3)}(z) = (3z^2/1+z+z^2)a_4^{(2)}(z)$. Thus, we have

$$a_4^{(3)}(z) = \frac{1}{3} [(10\nu - 4 + 5\mu)z^5 + (-25\nu + 7 - 5\mu)z^4 + (30\nu + 3)z^3 + (-25\nu + 7 - 5\mu)z^2 + (10\nu - 4 + 5\mu)z]. \tag{39}$$

Let $(\text{CSS})_{a_4^{(3)}}$ be the subdivision scheme corresponding to the Laurent polynomial $a_4^{(3)}(z)$; then, by Theorem 1, we get

$$\left\| \left(\frac{1}{3} (\text{CSS})_{a_4^{(3)}} \right)^1 \right\|_\infty = \max \frac{1}{9} \{ | -4 + 5\mu + 10\nu | + | 7 - 5\mu - 25\nu |, | 3 + 30\nu | \}. \tag{40}$$

Thus, $\|((1/3)(\text{CSS})_{a_4^{(3)}})^1\|_\infty < 1$ for $\nu \in ((-2/5), (1/5))$ and $\mu \in ((1/5) - (7\nu/2), 2 - (7\nu/2))$.

This implies that $(\text{CSS})_{a_4^{(3)}}$ is contractive and hence $(\text{CSS})_{a_4}$ is C^2 -continuous. This completes the proof. \square

If we put $\nu=0$ in the Laurent polynomial (30), then it gives one more factor of $(1+z+z^2)$. Hence, the following corollary is proved.

Corollary 1. *If $\nu = 0$ and $\mu \in ((4/5), (6/5))$, then $(\text{CSS})_{a_4}$ produces C^3 -continuous shapes.*

Corollary 2. *The continuity of $(\text{CSS})_{a_4}$ can be increased if we use the refinement rules corresponding to the following Laurent polynomial which is derived from the Laurent polynomial of (30):*

$$\begin{aligned} \alpha(z) = & \frac{1}{3^{n+2}} [C_0^n \{C_0^n (10\nu - 4 + 5\mu)\} + C_0^n \{C_0^n (-15\nu + 3) + C_1^n (10\nu - 4 + 5\mu)\}z \\ & + (C_0^n \{C_0^n (15\nu + 6) + C_1^n (-15\nu + 3) + C_2^n (10\nu - 4 + 5\mu)\} + C_1^n \{C_0^{n-1} (10\nu - 4 + 5\mu)\})z^2 \\ & + (C_0^n \{C_0^n (-20\nu - 10\mu + 17) + C_1^n (15\nu + 6) + C_2^n (-15\nu + 3) + C_3^n (10\nu - 4 + 5\mu)\} \\ & + C_1^n \{C_0^{n-1} (-15\nu + 3) + C_1^{n-1} (10\nu - 4 + 5\mu)\})z^3 \\ & + (C_0^n \{C_0^n (15\nu + 6) + C_1^n (-20\nu - 10\mu + 17) + C_2^n (15\nu + 6) + C_3^n (-15\nu + 3)\} \\ & + C_1^n \{C_0^{n-1} (15\nu + 6) + C_1^{n-1} (-15\nu + 3) + C_2^{n-1} (10\nu - 4 + 5\mu)\} + C_2^n \{C_0^{n-2} (10\nu - 4 + 5\mu)\})z^4 \\ & + \dots + (C_n^{n-2} \{C_2^2 (10\nu - 4 + 5\mu)\})z^{2n+4} \\ & + (C_{n-1}^n \{(10\nu - 4 + 5\mu) + (-15\nu + 3)\} + C_n^n (-15\nu + 3))z^{2n+5} \\ & + (C_n^n (10\nu - 4 + 5\mu))z^{2n+6}], \end{aligned} \tag{41}$$

where μ and ν are shape parameters and $n = 1, 2, \dots$

Remark 2. If we put $n = 2, n = 3,$ and $n = 4$ in (41), we get the Laurent polynomials of 3-point, 4-point, and 5-point

combined subdivision schemes which produce continuous shapes up to C^2 , C^3 , and C^4 smoothness.

Theorem 3 gives the following result.

Corollary 3. *The support of $(CSS)_{a_4}$ is $[-(5/2), (5/2)]$.*

Now, here we use the method proposed by Rioul [19] to find out the Hölders regularity of $(CSS)_{a_4}$.

Theorem 6. *If we choose $\mu = 1$ and $\nu = (-1/5)$, then the lower and upper bound of Hölder regularity of $(CSS)_{a_4}$ is 2.1079 and 2.369, respectively.*

Proof. From (30), we have

$$a_4(z) = \left(\frac{1+z+z^2}{3}\right)^3 z^{-5} \sum_{j=0}^4 m_j z^j, \quad (42)$$

where $m_0 = ((10\nu - 4 + 5\mu)/3)$, $m_1 = ((-25\nu + 7 - 5\mu)/3)$, $m_2 = ((30\nu + 3)/3)$, $m_3 = ((-25\nu + 7 - 5\mu)/3)$, $m_4 = ((10\nu - 4 + 5\mu)/3)$, $k = 3$, $\ell = 4$, $n = 3$, and $h = 0, 1, 2, 3, 4$. F_0, F_1, F_2, F_3 , and F_4 are matrices given by

$$(F_h)_{i,j} = m_{\ell+i-3j+h}. \quad (43)$$

Since $(F_0)_{i,j} = m_{4+i-3j}$, $(F_1)_{i,j} = m_{5+i-3j}$, $(F_2)_{i,j} = m_{6+i-3j}$, $(F_3)_{i,j} = m_{7+i-3j}$, $(F_4)_{i,j} = m_{8+i-3j}$, where $i, j = 1, 2, 3, 4$, thus, we have

$$\begin{aligned} F_0 &= \begin{pmatrix} m_2 & 0 & 0 & 0 \\ m_3 & m_0 & 0 & 0 \\ m_4 & m_1 & 0 & 0 \\ 0 & m_2 & 0 & 0 \end{pmatrix}, \\ F_1 &= \begin{pmatrix} m_3 & m_0 & 0 & 0 \\ m_4 & m_1 & 0 & 0 \\ 0 & m_2 & 0 & 0 \\ 0 & m_3 & m_0 & 0 \end{pmatrix}, \\ F_2 &= \begin{pmatrix} m_4 & m_1 & 0 & 0 \\ 0 & m_2 & 0 & 0 \\ 0 & m_3 & m_0 & 0 \\ 0 & m_4 & m_1 & 0 \end{pmatrix}, \\ F_3 &= \begin{pmatrix} 0 & m_2 & 0 & 0 \\ 0 & m_3 & m_0 & 0 \\ 0 & m_4 & m_1 & 0 \\ 0 & 0 & m_2 & 0 \end{pmatrix}, \\ F_4 &= \begin{pmatrix} 0 & m_3 & m_0 & 0 \\ 0 & m_4 & m_1 & 0 \\ 0 & 0 & m_2 & 0 \\ 0 & 0 & m_3 & m_0 \end{pmatrix}. \end{aligned} \quad (44)$$

Let $\rho(F_j)$: $j = 0, 1, 2, 3, 4$ be the joint spectral radii of matrices F_0, F_1, F_2, F_3 , and F_4 , respectively; then, we have

$$\begin{aligned} &\max\{\rho(F_0), \rho(F_1), \rho(F_2), \rho(F_3), \rho(F_4)\} \\ &\leq \rho \leq \max\{\|F_0\|_\infty, \|F_1\|_\infty, \|F_2\|_\infty, \|F_3\|_\infty, \|F_4\|_\infty\}. \end{aligned} \quad (45)$$

The eigenvalues of F_0, F_1, F_2, F_3 , and F_4 are required to calculate their joint spectral radii; therefore, $\rho(F_0) = \rho(F_2) = \rho(F_3) = \rho(F_4) = \max\{|m_0|, |m_2|\}$, $\rho(F_1) = \max\{|m_3 + m_0|, |m_1 + m_4|\}$.

The infinity norm of F_0, F_1, F_2, F_3 , and F_4 is

$$\|F_j\|_\infty = \max\{|m_2|, |m_3 + m_0|, |m_4 + m_1|\}, \quad (46)$$

where $j = 0, 1, 2, 3, 4$.

$$\begin{aligned} &\max\{|m_0|, |m_2|, |m_3 + m_0|, |m_1 + m_4|\} \\ &\leq \rho \leq \max\{|m_2|, |m_3 + m_0|, |m_4 + m_1|\}. \end{aligned} \quad (47)$$

If we use $\mu = 1$ and $\nu = (-1/5)$ in (47), we get

$$\max\{1, 0.333, 2, 2.6667\} \leq \rho \leq \max\{1, 2\}. \quad (48)$$

Hence, the lower bound of Hölders exponent is

$$r \geq 3 - \log_3(2.6667) = 2.10719. \quad (49)$$

The upper bound of Hölders exponent is

$$r \leq 3 - \log_3(2) = 2.369. \quad (50)$$

This completes the proof. \square

Theorem 7. *The limit stencil of $(CSS)_{a_4}$ which is defined in (18) is*

$$\left[\frac{5\mu + 5\nu - 3}{48}, \frac{27 - 5\mu - 5\nu}{48}, \frac{27 - 5\mu - 5\nu}{48}, \frac{5\mu + 5\nu - 3}{48} \right]. \quad (51)$$

Proof. To find out the limit stencil of $(CSS)_{a_4}$, we substitute $i = -1$ and $i = 0$ in the refinement rules (19) of $(CSS)_{a_4}$. Hence, we obtain the following refined points:

$$\begin{aligned} q_{-3}^{k+1} &= \left(\frac{5\mu}{27} + \frac{5\nu}{27}\right)q_{-2}^k + \left(1 - \frac{10\mu}{27} - \frac{10\nu}{27}\right)q_{-1}^k + \left(\frac{5\mu}{27} + \frac{5\nu}{27}\right)q_0^k, \\ q_{-2}^{k+1} &= \left(\frac{-5}{81} + \frac{5\nu}{81} + \frac{10\mu}{81}\right)q_{-2}^k + \left(\frac{20}{27} - \frac{5\mu}{27}\right)q_{-1}^k + \left(\frac{10}{27} - \frac{5\nu}{27}\right)q_0^k \\ &\quad + \left(\frac{-4}{81} + \frac{5\mu}{81} + \frac{10\nu}{81}\right)q_1^k, \\ q_{-1}^{k+1} &= \left(\frac{-4}{81} + \frac{5\mu}{81} + \frac{10\nu}{81}\right)q_{-2}^k + \left(\frac{10}{27} - \frac{5\nu}{27}\right)q_{-1}^k + \left(\frac{20}{27} - \frac{5\mu}{27}\right)q_0^k \\ &\quad + \left(\frac{-5}{81} + \frac{5\nu}{81} + \frac{10\mu}{81}\right)q_1^k, \\ q_0^{k+1} &= \left(\frac{5\mu}{27} + \frac{5\nu}{27}\right)q_{-1}^k + \left(1 - \frac{10\mu}{27} - \frac{10\nu}{27}\right)q_0^k + \left(\frac{5\mu}{27} + \frac{5\nu}{27}\right)q_1^k. \end{aligned} \quad (52)$$

The matrix form of the above system of four linear equations is

$$\begin{pmatrix} q_{-3}^{k+1} \\ q_{-2}^{k+1} \\ q_{-1}^{k+1} \\ q_0^{k+1} \end{pmatrix} \begin{pmatrix} \left(\frac{5\mu}{27} + \frac{5\nu}{27}\right) & \left(1 - \frac{10\mu}{27} - \frac{10\nu}{27}\right) & \left(\frac{5\mu}{27} + \frac{5\nu}{27}\right) & 0 \\ \left(\frac{-5}{81} + \frac{5\nu}{81} + \frac{10\mu}{81}\right) & \left(\frac{20}{27} - \frac{5\mu}{27}\right) & \left(\frac{10}{27} - \frac{5\nu}{27}\right) & \left(\frac{-4}{81} + \frac{5\mu}{81} + \frac{10\nu}{81}\right) \\ \left(\frac{-4}{81} + \frac{5\mu}{81} + \frac{10\nu}{81}\right) & \left(\frac{10}{27} - \frac{5\nu}{27}\right) & \left(\frac{20}{27} - \frac{5\mu}{27}\right) & \left(\frac{-5}{81} + \frac{5\nu}{81} + \frac{10\mu}{81}\right) \\ 0 & \left(\frac{5\mu}{27} + \frac{5\nu}{27}\right) & \left(1 - \frac{10\mu}{27} - \frac{10\nu}{27}\right) & \left(\frac{5\mu}{27} + \frac{5\nu}{27}\right) \end{pmatrix} \begin{pmatrix} q_{-3}^k \\ q_{-2}^k \\ q_{-1}^k \\ q_0^k \end{pmatrix}. \tag{53}$$

Symbolically, it can be written as

$$q^{k+1} = R_1 q^k. \tag{54}$$

Hence, the local subdivision matrix of the 4-point scheme $(CSS)_{a_4}$ is

$$R_1 = \begin{pmatrix} \left(\frac{5\mu}{27} + \frac{5\nu}{27}\right) & \left(1 - \frac{10\mu}{27} - \frac{10\nu}{27}\right) & \left(\frac{5\mu}{27} + \frac{5\nu}{27}\right) & 0 \\ \left(\frac{-5}{81} + \frac{5\nu}{81} + \frac{10\mu}{81}\right) & \left(\frac{20}{27} - \frac{5\mu}{27}\right) & \left(\frac{10}{27} - \frac{5\nu}{27}\right) & \left(\frac{-4}{81} + \frac{5\mu}{81} + \frac{10\nu}{81}\right) \\ \left(\frac{-4}{81} + \frac{5\mu}{81} + \frac{10\nu}{81}\right) & \left(\frac{10}{27} - \frac{5\nu}{27}\right) & \left(\frac{20}{27} - \frac{5\mu}{27}\right) & \left(\frac{-5}{81} + \frac{5\nu}{81} + \frac{10\mu}{81}\right) \\ 0 & \left(\frac{5\mu}{27} + \frac{5\nu}{27}\right) & \left(1 - \frac{10\mu}{27} - \frac{10\nu}{27}\right) & \left(\frac{5\mu}{27} + \frac{5\nu}{27}\right) \end{pmatrix}. \tag{55}$$

Now we calculate the eigenvalues of the subdivision matrix R_1 and denote them by λ_i : $i = 0, 1, 2, 3$. Thus, we have

$$\lambda_i = 1, \frac{1}{3}, \frac{1}{9}, \frac{10\nu + 1}{27}. \tag{56}$$

The matrix of the eigenvector corresponding to the eigenvalues is

$$W = \begin{pmatrix} 1 & -1 & 1 & -1 \\ \frac{5\mu + 5\nu - 3}{5\mu + 5\nu - 27} & \frac{-1}{3} & 1 & \frac{5\nu - 5\mu + 1}{15\mu + 15\nu - 27} \\ \frac{5\mu + 5\nu - 3}{5\mu + 5\nu - 27} & \frac{1}{3} & 1 & \frac{-(5\nu - 5\mu + 1)}{15\mu + 15\nu - 27} \\ 1 & 1 & 1 & 1 \end{pmatrix}. \tag{57}$$

By taking the inverse of the above matrix, we get

$$W^{-1} = \begin{pmatrix} \frac{27 - 5\mu - 5\nu}{48} & \frac{5\mu + 5\nu - 27}{48} & \frac{5\mu + 5\nu - 27}{48} & \frac{27 - 5\mu - 5\nu}{48} \\ \frac{-(5\nu - 5\mu + 1)}{20\nu - 16} & \frac{-3(5\nu + 5\mu - 9)}{20\nu - 16} & \frac{3(5\nu + 5\mu - 9)}{20\nu - 16} & \frac{5\nu - 5\nu + 1}{20\nu - 16} \\ \frac{5\mu + 5\nu - 3}{48} & \frac{27 - 5\mu - 5\nu}{48} & \frac{27 - 5\mu - 5\nu}{48} & \frac{5\mu + 5\nu - 3}{48} \\ \frac{-(5\nu + 5\mu - 9)}{20\nu - 16} & \frac{3(5\nu + 5\mu - 9)}{20\nu - 16} & \frac{-3(5\nu + 5\mu - 9)}{20\nu - 16} & \frac{(5\nu + 5\mu - 9)}{20\nu - 16} \end{pmatrix}. \tag{58}$$

Let δ be the diagonal matrix of eigenvalues; then,

$$\delta = \begin{pmatrix} 1 & 0 & 0 & 0 \\ 0 & \frac{1}{3} & 0 & 0 \\ 0 & 0 & \frac{1}{9} & 0 \\ 0 & 0 & 0 & \frac{(10\nu + 1)}{27} \end{pmatrix}. \tag{59}$$

Since $R_1 = W\delta W^{-1}$, therefore $R_1^k = W\delta^k W^{-1}$. Also, we have

$$q^{k+1} = R_1 q^k = R_1^2 q^{k-1} = R_1^3 q^{k-2} = \dots = R_1^k q^0, \tag{60}$$

which implies that

$$q^{k+1} = W\delta^k W^{-1} q^0. \tag{61}$$

Hence,

$$\lim_{k \rightarrow \infty} q^{k+1} = W \left(\lim_{k \rightarrow \infty} \delta^k \right) W^{-1} q^0. \tag{62}$$

Thus, we have

$$\begin{pmatrix} q_{-3}^\infty \\ q_{-2}^\infty \\ q_{-1}^\infty \\ q_0^\infty \end{pmatrix} = \begin{pmatrix} \frac{5\mu + 5\nu - 3}{48} & \frac{27 - 5\mu - 5\nu}{48} & \frac{27 - 5\mu - 5\nu}{48} & \frac{5\mu + 5\nu - 3}{48} \\ \frac{5\mu + 5\nu - 3}{48} & \frac{27 - 5\mu - 5\nu}{48} & \frac{27 - 5\mu - 5\nu}{48} & \frac{5\mu + 5\nu - 3}{48} \\ \frac{5\mu + 5\nu - 3}{48} & \frac{27 - 5\mu - 5\nu}{48} & \frac{27 - 5\mu - 5\nu}{48} & \frac{5\mu + 5\nu - 3}{48} \\ \frac{5\mu + 5\nu - 3}{48} & \frac{27 - 5\mu - 5\nu}{48} & \frac{27 - 5\mu - 5\nu}{48} & \frac{5\mu + 5\nu - 3}{48} \end{pmatrix} \begin{pmatrix} q_{-3}^0 \\ q_{-2}^0 \\ q_{-1}^0 \\ q_0^0 \end{pmatrix}. \tag{63}$$

Hence, we get the limit stencil of $(CSS)_{a_4}$, that is,

$$\left[\frac{5\mu + 5\nu - 3}{48}, \frac{27 - 5\mu - 5\nu}{48}, \frac{27 - 5\mu - 5\nu}{48}, \frac{5\mu + 5\nu - 3}{48} \right]. \tag{64}$$

Hence, it is proved. □

4.5. Properties of the 6-Point Subdivision Scheme. If we put $n = 2$ in (14), then we get the following 6-point combined subdivision scheme. We denote this scheme by $(CSS)_{a_6}$:

$$\left\{ \begin{aligned} q_{3i}^{k+1} &= \left(\frac{4\mu}{243} + \frac{4\nu}{243}\right)q_{i-2}^k + \left(\frac{56\mu}{243} + \frac{56\nu}{243}\right)q_{i-1}^k + \left(1 - \frac{40\mu}{81} - \frac{40\nu}{81}\right)q_i^k + \left(\frac{56\mu}{243} + \frac{56\nu}{243}\right)q_{i+1}^k + \left(\frac{4\mu}{243} + \frac{4\nu}{243}\right)q_{i+2}^k, \\ q_{3i+1}^{k+1} &= \left(\frac{-16\mu}{2187} - \frac{20\nu}{2187} + \frac{8}{729}\right)q_{i-2}^k + \left(\frac{-70}{729} + \frac{280\nu}{2187} + \frac{476\mu}{2187}\right)q_{i-1}^k + \left(\frac{560}{729} - \frac{664\mu}{2187} - \frac{56\nu}{2187}\right)q_i^k \\ &+ \left(\frac{280}{729} - \frac{56\mu}{2187} - \frac{664\nu}{2187}\right)q_{i+1}^k + \left(\frac{-56}{729} + \frac{280\mu}{2187} + \frac{476\nu}{2187}\right)q_{i+2}^k + \left(\frac{7}{729} - \frac{20\mu}{2187} - \frac{16\nu}{2187}\right)q_{i+3}^k, \\ q_{3i+2}^{k+1} &= \left(\frac{7}{729} - \frac{20\mu}{2187} - \frac{16\nu}{2187}\right)q_{i-2}^k + \left(\frac{-56}{729} + \frac{280\mu}{2187} + \frac{476\nu}{2187}\right)q_{i-1}^k + \left(\frac{280}{729} - \frac{56\mu}{2187} - \frac{664\nu}{2187}\right)q_i^k \\ &+ \left(\frac{560}{729} - \frac{664\mu}{2187} - \frac{56\nu}{2187}\right)q_{i+1}^k + \left(\frac{-70}{729} + \frac{280\nu}{2187} + \frac{476\mu}{2187}\right)q_{i+2}^k + \left(\frac{-16\mu}{2187} - \frac{20\nu}{2187} + \frac{8}{729}\right)q_{i+3}^k. \end{aligned} \right. \tag{65}$$

The Laurent polynomial of $(CSS)_{a_6}$ denoted by $a_6(z) = a_6^{(0)}(z)$ is defined:

$$\begin{aligned} a_6(z) &= \frac{1}{2187z^8}(1 + z + z^2)^3 \\ &= \left[(21 - 20\mu - 16\nu)z^{10} + (-39 + 44\mu + 28\nu)z^9 + (24\mu + 48\nu - 9)z^8 + (-54 + 276\nu + 84\mu)z^7 \right. \\ &\quad \left. + (-108\mu - 936\nu + 153)z^6 + (99 + 1200\nu - 48\mu)z^5 + (-108\mu - 936\nu + 153)z^4 + (-54 + 276\nu + 84\mu)z^3 \right. \\ &\quad \left. + (24\mu + 48\nu - 9)z^2 + (-39 + 44\mu + 28\nu)z + (21 - 20\mu - 16\nu) \right]. \end{aligned} \tag{66}$$

Theorem 8. Let $\{q_i^0\}_{i \in \mathbb{Z}}$ be the initial data; then, the refinement rules defined in (65) of $(CSS)_{a_6}$ produce the C^2 -continuous shapes if $\nu \in ((-1/4), (1/8))$ and its corresponding $\mu \in ((3/32) - (157\nu/32), (255/128) - (157\nu/32))$. It gives C^3 -continuous shapes for $\nu = 0$ and $\mu \in ((93/128), (87/64))$.

It produces C^4 -smooth shapes for $\nu = 0$ and $\mu \in ((3/5), (51/40))$. And it gives C^5 -smooth shapes for $\nu = 0$ and $\mu \in ((57/62), (33/31))$.

Proof. By Theorem 1, we have

$$a_6^{(n)}(z) = \left(\frac{3z^2}{1+z+z^2} \right) a_6^{(n-1)}(z), \quad i = 1, 2, 3, 4, 5, 6. \quad (67)$$

Hence,

$$\begin{aligned} a_6^{(1)}(z) &= \frac{1}{729} \left[(21 - 20\mu - 16\nu)z^8 + (3 - 4\nu + 4\mu)z^7 + (-24 + 56\nu + 52\mu)z^6 + (224\mu + 424\nu - 147)z^5 \right. \\ &\quad + (-39 - 200\nu + 200\mu)z^4 + (280\nu + 186 + 80\mu)z^3 + (-336\mu + 693 - 744\nu)z^2 \\ &\quad + (801 + 408\nu - 408\mu)z^1 + (-336\mu + 693 - 744\nu)z^0 + (280\nu + 186 + 80\mu)z^{-1} + \\ &\quad (-39 - 200\nu + 200\mu)z^{-2} + (224\mu + 424\nu - 147)z^{-3} + (-24 + 56\nu + 52\mu)z^{-4} \\ &\quad \left. + (3 - 4\nu + 4\mu)z^{-5} + (21 - 20\mu - 16\nu)z^{-6} \right]. \\ a_6^{(2)}(z) &= \frac{1}{243} \left[(21 - 20\mu - 16\nu)z^8 + (12\nu + 24\mu - 18)z^7 + (60\nu + 48\mu - 27)z^6 \right. \\ &\quad + (152\mu - 102 + 352\nu)z^5 + (90 - 612\nu)z^4 + (198 - 72\mu + 540\nu)z^3 \\ &\quad + (405 - 264\mu - 672\nu)z^2 + (198 - 72\mu + 540\nu)z^1 + (90 - 612\nu)z^0 \\ &\quad + (152\mu - 102 + 352\nu)z^{-1} + (60\nu + 48\mu - 27)z^{-2} + (12\nu + 24\mu - 18)z^{-3} \\ &\quad \left. + (21 - 20\mu - 16\nu)z^{-4} \right]. \\ a_6^{(3)}(z) &= \frac{1}{81z^2} \left[(21 - 20\mu - 16\nu)z^{10} + (-39 + 44\mu + 28\nu)z^9 + (24\mu + 48\nu - 9)z^8 \right. \\ &\quad + (-54 + 276\nu + 84\mu)z^7 + (-108\mu - 936\nu + 153)z^6 + (99 + 1200\nu - 48\mu)z^5 \\ &\quad + (-108\mu - 936\nu + 153)z^4 + (-54 + 276\nu + 84\mu)z^3 + (24\mu + 48\nu - 9)z^2 \\ &\quad \left. + (-39 + 44\mu + 28\nu)z + (21 - 20\mu - 16\nu) \right]. \end{aligned} \quad (68)$$

And when $\nu = 0$, we get the following Laurent polynomials from (67):

$$\begin{aligned} a_6^{(4)}(z) &= \frac{1}{27} \left[\begin{aligned} &(21 - 20\mu)z^8 + (-60 + 64\mu)z^7 + (-20\mu + 30)z^6 + (40\mu - 24)z^5 \\ &+ (147 - 128\mu)z^4 + (40\mu - 24)z^3 + (-20\mu + 30)z^2 + (-60 + 64\mu)z + (21 - 20\mu) \end{aligned} \right], \\ a_6^{(5)}(z) &= \frac{1}{9} \left[\begin{aligned} &(21 - 20\mu)z^6 + (-81 + 84\mu)z^5 + (-84\mu + 90)z^4 + (40\mu - 33)z^3 \\ &+ (-84\mu + 90)z^2 + (-81 + 84\mu)z^1 + (21 - 20\mu) \end{aligned} \right], \\ a_6^{(6)}(z) &= \left(\frac{3z^2}{1+z+z^2} \right) \frac{1}{9} \left[\begin{aligned} &(21 - 20\mu)z^6 + (-81 + 84\mu)z^5 + (-84\mu + 90)z^4 + (40\mu - 33)z^3 \\ &+ (-84\mu + 90)z^2 + (-81 + 84\mu)z^1 + (21 - 20\mu) \end{aligned} \right]. \end{aligned} \quad (69)$$

Then, by using Theorem 1 and denoting the subdivision schemes corresponding to the Laurent polynomials

$a_6^{(j)}(z)$: $j = 0, 1, 2, 3, 4, 5, 6$ by $(CSS)_{a_6^{(j)}}$: $j = 0, 1, 2, 3, 4, 5, 6$, respectively, we get

$$\left\| \left(\frac{1}{3} (\text{CSS})_{a_6^{(j)}} \right)^1 \right\|_{\infty} = \frac{1}{3} \max \left\{ \sum_{j \in \mathbb{Z}} |\alpha_{i+3j}^{[j,1]}|; i = 0, 1, 2 \right\}, \quad j = 0, 1, 2, 3, 4, 5, 6. \tag{70}$$

By solving $\|((1/3) (\text{CSS})_{a_6^{(j)}})^1\|_{\infty} < 1$ for $j = 0, 1, 2, 3, 4, 5, 6$, we get the required result. \square

Corollary 4. *The order of smoothness of $(\text{CSS})_{a_6}$ can be increased if we use the refinement rules corresponding to the following Laurent polynomial which is derived from the Laurent polynomial of (66):*

$$\begin{aligned} \alpha(z) = & \frac{1}{3^{n+5}} [C_0^n \{C_0^n (21 - 16\nu - 20\mu)\} + C_0^n \{C_0^n (-18 + 12\nu + 24\mu) + C_1^n (21 - 16\nu - 20\mu)\}z \\ & + (C_0^n \{C_0^n (48\mu + 60\nu - 27) + C_1^n (-18 + 12\nu + 24\mu) + C_2^n (21 - 16\nu - 20\mu)\} + C_1^n \{C_0^{n-1} (21 - 16\nu - 20\mu)\})z^2 \\ & + (C_0^n \{C_0^n (152\mu + 352\nu - 102) + C_1^n \times (48\mu + 60\nu - 27) + C_2^n (-18 + 12\nu + 24\mu) + C_3^n (21 - 16\nu - 20\mu)\} + \\ & C_1^n \times \{C_0^{n-1} (-18 + 12\nu + 24\mu) + C_1^{n-1} (21 - 16\nu - 20\mu)\})z^3 \\ & + (C_0^n \{C_0^n (-612\nu + 90) + C_1^n (152\mu + 352\nu - 102) + C_2^n (48\mu + 60\nu - 27) + C_3^n (-18 + 12\nu + 24\mu)\} + C_1^n \times \\ & \{C_0^{n-1} (48\mu + 60\nu - 2) + C_1^{n-1} (-18 + 12\nu + 24\mu) + C_2^{n-1} (21 - 16\nu - 20\mu)\} + C_2^n \{C_0^{n-2} (21 - 16\nu - 20\mu)\})z^4 \\ & \dots + (C_{n-2}^n \{C_2^2 (21 - 16\nu - 20\mu)\} + C_{n-1}^n \{C_1^1 (21 - 16\nu - 20\mu) + C_0^1 (-18 + 12\nu + 24\mu)\} + C_n^n (48\mu + 60\nu - 27))z^{2n+10} \\ & + (C_{n-1}^n \times \{(21 - 16\nu - 20\mu)\} + C_n^n (-18 + 12\nu + 24\mu))z^{2n+11} \\ & (C_n^n (21 - 16\nu - 20\mu))z^{2n+12}], \end{aligned} \tag{71}$$

where μ and ν are shape parameters and $m \in \mathbb{N}$.

Theorem 9. *The limit stencil of $(\text{CSS})_{a_6}$ is $[\xi_1, \xi_2, \xi_3, \xi_4, \xi_3, \xi_2, \xi_1]$, where*

Theorem 3 gives the following result.

Corollary 5. *The support of $(\text{CSS})_{a_6}$ is $[-4, 4]$.*

$$\begin{aligned} \xi_1 = & \frac{64(\mu^3 + \mu^2\nu - \mu\nu^2 - \nu^3) - 580\mu^2 - 930\mu\nu + 555\mu + 350\nu^2 + 555\nu}{756(20\mu + 145\nu - 6\mu\nu - 6\nu^2 + 240)}, \\ \xi_2 = & \frac{-(12\mu^3 + 40\mu^2\nu - 317\mu^2 + 44\mu\nu^2 + 45\mu + 16\nu^3 - 644\nu^2 + 45\nu - 961\mu\nu)}{42(20\mu + 145\nu - 6\mu\nu - 6\nu^2 + 240)}, \\ \xi_3 = & \frac{32\mu^3 + 88\mu^2\nu - 1396\mu^2 + 80\mu\nu^2 - 2138\mu\nu + 6525\mu + 24\nu^3 - 742\nu^2 + 6525\nu}{84(20\mu + 145\nu - 6\mu\nu - 6\nu^2 + 240)}, \\ \xi_4 = & \frac{-68(\mu^3 + \mu^2\nu - \mu\nu^2 - \nu^3) + 3719\mu^2 + 303\mu\nu - 25455\mu - 3416\nu^2 - 1830\nu + 45360}{189(20\mu + 145\nu - 6\mu\nu - 6\nu^2 + 240)}. \end{aligned} \tag{72}$$

Theorem 10. *If we choose $\mu = 1$ and $\nu = (-1/5)$, then the lower and upper bound of Hölder regularity of $(\text{CSS})_{a_6}$ are 2.1302 and 2.455, respectively.*

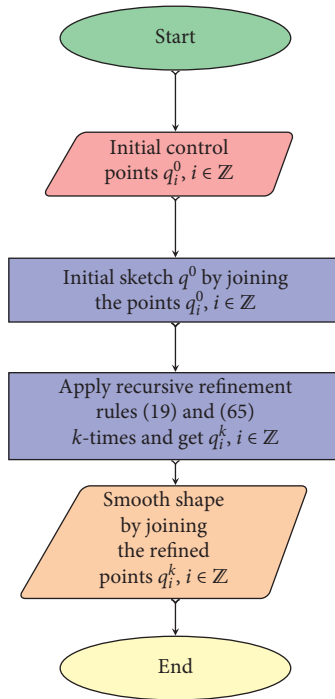


FIGURE 3: Flowchart to explain the geometric examples.

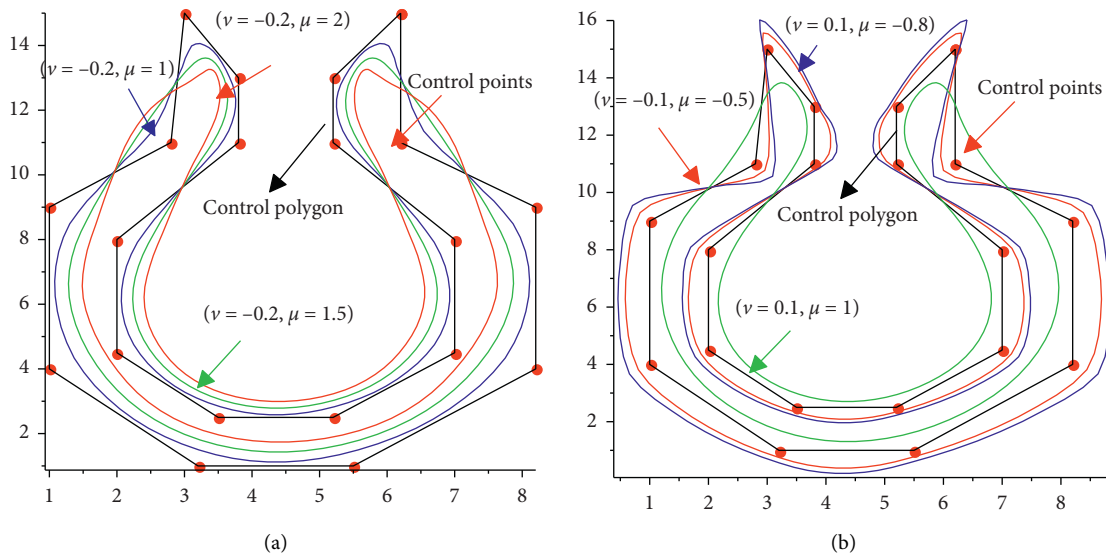


FIGURE 4: Continued.

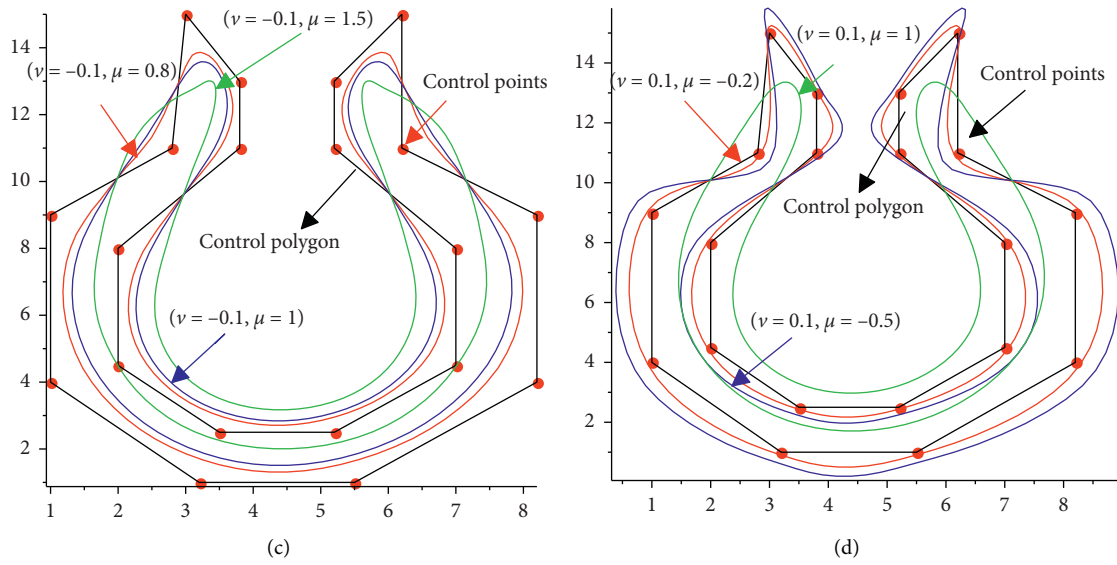


FIGURE 4: Coloured lines show the curves fitted by the combined subdivision schemes.

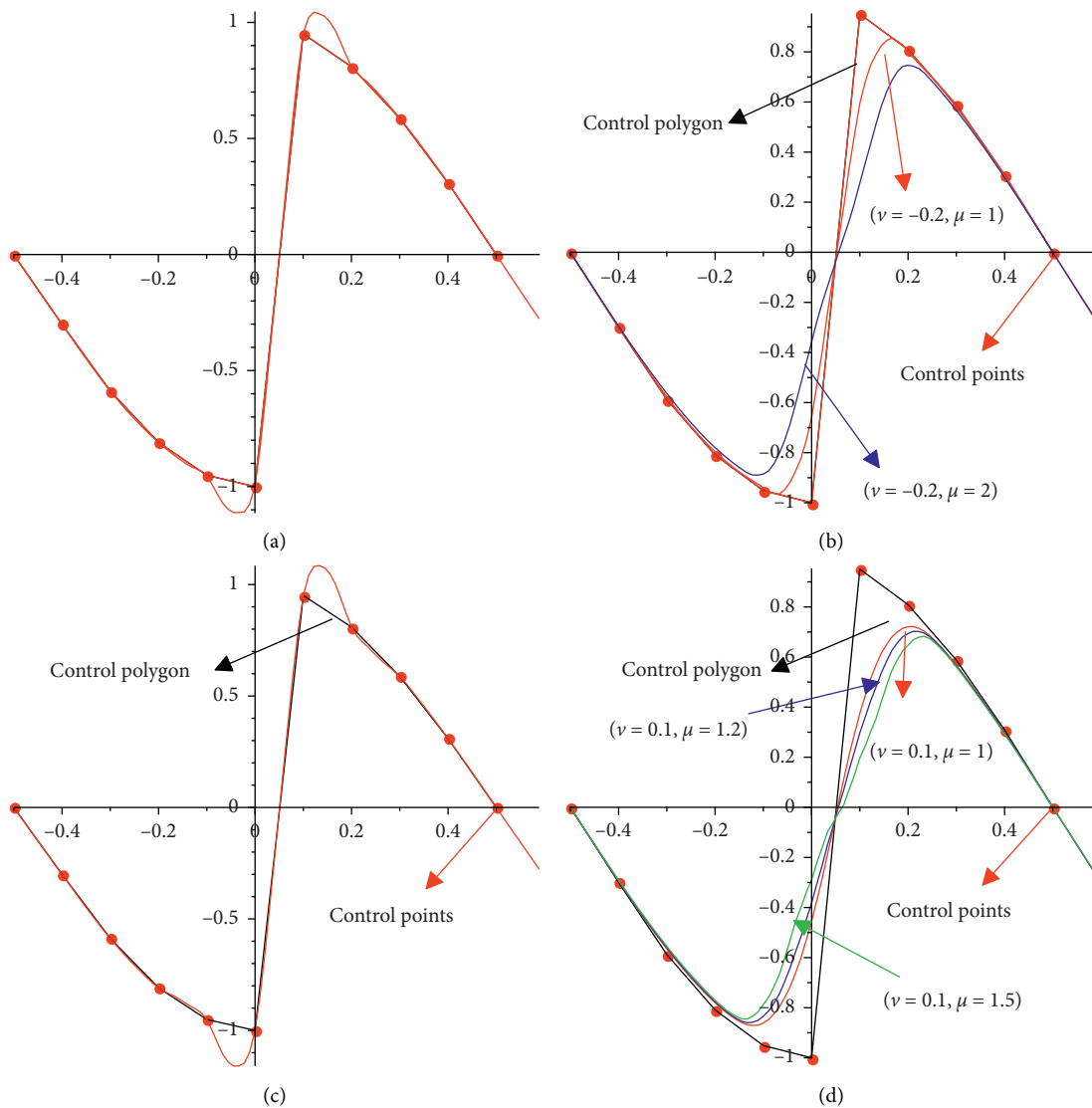


FIGURE 5: Red bullets are initial control points. Black solid lines are initial control polygons. Coloured lines show the fitted curves by our schemes in (b) and (d).

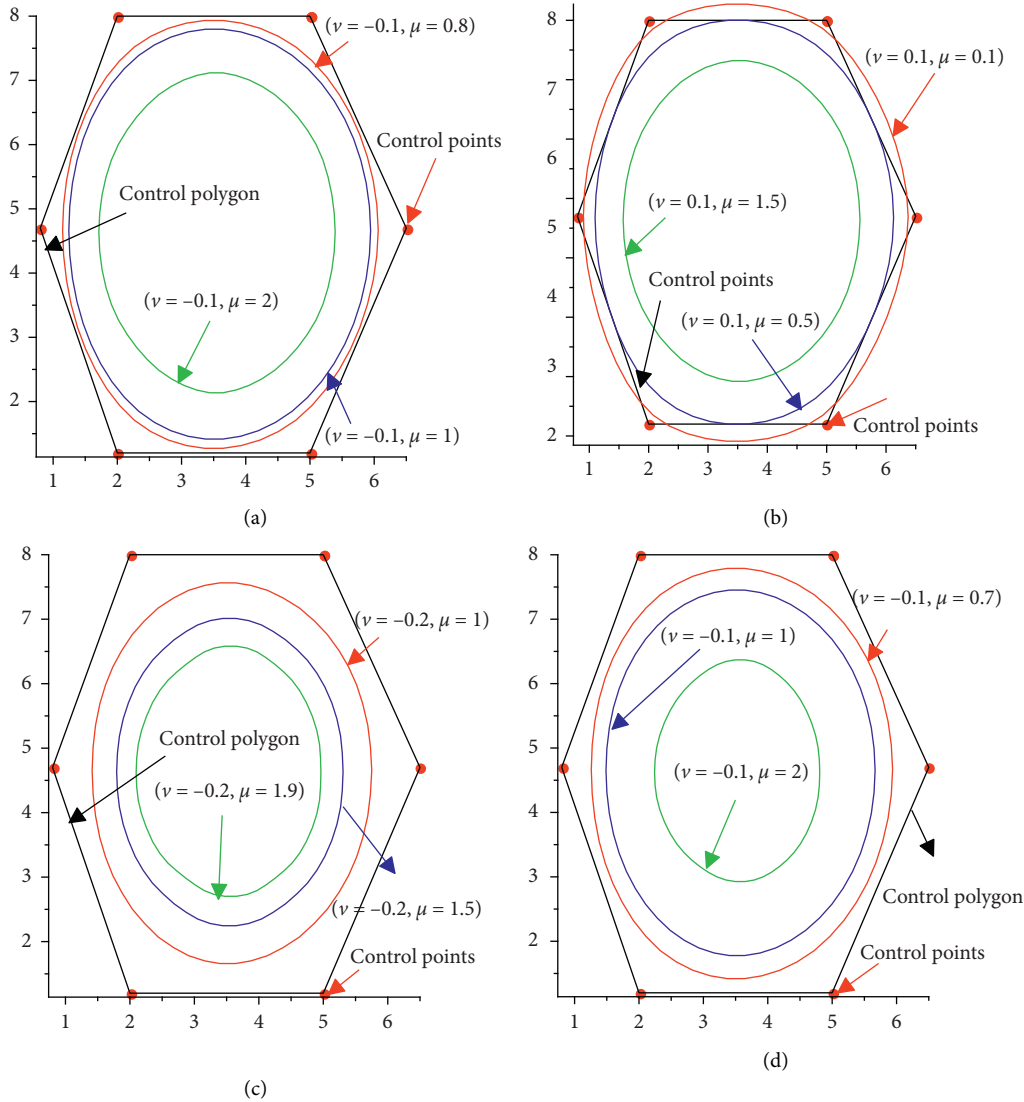


FIGURE 6: Red bullets show the initial control points. Black solid lines are the initial control polygon. Coloured lines show curves fitted by our subdivision scheme after two refinement steps. (a) 4-point combined scheme $\nu = -0.1, \mu = 0.1, 0.5, 1.5$; (b) 4-point combined scheme $\nu = 0.1, \mu = 0.1, 0.5, 1.5$; (c) 6-point combined scheme $\nu = -0.1, \mu = 1, 1.5, 1.9$; and (d) 6-point combined scheme $\nu = -0.3, \mu = 1, 1.3, 1.5$.

5. Geometrical Influence of $(CSS)_{a_{2n+2}}$ in Curve Modeling

In this section, we present models produced by the new combined 4-point and 6-point subdivision schemes. For modeling of 2D shapes by the combined schemes, we use the procedure which is explained in Figure 3 through a flow-chart. This procedure is used in the following numerical examples for curve modeling.

Example 1. In this example, we draw the initial sketch q^0 by using the initial data $\{q_i^0: i \in \mathbb{Z}\}$. The initial sketch and the initial data are shown by black polygons and red bullets in Figure 4. Curves fitted by the subdivision schemes $(CSS)_{a_4}$ and $(CSS)_{a_6}$ after four refinements steps for various values of μ and ν are shown in this figure. Figure 4(a) shows the curves fitted by a 4-point ternary combined scheme for $\nu = -0.2$

and $\mu = 1, 1.5, 2$. Figure 4(b) shows the curves fitted by a 4-point ternary combined scheme for $\nu = 0.1$ and $\mu = -0.5, -0.8, 1$. Figure 4(c) shows the curves fitted by a 6-point ternary combined scheme for $\nu = -0.1$ and $\mu = 0.8, 1, 1.5$. Figure 4(d) shows the curves fitted by a 4-point ternary combined scheme for $\nu = 0.1$ and $\mu = -0.2, -0.5, 1$.

Example 2. In this experiment, we input the initial data taken from the discontinuous function:

$$h(x) = \begin{cases} +\cos \pi x, & \text{if } x \in [0.5, 0[, \\ -\cos \pi x, & \text{if } x \in [0, 0.5]. \end{cases} \tag{73}$$

Curves fitted by the first two members of our class of schemes are shown in Figures 5(b) and 5(d), respectively, and the curves fitted by the first two members of the CETISS

are shown in Figures 5(a) and 5(c), respectively. We see that the CETISS produce Gibbs oscillations in the limit curves close to the discontinuity. It is also noted that our combined schemes do not produce Gibbs oscillations in the limit curves for certain values of the shape parameters.

Example 3. In this example, we take the initial data such that if we join this data by straight lines, we get a close polygonal shape. We smooth this shape by the first two members of our class of schemes and results are shown in Figure 6. This figure shows the flexible behaviour of our combined subdivision scheme. It also shows that shape parameters in the combined subdivision schemes provide grip on the limit curves.

6. Conclusion

In this research, we have constructed and analyzed a class of combined ternary subdivision schemes. The construction procedure is very simple and consists of only a few simple mathematical operations on the refinement rules of the two well-known classes of the schemes. But it gives us amazing results that are discussed theoretically and geometrically in detail. The class of schemes gives good smoothness and local control on the limit shapes. It also provides us a flexible environment to fit curves. The unnecessary oscillations in the limit curves of our combined schemes can be removed by changing the values of the shape parameters.

Data Availability

No datasets were generated or analysed during the current study.

Conflicts of Interest

The authors declare that they have no conflicts of interest.

References

- [1] G. Mustafa, R. Hameed, D. Baleanu, and A. Mahmood, "A class of refinement schemes with two shape control parameters," *IEEE Access*, vol. 8, no. 1, pp. 98316–98329, 2020.
- [2] N. Dyn, D. Levin, and J. A. Gregory, "A 4-point interpolatory subdivision scheme for curve design," *Computer Aided Geometric Design*, vol. 4, no. 4, pp. 257–268, 1987.
- [3] G. Deslauriers and S. Dubuc, "Symmetric iterative interpolation processes," *Constructive Approximation*, vol. 5, pp. 49–68, 1989.
- [4] C. Beccari, G. Casciola, and L. Romani, "An interpolating 4-point C^2 ternary non-stationary subdivision scheme with tension control," *Computer Aided Geometric Design*, vol. 24, no. 4, pp. 210–219, 2007.
- [5] M. F. Hassan, I. P. Ivriissimitzis, N. A. Dodgson, and M. A. Sabin, "An interpolating 4-point C^2 ternary stationary subdivision scheme," *Computer Aided Geometric Design*, vol. 19, pp. 1–18, 2002.
- [6] G. Mustafa, P. Ashraf, and J. Deng, "Generalized and unified families of interpolating subdivision schemes," *Numerical Mathematics*, vol. 7, no. 2, pp. 193–213, 2014.
- [7] S. M. Hussain, A. Rehman, D. Baleanu, K. s. Nisar, A. Ghaffar, and S. A. A. Karim, "Generalized 5-point approximating subdivision scheme of varying arity," *Mathematics*, vol. 8, no. 474, pp. 1–25, 2020.
- [8] S. S. Siddiqi and M. Younis, "Construction of m -point binary approximating subdivision schemes," *Applied Mathematics Letters*, vol. 26, no. 3, pp. 337–343, 2013.
- [9] R. Hameed and G. Mustafa, "Construction and analysis of binary subdivision schemes for curves and surfaces originated from Chaikin points," *International Journal of Analysis*, vol. 2016, Article ID 1092476, 15 pages, 2016.
- [10] G. Mustafa and R. Hameed, "Families of univariate and bivariate subdivision schemes originated from quartic B-spline," *Advances in Computational Mathematics*, vol. 43, no. 5, pp. 1131–1161, 2017.
- [11] O. Rioul, "Simple regularity criteria for subdivision schemes," *SIAM Journal on Mathematical Analysis*, vol. 23, no. 6, pp. 1544–1576, 1992.
- [12] G. Mustafa, P. Ashraf, and J. Deng, "Generalized and unified families of interpolating subdivision schemes," *Numerical Mathematics: Theory, Methods and Applications*, vol. 7, no. 2, pp. 193–213, 2014.
- [13] J. Pan, S. Lin, and X. Luo, "A combined approximating and interpolating ternary 4-point subdivision scheme," *Applied Mathematics Letters*, vol. 25, no. 12, pp. 2140–2146, 2012.
- [14] D. Gottlieb and C. W. Shu, "On the Gibbs phenomenon and its resolution," *SIAM Review*, vol. 39, no. 4, pp. 644–668, 1997.
- [15] S. Amat, J. Ruiz, J. C. Trillo, and D. F. Yanez, "Analysis of the Gibbs phenomenon in stationary subdivision schemes," *Applied Mathematics Letters*, vol. 76, pp. 157–163, 2018.
- [16] K. Rehan and M. A. Sabri, "A combined ternary 4-point subdivision schemes," *Journal of Computational and Applied Mathematics*, vol. 276, pp. 278–283, 2016.
- [17] N. Dyn, "Subdivision schemes in CAGD," in *Advances in Numerical Analysis II: Wavelets, Subdivision Algorithms, and Radial Basis Functions*, W. Light, Ed., Oxford University Press, Oxford, UK, 1992.
- [18] F. Pitolli, "Ternary shape-preserving subdivision schemes," *Mathematics and Computers in Simulation*, pp. 185–194, 2014.
- [19] P. Novara and L. Romani, "Complete characterization of the regions of C^2 and C^3 convergence of combined ternary 4-point subdivision schemes," *Applied Mathematics Letters*, vol. 62, pp. 84–91, 2016.

Research Article

A Nonstationary Ternary 4-Point Shape-Preserving Subdivision Scheme

Jieqing Tan^{1,2} and Guangyue Tong² 

¹*School of Mathematics, Hefei University of Technology, Hefei 230009, China*

²*School of Computer and Information, Hefei University of Technology, Hefei 23009, China*

Correspondence should be addressed to Guangyue Tong; 1285036868@qq.com

Received 26 October 2020; Revised 2 December 2020; Accepted 18 December 2020; Published 6 January 2021

Academic Editor: Ghulam Mustafa

Copyright © 2021 Jieqing Tan and Guangyue Tong. This is an open access article distributed under the Creative Commons Attribution License, which permits unrestricted use, distribution, and reproduction in any medium, provided the original work is properly cited.

This paper uses the continued fraction technique to construct a nonstationary 4-point ternary interpolatory subdivision scheme, which provides the user with a tension parameter that effectively handles cusps compared with a stationary 4-point ternary interpolatory subdivision scheme. Then, the continuous nonstationary 4-point ternary scheme is analyzed, and the limit curve is at least C^2 -continuous. Furthermore, the monotonicity preservation and convexity preservation are proved.

1. Introduction

Subdivision schemes are widely used in many areas, including CAGD, CG, and related areas. Most of the existing univariate subdivision schemes are binary, ternary, stationary, and linear. The classical binary 4-point scheme is one of the earliest and most popular interpolatory subdivision schemes [1, 2]. Hassan et al. present the 4-point ternary subdivision scheme in [3], in which the limit curves by the 4-point ternary subdivision scheme are continuous. Beccari et al. present a nonstationary subdivision scheme in [4, 5], which generates continuous limit curves. In graphic design, shape-preserving of curve/surface is essential. Monotonicity preservation and convexity preservation are two significant properties in maintaining shape-preserving. Dyn et al. analyze the convexity preservation of the 4-point interpolatory scheme in [6]. Many subdivision schemes cannot satisfy monotonicity preservation and convexity preservation in the current subdivision zoo. Cai presents binary and ternary 4-point interpolatory subdivision schemes that are continuous in nonuniform control points and discusses the limit curve's convexity preservation [7, 8]. Kuijt and van Damme present a local nonlinear interpolatory subdivision scheme which is monotonicity preserving in [9], and Kuijt and van Damme also research a type of shape-preserving 4-point interpolatory subdivision

scheme which interpolated nonuniform data in [10]. Tan et al. discuss the monotonicity preservation and convexity preservation of the binary subdivision scheme [11, 12]. Several subdivision schemes are designed to have their unique properties in [13–15]. Much research has been done on continued fraction theory and its application by Tan [16]. Ghaffar et al. discussed a new class of 2q-point nonstationary subdivision schemes and their application [17]. Ashraf et al. analyzed the ternary four-point rational interpolating subdivision scheme's geometric properties [18, 19]. More subdivision schemes are studied in [17, 20–22].

Nonstationary subdivision schemes have been studied [5, 22], but the limit curves are not monotonicity preserving and convexity preserving. Our paper aims to construct a nonstationary 4-point ternary interpolatory subdivision scheme, which is shape-preserving using a continued fraction. Section 2 uses a continued fraction to construct a nonstationary interpolatory subdivision scheme and then analyze the continuity. In Section 3, the monotonicity preservation of the limit curves is discussed. In Section 4, the convexity preservation of limit curves is discussed and proven. In Section 5, when the initial control polygon is open, we use the new rule for the endpoints to achieve better continuity. In Section 6, we use experiments to show that our scheme effectively handles cusps and shape preservation.

2. A Nonstationary Subdivision

2.1. A Stationary Subdivision

Definition 1 (see [3]). Given a set of the initial control points $P^0 = \{p_i^0 \in R^d\}_{i=1}^n$, let $P^k = \{p_i^k \in R^d\}_{i=1}^n$ be the set of control points at the order k subdivision. Define $\{P_i^{k+1} \in R^d\}_{i=1}^{3^{k+1}n}$ recursively by the following ternary subdivision rules:

$$\begin{cases} P_{3i}^{k+1} = p_i^k, & 1 < i < 3^k n, \\ P_{3i+1}^{k+1} = a_0^k p_{i-1}^k + a_1^k p_i^k + a_2^k p_{i+1}^k + a_3^k p_{i+2}^k, & 2 < i < 3^k n, \\ P_{3i+2}^{k+1} = a_3^k p_{i-1}^k + a_2^k p_i^k + a_1^k p_{i+1}^k + a_0^k p_{i+2}^k, & 2 < i < 3^k n, \end{cases} \quad (1)$$

where $a_0^k \equiv a_0 = -1/18 - 1/6u$, $a_1^k \equiv a_1 = 13/18 + 1/2u$, $a_2^k \equiv a_2 = 7/18 - 1/2u$, and $a_3^k \equiv a_3 = -1/18 + 1/6u$. u is a tension parameter. When $u \in (1/15, 1/9)$, the limit curve is C^2 -continuous.

2.2. A Nonstationary Subdivision. We use the continued fraction technique to construct a nonstationary 4-point ternary interpolatory subdivision scheme.

Definition 2. Given a set of the initial control points $P^0 = \{p_i^0 \in R^d\}_{i=1}^n$, let $P^k = \{p_i^k \in R^d\}_{i=1}^n$ be the set of control points at the order k subdivision. Define $\{P_i^{k+1} \in R^d\}_{i=1}^{3^{k+1}n}$ recursively by the following ternary subdivision rules:

$$\begin{cases} P_{3i}^{k+1} = p_i^k, & 1 < i < 3^k n, \\ P_{3i+1}^{k+1} = a_0^k p_{i-1}^k + a_1^k p_i^k + a_2^k p_{i+1}^k + a_3^k p_{i+2}^k, & 2 < i < 3^k n, \\ P_{3i+2}^{k+1} = a_3^k p_{i-1}^k + a_2^k p_i^k + a_1^k p_{i+1}^k + a_0^k p_{i+2}^k, & 2 < i < 3^k n, \end{cases} \quad (2)$$

where $a_0^k = -1/18 - 1/6u^k$, $a_1^k = 13/18 + 1/2u^k$, $a_2^k = 7/18 - 1/2u^k$, and $a_3^k = -1/18 + 1/6u^k$. u^k is a tension parameter:

$$\begin{aligned} u^k &= b_0 + \frac{c_1}{|b_1|} + \frac{c_2}{|b_2|} + \dots + \frac{c_k}{|b_k|}, \\ b_0 &= u + 1, b_j = \frac{(u + 1/4^{k+1})(1 + 1/8^{k-1}) - (u + 1/4^{k-1})(1 + 1/8^{k+1})}{(u + 1/4^k)(1 + 1/8^{k-1}) - (u + 1/4^{k-1})(1 + 1/8^k)}, \\ c_j &= \frac{(u + 1/4^{k-1})(1 + 1/8^k) - (u + 1/4^k)(1 + 1/8^{k+1})}{(u + 1/4^k)(1 + 1/8^{k-1}) - (u + 1/4^{k-1})(1 + 1/8^k)}, \quad u \in \left(\frac{1}{15}, \frac{1}{9}\right) (j = 1, 2, \dots, k). \end{aligned} \quad (3)$$

Theorem 1 (Pringsheim Theorem [16]). Let $f_n = b_0 + a_1/|b_1| + a_2/|b_2| + \dots + a_k/|b_k|$, if $|b_n| \geq |a_n| + 1$, so $f_n = b_0 + a_1/|b_1| + a_2/|b_2| + \dots + a_k/|b_k|$ is convergence.

Remark 1. According to Theorem 1, we know u^k is convergence. Due to $u^k = b_0 + c_1/|b_1| + c_2/|b_2| + \dots + c_k/|b_k| + \dots = u + (1/4^{k+1})/1 + (1/8^{k+1})$, we know the $\lim_{k \rightarrow +\infty} u^k = u, u \in (1/15, 1/9)$.

2.3. Convergence Analysis. This section's purpose primarily proves the continuity of (2) when the initial tension parameter $u \in (1/15, 1/9)$. To analyze our scheme's smoothness properties, we exploit Dyn and Levin's well-known results in [23], which relate the convergence of a nonstationary scheme to its asymptotically equivalent stationary counterpart. From Remark 1, we know $\lim_{k \rightarrow +\infty} u^k = u, u \in (1/15, 1/9)$, and the nonstationary subdivision scheme defined in (2) converges to the stationary subdivision scheme (1).

Proposition 1. The nonstationary subdivision scheme defined in (2) is asymptotically equivalent to the stationary scheme defined in (1) with $u \in (1/15, 1/9)$. Moreover, it generates C^2 -continuous limit curve.

Proof. If we want to prove that the proposed nonstationary subdivision scheme converges to a C^2 -continuous limit curve, we compute its second divided difference mask and show that the associated limit curves are C^0 -continuous.

The mask of nonstationary subdivision scheme is given by

$$\begin{aligned} m^k &= \frac{1}{18} [3u^k - 1, -3u^k - 1, 0, -9u^k + 7, 9u^k + 13, 18, 9u^k \\ &\quad + 13, -9u^k + 7, 0, -3u^k - 1, 3u^k - 1]. \end{aligned} \quad (4)$$

Its related first divided difference is

$$\begin{aligned} d_{(1)}^k &= \frac{1}{6} [3u^k - 1, -6u^k, 3u^k + 1, -6u^k + 6, 12u^k + 6, -6u^k \\ &\quad + 6, 3u^k + 1, -6u^k, 3u^k - 1]. \end{aligned} \quad (5)$$

Hence, the second divided difference mask turns out to be

$$d_{(2)}^k = \frac{1}{2} [3u^k - 1, -9u^k + 1, 9u^k + 1, -6u^k + 4, 9u^k + 1, -9u^k + 1, 3u^k - 1]. \quad (6)$$

In this way, according to Remark 1, it follows that

$$\lim_{k \rightarrow \infty} d_{(2)}^k = \frac{1}{2} [3u - 1, -9u + 1, 9u + 1, -6u + 4, 9u + 1, -9u + 1, 3u - 1]. \quad (7)$$

The mask $\lim_{k \rightarrow \infty} d_{(2)}^k$ tends to mask of the second divided differences of the stationary subdivision scheme defined in (1) with $u \in (1/15, 1/9)$.

Since the stationary subdivision scheme is C^2 -continuous when $u \in (1/15, 1/9)$, then nonstationary subdivision scheme associated with $d_{(2)}^\infty$ will be C^0 .

According to [16], if

$$\sum_k \|d_{(2)}^k - d_{(2)}^\infty\|_\infty < +\infty, \quad (8)$$

then the two different schemes are asymptotically equivalent, so it concludes that the scheme associated with $d_{(2)}^k$ is C^0 .

Since

$$\|d_{(2)}^k - d_{(2)}^\infty\|_\infty = \frac{1}{2} \max \left\{ |3u^k - 3u|, |-9u^k + 9u|, |-6u^k + 6u| \right\} = \frac{9}{2} |u^k - u|. \quad (9)$$

Next, we need to prove $9/2 \sum_{k=1}^{+\infty} |u^k - u| < +\infty$.

According to the structural characteristics of the u^k , we know $u^k > u^{k+1}$ and $\lim_{k \rightarrow \infty} u^k = u, u \in (1/15, 1/9)$. As $u^{k+1} < u^k$, $u^{k+1} - u > 0, u^k - u > 0$, thus $u^{k+1} - u/u^k - u < 1$, according to the comparison test, we know $\sum_{k=1}^{+\infty} |u^k - u| < +\infty$, so $9/2 \sum_{k=1}^{+\infty} |u^k - u| < +\infty$.

This completes the proof.

Hence, the nonstationary subdivision scheme defined in (2) is asymptotically equivalent to the stationary scheme defined in (1) with $u \in (1/15, 1/9)$. Limit curves generated by (1) are C^2 -continuous. According to Proposition 1, the limit curves generated by (2) are C^2 -continuous. \square

3. Monotonicity Preservation

The limit curves generated by (2) are C^2 -continuous, we next discuss the limit curves generated by (2) are monotonicity preserving.

Proposition 2. Given a set of the initial control points $P^0 = \{p_i^0 \in \mathbb{R}^d\}_{i=1}^n$ that satisfies $\dots p_{-1}^0 < p_0^0 < p_1^0 < \dots < p_{n-1}^0 < p_n^0 < \dots$, a nonstationary subdivision scheme for designing curves generates a new control point $P^k = \{p_i^k \in \mathbb{R}^d\}$ recursively at the level k by applying (2). Denoting $D_i^k = p_{i+1}^k - p_i^k, q_i^k = D_{i+1}^k/D_i^k, Q^k = \max\{q_i^k, 1/q_i^k\}, \forall k \geq 0, k \in \mathbb{Z}, i \in \mathbb{Z}$. Furthermore, if $1 \leq \lambda \leq 4, \lambda \in \mathbb{R}, 1/\lambda \leq Q^0 \leq \lambda$, then

$$D_i^k > 0, \frac{1}{\lambda} \leq Q^k \leq \lambda, \quad \forall k \geq 0, k \in \mathbb{Z}, i \in \mathbb{Z}. \quad (10)$$

Proof. We use mathematic induction to verify Proposition 2.

When $k = 0, D_i^0 = p_{i+1}^0 - p_i^0 > 0, 1/\lambda \leq Q^0 \leq \lambda$, then (10) is true.

Suppose that (10) is true for k , next we will verify it also holds true for $k + 1$.

$$\begin{aligned} D_{3i}^{k+1} &= p_{3i+1}^{k+1} - p_{3i}^{k+1} = \left(-\frac{1}{18} + \frac{1}{6}u^k\right)(p_{i+2}^k - p_{i+1}^k) \\ &\quad + \left(\frac{6}{18} - \frac{2}{6}u^k\right)(p_{i+1}^k - p_i^k) + \left(\frac{1}{18} + \frac{1}{6}u^k\right)(p_i^k - p_{i-1}^k) \\ &= \left(-\frac{1}{18} + \frac{1}{6}u^k\right)D_{i+1}^k + \left(\frac{6}{18} - \frac{2}{6}u^k\right)D_i^k + \left(\frac{1}{18} + \frac{1}{6}u^k\right)D_{i-1}^k \\ &= D_i^k \left[\left(-\frac{1}{18} + \frac{1}{6}u^k\right) \frac{D_{i+1}^k}{D_i^k} + \left(\frac{6}{18} - \frac{2}{6}u^k\right) + \left(\frac{1}{18} + \frac{1}{6}u^k\right) \frac{D_{i-1}^k}{D_i^k} \right] \\ &> D_i^k \left[\left(-\frac{1}{18} + \frac{1}{6}u^k\right)\lambda + \left(\frac{6}{18} - \frac{2}{6}u^k\right) + \left(\frac{1}{18} + \frac{1}{6}u^k\right)\frac{1}{\lambda} \right]. \end{aligned} \quad (11)$$

As $1 \leq \lambda \leq 4, u^k \in (1/15, 1/9)$, so

$$\begin{aligned} D_{3i}^{k+1} &> D_i^k \left[\left(-\frac{1}{18} + \frac{1}{6}u^k\right) \times 4 + \left(\frac{6}{18} - \frac{2}{6}u^k\right) + \left(\frac{1}{18} + \frac{1}{6}u^k\right) \right] \\ &= D_i^k \left(\frac{1}{6} + \frac{1}{2}u^k \right) > 0, \\ D_{3i+1}^{k+1} &= p_{3i+2}^{k+1} - p_{3i+1}^{k+1} = -\frac{2}{6}u^k D_{i+1}^k + \left(\frac{6}{18} + \frac{4}{6}u^k\right)D_i^k - \frac{2}{6}u^k D_{i-1}^k \\ &= D_i^k \left[-\frac{2}{6}u^k \frac{D_{i+1}^k}{D_i^k} + \left(\frac{6}{18} + \frac{4}{6}u^k\right) - \frac{2}{6}u^k \frac{D_{i-1}^k}{D_i^k} \right] \\ &> D_i^k \left[-\frac{2}{6}u^k \lambda + \left(\frac{6}{18} + \frac{4}{6}u^k\right) - \frac{2}{6}u^k \lambda \right] = D_i^k \left(\frac{4}{6}u^k(1 - \lambda) + \frac{1}{3} \right). \end{aligned} \quad (12)$$

As $1 \leq \lambda \leq 4, u^k \in (1/15, 1/9)$, so

$$\begin{aligned} D_{3i+1}^{k+1} &> D_i^k \left(\frac{1}{3} - 2u^k \right) > 0 \\ D_{3i+2}^{k+1} &= p_{3i+3}^{k+1} - p_{3i+2}^{k+1} = \left(\frac{1}{18} + \frac{1}{6}u^k\right)D_{i+1}^k + \left(\frac{6}{18} - \frac{2}{6}u^k\right)D_i^k \\ &\quad + \left(-\frac{1}{18} + \frac{1}{6}u^k\right)D_{i-1}^k \\ &= D_i^k \left[\left(\frac{1}{18} + \frac{1}{6}u^k\right) \frac{D_{i+1}^k}{D_i^k} + \left(\frac{6}{18} - \frac{2}{6}u^k\right) + \left(-\frac{1}{18} + \frac{1}{6}u^k\right) \frac{D_{i-1}^k}{D_i^k} \right] \\ &> D_i^k \left[\left(\frac{1}{18} + \frac{1}{6}u^k\right)\lambda + \left(\frac{6}{18} - \frac{2}{6}u^k\right) + \left(-\frac{1}{18} + \frac{1}{6}u^k\right)\lambda \right]. \end{aligned} \quad (13)$$

As $1 \leq \lambda \leq 4, u^k \in (1/15, 1/9)$, so

$$\begin{aligned}
 D_{3i}^{k+1} &> D_i^k \left[\left(\frac{1}{18} + \frac{1}{6}u^k \right) + \left(\frac{6}{18} - \frac{2}{6}u^k \right) + \left(-\frac{1}{18} + \frac{1}{6}u^k \right) \times 4 \right] \\
 &= D_i^k \left(\frac{1}{6} + \frac{1}{6}u^k \right) > 0.
 \end{aligned}
 \tag{14}$$

Now, we prove $1/\lambda \leq Q^k \leq \lambda$.
Since

$$\begin{aligned}
 q_{3i}^{k+1} &= \frac{D_{3i+1}^{k+1}}{D_{3i}^{k+1}} = \frac{-2/6u^k D_{i+1}^k + (6/18 + 4/6u^k)D_i^k - 2/6u^k D_{i-1}^k}{(-1/18 + 1/6u^k)D_{i+1}^k + (6/18 - 2/6u^k)D_i^k + (1/18 + 1/6u^k)D_{i-1}^k} \\
 &= \frac{-2/6u^k q_{i+1}^k + (6/18 + 4/6u^k) - 2/6u^k 1/q_{i-1}^k}{(-1/18 + 1/6u^k)q_{i+1}^k + (6/18 - 2/6u^k) + (1/18 + 1/6u^k)1/q_{i-1}^k}, \\
 q_{3i}^{k+1} - \lambda &= \frac{(-2/6u^k + \lambda/18 - 1/6\lambda u^k)q_i^k + (6/18 + 4/6u^k - 6\lambda/18 + 2/6\lambda u^k) - (2/6u^k + \lambda/18 + 1/6\lambda u^k)1/q_{i-1}^k}{(-1/18 + 1/6u^k)q_i^k + (6/18 - 2/6u^k) + (1/18 + 1/6u^k)1/q_{i-1}^k}.
 \end{aligned}
 \tag{15}$$

By (12), the denominator of the above expression is greater than zero. The numerator satisfies

$$\begin{aligned}
 \text{numerator} &< [(-2/6u^k + \lambda/18 - 1/6\lambda u^k)\lambda + (6/18 + 4/6u^k - 6\lambda/18 + 2/6\lambda u^k) - (2/6u^k + \lambda/18 + 1/6\lambda u^k)1/\lambda] \\
 &= (\lambda^2/18 - 1/3\lambda + 5/18) + (-1/6\lambda^2 - 1/3\lambda + 1/2)u^k.
 \end{aligned}
 \tag{16}$$

When $1 \leq \lambda \leq 4$, $-1/6\lambda^2 - 1/3\lambda + 1/2 \leq 0$, $\lim_{k \rightarrow +\infty} u^k = u$, $u \in (1/15, 1/9)$.

Then it can get $\text{numerator} < 1/18(\lambda^2 - 6\lambda + 5) + (-1/6\lambda^2 - 1/3\lambda + 1/2) \times 1/15 \leq 0$. So $q_{3i}^{k+1} - \lambda \leq 0$, $q_{3i}^{k+1} \leq \lambda$.
In the same way, we prove the $1/q_{3i}^{k+1} \leq \lambda$.

$$\frac{1}{q_{3i}^{k+1}} - \lambda = \frac{(-1/18 + 1/6u^k + 2/6u^k)q_i^k + (6/18 - 2/6u^k - 6\lambda/18 - 4/6\lambda u^k) + (1/18 + 1/6u^k + 2/6\lambda u^k)1/q_{i-1}^k}{-2/6u^k q_{i+1}^k + (6/18 + 4/6u^k) - 2/6u^k 1/q_{i-1}^k}.
 \tag{17}$$

By (13), the denominator of the above expression is greater than zero. The numerator satisfies

$$\begin{aligned}
 \text{numerator} &< \left(-\frac{1}{18} + \frac{1}{6}u^k + \frac{2}{6}u^k \right) \lambda + \left(\frac{6}{18} - \frac{2}{6}u^k - \frac{6\lambda}{18} - \frac{4}{6}\lambda u^k \right) + \left(\frac{1}{18} + \frac{1}{6}u^k + \frac{2}{6}\lambda u^k \right) \lambda \\
 &= \frac{1}{3} [(2\lambda^2 - \lambda - 1)u^k + (1 - \lambda)].
 \end{aligned}
 \tag{18}$$

When $1 \leq \lambda \leq 4$, $2\lambda^2 - \lambda - 1 \geq 0$, $\lim_{k \rightarrow +\infty} u^k = u$, $u \in (1/15, 1/9)$.

Then $\text{numerator} < 1/3[(2\lambda^2 - \lambda - 1) \times 1/9 + (1 - \lambda)] = 2/17(\lambda^2 - 5\lambda + 4) \leq 0$. So $1/q_{3i}^{k+1} \leq \lambda$.

Therefore, $1/\lambda \leq q_{3i}^{k+1} \leq \lambda$, $1/\lambda \leq 1/q_{3i}^{k+1} \leq \lambda$.
In the same way, we can prove $1/\lambda \leq q_{3i+1}^{k+1} \leq \lambda$, $1/\lambda \leq 1/q_{3i+1}^{k+1} \leq \lambda$. So $\lambda \leq Q^{k+1} = \max\{q_i^{k+1}, 1/q_i^{k+1}\} \leq \lambda$.
This completes the proof. \square

Theorem 2 (see [10]). *Given a set of initial control points $\{P_i^0\}_{i \in \mathbb{Z}}$ which are strictly monotonically increasing (strictly monotone decreasing), such that $D_i^0 \geq 0$.*

Let

$$D_i^k = p_{i+1}^k - p_i^k, q_i^k = \frac{D_{i+1}^k}{D_i^k}, Q^k = \max_i \left\{ q_i^k, \frac{1}{q_i^k} \right\}, \quad \forall k \geq 0, k \in \mathbb{Z}, i \in \mathbb{Z}. \quad (19)$$

Furthermore, the parameter λ satisfies $1/\lambda \leq Q^0 \leq \lambda, 1 \leq \lambda \leq 4$, and the limit curves generated by (2) are strictly monotone increasing.

4. Convexity Preservation

Now we discuss the convexity preservation of the nonstationary subdivision scheme. We consider convexity preservation and convex control polygon so the limiting curve generated by our scheme preserves convexity initial data.

Definition 3 (see [23]). *Given a set of control points $P^0 = \{p_i^0 \in R^d\}_{i=1}^n$, let $P^k = \{p_i^k \in R^d\}_{i=1}^{3^k}$, p_i^k is strictly convex at a point x_i^k , if $f[x_{i-1}^k, x_i^k, x_{i+1}^k] > 0$.*

In this section, we check the convexity preservation of the nonstationary subdivision scheme (2) with uniform initial control points.

Given a set of initial control points $\{P_i^0\}_{i \in \mathbb{Z}}, P_i^0 = (x_i^0, p_i^0)$ which are strictly convex, where $\{x_i^0\}_{i \in \mathbb{Z}}$ are equidistant points. For convenience, we make $\Delta x_i^0 = x_{i+1}^0 - x_i^0 = 1$. By the subdivision scheme (2), we have $\Delta x_i^{k+1} = x_{i+1}^{k+1} - x_i^{k+1} = 1/3 \Delta x_i^k = 1/3^{k+1}$. Denote $d_i^k = f[x_{i-1}^k, x_i^k, x_{i+1}^k] = 3^{2k-1} (p_{i-1}^k - 2p_i^k + p_{i+1}^k)$ as the second-order divided differences. In the following, we will prove $d_i^k > 0, \forall k \geq 0, k \in \mathbb{Z}, i \in \mathbb{Z}$.

Proposition 3. *Given that the initial control points $\{P_i^0\}_{i \in \mathbb{Z}}, P_i^0 = (x_i^0, p_i^0)$ are strictly convex, such that $d_i^0 > 0, \forall i \in \mathbb{Z}$, denote $r_i^k = d_{i+1}^k/d_i^k, R^k = \max\{r_i^k, 1/r_i^k\}, \forall k \geq 0, k \in \mathbb{Z}$. Furthermore, the parameter m satisfies*

$1 \leq m \leq 2, m \in \mathbb{R}$, then for $1/m \leq R^0 \leq m, P^k = \{p_i^k \in R^d\}$ recursively at the level k by applying (2), then

$$d_i^k > 0, \frac{1}{m} \leq R^k \leq m, \quad \forall k \geq 0, k \in \mathbb{Z}, i \in \mathbb{Z}. \quad (20)$$

Namely, the limit functions generated by the nonstationary subdivision scheme (2) are strictly convex.

Proof. We use mathematic induction to verify Proposition 3.

When $k = 0, d_i^0 > 0, 1/m \leq R^0 \leq m$, it is clear that (10) is true.

Suppose that (10) holds for k , next, we will verify it also holds for $k + 1$.

$$d_{3i}^{k+1} = 3^{2k+1} (p_{3i}^{k+1} - 2p_{3i+1}^{k+1} + p_{3i+2}^{k+1}) = 3^{2k+1} \left[\left(\frac{1}{18} + \frac{1}{2}u^k \right) d_{i-1}^k + \left(\frac{1}{18} - \frac{1}{2}u^k \right) d_i^k \right]. \quad (21)$$

As $d_{i-1}^k > 0, d_i^k > 0, u^k \in (1/15, 1/9)$, thus $d_{3i}^{k+1} > 0$.

$$d_{3i+1}^{k+1} = 3^{2k+1} \left[\left(\frac{1}{18} - \frac{1}{2}u^k \right) d_{i-1}^k + \left(\frac{1}{18} + \frac{1}{2}u^k \right) d_i^k \right]. \quad (22)$$

As $d_{i-1}^k > 0, d_i^k > 0, u^k \in (1/15, 1/9)$, thus $d_{3i+1}^{k+1} > 0$.

$$d_{3i+2}^{k+1} = 3^{2k+1} \left[\left(-\frac{1}{18} + \frac{1}{6}u^k \right) d_{i-1}^k + \left(\frac{4}{18} - \frac{2}{6}u^k \right) d_i^k + \left(-\frac{1}{18} + \frac{1}{6}u^k \right) d_{i+1}^k \right] = 3^{2k+1} d_i^k \left[\left(-\frac{1}{18} + \frac{1}{6}u^k \right) \frac{1}{r_i^k} + \left(\frac{4}{18} - \frac{2}{6}u^k \right) + \left(-\frac{1}{18} + \frac{1}{6}u^k \right) r_i^k \right] > 3^{2k+1} d_i^k \left[\left(-\frac{1}{18} + \frac{1}{6}u^k \right) m + \left(\frac{4}{18} - \frac{2}{6}u^k \right) + \left(-\frac{1}{18} + \frac{1}{6}u^k \right) m \right] = 3^{2k+1} d_i^k \left[\frac{1}{9} (2-m) + \frac{1}{3} (m-1)u^k \right]. \quad (23)$$

As $1 \leq m \leq 2, u^k \in (1/15, 1/9)$, thus $d_{3i+2}^{k+1} > 0$.

Next we will prove $1/m \leq R^{k+1} \leq m$.

Since

$$r_{3i}^{k+1} = \frac{d_{3i+1}^{k+1}}{d_{3i}^{k+1}} = \frac{(1/18 - 1/2u^k) d_{i-1}^k + (1/18 + 1/2u^k) d_i^k}{(1/18 + 1/2u^k) d_{i-1}^k + (1/18 - 1/2u^k) d_i^k}, \quad (24)$$

$$r_{3i}^{k+1} - m = \frac{(1/18 - 1/2u^k - m/18 + 1/2mu^k) + ((1/18 + 1/2u^k - (m/18 + 1/2mu^k)) r_i^k)}{((1/18 + 1/2u^k) + ((1/18 - 1/2u^k) r_i^k)}. \quad (25)$$

By (21), the denominator of (25) is greater than zero, and the numerator satisfies

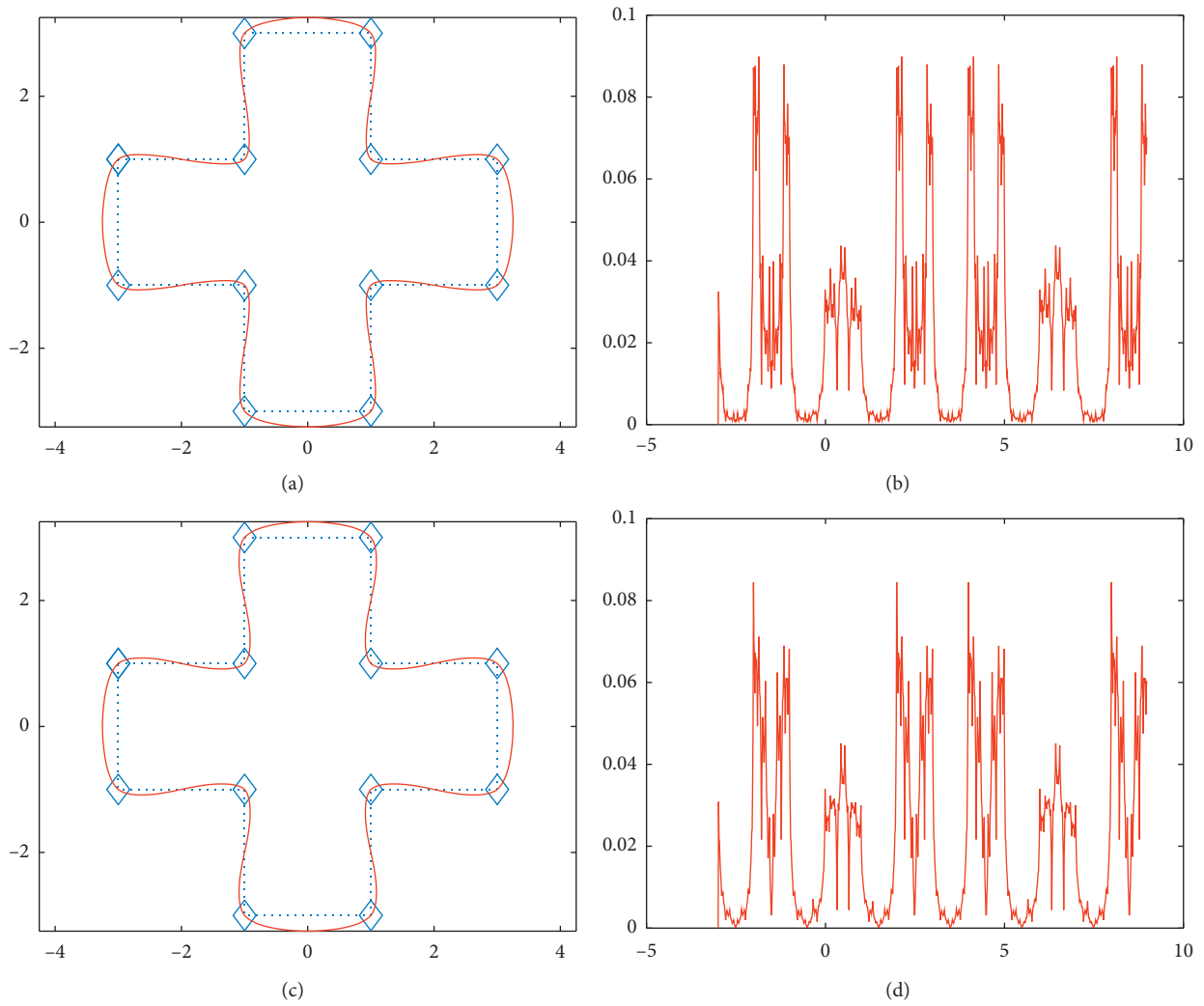


FIGURE 1: Limit curves and their curvature figures. (a) Stationary subdivision. (b) Curvature by (1). (c) Nonstationary subdivision. (d) Curvature by (2).

$$\begin{aligned} \text{numerator} &\leq \left(\frac{1}{18} - \frac{1}{2}u^k - \frac{1}{18}m - \frac{1}{2}u^k m\right) + \left(\frac{1}{18} + \frac{1}{2}u^k - \frac{m}{18} + \frac{1}{2}mu^k\right)m \\ &= -\frac{1}{18}(m^2 - 1)(1 - 9u^k). \end{aligned} \tag{26}$$

As $1 \leq m \leq 2, u^k \in (1/15, 1/9)$, thus numerator ≤ 0 , so $r_{3i}^{k+1} \leq m$.
In the same way, we can prove the $1/r_{3i}^{k+1} \leq m$.

$$\frac{1}{r_{3i}^{k+1}} - m = \frac{(1/18 + 1/2u^k - m/18 + 1/2mu^k) + (1/18 - 1/2u^k - m/18 - 1/2mu^k)r_i^k}{(1/18 - 1/2u^k) + (1/18 + 1/2u^k)r_i^k}. \tag{27}$$

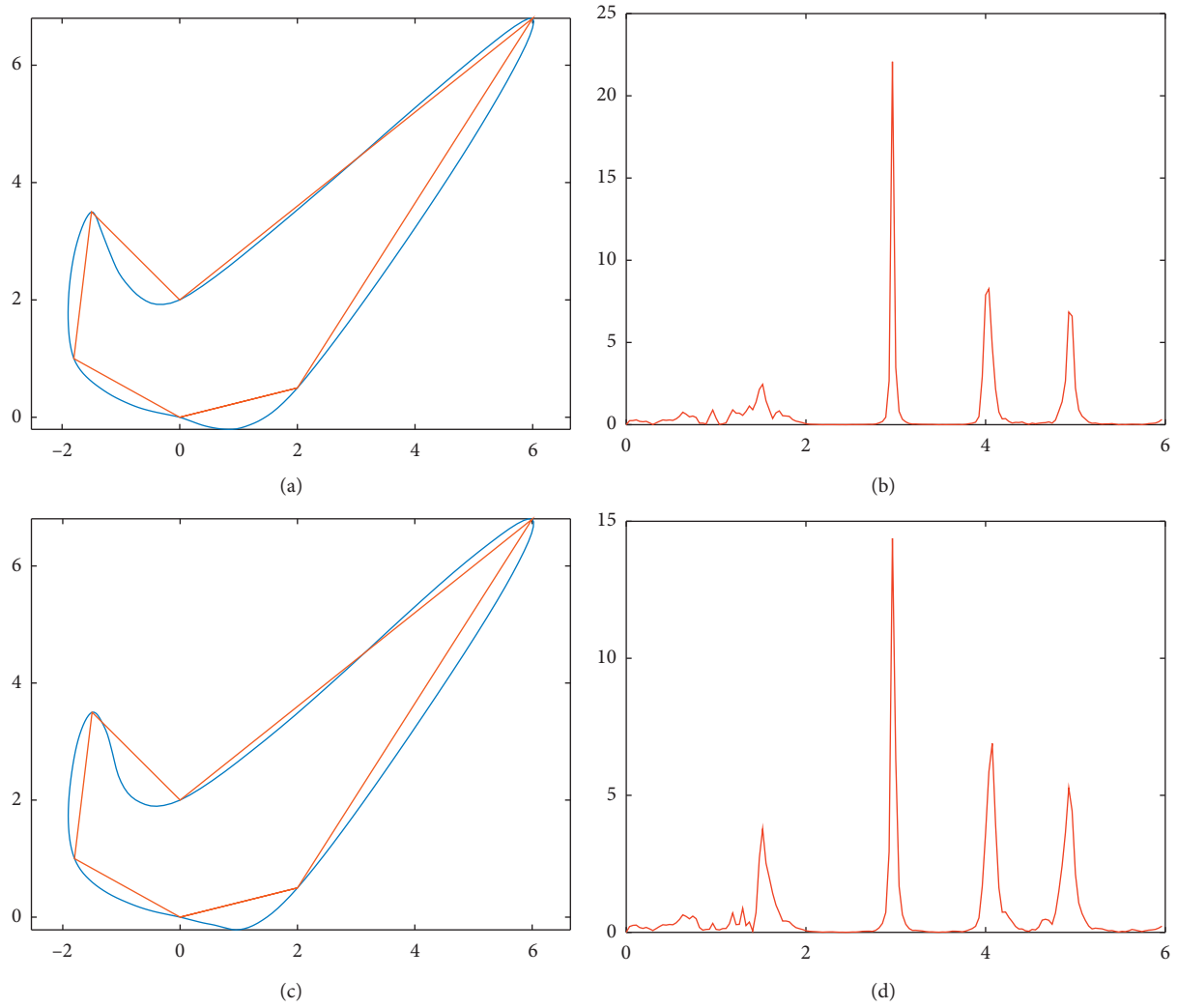


FIGURE 2: Limit curves and their curvature figures. (a) Stationary Nike by (1). (b) Curvature of stationary curvature (1). (c) nonstationary Nike by (2). (d) Curvature of stationary curvature (2).

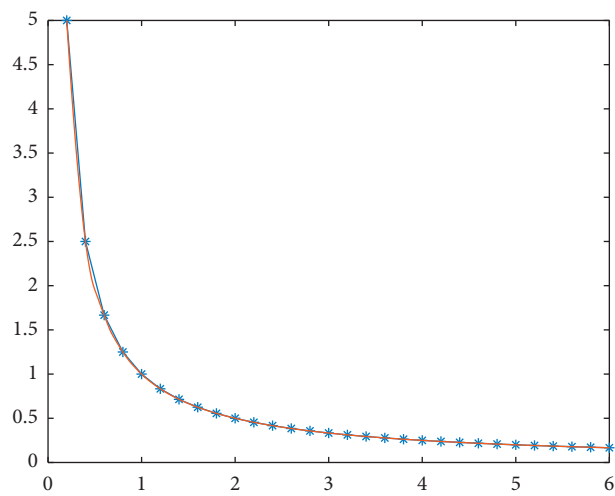


FIGURE 3: Limit curve by our scheme when $\lim_{k \rightarrow \infty} u_k = 1/12$. The initial polygon derives from $f(x) = 1/x$.

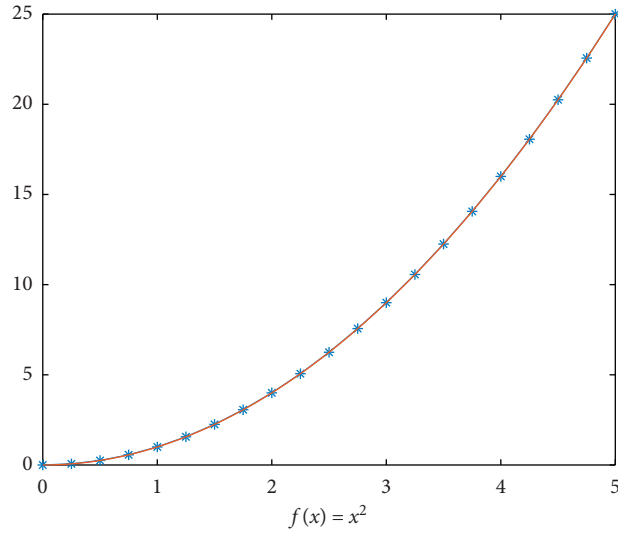


FIGURE 4: Limit curve by our scheme when $\lim_{k \rightarrow \infty} u_k = 1/12$. The initial polygon derives from $f(x) = x^2$.

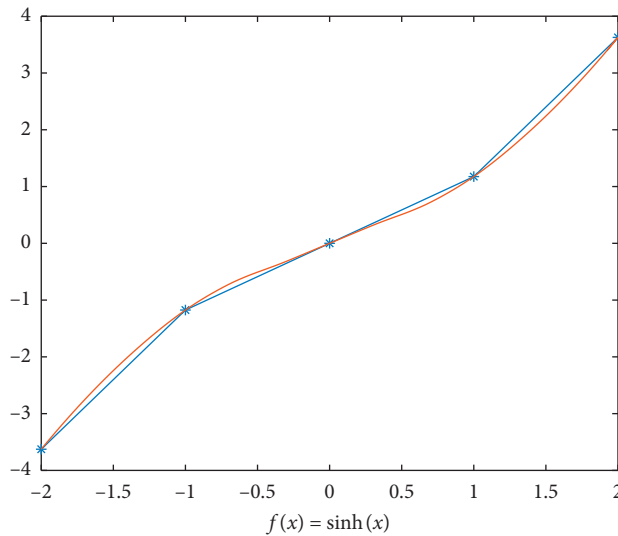


FIGURE 5: Limit curve by our scheme when $\lim_{k \rightarrow \infty} u_k = 1/12$. The initial polygon derives from $f(x) = \sinh(x)$.

By (22), the denominator of (27) is greater than zero:

$$\begin{aligned} \text{numerator} &\leq \left(\frac{1}{18} + \frac{1}{2}u^k - \frac{1}{18}m + \frac{1}{2}u^k m\right) + \left(\frac{1}{18} - \frac{1}{2}u^k - \frac{m}{18} - \frac{1}{2}mu^k\right) \frac{1}{m} \\ &= -\frac{1}{18m}(m^2 - 1)(1 - 9u^k). \end{aligned} \tag{28}$$

As $1 \leq m \leq 2, u^k \in (1/15, 1/9)$, thus $\text{numerator} \leq 0$, so $1/r_{3i}^{k+1} \leq m$. Therefore, $1/m \leq r_{3i}^{k+1} \leq m$.

In the same way, we can prove $1/m \leq r_{3i+1}^{k+1} \leq m, 1/m \leq 1/r_{3i+1}^{k+1} \leq m, 1/m \leq r_{3i+2}^{k+1} \leq m, 1/m \leq 1/r_{3i+2}^{k+1} \leq m$, so $1/m \leq R^{k+1} = \max\{r_i^{k+1}, 1/r_i^{k+1}\} \leq m$. This completes the proof.

From Proposition 3, the limit curves are generated by (2), which are convexity preserving. \square

5. Improved Subdivision Interpolation Scheme at Endpoints

If the initial control polygons are open, the new vertices near two endpoints cannot be calculated using (2), so we use the following subdivision schemes near the left endpoints and right endpoints to solve this problem.

The subdivision rules near the left endpoints are

$$\begin{cases} P_1^{k+1} = P_i^k, \\ P_2^{k+1} = \alpha_0^k P_1^k + \alpha_1^k P_2^k + \alpha_2^k P_3^k, \\ P_3^{k+1} = \beta_0^k P_1^k + \beta_1^k P_2^k + \beta_2^k P_3^k. \end{cases} \tag{29}$$

The subdivision rules near the right endpoints are

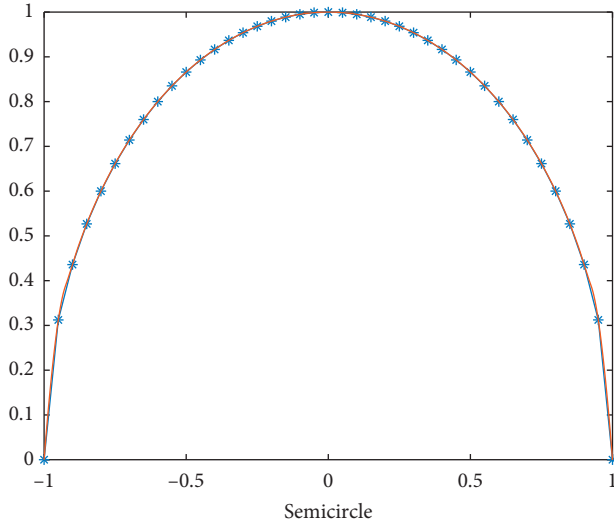


FIGURE 6: Limit curve by our scheme when $\lim_{k \rightarrow \infty} u_k = 1/12$. The initial polygon derives from semicircle.

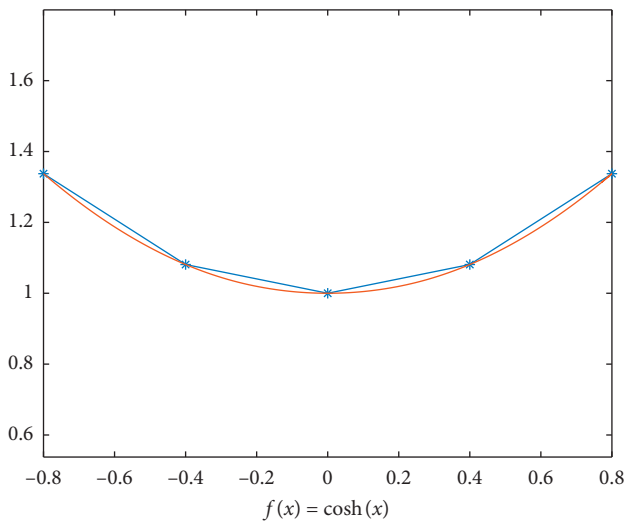


FIGURE 7: Limit curve by our scheme when $\lim_{k \rightarrow \infty} u_k = 1/12$. The initial polygon derives from $f(x) = \cosh(x)$.

$$\begin{cases} P_{3^{k+1}n}^{k+1} = P_{3^kn}^k, \\ P_{3^{k+1}n-1}^{k+1} = \alpha_0^k P_{3^kn}^k + \alpha_1^k P_{3^kn-1}^k + \alpha_2^k P_{3^kn-2}^k, \\ P_{3^{k+1}n-2}^{k+1} = \beta_0^k P_{3^kn}^k + \beta_1^k P_{3^kn-1}^k + \beta_2^k P_{3^kn-2}^k, \end{cases} \quad (30)$$

where

$$\begin{aligned} \alpha_0^k &= 3a_0^k + a_1^k, \alpha_1^k = a_2^k - 3a_0^k, \alpha_2^k = a_0^k + a_3^k, \\ \beta_0^k &= a_1^k + 3a_3^k, \beta_1^k = a_1^k - 3a_3^k, \beta_2^k = a_0^k + a_3^k. \end{aligned} \quad (31)$$

The improved interpolating subdivision scheme provides accurate endpoint interpolation. Wang and Qin in [24] have proved the limit curves by improved interpolating subdivision scheme are C^2 -continuous when the masks are

stationary scheme. However, according to Section 2, we can quickly get that (29) and (30) are C^2 -continuous.

6. Experiment and Conclusions

This paper uses the continued fraction technique to construct a nonstationary 4-point ternary interpolatory subdivision scheme. The smoothness analysis is discussed, which indicates that the limit curve generated by the nonstationary subdivision scheme is continuous. Shape-preserving of the curve is essential. Monotonicity preservation and convexity preservation are two significant elements in shape-preserving. We have been proved that our schemes can ensure monotonicity preservation and convexity preservation when the conditions are imposed on the initial points in Sections 3 and 4. Nonstationary subdivision scheme by (2) and stationary subdivision scheme by (1) generate limit curves that are semblable by eye. So the approach of curvature plots is used to check out the efficiency.

The initial control polygons cannot satisfy monotonicity preservation and convexity preservation in Figures 1 and 2. So the limit curves by our scheme are not shape-preserving. However, from Figure 1, the nonstationary subdivision scheme's curvature is better than the stationary subdivision scheme by (1); unfortunately, they are not obvious. Figure 2 shows that the shape of the curves and curvature of the nonstationary subdivision scheme by (2) are significantly better than those of the stationary subdivision scheme (1). By comparing the shape of the curve and curvature of Figure 1 with Figure 2, we can conclude that when the shapes of the control polygon are relatively flat, the shape and curvature of the nonstationary subdivision scheme by (2) are not significantly better than those of the stationary subdivision scheme by (1). Nevertheless, when the control polygon shapes are relatively steep or have cusps, the shape and curvature of the nonstationary subdivision scheme by (2) are significantly better than those of the stationary subdivision scheme by (1). Furthermore, Figures 3–5 show that if the initial control polygons are monotonicity preserving, our scheme's limit curves are also monotonicity preserving. From Figures 6 and 7, if the initial control polygons are convexity preserving, the limit curves are also convexity preserving by our scheme. So the experiments also show that our nonstationary subdivision scheme is shape-preserving.

Data Availability

All data used in this article are available from the corresponding author upon request.

Conflicts of Interest

The authors declare that they have no conflicts of interest.

Acknowledgments

This work was supported by the National Natural Science Foundation of China (NSFC) under the project nos. 61472466 and 61972131.

References

- [1] S. Dubuc, "Interpolation through an iterative scheme," *Journal of Mathematical Analysis and Applications*, vol. 114, no. 1, pp. 185–204, 1986.
- [2] N. Dyn, D. Levin, and J. A. Gregory, "A 4-point interpolatory subdivision scheme for curve design," *Computer Aided Geometric Design*, vol. 4, no. 4, pp. 257–268, 1987.
- [3] M. F. Hassan, I. P. Ivriissimitzis, N. A. Dodgson, and M. A. Sabin, "An interpolating 4-point C2 ternary stationary subdivision scheme," *Computer Aided Geometric Design*, vol. 19, no. 1, pp. 1–18, 2002.
- [4] C. Beccari, G. Casciola, and L. Romani, "An interpolating 4-point ternary non-stationary subdivision scheme with tension control," *Computer Aided Geometric Design*, vol. 24, no. 4, pp. 210–219, 2007.
- [5] C. Beccari, G. Casciola, and L. Romani, "A non-stationary uniform tension controlled interpolating 4-point scheme reproducing conics," *Computer Aided Geometric Design*, vol. 24, no. 1, pp. 1–9, 2007.
- [6] N. Dyn, F. Kuijt, D. Levin, and R. van Damme, "Convexity preservation of the four-point interpolatory subdivision scheme," *Computer Aided Geometric Design*, vol. 16, pp. 789–792, 1987.
- [7] Z. J. Cai, "Convergence, error estimation and some properties of four-point interpolation subdivision scheme," *Computer Aided Geometric Design*, vol. 12, pp. 459–468, 1995.
- [8] Z. Cai, "Convexity preservation of the interpolating four-point ternary stationary subdivision scheme," *Computer Aided Geometric Design*, vol. 26, no. 5, pp. 560–565, 2009.
- [9] F. Kuijt and R. van Damme, "Monotonicity preserving interpolatory subdivision schemes," *Journal of Computational and Applied Mathematics*, vol. 101, no. 1-2, pp. 203–229, 1999.
- [10] F. Kuijt and R. van Damme, "Shape preserving interpolatory subdivision schemes for nonuniform data," *Journal of Approximation Theory*, vol. 114, no. 1, pp. 1–32, 2002.
- [11] J. Tan, X. Zhuang, and L. Zhang, "A new four-point shape-preserving subdivision scheme," *Computer Aided Geometric Design*, vol. 31, no. 1, pp. 57–62, 2014.
- [12] J. Tan, Y. Yao, H. Cao, and L. Zhang, "Convexity preservation of five-point binary subdivision scheme with a parameter," *Applied Mathematics and Computation*, vol. 245, pp. 279–288, 2014.
- [13] M. A. Sabin and N. A. Dodgson, "A circle-preserving variant of the four-point subdivision scheme," in *Mathematics Methods for Curves and Surfaces, Modern Methods in Mathematics*, M. Daehlen, K. Morken, and L. L. Schumaker, Eds., pp. 275–286, Nashboro Press, Brentwood, TN, USA, 2004.
- [14] C. Deng and G. Wang, "Incenter subdivision scheme for curve interpolation," *Computer Aided Geometric Design*, vol. 27, no. 1, pp. 48–59, 2010.
- [15] C. Constanza and H. Kai, "Polynomial reproduction for univariate subdivision scheme of any arity," *Journal of Approximation Theory*, vol. 163, pp. 413–437, 2011.
- [16] J. Q. Tan, *Continued Fraction Theory and Its Application*, pp. 35–36, Science Press, Beijing, China, 2007.
- [17] A. Ghaffar, M. Bari, Z. Ullha, M. Iqbal, K. S. Nisar, and D. Baleanu, "A new class of 2q-point non-stationary subdivision schemes and applications," *Mathematics*, vol. 7, p. 639, 2017.
- [18] P. Ashraf, B. Nawaz, D. Baleanu et al., "Analysis of geometric properties of ternary four-point rational interpolating subdivision scheme," *Mathematics*, vol. 8, no. 3, p. 338, 2020.
- [19] P. Ashraf, A. Ghaffar, D. Baleanu, I. Sehar, K. S. Nisar, and F. Khan, "Shape-preserving properties of a relaxed four-point interpolating subdivision scheme," *Mathematics*, vol. 8, no. 5, p. 806, 2020.
- [20] L. Zou, L. Song, X. Wang, Y. Chen, C. Zhang, and C. Tang, "Bivariate thiele-like rational interpolation continued fractions with parameters based on virtual points," *Mathematics*, vol. 8, no. 1, p. 71, 2020.
- [21] R. Hameed, G. Mustafa, A. Liaqat et al., "A new approach to increase the flexibility of curves and regular surfaces produced by 4-point ternary subdivision scheme," *Mathematics Problems in Engineering*, vol. 2020, Article ID 6096545, 17 pages, 2020.
- [22] J. Tan, J. Sun, and G. Tong, "A non-stationary binary three-point approximating subdivision scheme," *Applied Mathematics and Computation*, vol. 276, pp. 37–43, 2016.
- [23] N. Dyn and D. Levin, "Analysis of asymptotically equivalent binary subdivision schemes," *Journal of Mathematical Analysis and Applications*, vol. 193, no. 2, pp. 594–621, 1995.
- [24] H. Wang and K. Qin, "Improved ternary subdivision interpolation scheme," *Tsinghua Science and Technology*, vol. 10, no. 1, pp. 128–132, 2005.

Research Article

Inverse Numerical Iterative Technique for Finding all Roots of Nonlinear Equations with Engineering Applications

Mudassir Shams ¹, Naila Rafiq ², Babar Ahmad,³ and Nazir Ahmad Mir¹

¹Department of Mathematics and Statistics, Riphah International University I-14, Islamabad 44000, Pakistan

²Department of Mathematics, NUML, Islamabad, Pakistan

³Department of Mathematics, Comsats University Islamabad, Islamabad 44000, Pakistan

Correspondence should be addressed to Mudassir Shams; shams6262@gmail.com and Naila Rafiq; nrafique@numl.edu.pk

Received 24 October 2020; Revised 24 November 2020; Accepted 2 December 2020; Published 4 January 2021

Academic Editor: Ghulam Mustafa

Copyright © 2021 Mudassir Shams et al. This is an open access article distributed under the Creative Commons Attribution License, which permits unrestricted use, distribution, and reproduction in any medium, provided the original work is properly cited.

We introduce here a new two-step derivative-free inverse simultaneous iterative method for estimating all roots of nonlinear equation. It is proved that convergence order of the newly constructed method is four. Lower bound of the convergence order is determined using Mathematica and verified with theoretical local convergence order of the method introduced. Some nonlinear models which are taken from physical and engineering sciences as numerical test examples to demonstrate the performance and efficiency of the newly constructed modified inverse simultaneous methods as compared to classical methods existing in literature are presented. Dynamical planes and residual graphs are drawn using MATLAB to elaborate efficiency, robustness, and authentication in its domain.

1. Introduction

A wide range of problems in physical and engineering sciences can be formulated as a nonlinear equation:

$$f(r) = 0. \quad (1)$$

The most ancient and popular iterative technique for approximating single roots of (1) is Newton's method [1] which has local quadratic convergence:

$$s^{(k)} = r^{(k)} - \frac{f(r^{(k)})}{f'(r^{(k)})}, \quad (k = 0, 1, \dots). \quad (2)$$

Nedzibove et al., in [2], presented the inverse method of the same order corresponding to method (2):

$$s^{(k)} = \frac{(r^{(k)})^2 f'(r^{(k)})}{r^{(k)} f'(r^{(k)}) + f(r^{(k)})}. \quad (3)$$

In the last few years, lot of work has been carried out on numerical iterative methods which approximate single root at a time of (1). There is another class of derivative-free iterative methods which approximates all roots of (1) simultaneously. The simultaneous iterative methods for approximating all roots of (1) are very popular due to their global convergence and parallel implementation on computer (see, e.g., Weierstrass [3], Kanno [4], Proinov [5], Petkovi'c [6], Mir [7], Nourein [8], Aberth [9], and reference cited there in [10–22]).

Among derivative-free simultaneous methods, Weierstrass–Dochive [23] method (abbreviated as WDK) is the most attractive method given by

$$s_i^{(k)} = r_i^{(k)} - w(r_i^{(k)}), \quad (4)$$

where

$$w(r_i^{(k)}) = \frac{f(r_i^{(k)})}{\prod_{\substack{j=1 \\ j \neq i}}^n (r_i^{(k)} - r_j^{(k)}), \quad (i, j = 1, 2, 3, \dots, n), \quad (5)$$

is Weierstrass' Correction. Method (4) has local quadratic convergence.

Nedzibove [2] introduced a new modification to (4), that is, an inverse method to WDK abbreviated as IWDK, i.e.,

$$u_i^{(k)} = \frac{(r_i^{(k)})^2 \prod_{\substack{j=1 \\ j \neq i}}^n (r_i^{(k)} - r_j^{(k)})}{r_i^{(k)} \prod_{\substack{j=1 \\ j \neq i}}^n (r_i^{(k)} - r_j^{(k)}) + f(r_i^{(k)})}. \quad (6)$$

The main aim of this paper is to construct a two-step inverse method of convergence order four.

2. Construction of Family of Simultaneous Method for Distinct Roots

We modify the Weierstrass method (4) as follows:

$$z_i^{(k)} = u_i^{(k)} - \frac{f(u_i^{(k)})}{\prod_{\substack{j=1 \\ j \neq i}}^n (u_i^{(k)} - u_j^{(k)}), \quad (7)$$

where $u_i^{(k)} = r_i^{(k)} - (f(r_i^{(k)}) / (\prod_{j=1}^n (r_i^{(k)} - r_j^{(k)})))$ and denote it by WDK2. Let us now convert method (7) into inverse iterative method as follows:

$$z_i^{(k)} = \frac{(u_i^{(k)})^2 \prod_{\substack{j=1 \\ j \neq i}}^n (u_i^{(k)} - u_j^{(k)})}{u_i^{(k)} \prod_{\substack{j=1 \\ j \neq i}}^n (u_i^{(k)} - u_j^{(k)}) + f(u_i^{(k)})}, \quad (8)$$

where
$$u_i^{(k)} = \left(\left((r_i^{(k)})^2 \prod_{\substack{j=1 \\ j \neq i}}^n (r_i^{(k)} - r_j^{(k)}) \right) / \left(r_i^{(k)} \prod_{\substack{j=1 \\ j \neq i}}^n (r_i^{(k)} - r_j^{(k)}) + f(r_i^{(k)}) \right) \right).$$

Thus, method (8) is a two-step inverse method abbreviated as IWM2.

2.1. Convergence Analysis. We prove here that convergence order of the IWM2 method is four.

Let $D \in C^n$ be an open convex subset, $\Gamma: D \rightarrow C^n$ and m times differentiable operator $(\Gamma_1(r), \dots, \Gamma_n(r))^T$ be continuous, and the sequence $(r^{(k)})_{k \in N}$ be defined by $r^{(k+1)} = \Gamma(r^{(k)})$:

$$r^{(k)} = (r_1^{(k)}, \dots, r_n^{(k)}) \iff r_i^{(k+1)} = \Gamma_i(r^{(k)}), \quad \forall i \in \{1, \dots, n\}, k \in N, \quad (9)$$

where norm in C^n is defined as $\|r\| = \max\{|r_1|, \dots, |r_n|\}$.

Theorem 1. *Let X and Y be normed spaces. Take an open convex subset D of X for a u times Fréchet differential operator Γ , i.e., $\Gamma: D \rightarrow Y$. Then, for any $x, y \in D$*

$$\begin{aligned} & \left\| \Gamma(y) - \Gamma(x) - \sum_{j=1}^{q-1} \frac{1}{j!} \Gamma^{(j)}(x) \left((y-x) \dots (y-x) \right)_{j\text{-times}} \right\| \\ & \leq \frac{\|y-x\|^q}{q!} \sup_{\zeta \in (x,y)} \|\Gamma^{(q)}(\zeta)\|. \end{aligned} \quad (10)$$

Using Theorem 1, we have the following.

Theorem 2. *Let $\beta \in D$ if*

- (i) $\Gamma(\beta) = \beta$
- (ii) $\Gamma(\beta) = \Gamma'(\beta) = \Gamma''(\beta) = \dots = \Gamma^{(u)}(\beta) = 0$

Then, there exists $s > 0$ such that, for any $r^{(0)} \in D, \|r^{(0)} - \beta\| < s$, the sequence $r^{(k+1)} = \Gamma(r^{(k)})_{k \in N}$ converges to β .

Proof. Let $s_0 > 0$ be such that

$$v_0 = \{r \in C: \|r - \beta\| \leq s_0\} \subset D. \quad (11)$$

$C_0 = \max\|\Gamma^{(u)}(r_0)\|_{z \in v_0}$, and there exists $0 < s \leq s_0$ such that

$$\frac{C_0 s^q}{q!} < s \iff \left(\frac{C_0}{q!}\right)^{(1/q-1)} < s, \quad (12)$$

where $v = \{r \in C^n: \|r - \beta\| \leq s\}$. Using hypothesis (2), $r \in v$; then, (ii) and Theorem 1 implies

$$\begin{aligned} \|\Gamma(r) - \beta\| &= \left\| \Gamma(r) - \Gamma(\beta) - \sum_{j=1}^{q-1} \frac{1}{j!} \Gamma^{(j)}(\beta) \left((r-\beta) \dots (r-\beta) \right)_{j\text{-times}} \right\| \\ &\leq \frac{1}{q!} \|r - \beta\|^q \sup_{\zeta \in (\beta,r)} \|\Gamma^{(q)}(\zeta)\|^q \leq \frac{C_0 s^q}{q!} < s. \end{aligned} \quad (13)$$

Thus, $\Gamma(r) \in v$. Using the above relation for $r = r^{(k)}$, we have

$$\|r^{(k+1)} - \beta\| = \|\Gamma(r^{(k)}) - \beta\| \leq \frac{C_0}{u!} \|r^{(k)} - \beta\|^q. \quad (14)$$

Using (14), recursively, we have

$$\begin{aligned} \|r^{(k)} - \beta\| &\leq \frac{C_0}{u!} \|r^{(k)} - \beta\|^q \leq \frac{C_0}{u!} \left(\frac{C_0}{u!} \|r^{(k)} - \beta\|^q\right)^q \\ &\leq \dots \leq \left(\frac{C_0}{q!}\right)^{1+q+\dots+q^k} \|r^{(0)} - \beta\|^{q^k} \\ &\leq \left(\left(\frac{C_0}{q!}\right)^{(1/q-1)} s\right)^{q^k} \rightarrow 0 \text{ for } k \rightarrow \infty. \end{aligned} \quad (15)$$

Thus, from inequality (14), $(r)_{k \in \mathbb{N}}^{(k)}$ is at least q . Now, consider IWM2 as a vector function, i.e., $\Gamma(r) = (\Gamma_1(r), \dots, \Gamma_n(r))$, where

$$\Gamma_i(z_i) = \frac{(u_i)^2}{u_i + \left(f(u_i) / \prod_{j \neq i}^n (u_i - u_j) \right)}, \quad \text{where} \tag{16}$$

$$u_i = \frac{(r_i)^2}{r_i + \left(f(r_i) / \prod_{j \neq i}^n (r_i - r_j) \right)}.$$

For a fixed point $\beta = (\beta_1, \dots, \beta_n)$, it is not difficult to prove $(\partial \Gamma_i(\zeta) / \partial r_i) = (\partial^2 \Gamma_i(\zeta) / \partial r_i \partial r_j) = (\partial^3 \Gamma_i(\zeta) / \partial^2 r_i \partial r_j) = 0$ and higher order partial derivative is not equal to zero. Thus, IWM2 has at least fourth-order convergence. \square

Theorem 3. Let ζ_1, \dots, ζ_n be simple roots of (1) and for sufficiently close initial distinct estimations $r_1^{(0)}, \dots, r_n^{(0)}$ of the roots, respectively; IWM2 has then convergence order 4.

Proof. Consider $\varepsilon_i = r_i^{(k)} - \zeta_i$, $\varepsilon'_i = u_i^{(k)} - \zeta_i$, and $\varepsilon''_i = z_i^{(k)} - \zeta_i$ be the errors in $r_i^{(k)}$, $u_i^{(k)}$, and $z_i^{(k)}$, respectively. For simplicity, we omit iteration index k . From first step of IWM2, we have

$$u_i - \zeta_i = r_i - \zeta_i - \frac{\left(r_i f(r_i) / \prod_{j \neq i}^n (r_i - r_j) \right)}{r_i + \left(f(r_i) / \prod_{j \neq i}^n (r_i - r_j) \right)}. \tag{17}$$

Thus, we obtain

$$\begin{aligned} \varepsilon'_i &= \varepsilon_i \left[1 - \left(\frac{\prod_{j \neq i}^n ((r_i - \zeta_j) / (r_i - r_j))}{1 + \left(f(r_i) / \prod_{j \neq i}^n (r_i - r_j) \right)} \right) \right] \\ &= \varepsilon_i \left[\frac{1 - \left(\prod_{j \neq i}^n ((r_i - \zeta_j) / (r_i - r_j)) \right) + \left(f(r_i) / \prod_{j \neq i}^n (r_i - r_j) \right)}{1 + \left(f(r_i) / \prod_{j \neq i}^n (r_i - r_j) \right)} \right]. \end{aligned} \tag{18}$$

Using the expression $\left(\prod_{j \neq i}^n ((r_i - \zeta_j) / (r_i - r_j)) \right) - 1 = \sum_{k \neq i}^n (\varepsilon_k / r_i - r_k) \prod_{j \neq i}^{k-1} ((r_i - \zeta_k) / (r_i - r_j))$ [2] in (18), we have

$$\varepsilon'_i = \varepsilon_i \left[\frac{\left((\varepsilon_i / r_i) \prod_{j \neq i}^n ((r_i - \zeta_j) / (r_i - r_j)) \right) - \sum_{k \neq i}^n (\varepsilon_k / r_i - r_k) \prod_{j \neq i}^{k-1} ((r_i - \zeta_k) / (r_i - r_j))}{1 + (\varepsilon_k / r_i) \prod_{j \neq i}^n ((r_i - \zeta_j) / (r_i - r_j))} \right]. \tag{19}$$

If we assume all errors are of the same order, i.e., $|\varepsilon_i| = |\varepsilon_k| = O(|\varepsilon|)$; then, we have

$$\varepsilon'_i = |\varepsilon|^2 \left[\frac{\left((1/r_i) \prod_{j \neq i}^n ((r_i - \zeta_j) / (r_i - r_j)) \right) - \sum_{k \neq i}^n (1/r_i - r_k) \prod_{j \neq i}^{k-1} ((r_i - \zeta_k) / (r_i - r_j))}{1 + (\varepsilon_k / r_i) \prod_{j \neq i}^n ((r_i - \zeta_j) / (r_i - r_j))} \right] = O(|\varepsilon|^2). \tag{20}$$

From second-step of IWM2, we have

$$z_i - \zeta_i = u_i - \zeta_i - \frac{\left(u_i f(u_i) / \prod_{j \neq i}^n (u_i - u_j) \right)}{r_i + \left(f(u_i) / \prod_{j \neq i}^n (u_i - u_j) \right)} \tag{21}$$

Thus, we obtain

$$\varepsilon_i'' = \varepsilon_i' \left[1 - \frac{\prod_{j \neq i}^n ((u_i - \zeta_j) / (u_i - u_j))}{1 + \left(f(u_i) / \prod_{j \neq i}^n (u_i - u_j) \right)} \right] = \varepsilon_i' \left[\frac{1 - \left(\prod_{j \neq i}^n ((u_i - \zeta_j) / (u_i - u_j)) \right) + \left(f(u_i) / \prod_{j \neq i}^n (u_i - u_j) \right)}{1 + \left(f(u_i) / \prod_{j \neq i}^n (u_i - u_j) \right)} \right] \tag{22}$$

As from the above argument $\left(\prod_{j \neq i}^n ((u_i - \zeta_j) / (u_i - u_j)) \right) - 1 = \sum_{k \neq i}^n ((\varepsilon_k' / u_i - u_k) \prod_{j \neq i}^{k-1} ((u_i - \zeta_k) / (u_i - u_j)))$ using in (22), we have

$$\varepsilon_i'' = \varepsilon_i' \left[\frac{\left((\varepsilon_i' / u_i) \left(\prod_{j \neq i}^n ((u_i - \zeta_j) / (u_i - u_j)) \right) \right) - \sum_{k \neq i}^n ((\varepsilon_k' / u_i - u_k) \prod_{j \neq i}^{k-1} ((u_i - \zeta_k) / (u_i - u_j)))}{1 + (\varepsilon_k' / u_i) \left(\prod_{j \neq i}^n ((u_i - \zeta_j) / (u_i - u_j)) \right)} \right] \tag{23}$$

If we assume all errors are of the same order, i.e., $|\varepsilon_i'| = |\varepsilon_k'| = O(|\varepsilon'|)$; then,

$$\begin{aligned} \varepsilon_i'' &= |\varepsilon'|^2 \left[\frac{\left((1/u_i) \prod_{j \neq i}^n ((u_i - \zeta_j) / (u_i - u_j)) \right) - \sum_{k \neq i}^n (1/u_i - s_k) \prod_{j \neq i}^{k-1} ((u_i - \zeta_k) / (u_i - u_j))}{1 + (\varepsilon_k' / u_i) \prod_{j \neq i}^n ((u_i - \zeta_j) / (u_i - u_j))} \right] = O(|\varepsilon'|^2) \\ &= O\left((|\varepsilon'|^2)^2 \right) = O(|\varepsilon'|^4). \end{aligned} \tag{24}$$

Hence, the theorem is proved. \square

2.1.1. Using CAS for Verification of Convergence Order. Consider

$$f(r) = (r - \theta)(r - \phi)(r - \varphi), \tag{25}$$

and the first component of $\Gamma_1(\mathbf{r})$ iterative schemes to find zeros of (25), $r^{(k+1)} = \Gamma(r^{(k)})$, simultaneously. In order to verify Theorem 2 conditions, we have to express the differential of an operator $\Gamma(r)$ in terms of their partial derivate of its component as $\Gamma_i(r)$:

$$\begin{aligned}
 & \frac{\partial \Gamma_1(\mathbf{r})}{\partial r_1} \quad \frac{\partial \Gamma_1(\mathbf{r})}{\partial r_2} \quad \frac{\partial \Gamma_1(\mathbf{r})}{\partial r_3}, \\
 & \frac{\partial^2 \Gamma_1(\mathbf{r})}{\partial r_1^2} \quad \frac{\partial^2 \Gamma_1(\mathbf{r})}{\partial r_1 \partial r_2} \quad \frac{\partial^2 \Gamma_1(\mathbf{r})}{\partial r_2^2} \quad \frac{\partial^2 \Gamma_1(\mathbf{r})}{\partial r_2 \partial r_3}, \\
 & \frac{\partial^3 \Gamma_1(\mathbf{r})}{\partial r_1^3} \quad \frac{\partial^3 \Gamma_1(\mathbf{r})}{\partial r_1^2 \partial r_2} \quad \frac{\partial^3 \Gamma_1(\mathbf{r})}{\partial r_1 \partial r_2^2} \quad \frac{\partial^3 \Gamma_1(\mathbf{r})}{\partial r_2^3} \quad \frac{\partial^3 \Gamma_1(\mathbf{r})}{\partial r_2^2 \partial r_3}, \\
 & \vdots \quad \vdots \quad \vdots \quad \vdots \quad \vdots \quad \dots,
 \end{aligned}
 \tag{26}$$

and so on.

The lower bound of the convergence obtained until the first nonzero element of the row is found. The Mathematica code is given for each of the consider methods as follows.

Weierstrass–Dochive Method (WDK):

$$\Gamma_1(r_1, r_2, r_3) := \mathbf{r} - \frac{f(\mathbf{r})}{\prod_{\substack{j=1 \\ j \neq i}}^n (r_i - r_j)}, \quad (i, j = 1, \dots, n),$$

In [1] := D[Γ₁[r₁, r₂, r₃], r₁]/.{r₁ → θ, r₂ → φ, r₃ → ϕ},

Out [1] := 0,

In [2] := D[Γ₁[r₁, r₂, r₃], r₂]/.{r₁ → θ, r₂ → φ, r₃ → ϕ},

Out [2] := 0, (27)

In [2] := D[Γ₁[r₁, r₂, r₃], r₂]/.{r₁ → θ, r₂ → φ, r₃ → ϕ},

Out [2] := 0,

In [3] := Simplify [D[Γ₁[r₁, r₂, r₃], r₁, r₂]/.{r₁ → θ, r₂ → φ, r₃ → ϕ}],

Out [3] := $\frac{1}{-\theta + \phi}$.

Modified Inverse Weierstrass Method:

$$\Gamma_1(r_1, r_2, r_3) := \frac{(\mathbf{r})^2 \prod_{\substack{j=1 \\ j \neq i}}^n (r_i - r_j)}{\mathbf{r} \prod_{\substack{j=1 \\ j \neq i}}^n (r_i - r_j) + f(\mathbf{r})},$$

In [1]: = $\frac{D[\Gamma_1[r_1, r_2, r_3], r_2]}{\{r_1 \rightarrow \theta, r_2 \rightarrow \phi, r_3 \rightarrow \varphi\}}$,

Out [1]: = 0,

In [2]: = $\frac{D[\Gamma_1[r_1, r_2, r_3], r_3]}{\{r_1 \rightarrow \theta, r_2 \rightarrow \phi, r_3 \rightarrow \varphi\}}$, (28)

Out [2]: = 0,

In [3]: = Simplify $\frac{[D[\Gamma_1[r_1, r_2, r_3], r_1, r_1]]}{\{r_1 \rightarrow \theta, r_2 \rightarrow \phi, r_3 \rightarrow \varphi\}}$,

Out [3]: = $\frac{2\theta(\theta - \phi)(\theta - \varphi)}{\theta\phi\varphi}$.

WDK2 Method:

$$\Gamma_1(r_1, r_2, r_3) := \mathbf{u} - \frac{f(\mathbf{u})}{\prod_{\substack{j=1 \\ j \neq i}}^n (u_i - u_j)}, \tag{29}$$

where $\mathbf{u} = \mathbf{r} - (f(\mathbf{r})) / \prod_{\substack{j=1 \\ j \neq i}}^n (r_i - r_j)$,

In [1] := D[Γ₁[r₁, r₂, r₃], r₁]/.{r₁ → θ, r₂ → φ, r₃ → ϕ},

Out [1] := 0,

∴ ,

In [13] := Simplify $\left[\frac{D[\Gamma_1[r_1, r_2, r_3], r_1, r_3, r_1, r_2]}{\{r_1 \rightarrow \theta, r_2 \rightarrow \phi, r_3 \rightarrow \varphi\}} \right]$,

Out [13] := $-\frac{12}{\theta^2}$. (30)

IWM2 Method:

$$\Gamma_1(r_1, r_2, r_3) := \frac{(\mathbf{u})^2 \prod_{j=1}^n (u_i - u_j)}{\mathbf{u} \prod_{j=1}^n (u_i - u_j) + f(\mathbf{u})}, \quad (31)$$

where $\mathbf{u} = (\mathbf{r}) \prod_{j=1}^n (r_i - r_j) / \mathbf{r} \prod_{j=1}^n (r_i - r_j) + f(\mathbf{r})$,

$$\text{In [1]} := \frac{D[\Gamma_1[r_1, r_2, r_3], r_1]}{\{r_1 \rightarrow \theta, r_2 \rightarrow \phi, r_3 \rightarrow \varphi\}},$$

$$\text{Out [1]} := 0,$$

∴,

$$\text{In [14]} := \text{Simplify} \left[\frac{D[\Gamma_1[r_1, r_2, r_3], r_1, r_1, r_1, r_1]}{\{r_1 \rightarrow \theta, r_2 \rightarrow \phi, r_3 \rightarrow \varphi\}} \right],$$

$$\text{Out [14]} := \frac{24}{\theta^3}. \quad (32)$$

(1) *Basins of Attraction.* To provoke the basins of attraction of iterative schemes WDK, IWDK, WDK2, and IWM2 for the root of nonlinear equation, we execute the real and imaginary parts of the starting approximation as two axes over a mesh of 250×250 in complex plane. Using $|r^{(k+1)} - r^{(k)}| < 10^{-3}$ as a stopping criteria and maximum number of iterations as 25. We allow different colors to mark to which root the iterative scheme converges and black in other case. Color brightness in basins shows less number of iterations. For the generation of basins, we consider the following four nonlinear functions, i.e., $f_1(r) = \log r + e^r + 1$ and $f_2(r) = \sin((r-1)/2)\cos((r-3)/2) + 1$.

The elapsed time from Table 1 and brightness in color in Figure 1(d)–2(d) shows the dominance behavior of IWM2 over WDK, IWDK, and WDK2, respectively.

The elapsed time from Table 1 and brightness in color in Figure 2(d) show the dominance behavior of IWM2 over WDK, IWDK, and WDK2, respectively.

3. Numerical Results

Some nonlinear models from engineering and physical sciences are considered to illustrate the performance and efficiency of WDK2 and IWM2 using CAS Maple 18 with 64 digits floating point arithmetic for all computer calculations. We approximate the roots of (1) rather than the exact roots which depend on computer precision ϵ , and the following stopping criteria are used to terminate the computer program:

$$e_i = \left\| r_i^{(k+1)} - r_i^{(k)} \right\|_2 < \epsilon, \quad (33)$$

TABLE 1: Elapsed time in seconds.

Method	WDK	IWDK	WDK2	IWM2
$f_1(r)$	0.12937	0.142207	0.323190	0.107267
$f_2(r)$	0.160921	0.23889	0.431936	0.153851

where e_i represents the absolute error. We take $\epsilon = 10^{-30}$. In Tables 2–5, CO represents convergence order of iterative schemes WDK2 and IWM2, respectively.

3.1. Applications in Engineering. In this section, we discuss some applications in engineering.

Example 1 (see [24]). Fractional Conversion.

As expression described in [25, 26],

$$f_3(r) = r^4 - 7.79075r^3 + 14.7445r^2 + 2.511r - 1.674, \quad (34)$$

is the fractional conversion of nitrogen, hydrogen feed at 250 atm. and 227 k.

The exact roots of (34) are

$$\begin{aligned} \zeta_1 &= 3.9485 + 0.3161i, \\ \zeta_2 &= 3.9485 - 0.3161i, \\ \zeta_3 &= -0.3841, \\ \zeta_4 &= 0.2778. \end{aligned} \quad (35)$$

The initial calculated values of (34) have been taken as follows:

$$\begin{aligned} r_1^0(0) &= 3.5 + 0.3i, \\ r_2^0(0) &= 3.5 - 0.3i, \\ r_3^0(0) &= -0.3 + 0.01i, \\ r_4^0(0) &= 1.8 + 0.01i. \end{aligned} \quad (36)$$

Table 2 clearly shows the dominance behavior of IWM2 over WDK2 iterative method in terms of CPU time in seconds and absolute error on same number of iterations k for nonlinear function. $f_3(r)$.

Example 2 (see [6]). Van der Waal's Fluid Model.

A Van der Waals fluid is the one which satisfies the equation of state:

$$P = \frac{R\theta}{v-b} - \frac{a}{v^2}, \quad (37)$$

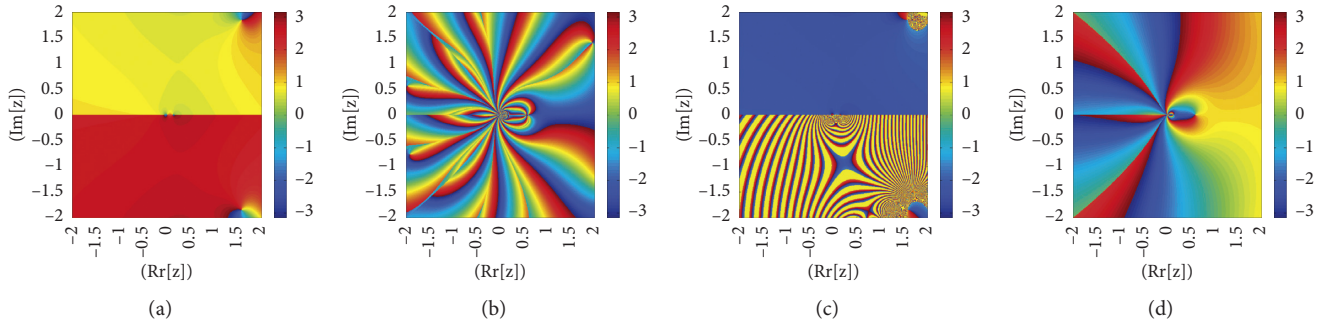


FIGURE 1: (a), (b), (c), and (d) show basins of attraction for nonlinear function $f_1(r) = r^3 + r - 40$ of the iterative methods WDK, IWDK, WDK2, and IWM2 respectively.

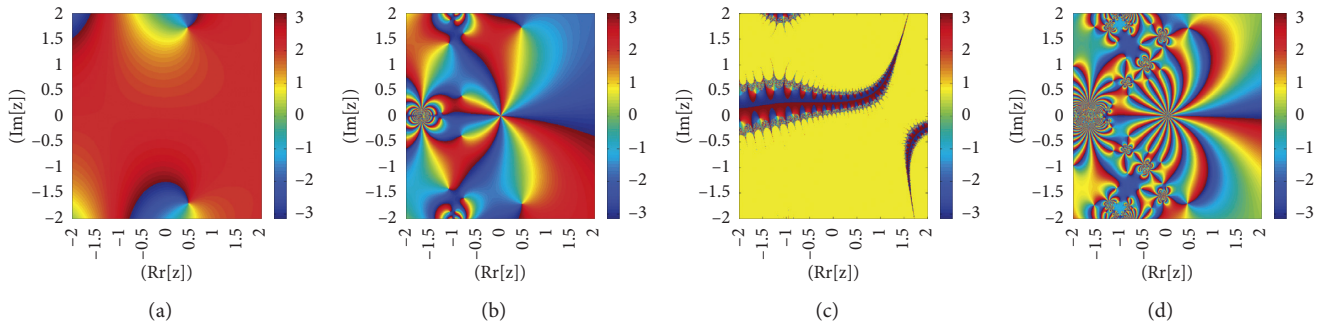


FIGURE 2: (a), (b), (c), and (d) show basins of attraction for nonlinear function $f_2(r) = \sin((r-1)/2)\cos((r-3)/2) + 1$ of the iterative methods WDK, IWDK, WDK2, and IWM2, respectively.

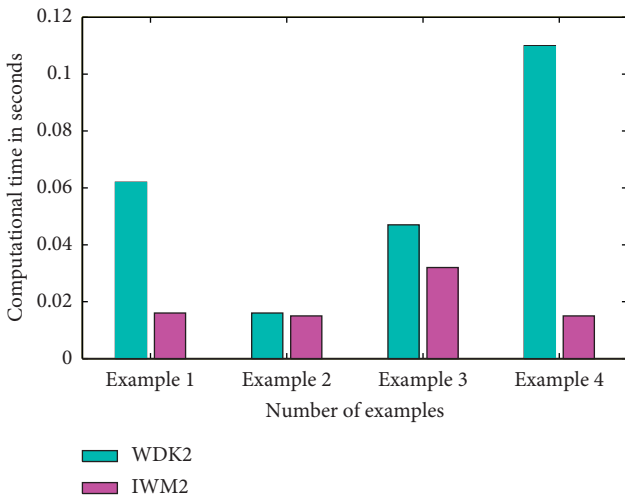


FIGURE 3: Computational time in seconds of WDK2 and IWM2 for nonlinear function $f_3(r) - f_6(r)$, respectively.

where R, a , and b are positive constants, P is the pressure, θ is the absolute temperature, and v volume. We obtain a nonlinear equation

$$\left(P + \frac{3}{v}\right)(3v - 1) = 8T, \quad (38)$$

by setting $P = (27b^2p/a)$, $T = (27Rb\theta/8a)$, and $r = (v/3b)$ Taking $P = 6$ and $T = 2$ in (37), we have

TABLE 2: Simultaneous finding of all roots.

Method	$e_1^{(6)}$	$e_2^{(6)}$	$e_3^{(6)}$	$e_4^{(6)}$
WDK2	0.0	0.0	$6.8e - 66$	$6.8e - 66$
IWM2	0.0	0.0	$1.2e - 89$	$2.4e - 86$

$$18r^3 + 13r^2 + 9r - 3 = 0 \quad (39)$$

or

$$f_4(r) = 18r^3 + 13r^2 + 9r - 3. \quad (40)$$

The exact roots of (40) are

$$\begin{aligned} \zeta_1 &= -0.476763 - 0.702381i, \\ \zeta_2 &= -0.476763 + 0.702381i, \\ \zeta_3 &= 0.2313104. \end{aligned} \quad (41)$$

The initial calculated values of (40) have been taken as follows:

$$\begin{aligned} r_1^0(0) &= -0.4 - 0.7i, \\ r_2^0(0) &= -0.4 - 0.7i, \\ r_3^0(0) &= 0.2. \end{aligned} \quad (42)$$

Table 3 clearly shows the dominance behavior of IWM2 over the WDK2 iterative method in terms of CPU time in

TABLE 3: Simultaneous finding of all roots.

Method	$e_1^{(3)}$	$e_2^{(3)}$	$e_3^{(3)}$
WDK2	8036.0	8036.0	20.2
IWM2	$4.9e-97$	$4.9e-97$	$1.7e-110$

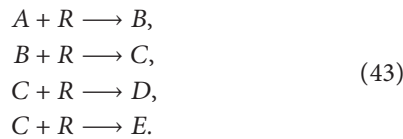
TABLE 4: Simultaneous finding of all roots.

Method	$e_1^{(3)}$	$e_2^{(3)}$	$e_3^{(3)}$	$e_4^{(3)}$
WDK2	0.2	0.4	0.5	0.7
IWM2	$4.8e-37$	$9.4e-36$	0.001	0.004

seconds and absolute error on the same number of iterations k for nonlinear function $f_4(r)$.

Example 3 (see [27]). Continuous Stirred Tank Reactor (CSTR).

An isothermal stirred tank reactor (CSTR) is considered here. Items A and R are fed to the reactor at rates of Q and $q-Q$, respectively. Complex reaction developed in the reactor is given as follows:



For a simple feedback control system, this problem was first tested by Douglas (see [28]). During his searching, he designed the following equation of transfer function of the reactor:

$$H_c \frac{2.98(r + 2.25)}{(r + 1.45)(r + 2.85)^2(r + 4.35)} = -1.
 \tag{44}$$

H_c being the gain of the proportional controller. This transfer function yields the following nonlinear equation by taking $H_c = 0$:

$$f_5(r) = r^4 + 11.50r^3 + 47.49r^2 + 83.06325r + 51.23266875 = 0.
 \tag{45}$$

The transfer function has the four negative real roots, i.e., $r_1 = -1.45, r_2 = -2.85, r_3 = -2.85$, and $r_4 = -4.45$

The initial calculated values of (45) have been taken as follows:

$$\begin{aligned}
 r_1^0(0) &= -1.0, \\
 r_2^0(0) &= -1.1, \\
 r_3^0(0) &= -2.2, \\
 r_4^0(0) &= -3.9.
 \end{aligned}
 \tag{46}$$

Table 4 clearly shows the dominance behavior of IWM2 over the WDK2 iterative method in terms of CPU time in seconds and absolute error on same number of iterations k for nonlinear function $f_5(r)$.

Example 4 (see [16]). Predator-Prey Model.

Consider the Predator-Prey model in which the predation rate is denoted by

TABLE 5: Simultaneous finding of all roots.

Methods	$e_1^{(3)}$	$e_2^{(3)}$	$e_3^{(3)}$
WDK2	9.3	9.3	7.5
IWM2	$3.9e-73$	$7.0e-73$	$1.3e-102$

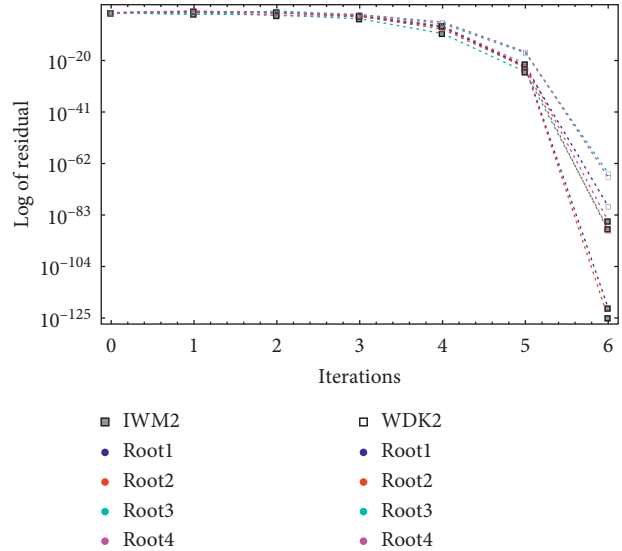


FIGURE 4: Error graph of WDK2 and IWM2 for $f_3(r)$, respectively.

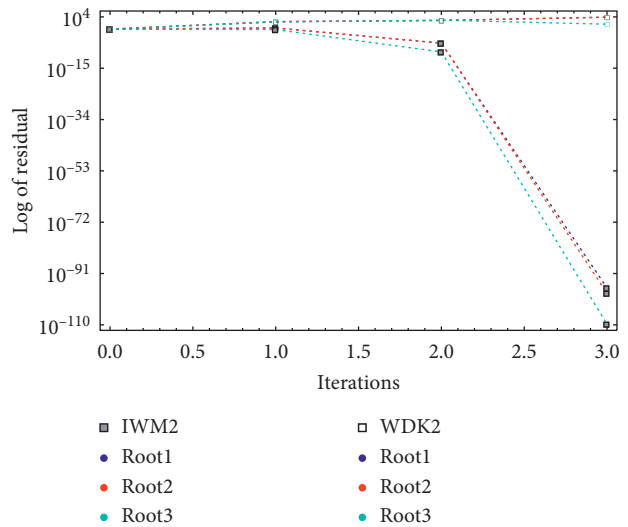


FIGURE 5: Error graph of WDK2 and IWM2 for $f_4(r)$, respectively.

$$P(r) = \frac{kr^3}{a^3 + r^3}, \quad a, k > 0,
 \tag{47}$$

where r is the number of aphids as preys [6] and lady bugs as a predator. Obeying the Mathusian Model, the growth rate of aphids is defined as $G(r) = r_1^*r, r_1^* > 0$. To find the solution of the problem, we take the aphid density for which $P(r) = G(r)$ implies

$$r_1^*r^3 - kr^2 + r_1^*a^3 = 0.
 \tag{48}$$

Taking $k = 30$ (aphids eaten rate), $a = 20$ (number of aphids), and $r_1^* = 2^{(-1/3)}$ (rate per hour) in (48), we obtain

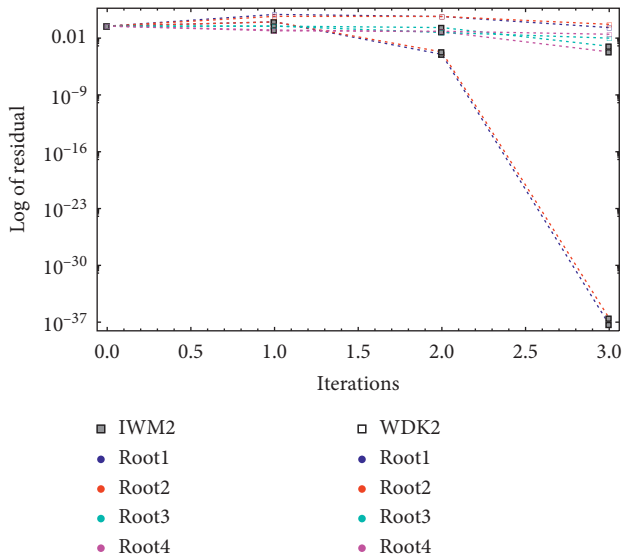


FIGURE 6: Error graph of WDK2 and IWM2 for $f_5(r)$, respectively.

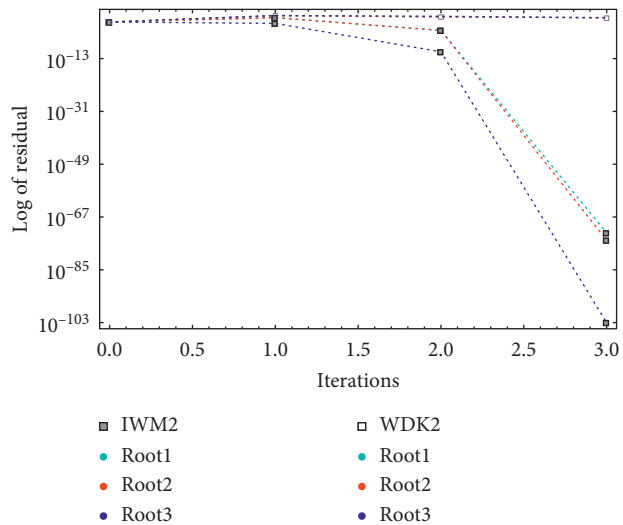


FIGURE 7: Error graph of WDK2 and IWM2 for $f_6(r)$, respectively.

$$f_6(r) = 0.7937005260r^3 - 30r^2 + 6349.604208. \quad (49)$$

The exact roots of (49) are

$$\begin{aligned} \zeta_1 &= 25.198, \\ \zeta_2 &= 25.198, \\ \zeta_3 &= 12.84. \end{aligned} \quad (50)$$

The initial estimates for $f_6(r)$ has been taken as follows:

$$\begin{aligned} r_1^0(0) &= 1.8 + 8.7i, \\ r_2^0(0) &= 1.8 - 8.7i, \\ r_3^0(0) &= 0.1 + 0.1i. \end{aligned} \quad (51)$$

Table 5 clearly shows the dominance behavior of IWM2 over WDK2 iterative method in terms of CPU time in

seconds and absolute error on the same number of iterations k for nonlinear function $f_6(r)$.

4. Conclusion

In this work, new two-step derivative-free inverse iterative methods of convergence order 4 for the simultaneous approximations of all roots of a nonlinear equation (1) are introduced and discussed. Dynamical planes and basins of attraction are presented to show the global convergence behavior of inverse simultaneous iterative methods and two-step classical Weierstrass method. Brightness in color in the dynamical planes of IWM2 shows less number of iteration steps as compared to classical simultaneous methods WDK2 for finding all roots of (1). The results of numerical test examples from Tables 2–5, CPU time from Figure 3, and residual error from Figures 4–7, corroborate with theoretical analysis and illustrate the effectiveness and rapid convergence of our proposed derivative-free inverse simultaneous iterative method as compared to the WDK2.

Data Availability

No data were used to support this study.

Conflicts of Interest

The authors declare that they have no conflicts of interest regarding the publication of this article.

Authors' Contributions

All authors' contributed equally in the preparation of this manuscript.

References

- [1] H. T. Kung and J. F. Traub, "Optimal order of one-point and multipoint iteration," *Journal of the ACM*, vol. 21, no. 4, pp. 643–651, 1974.
- [2] G. H. Nedzhibov, "Inverse Weierstrass-Durand-Kerner iterative method," *International Journal of Applied Mathematics*, vol. 28, no. 2, pp. 1258–1264, 2013.
- [3] P. D. Proinov and M. T. Vasileva, "On a family of Weierstrass-type root-finding methods with accelerated convergence," *Applied Mathematics and Computation*, vol. 273, pp. 957–968, 2016.
- [4] S. Kanno, N. Kjurkchiev, and T. Yamamoto, "On some methods for the simultaneous determination of polynomial zeros," *Japan Journal of Industrial and Applied Mathematics*, vol. 13, pp. 267–288, 1995.
- [5] P. D. Proinov and S. I. Ivanov, "Convergence analysis of Sakurai-Torii-Sugiura iterative method for simultaneous approximation of polynomial zeros," *Journal of Computational and Applied Mathematics*, vol. 357, pp. 56–70, 2019.
- [6] S. C. Chapra, *Applied Numerical Methods with MATLAB® for Engineers and Scientists*, McGraw-Hill, New York, NY, USA, 6th edition, 2010.
- [7] N. A. Ivanov, R. Muneer, and I. Jabeen, "Some families of two-step simultaneous methods for determining zeros of nonlinear equations," *ISRN Applied Mathematics*, vol. 2011, pp. 1–11, 2011.

- [8] A. W. M. Nourein, "An improvement on two iteration methods for simultaneous determination of the zeros of a polynomial," *International Journal of Computer Mathematics*, vol. 6, pp. 241–252, 1977.
- [9] O. Aberth, "Iteration methods for finding all zeros of a polynomial simultaneously," *Mathematics of Computation*, vol. 27, no. 122, p. 339, 1973.
- [10] M. Cosnard and P. Fraigniaud, "Finding the roots of a polynomial on an MIMD multicomputer," *Parallel Computing*, vol. 15, no. 1–3, pp. 75–85, 1990.
- [11] Y. M. Chu1, N. Rafiq, M. Shams, S. Akram, N. A. Mir, and H. Kalsoom, "Computer methodologies for the comparison of some efficient derivative free simultaneous iterative methods for finding roots of non-linear equations," *Computers, Materials & Continua*, vol. 66, no. 1, pp. 25–290, 2021.
- [12] V. K. Kyncheva, V. V. Yotov, and S. I. Ivanov, "Convergence of Newton, Halley and Chebyshev iterative methods as methods for simultaneous determination of multiple polynomial zeros," *Applied Numerical Mathematics*, vol. 112, pp. 146–154, 2017.
- [13] M. R. Farmer, *Computing the Zeros of Polynomials Using the Divide and Conquer Approach*, Ph.D Thesis, Department of Computer Science and Information Systems, Birkbeck, University of London, WC1, London, England, 2014.
- [14] S. I. Cholakov and M. T. Vasileva, "A convergence analysis of a fourth-order method for computing all zeros of a polynomial simultaneously," *Journal of Computational and Applied Mathematics*, vol. 321, pp. 270–283, 2017.
- [15] P. D. Ivanov and M. D. Petkova, "Convergence of the two-point Weierstrass root-finding method," *Japan Journal of Industrial and Applied Mathematics*, vol. 31, no. 2, pp. 279–292, 2014.
- [16] N. Rafiq, S. Akram, N. A. Mir, and M. Shams, "Study of dynamical behaviour and stability of iterative methods for non-linear equations with application in engineering," *Mathematical Problems in Engineering*, vol. 2020, p. 20, 2020.
- [17] N. A. Mir, M. Shams, N. Rafiq, S. Akram, and R. Ahmed, "On family of simultaneous method for finding distinct as well as multiple roots of non-linear polynomial equation," *PUJM*, vol. 52, no. 6, pp. 31–44, 2020.
- [18] N. A. Mir, M. Shams, N. Rafiq, S. Akram, and M. Rizwan, "Derivative free iterative simultaneous method for finding distinct roots of polynomial equation," *Alexandria Engineering Journal*, vol. 59, no. 3, pp. 1629–1636, 2020.
- [19] S. I. Cholakov, "Local and semilocal convergence of Wang-Zheng's method for simultaneous finding polynomial zeros," *Symmetry*, 2019, vol. 736, p. 15, 2019.
- [20] P. D. Proinov and M. T. Vasileva, "On the convergence of high-order Gargantini-Farmer-Loizou type iterative methods for simultaneous approximation of polynomial zeros," *Applied Mathematics and Computation*, vol. 361, pp. 202–214, 2019.
- [21] S. Akram, M. Shams, N. Rafiq, and N. A. Mir, "On the stability of Weierstrass type method with King's correction for finding all roots of non-linear function with engineering application," *Applied Mathematical Sciences*, vol. 14, no. 10, pp. 461–473, 2020.
- [22] A. Constantinides and M. Mostoufi, *Numerical Methods for Chemical Engineers with MATLAB Applications*, Prentice Hall PTR, Englewood Cliffs, NJ, USA, 1999.
- [23] Weierstrass and K. Neuer Beweis des Satzes, "Dass jede ganze rationale Function einer Ver"anderlichen dargestellt werden kann als ein Product aus linearen Functionen derselben Ver"anderlichen," *Sitzungsber. K"onigl. Preuss. Akad. Wiss. Berlin II*, vol. II, pp. 1085–1101, 1891.
- [24] M. Shams, N. A. Mir, N. Rafiq, and S. Akram, "On dynamics of iterative techniques for non-linear equations with application in Engineering," *Mathematical Problems in Engineering*, vol. 2020, p. 17, 2020.
- [25] I. K. Argyros, A. A. Magreñán, and L. Orcos, "Local convergence and a chemical application of derivative free root finding methods with one parameter based on interpolation," *Journal of Mathematical Chemistry*, vol. 54, no. 7, pp. 1404–1416, 2016.
- [26] M. Ivanov, "An improved memory method for the solution of a nonlinear equation," *Chemical Engineering Science*, vol. 44, no. 7, pp. 1495–1501, 1989.
- [27] N. A. Mir, M. Shams, N. Rafiq, M. Rizwan, and S. Akram, "Derivative free iterative simultaneous method for finding distinct roots of non-linear equation," *Ponte*, vol. 75, pp. 178–186, 2019.
- [28] J. M. Douglas, *Process Dynamics and Control, Vol. 2*, Prentice-Hall, Englewood Cliffs, NJ, USA, 1972.